Fibre reinforced ceramic moulding composites manufacture and characterisation.

Ren, Guogang

FIBRE REINFORCED

CERAMIC MOULDING COMPOSITES

MANUFACTURE AND CHARACTERISATION

by

Guogang Ren

DEPARTMENT OF MATERIALS
QUEEN MARY AND WESTFIELD COLLEGE
UNIVERSITY OF LONDON

This thesis is submitted for the degree of

Doctor of Philosophy of the University of London

December 1999

Abstract

Ceramic materials have considerable attraction for use in applications where the service temperatures are high and where fire performance and non-combustibility are important. Unfortunately most monolithic ceramic materials are extremely brittle which limits their use for structural applications. The development of fibre and particulate reinforced ceramic composites provides a route to achieving increased toughness in the materials, although this is often at the expense of ultimate strengths and/or the process-ability of the materials. Many reinforcing fibres used with ceramics are inherently expensive and manufacturing routes to produce fibre reinforced materials can involve high processing temperatures and are consequently expensive. A key goal of this research therefore is to develop a new type of ceramic matrix composites that combine toughness, strength and process-ability to provide a cost effective structural material.

The research described in this thesis has been concerned with the development and characterisation of a series of ceramic compounds that can be moulded at modest temperatures (130-160 °C) and pressures in a manufacturing system that replicates dough moulding compounds (DMC) as used for polymeric matrix composites. The conventional polyester matrix of polymeric DMC has been replaced by a soluble inorganic system which is compounded with fibres, fillers and hardening agents to produce a paste-like or doughy substance. The handle-ability of the material is determined by the viscosity of the matrix and the type or amount of fillers and additives present.

The research has involved a careful set of experiments in which the formulation of the ceramic DMC has been systematically varied in order to achieve an optimum viscosity for storage and handling together with a further series of experiments studying the hardening and cure of the compounds. The mechanical properties of the compounds have been measured and additional formulation changes have been introduced to maintain desirable processing characteristics while improving mechanical properties, and in particular the impact resistance using instrumented falling weight impact machines. Finally the fire properties of the compounds have been studied using cone calorimetry and indicative furnace testing.

The structure of the compound has been studied throughout the programme with various microscopic techniques and thermal analysis systems used to characterise the materials, their dispersion and changes that occurred during processing and after high temperature exposure.

The final result of the programme has been the identification of a range of material formulations that can provide a tough moulding compound, capable of high temperature service use, that possesses useful structural properties and which can be processed cheaply at modest temperatures using low cost materials.

Acknowledgements

I wish to express my thanks to my supervisor Dr Paul J. Hogg for his guidance, continuous and endurable encouragement freely offered during the course of this project. I am also indebted to Dr. Dave H. Woolstencroft for his persistent support during the research programme.

Special thanks go to Mr Ali Ahmadnia, Dr Marcel Kay, Dr Gary Bibo, Dr S. N. Sapalidis, Dr Ata Yoosefi-nejad, Dr Keizo Akutagawa, Dr Angus Evans, Dr Chris Lobley, Mr Simon Aramah, Mr Robert Neumann, Mr Roy Trew, Mr Anthony Cronin, Mr Duncan Oddy, Dr Matt German, Dr Iain Gibson, Dr Tom Buckland, Dr Karin Hing, Dr Jie Huang, Dr Kang Qiang and Dr Fariborz Kiannejad. Thanks also go to Mr Colin Langdown for his long term help to my material manufacture.

Thanks also go to Crosfield Co., Cem-FIL International, Croxton&Garry Co. and many other companies for providing me with raw materials for this research.

Thanks also go to, Dr M J Reece, Dr Andy Bushby, Dr Zhenxiao Guo, Professor Craig Davies, Professor K E Tanner for their advice, help and supports. Lots of help and assistance also come from Mr Robert Whitenstall, Dr Zofia Luklinska and Mr Mick Willis for the optical microscope, SEM and TEM works.

Thanks also go to Mrs Sandra Wells, Mrs Yvonne Johnson, Mrs Catherine Jones and Miss Catherine Pedley for their always warm help.

Last but not least, I would like to express my sincere gratitude to my wife and my daughter for their unfailing support and encouragement.

CDMC

to my parents,
Li Cuixiang and Ren Xuezhong

to my uncle,
Ren Xuezhong and his family

to my wife and my daughter
Song Yuzhi and Ren Yuan

CDMC

Contents

List of Tables

Chapter 4 Materials and compounding

Chapter 5 Moulding Technology

Chapter 6 Mechanical Characterisation

Chapter 7 Optimisation of the Mechanical properties

Chapter 8 Fire Performance

List of Figures

Chapter 4 Materials and Compounding

Chapter 6 Mechanical Characterisation

Chapter 8 Fire Performance

Chapter 9 Potential Applications

Abbreviations

AR-glass	Alkaline resistant glass.	
BET	Abbreviation of names of Brunauer, S; Emmett, PH and Teller, EJ.	
BV	Brookfield Viscometer	
CDMC	Ceramic dough moulding compound / composites	
C-glass	Glass with more alkalinity in composition	
C_3S	Tri-calcium silicate	$3CaO \cdot SiO_2$
C_2S	Di-calcium silicate	$2Ca \cdot SiO_2$
C_3A	Tri-calcium Aluminate	$3CaO \cdot Al_2O_3$
C_4AF	Tetra-calcium aluminoferrite	$4CaO \cdot Al_2O_3 \cdot Fe_2O_3$
DMC	Dough moulding compound	
DSC	Differential scanning calorimeter	
DWT	De-watering time	
E-glass	Glass used for electrical applications	
EHC	The effective heat of combustion.	
FTIR	Fourrier transmission infrared spectroscopy	
HDT	Heat distortion temperature	
HRR	The heat release rate	
IMO	International Maritime Organisation	
MLR	Mass loss rates	
MS	Mass stability	
NCF	Non-crimped fabrics	
P	Load	
PE	Polyethylene	
PP	Polypropylene	
ROMT	The range for optimisation of moulding temperatures	
RSR	Rate of smoke released	
R.T.	Room temperature	
SEA	Specific extinction area	
SEM	Scanning electron microscopy	
SiC	Silicon carbonate	
SMC	Sheet moulding compound	
THR	The total heat release	

Nomenclature

a	Acceleration
$\mathbf{a_m}$	Molecular cross-sectional area, one gas molecule in square angstroms, $N=6x10^{23}$ $\mathbf{a_m}$ = 16.3 A.
$\mathbf{a_m}$	A semi-empirical calibration related to the mirror radius
$\Delta\mathbf{a_f}$	A total cross-sectional area of a group of parallel fibres lying at an angle θ to the applied load is equivalent to a group of fibres of area $\Delta a'_f$ aligned in the direction of the applied load.
$\mathbf{A_{from}}$	A particular intersection area
$\mathbf{A_{voids}}$	Void contents of the area in the section cut from the specimens
A	Area.
C	constant
cps	SI unit of dynamic viscosity, centipoise (= $1x10^3$ Pa s = $1x10^3$ kg/m s)
D	Diameter
$\mathbf{D_f}$	Glass fibre density
$\mathbf{d_n}$	Average particle diameters
$\mathbf{d_s}$	Average surface and diameter
$\mathbf{d_p}$	Average pore diameter
$\mathbf{d_{water}}$	The density of water at testing temperature
$\mathbf{d_{CDMC}}$	The density of ceramic moulding composites
dv/dx	The speed at which the intermediate layers move with respect to each other
-dm/dt	Specimen mass loss rate(kg/s)
E	Impact energy absorption
$\mathbf{E_{II}}$	Elastic modulus of unidirectional short fibre composites
$\mathbf{E_c}$	Elastic modulus of composites
$\mathbf{E_B}$	The binding energy (E3-23, E3-24)
$\mathbf{E_b}$	Modulus of elasticity, in GPa
$\mathbf{E_k}$	The actually measured kinetic energy
$\mathbf{E'_k}$	The energy of the emitted electrons
$\mathbf{E_{CDMCm}}$	The matrix modulus for the CDMC
$\mathbf{E_{ARf}}$	Elastic modulus of AR-glass fibre
$\mathbf{E_f}$	Elastic modulus of glass fibre
$\mathbf{E_m}$	The elastic modulus of matrix

G_1	The weight of specimen after drying
G_2	The weight after immersed in to water for 24 hours
G_3	The weight of the specimen with immersed into water and then dried afterwards
g	The free fall acceleration constant
$\Delta h_{c,eff}(t)$	a time-verying value of the effective heat of combustion
K	A constant which is a function of the spherical particles diameter and the bond strength between two particles
L	Length
m	The mass
M	Torque input by instrument
m_i	The specimen mass at sustained flaming(kg)
m_1	The weight of specimen in air
m_2	The weight of specimen and plus the thread in air
m_3	The weight of specimen and thread in water
M_f	The modulus of normal E-glass fibre used in polymer composites
M_m	The modulus of phenolic and polyester resin
Δp	Orifice pressure differential (Pa)
P_f	Weight percentage of glass fibre
P_0	The saturated glass pressure
r_o	The oxygen/fuel mass ratio
R_c	Radius of container (cm)
R_b	Radius of spindle (cm)
S_{BET}	Use BET method to work out the surface area
S	Shear rate
S_c	The tensile strength to in-situ individual fibre
ΔT	The temperature difference
t^1_d	Delay time of the CO_2 analyser
T	The mean furnace temperature (°C)
t	The time (in minute)
T_e	The absolute temperature of gas at the orifice meter (K)
t_d^1	Delay time of the CO_2 analyser(s)
t_d^2	Delay time of the CO analyser(s)
t_d^3	Delay time of the H_2O analyser(s)
V_0	The velocity at the time t_0

V_f	Fibre volume fraction of CDMC
V_{CDMC}	Volume of CDMC composite
V_m	Volume fraction of matrix
V_f	The volume fraction of glass fibre
W_f	Weight of glass fibre
W_{CDMC}	Weight of CDMC composite
W_{water}	The weight of water in CDMC compound before moulding
W_L	Water lost during moulding from CDMC
W_{CDMC}	The weight of CDMC after moulding
W_S	Absorption of water in mg/cm^2
$W_{p\cdot c}$	Water absorption ratio
X_{CO}	CO reading , mole fraction
X^1_{CO}	CO reading before delay time correction
X_{O_2}	Oxygen analyser reading, mole fraction O_2
$X_{O_2}^{\circ}$	Initial value of oxygen analysis reading
X_{O2}	Oxygen reading, mole fraction
X'_{O_2}	The oxygen analyser reading before a delay time correction
X^1_{O2}	Oxygen reading before delay time correction
X_{CO2}	CO_2 reading, mole fraction
α_m	Coefficient of the thermal expansion for ceramic matrix
α_f	Coefficient of the thermal expansion for glass fibre
η	Connection factor for glass fibre volume fraction
η_l	Fibre length correction factor
η_0	Correction factor related to fibre directions and fibre position in Composites
η_m	Correction factor for matrix shrinkage and cracking
η_v	Correction factor for voids contained in matrix and between interfaces
ϕ	Fraction of total volume occupied by shares
Φ	The diameter of the single fibre
μ	Coulomb friction coefficient
υ_a	The moles of gas absorbed per gram of absorbent when gas pressure

υ_m	Mono-layer capacity of the surface
υ_p	Specific pore volume (ml/g)
$\sigma_{residual}$	Residual stress between glass fibre and the matrix in CDMC
σ_c	The crushing strength
τ	Shear stress
τ_0	Starting shear stress relating to fibre roughness
Γ_f	The fracture energy of the fibre
ω	Angular velocity of spindle (rad/sec.)
ξ	Geometrical parameter depending on fibre shape and arrangement
Ψ	A function of E_f, V_f, and E_m

Chapter 1

INTRODUCTION

In a fibre reinforced ceramic moulding compound, the main constituent materials are reinforcement (glass or carbon fibres) and a ceramic matrix. If the matrix is a metal silicate then this could be tailored to provide stability at elevated temperatures over 1200 °C. The selection of the reinforcement for applications therefore, becomes a key factor for the mechanical properties at low and medium temperature ranges (room temperature to 600 °C).

It is known that bulk silica-based glasses (E, C and AR-glass) start to decline in strength when they are subjected to temperatures greater than 250 °C, and they have softening temperatures around 800 to 850 °C (Hull D, 1996). For non-structural applications, with working temperatures lower than 800 °C, these materials could have advantages in terms of low cost and easy manufacture. In the temperature range between 300 °C to 800 °C, the glass fibres encapsulated in a ceramic compound are expected to give reasonable strength and to inhibit crack initiation.

When the temperature is over 800 °C, normal glass fibres become soft and can melt if the temperature continues to increase to over 1200 °C. In a silicate matrix composite, the glass fibres could fuse with the matrix.

The general concept of materials selection for heat protection and fire resistance has been illustrated in Fig. 1.1. As indicated, conventional polymer based composites could not be used when the temperatures exceed 200 °C with what ever reinforcement is used. Thermal degradation is fully controlled by the polymer matrix system although slight improvements in HDT can be made by a carefully selecting fillers and fibres. For instance in polymer DMC/SMC, 300 °C is the best HDT achieved by selecting suitable matrix and fillers.

Other fibres, for example, carbon fibre, can retain strength at elevated temperatures as high as 1700 ℃ depending on the coating systems. However, compared with glass fibres, carbon fibres are too expensive for most applications. In terms of cost effectiveness, for applications in civil and general engineering, glass fibres should be the first choice for heat resistance, thermal insulation and fire barrier requirements.

High performance fibres like Al_2O_3 fibre (melting temperature 2050 °C), SiC fibre (sublimes 2700 °C), retain their properties to very high temperatures, providing no adverse reaction occurs with the matrix materials either during processing or in service. The very limited applications again is due to their high price.

The problem raised here has been that most of these high performance ceramic composites were manufactured with expensive reinforcements and matrix systems through very slow and multi-stepped preparation and sintering processes such as chemical infiltration and tape casting followed by high temperature treatment. Compared to other composites such as polymer composites, the processes used for making a modern ceramic composites are both time consuming and very expensive. Although newly developed ceramic/composites injection moulding process significantly improves the greenware manufacturing efficiency, it is still limited by the small product size, high initial tooling investment, and the need for high temperature sintering after moulding.

Because of this, it would be beneficial to find an efficient ceramic composites manufacturing method with relatively low cost. Therefore, the purpose of this research is to combine an efficient, low cost route provided by traditional fibre/polymer composites manufacturing process, particularly DMC, with the high performance properties of a low cost ceramic composites.

More clearly, the basic drive for developing a ceramic moulding composite in this research was to produce a material not only providing mechanical properties similar to conventional polymer DMC, but also working at higher temperatures (up to 600~900 °C).

The matrix system is based on the liquid metal silicates, which have the capability to be chemically cross-linked by mineral salt hardeners (such as Al-Phosphate) at low temperatures (<200 °C). The real function of this hardening material is to trigger the silicate polymerisation (cross-linking), accelerate the sol-gel formation process, provide enough bonding strength for the glass fibre and the whole composite structure.

In more detail, the ceramic moulding composite investigated here is a ceramic based glass - glass/ceramic composite with a modified DMC manufacturing technique and compatible mineral fillers. With a specially formulated ceramic matrix system and alkali resistant glass fibre (AR), the ceramic dough moulding compound (CDMC) has improved ductility, compared with the traditional ceramics and glasses. The complete process of developing a ceramic moulding compound can be described as a sequence of the raw material preparation, manufacturing and moulding, testing of physical, mechanical properties and fire performance. The polymerisation of the silicates has been also investigated primarily using TEM and other methods in order to determine a basic composition for different moulding temperatures.

This thesis consists of 10 Chapters. In Chapter 2, the background of the ceramic matrix, fibre reinforcements and general relevant composite processes are presented as Literature Review; Chapter 3 is the testing experimental methods; The material technologies of compounding and moulding are in Chapter 4 and 5. The characterisation and optimisation of mechanical properties are in Chapter 6 and 7. The material's fire resistance and heat performance are presented in Chapter 8. Some application trials are in Chapter 9. Finally Chapter 10 is the Conclusion. The general research steps are shown schematically in Fig. 1.2.

The evaluation of formulations and optimisation of mechanical properties have been carried out by mechanical tests such as tension, flexure and impact on the manufactured CDMC panels. The mechanical properties are optimised by tailoring formulations and moulding conditions. It is clear that with a brittle matrix, the mechanical properties are highly effected by the fibre types and fibre/matrix interfacial properties which reflect the formulation, moulding conditions and post curing.

The fire performance of the material, however, is controlled by the formulation, especially the type, volume content of polymers, fibre reinforcement, filler types and structure of the products. The material's thermal properties can be determined by the stability of the material and the interfacial properties at elevated temperatures.

This new compound was used to produce a number of trail mouldings of representative industrial components including Heat Shield (Al mould), Heat Shield Cap (steel mould), a double curvature track line fairing (Carbon graphite mould). These illustrated the advantages of low cost, easy manufacturing, proper mechanical properties and excellent fire and heat resistance for the CDMC.

Matrix system selection according to application temperatures

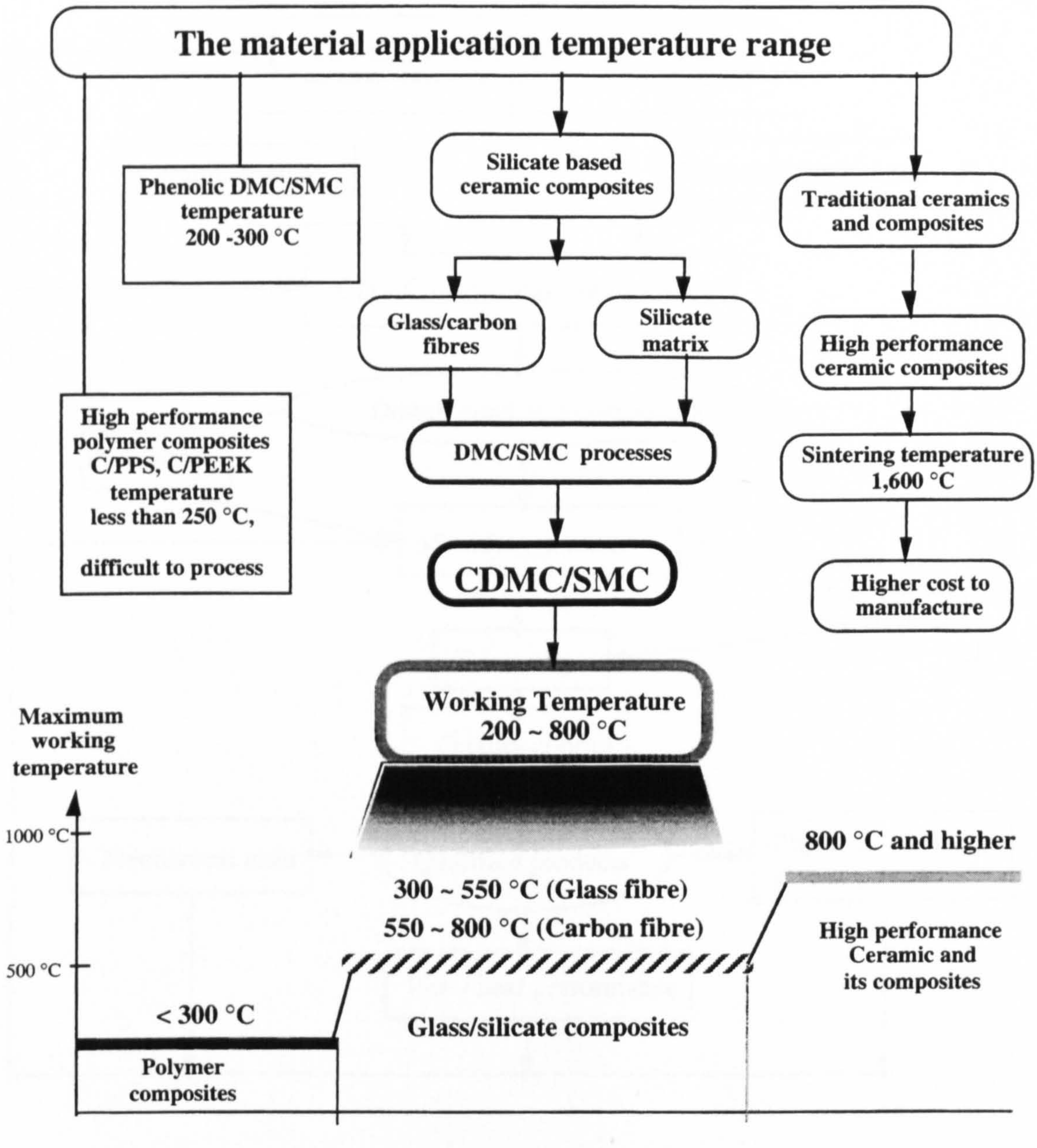

Fig. 1.1 Indication of working temperature ranges for different classes of composite materials and basic principles of selecting the matrices for polymer/glass fibre/carbon fibre/ceramic matrix composites in terms of different application temperatures.

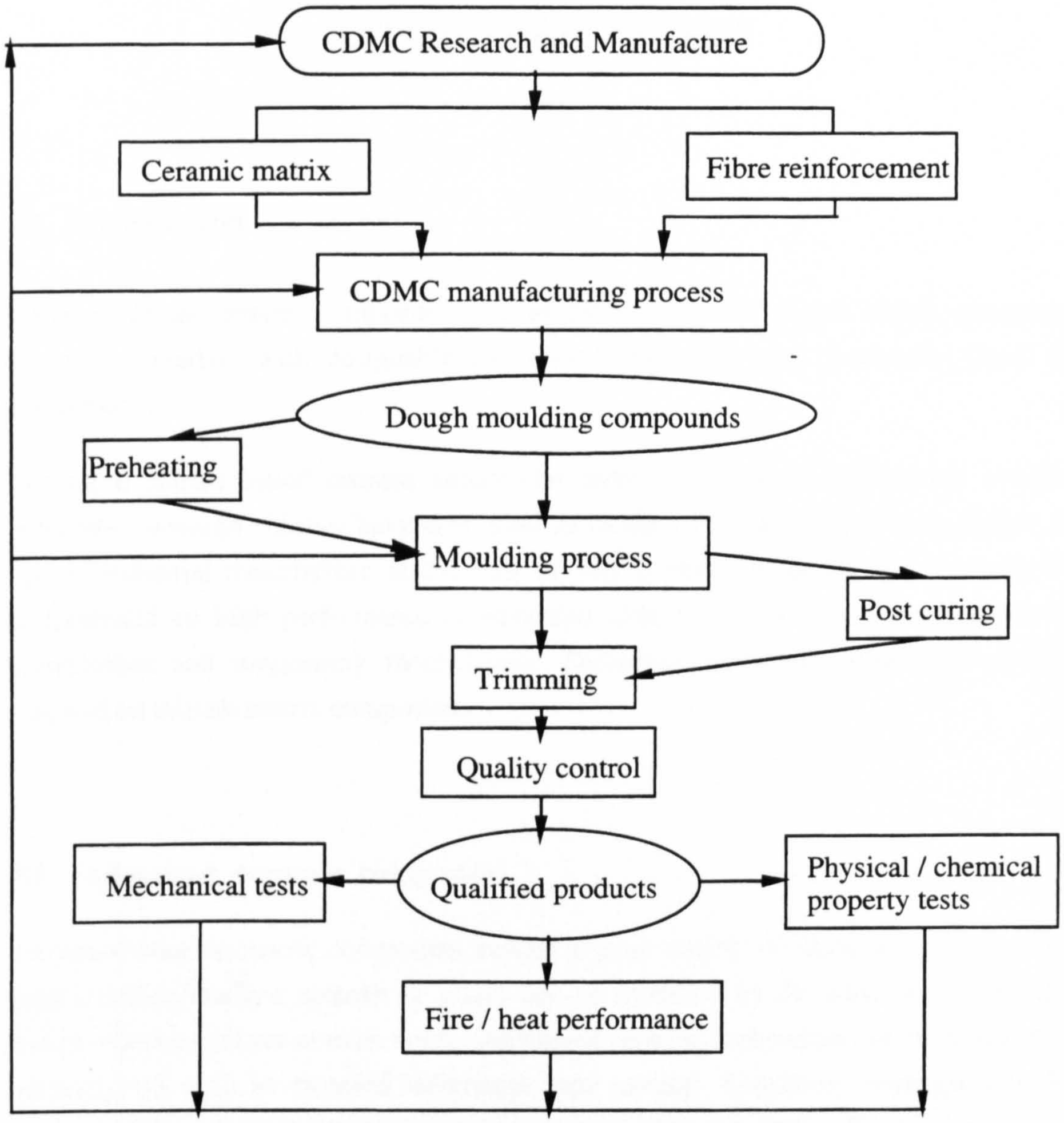

Fig. 1.2 Total schematic view of the manufacturing, moulding and testing of the CDMC in this research programme.

Chapter 2

LITERATURE REVIEW

2.1 Introduction

Fibre reinforced ceramic composites such as fibre reinforced silicate matrix composites are new materials with designable mechanical properties and inherently good fire performance.

For metal silicate based ceramic composites there is not much information available presently, although silicates have been used as binders for many years, long before the age of industrial manufacture at the turn of this century. Most ceramic research has concentrated on high performance or advanced ceramic composites, especially on the manufacture and toughening mechanisms. There has been little systematic research reported on silicate matrix composites.

2.2 Advanced ceramic composites

Advanced ceramic matrix composites include a great variety of materials. Typically, a matrix (polycrystalline ceramic or glass) can be modified by the addition of particles, flakes, whiskers, fibres or even voids. Advanced ceramic composites can be produced in several ways such as chemical infiltration, tape casting, fibre/slurry impregnation, hot press moulding, injection moulding and so on. One of the relatively efficient methods for producing high performance fibre/ceramic composites e.g. Al-Si-B-O/Al-Si-O-C, SiC/SiC/Al_2O_3, SiC/Al_2O_3, SiC/Cr, SiN, SiC_W-Al_2O_3 is tape casting/impregnation with continuous fibre systems (Fig. 2.1) (Hull and Clyne, 1996).

In the process, the tapes are cast from a formulated slurry consisting of a liquid, a ceramic powder, an organic polymer, a plaster, or a dispenser. Laminates of a wide variety of architecture and compositional ranges have been produced by stacking the individual layers and then consolidating them (Haug and Schafer, 1992). The great flexibility in

designing and tailoring these multi-component systems permits control and enhancement of many significant properties. The principle that underpins ceramic composites is that by introducing a second phase in a ceramic matrix, a different failure mechanism can be trigged that prevents catastrophic failure (or improves other special functionality such as fire or thermal performance).

The intrinsic high stiffness, high hardness, chemical inertia and fire resistance of ceramics are derived from the strength of their chemical bonding (Chant, Bleay. 1995). This bonding permits little or no movement of dislocations, even at modest temperatures, and leads ultimately to brittleness. Because a distribution of flaw sizes is evident in real materials, ceramics exhibit a distribution of strength values. From a design engineer's perspective, ceramics are unreliable (Strand, 1986). Pure glass/ceramics are very brittle materials, although they still could be toughened by some limited methods such as increasing fracture surface area, changing the fracture mode (e.g., mode I to mode II or III), and mechanical interlocking. However, there are many limitations on the actual use of these toughening techniques.

Producing a rough fracture surface is most readily achieved in ceramic composites by: the interaction of tough second-phase particles which hinder crack propagation; weak interfaces in certain materials (fibres and whiskers) which deflect cracks; residual stresses at second phases which affect crack propagation; micro cracking leading to crack branching and deflection; and elastic mismatches between phases leading to induced stresses and crack deflection. The concept of "a process zone" can be applied to the vicinity of a crack tip where such processes occur. Removing energy from the advancing crack depends on the volume fraction of transformable particles, fibres and number of micro crack nuclei. For fibre reinforced ceramics, toughness also relies on the level of fibre bonding, the spacing of critical flaws on fibres, fibre bridging and pull out length, and features of ductile fillers in the overall composites.

A very effective technique for dissipating energy during fracture of a ceramic composite is through whisker or fibre pullout. Extracting a fibre from a matrix in a composite against frictional stresses, can absorb large amounts of energy, since quite large areas are involved (i.e. the fibre lateral area). However, the manufacturing methods are very complicated and extremely expensive (high temperature sintering) for these advanced ceramic composites. The large amount of energy consumption by ceramics such as Al_2O_3 is illustrated in Fig. 2.2.

In comparison, liquid silicate ceramics can be thermally and chemically cured/hardened at relatively low temperatures, and produce reasonable mechanical properties with low

energy consumption and this results in a low cost. The composites formed with low cost glass fibre or carbon fibre have presented all the features of brittle ceramic matrix composites.

2.3 Ceramic composites used for fire protection and heat insulation

Ceramic composites have been widely used in fire protection and heat insulation in aerospace industry (Banas, 1996) since the early 60's. The most complicated application has been the space shuttle thermal protection system. Although some other polymer composites such as phenolic composites have been used in the orbiter's rockets, these were not economical for the development of NASA's space shuttle orbiters since the polymer insulation layer would be burned off during re-entry. The temperature when the space shuttle encountered re-entry was as high as 1260 °C.

The raw materials for reusable insulation tiles were mainly composed of 99% pure silica fibre derived from high quality sand. They were light weight with a very low coefficient of thermal expansion, and a high temperature stability. They were selected for making a small block of tile which could be heated to as high as 2268 °C, as shown in Fig. 2.3. These surface layers for the space shuttle have to be made through extremely complicated manufacturing processes.

The two most famous insulation systems used in the space shuttle were LI-900/LI-1200 and FRCI-12 containing mainly silica fibre and SiC particles or fibres (Fig. 2.3 - 2.4). The manufacturing processes started with making a billet from a slurry; followed by removal of entrapped air bubbles by vibration. The billet was compressed to the final cast size. After the billets were dried, the peak sintering temperature was 1327 °C, which maintained the silica in an amorphous state.

That was a very expensive and very complicated manufacturing process. For the space shuttle the cost of these materials were acceptable, but for normal civil and industrial applications, they are far too expensive both in terms of the raw materials and the quality control required.

Therefore, for normal industrial and civil applications, an affordable ceramic based insulation material is required which can provide a certain level of ductility. From an initial investigation, silicate moulding compounds could fulfil these tasks and involve a

lower cost manufacturing process with relatively good insulation properties and desirable mechanical properties.

2.4 Manufacture of chopped fibre reinforced DMC

Chopped fibre composites are widely used for making many flat and irregular or complicated shapes which are difficult to produce from continuous fibre composites due to their poor flowability. Although open and closed processes such as DMC are less efficient in use of fibres, they have higher output rates and lower costs than continuous fibre processes. The chopped fibre composites can also be produced with few surface flaws, and with three-dimensional orientation reinforcement as shown schematically in Fig. 2.5. With a 3-D fibre orientation, the mechanical properties of composites in any direction are proportional to the amount of fibre by volume oriented in that direction. As fibre orientation becomes more random, the mechanical properties in any one direction become lower.

Polymer DMC is a mixture of a chopped fibre (glass/carbon , etc.) and resin (UP resin/phenolics/epoxy, etc.) with additives and a large quantity of fillers, in the form of dough, supplied in bulk form or as an extruded rope for compression (as shown in Fig. 2.6), transfer or injection moulding. Manufacturing of the moulding compound begins with mixing of a fibre-free paste. Batch mixers are ordinarily used for this operation to mix a large amount of solid ingredients which are difficult to compound. A high-speed turbine mixer with a saw tooth disc blade is frequently used to make the paste itself as shown in Fig. 2.7. The thickening agents and catalysts are often added near the end of the mixing to reduce their extent of reaction. Afterwards, the paste is transferred to a double arm or planetary mixer and chopped glass roving. About 6 ~ 25 mm in length and 20 to 30 % fibre in volume, are added into the compound. For industrial production, polymer DMC is manufactured by feeding the paste premix into a Z-blade mixer, where chopped glass is distributed. The resulting 'dough' is either extruded in a sausage like shape, or formed into large lumps, and then packed in diffusion tight foil.

The DMC manufacturing route was used as a possible production method for the ceramic moulding composites. In the initial research of this project, it is shown that this process and moulding technique are ideal for manufacturing and moulding processes of chopped

fibre/ceramic moulding composites, providing some necessary modification is introduced based on the features of ceramic matrices.

The ceramic materials have to be changed in the following ways in order to improve their engineering reliability (Kelly and Macmillan, 1986). Firstly, by decreasing the sensitivity to flaws; secondly by increase reliability and to realise the potential strength of ceramics. It was considered that one of the ways to realise these would be applying or adding reinforcement to form a second or third phase in a composite structure.

The general concept of this research is to combine low cost and low temperature ceramic compounds (part I) with the DMC manufacturing method (part II) to produce products with optimal mechanical and thermal properties. For mechanical properties, the aim is to reach the properties of phenolic/polyester DMC listed in Table 2.1. For the thermal properties, it is to retain the properties of matrix systems of ceramic silicates, but with better thermal shock resistance.

2.5 Silicate based composites

Silicate based primitive composites have been manufactured for hundreds of years. The Chinese and Egyptians had used natural fibre or fabrics such as the crop fibres mixed with metallic silicates or clay to make their houses and wells as early as 8,000 BC. Particularly, the Chinese used silicate clays combined with $Ca(OH)_2$ / CaO and sand to build the bases or foundations with stones, bricks for the great wells, roads, and buildings over several thousand years.

In modern industries, silicate based composites have been widely used in building construction and decorative panels, while their main reinforcements once were asbestos fibres and other mineral fibres. Since health regulations world-wide banned the use of asbestos, people have tried many alternatives to replace asbestos and other harmful mineral fibres for composites.

Although the fire performance of metallic silicates has been known for many years, it was only recently that they have started to be used in the fire resistant materials arena, since they have always been brittle and fragile. It was the development of composite research and the wide range of applications of polymer composites which are so weak when facing fire, that promoted the renewed interest in these materials. Also public concern and the

potential for the massive loss of human life in fire disasters, has promoted a new impetus in the development of new fire resistance materials.

2.5.1 Silicate matrix composites in general

Silicates can be found in the form of liquids, powders and glasses. They also exist in fibrous structures and in some metallic silicates, which generate different forms of composites. Accordingly silicates can be matrix or reinforcement in their composites according to the form of silicates and the manufacturing processes.

Low temperature hardening processes using liquid silicates as binder, were reported in later 80' and early 90' (Mackenzie, 1991). With blast furnace slag powder as a filler, the silicate matrix was reinforced with glass or polymeric fibres. Final curing temperatures can be below 100 ℃ after humid atmosphere treatment. The process was so called wet curing. Room temperature setting has used Na-silicates and mineral materials with acidic gas (CO_2/SO_2) to help to develop a full strength.

There have been many silicate/glass based composites systems reinforced with mineral fibres developed during 80's and 90's in UK, USA, Japan, Canada, New Zealand and other countries. Some of them used liquid silicates as a binder to bond chrysotile asbestos into a robust, dimensionally-stable lightweight ceramic materials (JP05097495A2, 1994; Mackenzie, 1994; Tredway, Musson, Chen 1996). The method was to fuse liquid metallic silicates and ground waste glass to form a material without fibre emissions and with enhanced mechanical properties. These materials formulations are listed in the Table 2.2.

The benefit of this was that the fibre bundles were stabilised through fusion with a glassy matrix, significantly reducing the respirable fibre concentration. The SEM analysis of this system proved that any resulting dust was free of fibres. The valuable thermal treatment could also convert the chrysotile into crystalline forsterite, which should destroy its cell toxicity. The manufacturing processes are displayed in Fig. 2.8 developed in USA/Japan and Fig. 2.9 developed in UK.

In early 90's, a series of silicate composites were designed as fire proof structural laminate with specific mechanical properties. One of these systems was CS3000-FR/HR (Claymore Systems data sheet, 1994, 1996) rated as non combustible in accordance with British Standard 476 Part 4. Further tests proved that the materials after exposure to

temperatures up to 1000 °C showed minimum deterioration, and produced negligible levels of smoke and no toxic emissions.

Since solid silicates as a general mineral composition, possess good thermal performance, their composites are widely used in coating industries for improving fire resistance. As an example, a fire resistant inorganic coating composite was made by a Canadian firm for high speed aeroplanes (US4888057). It provided an intumesecent feature when subjected to high temperature and fire to form a continuous heat insulation structure which was retained for prolonged periods at temperatures up to 1000 °C. For instance, a coating system with multiple layers on an Al panel with the thickness of coating from 1.9 to 3 mm was heated up to more than 1000 °C, the time for the back surface to reach 300 °C was > 30 minutes. When it was heated for 30 minutes up to 900 °C, the coating layer swelled to about 4 to 5 mm.

A coloured fire resistant composite was developed by a group of Japanese researchers (JP-5-163051/A2-930629) in 90's. Panels were manufactured by a moulding process and curing at elevated temperatures generated enough strength for building materials. The process is shown in Fig. 2.10.

Shrinkage has been always a problem for the manufacture of metallic silicate composites. During sintering and moulding the density of the materials increases tremendously. Materials shrinkage makes it difficult to introduce dimensional stability into the components. Because of this, the surface qualities of the moulded or sintered parts can not be controlled. A Japanese research group developed a dimensional stable material based on a silicate composite with the blast furnace slag as its main filler (Huda 1994). This water proof composite material has achieved following properties:

Bending strength	29.4	MPa
Young's modulus	19.6 ~ 29.4	GPa

The use of fine aggregates could also improve workability during moulding of kneaded materials and reduce the shrinkage caused by drying of the hardened materials. Other expandable inorganic materials in cement applications have been reported such as the use of pre-hydrated high alumna content cement as an expansion additive to compensate for shrinkage compensating (Fu, Xie, Gu, Beaudoin, 1994).

In the above discussion, silicates were used as a binding agent. In later research the silicates were used for improving the strength of greenware which was in the form of a liquid meta-silicate solution for ensuring compatibility with ceramics or concrete (Yanakiev, 1990). The silicates could be used to mix with original composition to produce better and stronger greenware. With acid treatment, articles with a 3-dimensional porous structure in their framework can be obtained after sintering. An other route for making porous structures was using SiN_4 mixed with $Na_2O{\cdot}SiO_2{\cdot}H_2O$, Al_2O_3 and Y_2O_3 as sintering aids (JP 63256575). The final sintering resulted in a honeycomb-shaped ceramic article having micro-pores on the cell wall (JP 63256578). The process is shown in Fig. 2.11-2.12.

Silicates are often hardened by means of esters, which hydrolyse and subsequently gel the silicates (Nicholas, 1972; Roberts, 1972). These were used to stabilise soils in underground construction projects (O'Connor, Krizek, and Atrmotzidis, 1978) and used extensively in spiral-tube winding, fibre drums, and sailing, laminating metal foil to paper and in corrugated boxes used in manufacturing of refractory and acid-resistant mortars and cements used in palletising, granulating and as a carrier for water based coating (Classer and Lee, 1971).

2.5.2 General features of silicates for composite processing

Viscosity characteristics of liquid silicates are very important since they reflect the solid content, mole ratio of SiO_2:Na_2O, particle sizes, level of gel and sol formation, etc. For example, the silicate solutions in a mole ratio (SiO_2:Na_2O) of 2.65 can be manufactured in an autoclave at a temperature of 160 ℃ by dissolving fine ground sand in a NaOH solution. The solid level of the solutions sold commercially is normally between 25 - 40%(wt.). Figure 2.13 shows how the viscosity of silicate solutions increased with an increase in the solid level. Meanwhile, the higher the ratio of SiO_2:Na_2O, the greater the rate of viscosity increase with the solid content.

Silicate powders are made from liquid silicate solutions. The ratio of the SiO_2:Na_2O in powders are determined by the ratio in precursor liquids. In a high ratio SiO_2:Na_2O solution, evaporating of water, increases the viscosity to a point where solid forms. The rate of evaporation of a solution containing soluble silicates and the rate of solid silicates dissolving into water are a function of particle size, SiO_2:Na_2O ratio and water content. In

Table 2.3, powdered soluble silicate can be made in a wide range of SiO_2:Na_2O ratios and solution rates for diverse applications.

As discussed above, the ratio of SiO_2:Na_2O and the content of silicates in water solution give different viscosity for the solution. Therefore, the solid silicates have been used to adjust viscosity in liquid solution and binder for ceramic slurries. Many of the metallic silicates in solid or liquid systems such as K-silicates, Na-silicates, Al-silicates and $MgCl_2$ etc. are developed for these applications (Shchetanov, Mizyurina, Gribkov, Shalin, Chanov, 1996). A Chinese paper reported on the use of silicates as thickening, diluting agents and bonding agents for analysis of black talc slurry (Wu, 1994). It was found that by adding metallic-silicates with different ratio of SiO_2 and Na_2O, the whole system was thickened or diluted as desired.

The fibre/silicate composites are classified as the ceramic composites (Bentur and Mindess, 1990; Balaguru, Shah, 1992). Since we are going to use the process of DMC from the polymeric composite industry to produce fibre/ceramic moulding compounds, the materials we investigated and produced have been named as ceramic dough moulding compounds (CDMC).

2.6 Background to the matrix system-Silicates

What are silicates? Silicates (M_x·$mSiO_2$·nH_2O) are a vast family in inorganic chemistry and are derived from silicon (Si). Silica (SiO_2) and silicates have been intimately connected with the evolution of mankind from prehistoric times: the names derived from the Latin *Silex*, gen. *silicis*, flint, and serve as a reminder of the simple tools developed in Palaeolithic times (~500,000 years ago) (Greenwood, Earnshaw,1984). The name of the element, silicon, was proposed by Thomas Thomson in 1831, the ending *on* being intended to stress the analogy with carbon and boron.

Naturally occurring silicate minerals makes up more than 90% of the earth's crust. Although tens of thousands types of metallic-silicates chemically exist, they are only a small part of the natural resources on the surface of the earth. These minerals are slightly soluble and are in chemical equilibrium with the mineral components (Grayson, 1985). Because of this slight solubility, concentrations of dissolved silica usually are 10 ~ 100 PPM in mineral water. The soluble silicates have the general formula (C2-1):

$$M_2O{\cdot}mSiO_2{\cdot}nH_2O \qquad C2\text{-}1$$

M - an alkali metal, **m**, **n** are the number of moles of SiO_2 and H_2O relative to one mole of M_2O, the **m** has been called the ratio of the silicate. Sodium silicate is the most soluble common silicate, and the commercial form of this silicate generally is a glass dissolved in water to form a viscous alkaline solution (m = 0.5 ~ 4.0), the commercial water glass has an **m** value of 3.3.

Although the knowledge of soluble glass could be traced to antiquity, soluble silicates started their industrial development in the early 19th century in Germany and were first produced in North America during the Civil War, when they were in laundry soaps as a replacement for resin.

The production method was that sodium carbonate (soda ash) and sand were fused in an open hearth furnace to produce a glass which was then cooled, crushed and dissolved, and this formed the basis of modern manufacturing methods. Commercial availability of those glass solutions gradually led to the development of adhesives and binders after the turn of the century.

Apart from additives in washing powder and detergents, soluble silicates developed an important market after World War II in manufacturing synthetic pigments and fillers, silica gels and sols, synthetic clays and zeolites. It was well known that soluble silicates have miscellaneous usage's in cements, coatings, bleaches, water treatment, and soil stabilisation. These are based on their capability to form gels/sols and to react with multivalent metal ions or oxide surfaces in solution. After World War II, the main market for liquid silicates was adhesives and surface active agent.

2.6.1 Structure of soluble silicates

Silicates are composed of silicon and oxygen. The bulk of soils, rocks, clays, and sand come under the mineral silicate classification. The basic building block of a metallic silicate is SiO_4^{4-} , a tetrahedron structure giving various arrangements for silicate ceramics (Fig 2.14) (Callister, 1993). Table 2.4 shows some of the structures in different silicates (Engelhardt and co-workes, 1975).

Synthetic silicates and silica are made up of oligomers of the basic building block of SiO_4^{4-} with tetrahedral structure. Silicate polygons can construct more complex structures according to Pauling's rules. The Q^s structure notation refers to the connectivity of silicons (Von, Engelhardt and co-workers 1975). The superscript represents the number of nearest-neighbour silicon atoms.

2.6.2 Silicates in solutions

The distribution of silicate species in solution has long been of interest because of the wide variations in the typical properties. Studies in 1920's led to a dual description of silicate components (Harman, 1928). Prior to 1928, sodium silicate solutions were thought to be composed of products of hydrolysis, colloidal silicic acid, hydroxide ions, and sodium ions. However, through the analysis of the properties of solutions with various ratios of SiO_2:Na_2O, the silicate solutions also contain crystalloidal silica (Nauman and Debye, 1928).

Later research in light scattering showed that stable silicate solutions did not contain very large particles. In the 1970's, other indirect methods of studying silicates species in solution indicated that these are a complex mixture of silicate anions with varying degrees of polymerisation in a dynamic equilibrium (Engelhardt and Co-workes, 1975). Recently, the NMR spectra for a range of silicate ratios were measured, and the various silicon centres could be identified and relative concentrations could be estimated.

The following representations of the polymeric species in silicate solutions have been proposed, i.e., for $H_{2x}\ Si_yO_{(2y+x)}$ or its ionised forms: number of non bridging oxygen = 2x; number of bridging oxygen atoms = 2y + x. The most common species in $Na_2O{\cdot}SiO_2{\cdot}H_2O$ family are shown in Fig. 2.15. A general formulation could be presented as:

$$\mathbf{Na_2O{\cdot}SiO_4{\cdot}xH_2O} \qquad \text{C2-2}$$

x = n - 1, contain silicate monomer; x = 4, sodium meta-silicate pentahydrate (CN No. 10213-79-3/PQ Co.); x = 5, sodium meta-silicate hexahydrate (CN No. 35064-64-3/PQ Co.); x = 7, sodium meta-silicate octahydrate (CN No. 27121-04-6/PQ Co.); x = 8, sodium silicate meta-silicate nonahydrate.

Silicate glasses (Zhdanor, Stekla, 1978), that contain SiO_4 tetrahedra are similar to other forms of silica, crystalline silicates and glasses (Crosfield Chemicals, 1994-1995). The tetrahedra may be monomers or polymerised with up to four other tetrahedra sharing oxygen atoms to form Si-O-Si bridges (siloxane bond).

Soluble silicate solutions contain mixtures of silicate anions, ranging from monomer SiO_4^{4-} and dimer $Si_2O_5^{2-}$ through to high molecular weight polymers containing a large number of Si atoms. On evaporation, these polymers coalesce causing steep rises in solution viscosity which is why more siliceous materials are often used as adhesives.

It is suggested that the principal factors in commercial silicate glass dissolution are temperature, glass composition and surface area. The dissolution of silicate glass involves a two-step mechanism (El-Shamy and Lewins, 1972):

Ion exchange $\equiv SiONa + H_2O \Leftrightarrow \equiv SiOH + Na^+ + OH^-$ C2-3

Network breakdown: $\equiv SiOSi \equiv + OH^- \Leftrightarrow \equiv SiO^- + HOSi \equiv$ C2-4

The solubility trend is $K^+ > Na^+ > Li^+$. The presence of multivalent metal ion impurities, e.g. Al^{3+}, Ca^{2+}, or Fe^{3+}, in the alkali silicates reduces the solubility of the glass (Douglas, 1972).

2.7 Polymerisation of silicates

Polymerisation of silicates has been of great interest to technologists for a wide range of applications. The complex silanol polymerisation process may be simplified as C2-5:

$$\equiv SiOH + \equiv SiO^-H^+ \xrightarrow{K_1} \equiv SiOSi \equiv + H_2O\uparrow \qquad \text{C2-5}$$

This empirical representation becomes less valid at pH>10. Other factors influencing colloidal systems are ionic strength, dielectric constant, and temperatures. Larger particles grow at the expanse of smaller particles, especially at higher pH value, the tendency of smaller particles to condense at the surface of the large particles is more (Schwertz and Muller, 1958).

Low pH values and higher ionic strengths lead to the growth of smaller particles. If the concentration of SiO_2 is sufficiently high, inter particle aggregation and ultimately network formation will occur, i.e., gelation, yielding a continuous structure throughout the medium (Balyakov and Co-workers, 1974).

2.7.1 Chemical mechanisms of silicate condensation

The mechanism of silicate polymerisation can be divided into 3 stages, as shown in Fig. 2.16. They start with monomers and then grow into particles, if the condition is right they can link up together and form chain and networks. The reaction involves the condensation of silinol groups (C2-6) and results in an increase in molecular weight of silica (Carmen, 1940):

$$\text{-SiOH} + \text{HOSi-} = \text{-SiOSi-} + H_2O \qquad \text{C2-6}$$

The formation then growth of spherical particles is one kind of polymerisation. Aggregation of particles to form viscous sols and gels is another kind of polymerisation which may occur and lead to form chains or networks under other conditions. Succeeding steps in polymerisation from monomer to large particles and gels have been represented schematically by Ilea (1974) as in Figure 2.17. An intermediate covalent stage and even more extensive complexes involving 6 co-ordinated silicon were postulated in the pH between 2 - 10 as shown in Fig. 2.18 (Weyl, 1951).

When polymerisation takes place above pH 7, the ionisation of polymer species is much faster so that the monomer polymerises and decreases in concentration vary rapidly at 25 °C. Meanwhile, the particles grow rapidly to a final size that depends mainly on temperature. The higher the temperature, the bigger the particle size (Ilea, 1955).

It was observed that at pH 8 the polymerisation of silicic acid has an "induction period" during which there is little or no polymerisation of monomer. And the "reactive silica" was mainly $Si(OH)_4$ monomer (Baumann, 1959). At this pH stage, the polymerisation of monomer involves a reaction between $Si(OH)_4$ and $\equiv SiO^-$ ions.

2.7.2 The self-condensation

Self condensation of monomer catalysed by OH^- ion involves the formation of oligomers and is commonly written as:

$$2Si(OH)_4 \xrightarrow{OH^-} (OH)_3SiOSi(OH)_3 + H_2O \qquad \text{C2-7}$$

The greater the member of siloxane linkages and the fewer OH^- groups on a silicon atom, the stronger the acidity (C2-8) (Ilea, 1984):

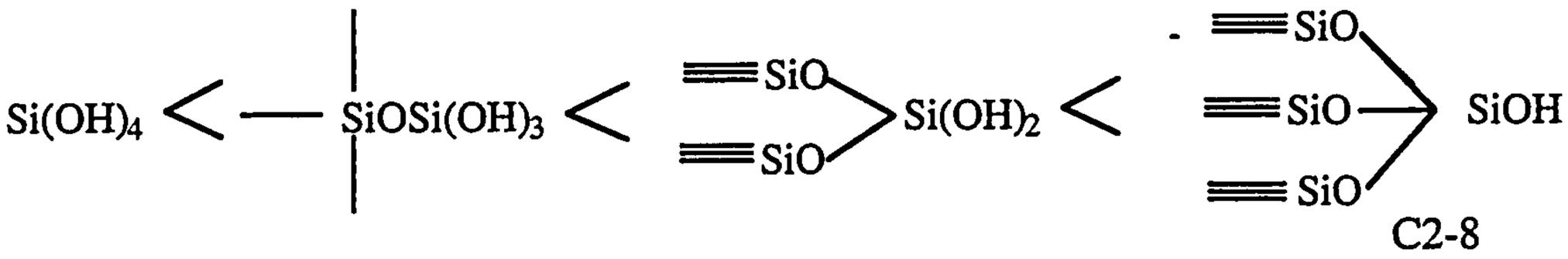

C2-8

Polymerisation also involves intermediate ionisation to $\equiv SiO^-$ or $\equiv Si^+$ to below or above pH 2. The key point is that condensation involves the reaction of an $\equiv SiO^-$ ion with the non-ionised silanol group:

$$\equiv Si^- + HOSi \equiv \longrightarrow \equiv SiOSi \equiv + OH^- \qquad \text{C2-9}$$

When monomer polymerises in alkaline solution in pH range 8-10 colloidal silica particles form quickly and grow spontaneously (Ilea, 1984).

2.8 Physical characteristics of gel and powder

Silica gel and powders consist of silica particles, ranging from 1 to 100 nm in diameter.

- **Silica gel -**

A coherent, rigid three dimensional network of continuous particles of colloidal silica can be formed by polymerisation of silicic acid and through aggregation of colloidal silica. Most common four types of Gels are:

- Alcogel - pores filled with alcohol;
- Aqua gel - pores filled with water;
- Xerogel - liquid medium has been removed, structure compressed;
- Aerogel - A type of Xerogel, liquid removed, structure kept.

- **Silica powder -**

Silica powder consists of small granules of silica gel or sub micron particles that are linked together in extremely weak networks. There are about 7 types of silica powders: pulverised gels, spheroidal gels, precipitated silica, aerosols or pyrogenic silica, organophilic silica, aluminosilicate anions (Buzagh and Von, 1950).

The average particle diameters can be calculated as d_n, the number - average diameter and d_s, the surface - average diameter:

$$d_s = \frac{\sum_{i=1}^{i=k} n_i d_i^3}{\sum_{i=1}^{i=k} n_i d_i^2} \qquad \text{E2-1}$$

Where n_i is the number of particles in its range of sizes, the mean diameter of each being d_i , and k is the number of size range.

Another important property is the surface area of the gel or powder. The BET (Brunauer, Emmett, and Teller) method of calculation specific surface area from an absorption isotherm used nitrogen as the absorbed at 196 °C. BET equation (Burnaner, 1945):

$$\frac{p}{v_a(p_0 - p)} = \frac{1}{v_m c} + \frac{(c-1)p}{v_m c p_0} \qquad \text{E2-2}$$

υ_a is the moles of gas absorbed per gram of absorbent when the gas pressure is p, υ_m is the mono-layer capacity of the surface, p_o is the saturated gas pressure, c is constant.
The area determined by the equation E2-3:

$$S_{BET} = v_m a_m N \times 10^{-20} \qquad \text{E2-3}$$

a_m is the molecular cross-sectional area of one gas molecule in square angstroms, N = 6 x 1023, a_m = 16.3 A for oxide surface. Fully hydroxlated powder was dehydrated and the example was showed in Table 2.5 based on the BET equation.

From these data, with the elevating temperature, the surface area was decreased, means the particle size was increased and the SiOH was consumed from 10 to 2.

- **Porosity of gel and powder**

They are characterised by specific surface area m^2/g, specific pore volume (u_p, ml/g), average pore diameter d_p, pore size distribution $\Delta v_p / \Delta d_p = f(\bar{d}_p)$ and degree to which entrance to larger pores is restricted by smaller pores ("bottle-necks" or "ink-bottle" pores) (Linsen and Heuvel, 1967). Because absorption characteristics change with pore size, Dubinin (Dubinin, 1968) classified porosity in the terms of micropores, mesopores, and macropores.

	Diameter (A)	Specific surface area (m^2/g)
Micropores	10 - 28	7500
Mesopores	30 - 2000	500-10
Macropores	2000 - 4000	<10

2.8.1 Particle size and packing

All silica gel and precipitates tend to be compressed by the shrinkage forces of the surface tension of water as it dries out of pores. Unless special precautions are taken to strengthen the structure and reduce the surface-tension forces, the wet precipitate or gel is strongly compacted to about the same co-ordination number 6.

Loss of surface area of SiO_2 particles by particle packing can be achieved by pressure such as 1500 MPa. The approximate relation between pressure and the co-ordination number of silica particles was listed in Table 2.6. Depending on the pore radius, the silica gels can be subdivided into four groups (Coelingh, 1939; Brunauer, 1954) listed in Table 2.7.

There are some methods to measure the pore volume: liquid nitrogen pressure approaches $p/p_o=1$ (Kiselev's method) (Everett and Stone, 1958); flow method by a nitrogen-helium mixture containing 96.7% nitrogen (Lard and Brown, 1972); the oil absorption test, long used to evaluate carbon blacks, pigments and fillers, can give as indication or pore volume which used a non-volatile liquid that steadily penetrates the pores in silica. The amount of "oil" absorbed by a silica powder is an indirect measure of porosity.

2.8.2 Aggregate strength: inter-particle bonding

The conversion of a spherical sol particle to an uniform gel is through the formation of a Si-O-Si bond or an inter-particle bonding as shown in Figure 2.19 (Suger and Guba, 1954). When particles collide, there are neutral $\equiv SiOH$ groups as well as $\equiv SiO^-$ ionised groups on the surface of the particles which condense to form the *Si-O-Si* linkages by the same mechanism involved in the polymerisation of low molecular weight species. The presence of the soluble silica or monomer then plays a role of further cementing the particles together. From the bond formation of particles showed in Fig. 2.20, the particles can link together into chains then develop into rods or fibre structures or a solid structure or a fibrous network (Iler, 1984).

An important step in the formation of a rigid gel is the strengthening of the inter particle bonds. When two silica particles unite in water, they grow together because the solubility of silica in the crevice at the point of contact is less than that of the silica over the surface of the particle.

The formation of inter particle "necks" can occur by 2 processes: the solution / re-deposition process and the deposition of additional silica from supersaturated solution. The mechanical strength of coalescence of particles in gel structures having same particle size and a packing arrangement can be measured from equation developed by Kaiser (Meissner, Michaels, and Kaiser, 1964). It was indicated that the higher the porosity, the lower the related strength (Table 2.8).

$$\sigma_c = PD^{-2} = K\phi \exp(7.2\phi) \qquad \text{E2-4}$$

σ_c is the crushing strength; P is crushing load; D is diameter of agglomerate; ϕ is fraction of total volume occupied by shares; K is a constant which is a function of the spherical particles diameter and the bond strength between two particles.

Gel strength and hardness were real concern when in 1950's. Many procedures of increasing mechanical strength, reducing shrinkage, with higher porosity had been devised for soluble silicates (Vail, 1952). Slow drying was essential in order to keep the gel lumps from shattering because of greater shrinkage of the exterior portions. If water in the gel is replaced with an organic liquid having a lower surface tension, the gel shrinks less during drying, leaving larger pores. Another approach is to use a compound which releases acid slowly then mixed with concentrated sodium silicate solution reacted and set in a day to an extremely hard gel.

The effects of cations to accelerate gelling increased in order Li^+, Na^+, an K^+ and of anions in the order NO^{3-}, Cl^-, Br^-, and I^-. For some un-explained reason I^- had about five fold the effect of NO^{3-} (Mookerjee and Niygi, 1975).

2.9 Polymerisation of catalysed silicates

The most industrialised polymerisation of silicates is catalysed by substances such as acid gases and liquid acids, metallic minerals, salts, even organic or polymers.

2.9.1 Catalysis by gases and liquid acid

- Acidic gas

Silicates can be hardened by acidic gases such as CO_2 and SO_2 at different temperatures. The silicate/CO_2 system is very popular for foundry industry which offers many advantages. As a bonding agent, liquid silicate mixed with sand can be hardened in situ immediately after compacting, exposing the core or mould to carbon dioxide (Crosfield Chemical, 1994).

The chemical mechanism of the silicate/CO_2 system was that, the surface film of the M-silicate coating reacts with carbon dioxide, forming a hydrated silica gel membrane which is a semipermeable type of structure. Secondly, water is lost from the underlying sodium silicate, brought about by the flow of the carbon dioxide gas stream. It is considered to set the silicate by two possible processes (Nichols, 1972, Ruskin and Cihlar, 1987):

a. Physical dehydration of the silicate solution by the drying action of the CO_2.

b. Neutralisation of the silicates and gel formation by chemical reaction with the CO_2.

As the drying temperature increases from 60 °C to 110 °C, $NaCO_3^-$ is formed initially and then converted to $NaHCO_3$ on further processing. Generally, shorter gassing time gives lower initial strengths which considerably increase on standing. With longer gassing period, higher initial strength tends to be obtained, but the strength build-up during storage is reduced. CO_2 gas was proved the most convenient and efficient gas to harden the silicates (Mackenzie and Ranchod, 1991). Samples gassed with CO_2 contain bicarbonate and carbonate species which decomposed on heating in at least four stages up to 1000 °C. IR spectroscopy suggests that the more thermally stable species may be silicate carbonates.

- Silicate/SO_2 system

The silicate/CO_2 and silicates/SO_2 systems work well both in normal and high temperatures (Mackenzie, 1989). The method is to bubble SO_2 into a sodium silicate solution in order to produce solidification. X-ray diffraction indicate the presence of crystalline $Na_2SO_3 \cdot 7H_2O$, and a smaller amount of $Na_2S_2O_5$ which is on an amorphous component.

- Liquid acid as catalyst

The development of liquid setting agents is concentrated in poly-alcohol esters and alkaline carbonate esters. Poly-alcohol esters are the acetates of glycerol and ethylene glycol. This setting agent are usually 8% - 14% based on the weight of Na-silicate. In common with most chemical reactions the setting rate of the liquid silicate/ester system is temperature dependent - the lower the temperature of the system the slower the rate of set.

2.9.2 Solidified by metallic acids

Metallic acids are powdered setting agents such as heavy metal silicides, when mixed with liquid silicates, react to form a hard mass. The reaction mechanism is complicated and the relationships among these metallic solids and liquid silicates remains unknown.

- Calcium silicates

This occurs in a variety of chemical forms as by-products of blast furnace slag or by products of magnesium and ferrochrome in form of gamma-dicalcium silicates which are extremely reactive when freshly prepared. The activity can be lost with the time by the action of air and moisture.

- Portland Cement:

This contains a high proportion of calcium silicates and other metallic minerals which are extremely efficient as setting agents. Table 2.9 represents the chemical constituents for various types of Portland cement (Richard and Smith, 1985). When it is ground to a powder and mixed with water, it forms a stone like mass which results from a series of chemical reactions with the crystalline constituents hydrate, forming a materials of high hardness that is extremely resistant to compressive load.

During hydration, cement forms a non crystalline paste that has good adhesive properties. After its setting, it consists of submicron-sized crystals in a gel-like materials that possesses a high surface area value. The composition of the four main compounds in Portland cement are (Lee, 1970; Bushby, 1991):

Tri-calcium silicate	$3CaO \cdot SiO_2$ (C_3S)	C2-10
Di-calcium silicate	$2Ca \cdot SiO_2$ (C_2S)	C2-11
Tri-calcium Aluminate	$3CaO \cdot Al_2O_3$ (C_4A)	C2-12
Tetra-calcium aluminoferrite	$4CaO \cdot Al_2O_3 \cdot Fe_2O_3$ (C_3AF)	C2-13

Hydration of Portland cement contributes to forming the cement paste and developing the final rigid mass. C_3S is the most dominating component in the hydration process (C2-14):

$$2(3CaO \cdot SiO_2) + 7H_2O = 3CaO \cdot SiO_2 \cdot 4H_2O + 3Ca(OH)_2 \qquad \text{C2-14}$$

$3CaO{\cdot}2SiO_2{\cdot}3H_2O$ is tobermorite gel. After mixing the C_3S and water, lime and silica ions enter into solution, and it begins to form at the surface of the C_3S crystals and proceeds to cover them. As ions diffuse through this layer, nucleation and growth of the portandite and tobermorite gel crystals continue. Similar reactions happen between in C_2S and water:

$$2(2CaO{\cdot}SiO_2) + 5H_2O = 3CaO{\cdot}2SiO_2{\cdot}4H_2O + Ca(OH)_2 \qquad \text{C2-15}$$

- By aluminium phosphates

Hardeners for soluble silicates are produced by a drying process of a salt containing phosphoric acid $Al_2(PO_4)_3$. A condensation reaction of P_2O_5 and Al_2O_3 lead to different hardeners depending on the processing temperature and the P_2O_5/Al_2O_3 ratio. In an alkaline environment the hardeners are dissolved and the polymerisation of -O-Si-O-Si- reaction would occur.

2.10 Chemical Activity

Soluble silicate and polymer-metal ions interact in solution. Since the reaction happens among metal ions in solution and polymeric silicate species, it has been shown that silica-gel surfaces form complexes with multivalent metal ions that indicate a correlation between the liquid properties of the surface OH groups on silica gel and metal-ion hydrolysis (Zhdanor, 1978). For Cu^{2+}, Fe^{3+}, Cd^{2+} and Pb^{2+} their solution activity can be increased. The existence of Ca^{2+} and Mg^{2+} decreases the solution activity.

2.10.1 The nature of silica surface

There are three types of silica surface (Barby, 1926). A fully hydroxylated surface terminated with silanol (SiOH) groups. All silica dried from water at less than 150 ℃ are of this type. Secondly, a siloxane surface consisting mainly of oxygen atoms, each bonded to adjacent silicon atoms. Pyrogenic silica condensed form the vapour state are of this type. Also, hydoxylated silica which have been dehydrated at around 1000 ℃ develop a siloxane surface by removal of water forming adjacent silanol groups. And

thirdly, an organic surface formed by chemical or physical attachment of organic molecules or radicals.

2.10.2 Reaction with phosphoric, boric acids and sulphuric acids

- The reaction of silica with phosphoric acid is a condensation reaction with elimination of water. Silicon phosphate has long been known as a water soluble material.

- The reaction of boric acid with silica appears to parallel those of phosphoric acid, on dehydration at high temperature, Si-O-B bonds are formed in the resulting mixed-oxide glass. The Si-O-P and Si-O-B bonds are hydrolysed in aqueous solution (Lorentz et al, 1962).

- Silicon dihydrogen sulphate [$SiO(HSO_4)$] was obtained by dehydrating "dihydroxy" silicon dihydrogen sulphate [$(HO)_2Si(HSO_4)$], with concentrated sulphuric acid (Bount, 1976).

2.10.3 Reaction with metallic materials

- Iron and uranium

Monomeric silica does not react with most metal ions in water at low pH where $Si(OH)_4$ existed. For reaction to occur hydrolysis to a basic metal ion must first take place (Porter and Weber, 1971):

$$H_2O + Fe^{3+} = Fe^{2+}OH + H^+ \qquad \text{C2-16}$$

Second step:

$$(\text{-}SiOH)_m + Fe^{3+} = (\text{-}SiOH)_{m-n}(\text{-}SiO)_nFe^{3-n} + nH^+ \qquad \text{C2-17}$$

Very few metal ions form basic ions at the pH of 2 (iron and uranium are the only ones), where monomeric $Si(OH)_4$ is most stable, the reaction between silica and uranol ion as follows (Weber, Jr., and Stumin, 1965):

$$UO_2 + Si(OH)_4 = UO_2Si(OH)^{3+} + H^+ \qquad \text{C2-18}$$

- Reaction with chromium

Hexavalent chromium as H_2CrO_4 appears to form a complex with $Si(OH)_4$ (Iler, 1952), The H_2CrO_4 dimerised the silica quantitatively and the excess had no further effect:

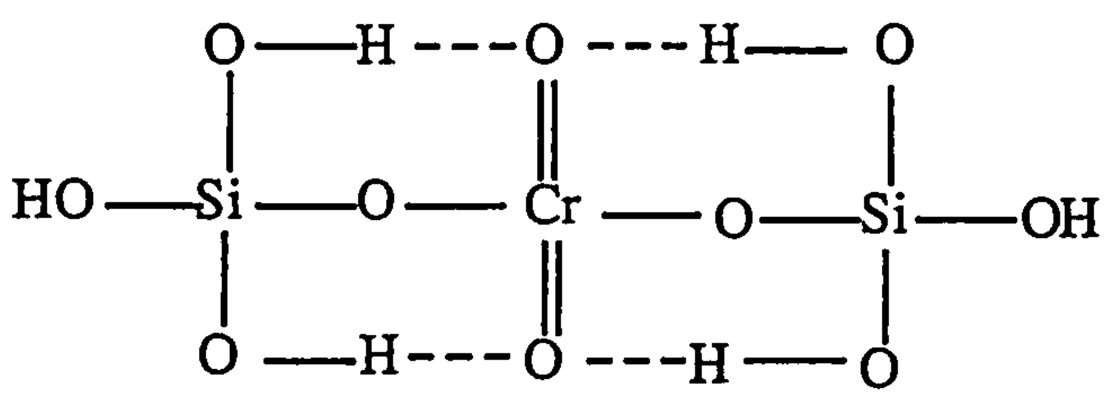

C2-19

- Reaction with aluminium

There is an affinity for the internal reaction between oxides of aluminium and silicon. Aluminium oxide is far less soluble than silica in water at 25 °C, pH 5-8 (Okura, Goto, and Murai, 1952). It is necessary to spend time to allow monomeric silica, $Si(OH)_4$, to react with Al^{3+} ion at 25 °C to form colloidal aluminium silicate:

$$2\ Si(OH)_4 + 2\ Al^{3+} + H_2O = Al_2Si_2O_5(OH)_4 + 6\ H^+ \qquad \text{C2-20}$$

There is a reaction between $Si(OH)_4$ and crystalline $Al(OH)_3$ by which several reaction layers of SiO_2 are built up, with simultaneous decrease in pH of the suspension.

2.11 Manufacturing silicates

In UK, these silicates are manufactured to be used in wide variety of industries:

Detergent manufacture	24%
Paint manufacture	24%
Catalysts	11%
Foundry binders	11%
Cements	7%

Most of the UK's liquid silicates are produced by Gossage's method from Sibia sand by reaction with sodium carbonate to yield a glass:

$$Na_2CO_3 + xSiO_2 \xrightarrow{>1500^0C} Na_2O \cdot xSiO_2 + CO_2 \qquad \text{C2-21}$$

x - the mole ratio.

Crystalline products and their compositions are shown in Fig. 2.21. Highly siliceous phases are slow to attain equilibrium structures and compositions, but a few of the naturally occurring members (Kenyaite, Maketite, and Kanemite) have attained equilibrium over geological time.

Soluble silicate glasses are manufactured in oil-gas-fired open-hearth regenerative furnaces in modern industry. Glass is obtained by reaction of quartz sand and sodium carbonate (soda ash) at a temperature of 1200 ℃ in the molten batch and a manageable melt viscosity. The reaction rate of quartz with Na_2CO_3 is controlled by silica diffusion. As Na_2CO_3 melts and reacts with the sand grains at the slow process of quartz network breakdown. The raw materials of sand and soda ash for manufacture of the soluble silicate must be of high purity. The impurities observed in 3.3 ratio solution can be shown in Table 2.10.

2.12 Possible fibre selection

Since silicate composites have a basic structure similar to both ceramic composites and cementitious materials, the glass fibres can be directly adapted from fibre reinforced cement and concrete applications. At the same time since dough moulding compound reinforced with chopped glass has been well established, we have used the similar manufacturing and moulding techniques to make and mould ceramic moulding compound.

One of the major interests for ceramic matrix composites is that the thermal behaviour is not dependent on the matrix as for polymer composites, but depends on the reinforcement at the temperature range 200 to 800 °C. At higher temperatures, the thermal behaviour was both dependent on the composition of the ceramic matrix and reinforcements. Therefore, there was always a concern of the thermal behaviour of reinforcements for ceramic composites. For example, glass typically starts softening at about 550 to 730 °C, it resists to creep only up to about 280 °C.

Polymeric fibres (e.g. PP&PE, Kevlar^{TM}) do not have good thermal properties. Ceramics such as alumna (T_m ~ 2027 °C) show little creep below 830 °C, while SiC and Carbon fibres were in general highly creep resistance to over 930 °C, depending on the detail of their microstructures. But they are very expensive to use.

2.12.1 General fibres

A wide range of fibres of different mechanical, physical and chemical properties have been used for reinforcement of low cost ceramics such as cementitious matrices. The individual fibre may be subdivided into two groups: discrete mono-filaments separated one from the other, such as steel fibre, and fibre assemblies, usually made up of bundles of filaments, each with a diameter of ~20 μm or less. The bundled structure is typical whether it is inorganic or organic such as glass fibre, ceramic fibre and carbon fibre, Kevlar fibre, and metallic fibres.

Continuous reinforcement, in the form of long fibres or fabrics are incorporated in the matrix in many ways. For example, the non-crimped fabrics were impregnated by ceramic matrix for making CS3000, a fire proof composites panels. Discrete, short fibres, usually

less than 50 mm long (or 1 inch or half inch long), which are incorporated in the matrix by methods such as spraying and mixing as premix. The reinforcing array could be further classified according to the dispersion of the fibres in the matrix. In this form the distribution of the fibres in the matrix is more uniform, and the chopped fibre tend to assume a more random orientation. In DMC, the fibre orientation seemed to be arrayed in 3 dimension, however, since the influence of the moulding pressure and flatten flow during the moulding, the fibre mainly distributed in 2-dimensions.

The problem that exists with all traditional glass fibres is their chemical resistance to water or boiling water and especially, alkaline media. A 10-micron-diameter E-glass filament typically loses 0.7-0.9 % of its weight when left in hot water for few days (Yellow Pages: Industry overview). To slow erosion, protective moisture-resistant coatings, such as silane compounds, are applied during fibre manufacturing. Corrosion-resistant glass, known as C-glass or ECR glass, loses much less of its weight when exposed to an acid solution than does E-glass. Although C-glass and S-2 glass show good corrosion-resistance to sulphuric acid, their resistance to alkaline environment especially to NaOH is unknown.

2.12.2 Alkali resistant glass fibres (AR-glass)

Glass fibres used in conventional polymer composite industries were borosilicate glass fibres (E-Glass) and the soda-lime-silica glass fibres (A-glass) which used to reinforce brittle cement materials. These fibres had very high tensile strengths and relatively high elastic modulus. However, since their chemical compositions were not suitable (Table 2.11) for the cement-based matrix with high alkalinity (pH >11.5), the research took the two logical developmental paths during past 20 years:

- Developing fibres that are durable in alkaline environment, leading to an alkaline-resistant glass (AR-glass) fibres.
- Focused on the development of a less alkali matrix, leading to a development of a polymer modified mortar matrix and use of-alkaline special cements.

There has been intensive research to compare the glass fibre's (E and AR glass) resistance to alkalinity liquid produced by cements or concrete for the last thirty years by the British Building Research Establishment (Majumdar, 1973, 1975). It has been proved that at room temperature, AR-glass composites have much better property retention while the

properties of E-glass fibre/cement or concrete decreased tremendously. There is no report about glass fibre resistance to alkali at elevated temperature being found up to now.

Alkali-resistant glass fibre with more than 16% Zirconia in composition such as the Cem-FIL chemical resistance fibres produced considerably durability of the fibre in an alkaline environment. The Zirconia in composition enables AR fibre to resist the very high alkalinity produced by the hydration of alkaline resin matrices.

No investigation has been reported on the interface between glass fibre and ceramic matrix under alkaline conditions and the moulding temperature range 100 ℃ - 200 ℃ in liquid alkali system. However, one or two researchers have noticed that the interfacial bonding and chemistry of coupling agents in polymer matrix composite (e.g. γ-APS) are affected by pH, or environmental conditions (Jang and Ishida, 1988) when the composites are in application. There is no report can be found now on researches in the formation of interfaces in ceramic composites under high alkali media while at the temperature higher than 100 °C.

2.13 Summary

Mineral silicate related materials have a long history being used as binders by humans for more than 5000 years. They have existed on the surface of the earth since the earth cooled down to the current temperatures, billions of years ago. Their main chemical core structures are the same as -[O-Si-O-Si-]O- . More complex chemical structures were produced when the material was at higher temperatures, after mixing with other materials.

When the metallic-silicate powder or liquid are exposed to different environments such as acid or alkali, they would be condensed or polymerised into small particles first, then they form a sol. If it is in acid or pH <7~8, a gel would be formed and further leads to networks. Only in the case of salt presence, the silicates can be gelled with the pH>7~8. With the evaporation of moisture or water under the higher temperature, it also provide the opportunity to move the sol to gel with the help of salt, but produced large particles with less or short chain structures. According to the theory, at low pH, produced small particles and formed more strong chain structure; while the at higher pH, produced large particles and formed weak or short chain.

The silicate composites have also been used since pre-historical times for buildings and walls with mineral fibre or natural fibres. Modern fibre reinforced silicate composites in this thesis were developed from both heat insulation / resistance materials and fibre reinforced ceramics sol/gel materials. Started from 10 years ago, the main application has been focused in the fire proof/ barrier, heat resistance / insulation areas plus the engineering and design requirements.

For the fibres used in the composites, mainly chopped glass fibre and short mineral fibres for a concern of the cost. The continuous development of AR-glass fibre has provided more and more suitable low cost reinforcements for the matrix.

Although the research is going to be emphasised mainly on the compounding process used for making CDMC, its mechanical characterisation and the ceramic's common problem of "brittleness" will also be primarily investigated and the achievement can be seen in following chapters.

Table 2.1 Mechanical, physical and other properties of polyester and phenolic DMC [Their glass fibre content is around 25 %(wt.)].

Properties		Polyester DMC	Phenolic DMC
Mechanical properties	Tensile strength (MPa)	70 - 90	65 - 70
	Tensile modulus (GPa)	8 - 10	9 - 11
	Flexural strength (MPa)	120 - 150	80 - 90
	Flexural modulus (GPa)	7 - 9	7 - 9
Energy absorption in impact (J) (4.0 mm thick)		35	25 - 30
Physical properties	Density	1.70	1.70
	Water absorption (%)	0.2	1-2
Fire properties	Oxygen index (%)	20 - 30	75 - 95

Table 2.2 The general formulation for the liquid silicate composites made from waste materials and inorganic/mineral fillers.

Formulation	Materials used			
	USA	Japan	UK	Canada
Liquid silicates	x	x	x	x
Chrysotile asbestos	x	x		
Ground waste glass	x	x	x	
Inorganic/minerals	x	x	x	x
SiC powder				x
Furnace slag		x		
Pigment		x		
Polymers		x		
Glass fibres		x	x	

Table 2.3 Solution rates of amorphous sodium silicate powders (3 parts water + 1 part silicate powder).

Silicates SiO_2:Na_2O ratio	Particle Size(μm)	Time to dissolve at 25 °C			Time to dissolve at 50 °C		
		50%	75%	100%	50%	75%	100%
3.32, anhydrous	230(65)	60 h			155 min		
2.22, anhydrous	230(65)	10 h	70 h		17 min	1 h	
2.0, hydrated (18.5 wt % H_2O)	149(100)	27 s	54 s		15 s	22 s	29 s

Table 2.4 Summary of the structures in different silicates.

Silicate type	Unit structure	Name	Registry No	Formula	Q^s structure
Discrete, noncyclic orthosilicate	SiO_4^{4-}	Zircon	(14940-68-2)	$ZrSiO_4$	Q^0
Pyrosilicate	$Si_2O_7^{6-}$	Thortveitite	17442-06-7	$Sc_2Si_2O_7$	Q^1Q^1
Discrete, cyclic tetramer	$Si_3O_9^{6-}$	Benitoite	15491-35-7	$BaTiSi_3O_9$	$(Q^2)^3$
Cyclic hexamer	$Si_6O_{18}^{12-}$	Beryl	1302-52-9	$Be_3Al_2Si_6O_{18}$	$(Q^2)^6$
Infinite chain pyroxenes	$(SiO_3^{2-})_n$	Diopside	14483-19-3	$CaMg(SiO_3)_2$	$(Q^2)^n$
Amphiboles	$(SiO_{11}^{6-})_n$	Tremolite	14567-73-8	$Ca_2Mg_5(Si_4O_{11})_2(OH)_2$	Q^3Q^2
Sheet	$(SiO_5^{2-})_n$	Talc	14807-96-6	$Mg_3(OH)_2Si_4O_{10}$	$(Q^3)^n$

Table 2.5 The physical and chemical relationships of gel and powder among dehydration temperature, surface area, SiOH groups based on the BET equation.

Dehydration Temperature (°C)	Surface area (m^2/g)	SiOH Groups (n/m^{-2})	Constant c
120	182	10	104
620	170	3	53
810	141	2	45

Table 2.6 Relationship among the pressure, surface area and porosity of SiO_2 particles with starting particle diameter 4 nm.

Pressure (tons/in^2)	Surface (m^2/g)	Co-ordination Number	Porosity (cm^3 pores/cm^2 body)
0	636	3	-
10	522	5.6	0.51
50	373	9.8	0.33
100	219	-	0.204

Table 2.7 The influence of pore dimension in gel to the classification of absorption of particle sizes.

Pores dimension in gel	Exhibiting	Capillary	p/p_0
<2 nm	Absorption	No	
2 nm	Hysteresis for water	Small molecules	0.5 - 0.8
3 - 10 (Micropores)	Hysteresis for Large molecules	Absorption	Higher
>10 nm		Absorption	Unity

Table 2.8 The relationship between porosity and strength of packed silicates.

Porosity (cm^3/cm^3 of gel)	Strength Relative
0.26[a]	100
0.30	71
0.5[b]	12
0.6	5

a. Regular close packing

b. Open packing

Table 2.9 Chemical constituents for various types of Portland cement.

Type of cements	$3CaO \cdot SiO_2$	$2CaO \cdot SiO_2$	$3CaO \cdot Al_2O_3$	$4CaO \cdot Al_2O_3 \cdot Fe_2O_3$	$CaSO_4$	MgO	Free CaO
Type I	45	27	11	8	3.1	2.9	0.5
Type II	44	31	5	13	2.8	2.5	0.4
Type III	53	19	11	9	4	2	0.7
Type IV	28	49	4	12	3.2	1.8	1.9
Type V	38	43	4	9	2.7	1.9	0.5

Table 2.10 Range of composition of typical sodium silicate glasses (3.3:1 = SiO_2:Na_2O).

Assay	WT %	
	Low	High
Na_2O	**23.21**	**23.89**
SiO_2	**75.36**	**76.00**
K_2O	0.00	0.10
Fe_2O_3	0.005	0.30
TiO_2	0.004	0.052
Al_2O_3	0.15	0.51
CaO	0.032	0.017
MgO	0.004	0.10
CdO	0.00012	0.0022
NiO	0.00008	0.0026
Se_3	0.008	0.19
CO_2	Nil	0.23
Cl	0.025	0.12
Ignition less	0.03	0.36
Ratio by wt SiO_2:Na_2O	3.154	3.246

Table 2.11 Chemical compositions of selected glass fibres.

Component	A-Glass	E-Glass	Cem-FIL Glass	NEG. AR-Glass
SO_2	73.0	54.0	62.0	61.0
Na_2O	13.0		14.8	15.0
CaO	8.0	22.0	5.6	
MgO	4.0	0.5		
K_2O	0.5	0.8		2.0
Al_2O_3	1.0	15.0	0.8	
Fe_2O_3	0.1	0.3		
B_2O_3		7.0		
ZrO_2			16.7	20.8
TiO_2			0.1	
Li_2O				1.0

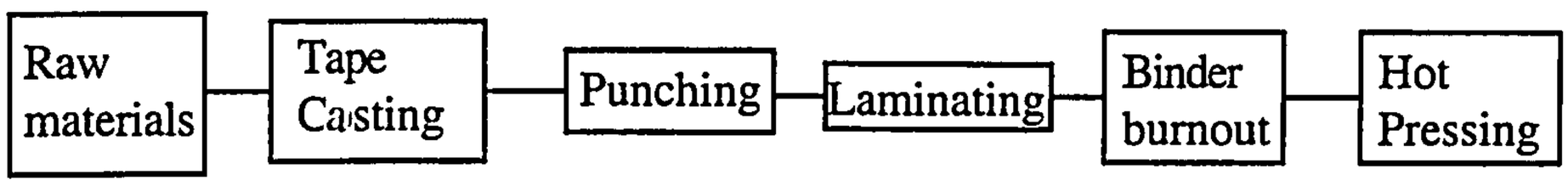

Fig. 2.1 Flow chart of high performance ceramic composites manufacturing process: tape casting.

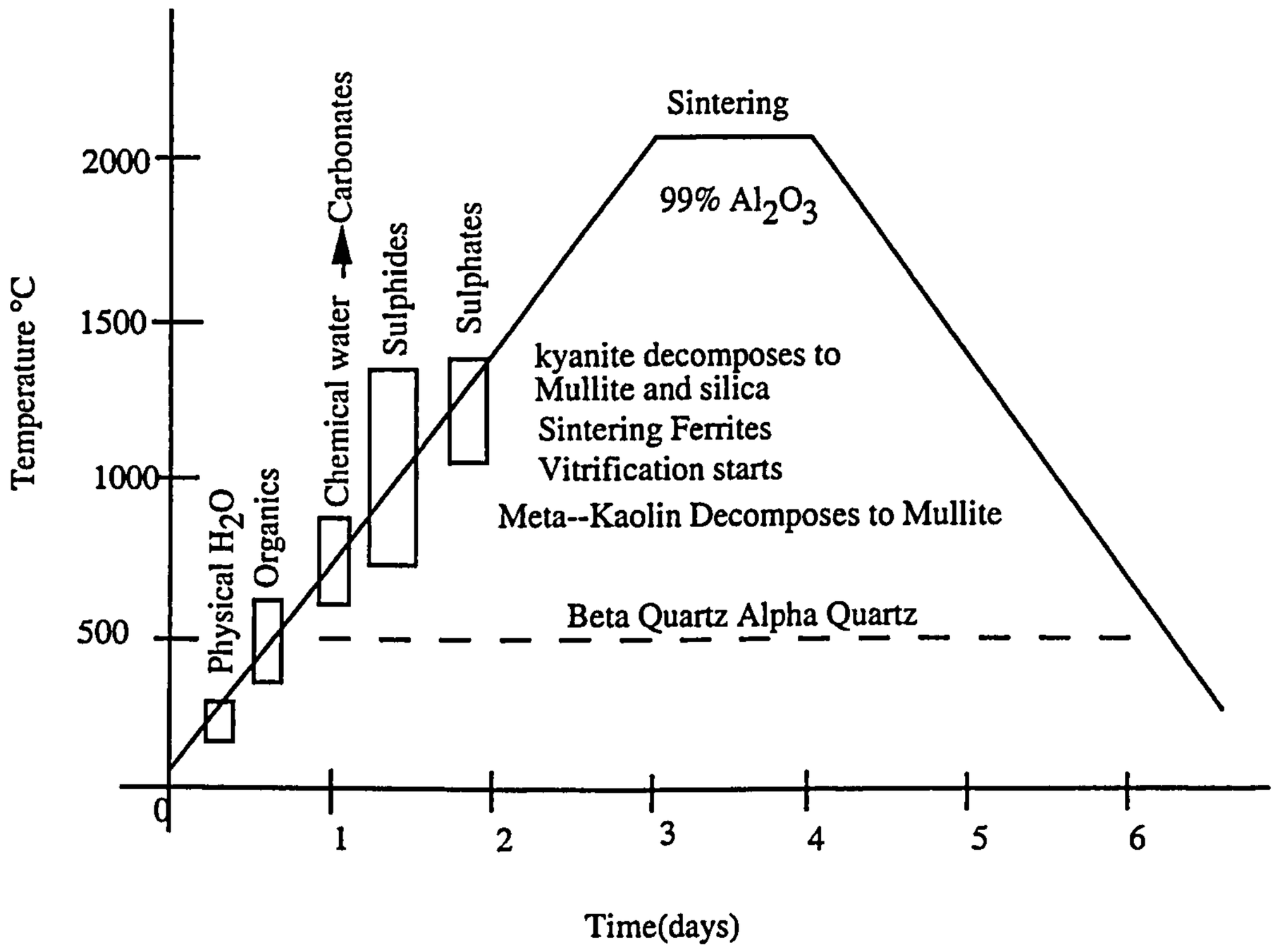

Fig. 2.2 Temperature rising degrees and time for ceramic sintering processes. The high temperature maintenance in furnace for longer duration consumed large amount of energy for different stages of phase changes (Remmey Jr., 1994).

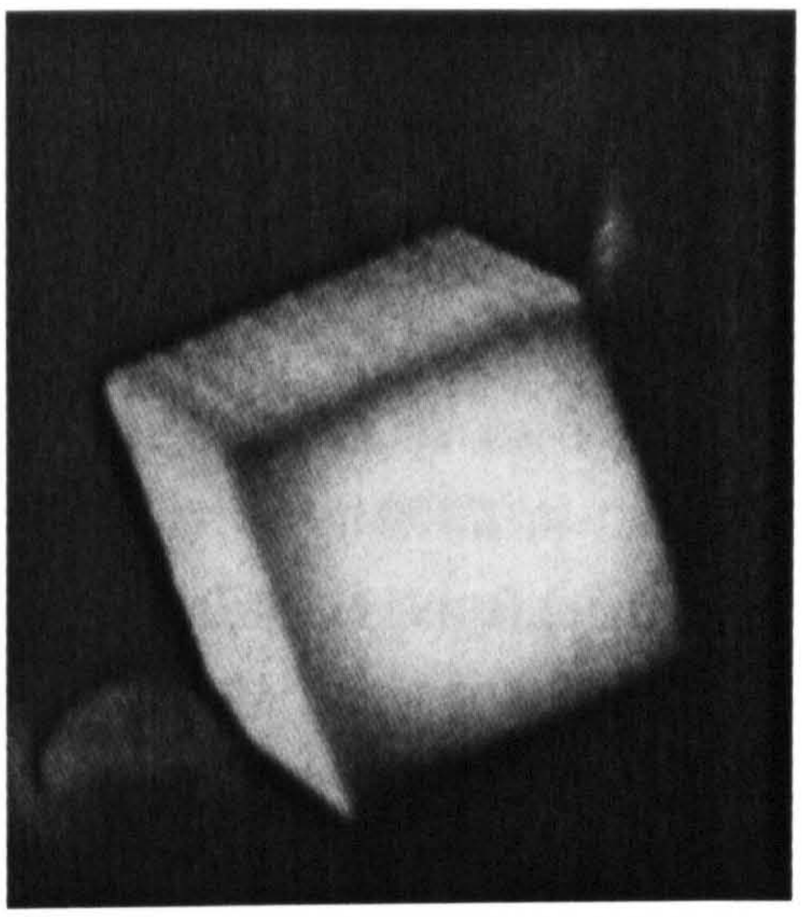

Fig. 2.3 White hot at 2268 °C, the glow from a cube of fibre ceramic tile insulation held by a technician's bare hand.

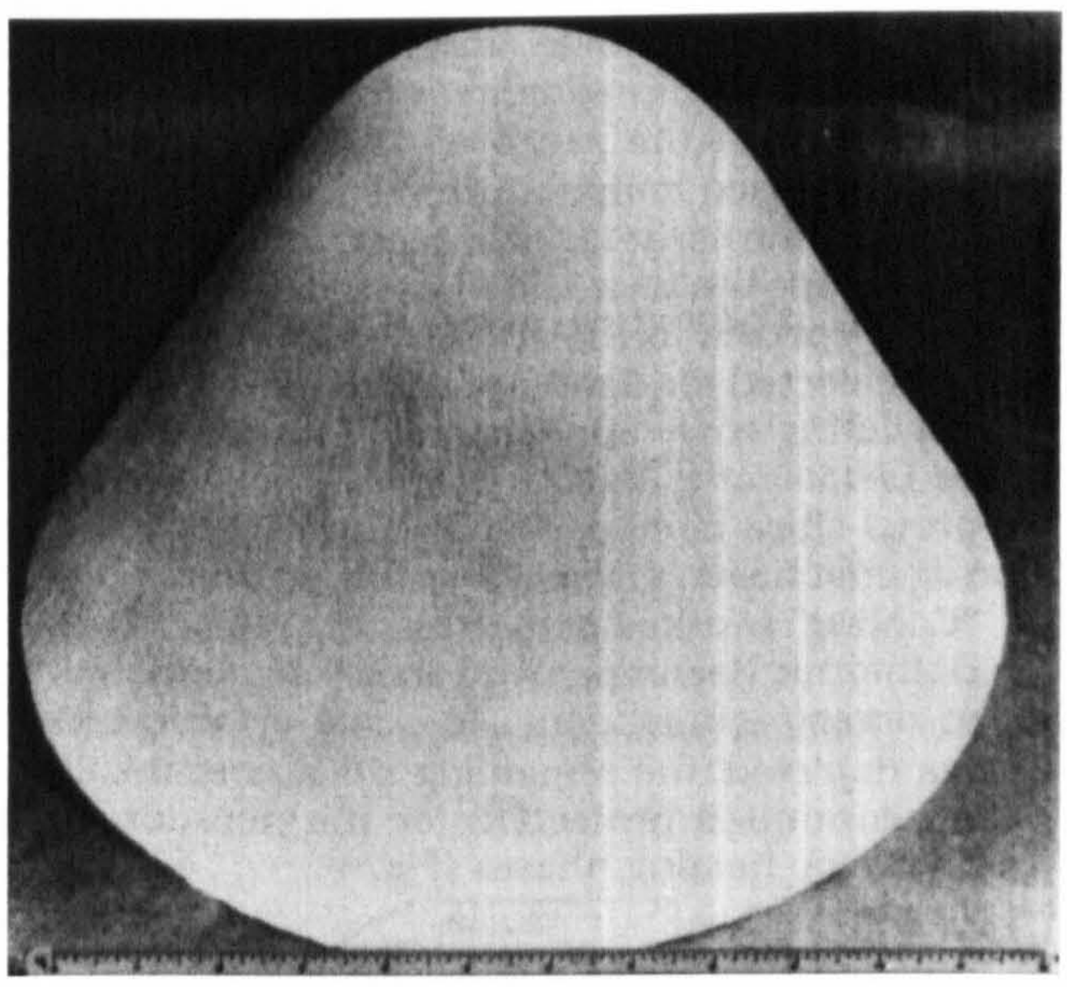

Fig. 2.4 The Conical Apollo radome was built of fused silica composites in the early 1960s. This early ceramic structure was 100 % inorganic and nonablative.

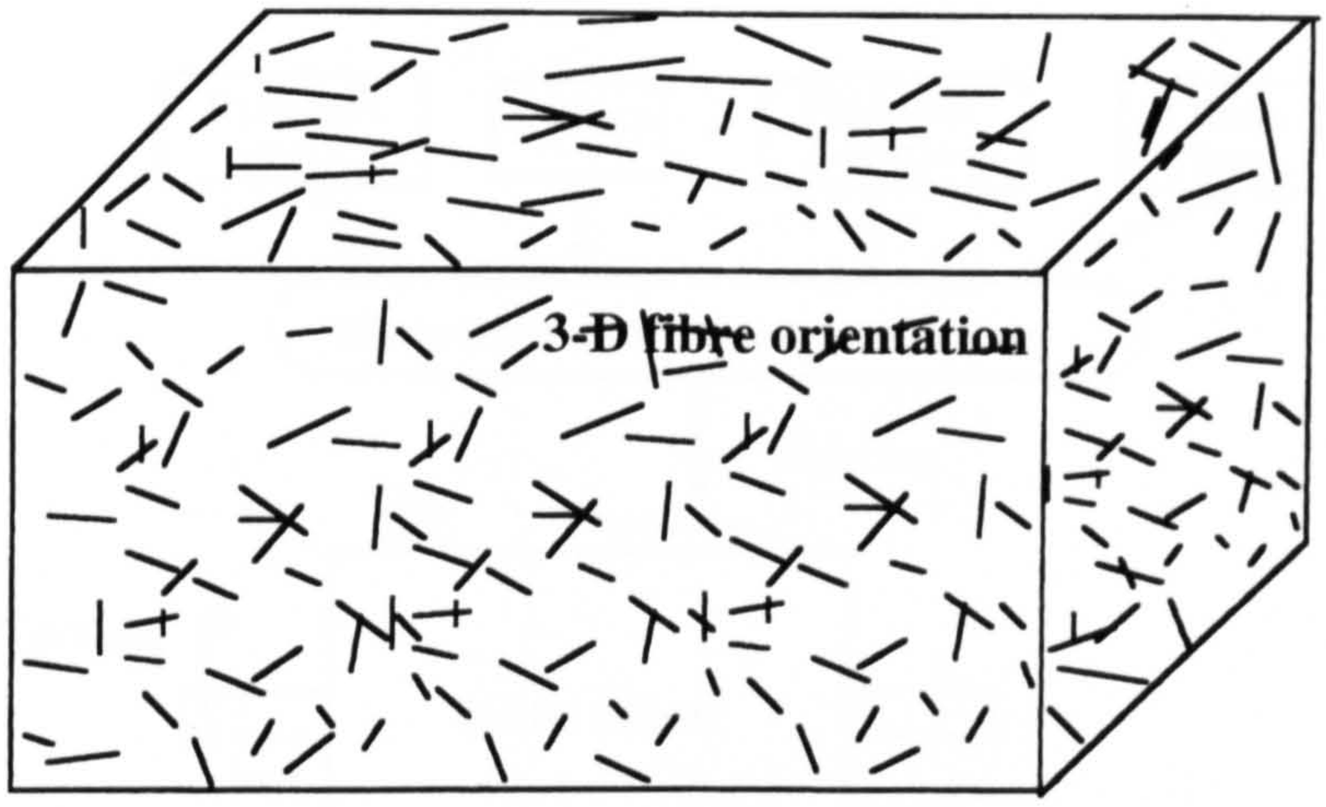

Fig. 2.5 Three dimensional fibre orientation in chopped fibre composites such as DMC.

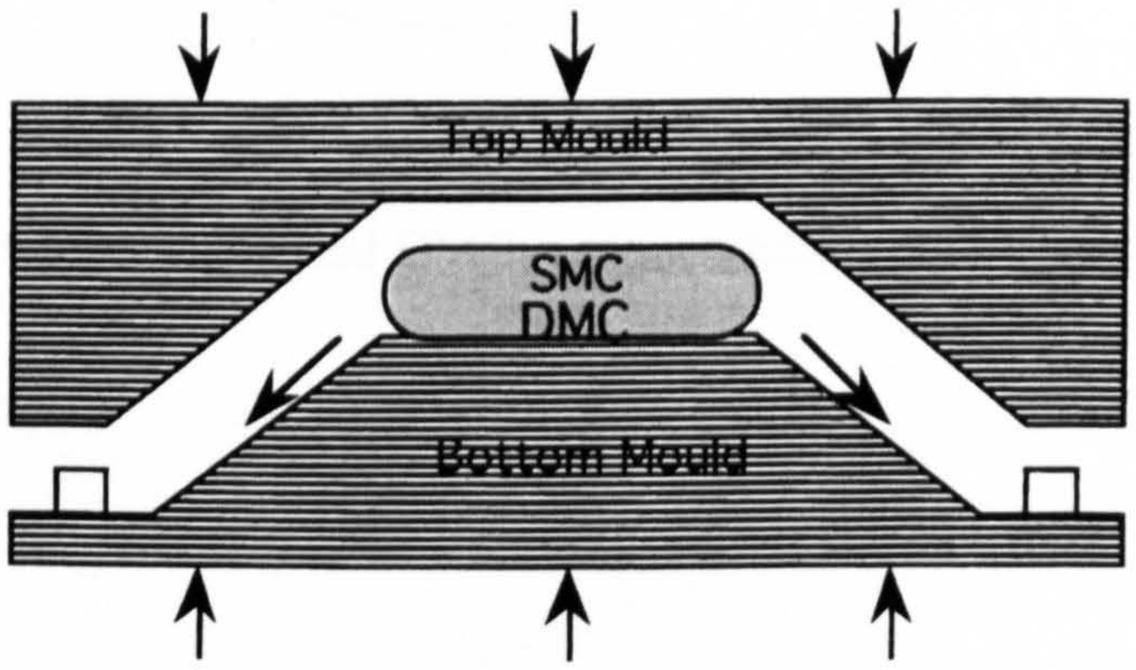

Fig. 2.6 Illustration of general compression moulding outline used for DMC composites.

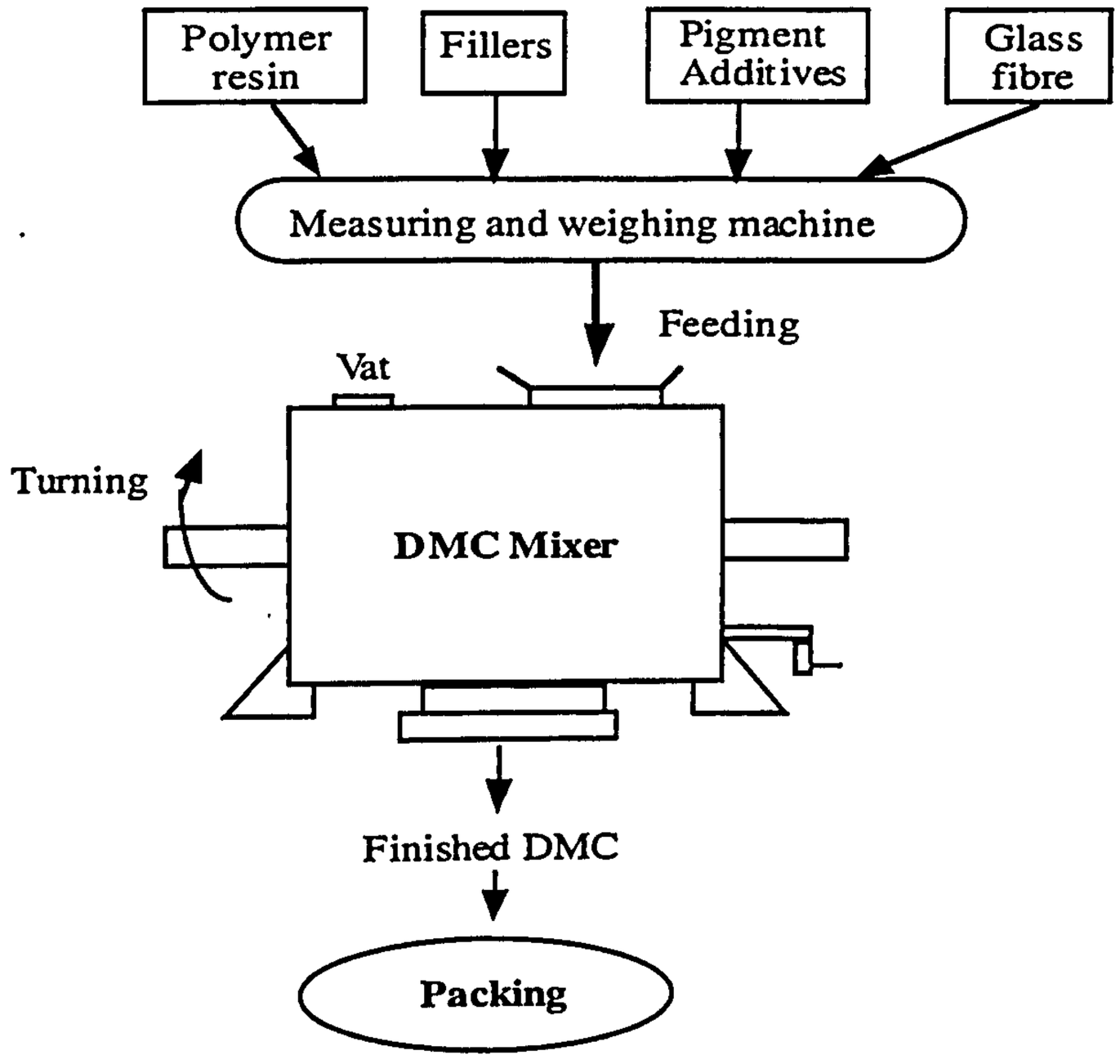

Fig. 2.7 Schematic show of a typical DMC compounding process (Murphy, 1994).

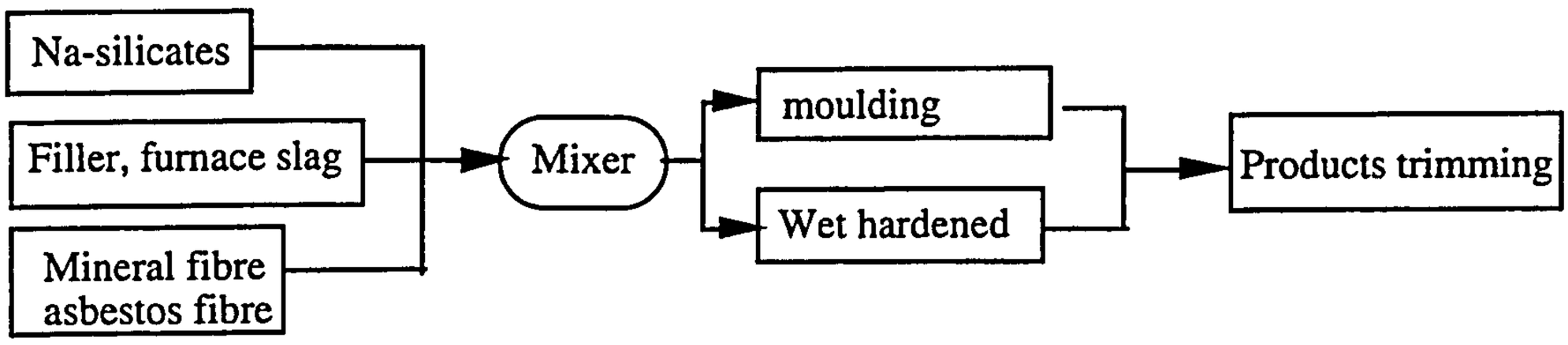

Fig. 2.8 Silicates, mineral fibre/asbestos, furnace slag composites manufacturing process developed in USA and Japan during 80's.

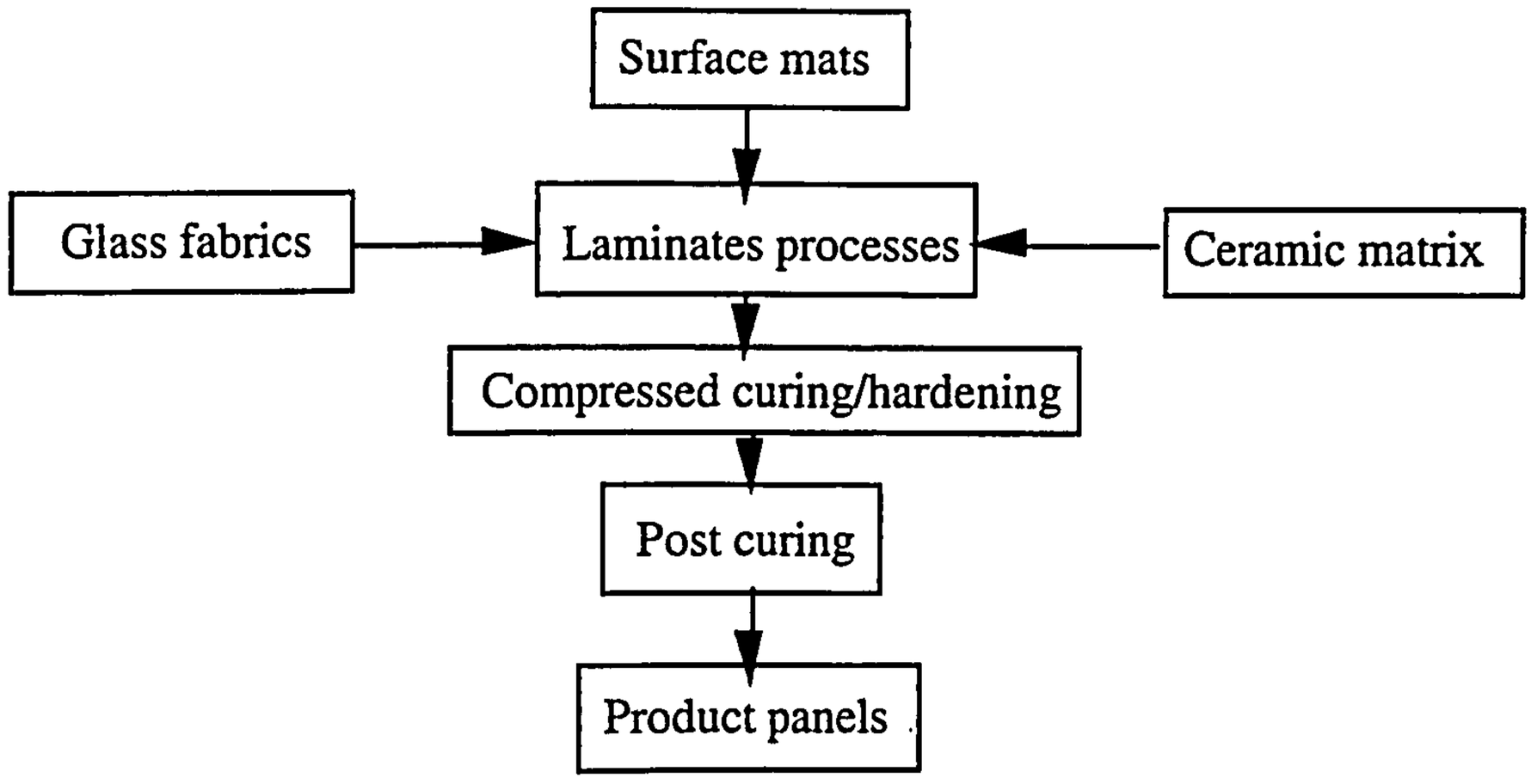

Fig. 2.9 Manufacturing method used in glass fibre fabrics-ceramic laminates by Claymore Systems in UK in early 90's.

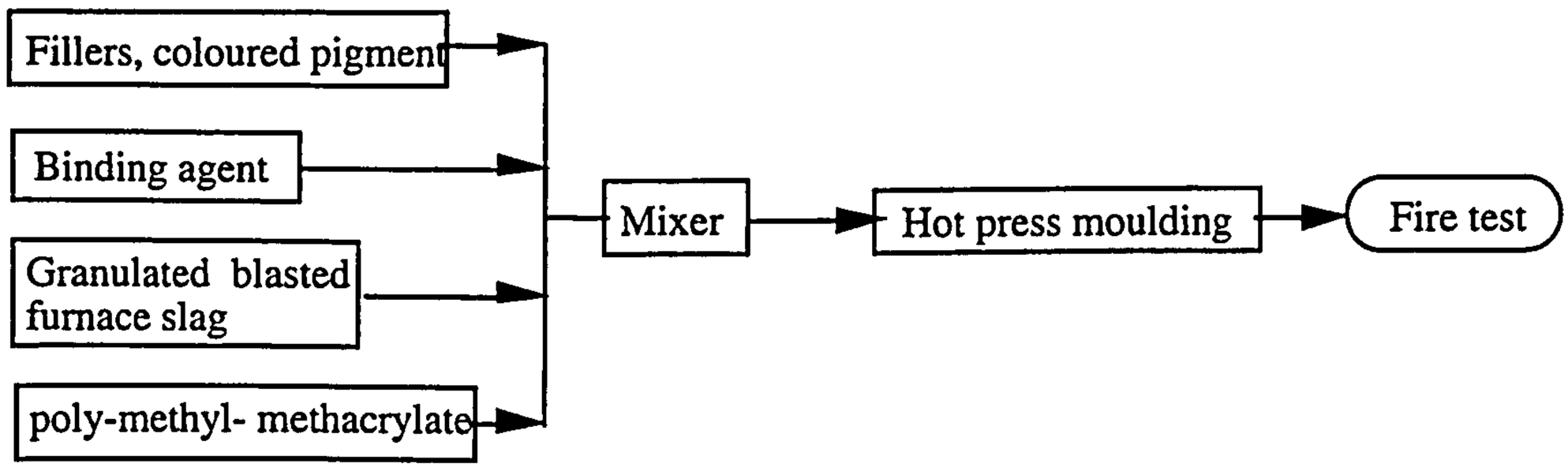

Fig. 2.10 A coloured fire resistan t composite manufacturing process scheme.

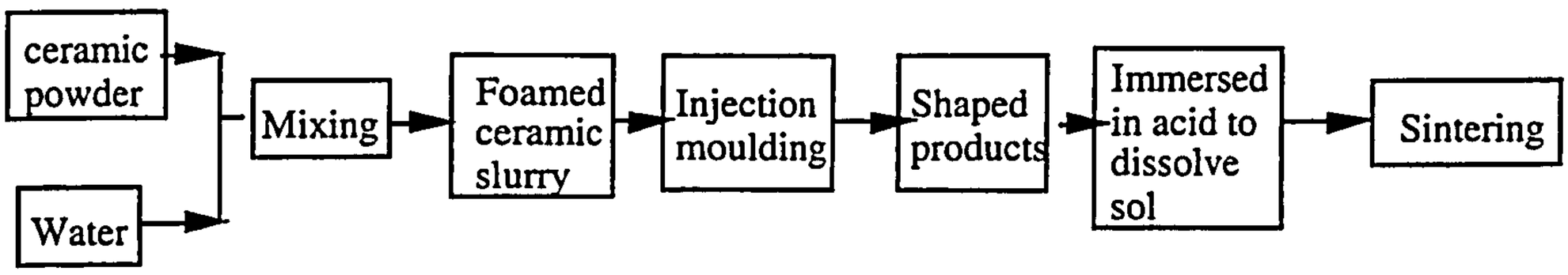

Fig. 2.11 Ceramic manufacturing process with acid treatment to produce porous structure.

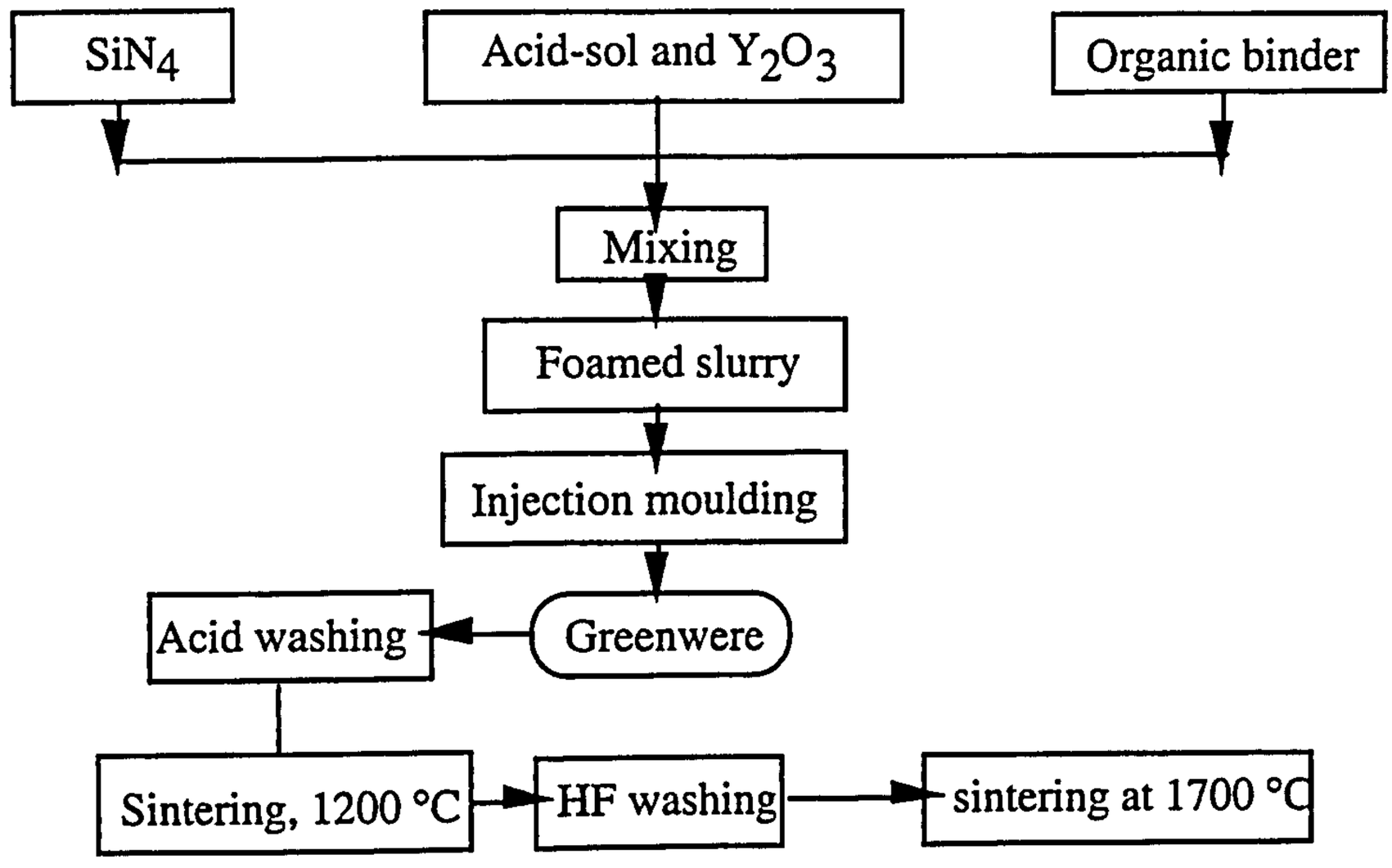

Fig. 2.12 Detailed manufacturing process for silicates as a binder.

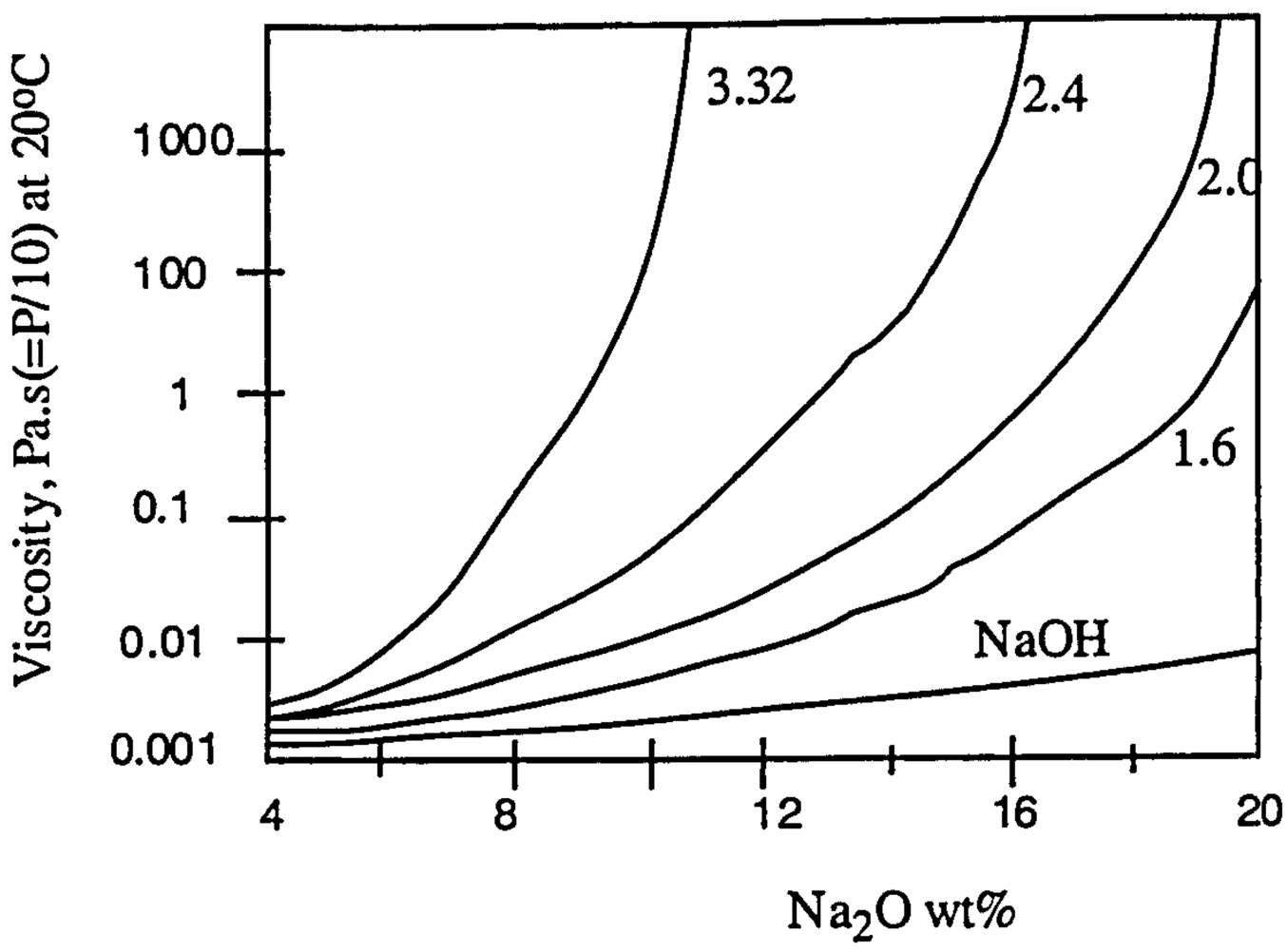

Fig 2.13 Viscosity of sodium silicate solutions at various ratios vs. percent of the Na_2O solid.

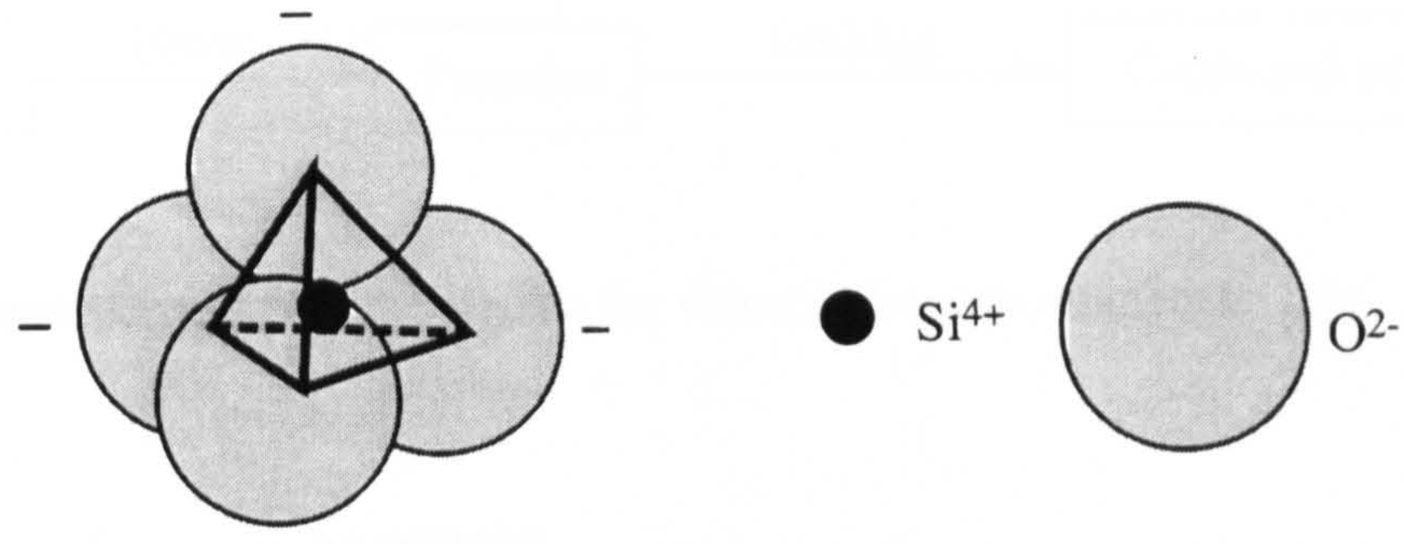

Fig 2.14 Basic structure of silicon-oxygen(SiO_4^{4-}) tetrahedron.

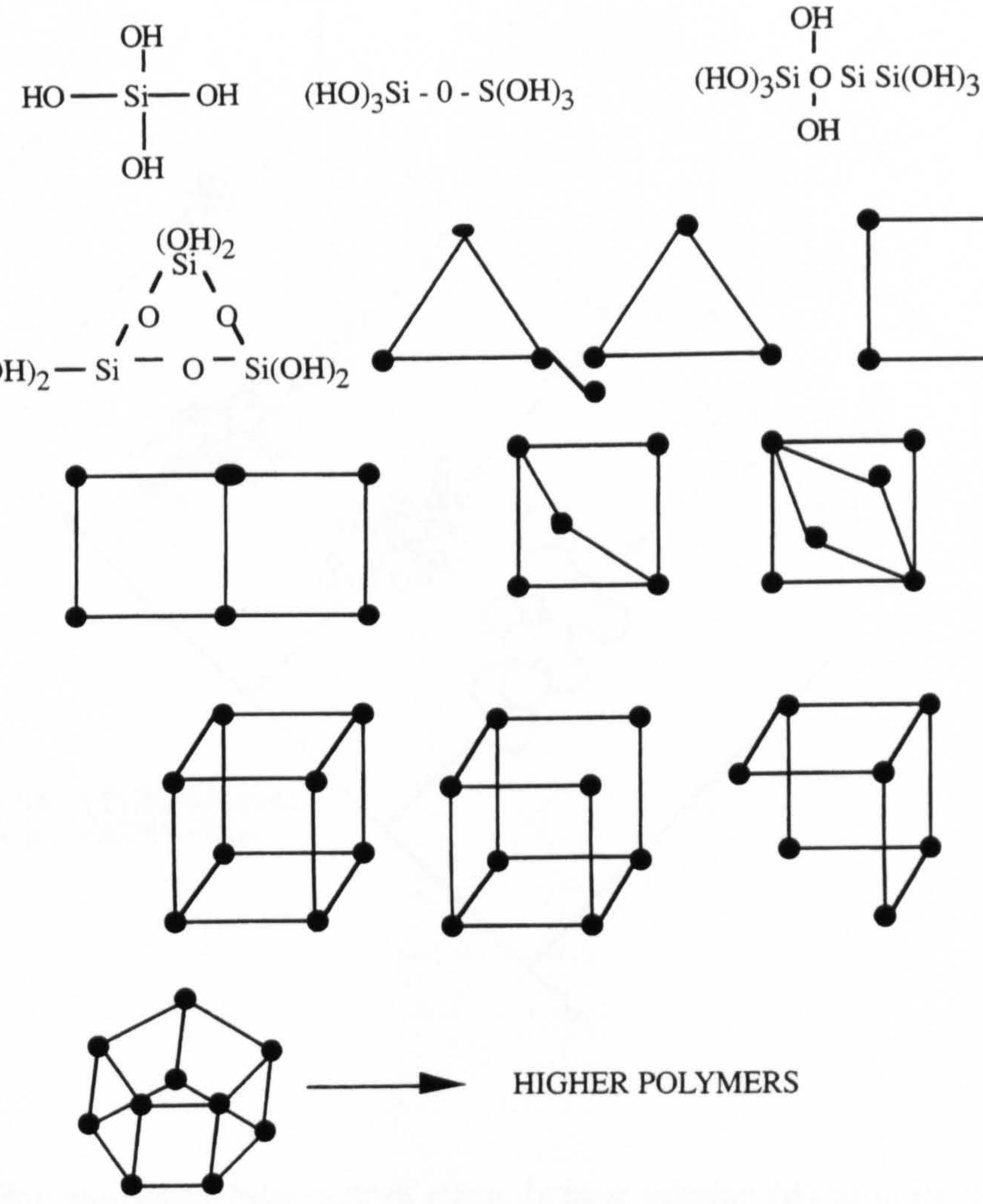

Fig. 2.15 Some of the simpler polysilicate species identified in sodium silicate solutions.

Fig. 2.16 Three steps of polymerisation for silicates from monomers to gels.

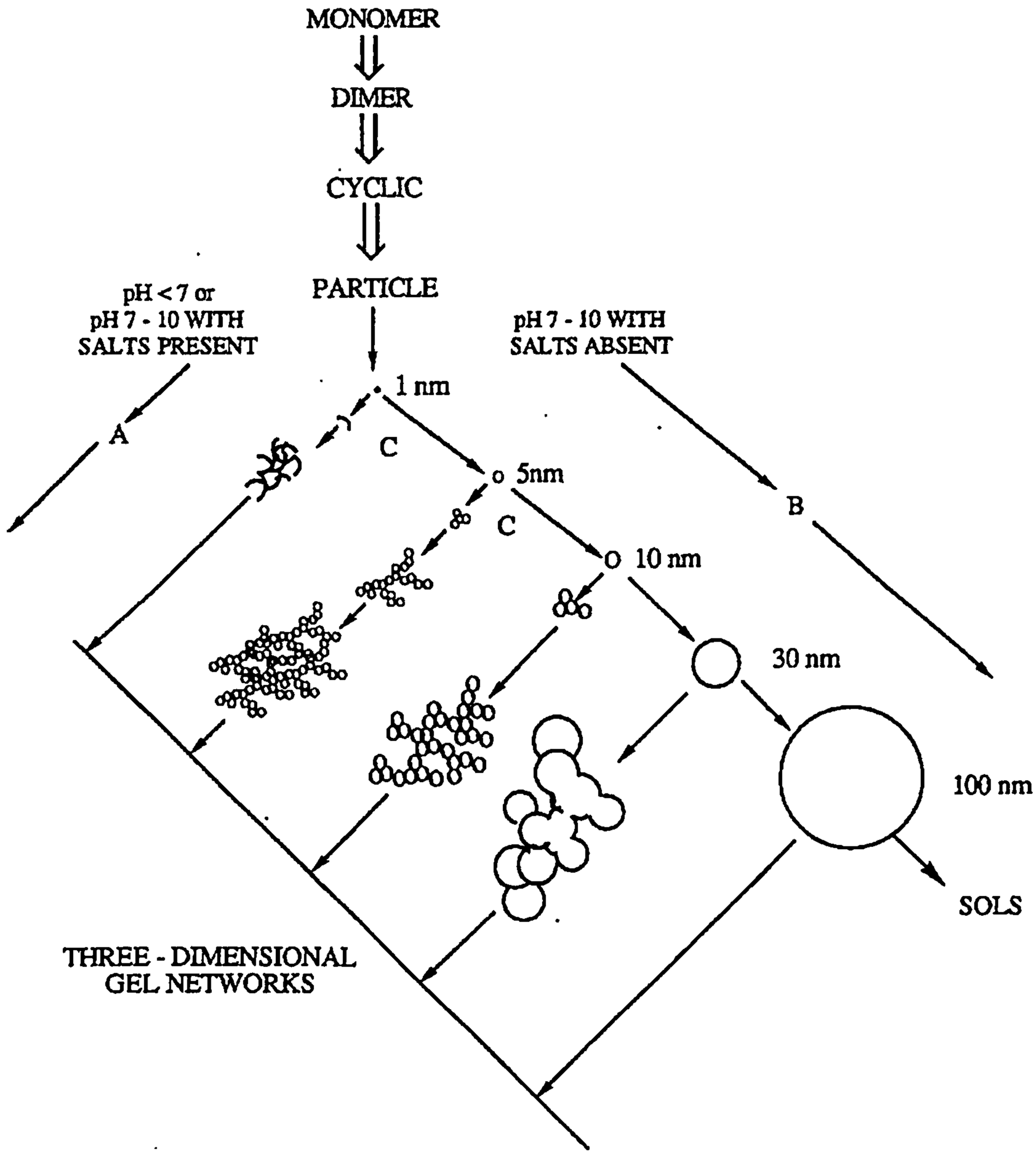

Fig. 2.17 Polymerisation behaviour of silica. In base solution (B) particles in sol grow in size with decrease in numbers; in acid solution or in presence of flocculating salts (A), particles aggregate into three-dimensional networks and form gels (Iler, 1984).

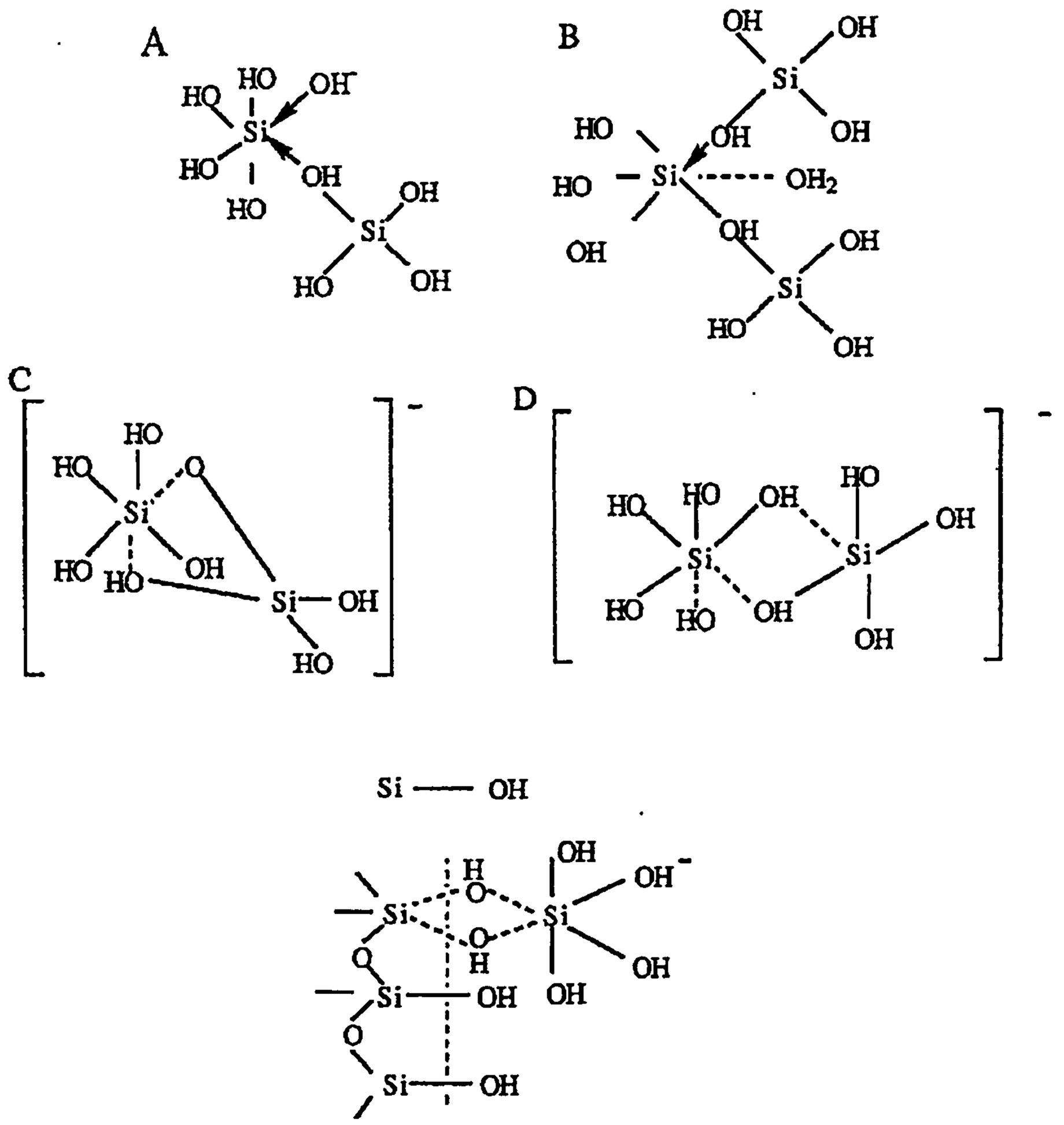

Fig 2.18 Possible intermediates in polymerisation of silica: A. two silicon anionic complex involving OH^- ion; B, three-silicon cationic complex involving H^+ ion; C+D, suggested alternates to A; E, intermediate at silica surface.

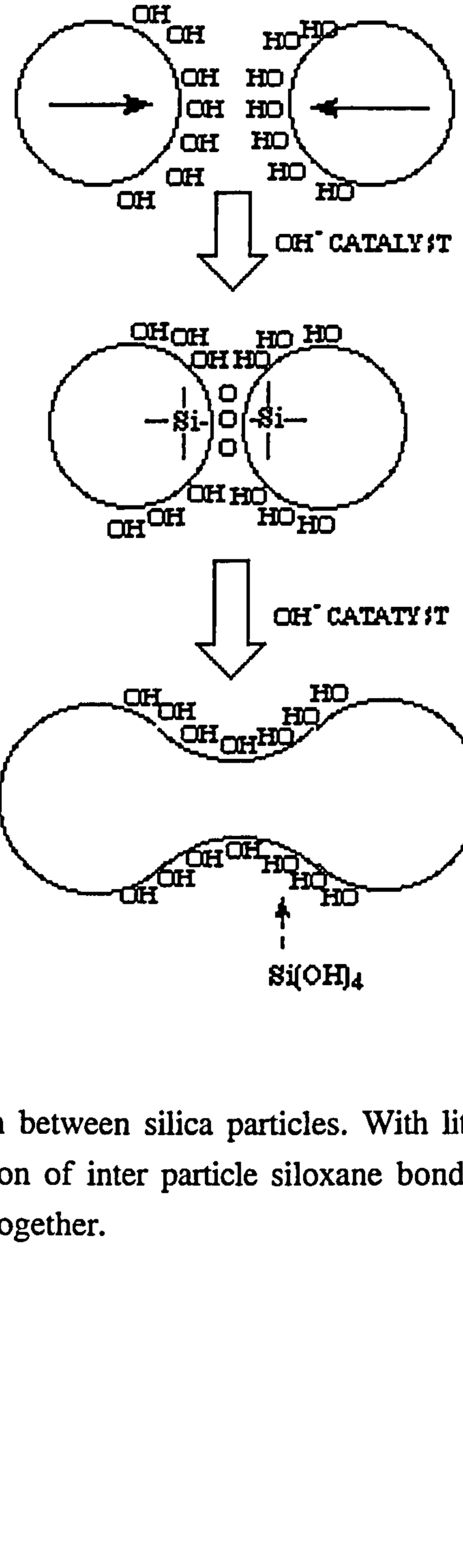

Fig. 2.19 Bond formation between silica particles. With little or no charge repulsion, collision results in formation of inter particle siloxane bonds, catalysed by base. Once bonded, the particle grow together.

COORDINATION NUMBER		VOLUME %		PORE VOL
		SOLID	PORES	cm^3/g
12		74.5	25.5	0.155
6	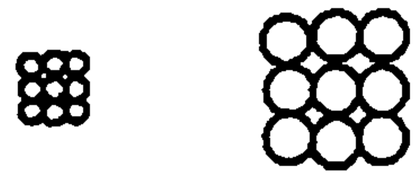	52	48	0.42
3	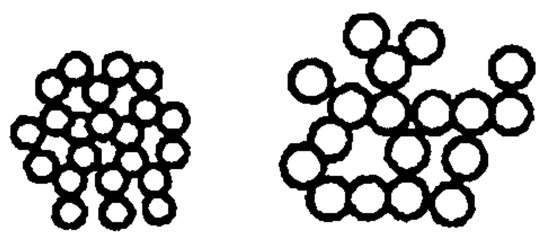	5	95	8.6
3-2-3	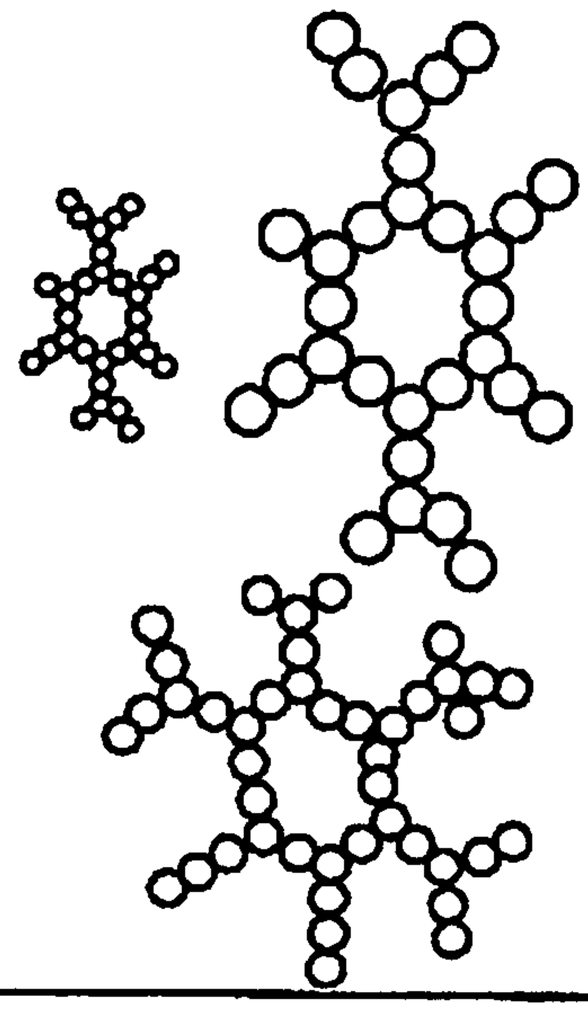	1.3	98.7	35
3-2-2-3		0.83	99.17	54

Figure 2.20 The size of the ultimate particles and the co-ordination number (number of particles touching each particle) control the pore volume and average pore diameter.

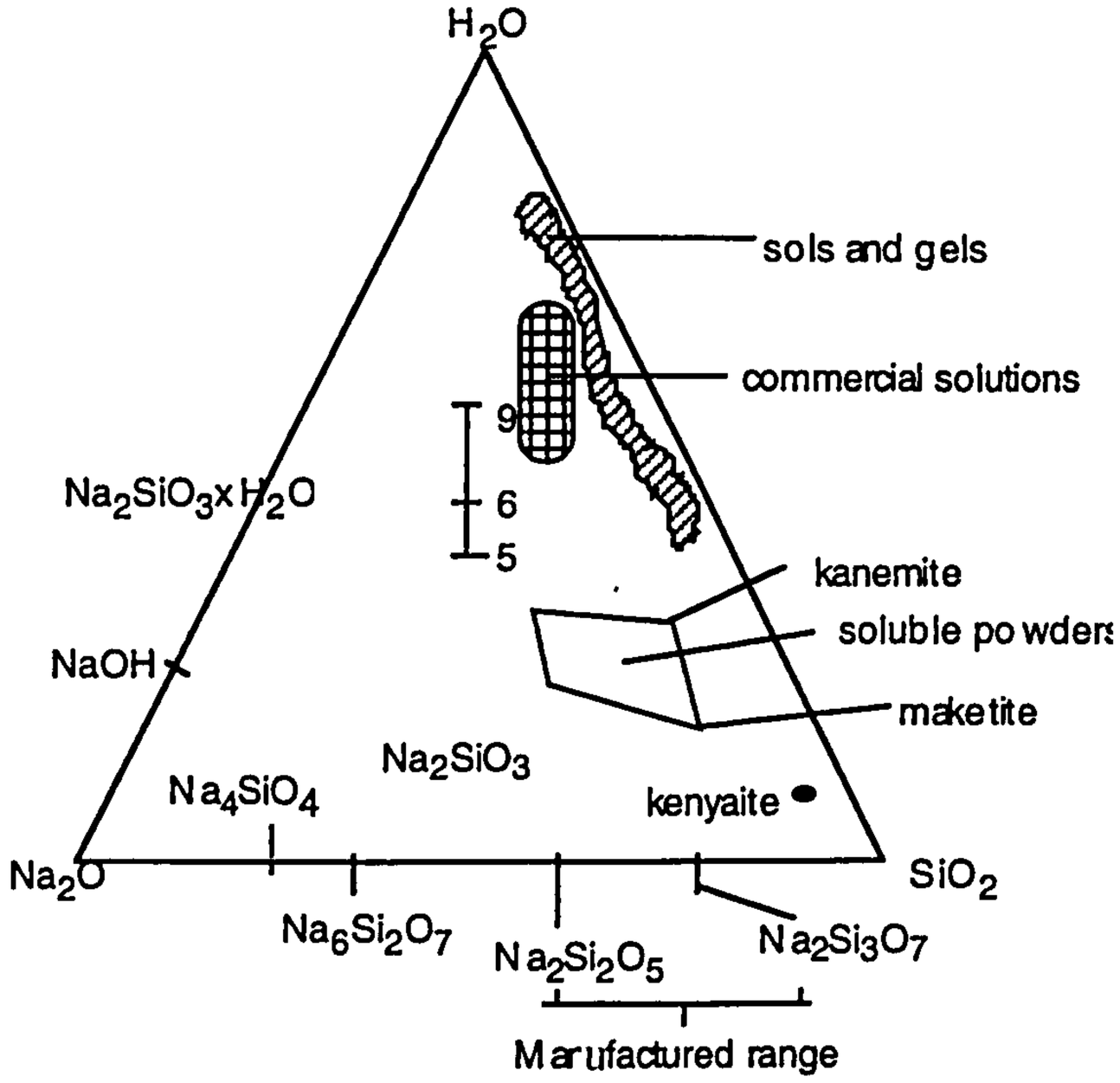

Fig. 2.21 Chemical distribution of sodium silicate products based on the manufacture formulation and the final composition.

Chapter 3

TESTING AND EXPERIMENTAL METHODS

3.1 Introduction

It is necessary to use a range of experimental methods for measuring mechanical, physical, and thermal properties of the ceramic moulding compounds, in order to evaluate and to optimise the formulation, process-ability, mould-ability and properties of the final products. Some of the tests used standard testing methods, but some of others did not, as no standard method was available. In the latter case, details of the test protocols have been given.

3.2 Viscosity measurement

A key property that must be measured and controlled is the material's viscosity in order to optimise the manufacturing and moulding processes. The viscosity of a ceramic dough compound has characteristics similar to polymeric systems. To measure the viscosity, a Brookfield Viscometer (BV) was employed. The BV is of the rotational variety (Fig. 3.1), measuring the torque required to rotate an immersed element (the spindle) in a fluid. The spindle is driven by a synchronous motor through a calibrated spring; the deflection of the spring is indicated by a digital displayer. By utilising a multiple (four or eight) speed transmission and interchangeable spindles, a wide viscosity range can be measured (Brookfield Engineering Lab.).

For a given viscometer model, the highest viscosity was measured by using the smallest spindle at the slowest speed. Generally, for polymer and ceramic matrix systems in processing, the viscosity range is from 200 cps to 20,000 cps. For mixtures of ceramic pastes with catalysts, hardeners, fillers, additives, the viscosity range can extend from

1000 cps to a maximum $1.0x10^7$ cps after several days, which is almost the maximum range of a normal viscometer. The BV used in the study was Model DV-II+ with high viscosity measurement spindles and a viscosity measurement range from 50 cps to 8.0 x 10^7 cps.

- Basic principles

Newton assumed that a force was required to maintain a difference in speed between two layers in a liquid that was proportional to the difference in speed through the liquid. This can be expressed by Equation E3-1 as shown schematically in Fig. 3.2.

$$\frac{F}{A} = \eta \frac{dv}{dx} \qquad \text{(E3-1)}$$

η is a constant for a given material called "viscosity", here the unit used was cps. F/A indicates the force per unit area required to produce the shearing action as "shear stress - τ", the unit is "dynes per square centimetre" (dynes/cm^2). The dv/dx is the speed at which the intermediate layers move with respect to each other as "shear rate - S".

Therefore, the viscosity of the materials can be defied mathematically by E3-2:

$$\eta = viscosity = \frac{F/A}{dv/dx} = \frac{\tau}{S} \qquad \text{(E3-2)}$$

The friction of two liquid layers becomes apparent when a layer of fluid is made to move in relation to another layer. The greater the friction, the bigger the amount of force required to cause this movement. This shearing occurs whenever the fluid is physically moved.

For cylindrical spindles τ and S are defined as Equation E3-3 and E3-4:

$$S = \frac{2\omega R_c^{\,2} R_b^{\,2}}{X^2\left(R_c^{\,2} - R_b^{\,2}\right)} \qquad \text{(E3-3)}$$

$$\tau = \frac{M}{2\pi R_b^{\,2} L} \qquad \text{(E3-4)}$$

where ω is angular velocity of spindle (rad/s); R_c is radius of container (cm); R_b is radius of spindle (cm); X is radius at which shear rate is being calculated; M is torque input by instrument; L is effective length of spindle.

A flow chart listing viscosity measurements as required for a full characterisation of the materials for measurements is shown in Fig. 3.3.

- Newtonian and Non-Newtonian viscosity:

Pure liquid silicates, are similar to a Newtonian fluid. A Newtonian fluid relationship between shear stress and shear rate is shown in Fig. 3.4. But when the fillers and hardeners are added to a ceramic slurry system, the rheology of the matrix mixture would be changed and they may exhibit non-Newtonian behaviour depending on the types of additive introduced into the basic ceramic system.

Non-Newtonian fluids are described as plastic fluids that fall into two categories: thixotropic and rheopexic fluids. They exhibit different shear-force curves and viscosity-shear curves. Fig. 3.5 shows one of the examples of shear-force and viscosity-shear curve for non-Newtonian fluids. Some results of the system slurry with only one filler in next chapter indicated that some fillers did not greatly change the viscosity of a liquid silicate system.

- Rheology of the matrix

Pure liquid silicates are close to Newtonian fluids, and the viscosity is stable in a sealed container at ambient temperature (400 - 500 cps). However, the slurry of the liquid silicates with silicate fillers becomes a medium to highly viscous Non-Newtonian fluid when hardeners and some mineral fillers cause interactions between these inorganic molecules. This ultimately results in cross-linking after the mixing process. It can be noticed that mixing initially leads to a slight viscosity decrease and shortly afterwards a rapid increase in viscosity. A schematic indication of rheological development in the matrix slurry during the entire manufacturing process is shown in Fig. 3.6.

3.3 Physical properties

Relevant physical properties of the CDMC moulded panels are density, water evaporation, water absorption and void content.

3.3.1 Density measurement

The densities of the CDMC panels were measured by the traditional Archimedes Method (D 792-86/A). The mechanism involved weighing the specimens both before and after immersing into pure water. The density of a specimen is given by:

$$d_t = \frac{d_{water} \cdot m_1}{m_2 - m_3} \qquad \text{(E3-5)}$$

Where:

m_1 = the weight of specimen in air;
m_2 = the weight of specimen and plus the thread in air;
m_3 = the weight of specimen and thread in water;

d_{water} = The density of water at testing temperature;
$d_t = d_{CDMC}$ = The density of specimen.

The densities of the CDMC panels in this research were measured at room temperature based on the procedure of ASTM D792 and with the results calculated according to E3-5. Specimens were cut from moulded panels in a way as shown in Fig. 3.7.

3.3.2 Water evaporation

The water evaporation and retained water in the CDMC during and after moulding were measured and calculated with equation E3-6. The water retained in the moulded product was calculated from the whole water contained in the compound before moulding, the weight loss between the compound during moulding and the final products after moulding.

$$Water(\%) = \frac{W_{water} - W_L}{W_{CDMC} - W_L} \times 100\% \qquad \text{(E3-6)}$$

Water(%) is the water percentage contained in the CDMC panel after moulding. W_{water} is the weight of water in the compound before moulding. W_L is the water lost during moulding from the compound. W_{CDMC} is the weight of the CDMC panel after moulding.

3.3.3 Void Content

The void content of the CDMC panel after moulding can be measured by several methods, such as N_2 absorption, pressure differentials and image analysis. In this research, image analysis was used. The method involved cutting different slices from the specimen coupons. From these cut sections of the test specimens, the outline of the voids from one section was drawn by the computer either connected with a SEM or an image analyser.

$$Void\% = \frac{A_{Voids}}{A_{Fram}} \times 100\% \qquad \text{(E3-7)}$$

Then the computer could calculate the void content for the area on the section (A_{voids}) cut from a specimen, using equation E3-7. Since this measurement of the void content relates to a particular intersection area (A_{fram}), many sections have to be measured in order to obtain a statistical average (void %). In this work, each moulded sample normally provided more than 7 sections.

3.3.4 Water absorption

The absorption of water by a CDMC panel is complex and directly depends on the volume fraction of pores and water paths. The water absorption also depends on factors such as the glass fibre volume fraction, moulding temperature used, fillers involved and organic additives.

Generally speaking, to determine the water absorption:

a. If a material is insoluble in water,

$$W_{p\bullet c} = \frac{G_2 - G_1}{G_1} \times 100\% \qquad \text{(E3-8)}$$

b. If a material contains soluble substance in water,

$$W_{p\bullet c} = \frac{G_2 - G_3}{G_3} \times 100\% \qquad \text{(E3-9)}$$

Where,

G_1 = The weight of specimen after drying (mg.).

G_2 = The weight after immersed in to water (mg.) for 24 hours.

G_3 = The weight of the specimen with immersed into water and then dried afterwards.

S = Surface area of materials (cm^2).

W = The water absorbed (mg).

W_S = Absorption of water in mg/cm^2.

$W_{p\cdot c}$ = Water absorption percentage of a CDMC.

The size of specimen required for this test is 50x50 mm^2 , dried at 70 ℃ for 4 hours (or 105 °C for 1 hour). Then after the specimen were immersed in pure water (20 ℃) for 24 hours, they were taken out of the bath and were weighed within 1 minute.

3.3.5 Differential scanning calorimeter (DSC)

Thermal analysis is a method which studies the changes in structure and properties of a material with temperature. It can provide information on changes in physical or chemical conditions in an organic or inorganic material.

A Perkin-Elmer 7 Series DSC was employed to determine the thermal properties of ceramic matrix, fillers, hardeners and binders. The apparatus is a computer-controlled instrument operating with a DEC workstation. The operation was based on the Perkin-Elmer power compensated 'Null-balance' DSC principle. The sample and reference are heated or cooled, simultaneously in separate but identical holders with separate heaters and platinum resistance temperature sensors. The energy which was absorbed by a sample was compensated by adding or subtracting an equivalent amount of electrical energy to a heater located nearby. This was done to keep the temperature identical to that of the reference and the set point. The difference in electrical energy required between samples and reference is collected and plotted against temperature.

The CDMC matrix, hardeners (such as Fabutit 320 and 328), fillers (such as $CaCO_3$, MT, FW325, P60) and liquid silicates (Crystal 079) were weighted accurately between 9.0 to 10.0 mg. They were put into the sample Al pans and were encapsulated by clamping the covers. All measurements were done with a nitrogen purge gas at a scanning rate of 20 ℃ per minutes.

3.4 Tests for mechanical properties

Mechanical characterisation of the CDMC was carried out by a screw driven displacement controlled mechanical test machine, Instron 1122. A minimum of 5 - 7 specimens for each measurement, were cut using a special diamond tipped blade for ceramic composites and glass fibre reinforced polymer composites. These specimens were tested for different formulations, moulding conditions and duration of post-cure in terms of tensile, flexural, and instrumented falling weight impact.

3.4.1 Tension

Tensile properties were obtained using a standard of tensile test for fibre reinforced composite materials. BSI 1003 which is equivalent to the ISO /DIS 3268.

The CDMC specimens were prepared by the Type III method with end taps to prevent failure close to the grips. The dimension of tensile testing specimens and a photo of the CDMC testing specimen are shown in Table 3.1 and Fig. 3.8 - 3.9. The tensile specimens in this research were kept at room temperature for about 30 days after moulding to reach their maximum properties before tests.

When loading to failure, the cross head speed for type III specimen was 2.0 mm/min. When measuring elongation in order to determine the modulus of elasticity in tension, a 0.2 mm cross head speed was used. The dimensions of the specimens were measured, width **b** to the nearest 0.1 mm and the thickness **h** to the nearest 0.02 mm at the mid-point of the specimen and within 5 mm of each end of the gauge length. Tensile strength was calculated at maximum force.

3.4.2 Flexure (ISO-178)

This test is used for determining the flexural properties of a fibre reinforced composite materials.

The CDMC in the form of rectangular bars of standard dimensions which were cut from the moulded CDMC panels as shown in Fig. 3.10. The apparatus was an Instron 1122 with 5 kN load cell. Cross-head speed used was 2.0 mm/min. All the flexural specimens in this research were kept at room temperature for about 30 days after moulding to reach their maximum properties before test.

The dimension of testing specimens was designed with minimum length L more than 16 times of thickness. The width b is also a function of thickness, as shown in Table 3.2. The results were calculated using E3-10 and E3-11. The corresponding flexural stress - strain curves for some specimens moulded at different moulding temperatures were then calculated based on their force-deflection histories.

$$\sigma_f = \frac{3FL}{2bh^2} \qquad \text{(E3-10)}$$

$$E_b = \frac{L^3}{4bh^3} \cdot \frac{\Delta F}{\Delta d} \qquad \text{(E3-11)}$$

$\mathbf{E_b}$ is the modulus of elasticity, in GPa.

During a flexural test three different types of breaks can occur:

a. Initiated on the surface under tension;

b. Initiated on the surface under compression;

c. By internal shear failure.

3.4.3 Impact (ISO 6603/2)

A falling weight impact test was selected for this programme, using ISO 6603/2 standard. This test uses a small plate supported on a circular loading jig. This mode of testing allows the composite to develop damage over a large area if the damage process is available for this to happen. The alternative testing methods, such as charpy tests, restrict the damage area to a local zone at the point of impact and have been shown to be less relevant for the study of the chopped fibre reinforced composites.

The force-time, energy-time, velocity and deformation data were obtained throughout the event with a striker which was fitted with a force transducer. These data were then transferred to a computer for the data analysis. In this way, the force-time, energy-time, displacement-time, force-deformation histories, etc. can be obtained.

This low velocity drop-weight impact test involved a striker which was much heavier than the specimen and which was dropped from a certain height onto the specimen surface. The fixed plate configuration is normally used as shown in Fig. 3.11.

Techniques traditionally used for measuring the energy absorption in fracture of metals involve complete failure of the specimen (e.g. Charpy) (ISO 179, 1982) and this data may not be relevant to composites in terms of its application. To obtain more meaningful data, fracture toughness tests are often carried out. However, to put these results into perspective, tests such as impact are conducted to provide practical information regarding to the material's toughness. All the materials configurations manufactured for the programme were tested with impact specimens, size of 60 x 60 mm^2. The thickness of specimens was between 3.0 to 4.0 mm.

The incident energy and velocity of the striker were varied by altering the height of the mass above the specimen, according to a diagram shown in Fig. 3.12. The force:

$$P = mg - F = ma = m\frac{dv}{dt} \qquad \text{(E3-12)}$$

The theoretical velocity at impact at time t

$$V_t = V_0 + gt - \int_0^t \frac{F}{m} dt$$

$$V_t = \sqrt{\frac{2E}{m}}$$

The theoretical impact energy E is determined at the time t by,

$$E = FV_0 t + \tfrac{1}{2} gFt^2 - \tfrac{1}{m}\int_0^t F^2 t \cdot dt \qquad \text{(E3-13)}$$

$$E = m \cdot g \cdot h \qquad \text{(E3-14)}$$

Where

a = Acceleration;

F = The force on striker;

g = The free fall acceleration constant;

m = The mass of the striker;

V_0 = The velocity at the time t_0;

V_t = Velocity at time t;

x = The displacement.

The contact force-time, energy-time histories and force-deformation were recorded using an instrumented striker, with a plate motion determined using the equation of motion. All

the impact data was recorded and analysed by the CEAST software in a PC computer. The testing parameters are listed in Table 3.3. Fig. 3.13 shows two impact force-deformation curves of the CDMC reinforced by 12 mm and 6 mm glass fibre respectively with impacting energy 15.9 J. The specimens thickness was 4 mm.

3.4.4 Interfacial shear strength: micro-indentation

We have mentioned above that the fibre diameter in the CDMC specimens is 14 μm which was supplied by Cem-FIL and the type used was AR50/1. Micro-indentation tests were performed using a Berkovich Indentor in order to measure the interfacial shear strength shown in Fig. 3.14. The cross-head speed of the indentor was set to 0.2 μm/s for all the experiments presented. The maximum displacement is 200 μm and the precision 0.05 μm. The load measurement has a precision of 1 mN. The loaded range is from 200 to 600 mN. During the test, both load and penetration depth are continuously recorded. In the diagram, τ is the interfacial shear strength; L is the thickness of the specimen or the fibre length; F is the load applied to the fibre, and Φ is the diameter of the single fibre. The interfacial shear strength can be calculated by equation E3-15. If the fibre selected is parallel to that of movement of indentor, the L could be the thickness of the specimen.

$$\tau = F/(\Phi\pi L) \rightarrow L = F/(\pi\Phi\tau) \qquad \text{E3-15}$$

3.5 Tests for fire performance

Fire performance in this research was carried out in two areas, fire penetration using a small furnace built to reproduce International Maritime Organisation (IMO) test conditions, and materials reaction to fire using a Cone Calorimeter test.

3.5.1 Fire resistance

Experimental fire tests were carried out using a relatively small stack-bonded ceramic wool lined furnace, at QMW, that was gas fired by a multi-nosed burner arranged so that the jet from the burner did not impinge directly on the surface of the specimens. This has been configured to match the fire test conditions specified by both British Standards and IMO fire tests which call for testing on 1.0 m^2 panels. Combined with this, there is a greater acceptability of smaller furnaces for testing specimens of elements that are at full size, capable of being tested in smaller furnaces (BS 476, Part 20/ISO 843). The CDMC test pieces (3.0 x 300 X 170 mm^3) are mounted in a specially designed frame forming the door of the furnace. The furnace is computer controlled to follow a specified temperature / time programme. The reference temperature is taken as a mean value from four control thermocouples set 100 mm from the hot face of the front panel. Each test specimen was instrumented with thermocouples on the hot and cold faces. The output of each individual thermocouple was continuously monitored for upwards of 60 minutes and recorded using a data logging system. The fire penetration test equipment (Fire penetration furnace structure) is shown schematically in Fig. 3.15.

Based on BS476: Part 20, the heating conditions of the standard temperature/time curve and the maximum allowable temperature have been shown in Fig. 3.16. It should be governed by equation:

$$T = 345\log_{10}(8t + 1) + 20 \qquad \text{(E3-16)}$$

Where T is the mean furnace temperature (°C), t is the time (in minutes) up to a maximum of 360 min.

3.5.2 Material's fire reaction

The materials fire reaction was examined by a Cone Calorimeter, which has been developed for usage as both production and research equipment for measuring the fire properties of materials (ISO 5660).

A schematic diagram of the cone calorimeter is shown in Fig. 3.17. According to ISO/DIN 5665, the equipment comprises a load cell for weighing the mass, a cone heater and a system for collecting the combustion products (soot, gas sampling, temperature and pressure measurement). The cone-shaped heater produces a uniform heat flux on the sample surface (100 mm x 100 mm) (L. Sarvarant and E. Mikkola, 1986). The heat flux can be adjusted between 1 and 100 kWm^{-2} which corresponds well to different fire situations. In this study a heat flux of 75 kWm^{-2} was used. This causes the surface temperature to rise tremendously in very short time. The results are obtained as time-dependent curves of different parameters.

This testing method is based on the net heat of combustion being proportional to the amount of oxygen consumed. That is approximately 13.1 x 10^3 kJ of heat being released per kg of oxygen consumed. Specimens are burnt with an applied heat flux in the range 0 - 100 kW/m^2 rate radiator under the conical heater. The testing measurements included heat release rate (HRR); CO and CO_2 production rates and yields; mass stability and mass loss rates; the effective of heat combustion; rate of smoke released and specific extinction area.

Gas analysis instrumentation built into the Cone Calorimeter can give the composition distribution for the exhaust gas system. The schematic gas flow chart of cone calorimeter is shown in Fig. 3.18.

HRR [IMO resolution A517(13)] is defined as the amount of heat released by a burning body in unit time. It is one of the fundamental properties of a fire and should always be taken into account in any assessment of fire since it significantly affects the development of fire in a building. The HRR can be calculated from equation E3-17, E3-18:

$$q(t) = (\Delta h_c / r_o)(1.10)C\sqrt{\frac{\Delta p}{T_e}} \cdot \frac{T^o_{O_2} - X_{O_2}}{1.105 - 1.5X_{O_2}} \qquad \text{E3-17}$$

where

$$C = \frac{10.0}{12.54 \times 10^3 (1.10)} \cdot \sqrt{\frac{T_e}{\Delta p}} \cdot \frac{1.105 - 1.5X_{O_2}}{X^o_{O_2} - X_{O_2}} \qquad \text{E3-18}$$

where, C, calibration constant for oxygen consumption analysis; T_e is the absolute temperature of gas at the orifice meter(K); Δp is orifice pressure differential (Pa); q is the

heat release rate; X_{O_2} is oxygen analyser reading, mole fraction O_2; $X_{O_2}^{\circ}$ is initial value of oxygen analysis reading; X'_{O_2} is the oxygen analyser reading before a delay time correction; r_o is the oxygen/fuel mass ratio.

The CO production rate could be derived from following equation E3-19:

$$X_{CO}(t) = X^1 co\left(t + t_d{}^2\right) \qquad \text{E3-19}$$

Where X_{CO}: CO reading , mole fraction; X^1_{CO} : CO reading before delay time correction; $t_d{}^1$: delay time of the CO_2 analyser(s); $t_d{}^2$: delay time of the CO analyser(s); $t_d{}^3$: delay time of the H_2O analyser(s).

CO_2 production rate could be derived from following equations (W. J. Parker, 1982):

$$X_{O_2}(t) = X^1 o_2\left(t + t_d\right) \qquad \text{E3-20}$$

$$X_{CO_2}(t) = X^1 co_2\left(t + t^1{}_d\right) \qquad \text{E3-21}$$

Where

X_{O_2}: Oxygen reading, mole fraction; $X^1_{O_2}$ is oxygen reading before delay time correction; X_{CO_2} is CO_2 reading, mole fraction; t^1_d delay time of the CO_2 analyser.

The effective heat of combustion (EHC) and mass loss rate can be used to prove additional information on the fire behaviour of materials, which could be calculated by equation E3-22, a time-verying value of the effective heat of combustion $\Delta h_{c,eff}(t)$:

$$\Delta h_{c.eff}(t) = \frac{q(t)}{-dm\,/\,dt} \qquad \text{E3-22}$$

Where, m is the specimen mass (kg), at end of the test; (-dm/dt) is specimen mass loss rate (kg/s).

3.6 Equipment and mechanism of SEM, TEM and X-ray

SEM and TEM microscopes and X-ray diffraction have been used for examining microscopic structures and chemical composition. Fig 3.19 shows the various analytical mechanisms available with SEM and TEM. Particularly, for investigating the polymerisation of the matrix by X-ray microanalysis, the results have been presented in the form of diagrams which represent different ratios of composition on the surfaces of the matrix cured at different temperatures.

SEM studies were undertaken on fractured surfaces of tested specimens and on polished sections cut from the CDMC panel without testing, and mounted in a room curing epoxy resin. The specimens were then polished by grinding machines on a series of successively finer silicon carbide polishing wheels. Final polishing was performed on cloth wheels impregnated with diamond paste (1 μm particles). Specimens polished with 1 μm paste were found to produce the optimum contrast between fibres and matrix.

As an example, Fig. 3.20 shows a SEM micrograph of a surface of ceramic moulding composite. Some reinforced glass fibres can be observed in a porous ceramic moulding composite.

The surface composition of the ceramic matrices hardened at different temperatures was investigated using quantitative energy dispersive spectroscopy (EDS) X-ray microanalysis in the SEM (Williams DB, 1984, 1996). The quantitative calculation for the X-ray microanalysis was based on the technique and equation developed by Cliff-Lorimer in 1975. They showed that quantification was possible using a simplification of a traditional ratio equation, by simply using the ratio of the intensities gathered from two elements simultaneously in the microanalysis.

The Cliff-Lorimer ratio technique uses equation E3-23 as a base for two elements A and B in a Binary system.

$$\frac{C_A}{C_B} = k_{AB}\frac{I_A}{I_B} \qquad \text{(E3-23)}$$

The term k_{AB} is often termed the Cliff-Lorimer factor. It is actually not a constant. It varies according to the EDS system and kV. For a binary system, it can be assumed that A and B constitute 100% of the specimen,

$$C_A + C_B = 100\% \qquad \text{(E3-24)}$$

For a ternary and higher order systems (C_A+C_B+C_C =1):

$$\frac{C_B}{C_C} = k_{BC}\frac{I_B}{I_C} \qquad \text{(E3-25)}$$

Related k factors:

$$k_{AB} = \frac{k_{AC}}{k_{BC}} \qquad \text{(E3-26)}$$

It is a convention that the units of composition are expressed as %(wt.).

Energy-Dispersive X-ray Spectrometer (EDS) is a modern analytical technique for a quantitative microanalysis or identification of unknown compounds on the surface of CDMC mixtures. While in this project, the EDS has been used in quantification and identification of leached compound (Na_2O/NaOH) on the surface of CDMC and obtaining compositional information on the CDMC matrices moulded in different temperatures.

3.7 Summary

Most of the testing methods for obtaining the mechanical, physical, chemical and fire /thermal properties for the CDMC have been listed in the Table 3.4 as a summary of this Chapter.

These test processes and results have provided an general evaluation for the CDMC processing, moulding and formulation design. These are the bases for further improvement and achievement to be done for the CDMC.

Table 3.1 Dimension of the type III tensile test specimen.

Item	Mean	Type III
F	Overall length minimum	250 mm
h	Thickness (for the CDMC panels)	3.0 - 4.5 mm
b	Width of the middle parallel part	25 mm
L_0	Gauge length	100 mm
E	Distance between grips	170 mm
D	Distance between end pieces	150 mm
T	Minimum length between end pieces	50 mm

E_T is the initial tangent modulus of elasticity, in megapascals;

F_1 is the change in force in Newton;

L_o is the gauge length of the extensometer, in millimetres;

R is the magnification ratio of the extensomter;

A is the initial cross sectional area of the test specimen, in square millimetres;

Z_1 is the change in the apparent extension, in millimetres, taken from the chart for the change in force F_1.

Table 3.2 The dimension of the flexural specimens of the CDMC. The number of test specimens was 5 to 7.

Thickness, h	Width, b	Length, L
$1 < h < 10$ (h = 3.0-4.5 mm for the CDMC)	15	>16xh

Table 3.3 Impacting testing perimeters of drop weight method. All the impacting specimens were prepared by the size of 60 x 60 mm^2. The thickness of specimens was between 3.0 to 4.0 mm.

impacting conditions	**I**	**II**
Striker mass (kg)	0.78	2.316
Impacting height (m)	0.68	0.70
Impacting velocity (m/s)	3.6	3.71
Impacting energy (J)	5.2	15.9

Table 3.4 A list of mechanical, physical, fire and fire reaction tests, test specifications, standards and testing machines used in the research.

Type of test	Test specifications	Test standard	Test machine
Mechanical tests	Tension	BSI 1003/ISO /DIS 3268	Instron 1122
	Flexure	ISO-178	Instron 1122
	Impact	QMW	CEAST machine
	Shear strength between fibre/matrix	Micro-indentation	Berkovich Indentor
Physical properties	Density	D 792-86/A	Oertling R51 Mark II
	Water absorption		Oertling R51 Mark II
	Voids content		Image analysing system
Fire performance	Fire penetration	BS476: Part 20 (IMO)	Furnace
	Materials fire reaction	ISO/TR 3814; ISO/DIN 5665	Cone Colorimeter
Viscosity	Viscosity of matrix slurries	Non-Newtonian	Model DV-II Viscometer
TEM	Micro-structure	Standard operating procedures	TEM 100X/100 Kev, 46 cmc/L
SEM	Micro-graphs	Au or carbon coated samples	
X-ray	Substance identification	SEM/TEM	
DSC	Thermal analysis	D3418	
TGA	Thermal gravimetric analysis		

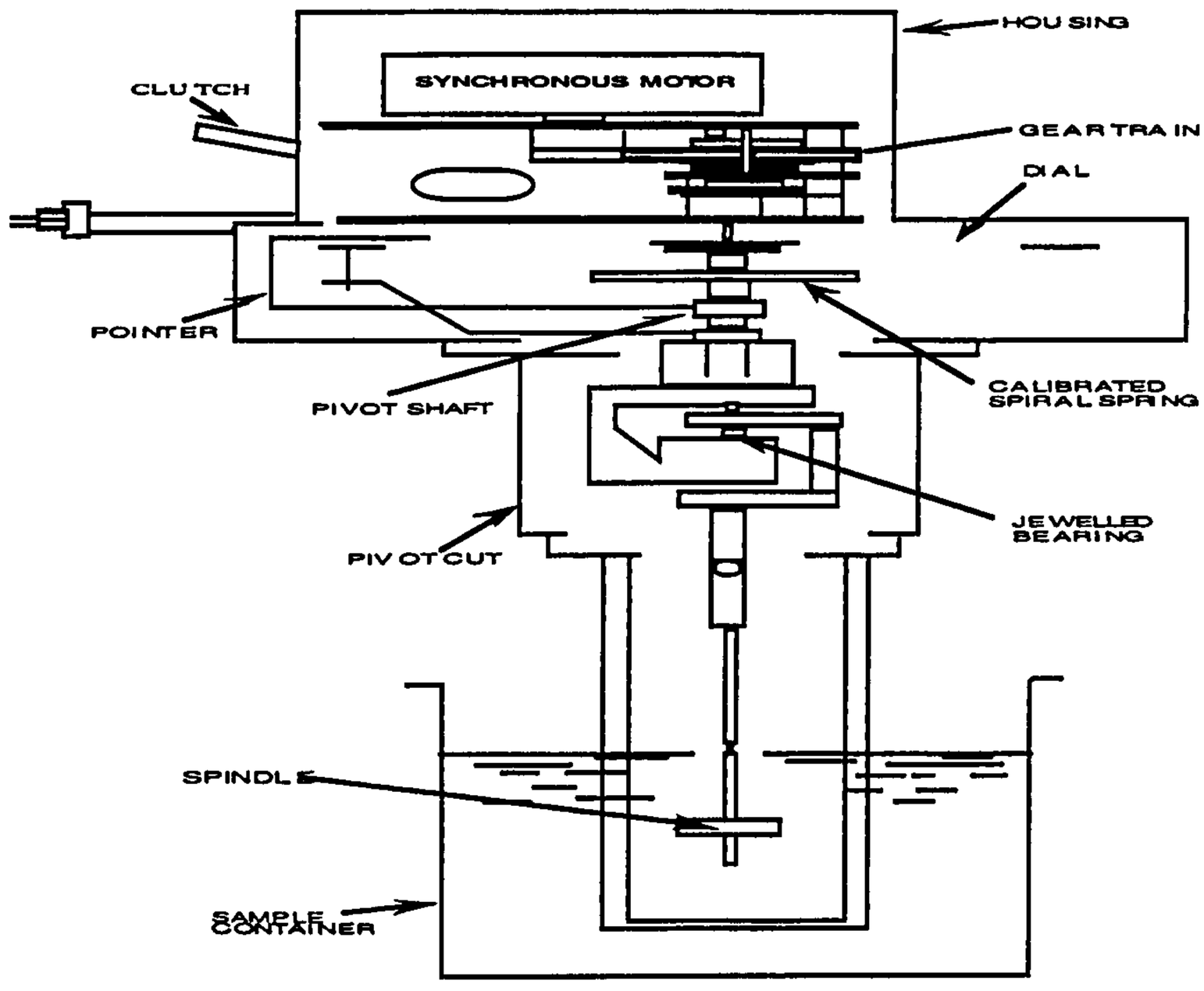

Fig. 3.1 A schematic drawing of the structure / working mechanism of the Brookfield Viscometer, Model DV-II+.

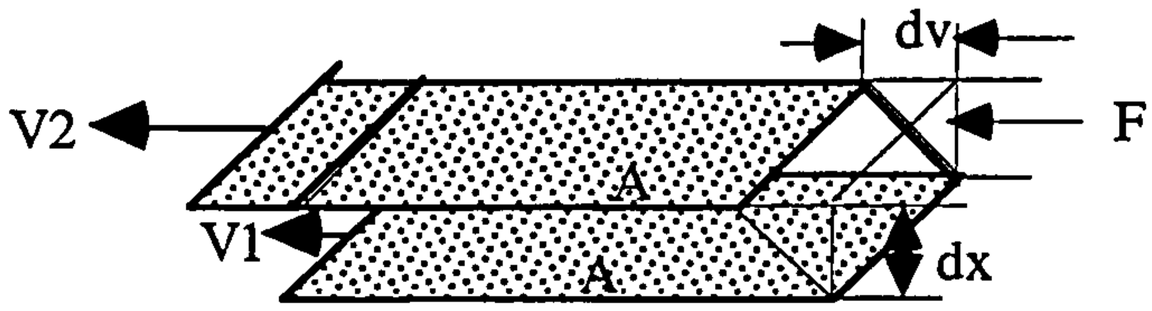

Fig. 3.2 Newton defined viscosity by considering the model of two layers in liquid water at room temperature.

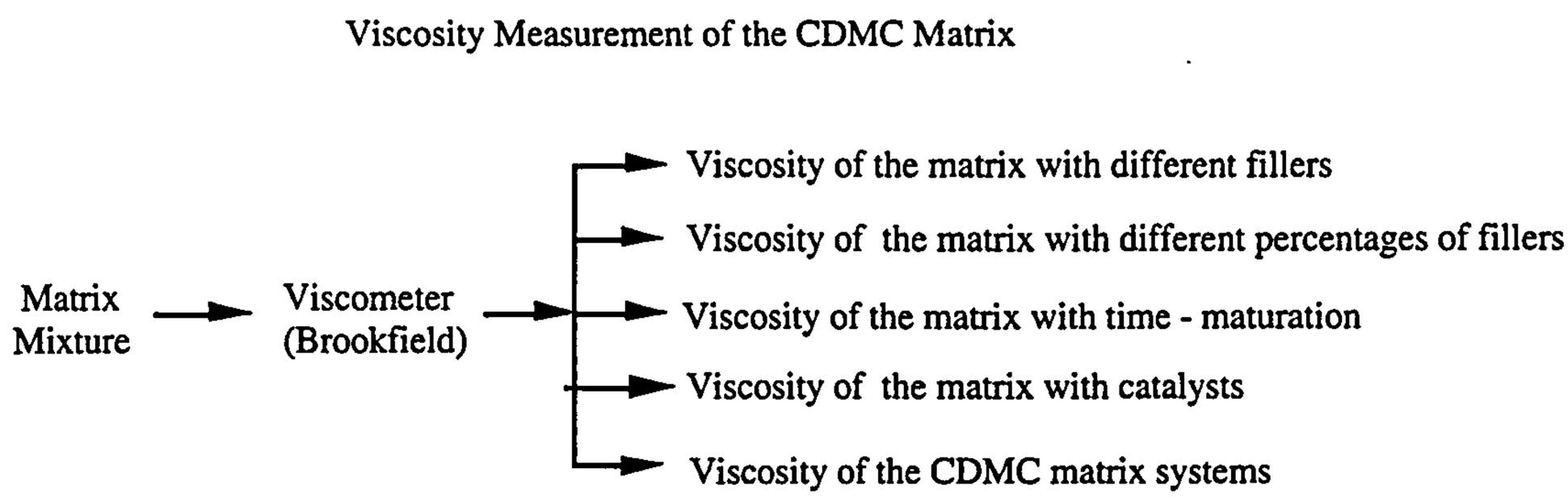

Fig. 3.3. This chart shows the categories of viscosity measurement in this work.

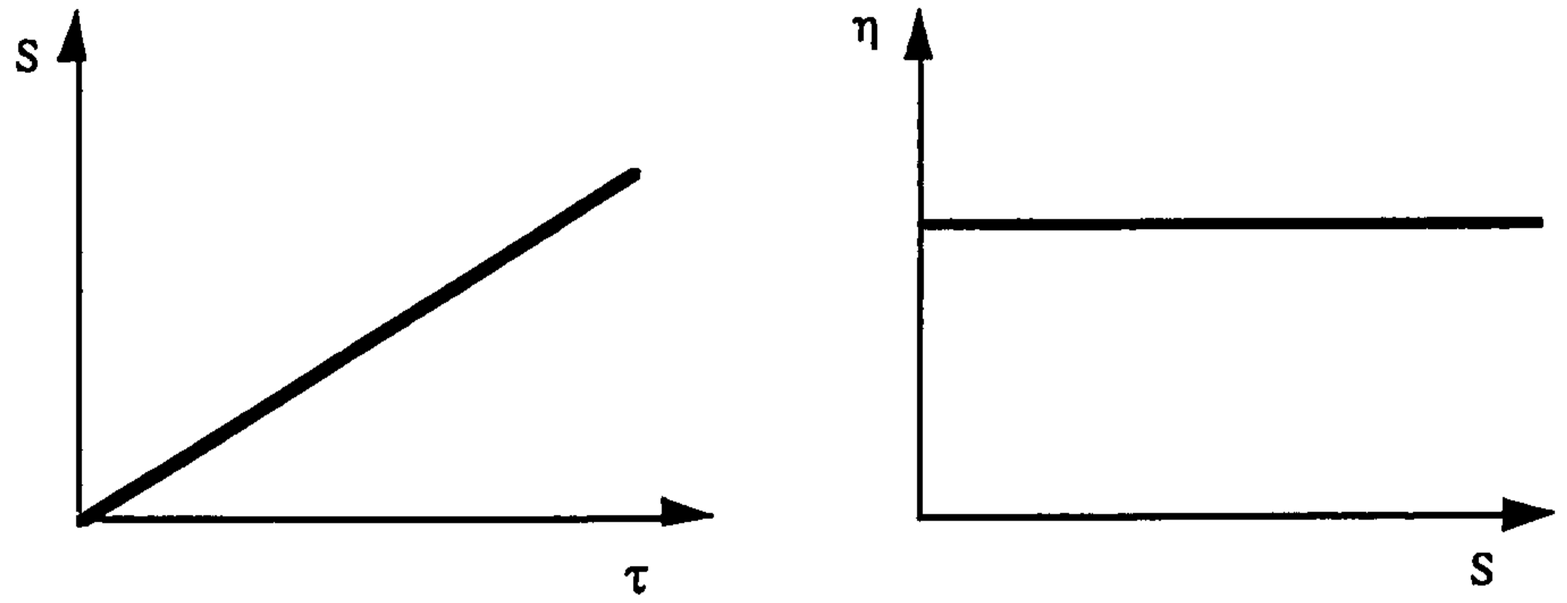

(A) (B)

Fig. 3.4 Newtonian fluid relationship between shear stress (τ) and shear rate (S) is a straight line (A), and viscosity (η) is independent of shear rate (B).

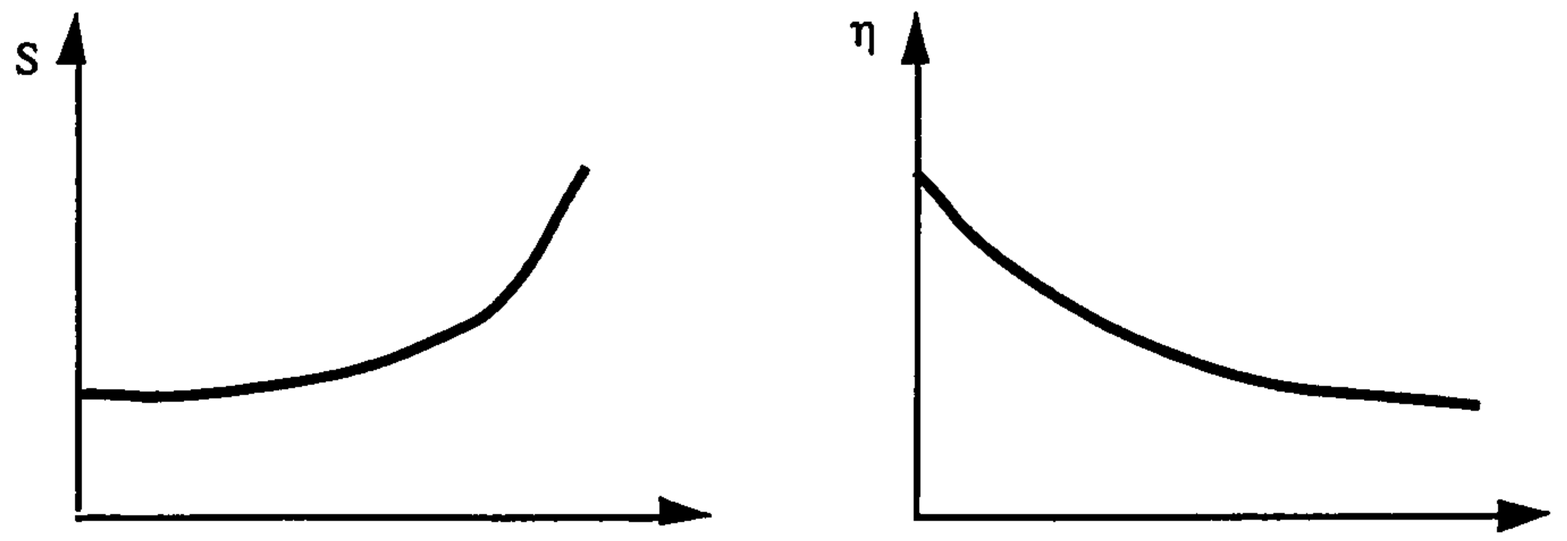

(A) (B)

Fig. 3.5 One type of non-Newtonian fluid, pseudo plastic fluid, (A) shear rate increases with shear force; (B) a decrease in viscosity (η) with an increase in shear rate (S).

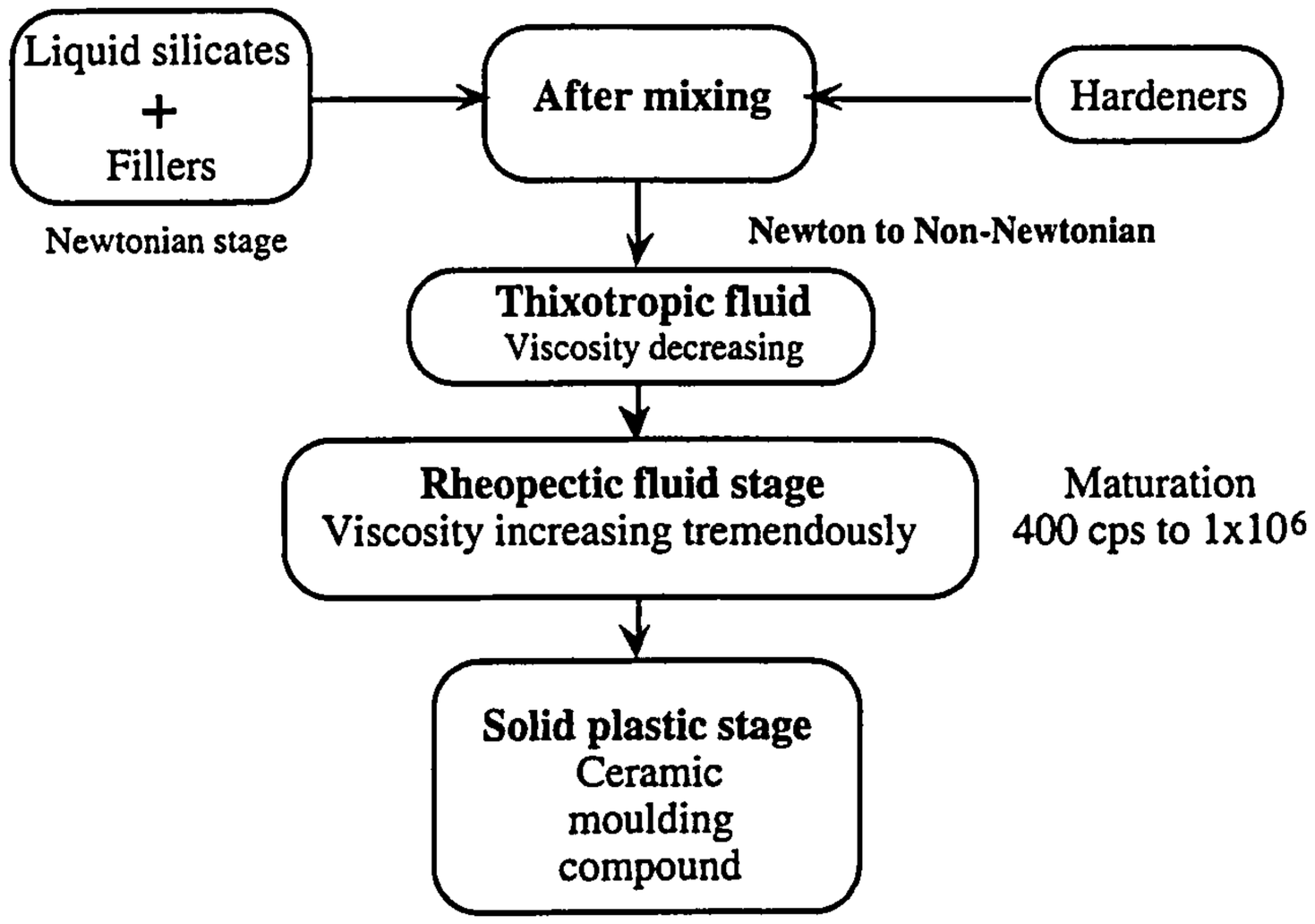

Fig. 3.6 A schematic indication of the expected rheological development in the ceramic matrix slurry during the period of moulding.

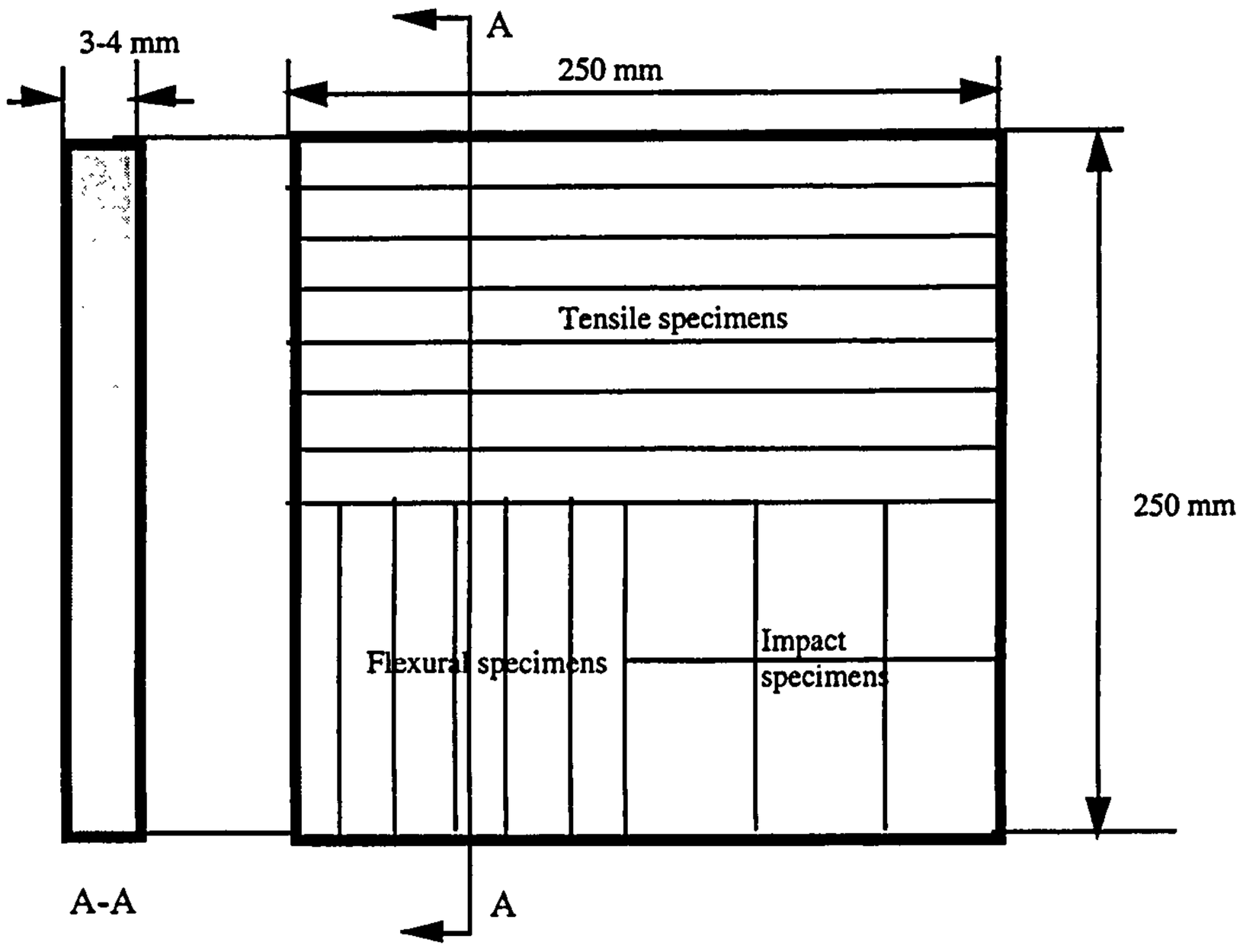

Fig. 3.7 The specimens were cut from the moulded panels for different mechanical, and physical tests and measurements.

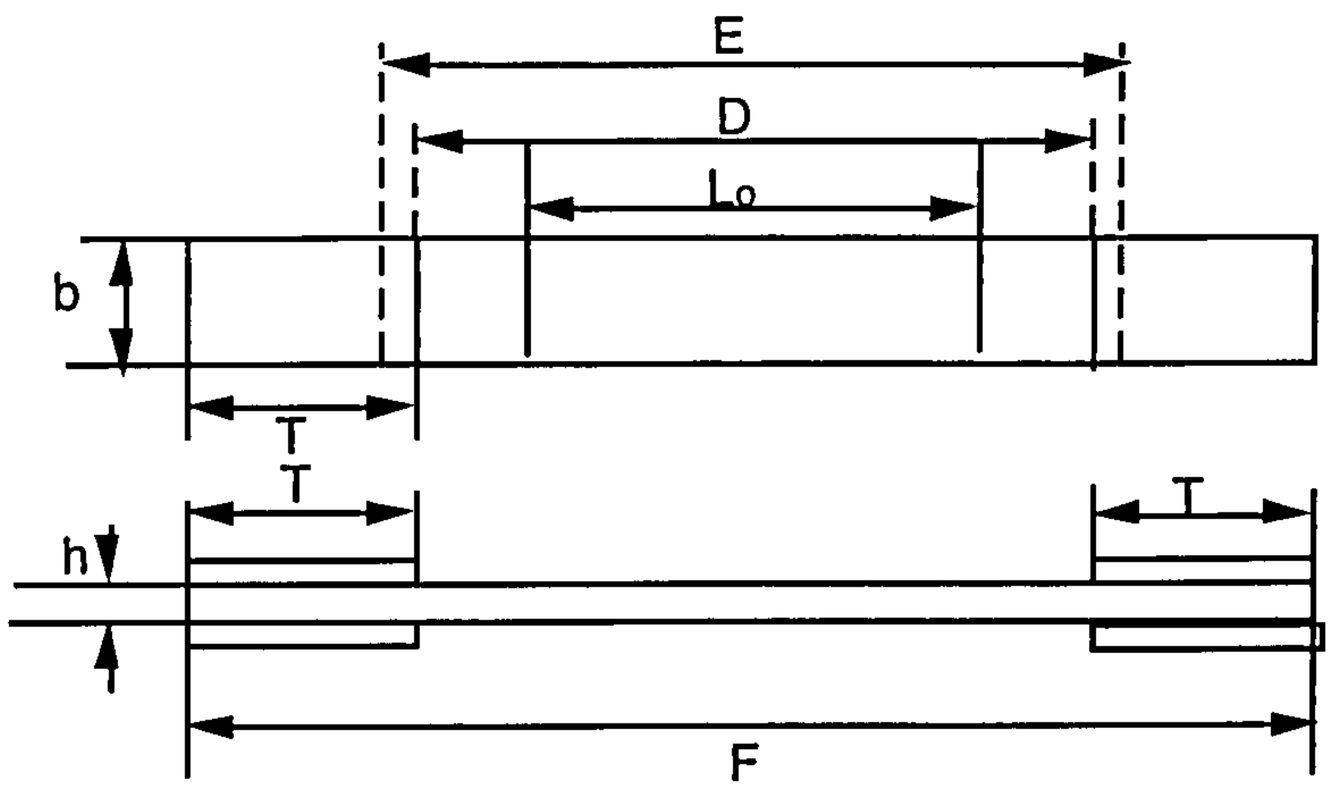

Fig. 3.8 Type III specimen for tensile test.

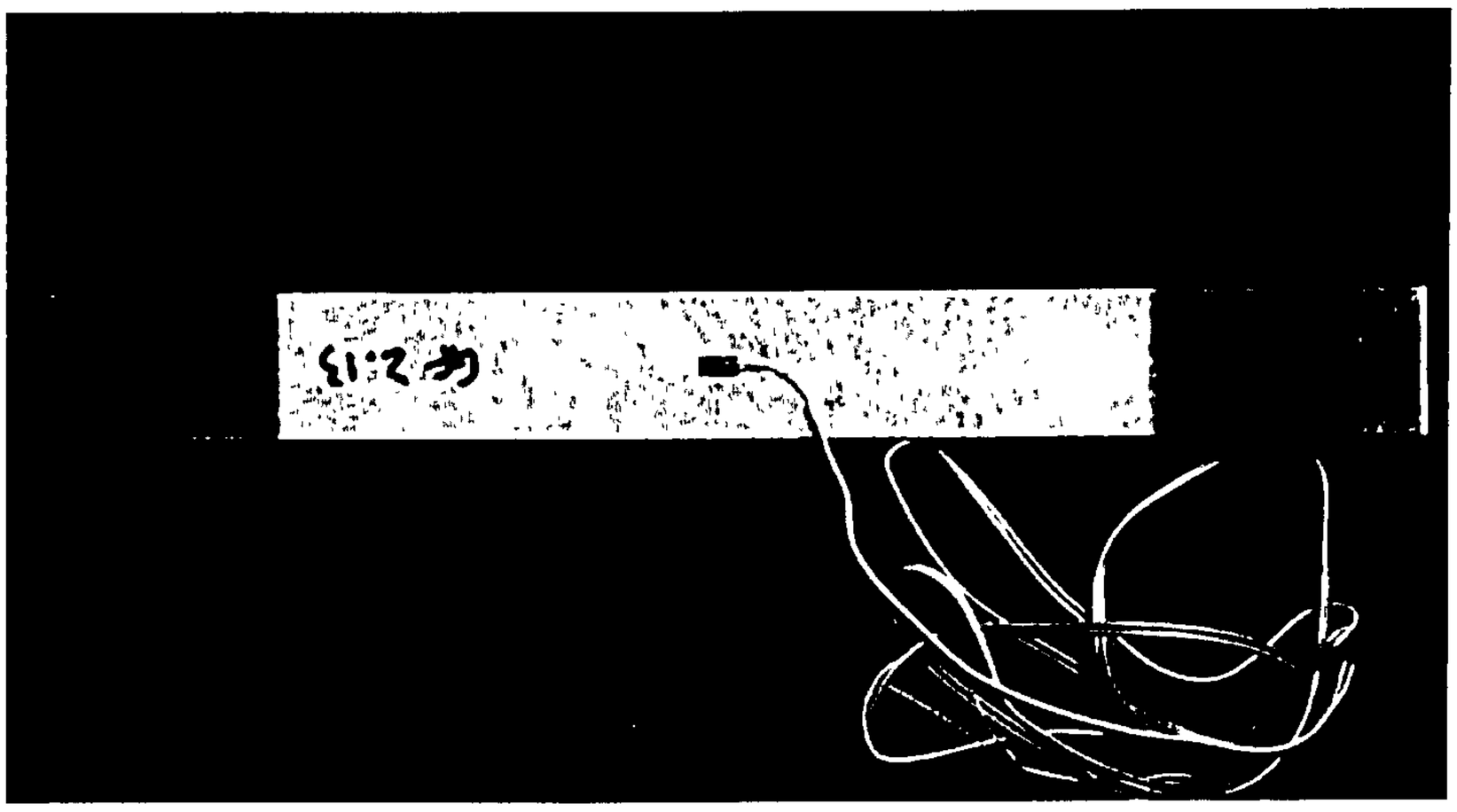

Fig. 3.9 A tensile specimen of the CDMC with end taps and mounted strain gauge.

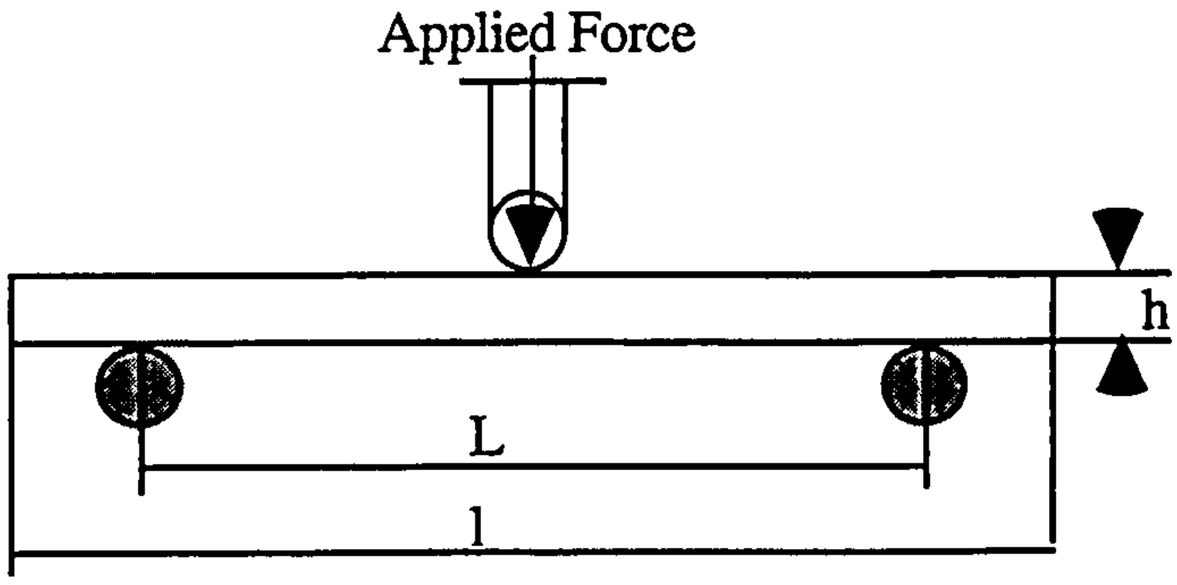

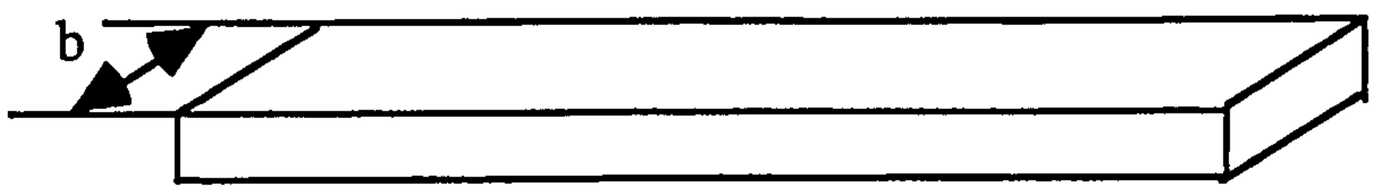

Fig. 3.10 A schematic drawing of a specimen for flexural test, three point bending.

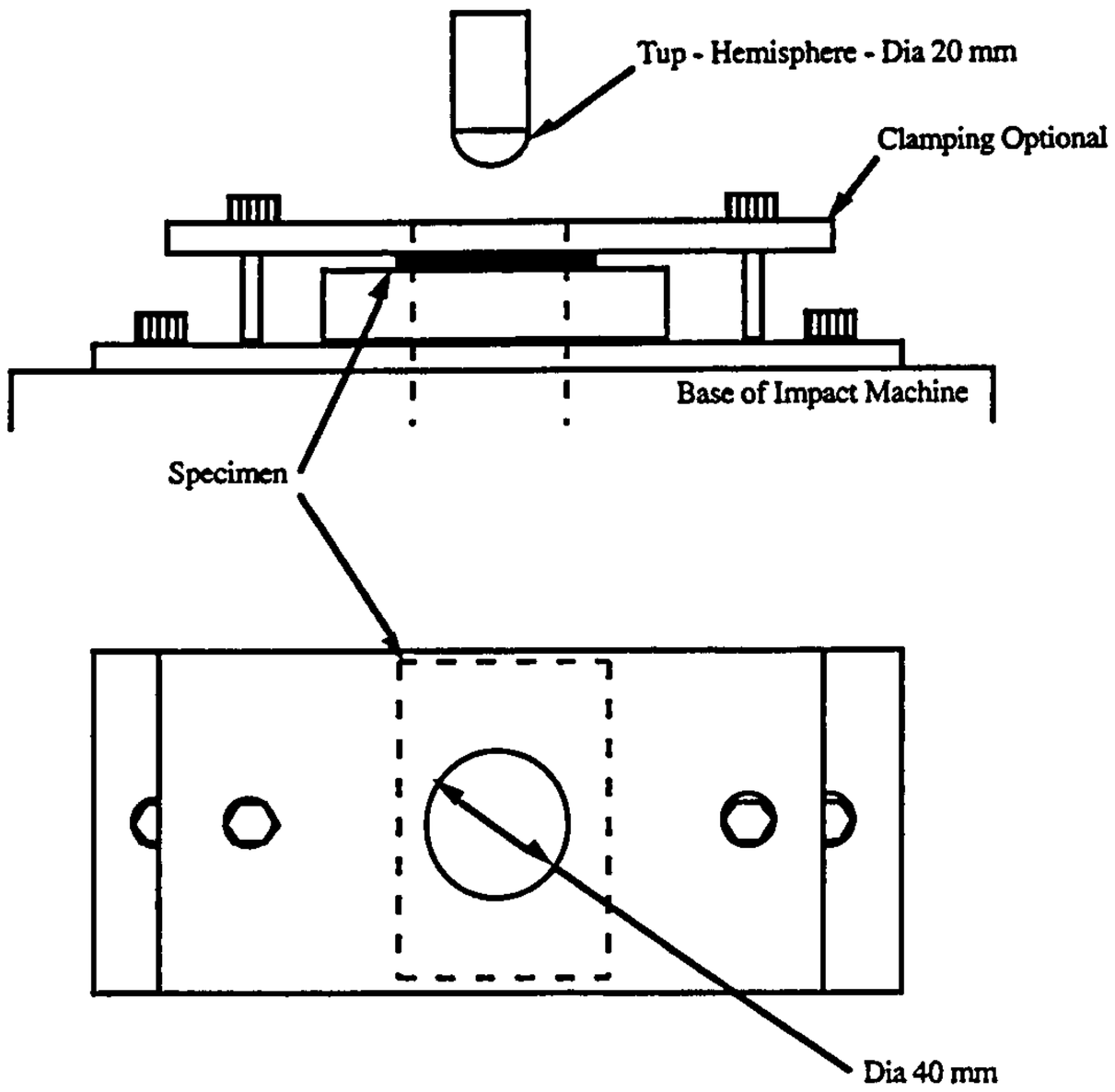

Fig. 3.11 Schematic representation of the miniature (QMW) impact support conditions.

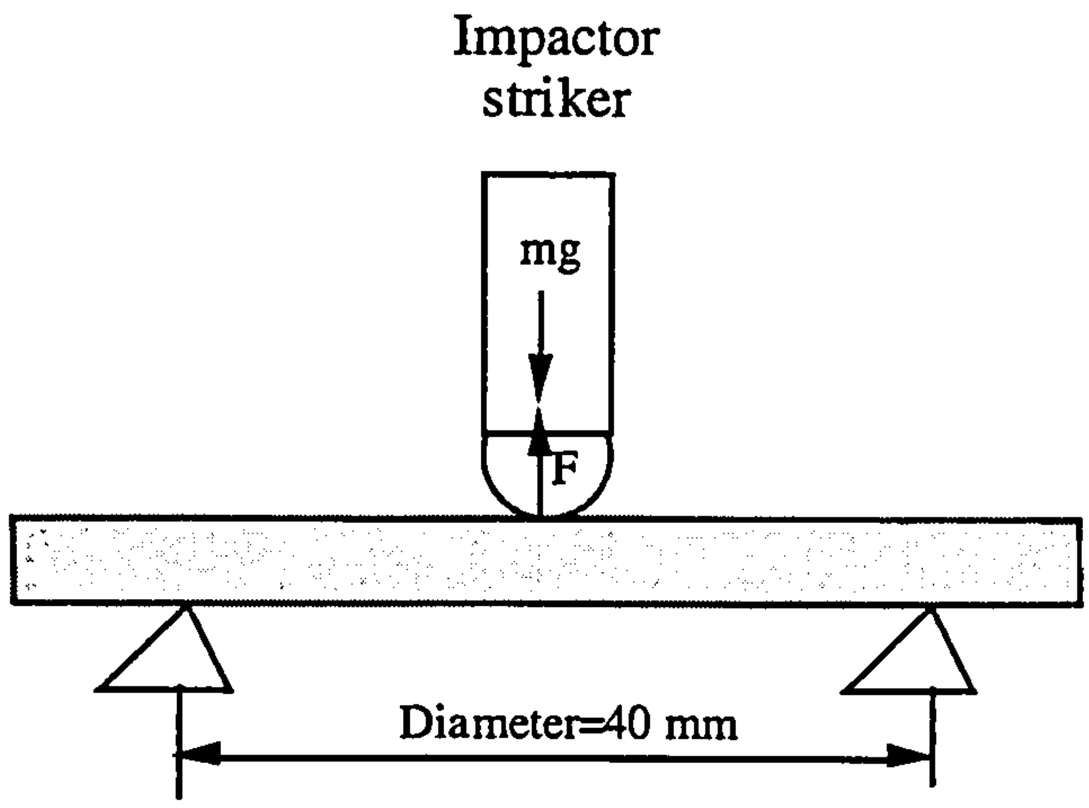

Fig. 3.12 The basic demonstration of the impacting mechanism during drop weight impacting test.

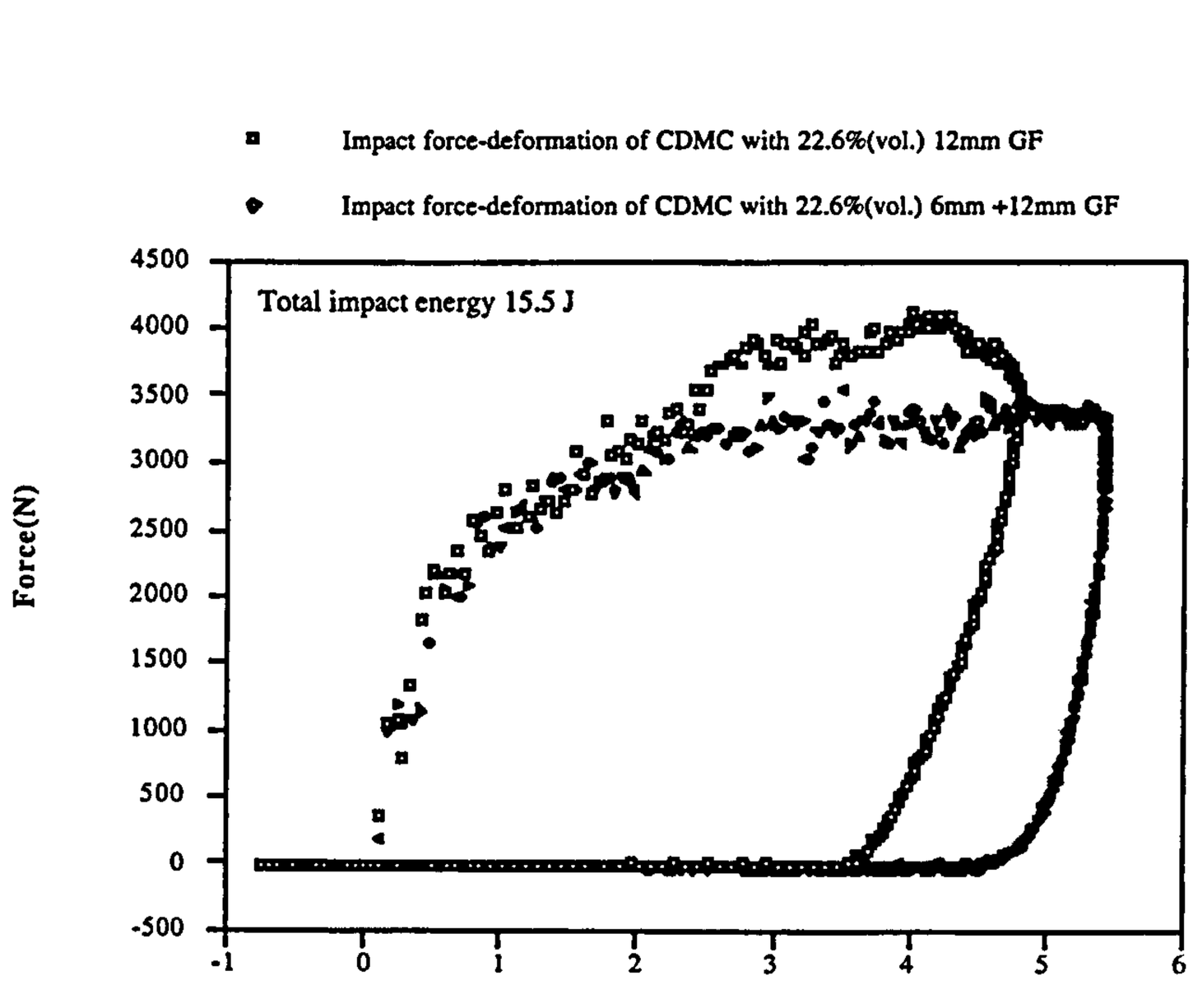

Fig. 3.13 Impact force-deformation of the CDMC with 22.6%(vol.) AR62/2-glass fibre. The fibre lengths are 12 mm and 12 mm + 6 mm respectively. The specimen dimension was 60 mm x 60 mm x 4 mm, moulded at the temperature 140 °C.

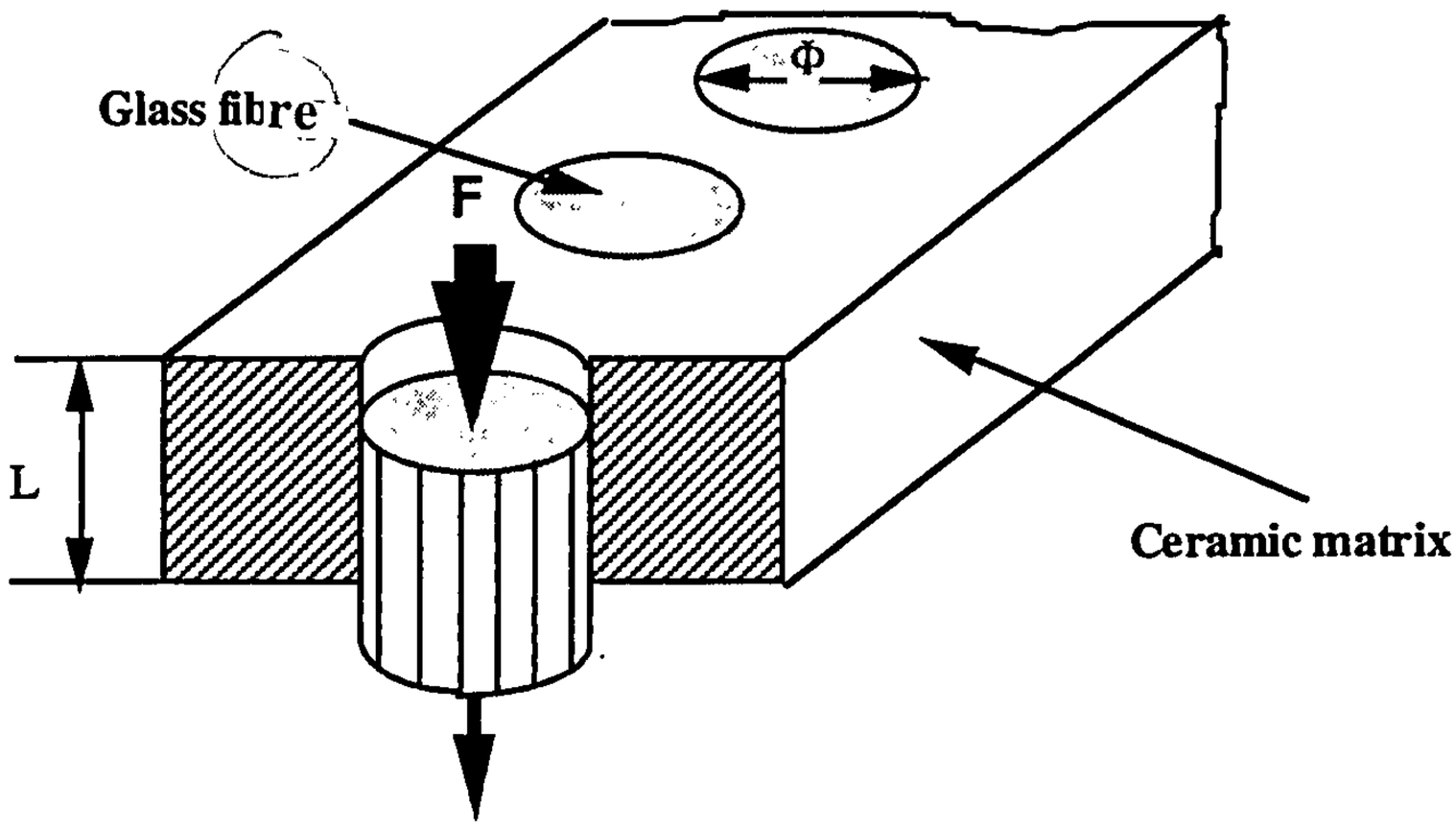

Fig. 3.14 Testing mechanism of a fibre push-out for shear strength between glass fibre and ceramic matrix.

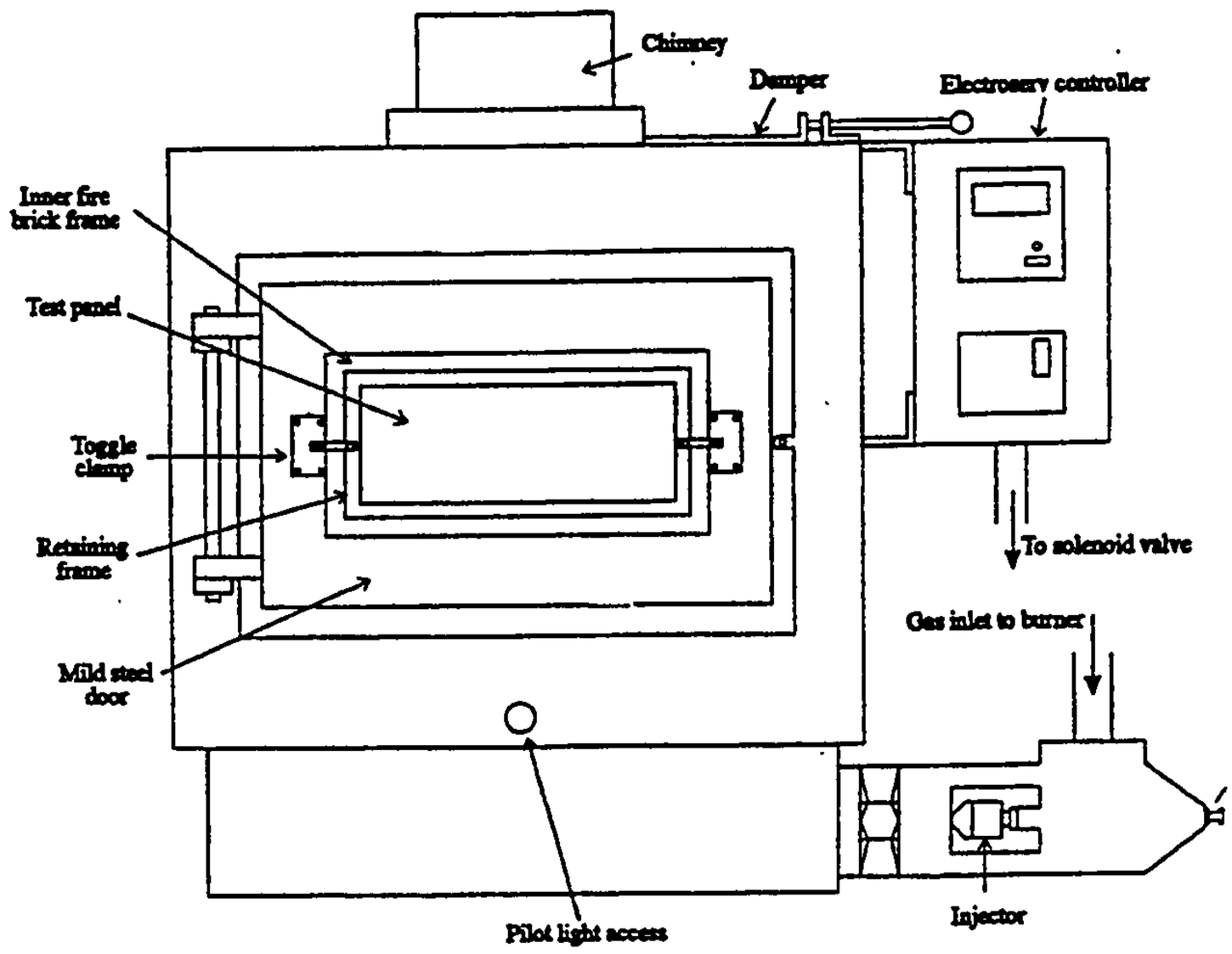

Fig 3.15 Schematic view of furnace structure used for fire penetration test, small scale IMO testing equipment.

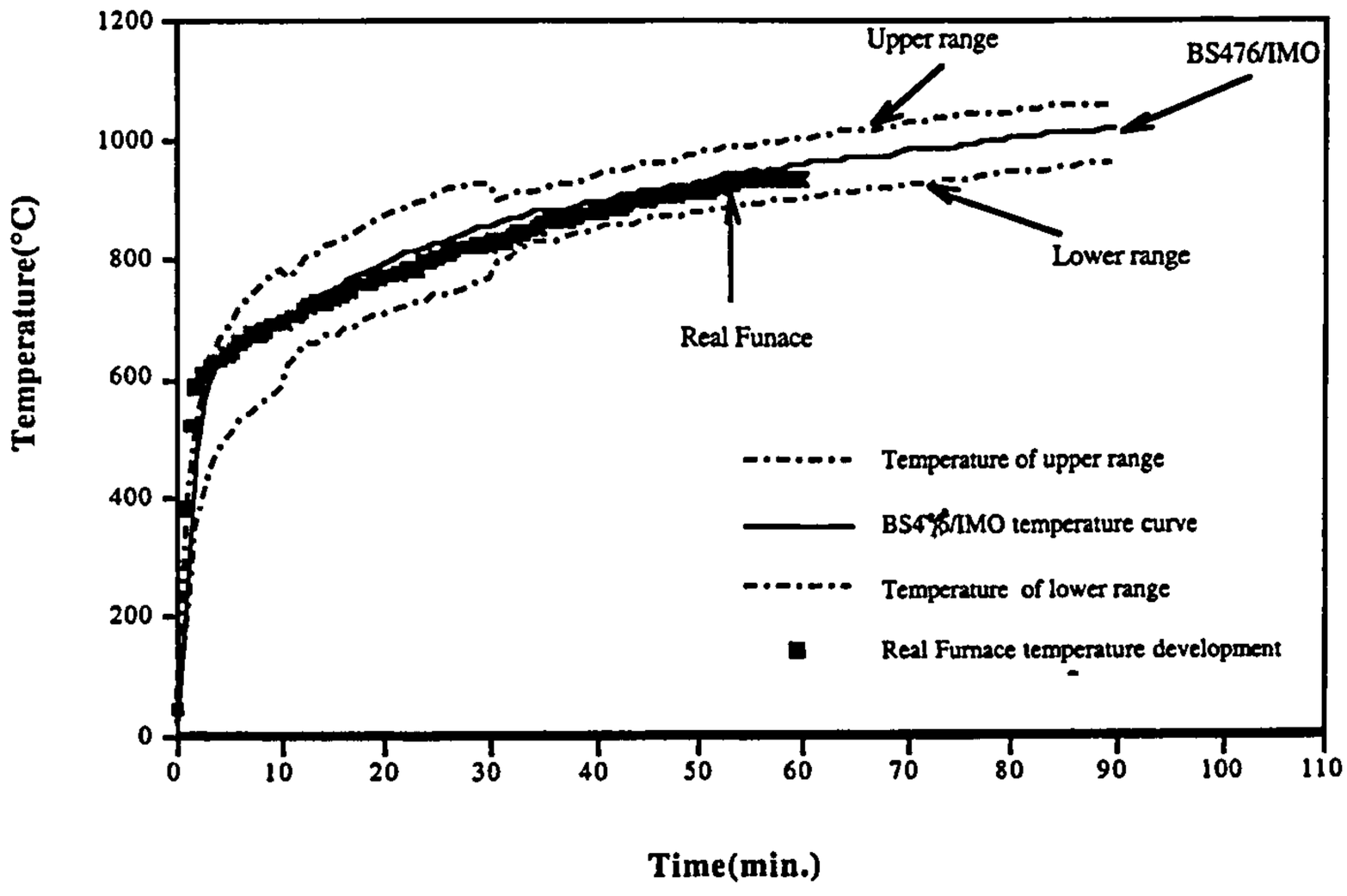

Fig. 3.16 Typical furnace temperature-time curve compared with BS476/IMO standard curve and the maximum and minimum allowable temperature.

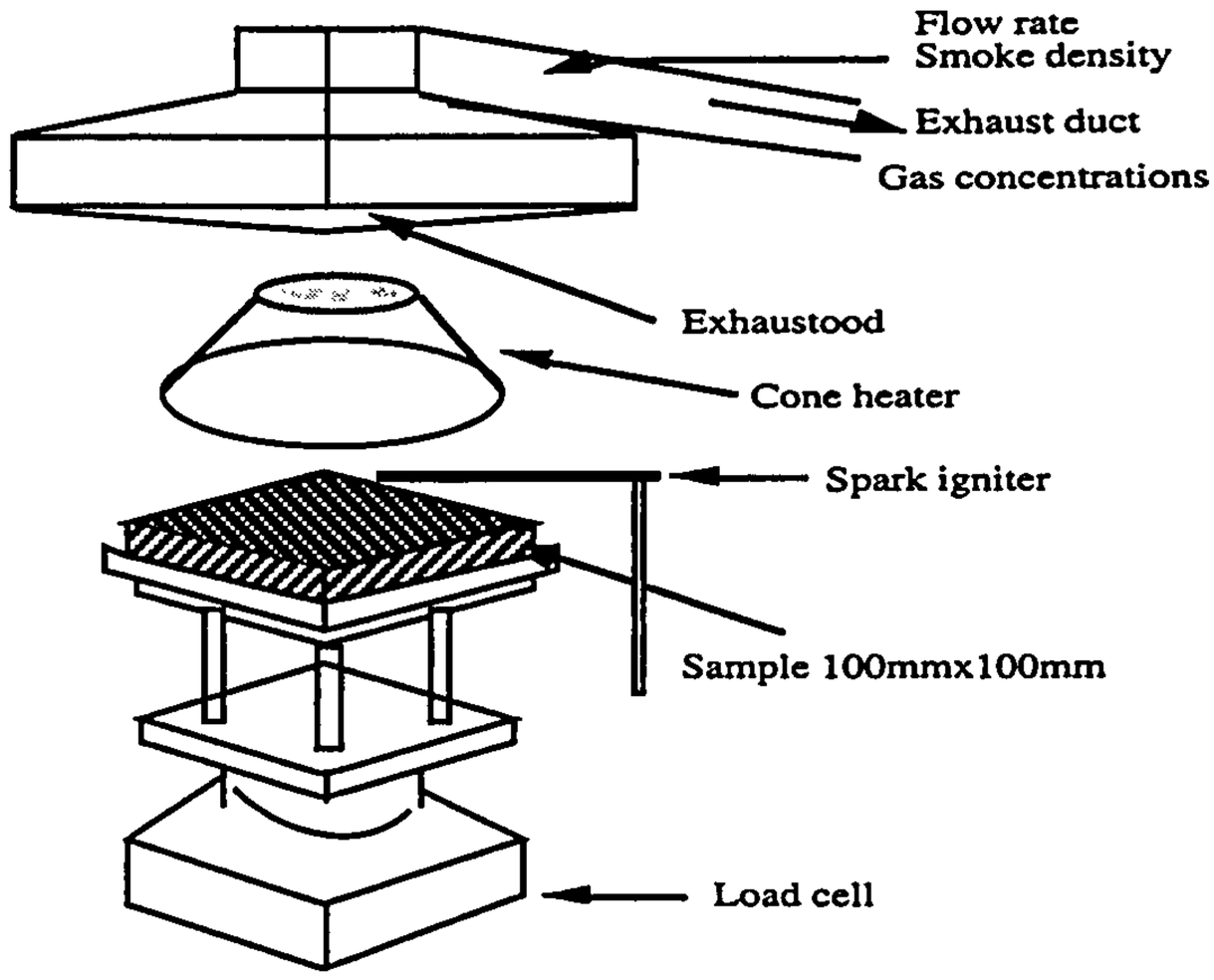

Fig. 3.17 A schematic structure view of the Cone Calorimeter heating system, materials reaction to fire.

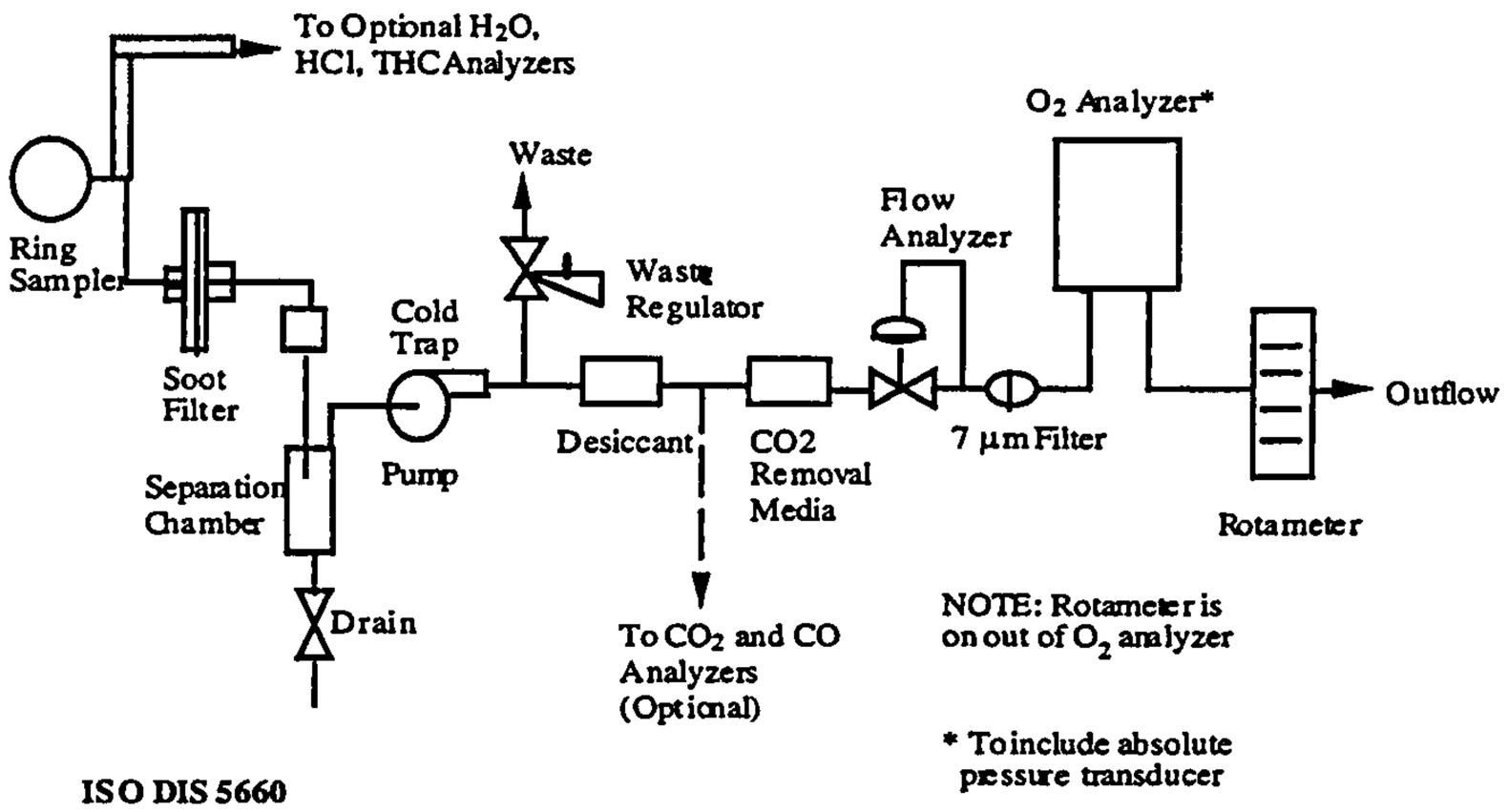

Fig. 3.18 The exhausting gas collection and analysing system in the Cone Calorimeter.

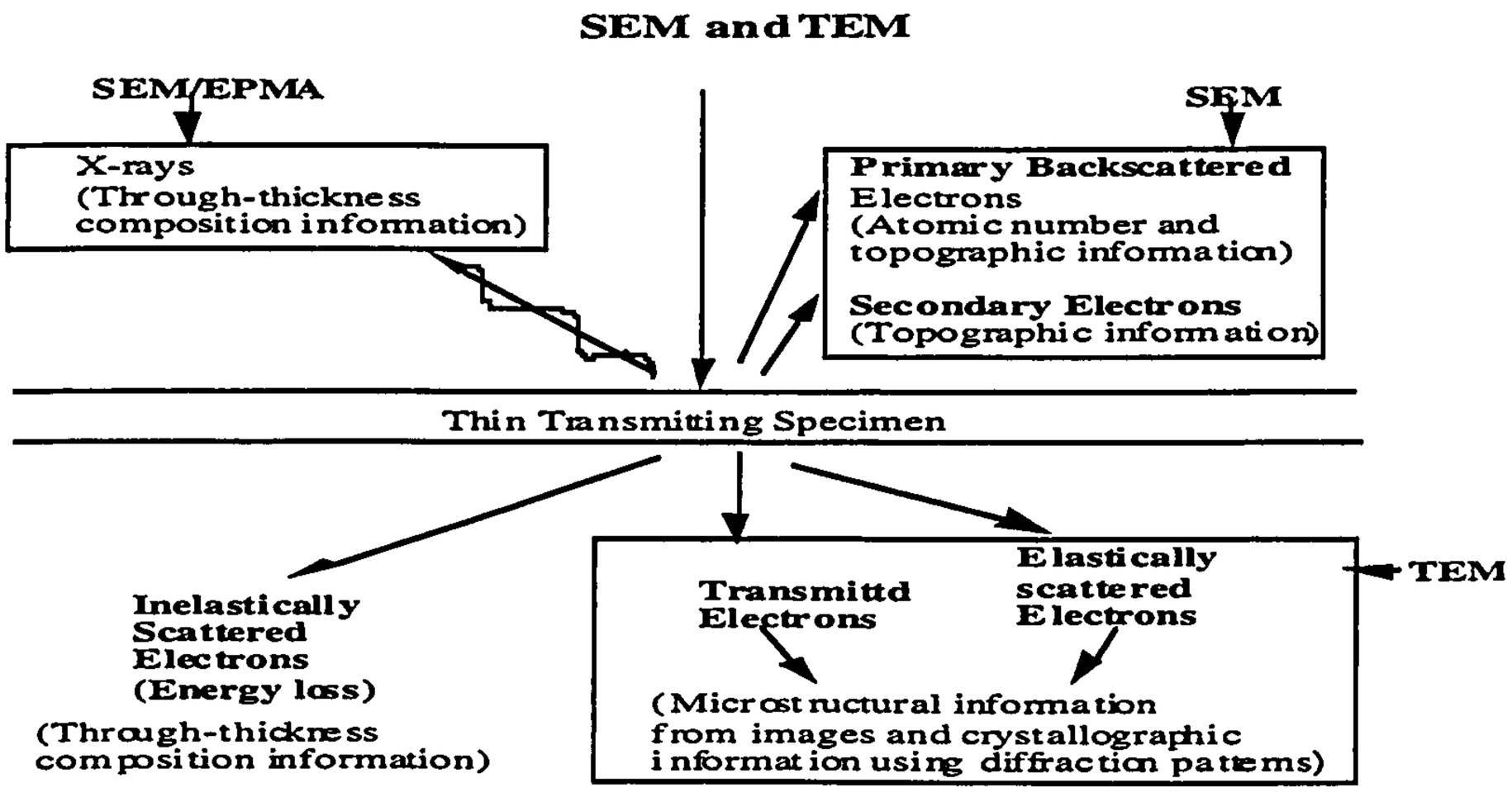

Fig. 3.19 Analysis mechanisms of SEM, TEM and related x-ray.

Fig. 3.20 A SEM photograph of a polished surface of the CDMC.

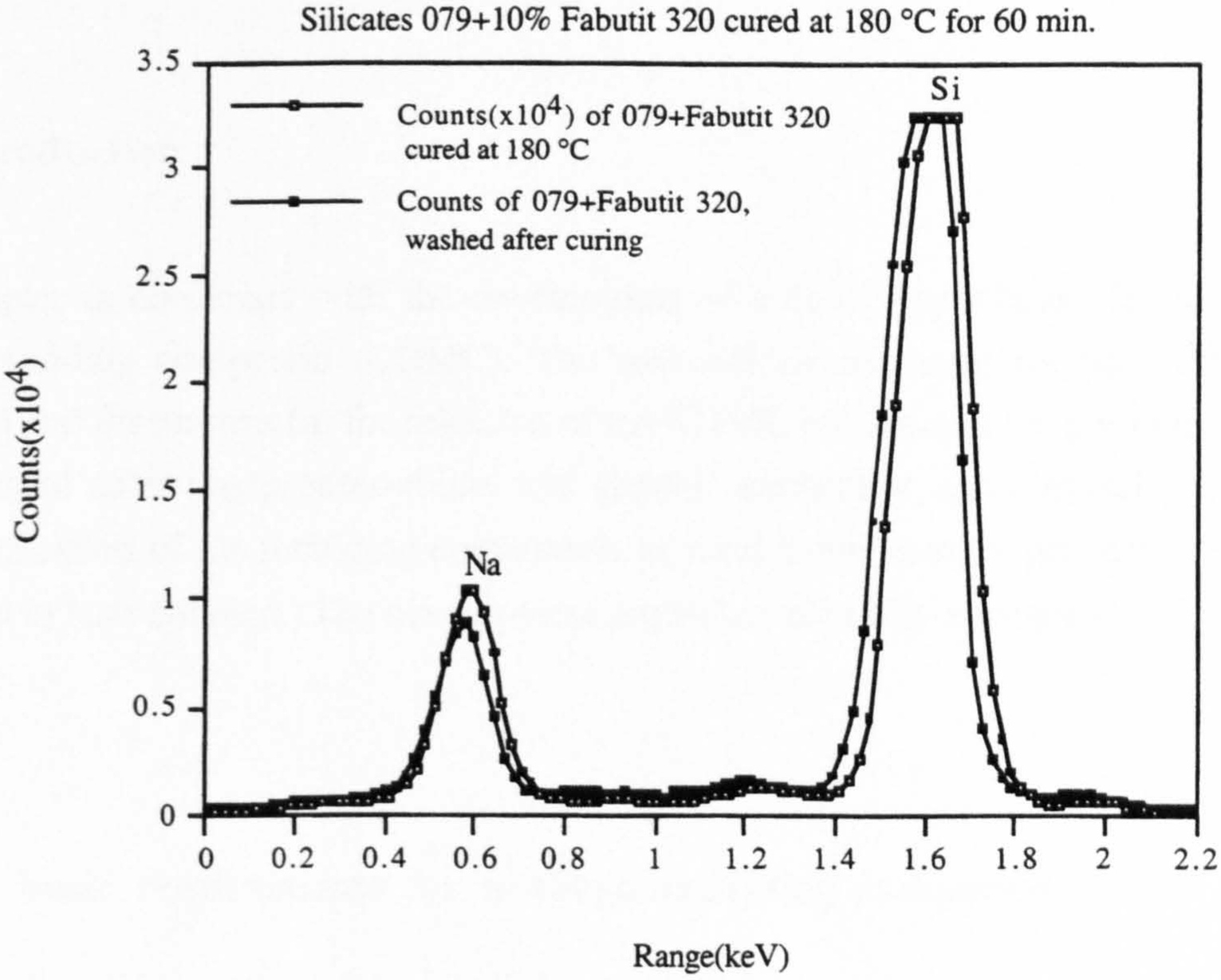

Fig. 3.21 EDS compositional analysis made by SEM. The ceramic resin matrix cured at 180 °C, unwashed particles and washed particles after curing. The ratio of Na:Si kept stable or unchanged.

Chapter 4

MATERIALS AND COMPOUNDING

4.1 Introduction

This chapter is concerned with the development of a basic formulation for a ceramic dough moulding compound (CDMC). The essential requirements for the CDMC are discussed and the reasons for the selection of the CDMC constituents are presented from a standpoint of achieving process-ability and general mechanical and physical properties. The optimisation of the moulding compounds to meet more specific property criteria is discussed in later chapters. The development procedure is briefly introduced in Fig. 4.1.

4.2 The basic requirements for a dough moulding compound

A dough moulding compound is a material that is handlable in its unprocessed state at room temperature. It has a storage capability and will flow at processing temperatures. This flow-ability allows it to be transformed in the moulding process into a required shape and then cured into a solid material form with structural properties. These requirements are common irrespective of whether the material is based on polymer or ceramic matrices.

The handlability of the material at room temperature, and its ability to be moulded and to flow at processing temperatures are best described by referring to an idealised viscosity - time plot as shown in Fig. 4.2. The indicative lines illustrate a typical viscosity history of a polymeric matrix DMC and the target behaviour curve for the ceramic matrix system under development. Specific data points from such target curves are given in Table 4.1.

The CDMC will be a matrix system which is based on liquid silicates. This matrix will be liquid initially and, via some curing process, transform into a cross-linked three dimensional structure to provide the basis for the structural performance. The strength of the CDMC will be provided by fibres, while the viscosity control will be achieved by the introduction of fillers. Fillers will also provide a route to keep costs low, to improve dimensional stability -and ultimately to introduce functionality of various kinds into the composites (e.g. to optimise fire resistance).

The options available to formulate a CDMC are enormous and, as such, a decision was taken at an early stage in this programme to rationalise the development of a range of materials based on a relatively standard base formulation. This consisted of a mixture of liquid silicates, a curing or hardening agent and a base filler. All other fillers are added to introduce additional properties.

4.3 Ceramic resins

The CDMC concept is possible because in liquid silicates, we have a material form that is soluble in water but which can be transformed into an insoluble, polymeric form. Sodium silicates in solution therefore, form the most essential ingredient in our standard matrix formulation. The major drawback of using soluble silicates in solution is that, after or during the hardening process, it is necessary to lose water from the compound. If water is retained by the composite, this will provide a route for dimensional instability and possible cracking of the material.

The silicates are available commercially with a variety of different water to solid silicate ratios. A list of solutions supplied by a manufacturer, Crosfield, is given in Table 4.2. In order to achieve the minimum water content in the final product, solution 079 has been selected as a base liquid for the CDMC. The solution as it stands could be used in conjunction with a suitable hardener to achieve a solid product. However the water content is likely to be too high and the hardened matrix will shrink, exhibit little dimensional stability and probably crack.

The next part of the formulation is therefore to tailor additional silicates in solid form. Again a range of solid silicates are available commercially that could be added to the silicate solution to increase the solid content. The concern is however that dissolving in further silicate would result in adopting the characteristics of a gel and ultimately a water glass, which makes the material unsuitable as a carrier liquid for the CDMC. This difficulty has been overcome by selecting from a list of solid silicates, a compound called P60 as identified in the list of Table 4.3. The reason for selecting P60 is that this silicate will not dissolve in the silicate solution at room temperature, but will do so at elevated processing temperatures. The net result of this is that at first the viscosity of the suspension is increased but the material is still capable of flow and can still act as a carrier for additional compounds such as fibres and structural fillers. The silicate will dissolve at processing temperatures which will result in a reduction in viscosity and an increase in the overall silicate to water ratio. The effect of adding the solid P60 on the liquid viscosity is similar to that of adding other filler types and will be shown alongside alternative fillers in the next section. However, at this point it is simply worth noting that a P60 content of 5-10%(vol.) was used throughout.

4.4 Hardeners

Once a basic liquid composition has been identified then attention has to be given to the mechanisms for hardening the liquid and converting it to a 3-D network inorganic polymer.

Commercial hardening agents are available which take many forms. Based on previous experience with liquid silicate systems and the target processing temperatures, a modified aluminium phosphate compound sold commercially as Fabutit was identified as being appropriate. A type of very fine Fabutit powder (320) has been examined by SEM and its physical status is shown in the SEM micrograph in Fig. 4.3. This compound effectively reacts with the liquid silicates to initiate or to create cross-linking 3-D chemical structures. A group of brief indicative formula for the chemical reactions that might be involved is shown in Fig. 4.4.

The basic matrix system with hardener (silicates : hardener = 100:5) was examined by the TEM and showed small particle islands of phosphate in a two phase structure in a matrix cured at 200 °C as shown in Fig. 4.5. The poly-silicate glass presents a continuous phase while the hardener powder islands are distributed in the matrix. Surrounding the Fabutit particles which are sized around 1 - 5 μm, the needle like structure of silicates appeared in the continuous glass phase. It was determined by TEM X-ray diffraction that the composition of the mixture consisted of sodium silicates, sodium hydrate and aluminium phosphate. The silicate structure appeared amorphous while the Fabutit was crystalline structure, as in its original powder form.

The Fabutit is added to the silicate solution as solid particles. This compound does not dissolve and accordingly must interact with the silicates via reactions at the particle surface. The Fabutit will increase the viscosity of the suspension both by virtue of its particulate nature and also by stimulating the polymerisation of the silicates illustrated in the group of indicative chemical reaction formulae. The viscosity versus time for the standard matrix system with different percentages of hardener - Fabutit 320 is shown in Fig. 4.6. All the viscosity curves were increasing with time. The more hardener added, the higher the viscosity increase rate.

In order to obtain additional information on changes in physical and chemical structure, a DSC analysis of the hardener-Fabutite 320 was obtained. The DSC examination can determine the material's physical changes or chemical reactions within the materials by detecting any energy loss or absorption. Normally, a DSC result can also help to explain the thermal behaviour of the tested materials. The tested temperature range is from 50 - 400 °C as shown in Fig. 4.7 and this covered the moulding temperature range from 99 to 200 °C. It showed that at the moulding temperature below 250 °C, nothing would happen to chemical structure of the Fabutit 320 if it is heated up independently. For instance, the evaporation of unbound water or moisture occurred at the temperatures below 150 °C. Then the structure may change at the temperatures around 240 to 275 °C.

It is important that addition of the Fabutit does not result in a rapid reaction at room temperature, and does not as a consequence result in an unacceptable increase in viscosity. Based on the data shown in Fig. 4.6, a Fabutit content of 5% in the matrix was chosen as fixed level for a duration of this programme.

4.5 Fillers

Fillers are very important constituents for all polymer and ceramic compounds in terms of costs, physical, chemical and mechanical properties. Based on the requirement of the compound, the fillers used are low cost minerals. The combination of liquid silicates, Crystal P60 and Fabutit hardener results in a stable system where the viscosity of the matrix can be allowed to increase in a controllable way. This actually forms the processing base for the matrix. However, the viscosity of this slurry is still too low for practical use and also the matrix would be too expensive for many applications. It is accordingly necessary to include some form of particulate fillers as part of the standard matrix formulation to raise the stable viscosity to the appropriate level and to dilute the silicate liquid content. This dilution reduces cost and improves dimensional stability for a moulded product. Ideally the matrix would cure but not shrink during moulding.

4.5.1 Effects on viscosity of the matrix

In order to develop a standard formulation it was considered desirable to select fillers that would be a constant factor in all formulations but where additional or alternative filler types could also be added to modify the formulation for specific functional needs.

Candidate filler types for adding to the compound include: Calcium Silicates (Wallonstonite = FW), Martinel Trihyde ($Al(OH)_3$ = MT), Calcium carbonate (Millicarb), Talc (Migsil) and Silica/silica glass (Spheriglas), SiC and SiN, etc. Some of these fillers have been used to formulate a range of trial compounds whose viscosity have been measured using a Brookfield viscometer, listed in Table 4.4.

The effects of adding a series of candidate fillers on the viscosity of the matrix suspensions are shown in Fig. 4.8. The effects of the fillers are reasonably constant with time as shown in the Fig. 4.9 and Fig. 4.10 which indicate respectively the effects of adding different composition of two fillers, Wollanstonite and MT for a period of time. It should also be noted that the viscosity result in Fig. 4.8 refers to a compound with added Fabutit hardener and there is no short term (2 hours) effect of filler additives reacting with the hardener to increase viscosity.

Based on these viscosity measurements it was apparent that a maximum filler content (irrespective of filler type) of about 30-50% was permissible before the viscosity of the compound became too high for easy processing.

From the range of fillers studied, the Wollanstonite (FW) was selected as a standardised base filler system. FW is essentially a calcium silicate and is not soluble in the liquid silicates but will bond well with the matrix when it cures. FW is furthermore available in a more fibrous form to select for different applications and this provides additional benefits in terms of viscosity and reinforcement for a final composite. A Wollanstonite powder has been examined by SEM and is shown in Fig. 4.11.

A minimum level of 15 - 20%(wt.) FW was added to all matrix compositions with a total filler content as high as the maximum 50%. MT was added for special requirements such as for the fire performance. Other fillers including P60, Fabutit, etc. were adjusted according to the needs for cost, mechanical and thermal properties.

In the manufacturing process, materials selection and preparation determined the viscosity of ceramic slurries. A well controlled viscosity can be a pass ticket for a further successful moulding or achieving qualified products. The viscosity has a significant influence on the mechanical properties and the production efficiency.

For liquid silicates and their slurries, viscosity development takes place in two stages as shown in Fig. 4.12. One is an Newtonian stage, the other is an Non-Newtonian stage. In this research, the main discussion is the effects on the matrix viscosity by hardeners which is in the Non-Newtonian fluids stage.

4.5.2 Mechanical properties of the CDMC: effects of different fillers

Originally, the major selection criteria for fillers was their chemical and physical compatibility with a base matrix. Based on this, the fillers evaluated were Wallonstonite, MT, Spheriglass powder, Millicarb and Talc. The reason to use these fillers was that they

were stable, commercially available, low cost and were often used in polymer and ceramic composites. Within this group, MT was believed to be one of the best fire retardant minerals, as a large amount of chemically bonded water is released when subjected to heat or fire. The Wollanstonite, Spheriglass and Talc are minerals having the basic chemical structure of mineral silicates compatible with the liquid silicates and thermally stable over 1000 °C. All fillers were examined in the CDMC composites in this section, using each single filler individually to replace all other fillers in the matrix.

The tests were carried out in two sections. Section I used general fillers, they were Millicarb, MT and TiO_2 powders which are not in the domain of silicate minerals. The section II used a crystobalite, a T85 (ceramic foamed particles), a grinding glass powder (Spheriglass), a fibrous Wollanstonite, a powdered Wollanstonite and a Talc, which all have similar mineral structures. The flexural properties for section I fillers and section II fillers were shown in Fig. 4.13 and 4.14.

It was found that the CDMC with fibrous FW has the higher flexural strength which was 57 MPa and the Talc filled CDMC achieved the highest modulus of 35 GPa. The metallic silicates such as glass powder containing Ca^{2+}, Al^{3+} silicates and Talc are more compatible with the matrix system and lead to slightly better flexural properties.

In order to establish a standard matrix system, fillers needed to be not only compatible with silicates but also assist the manufacturing process, while providing desirable mechanical properties after moulding. It was found that FW, Talc, $CaCO_3$ and TiO_2 present the best or reasonable mechanical properties, while all of them were compatible with the manufacturing procedures. As a result of this investigation, therefore, in formulation SF-II (later used as standard formulation), FW was selected as the main filler, for achieving best manufacturing feature and mechanical properties.

4.6 The base line formulation

The base line formulation for the matrix designated as SF-II was selected on the basis of the test results and the matrix formulation listed in Table 4.5. All the other matrix compositions with different functions for various applications can be derived from this matrix formulation. SF-II was formulated with liquid silicates, hardener and mineral fillers based on their effects on viscosity.

A typical viscosity curve of the standard matrix effected by Fabutit and other mineral fillers to the matrix system after one hour is shown in Fig. 4.15. Adding the Fabutit to the mixture increases the viscosity quickly as designed and expected. The final viscosity of matrix reached around 1.0 $x10^7$ cps after mixing for 2 ~ 3 days, the viscosity of the material is stable and the material is ready to be moulded.

4.7 Glass fibre

Alkali-resistant glass fibres provided by Cem-FIL with more than 16% Zirconia in their composition are durable in an alkaline environment. Some of the properties of selected glass fibres are listed in Table 4.6 and different types of chopped AR-glass fibre, roving and E-glass fibres which have been used are listed in Table 4.7.

During a preliminary study, E-glass fibre and Cem-FIL AR-glass were used to compare their chemical resistance and mechanical properties. These Cem-FIL fibres are able to resist a very high alkalinity produced by the hydration of alkaline matrices while under the same conditions, the E-glass can be severely corroded and results in a decrease in mechanical properties.

Vetrotex E-glass (Tex 2450 for polymer SMC/DMC), Cem-FIL 50/1, 62/2 rovings are typical E-glass and AR-glasses for chopped fibre composites and have been used throughout this research. The Cem-FIL roving are used in spray process for cementitious and concrete composites. Cem-FIL Chopped Strands, consist of a continuous filament, chopped to pre-selected lengths (6 mm, 12 mm, 24 mm). Some Cem-FIL chopped AR62/2 glass fibres with length 12 mm are shown in Fig. 4.16.

4.8 Glass fibre volume fraction

The volume fractions of the glass fibres in the CDMC are defined by its formulation before moulding, the weight difference before and after moulding and the density of a moulded CDMC panel. The weight difference is the water evaporated during the moulding.

For example, Matrix + 22.6%(vol.) GF system can be formulated by 436 g of glass fibre, 1342 g of ceramic compound (solids) (all together 1778 g). AR-Glass fibre density is around $D_f = 2.68$. For this particular case, the volume of glass fibre used:

$$V_{fibre} = \frac{W_f}{D_f} = \frac{436}{2.68} = 176.49 cm^3 \qquad \text{E4-1}$$

The measured density for composite: $D_{CDMC} = 2.2365$ (measured after moulding), therefore,

$$V_{CDMC} = \frac{W_{CDMC}}{D_{CDMC}} = \frac{1778}{2.2365} = 795.17 cm^3 \qquad \text{E4-2}$$

Volume fraction of glass fibre:

$$V_f = \frac{V_f}{V_{CDMC}} = \frac{176.49}{795.17} = 22.2\%(vol.) \qquad \text{E4-3}$$

Matrix volume fraction:

$$V_m = 1 - V_f = 1 - 22.2\% = 77.8\ \%(\text{vol.})$$

Weight % of glass fibre: $P_f(\%wt) = \frac{W_f}{W_{CDMC}} = \frac{473}{1778} = 26.6\%(wt)$ E4-4

From E4-4 and E4-1, the relationship between V_f and P_f can be deducted as following in E4-5:

$$V_f = \frac{V_{fibre}}{V_{CDMC}} = \frac{W_f / D_f}{W_{CDMC} / D_{CDMC}} = \frac{W_f \bullet D_{CDMC}}{W_{CDMC} \bullet D_f} = \frac{D_t}{D_f} \bullet P_f \qquad \text{E4-5}$$

For example in this formulation we can work out the volume fraction of glass fibre in order to examine the equation E4-5:

$$V_f = \frac{2.2365}{2.68} \times 26.6\%(wt) = 22.2\%(Vol.) \qquad \text{E4-6}$$

If we assume the D_f and D_{CDMC} is fixed here, the simplified equation of E4-5 can be deducted as:

$$V_f = 0.835 \times P_f \qquad \text{E4-7}$$

D_f : density of the glass fibre;

D_{CDMC}: density of the CDMC, measured;

V_f : fibre volume fraction in the CDMC;

V_{CDMC} : volume of the CDMC composite;

V_m : volume fraction of the matrix in the CDMC;

W_f : weight of the glass fibre;

W_{CDMC} : weight of the CDMC;

P_f : weight percentage of the glass fibre.

The equation E4-7 is the relationship between a glass fibre volume fraction and the weight percentage. The results of this equation and experimental density test for the CDMC made it clear that the density of 22.6 %(vol.) CDMC (8.0 MPa, 130 ℃ moulded) is less than the density of glass fibre, due to the less dense matrix system (D_{CDMC} = 2.22-2.24).

With a weight and volume fraction increase for a particular glass fibre, the volume fraction of the matrix would be decreased. It was noted that when the weight percentage of glass fibre exceeded 30%(wt.), it can be difficult to process and to mould with the composites.

4.9 The CDMC formulation

The combination of the standard matrix, SF-II with glass fibres produced a moulding compound, which was identified as a ceramic dough moulding compound (CDMC) before it is hardened after moulding. The overall manufactured formulations and combination of the matrix with selected glass fibres and fillers are revealed in Fig. 4.17.

An SEM micrograph of the matrix is shown in Fig. 4.18 and reveals a continuous silicate matrix phase and particles which were originally mineral powders (FW, Fabutit, and etc.) uniformly distributed.

CDMC with E-glass fibre and AR-glass have been studied in order to compare the mechanical properties. The mould-ability of the E-glass composite and the comparisons of E-glass and AR-glass in the composites have also been examined and will be discussed in the Chapters on the mechanical properties of the CDMC.

The glass fibre fraction in the composites is adjustable with volume fraction from 0 % to 25 or 30 %(wt) which is a point that it started to be difficult to obtain a full wet-out of the fibre and the quality of the CDMC can not be guaranteed.

4.10 Compounded CDMC

The general aim of the manufacture for CDMC moulding has been shown in Fig. 4.19. The conditions high lighted in the Figure are required for the compound to flow in the mould. The flow ability during moulding for complex parts by using this compound was demonstrated by the moulding carried out later. The CDMC of a small quantity normally can be made with a food mixer as shown in Fig. 4.20.

Varieties of formulated CDMC were manufactured with a standard compounding and moulding process which has been schematically shown in Fig. 4.21.

All the manufacturing operations were carried out at the room temperature. Before moulding, the compound needs to be matured. The matured CDMC has a viscosity which is ready for moulding as shown in Fig. 4.22. It can be different shapes as required for moulding processes for different shapes of products.

If the viscosity is too high for some applications, the compound should be heat treated to achieve good moulding viscosity. Two methods could be used for pre-treatment:

- Preheating the ceramic moulding compound

The material can be softened prior to mould by a micro wave or other methods which will shorten the moulding time. The advantage of a preheated DMC is that this improves the matrix flow to details in the mould, causing less pores and vacancies, and allowing the use of a low moulding pressure. This also reduces the risks of the fibre shearing damage while a matrix is still rigid. The disadvantage is that the degree of heating of the CDMC (if

by microwave) was difficult to control and an uniform temperature profile is difficult to achieve quickly.

- Slow moulding

The CDMC compound can also be moulded directly without any preheating by spending a longer time to fully close the mould. But it might produce a less smooth surface, and a increased risk of damaging the mould and fibre, because a high moulding pressure has to be adopted.

4.11 Summary

The feasibility for processing the formulated matrices and raw materials for the CDMC were investigated in this chapter. The rheology and features of the compound made the compounding and moulding possible and approved applicable. Proper composition of matrix system and reinforced glass fibre have been formulated together based on the viscosity effected by hardeners and mineral fillers. Matrix system SF-II has been selected as a general matrix for further combination with the glass fibre into the composites.

The viscosity of the compound slurry played an important role in processing the CDMC. And an increased viscosity of mixture is ideal for a stage of the compound moulding. The matrix initial viscosity was, as expected, low enough to wet out the chopped glass fibre. Then the viscosity of premixed paste added with chopped fibre glass can increase significantly (>$1x10^6$ cps).

Table 4.1 The viscosity requirement for the CDMC compounding.

Time (days)	Directly after compounding	One day after compounding	One week after compounding
Viscosity, cps	5000 ~ 10000	6×10^5	$>= 1 \times 10^6$

The final viscosity of the compound expected to be > or = 1×10^6 cps.

Table 4.2 The chemical and physical features of the liquid silicates.

Grade	SiO_2:Na_2O (Wt)	Total solid %	Viscosity at 20 °C cps	Na_2O %	SiO_2%
079	3.30	38.1	500	8.85	29.25
074	3.37	36.2	150	8.25	27.90
070	3.30	34.4	70	8.00	26.40

Table 4.3 The formulation of the powder silicates (Specification of Crosfield, 1994).

Grade	Mean Wt Ratio SiO_2:Na_2O	Mean Mol Ratio SiO_2:Na_2O	Mean Na_2O %	Mean SiO_2 %	Mean Total Solids %	Bulk Density g/Litre
Crystal C Powder	2.00	2.06	27.00	53.00	80.0	400-500
Crystal M Powder (P60)	3.30	3.41	18.50	61.50	80.0	550-650
Crystal AL Powder	2.00	2.06	28	56.00	84.0	80-120

Table 4.4 The viscosity test compositions of the ceramic slurries in the compounding control process, tested at 20 °C.

Slurry composition	Hardener used	Percentage %(wt.)		Testing condition
		Hardener	Filler	
Silicate 079+FW*	Fabutit 320	5	5-60	R.T.***
Silicate 079+MT	Fabutit 320	5	5-60	R.T.
Silicate 079+Silica	Fabutit 320	5	5-65	R.T.
Silicate 079+Talc	Fabutit 320	5	5-65	R.T.
Silicate 079+Millicarb	Fabutit 320	5	5-65	R.T.
silicate 079+P-60	Fabutit 320	5	5-65	R.T.
Silicate 079+FW			5, 10, 20	R.T.
silicate 079+MT**			5, 10, 20	R.T.
Silicate 079+Fabutit 320	5, 10, 12.5, 15, 17.5, 20%			R.T.

* FW - Wallonstonite FW 325.
** MT - Martinal Trihyde.
***R.T. Room temperature.

Table 4.5 The formulation of SF-II + AR/E-glass fibre for the CDMC for general applications.

Formulation II	%(wt) of different raw materials
Crystal 079	35.0 %
Wallonstonite (FW)	15.0-20.0 %
P-60	4 %
Hardener	2-5 %
Glass fibre (E-glass or AR-glass)	0 - 35

Table 4.6 Some properties of A-glass, E-glass, AR and NEG glass fibres.

Properties	A-Glass	E-Glass	Cem-FIL AR-Glass	NEG AR-Glass
Specific gravity	2.46	2.54	2.70	2.74
Tensile strength (MPa)	3130	3448	2482	2448
Modulus of elasticity(GPa)	65	72	80	79
Strain at break (%)	4.7	4.8	3.6	2.5

Table 4.7 Different types of chopped AR-glass fibre, roving and E-glass fibre used for the CDMC in this research (Vetrotex and Cem-FIL technical specification, 1994 and 1996).

Products	*Cem-FIL 50/1	Cem-FIL 62/2		*Vetrotex roving E-glass
Length of the fibres	12 mm	6 mm	12 mm	12 mm
Colour	Pink	Green	Green	White
Filament diameter	14 μ	14 μ	14 μ	12 μ
Filaments per Strand		102	102	64
Strand Tex (g/km)	76	38	38	
Loss on Ignition %	1.5	1.7	1.7	1.7
Roving Tex	2450			2400

*Cem-FIL 50/1 roving was chopped by a SMC machine to 12 mm length when used in the CDMC.

*Vetrotex SMC roving was chopped to 12 mm length by a SMC machine when used in the CDMC.

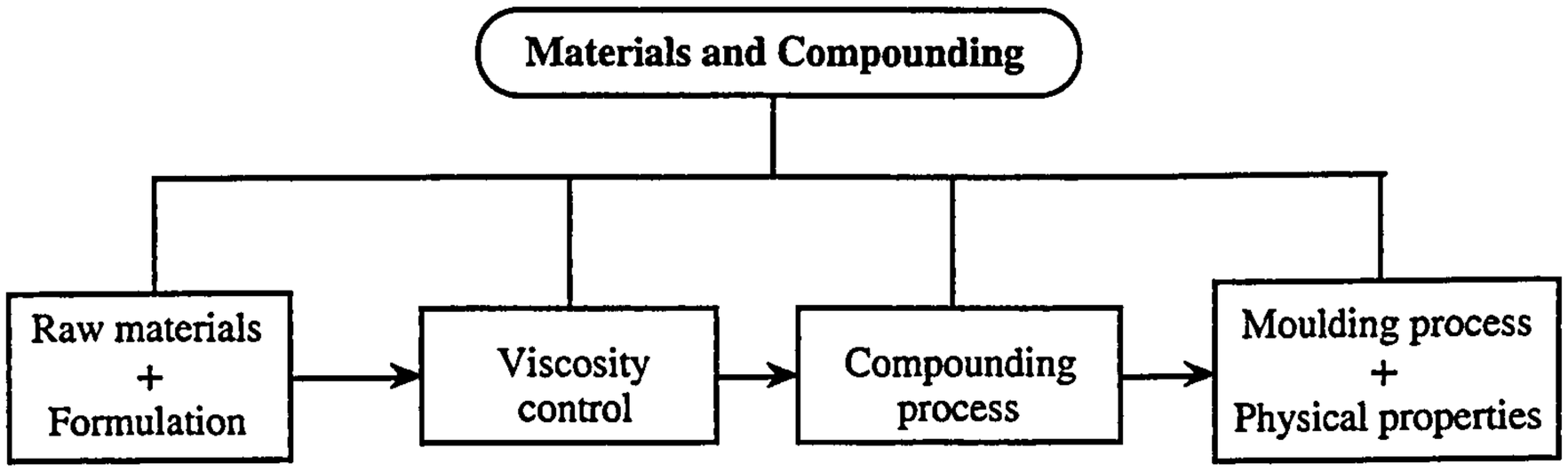

Fig. 4.1 Development review at the stage of materials and compounding.

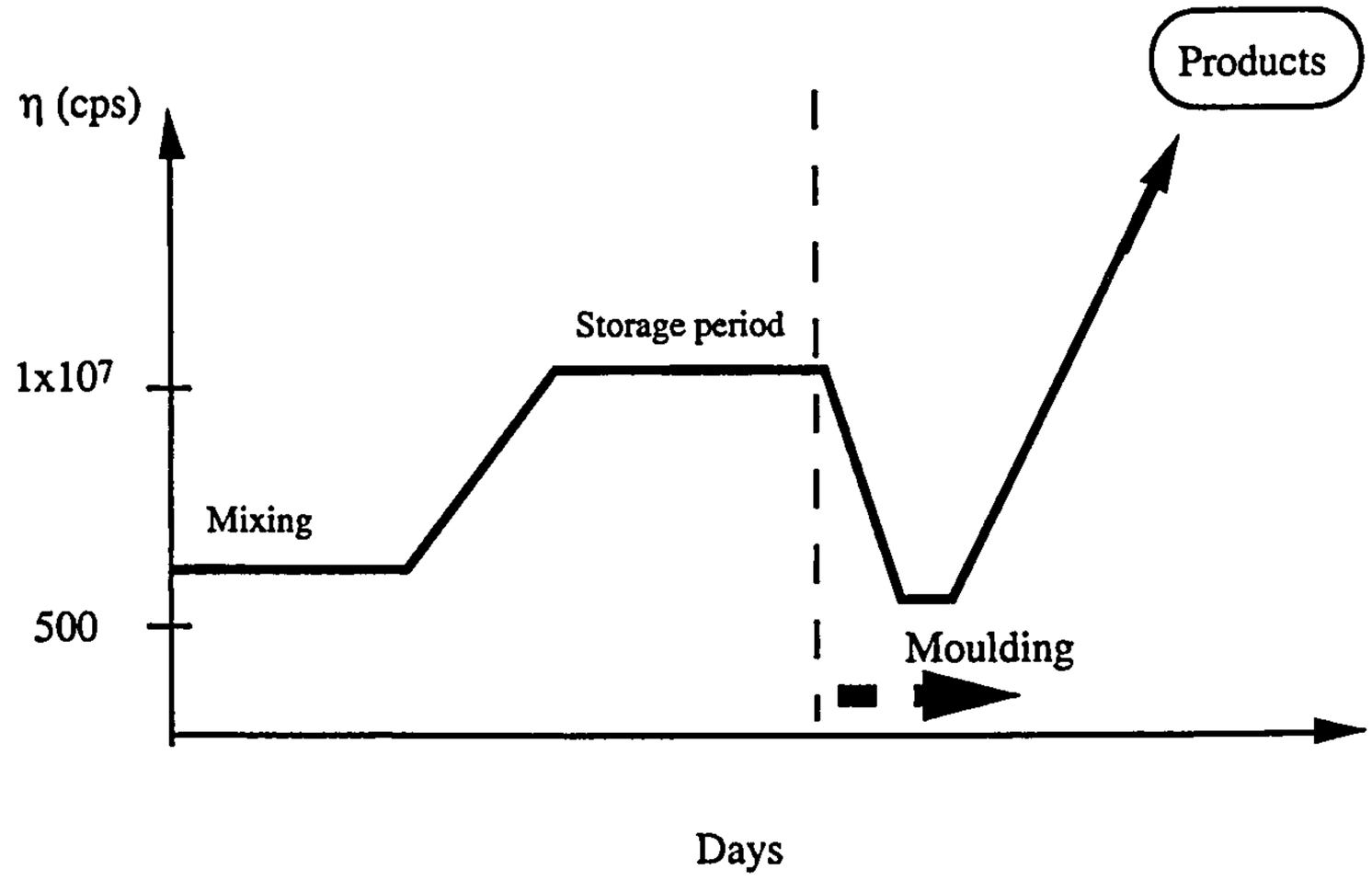

Fig. 4.2 The ideal viscosity development of polymer and ceramic matrices for the DMC/SMC with similar conditions of compounding, thickening control and moulding.

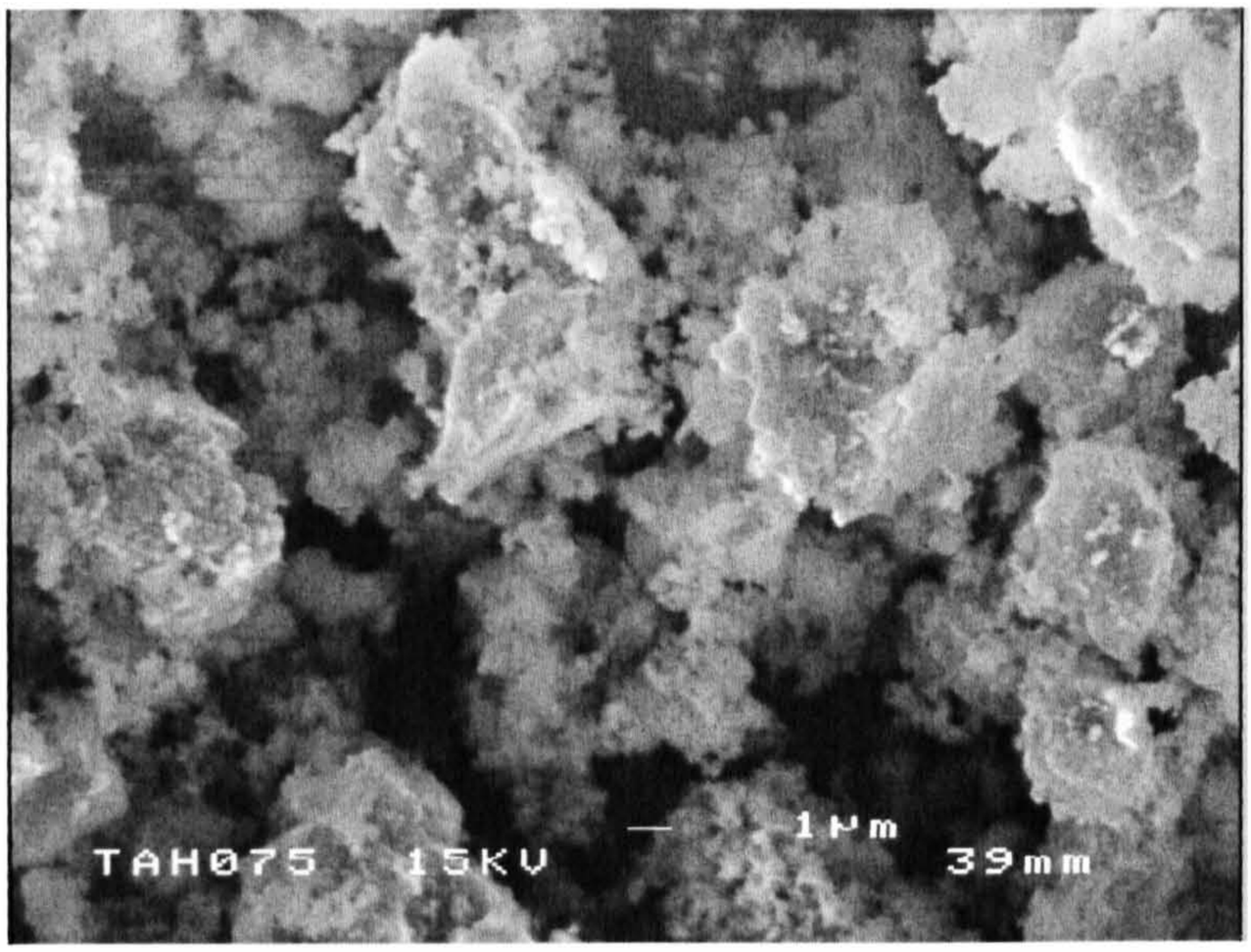

Fig 4.3 A SEM diagram shows the very fine Fabutit powder.

$$H_2O + M_2O{\cdot}xSiO_2 + H_3PO_4 \longrightarrow xH_2SiO_3{\cdot}H_2O + M_2HPO_4$$

$$M_2O{\cdot}xSiO_2 + Al_2O_3 + H_2O \longrightarrow xH_2SiO_3{\cdot}Al(OH)_3\ HO + M_2HAlO_3$$

$$M_2O{\cdot}xSiO_2 + H_2O + CO_2 \longrightarrow xH_2SiO_3{\cdot}H_2O + M_2CO_3$$

$$H_2SiO_3 + n(H_2SiO_3)$$

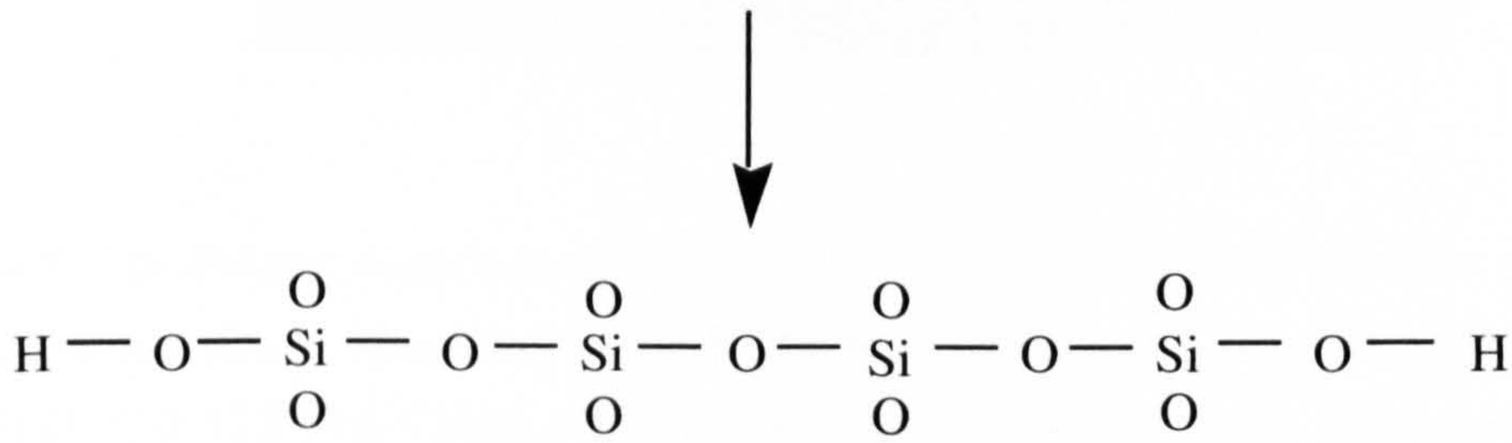

Fig. 4.4 The possible chemical reactions involved in cure of silicates with phosphates (M = Li, Na, K).

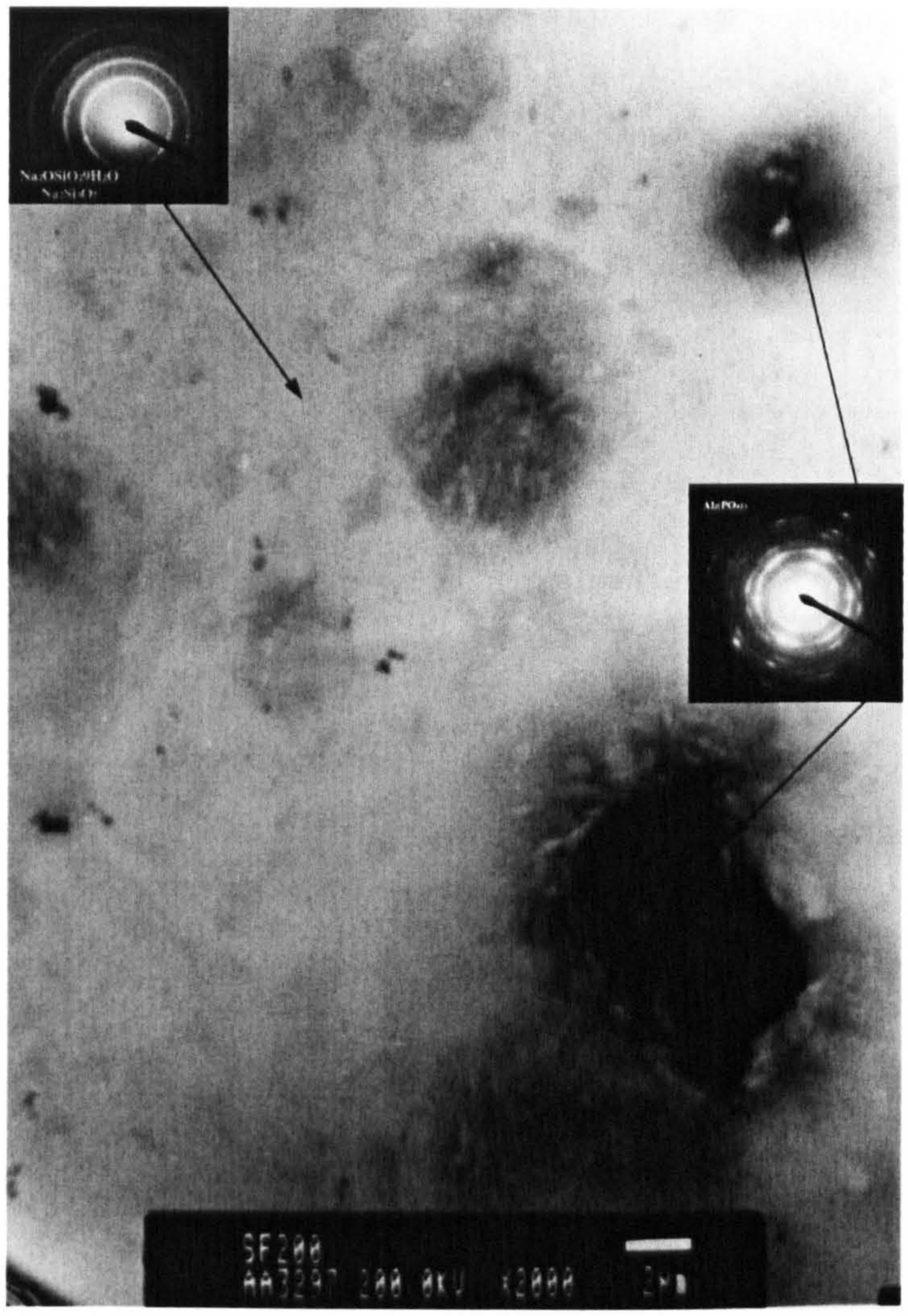

Fig. 4.5 The Fabutit islands in the matrix of silicates/Fabutit. The silicates appeared to be a continuous phase identified by TEM to be a mixture of $Na_2OSiO_29H_2O$ (19-1239), $Na_2Si_3O_7$ (19-1237/18-1240), while the Fabutit island phase was identified with TEM to be a $Al_2(PO_4)_3$ (20-44A) surrounded with the sodium silicate structure.

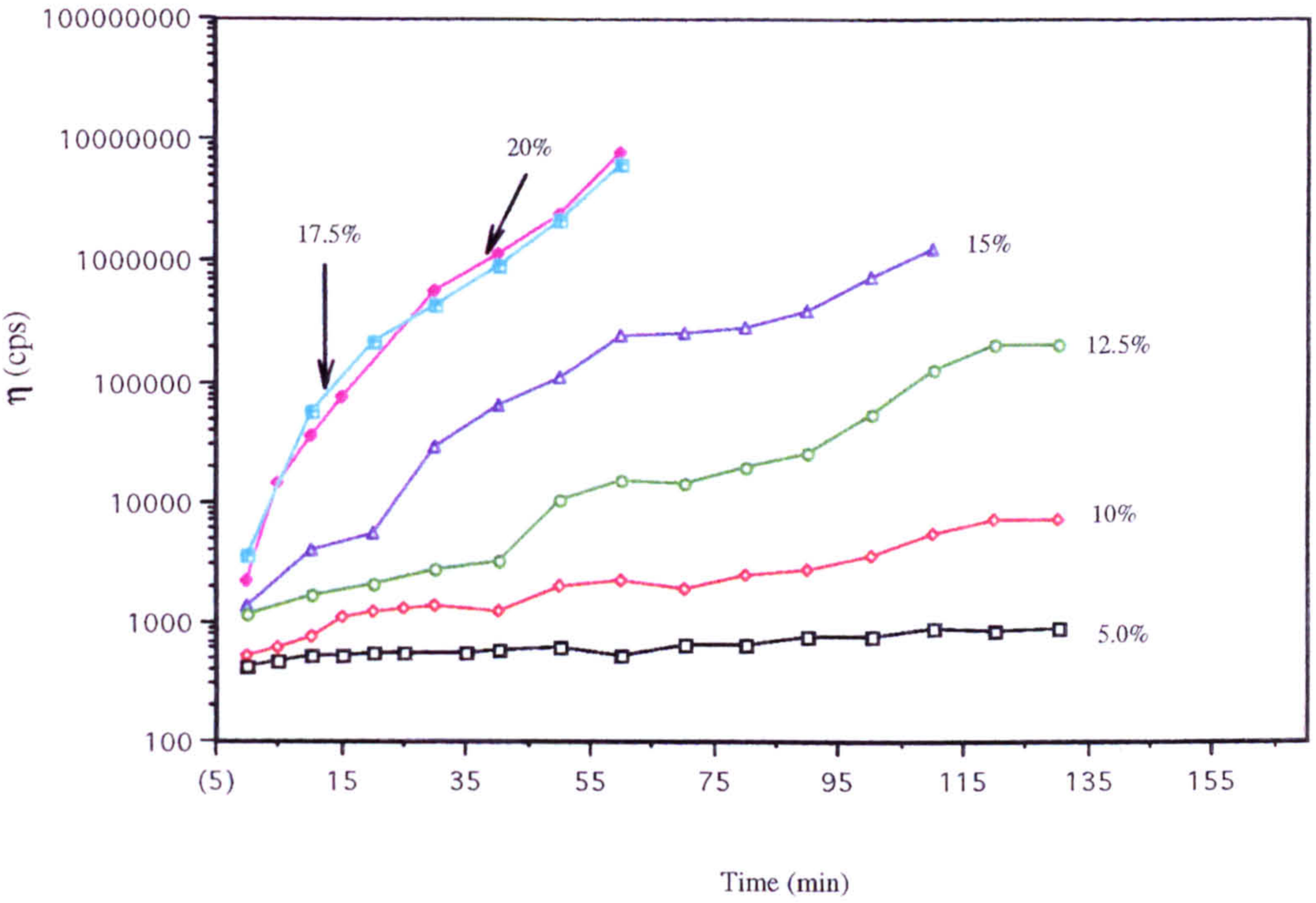

Fig. 4.6 The viscosity-time of the matrix system with 5 - 20%(wt.) Fabutit. Measured at room temperature.

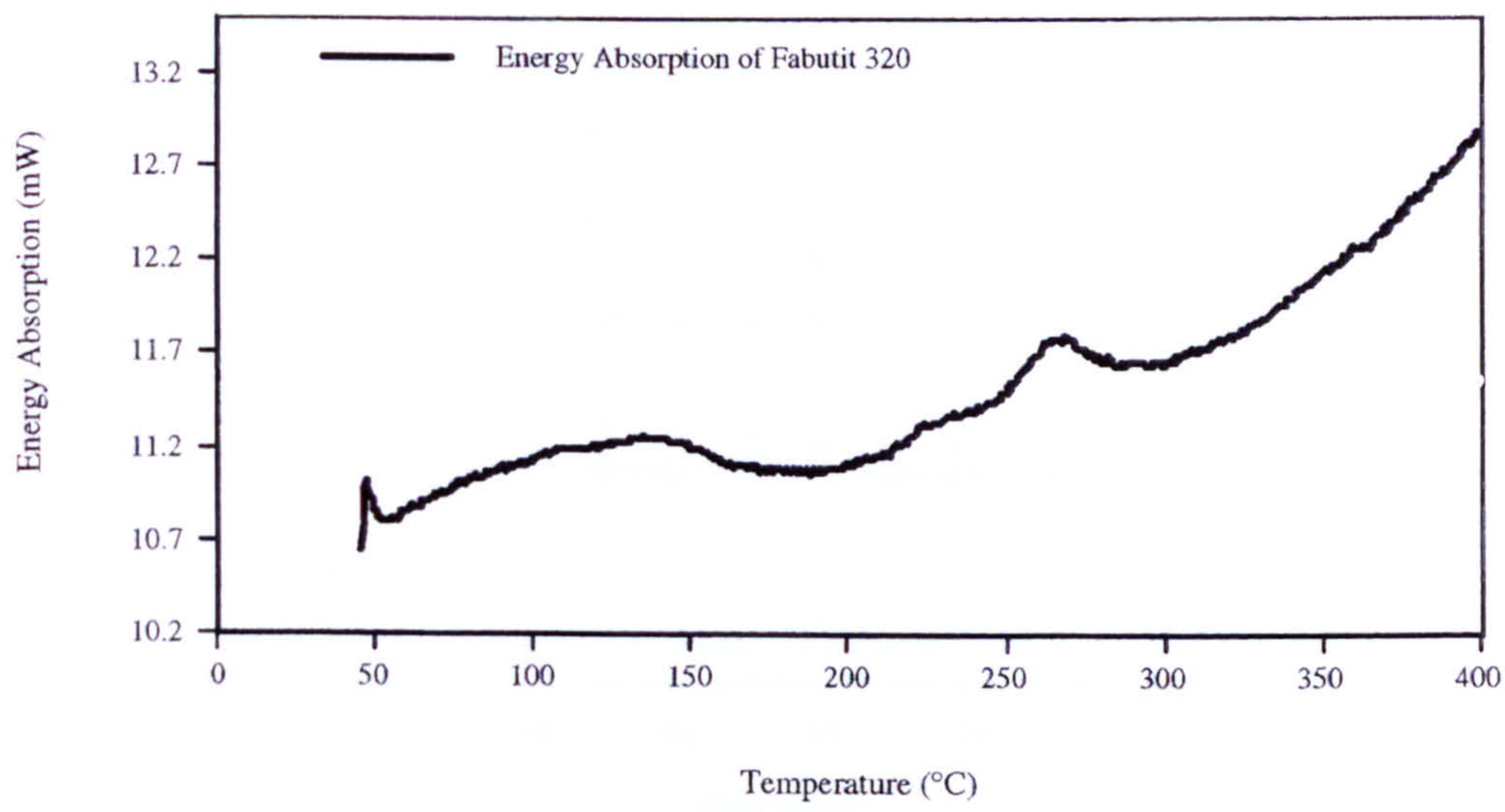

Fig. 4.7 The DSC graph of a hardener (Fabutit 320) used in matrix systems. The hardener was examined from temperature 50 °C to about 400 °C.

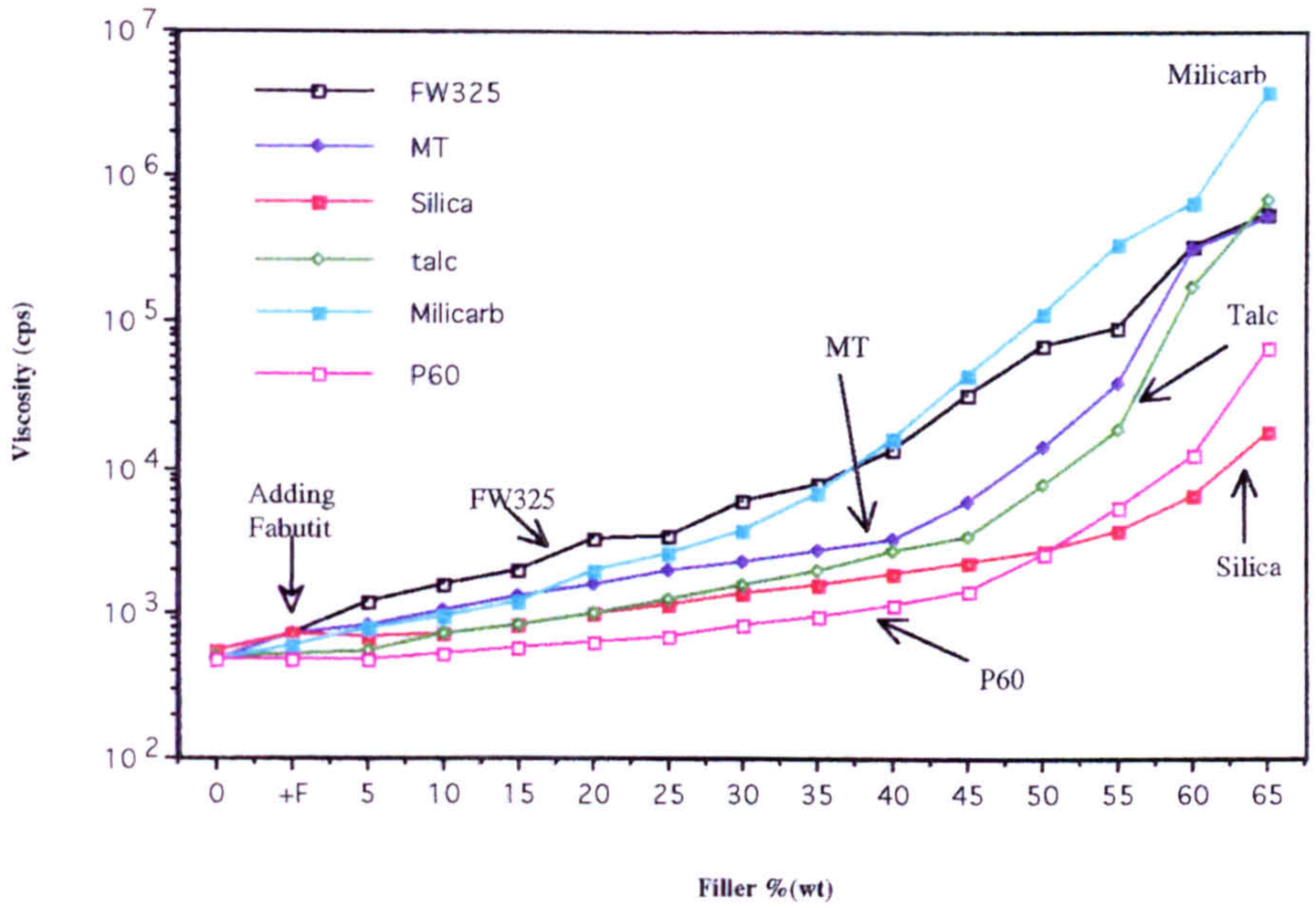

Fig. 4.8 The viscosity of the matrix with hardener, FW, MT, Millicarb, P-60, silica and talc vs. the percentage of fillers measured at room temperature (20 °C). At the X-axis "+F" is the point added the hardener.

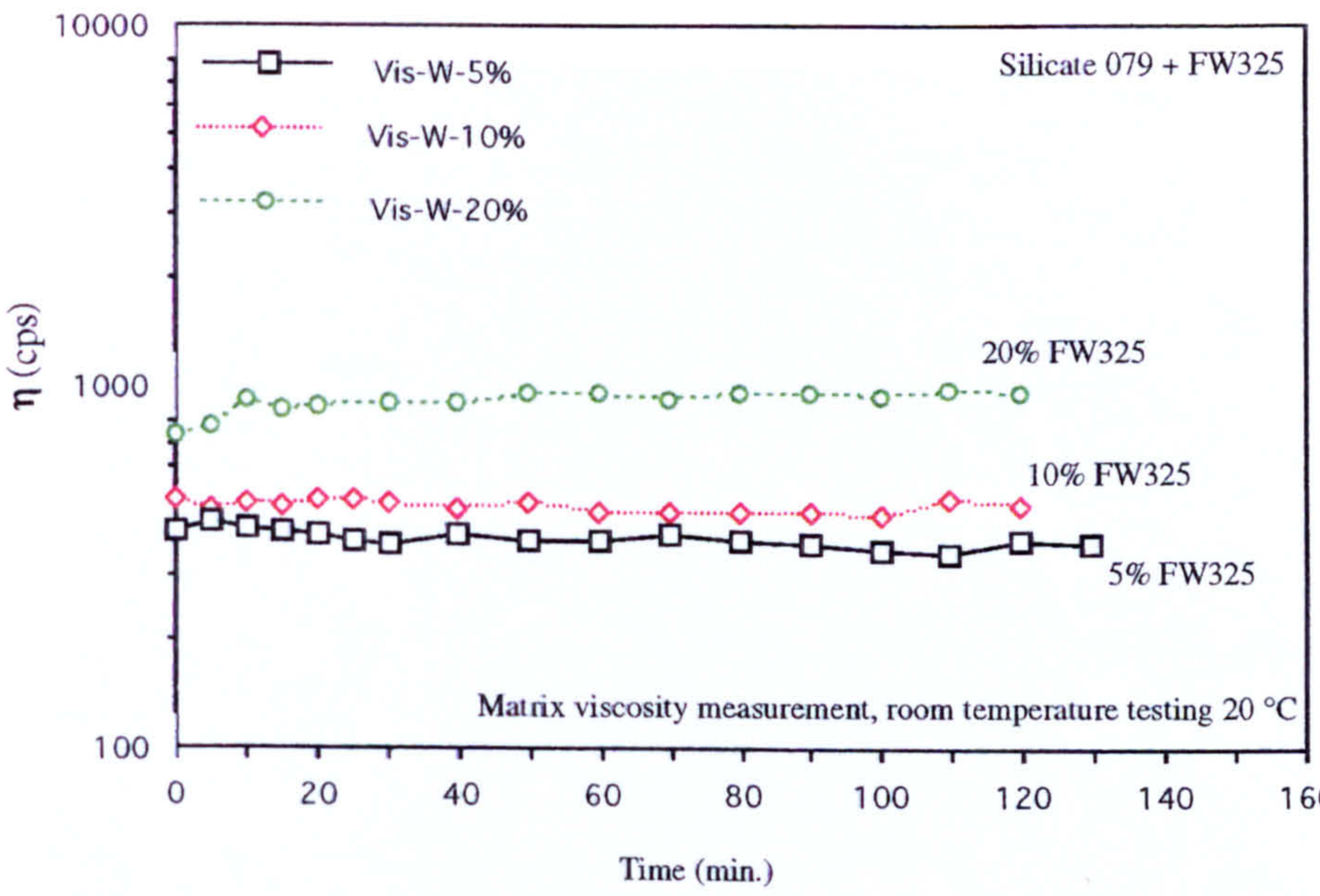

Fig. 4.9 The viscosity of the matrix, Crystal 079 + 5-20%(wt) FW325 measured at room temperature (20 °C).

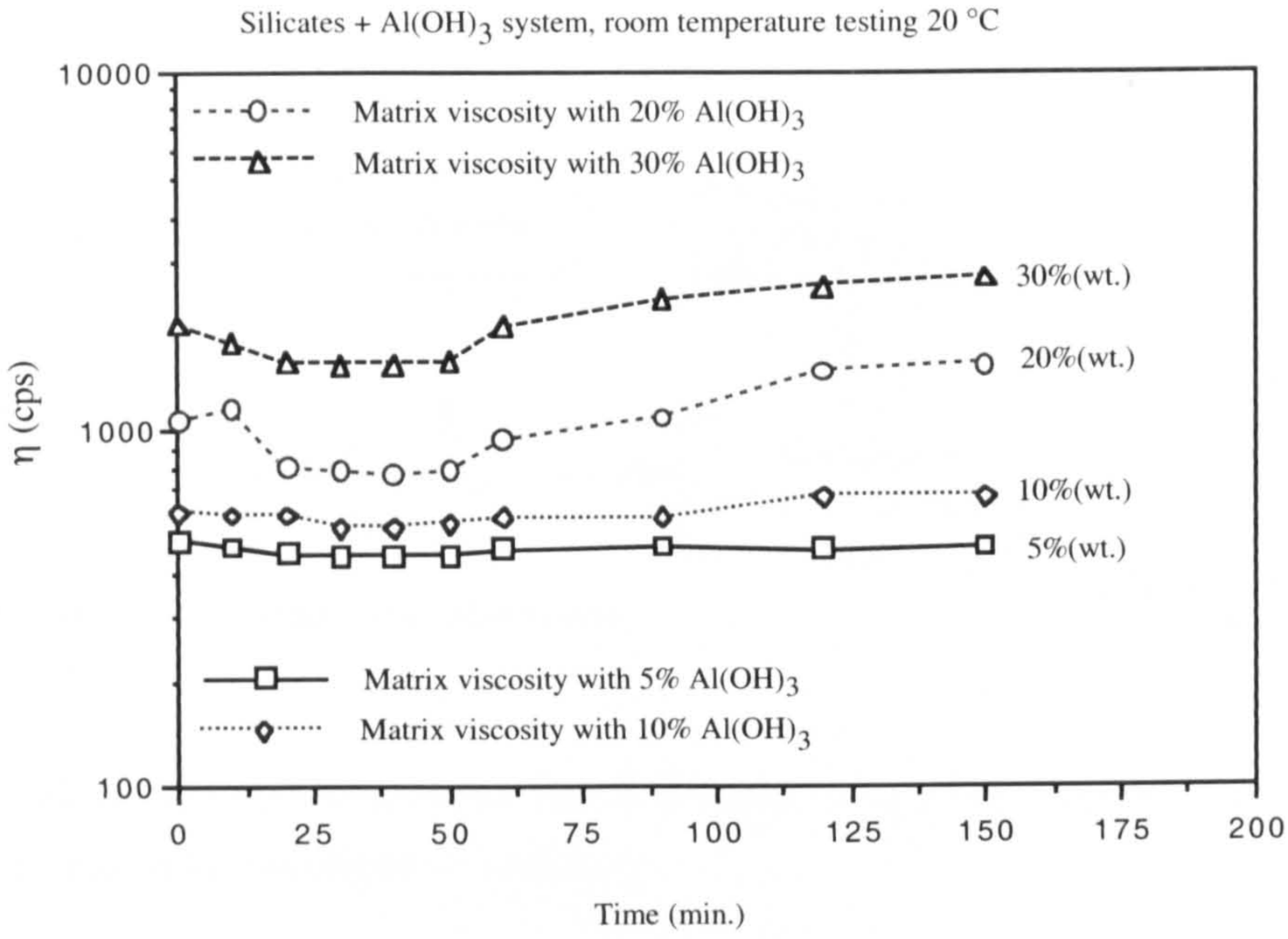

Fig. 4.10 The viscosity of liquid silicates with 5-30%(wt.) Martinel Trihyde (MT) as filler and was measured at room temperature (20 °C).

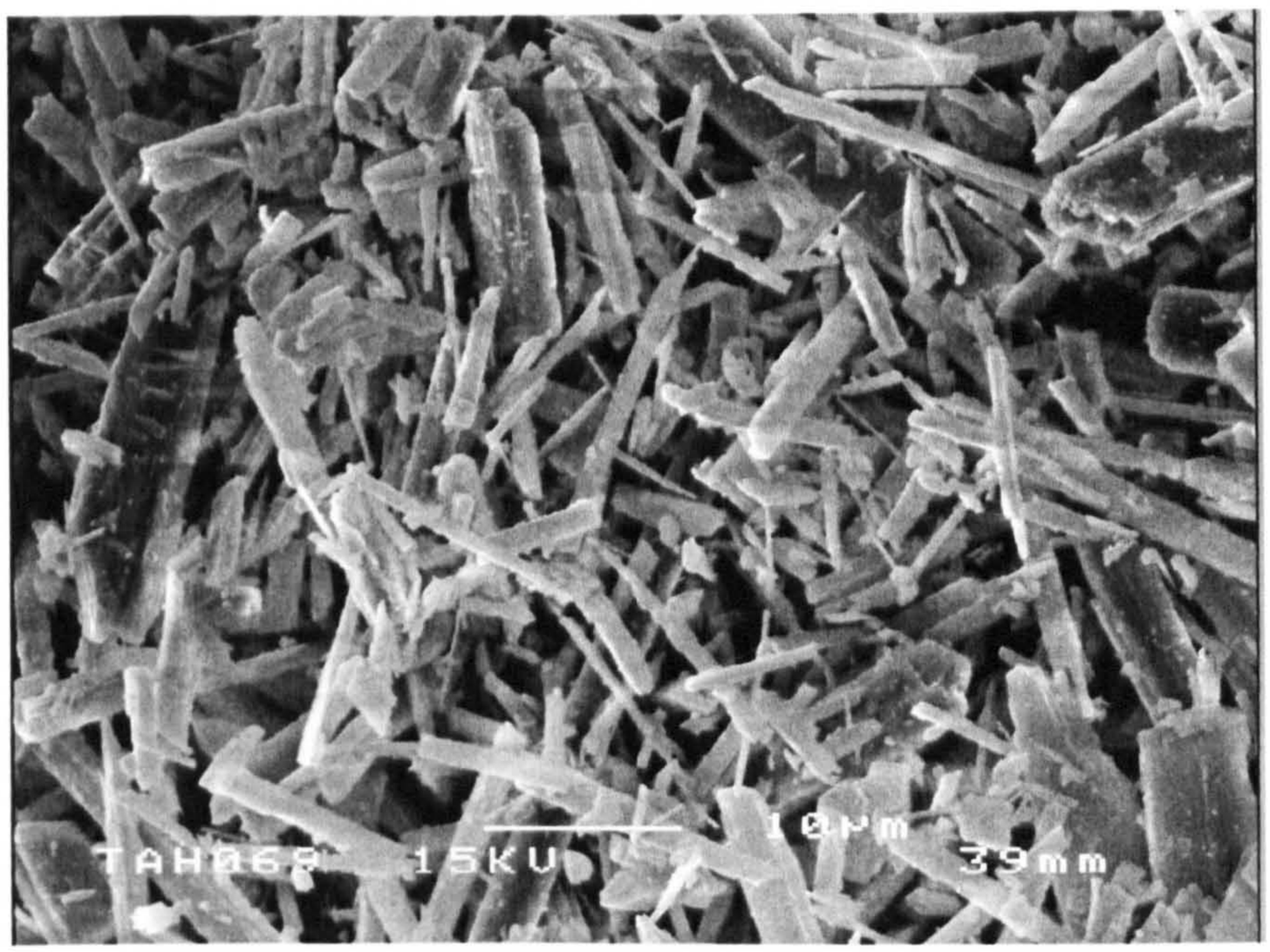

Fig. 4.11 A SEM micrograph of the fibrous Wollanstonite.

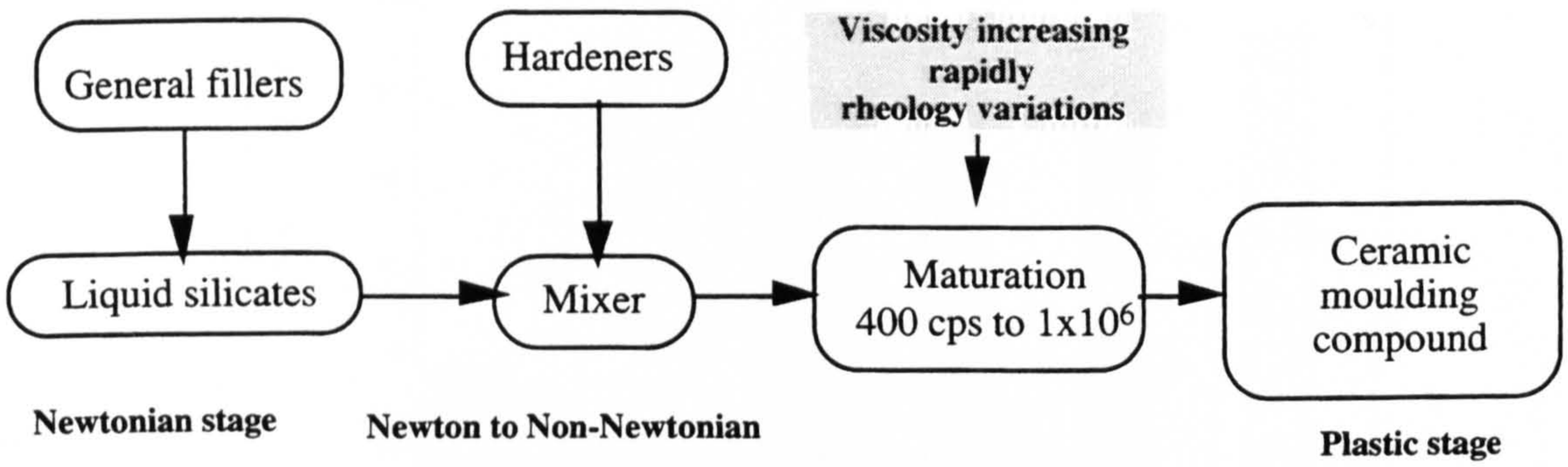

Fig. 4.12 Rheology development of liquid silicates from a Newtonian stage to a Non-Newtonian stage with variations of rheology.

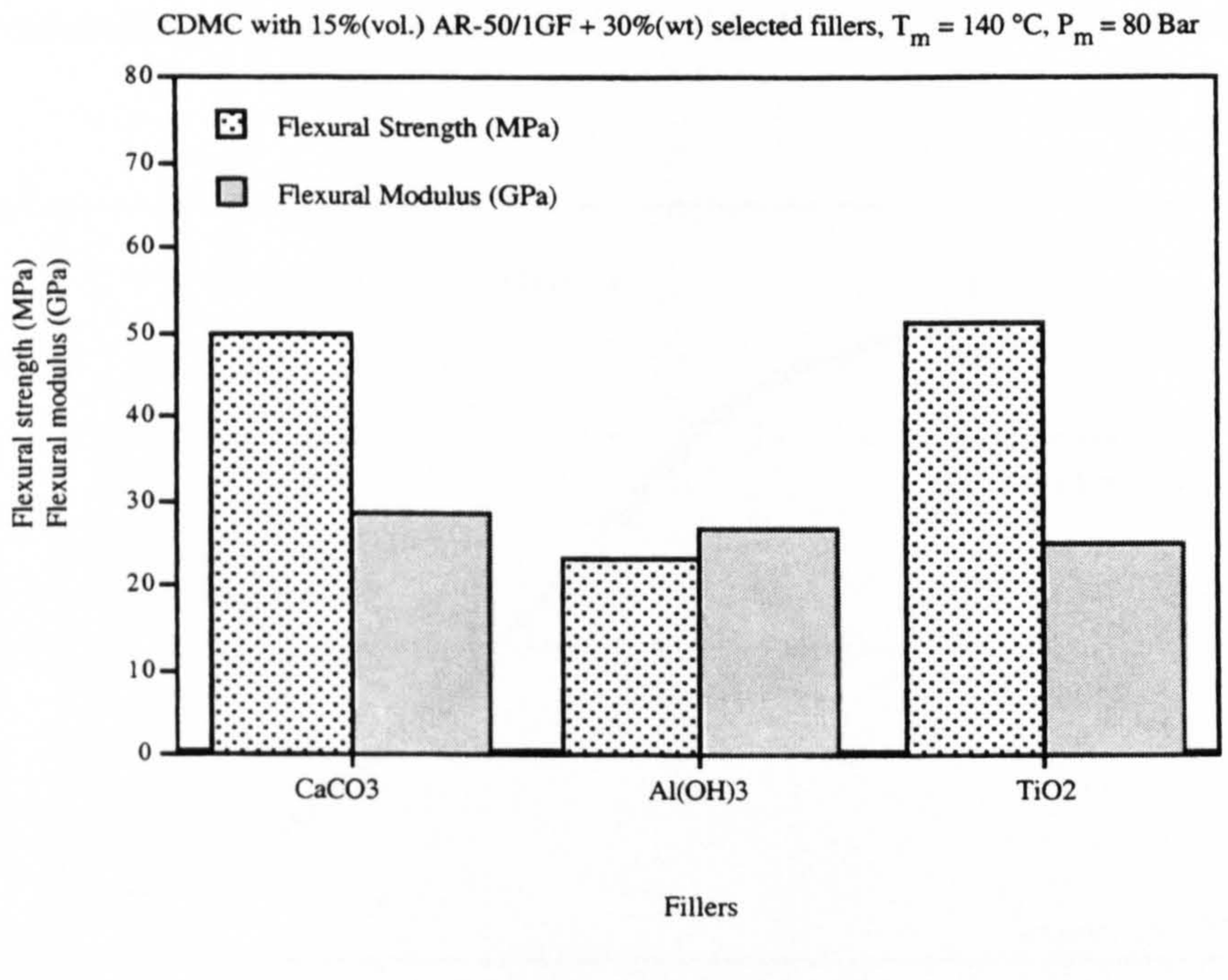

Fig 4.13 Flexural properties of the CDMC effected by different fillers, Millicarb ($CaCO_3$), MT and TiO_2 using combination of ceramic matrix + 15%(vol.) AR50/1GF, moulded at temperature of 140 °C.

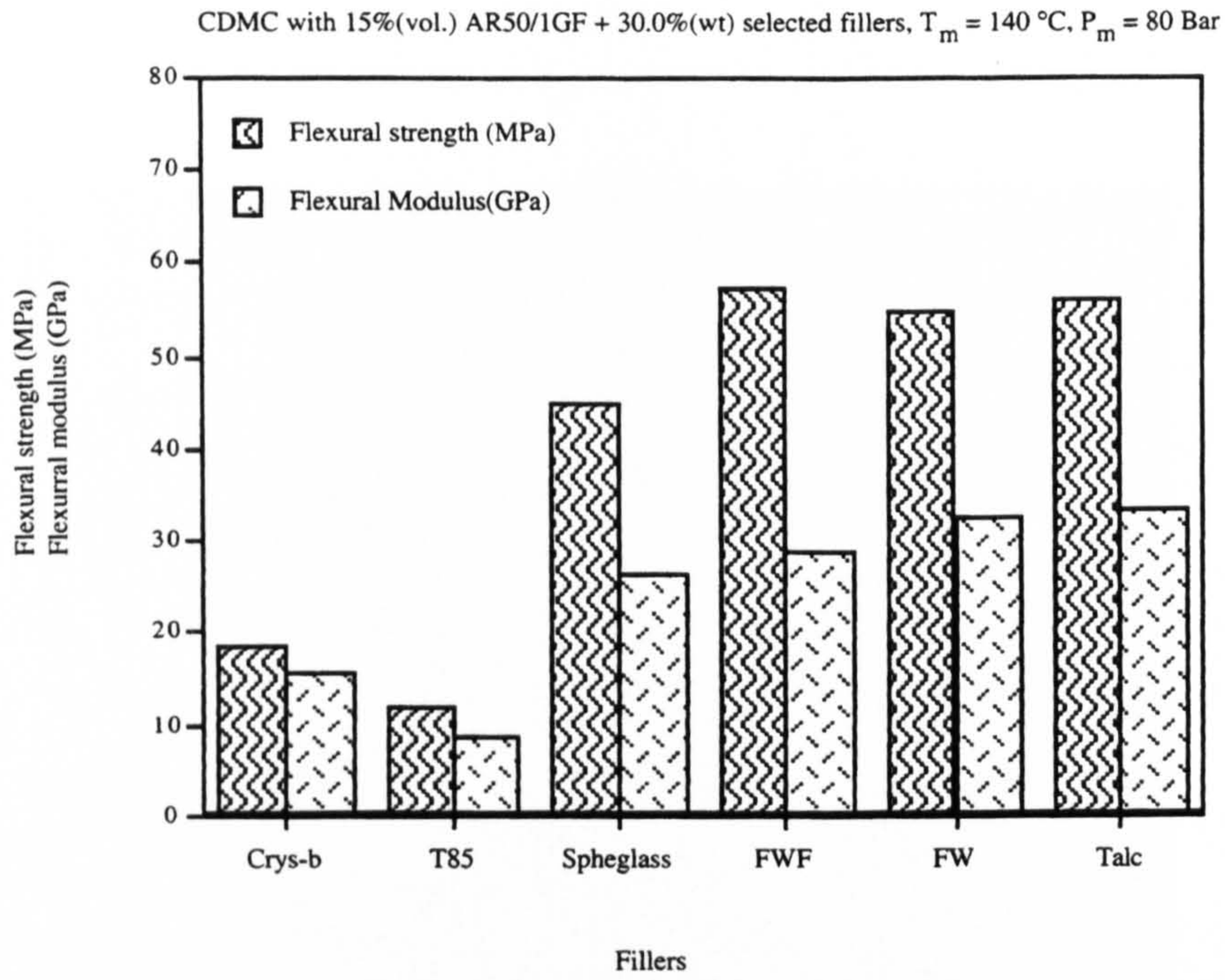

Fig. 4.14 Flexural properties of the CDMC effected by different metallic silicate fillers based on combination of ceramic matrix + 15%(vol.)AR50/1 GF, moulded at 140 °C.

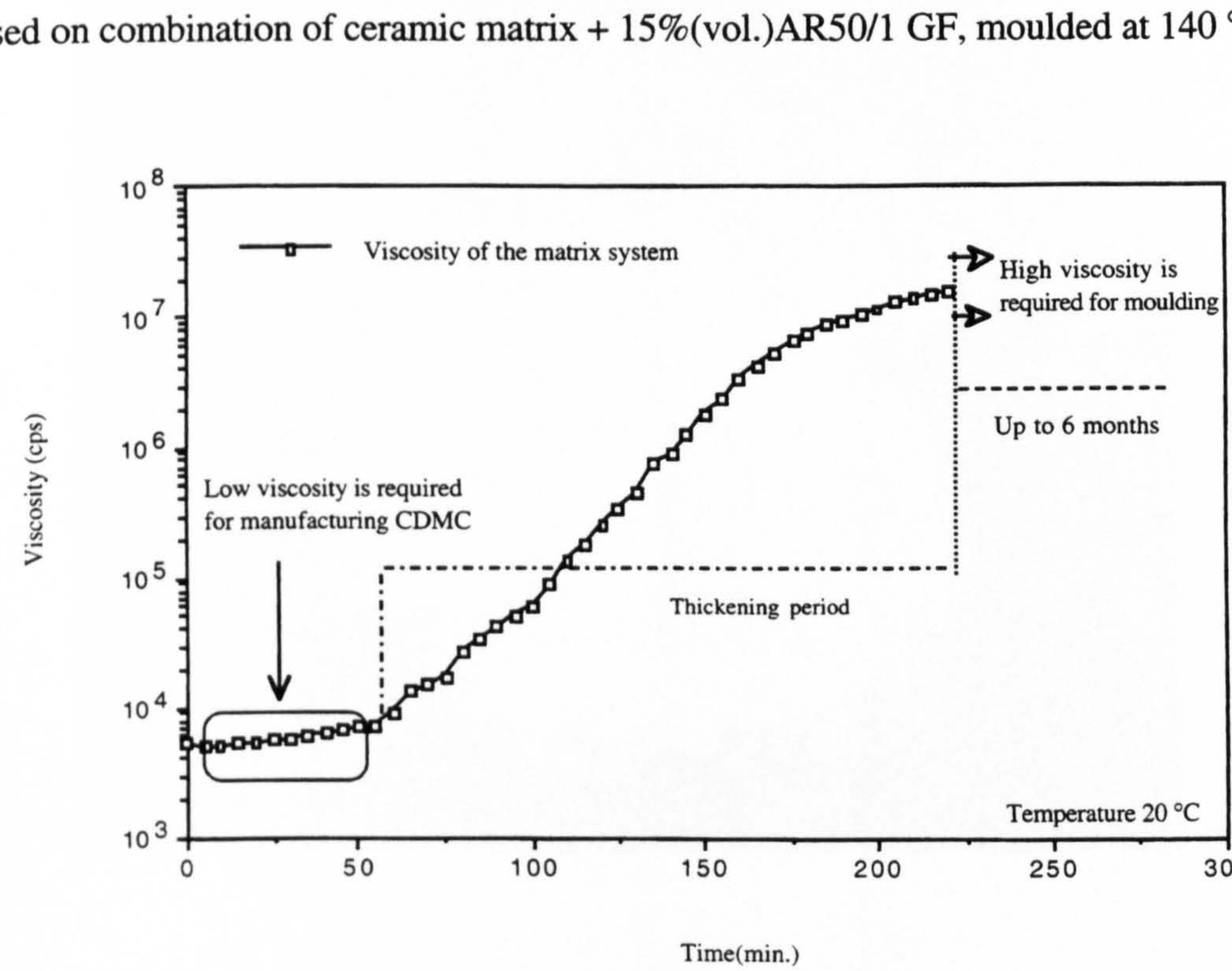

Fig. 4.15 The viscosity curve of a typical compund slurry system vs. time using 5.0%(wt.) Fabutit as a hardener, measuring temperature 20 °C.

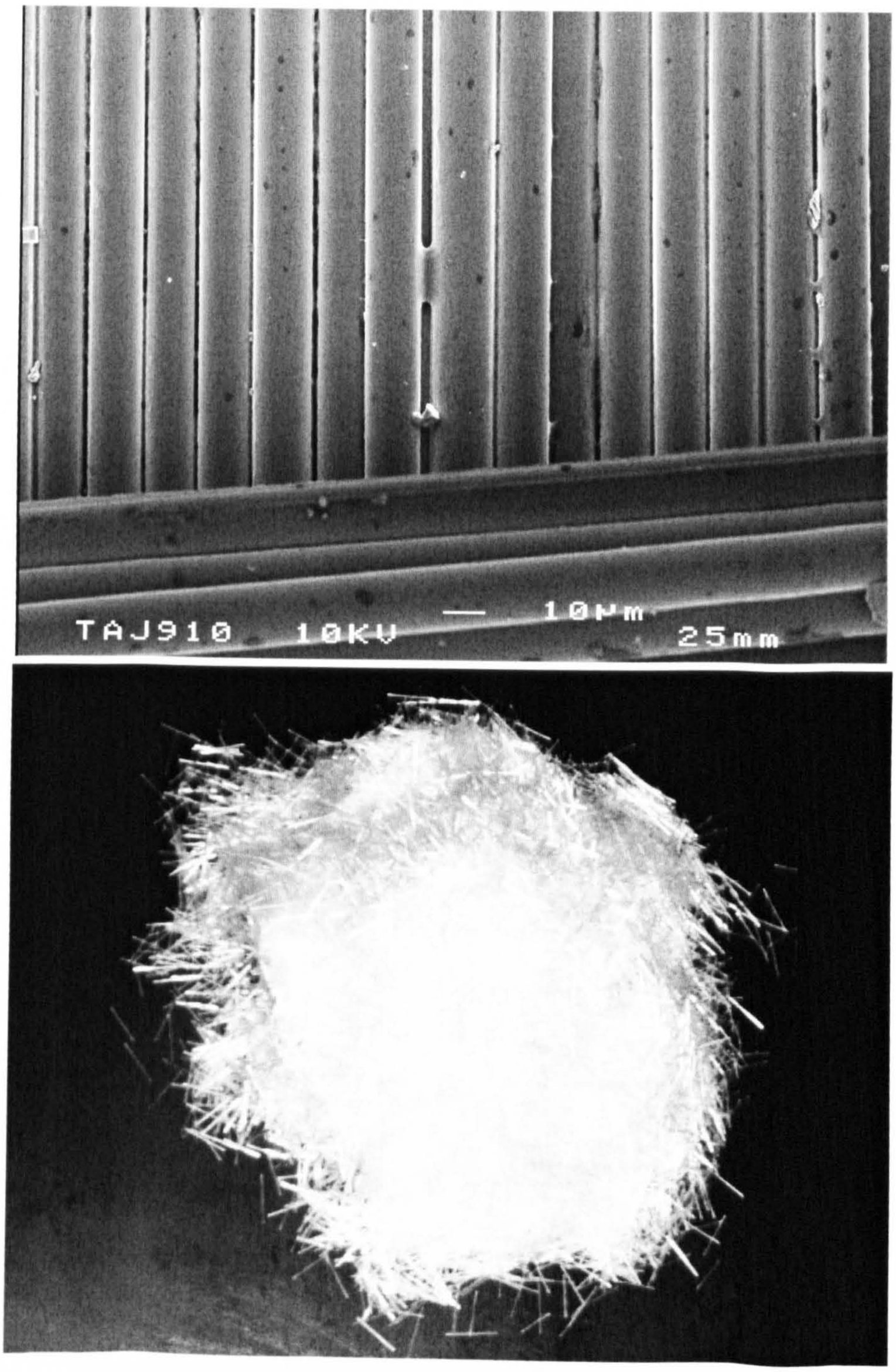

A

B

Fig. 4.16 A SEM micrograph (**A**) and a photo (**B**) of same AR 62/2 chopped fibre with length 12 mm.

Manufacturing glass fibre reinforced ceramic moulding compound

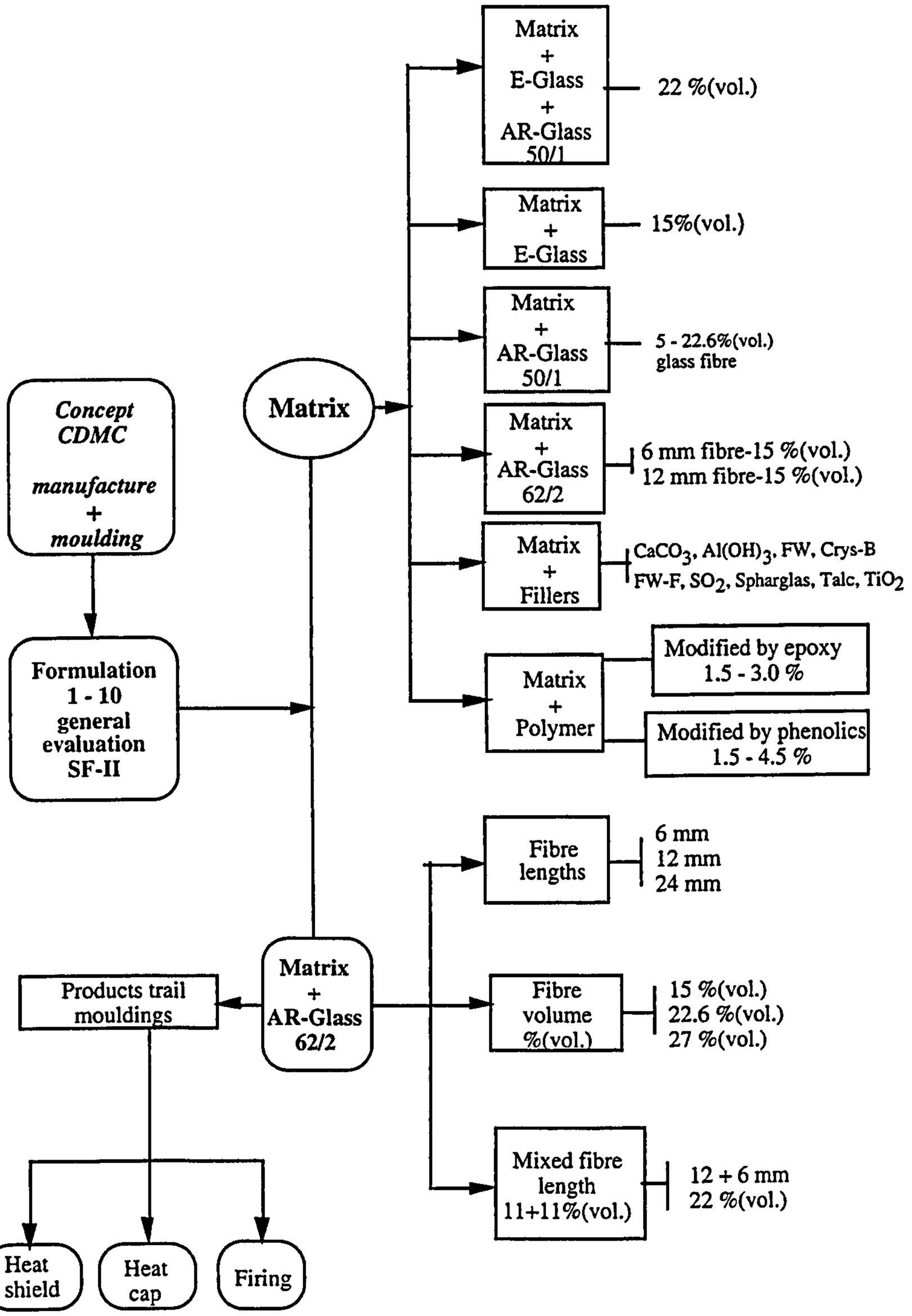

Fig. 4.17 This diagram shows the progress in manufacture of the CDMC: concept formation, formulation optimisation from preliminary formulations and some CDMC produced in the work.

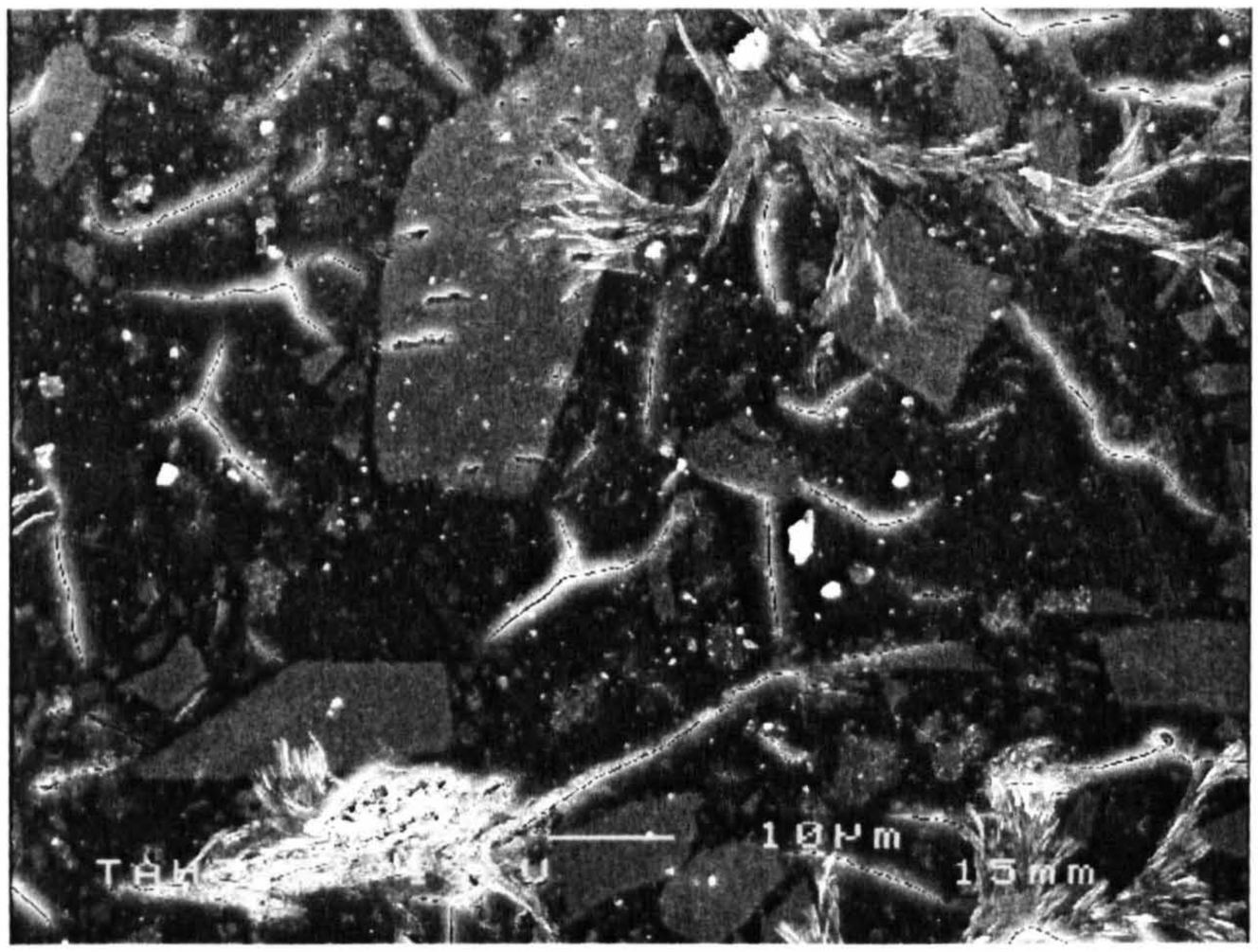

Fig. 4.18 A matrix SEM micrograph shows some of the filler particles in the continuous phase of the CDMC matrix.

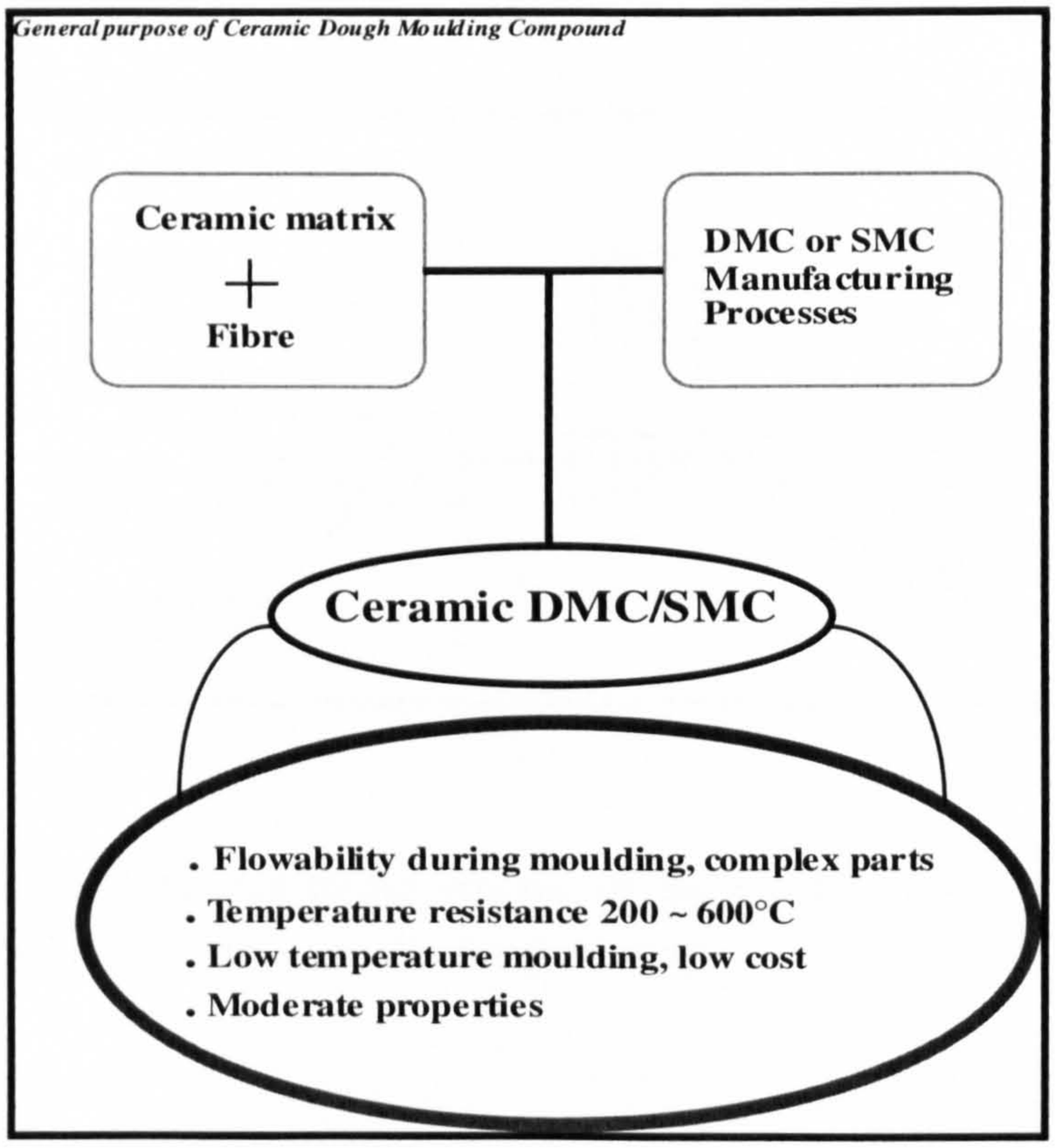

Fig. 4.19 The general concept, requirement and aim of the compounding and moulding.

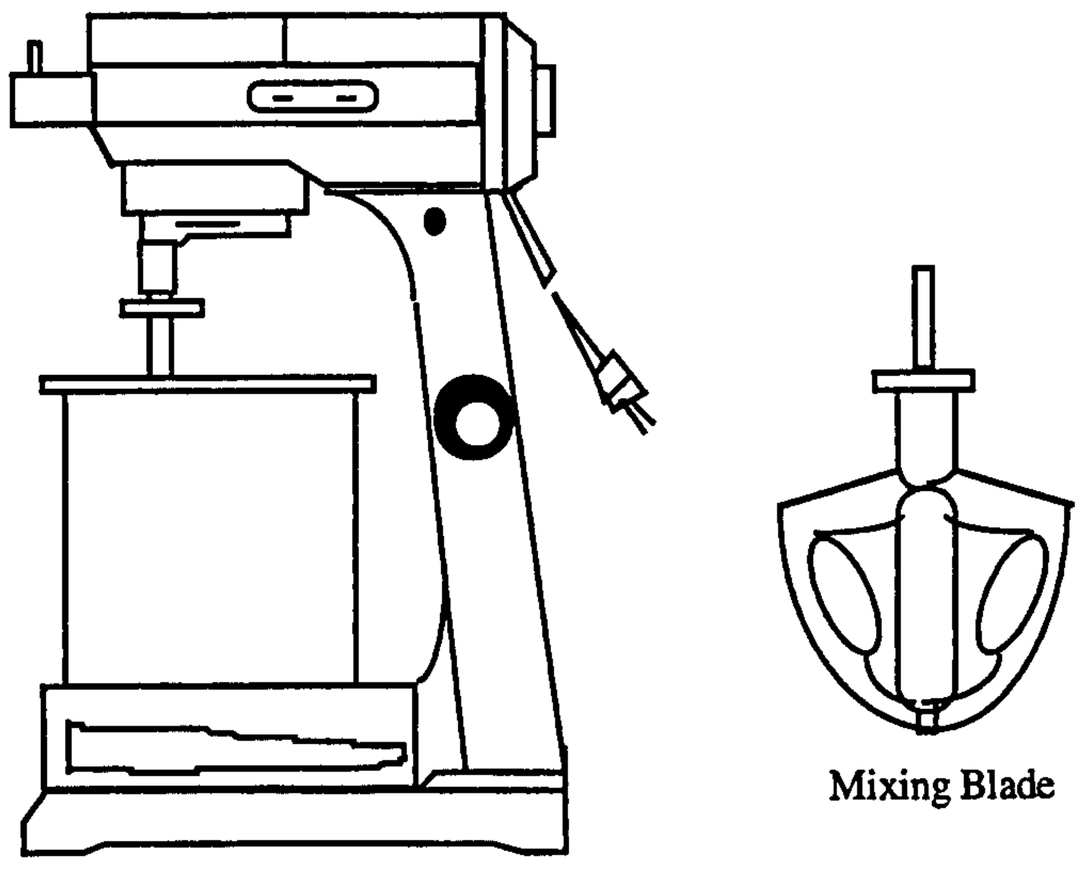

Fig. 4.20 Schematic drawing of a small mixer used for mixing the CDMC.

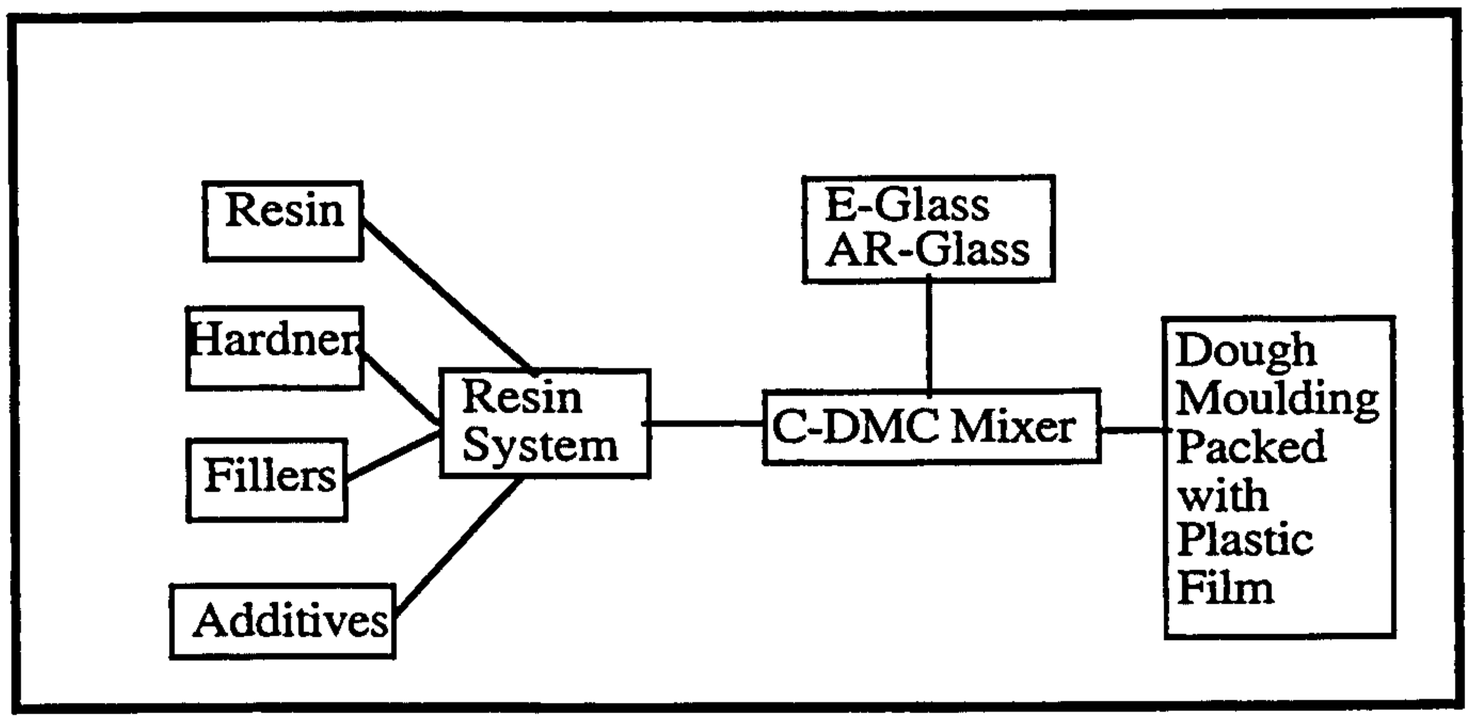

Fig. 4.21 Schematic manufacturing process of the CDMC, through combination of reinforcement and resin matrix, and the dough making.

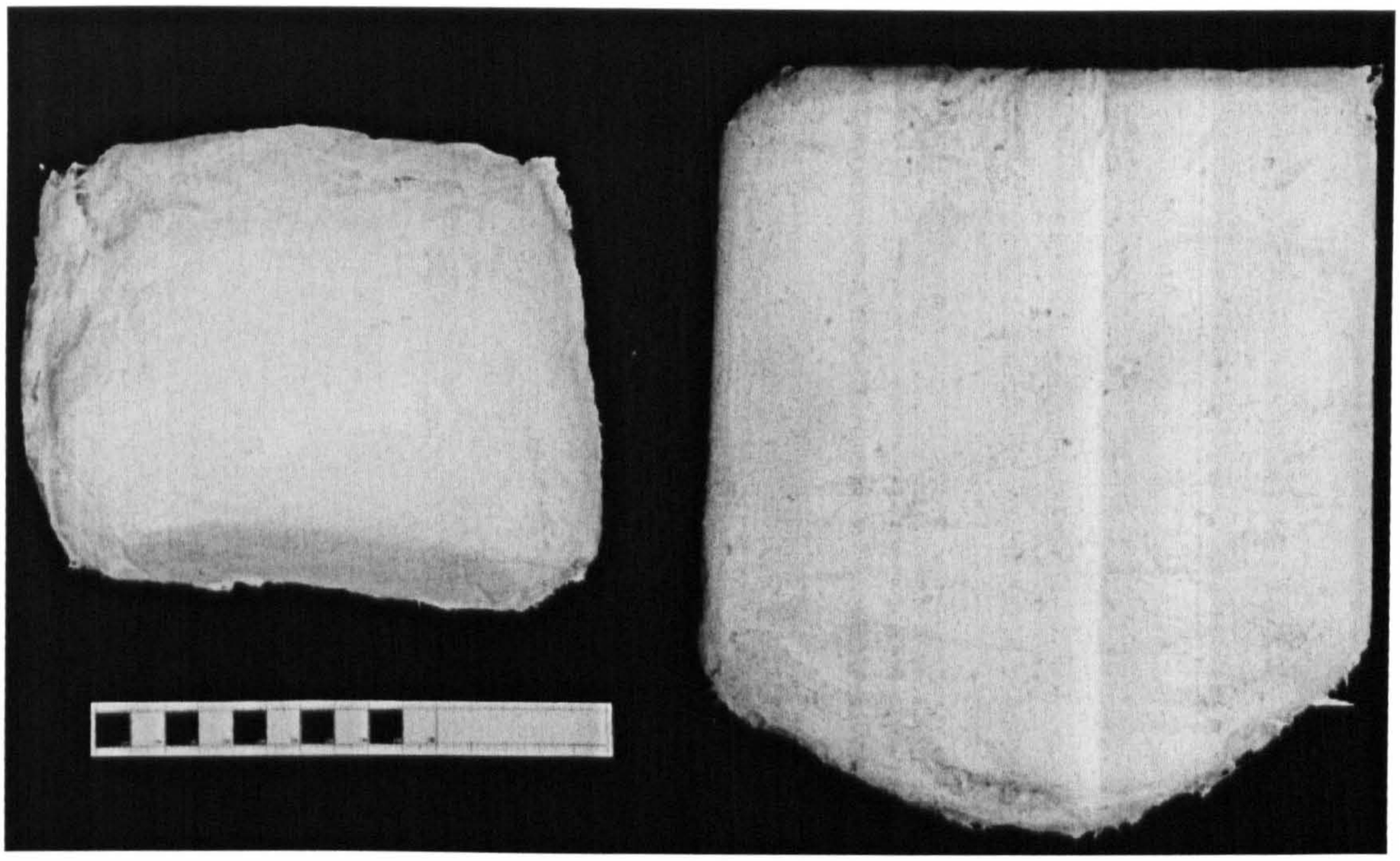

Fig. 4.22 The CDMC matured and ready to be moulded.

Chapter 5

MOULDING TECHNOLOGY

5.1 Introduction

The investigation of the moulding technology for CDMC involved firstly, the compound suitability for moulding into useful shapes with existing moulding techniques; secondly the determination of the best range of moulding temperatures for achieving reasonable mechanical properties; thirdly, the use of data from mechanical (flexure), physical (water absorption, density, porosity, etc.) tests and thermal analysis (DSC) to support the approach of using low temperatures to mould the ceramic composites. The determination of an optimum range of moulding temperatures was the primary objective of this chapter.

The optimised moulding condition was assessed by using the standard matrix with both 15%(vol.) AR and E-glass fibres and 22.6%(vol.) mixed glass fibre (AR to E-glass in ratio of 12:10). The whole optimisation scheme with moulding variations in different temperatures, pressures and time is shown schematically in Fig. 5.1. The optimisation covered 3 groups of process variables: firstly, the matrix is combined with glass fibres moulded at temperatures ranging from 99 - 180 °C; the second section involved moulding pressures ranging from 0 - 17.0 MPa (0-170 Bar) and mould closure times from 30 - 90 minutes using the standard matrix and 15%(vol.) AR50/1 chopped glass fibre; the third stream, took the matrix with E-glass fibre and AR-glass fibre respectively, moulded at temperatures from 130 - 190 °C. The further investigation of detailed mechanical properties of the matrix with two types of AR-glass fibres (AR-50/1 and AR62/2) is reported in Chapter 6 and Chapter 7.

The principal requirements for the moulding process were identified as: the fibre shall not be damaged severely; the material attains sufficient density for optimum mechanical properties; the process should be applicable to a variety of fibre/matrix combinations and complex shaped products. All the combinations of composite formulation were moulded

within the temperature range 99 - 200 °C. The moulding pressure and mould holding time were also studied within the range of 0 - 17.0 MPa and 30 - 90 minutes.

For the moulding compound itself, there are two major steps in the moulding process: firstly, compound viscosity falls, the material flows to fill the mould and the required shape is formed. During the second stage, the viscosity of the compound increases and the material consolidates as discussed in Chapter 3.

5.2 Moulding facility

A Palamine hydraulic press was used to mould the flat panels which were used for mechanical and fire tests. For routine mechanical testing the CDMC was usually moulded into plates with dimension of 285 x 285 x 4.0 mm^3. The mass of the material used for a moulding ranged from 800 g to 900 g depending on the thickness and density of a plate required. Fig. 5.2 shows the mould used for making the CDMC panels.

5.3 Material flow-ability during moulding

The moulding compound flows under pressure and elevated temperatures, and benefits from reduced matrix viscosity at elevated temperatures. The chopped AR-glass fibre with a length of 12 mm, Tex 2450 was used to examine the flow-capability within the mould. The process of moulding can be illustrated by the material flowing with glass fibre bundles travelling from the centre area to an edge area as shown in Fig. 5.3 - 5.4. The glass fibre bundles are rotated when reached at the edge of the mould under the moulding pressure. A matrix rich area was formed on the surface of this CDMC plate. The fibre bundles can be seen around corners of the moulded part which are uniformly distributed. The viscosity of the matrix affects the final orientation distribution mainly through its effect on the way in which the mould fills. This in turn, determines the distribution of elongational and shear fields (Hull and Clyne, 1996).

The moulding process begins with weighing the compound, and the charge may occupy around about 55% ~ 75% of the mould surface area before moulding. The greater the percentage coverage of the mould chamber, the better, since the longer the distance the compound has to travel, the greater the risk of the fibre damage. Nevertheless in real production, it is not always possible to maximise the mould cover area, the coverage may

also depend on local thickness, overall size and complexity of a product. Many other important factors such as compound formulation/flow-ability, moulding conditions, property requirements, manufacturing efficiency, etc. have to be considered at the same time for a particular product.

5.4 Preliminary optimisation of process variables

Three important factors during moulding are: temperature, pressure, and mould closure time. The objective was to use measured mechanical and physical properties of specimens moulded under different process conditions to determine the optimum process conditions.

The range of moulding temperatures, pressures and mould holding times investigated were from 99 °C - 180 °C, 0.0 - 17.0 MPa, 30 - 90 minutes respectively.

5.4.1 Moulding temperatures

The influence of moulding temperature, on materials flexural properties, mould closing and closure time, water evaporation rate and material's water absorption were investigated with a CDMC having AR-glass fibre. All data is generated or based on the moulding temperatures from 99 - 180 °C.

5.4.1.1 Flexural property and density

The flexural properties and density of the CDMC at the moulding temperatures ranging from 99 °C - 180 °C were examined. All load-deflection curves were linear to failure. The highest flexural property and density were achieved with the samples moulded at a temperature of 150 °C, as shown in Fig. 5.5 for flexural properties and Fig. 5.6 for densities. The flexural properties of the material against their densities are shown in Fig. 5.7, a small increase in density generated at different moulding temperatures would produce quite big influences on both strength and modulus.

The densities of the CDMC when moulded with various moulding temperatures follow a similar trend to the flexural properties. Over a temperature increase from 99 to 180 °C, the maximum density of 2.32 was achieved at the optimum moulding temperature of 150 °C.

The maximum flexural strength, at a moulding temperature of 150 ℃ was about 80 MPa, and modulus was about 43.0 GPa. At higher moulding temperatures, the flexural properties and densities were reduced. Based on these results, the material's flexural strength is approximately proportional to the density. The polished surfaces of typical specimens moulded at 120, 150 and 180 °C are shown as SEM micrographs in Fig. 5.8. When the CDMC was moulded at different temperatures, they exhibited different void contents and different interfacial bonding between fibre and matrix. This also appeared to affect the level of initial cracking within the composite. Interfacial phenomena generated by different moulding temperatures affects the mechanical properties and this will be further discussed in Chapter 6 and 7.

5.4.1.2 Mould closure time

To undertake an industrial moulding process it is necessary to know the duration of the moulding at different moulding temperatures. This is partially determined by how quickly the compound heats up and begins to flow. The time needed to close the mould is defined by the time taken for press platens on the top and bottom both touching the male and female moulds and the time until the press settled in a stable position where the CDMC completely filled the mould cavity. Fig 5.9 shows the time needed to close the mould at normal moulding temperatures ranging from 99 - 180 °C. The higher the moulding temperature used, the less time would be needed to close the mould. This factor is obviously dependent on mould dimensions and details such as the thickness and amount of compound charged for an individual mould system. For example at the moulding temperature 99 °C the mould would not be fully closed in 130 seconds. But at a moulding temperature of 180 °C, only 30 ~ 40 seconds are needed to close the mould.

5.4.1.3 Water evaporation

The water evaporation rate during moulding is related to the moulding temperature. The water remaining as a percentage of the CDMC after moulding is shown in Fig. 5.10 and the time for water to stop being released during moulding is shown in Fig. 5.11. Water release rates can be divided into 3 categories: mild, medium and violent which corresponding to low, medium, and high moulding temperatures since the speed of heat transfer is proportional to the temperature difference between mould and compound. It means that to release water from the compound, a certain amount of energy is needed. The water retained in specimens moulded at lower temperature less than 130 °C, was from 30%(wt.) - 12%(wt.). Although those moulded at 99 - 120 ℃ can be post-hardened at room temperature, the Si-O-Si chain may be difficult to increase in length in the short

period. The benefits may be, the formation of a weak interfacial bond between fibre and matrix, with non-corroded fibres, producing a considerably higher strength and a higher strain to failure.

- Evaporation at low moulding temperatures (<120 °C):

When moulding at a temperature lower than 120 °C, less than 20% of the total unbound water was released from the compound. The water release process should obey the chemical formula as shown in C5-1, although a certain balance will be reached. It is clear that the more heat provided at higher temperatures, the more the equilibrium would swift towards the right side, allowing more network chains to be connected.

$$Si-OH+Si-OH \xrightarrow{High(T°C)} Si-O-Si+H_2O\uparrow \qquad \text{C5-1}$$

An advantage of this lower temperature moulding is that there is insufficient energy to break the bonds of the sizing layer between the glass and matrix, which does not bond to the matrix and produces a weak interface.

- Medium moulding temperatures (130 - 160 °C):

The moisture level in the final moulded compound was from 10.0 - 4.0 %(wt.) as plotted in Fig. 5.10. This shows the proper water contents range for optimising the mechanical properties which corresponding to this optimised moulding temperature range. At this range, the density of the CDMC was the highest especially when moulded in 150 °C. Therefore, based on the general data on densities, flexural properties and moulding time requirement, the optimised temperature range for moulding CDMC was defined from 130 °C - 160 °C. Meanwhile within this temperature range, the time for releasing required amount of water is around 50 minutes. This has been shown in Fig. 5.11. This optimised moulding temperature range and corresponding moulding time as well as the maximum mechanical properties achieved will be further discussed in next Chapter.

- High moulding temperatures (160° - 180 °C):

For the compound moulded within this temperature range, the water evaporation rate was extremely high and can be presented with the form of final moisture level (water remained in the final compound which resulted in a material's rapid solidification. A fused interface can be observed, indicating a good bonding between fibre and matrix. The large voids

formed were due to matrix hardening rapidly and a quick build up of structure. Meanwhile, the fibres may act as bridges while the matrix hardens, and shrinks, leaving voids as capillaries for further water evaporation. It was noticed that just 20 - 30 minutes was needed to evaporate almost all the water. The higher the moulding temperatures, the less de-watering time (DWT) needed and resulted in the higher water evaporation rate.

5.4.1.4 Porosity and water absorption

The link between void content and moulding temperature follows a similar trend to that of densities and mechanical properties, while voids themselves effect the absorption of water. Between the moulding temperatures of 130 - 150 °C, the lowest void content and maximum density in the CDMC were achieved. The void content was measured using image analysis as described in Section 3.3.3. Some typical polished sections of specimens have been shown in Fig. 5.8 for the CDMC moulded at temperatures of 120 °C, 150 °C and 180 °C. Different morphologies of void formation can be observed with the changes in moulding temperatures. Moulding at 150 °C formed dense structures and less voids. The specimens moulded at 180 °C had a void content of 6.0%. These polished CDMC images (every specimen had 5 - 7 images taken from different areas) were analysed by a computerised image analyser. The relationships among void contents, water absorption and moulding temperatures are listed in Table 5.2 for 22.6 %(vol.) glass CDMC and revealed that the smallest void contents and water absorption were obtained when the moulding temperatures were between 130 - 150 °C. Within them a pure matrix sample without fibre moulded at 130 °C contained voids at the level of 0.88 % and absorbed 0.4 - 1.5 % of water. The relationship between the flexural properties, void contents and densities for pure matrix are listed in Table 5.3. These results reveal that for the ceramic matrix, porosity and density determines the mechanical properties. The average void content and water absorption for the CDMC measured in this way were also plotted against moulding temperatures in Fig. 5.12.

A corresponding set of samples were used to measure the water uptake in the just-moulded condition. Samples were immersed in water at room temperature for 24 hours (see section 3.3.4). The water absorbed is then plotted against moulding temperatures as shown in Fig. 5.12.

The water absorption is changing as void content varies. At moulding temperatures below 140 °C, the absorption appears independent of void content and is linked only to the moulding temperatures. Another interesting phenomena is that although the void content

of the CDMC when moulded in the low temperature range (99 - 130 °C) was lower compared to the void content when moulded at the high temperature range (160 - 180 °C), the water absorption rates were much higher. This might be due to the incompletion of polymerisation of silicate when moulded at lower temperature range. When the specimens were moulded below 140 °C, although the void contents were very low and yet the water absorption increase dramatically. The explanation might be that at the lower moulding temperatures, the cross linking and network formation in the silicates may be incomplete. It is possible that the network is accordingly more open and capable of absorbing water easily.

The high absorption with low void contents at the lower moulding temperatures may also link to effects of the fibre/matrix debonding which provides the path for water defusing into depth of the composites.

5.4.1.5 Supporting data from DSC for the ceramic matrix

DSC analysis of the fillers in matrix can provide additional information on any changes in the physical and chemical structure for the moulding temperatures ranging from 99 to 200 °C. The data may also help to explain the thermal behaviour of the panels during fire or heat insulation up to 400 °C. The main objective of using DSC for the fillers was to obtain thermal information on the raw materials, such as resin, fillers and hardeners, in order to predict thermal behaviour for the composites.

Typical DSC traces obtained from sample fillers are shown in Fig. 5.13. The inorganic fillers, such as FW did not give any change within this temperature range. For P60, the water was released when the temperature reached 100 °C, followed by very slow water evaporation and possibly structural change all the way to the highest temperatures.

The energy absorption curves produced here may represent the water evaporation from the fillers which could be added into matrix. This process must also connect with the silicate polymerisation in the matrix within this temperature range. This needs to be further investigated and explained.

Although the chemical structure of the fillers when processed in different temperatures have to be also confirmed by other facilities such as X-ray or FTIR, these data may still

support the concept of water release from the raw materials within the moulding temperature range and from the matrix when subjected to fire or heat.

5.4.2 Flexural properties of matrix effected by density and porosity

It is known that CDMC's flexural properties are linked to its porosity / density which has been shown above. Since the density and porosity in turn are mainly determined by the matrix, it is interesting to investigate the links between density / porosity and mechanical properties for the pure matrix. These are examined by testing the flexural properties for 6 matrix specimens randomly selected from a common moulded matrix panel at 130 °C. The specimens reflect the scatter in void contents and also in mechanical properties. For each specimen tested in flexure, the material close to the fractured zone was polished, then examined by SEM as shown in Fig. 5.14.

The flexural properties for individual values of porosity / density of the matrix specimens are compared in Table 5.3 in the order of densities. Both trends in flexural modulus and strength were related to their density or porosity; the higher the density and lower the porosity, the higher the flexural properties, especially for the flexural strength. These are shown in Fig. 5.15 for the flexural properties effected by porosity and Fig. 5.16 for flexural properties effected by density. The densities here are the density of that small block close to the fractured area. Since it is impossible to get the exact densities at the fractured site, the correlation between a flexural property and its density in some specimens are not that perfect.

The corresponding SEM images for different void sizes in (Fig. 5.14) are from the photo number 1 to 6, the porosity and the size of pores were gradually increased from very few pores to some small pores, then to large amounts of big pores. With the pore diameter increased, the flexural modulus and strength decreased significantly. When the porosity increased from zero to about 15 %, both the strength and the modulus decreased about 40 %, density was decreased at almost same rate as porosity increased.

5.4.3 Moulding pressure and time

- Moulding pressure

The flexural properties and densities of the CDMC with 15%(vol.) AR-glass 50/1 moulded at different pressures 0.0 - 17.0 MPa (170 Bar) were measured as shown in Fig. 5.17 - 5.18. Other moulding conditions were kept constant at 140 ℃ with a holding time of 1.0 hour.

The moulding pressures were in a low and medium range compared with those used in the manufacture of polymer moulding composites. Since water evaporation was always involved in the process, the pressure applied to the mould may delay water release, and can alter the density or porosity of the moulded products, which in turn influences the mechanical properties. The flexural properties vs. material densities are plotted in Fig. 5.19 and show the influence of density on flexural properties under different moulding pressures.

At lower moulding pressures, i.e. 0 to 4.0 MPa , the flexural properties remained consistent around 15 ~ 20 MPa with 15%(vol.) AR50/1 glass fibre. The materials contained a certain amount of pores and the densities were around 1.0 ~ 1.5. As the pressure is increased from 4.0 - 8.0 MPa, the flexural strength increased to a maximum around a moulding pressure of 8.0 MPa. This was followed by a decrease in properties up to around 12.0 MPa. There after both flexural properties and densities were relatively constant. The flexural properties and densities are clearly related each other when moulded at same pressure and temperature.

- Mould holding time

The effects on flexural properties of different periods of moulding time (30 minutes, 60 minutes and 120 minutes) were examined. It seemed that mould holding time did not give much influence on the mechanical properties as shown in Fig. 5.20.

It is noticed that the longer the moulding time, the better the surface smoothness. Observation found that the CDMC panel was distorted by the shrinkage on cooling for panels moulded with less than 30 minutes holding time. This may be caused by a inadequate time for sufficient structural cross link and water to release.

5.5 Post hardening

Since the curing temperature was relatively low (from 99 to 180 °C), it was impossible to release all the water within a short time especially at the lower moulding temperatures. Therefore, for products moulded at the low moulding temperatures, post curing becomes important for property control.

Post-curing characteristics of the CDMC moulded at 99 ℃ have been examined by measuring weight loss after moulding as panels produced at this temperature had highest residual water content. Water content of moulded panels at room temperature was constantly examined. With continuous evaporation at room temperature after moulding, the panel surface from plane and smooth gradually became as an rough surface with shrinkage marks around the glass bundles. Fig. 5.21 shows the average water released from CDMC moulded at 99 °C. The evaporation or absorption of the moisture seemed reached balance and kept stable after 28 days.

An example of the CDMC moulded at 99 °C, shows that water evaporated from the compound during moulding for one hour was just about 5 % of total water contained. The water percentage reduced from 27%(wt) to 22.6%(wt). This continuation of the low moulding temperature and the post curing process caused extreme shrinkage and distortion to the CDMC over a period of time, as shown in Fig. 5.22.

5.6 The matrix shrinkage during moulding

Matrix shrinkage has been found to be one of the important reasons for the formation of the voids, micro-cracks and product distortion during moulding, which give changes to mechanical and physical properties. Nevertheless, all ceramic materials presented the steps of particle formation, dimensional shrinkage and inter neck linkage. One of the CDMC's SEM micro graph and a diagram are shown in Fig. 5.23 and illustrate this general process and schematically in Fig. 5.24. For the CDMC panels, the higher the moulding temperature used, the more voids are left.

The smooth voids and gaps might be caused by a surface tension during water release from the compound which raised the stress concentration from the action of capillary forces. It becomes operative when pores started to empty by a liquid-air interface in the

form of menisci distributed in the pores of the drying matrix which is surrounding fibres. There are probably two steps of volume shrinkage or plastic deformation and crack generation.

At first stage, the decrease of a volume was equal to a volume of evaporated liquid/water at temperature above 100 °C. The free water which was not chemically combined with matrix might start to release into the pores produced by the matrix curing shrinkage. This shrinkage was partly caused by surface tension of water in matrix and neck for matrix among and around outside of individual fibres.

There was enough liquid to fill the pores at the first stage during moulding and no liquid-air interface occurred and no capillary forces were operating. During the second stage with opening the mould for breathing, the water gradually released from the matrix system, the water volume was reduced. With the big volume of water loss, numerous concave were formed in the pores, and the capillary attraction presses the particles or around fibres together. For particles and fibres in contact, the volume reduction might result first in an elastic deformation of the system and then when the system becomes rigid, an irreversible, collapse or cracking may occur during drying, owing to release the stress concentration under the press pressure. These stresses generally produced fragmentation of the gel (cracking unless special precautions were taken). In the CDMC composites, it can be more complicated because the fibre/matrix interface assists the formation of voids and shrinkage cracks. And this cracking process is going to be discussed further in Chapter 6.

5.7 Initial optimisation of the moulding conditions

The optimisation of moulding conditions has concentrated on moulding temperatures in a range of 99 to 180 °C. When the temperature was higher than 160 °C, the surface of glass fibre would be chemically active and form a better interface with the matrix. This will be discussed more in next chapter. When the moulding temperatures are lower than 120 °C, the water evaporation rate and the matrix hardening process are too slow for a standard moulding time (60 minutes) and around 20 %(wt.) water still remained in the moulded panels. Although the possibility of producing a high strength material is greater at lower moulding temperatures due to the intact fibre - matrix interface, the surface roughness and dimensional instability after moulding, made them difficult in practice. Therefore, considering all the factors and properties they can achieve, the best moulding temperature should be in the range of 130 °C to 150 °C.

The range of the moulding pressure used was from contact moulding to 17.0 MPa, and this produced the panels with different densities. Low to medium pressures were recommended for the energy and safety considerations. The mould holding time of one hour is sufficient for a good moulding practice. The optimised moulding condition was listed in Table 5.4 for the CDMC.

5.8 Summary

The CDMC is mouldable using selected moulding conditions:

1) At lower temperatures 99 - 120 °C, quality products were difficult to obtain because not enough energy was supplied to drive off water unless post-curing/hardening was employed. This was also linked to distortion of products if proper fixture was not employed after moulding.

2) At temperatures 130 - 150 °C, the moulded products had a smooth surface finish. In this range, the moulding pressures can give contribution to control the materials' voids content, density and surface quality, especially within the pressure range from 8.0 ~ 12.0 MPa. The voids remained at a minimum at the temperature range 130 °C - 150 °C. Some shrinking residual stresses generated micro-cracks around fibre and fibre bundles, providing opportunities for fibre sliding, pull-out during its mechanical tests.

3) By increasing the moulding temperatures, the time for closing mould was reduced. But there was an increase in porosity which is in a form of smooth voids. This resulted in a better interfacial bonding and brittleness. The cause of this porosity phenomena is due to matrix shrinkage and rapid hardening of the structure in material at the elevated moulding temperatures. Some panels moulded in different conditions have been illustrated in Fig. 5.25 for showing this success of moulding process.

Table 5.1 Pre-designed moulding condition for the CDMC.

Items	Moulding condition
Temperature, °C	99 ~ 180
Pressure, MPa	0.0 ~ 17.0 (0 - 170 Bar)
Mould holding time, minutes	30 ~ 190

Table 5.2 Void content of the CDMC moulded at different temperatures examined by an image analyser. And the related water absorption is listed as well. All listed values were mean values; panels were moulded at 130 - 180 ℃ (P_m = 8.0 MPa for 60 minutes). The specimens were polished and the mean values of 5 specimens for each temperature were calculated.

Moulding temperature (°C)	Voids area	Frame area	Area fraction of void content %	CDMC water absorption, %
180	1.246	19.265	5.93 %	4.9
170	3.883	24.254	12.6 %	7.8
160	0.666	20.405	3.25 %	1.8
150	0.196	16.611	1.18 %	0.49
130	0.196	20.405	0.45 %	1.92
Pure matrix (130 °C)	0.145	16.611	0.88 %	0.40 - 1.50

Table 5.3 The relationship and comparison among individual porosity / density of the matrix specimens and properties are compared. The porosity were obtained by the technique of photo-image analysis.

Single specimen of Moulded product of the matrix system	Porosity(%)	Density	Flexural strength MPa	Flexural modulus GPa
No. 1	0.01	2.30	89.2	45.00
No. 2	2.1	2.30	53.8	34.50
No. 3	5.6	2.28	55.4	28.70
No. 4	8.2	2.17	51.0	32.20
No. 5	10.9	2.03	49.0	28.47
No. 6	14.7	1.99	49.7	25.18

Table 5.4 The primarily optimised moulding conditions for the moulding compound.

Item	Moulding condition (optimised)	Unit
Temperature	130.0 ~ 150.0	℃
Pressure	8.0	MPa
Mould holding time	60.0	Minutes

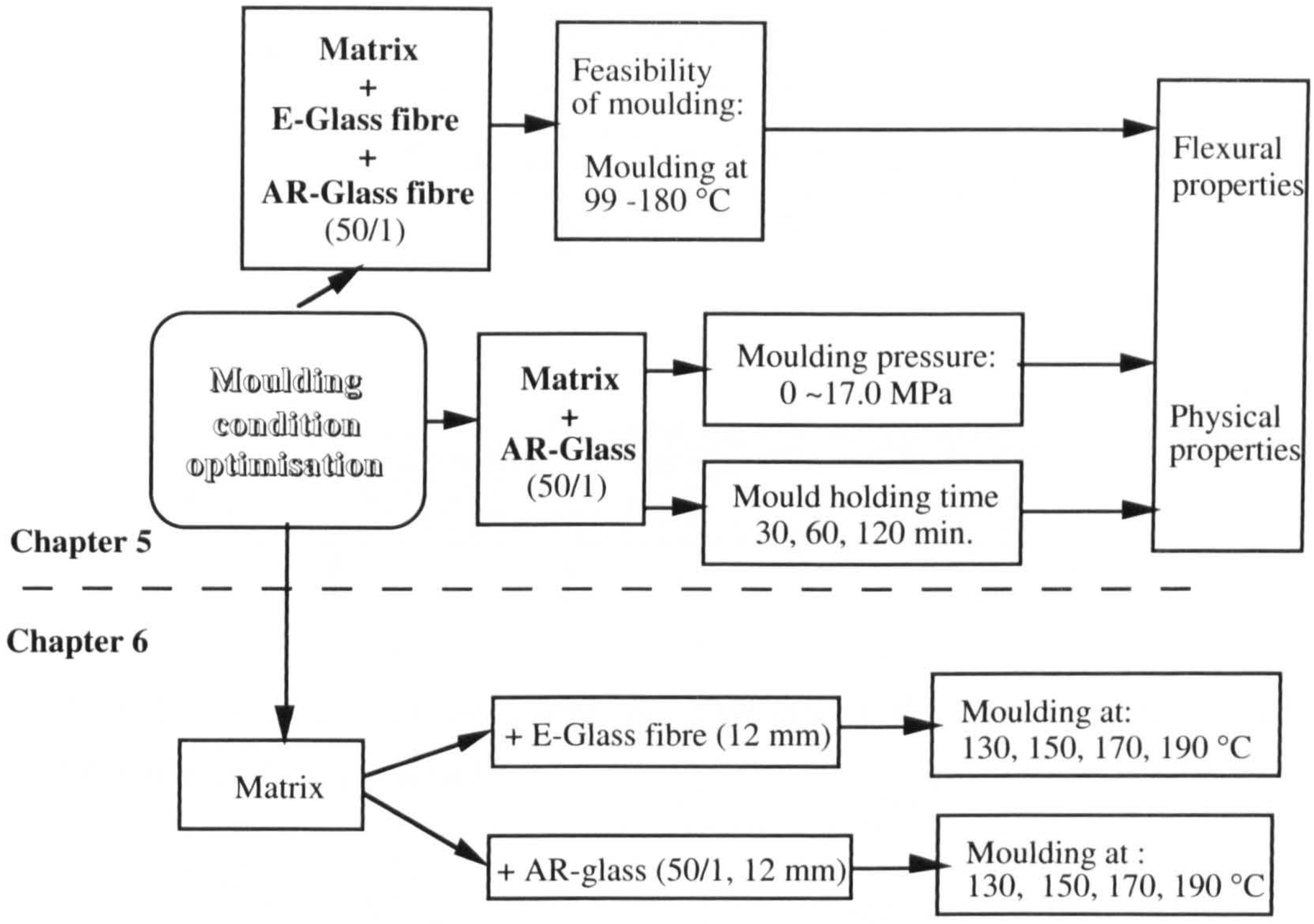

Fig. 5.1 Schematic flowing chart shows the routes of optimisation of moulding conditions through chapter 5 and 6. The CDMC with mixed glasses and AR-glass and E-glass were moulded at different temperatures, pressures, and mould closure times.`

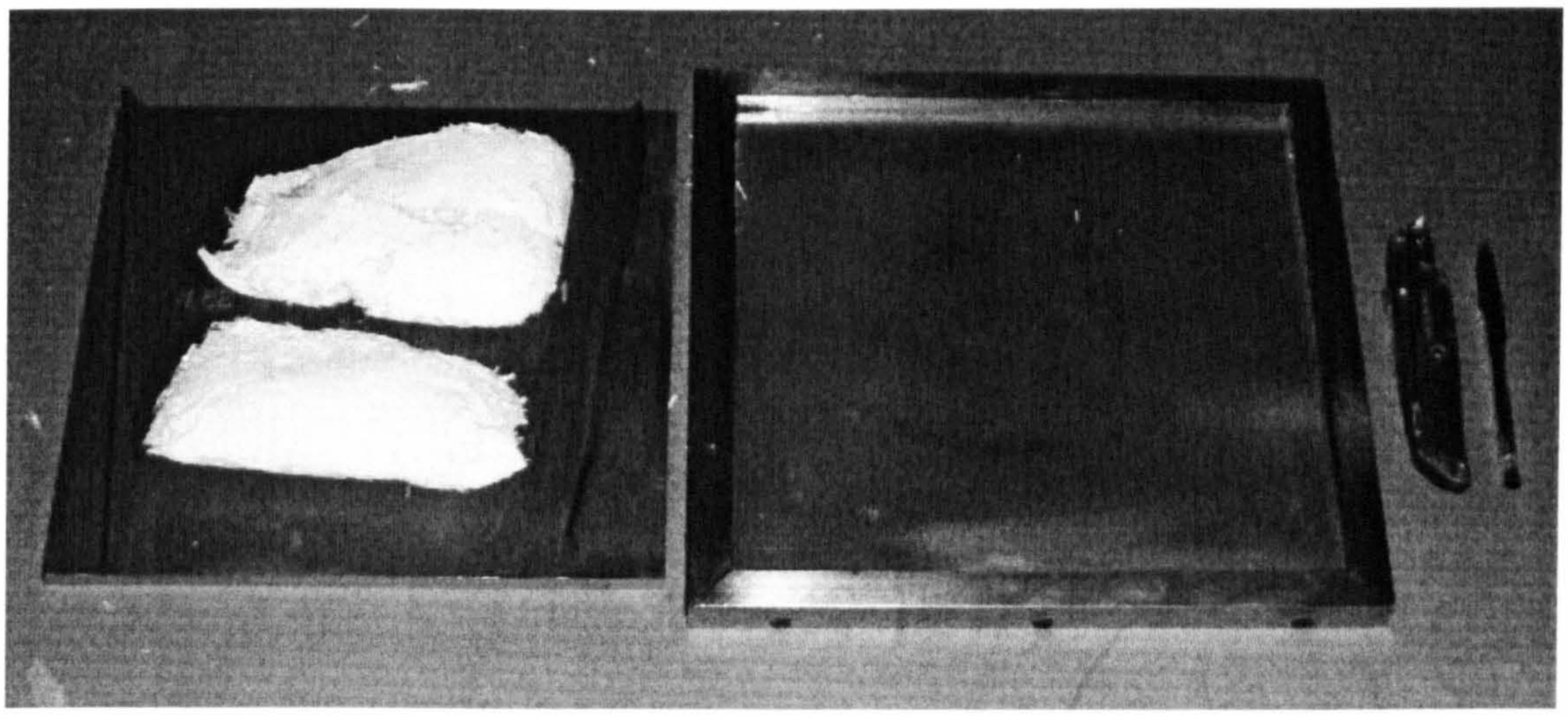

Fig. 5.2 The CDMC and the mould used for making panels.

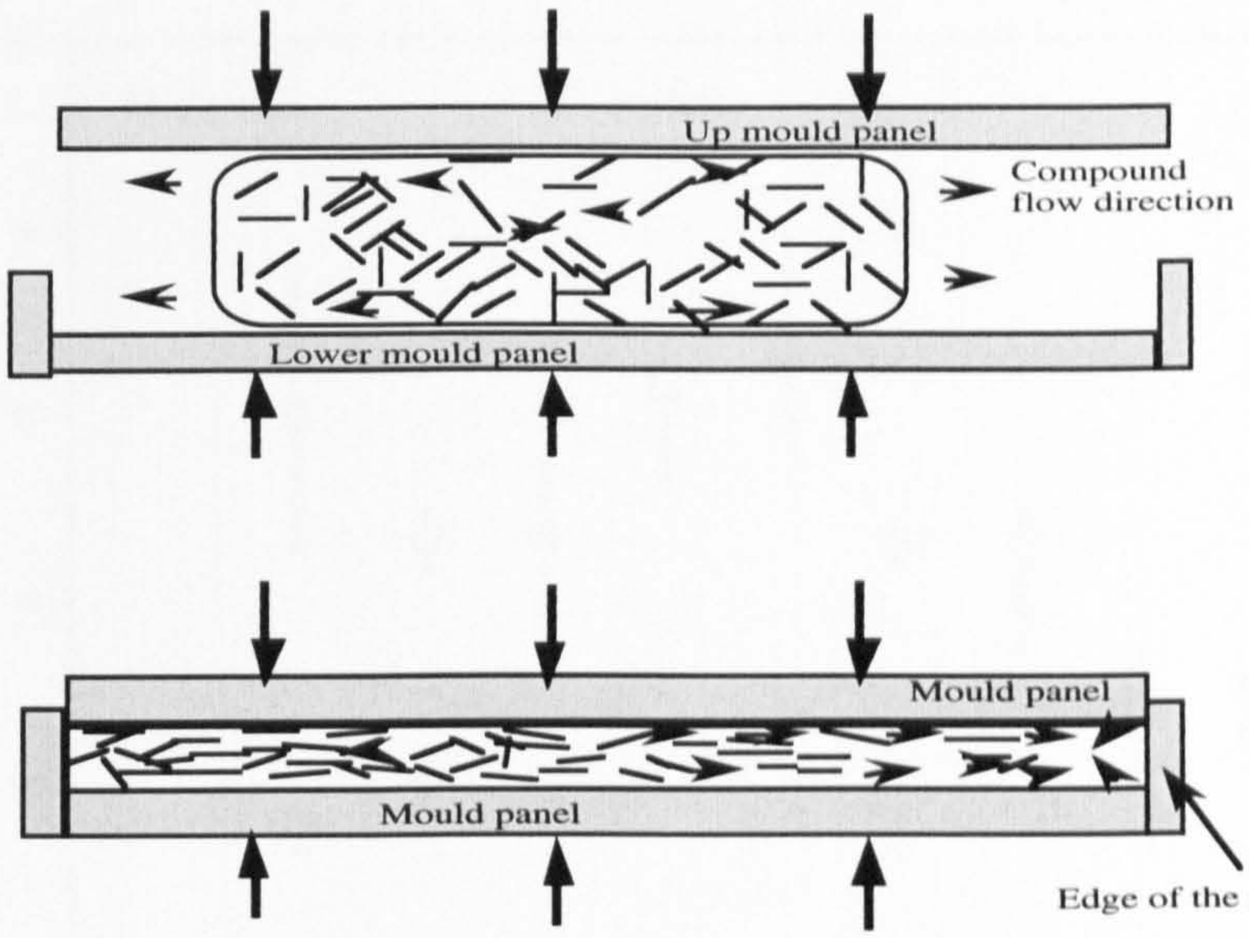

Fig. 5.3 Schematic view of the compound flow during the start and the end of the moulding at elevated temperatures.

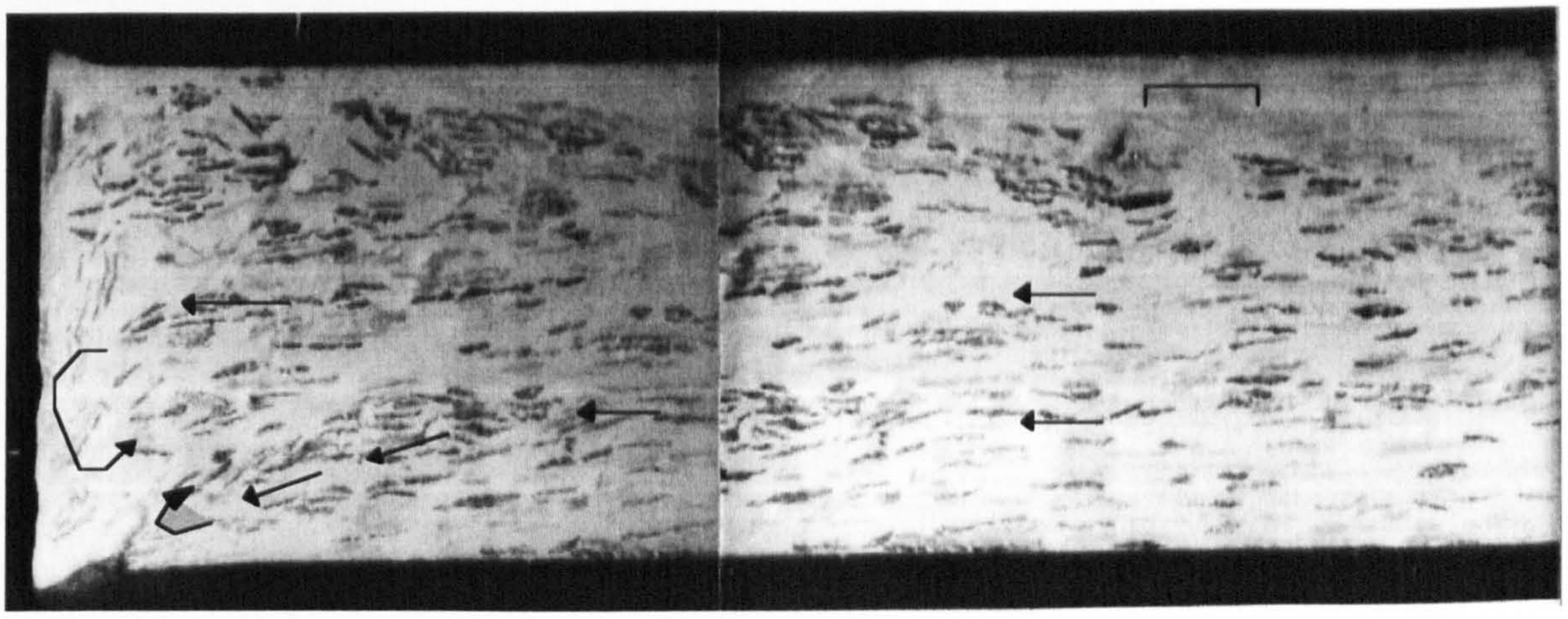

Fig. 5.4 The optical micro-graph of a CDMC with flow pattern of chopped fibre bundles throughout the cross-section of moulded panel with thickness of 3.1 mm. The orientation pattern of the fibre bundles indicated their travelling experience as a horizontal levelling distribution.

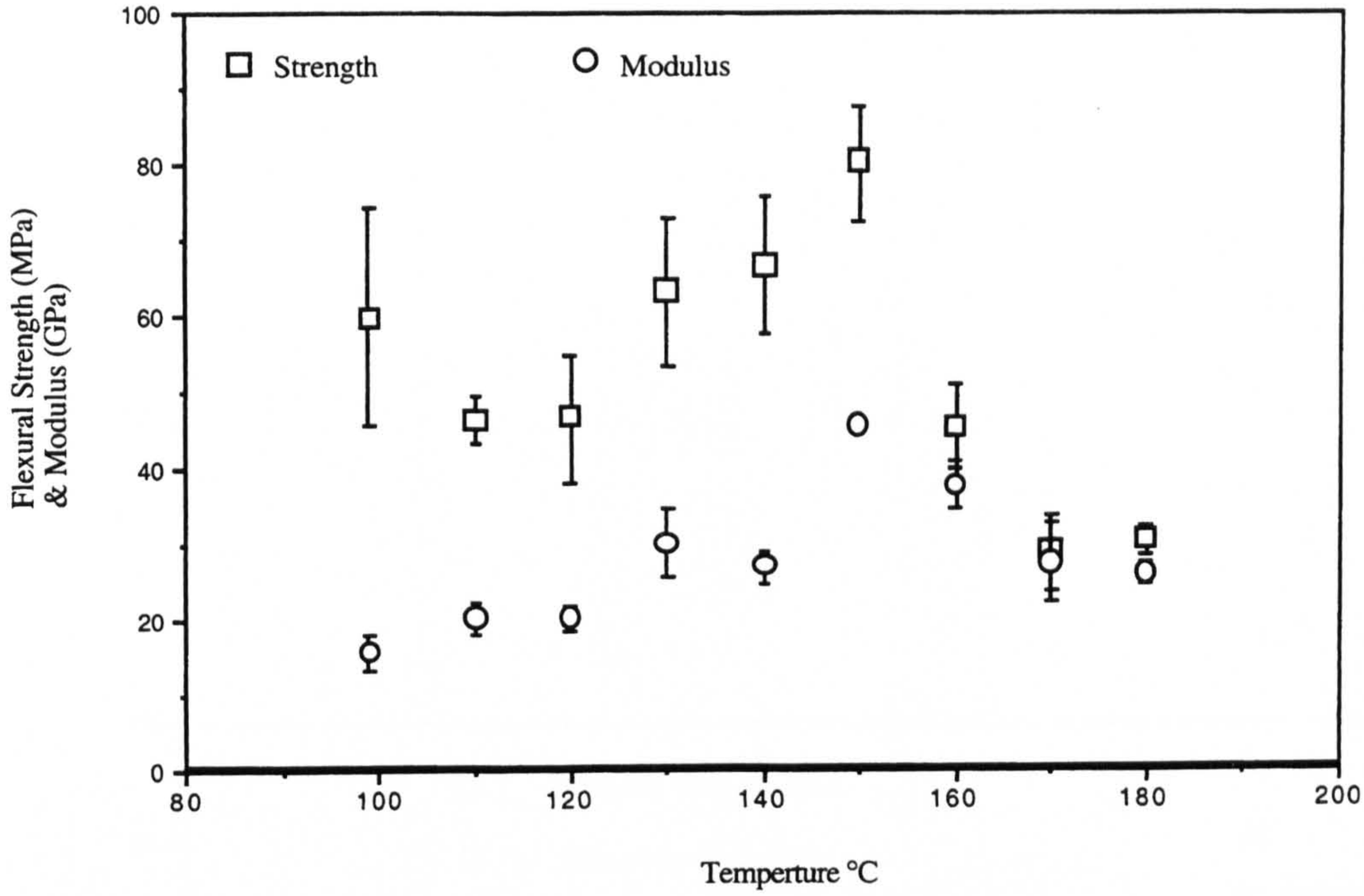

Fig. 5.5 Flexural properties of the CDMC were obtained under the moulding temperature from 99 °C - 180 °C (P_m = 80 Bar for 1.0 hour). The CDMC was with 22.6 %(vol.) glass fibres (length 12 mm).

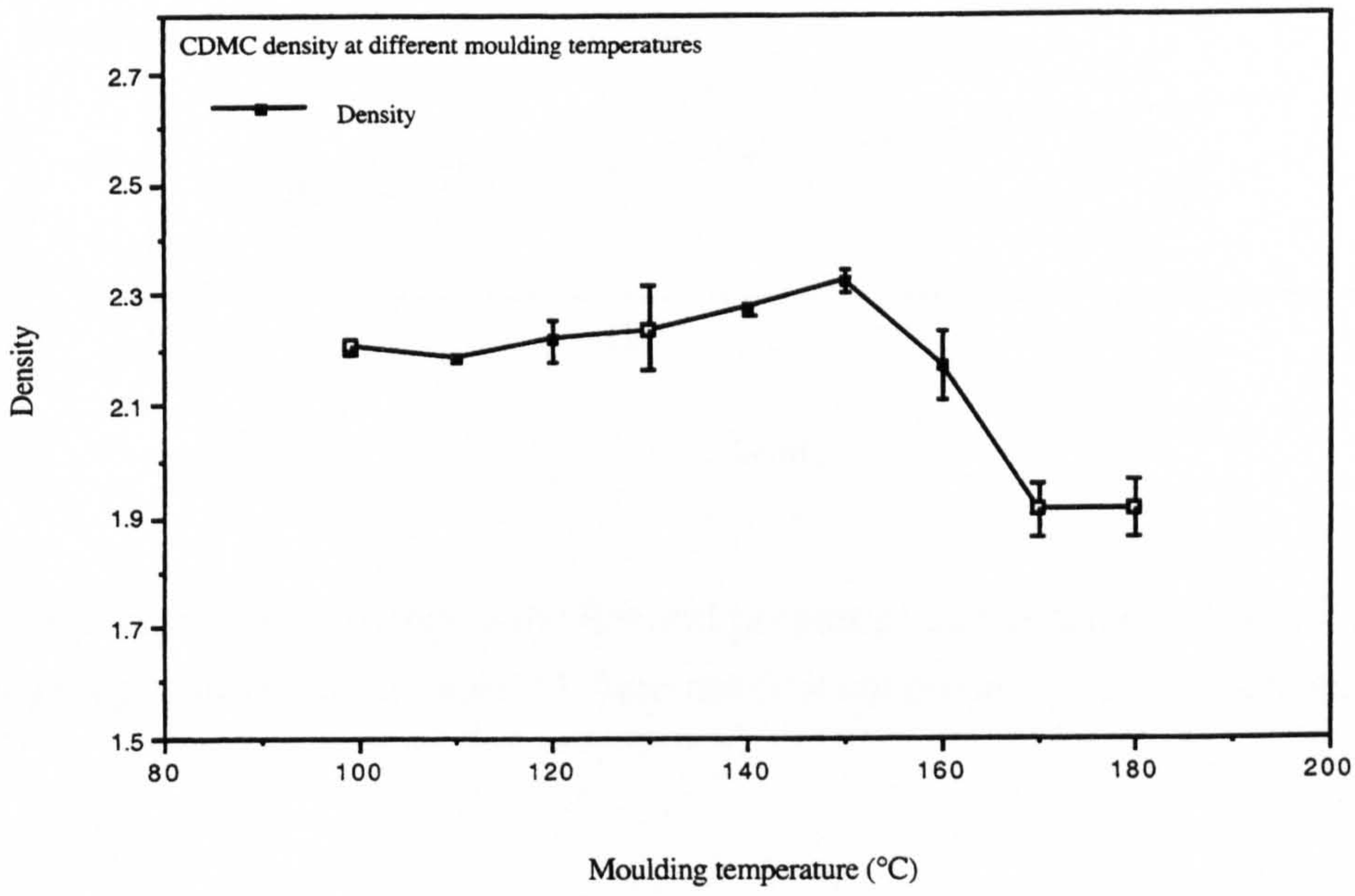

Fig. 5.6 Density (g/cm^3) distribution of the CDMC with the moulding temperatures from 99 ℃ - 180 ℃ (P_m = 8.0 MPa for 1.0 hour). The CDMC was with 22.6%(vol.) glass fibre (length 12 mm).

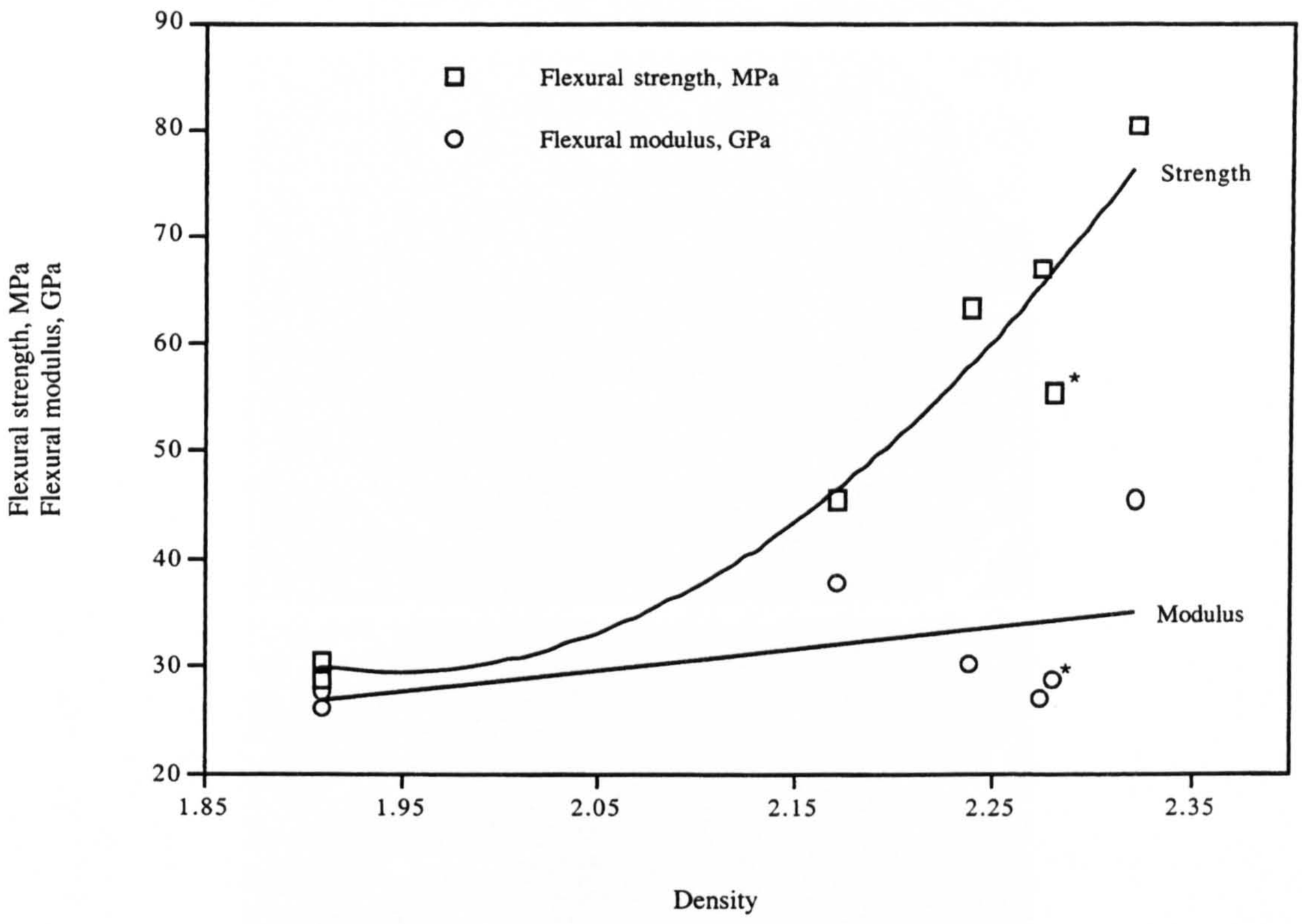

Fig. 5.7 The relationship between the flexural properties and densities of the CDMC. The flexural strength and modulus with " * " are the flexural properties of the pure matrix.

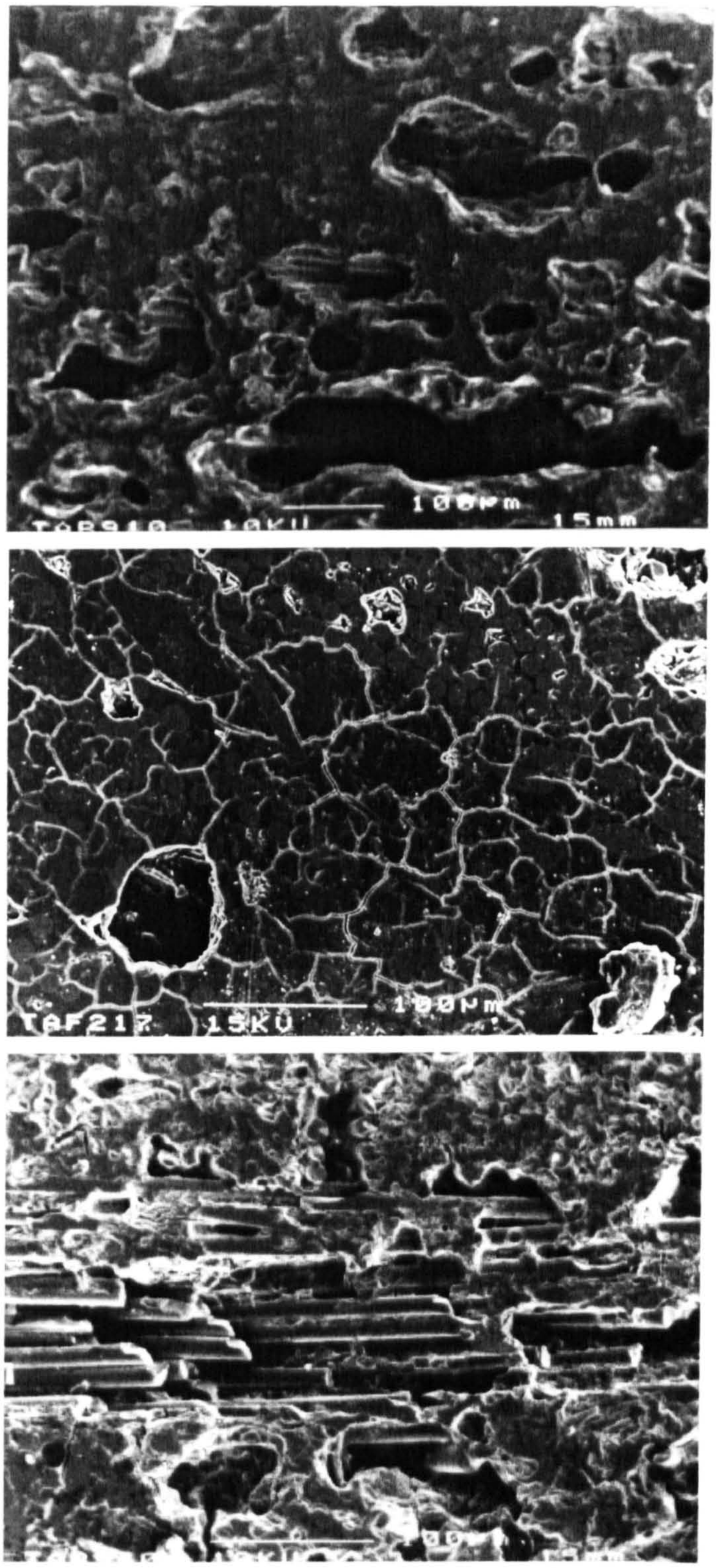

A: 180 °C
B: 150 °C
C: 120 °C

Fig. 5.8 SEM analysis of polished sections of specimens moulded at different temperatures, from top 180 °C (**A**), 150 °C (**B**) and bottom 120 °C (**C**), CDMC is with AR-glass (50/1) glass fibre.

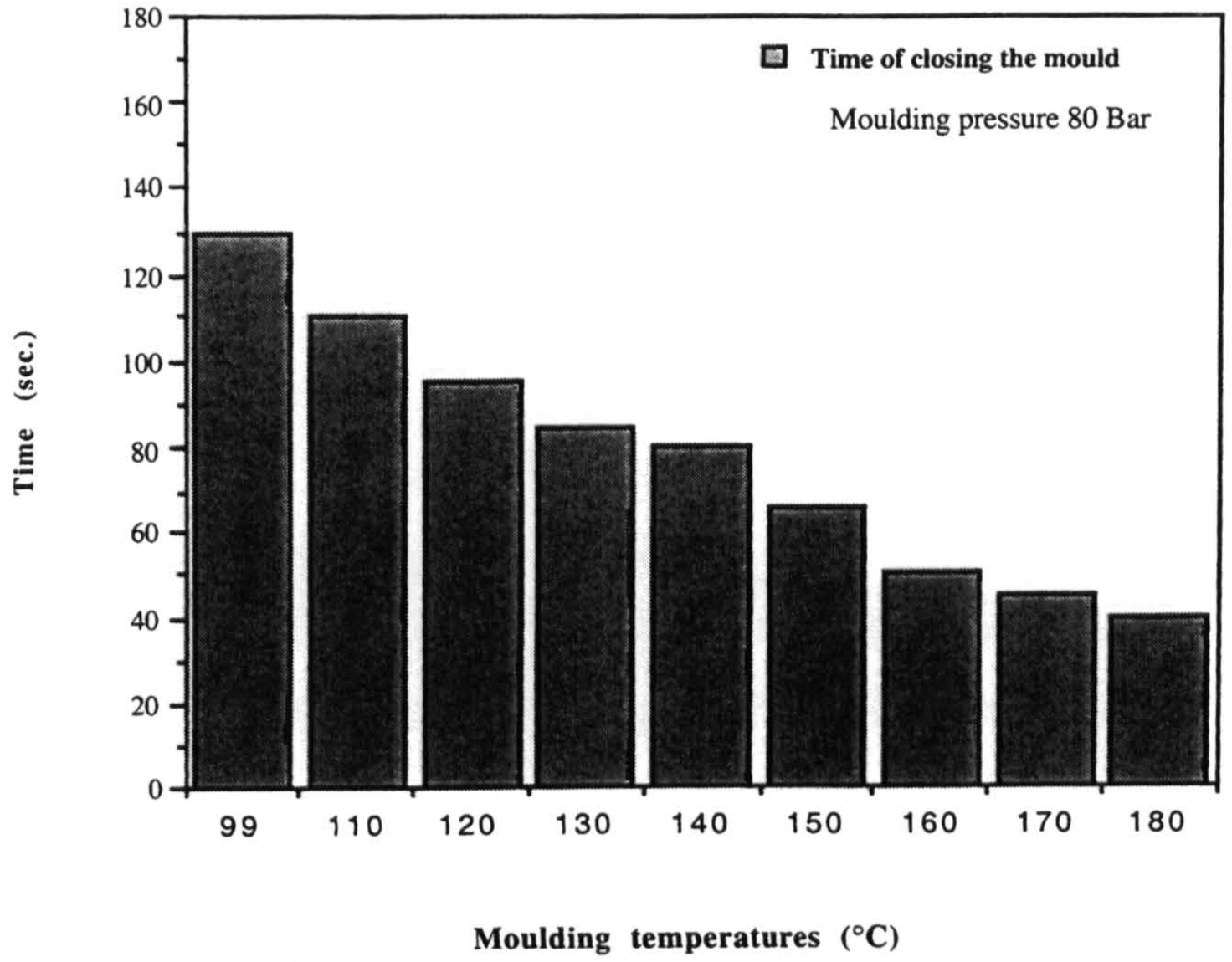

Fig. 5.9 Time needed to close the mould at moulding temperatures from 99 - 180 °C for the CDMC with 22.2%(vol.) glass fibre and the moulding pressure used was 8.0 MPa.

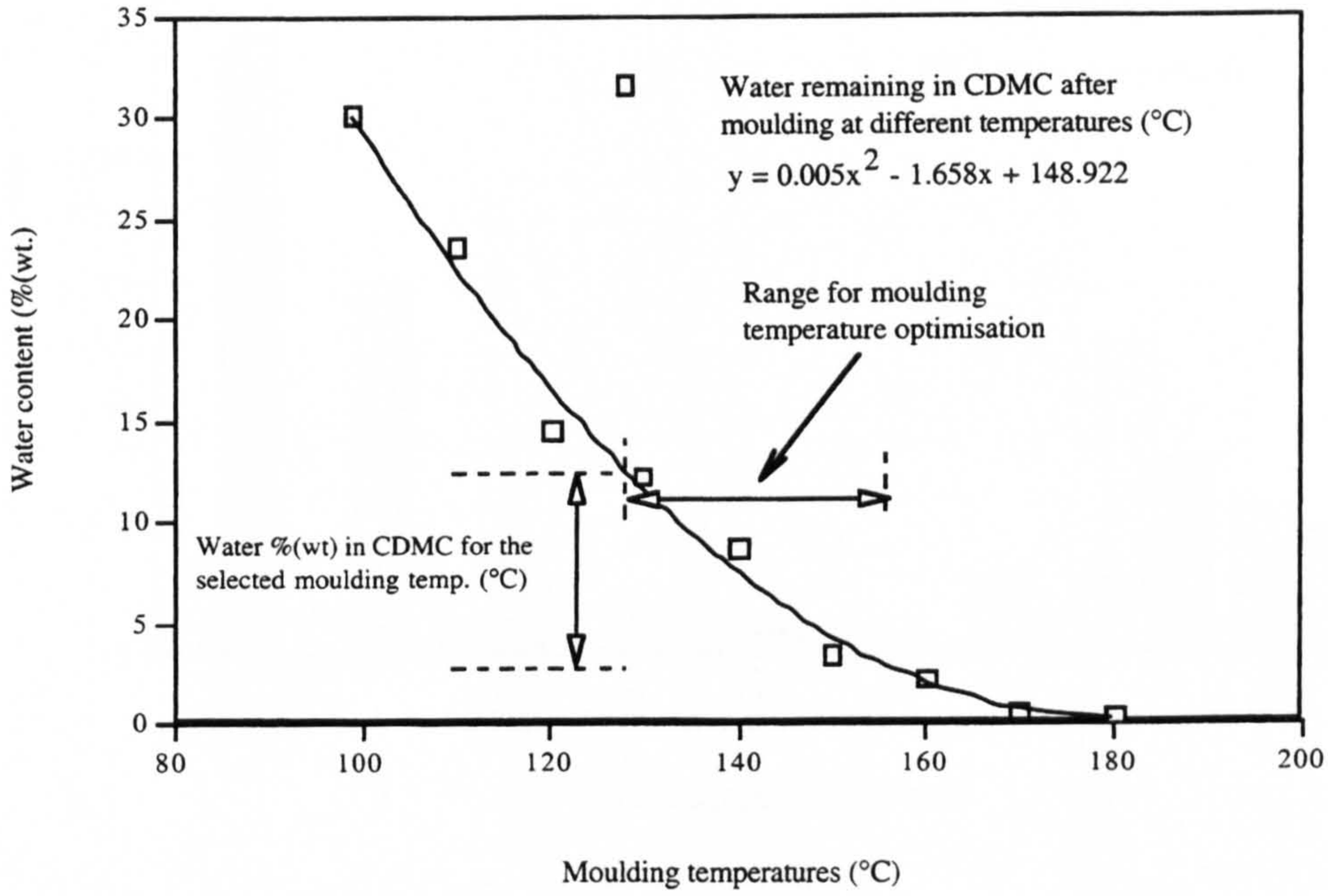

Fig. 5.10 Water remained [%(wt.)] in the CDMC after moulding at different moulding temperatures.

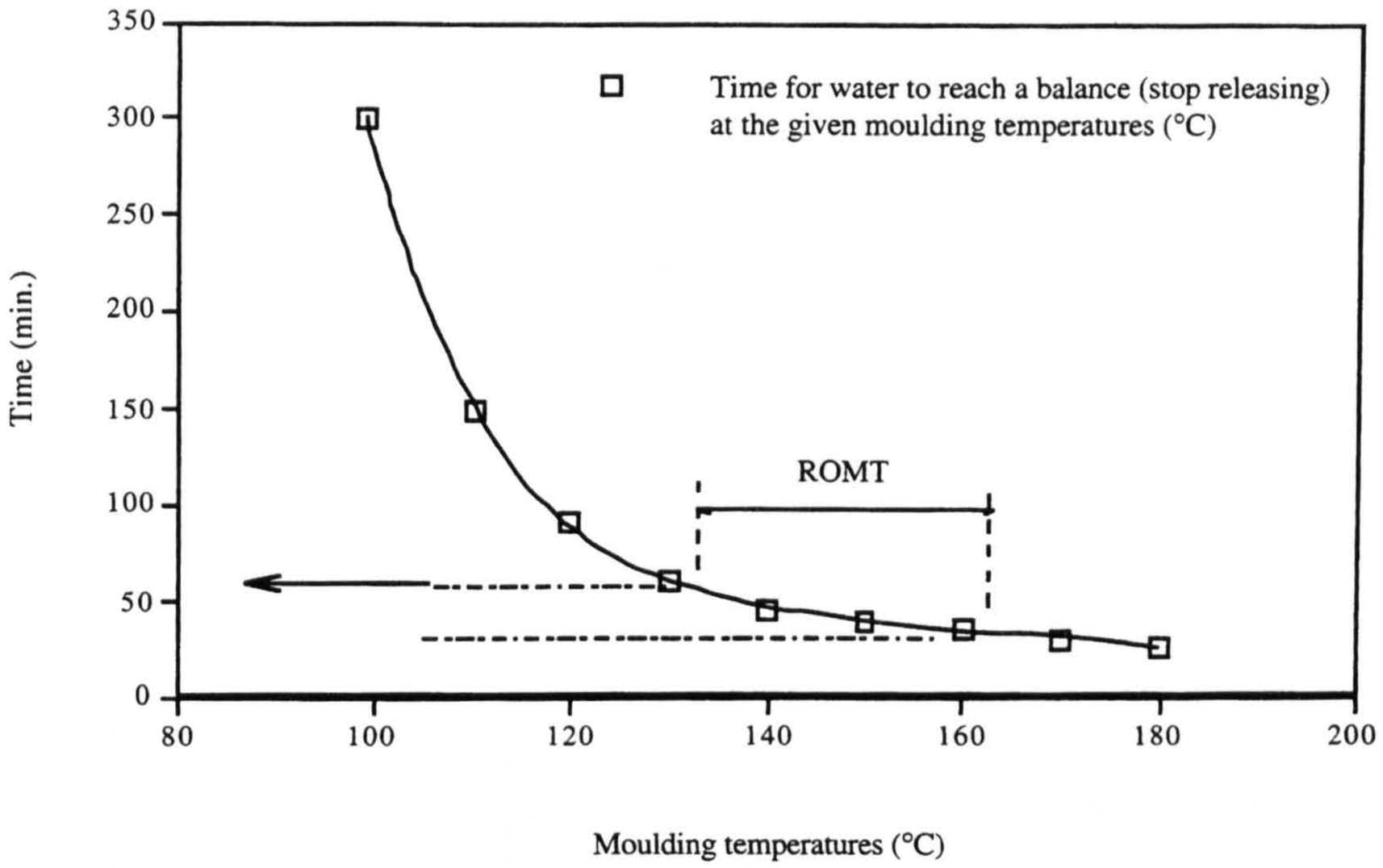

Fig. 5.11 Time (min.) to achieve equilibrium water content during moulding at the given moulding temperatures. The range for optimisation of moulding temperatures (ROMT) can be determined if 60 minutes is the moulding period.

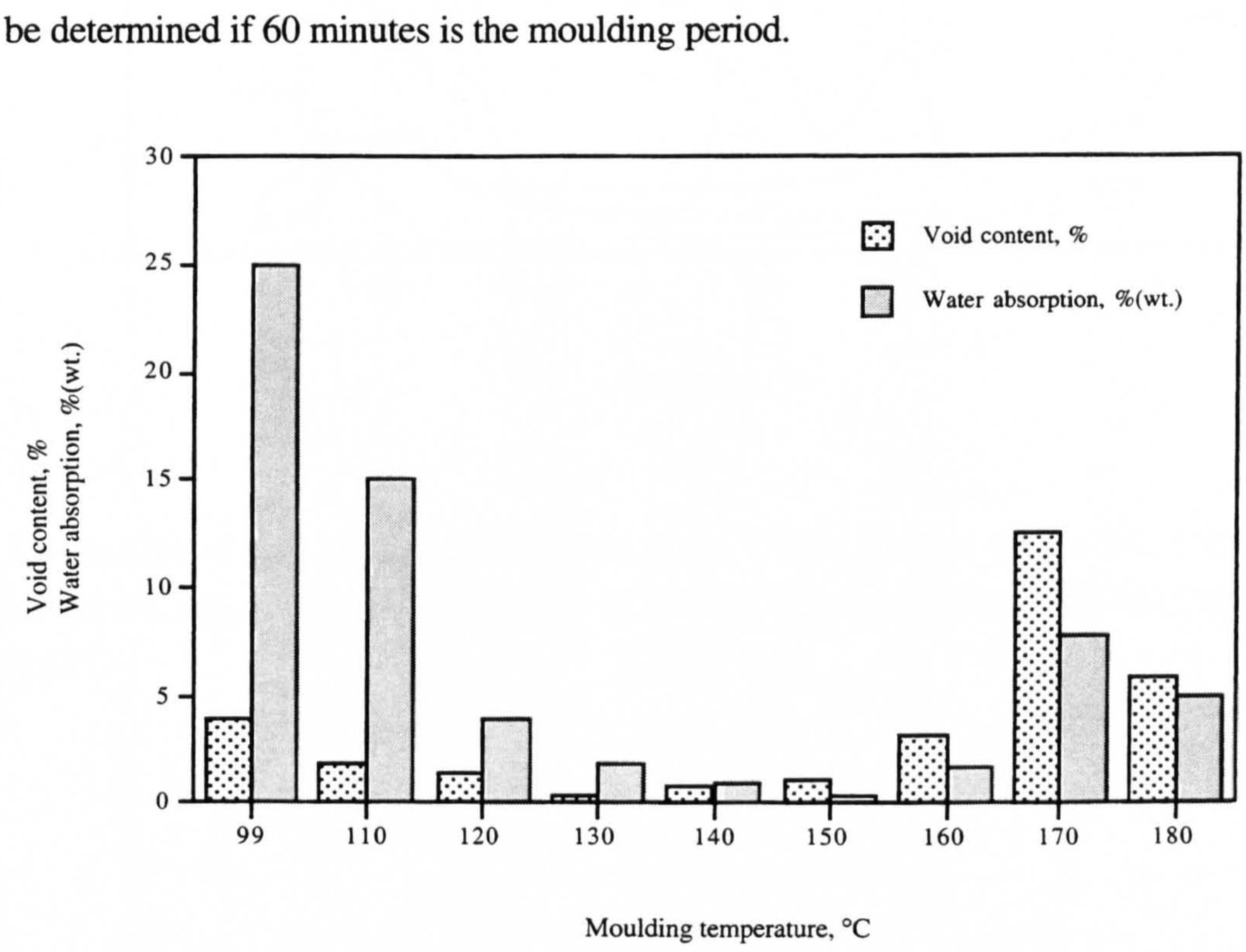

Fig. 5.12 The illustration of average voids contents and water absorption vs. moulding temperatures. The materials moulded at 99 - 180 °C (P_m = 8.0 MPa for 60 minutes), with 22.6%(vol.) glass fibre.

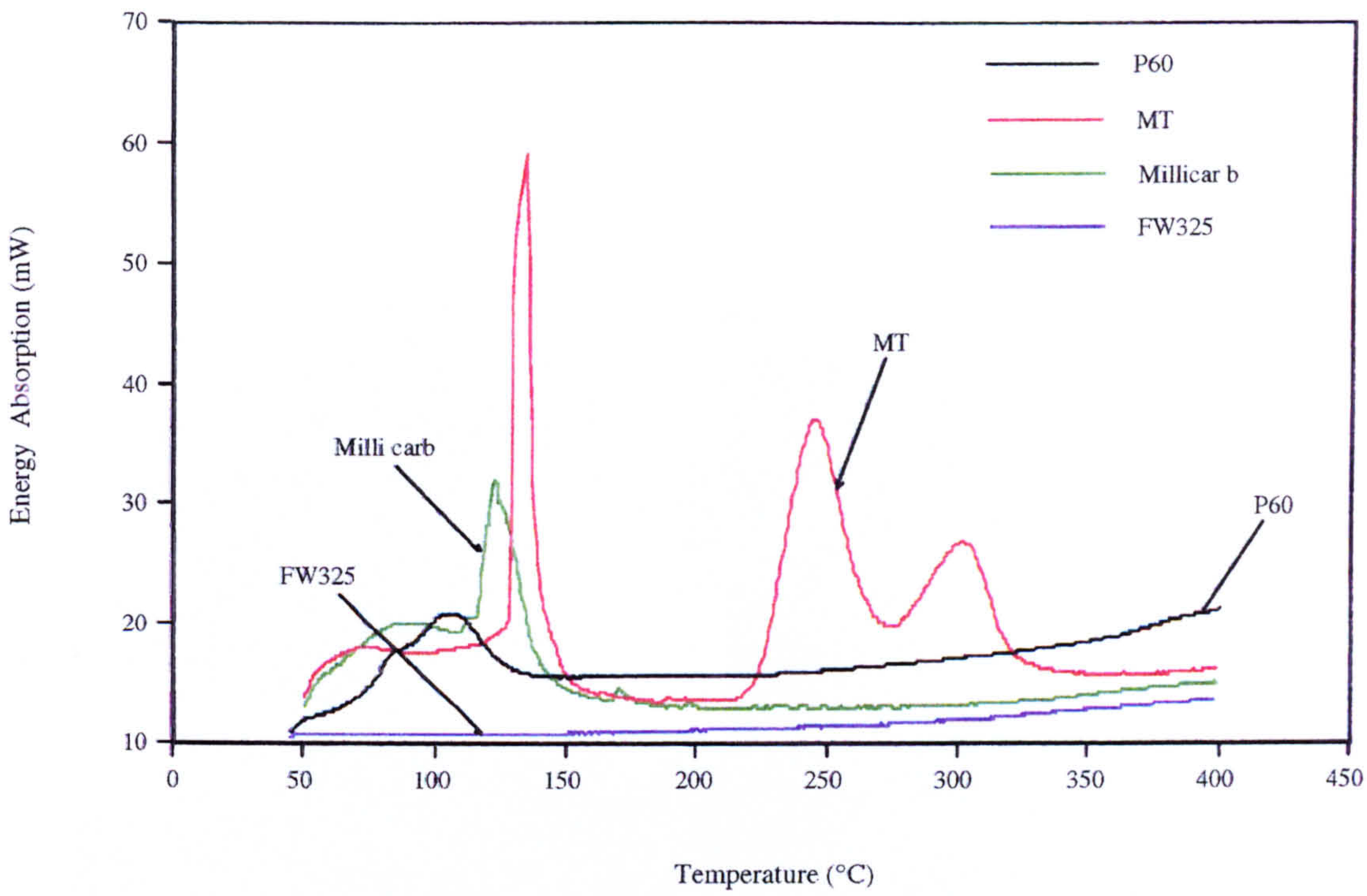

Fig 5.13 Results of DSC energy absorption of the fillers used in this work. They were examined in the temperature range from 45 °C to 400 °C. Materials are P60, MT, Millicarb and FW325.

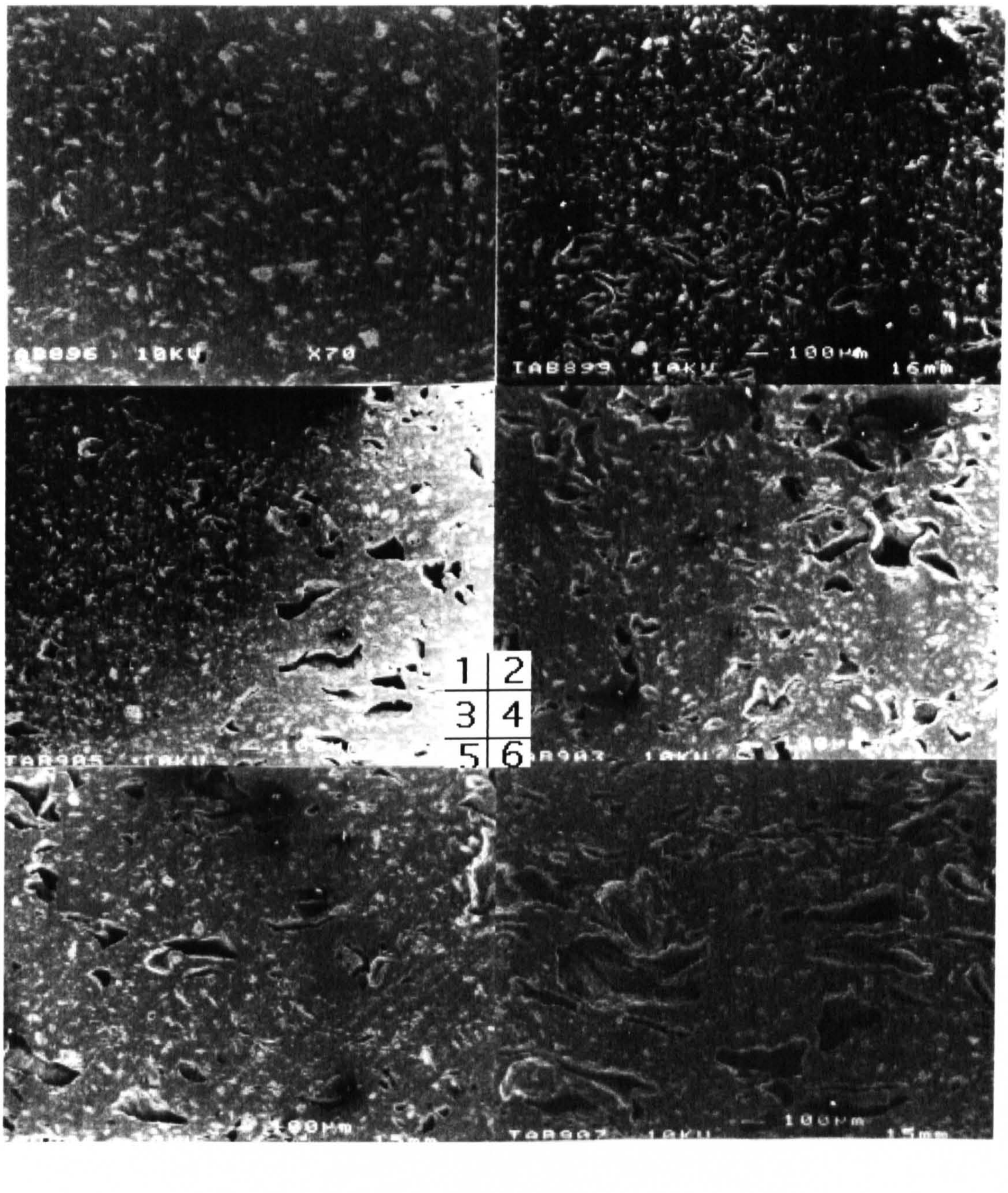

Fig. 5.14 SEM photographs of flexural specimens of pure ceramic matrix, No 1 to 6 is corresponding to their fractured specimens in Table 5.3. The matrix panel was moulded at temperature 130 ° (P_m = 8.0 MPa, 60 minutes).

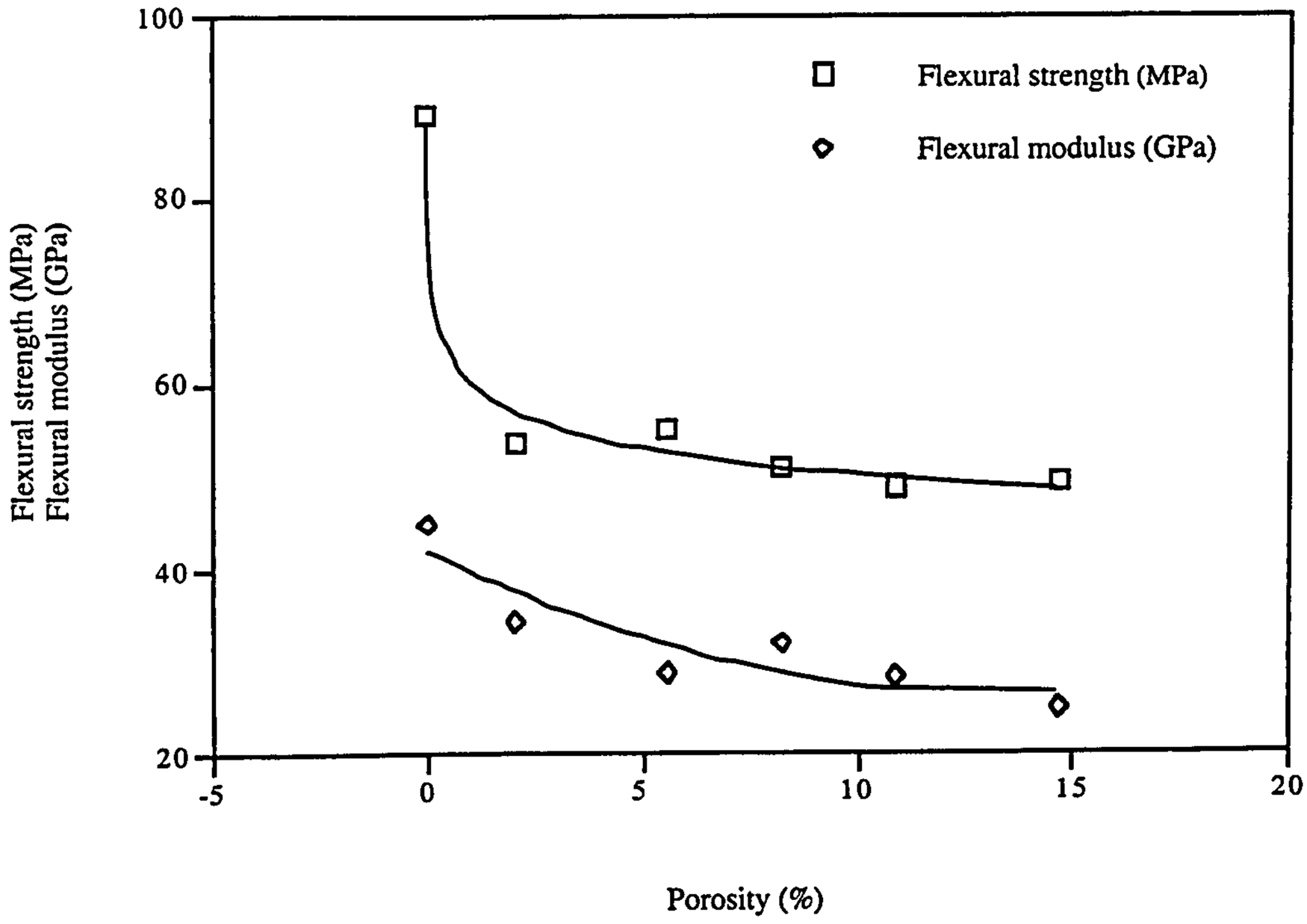

Fig. 5.15 The effect of the matrix porosity on flexural properties.

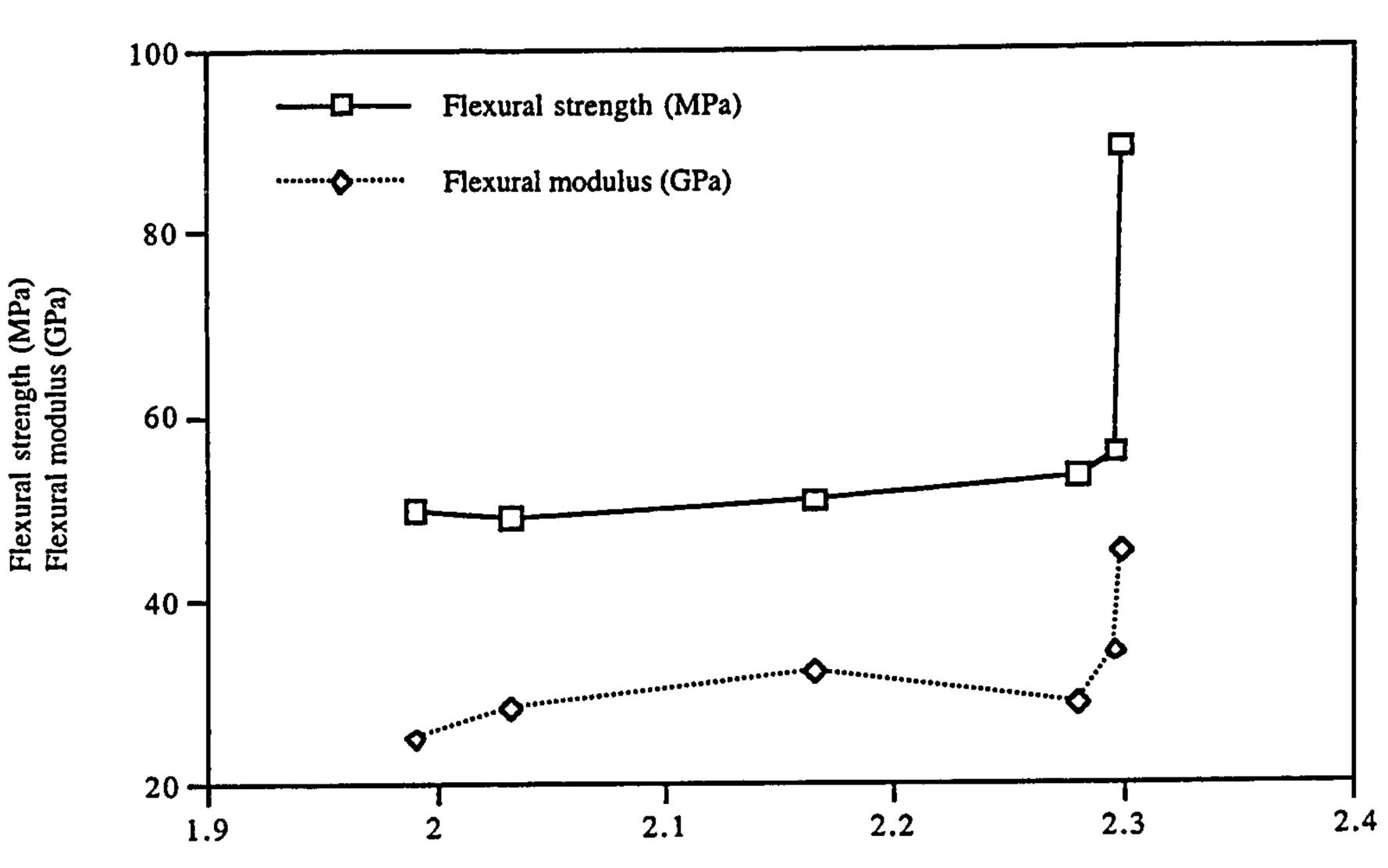

Fig. 5.16 The effect of the matrix density on flexural properties.

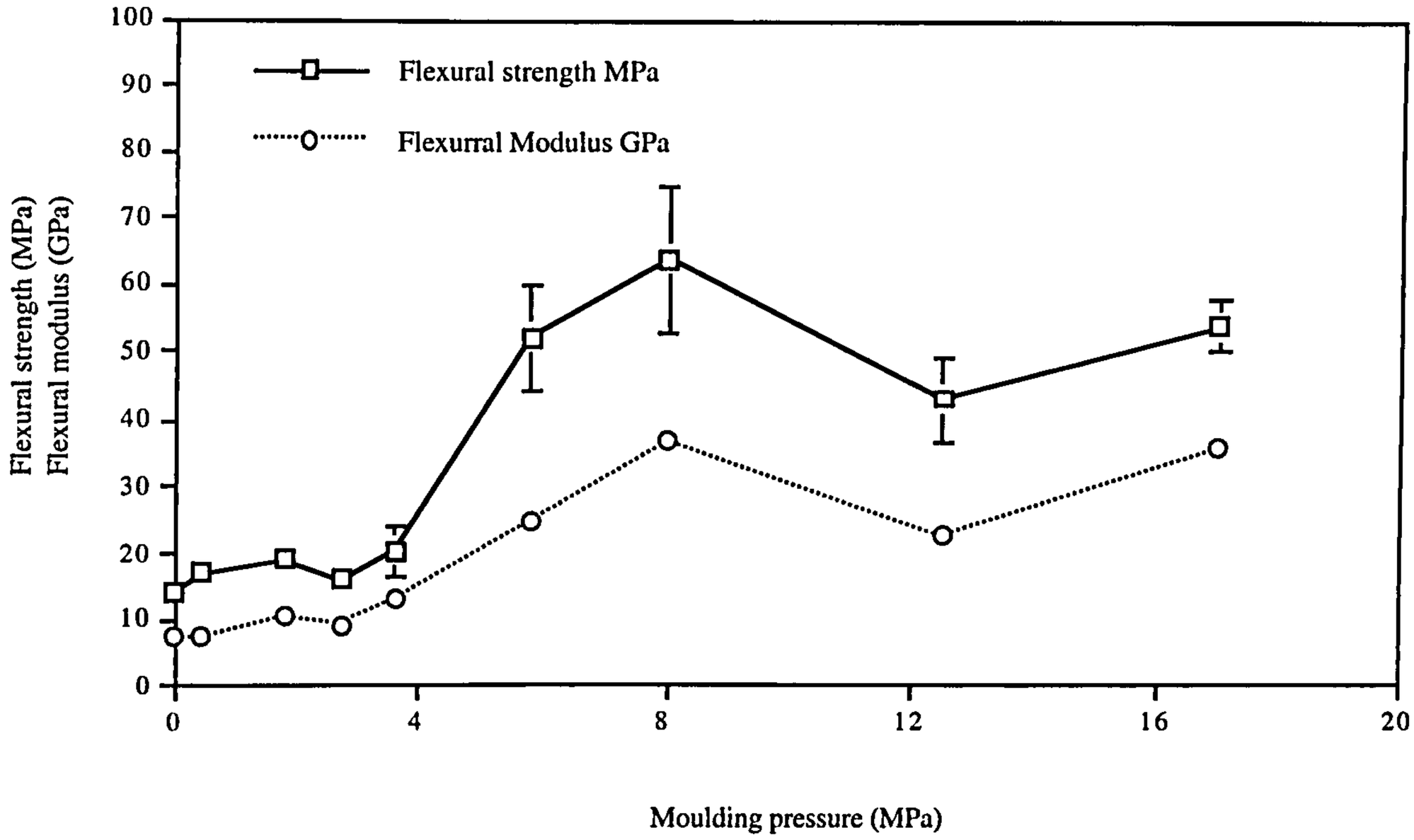

Fig. 5.17 Flexural properties of the CDMC with 15%(vol.)AR50/1 GF effected by the moulding pressures (from 0.0 to 17.0 MPa), T_m = 140 °C, holding time for 1.0 hour.

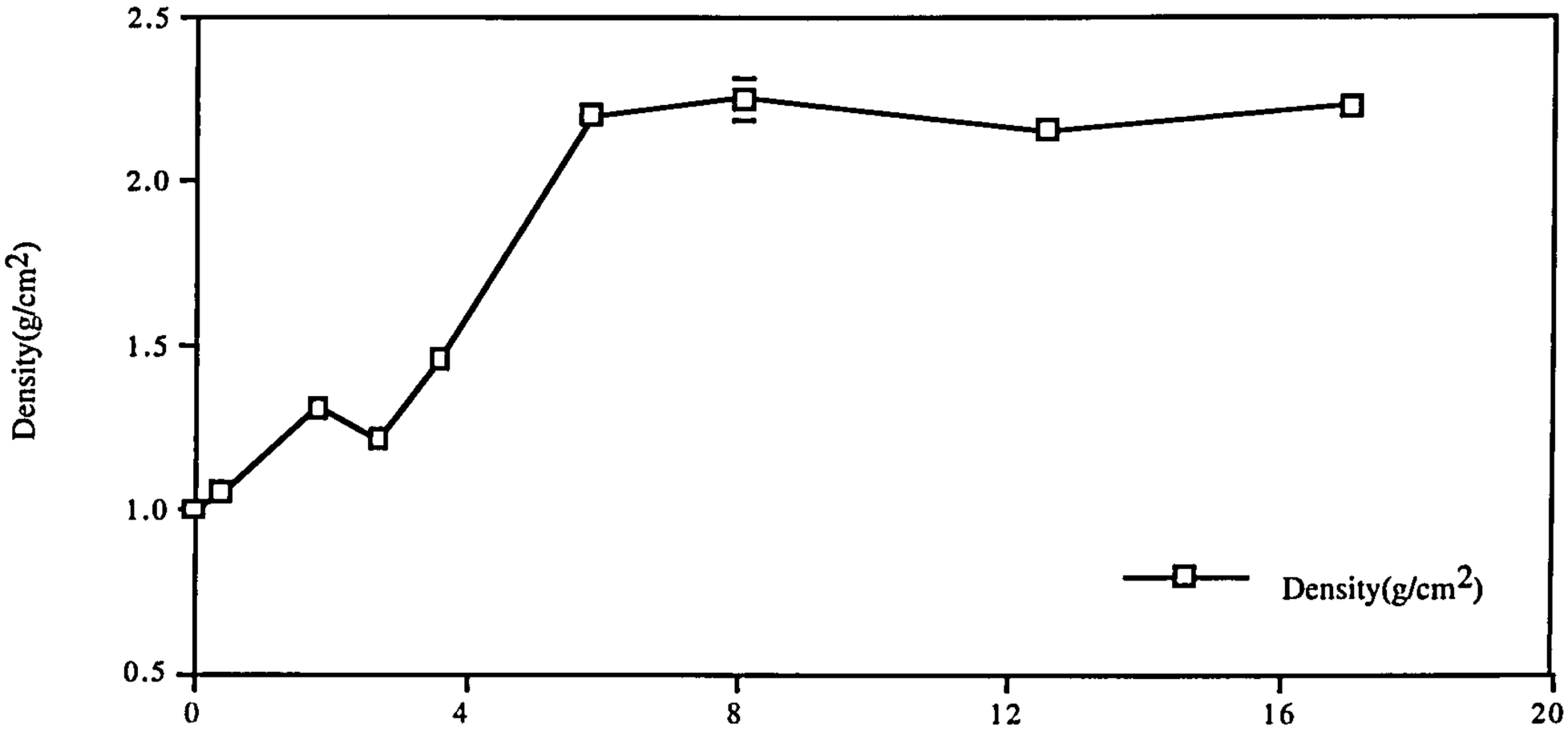

Fig. 5.18 Density (g/cm^3) of the CDMC panels effected by the moulding pressures. Moulding temperature was 140 °C for 60 minutes.

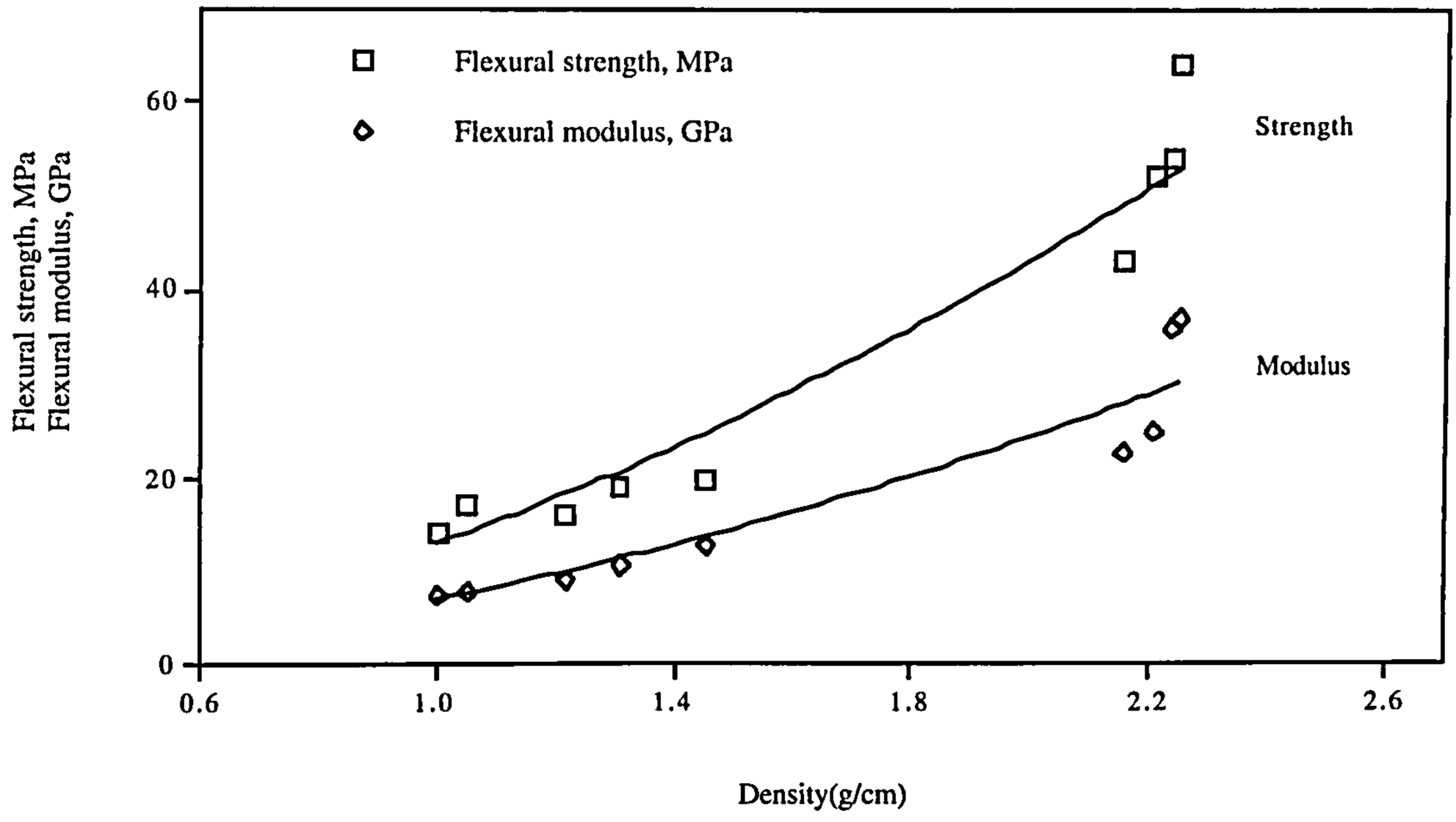

Fig. 5.19 Material flexural strength and modulus effected by densities which were generated by different moulding pressures.

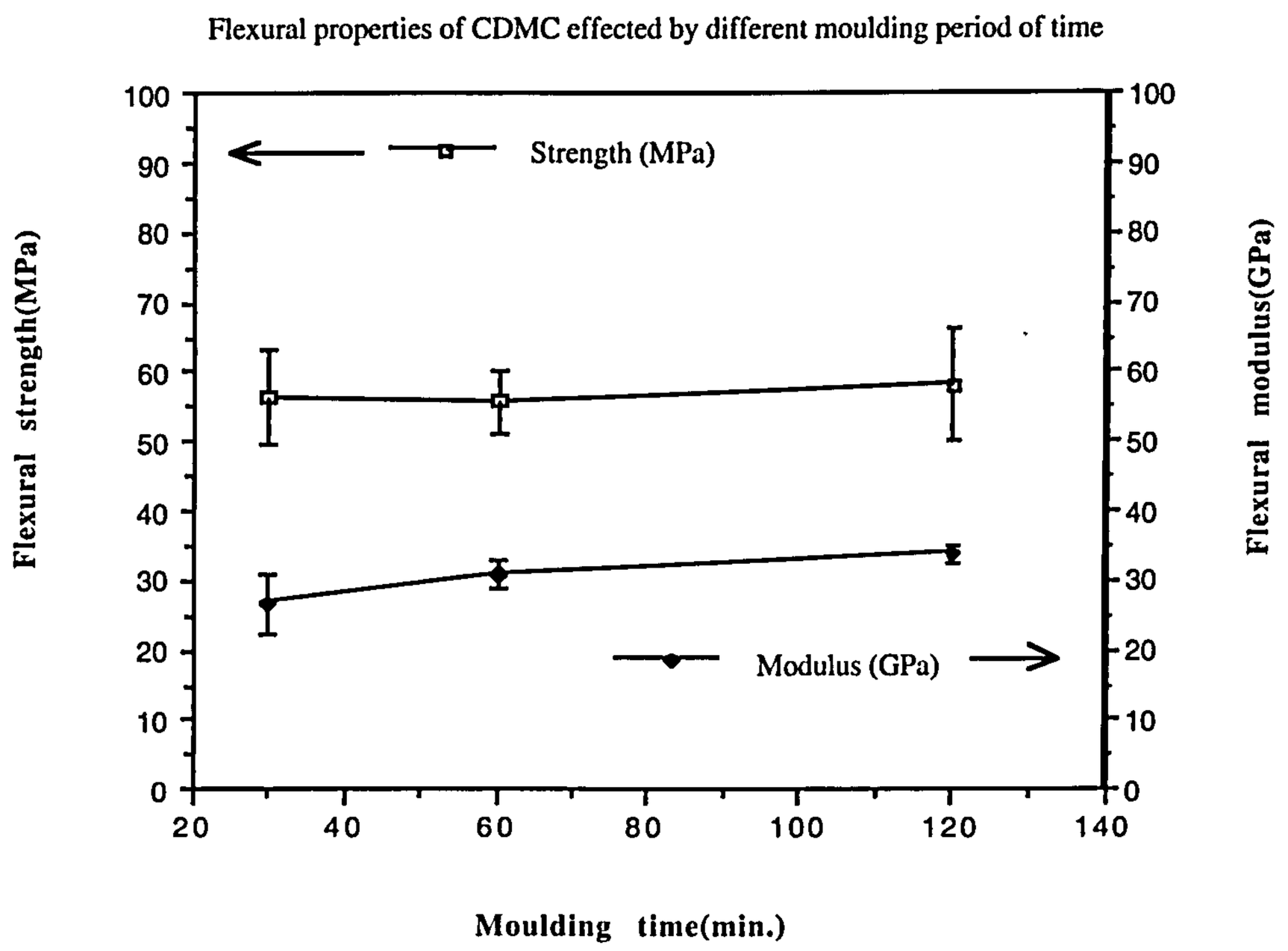

Fig. 5.20 Flexural properties effected by the mould holding time. Moulding temperature 140 °C, pressure 8.0 MPa. Glass fibre volume fraction was 15%(vol.) AR-glass fibre 50/1.

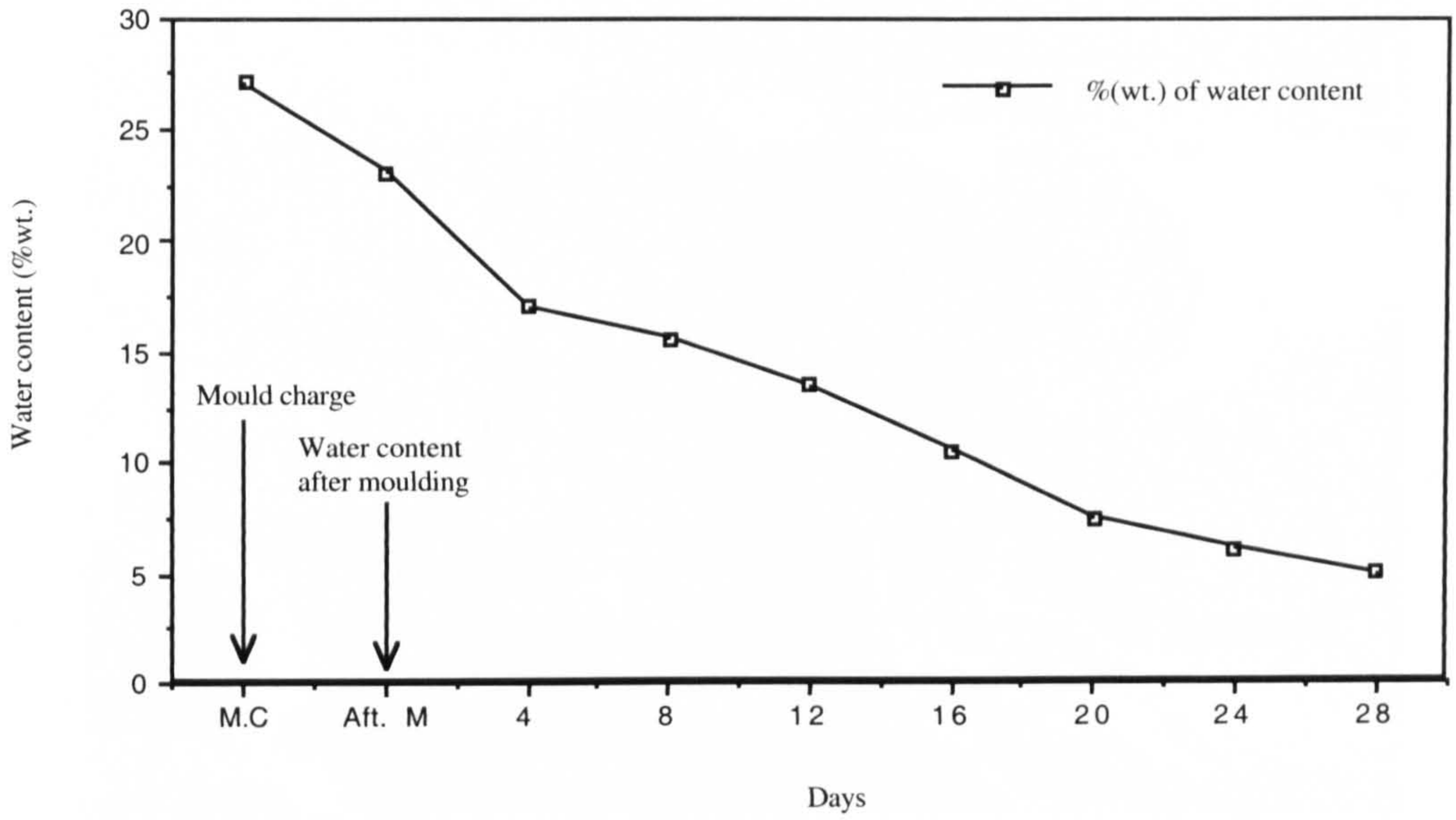

Fig 5.21 The average water content (%) of CDMC against time (days) after storage at room temperature. The CDMC with 22.6%(vol.) glass fibre moulded at 99 ℃ for one hour.

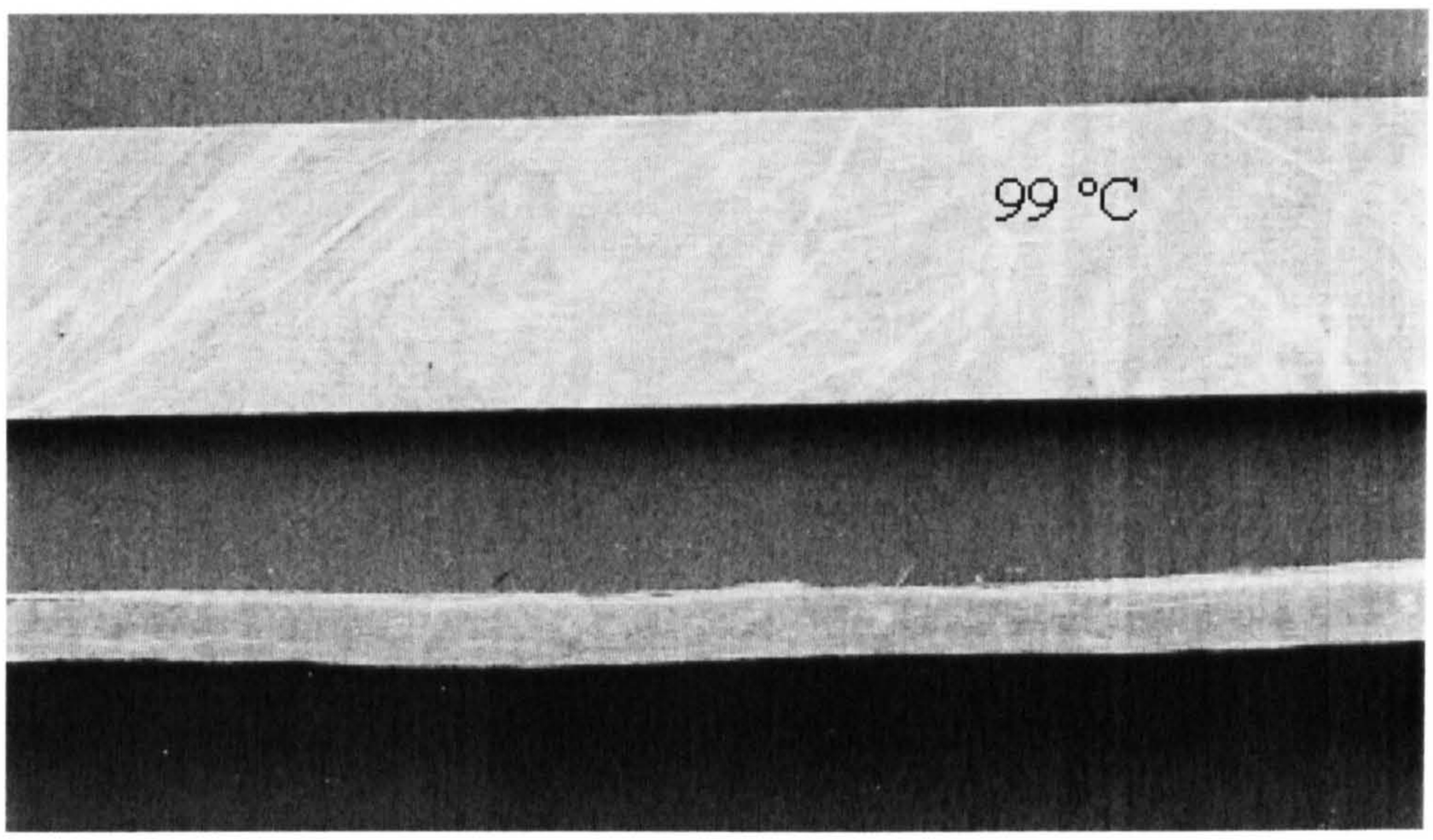

Fig. 5.22 The illustrated panel was moulded at 99 ℃ and room temperature post-cured. Distortion and dimensional shrinkage was observed after a mouth.

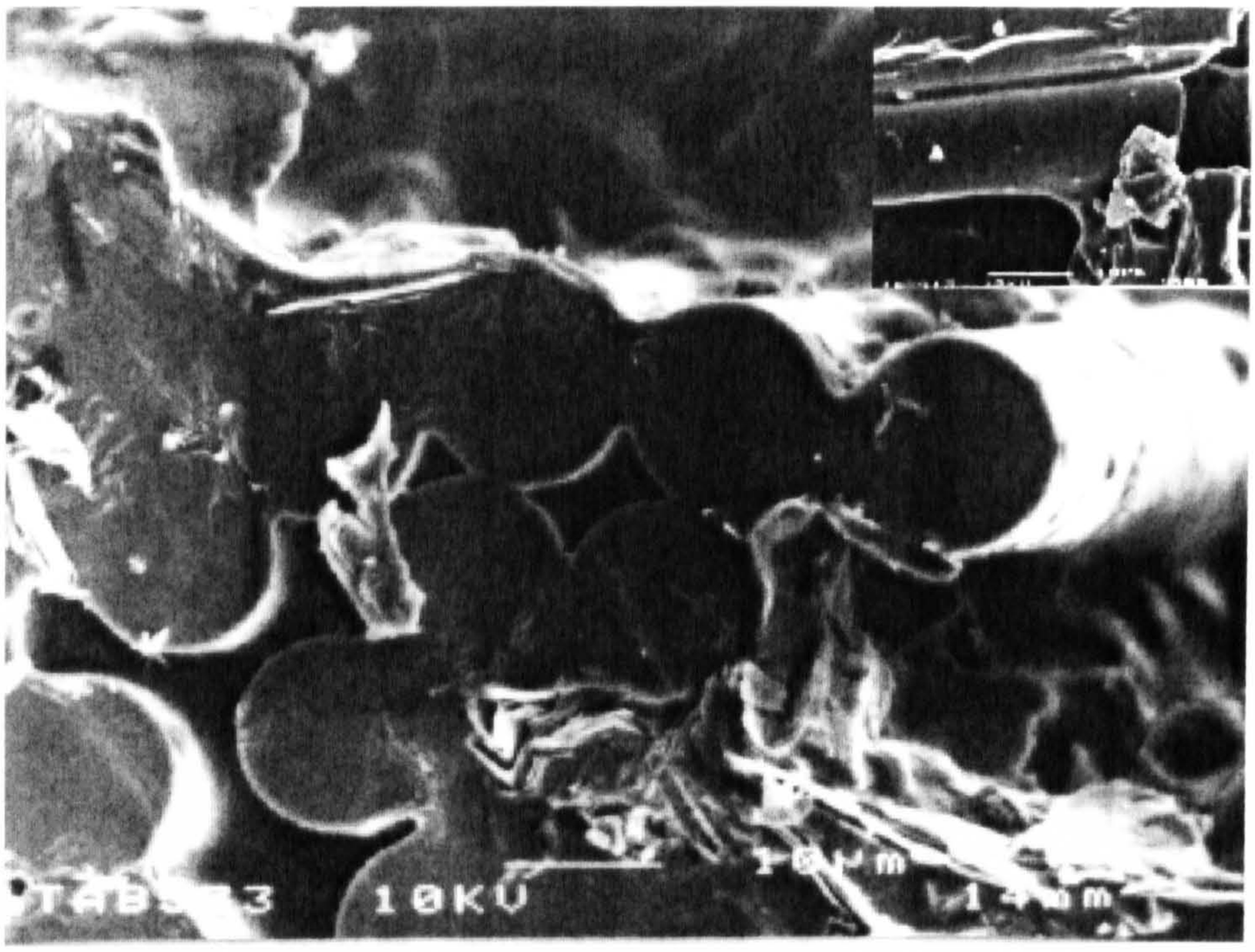

Fig. 5.23 The typical matrix shrinkage among fibre bundle in specimen moulded at 170 °C. The insert section shows a particular fibre surrounded with gelled ceramic matrix.

Fig. 5.24 Capillary forces during drying of a wet particulate material around glass fibre, produce inter-linking among fibres by the sol-gel formation of ceramic matrix.

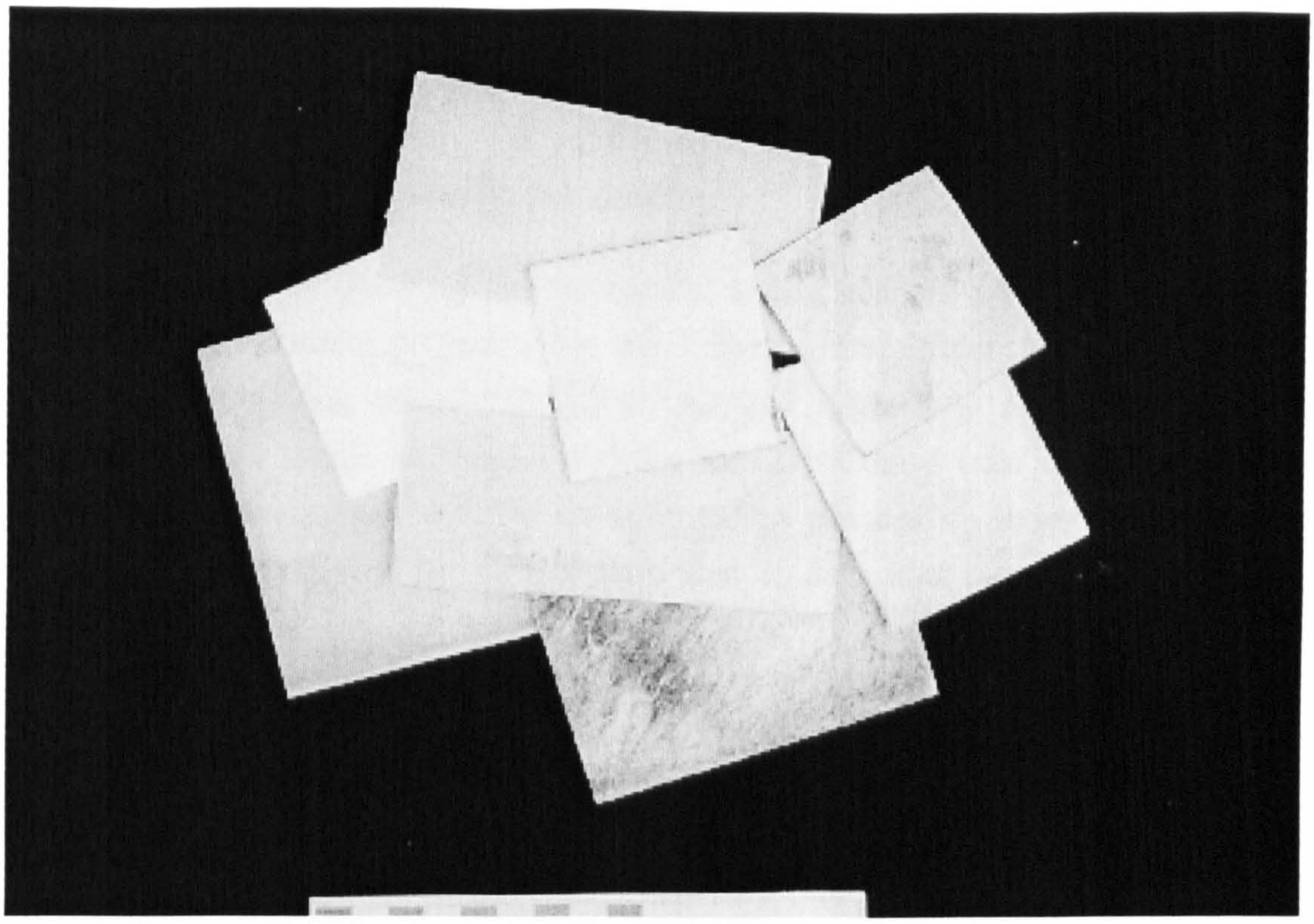

Fig. 5.25 Some of the moulded CDMC panels. They were all moulded at optimised moulding conditions.

Chapter 6

MECHANICAL CHARACTERISATION

6.1 Introduction

The general mechanical characteristics of the CDMC investigated and discussed in this chapter are affected by fibre volume fractions, fibre lengths and types, moulding conditions and fibre-matrix interfacial properties.

A schematic diagram showing the mechanical testing plan is presented in Fig. 6.1. Evaluation of mechanical properties for the CDMC with different fibre (AR) volume fractions and moulding temperatures (both AR and E-glass) is a major task in this Chapter. Flexural, tensile and impact tests for the CDMC have been carried out for the mechanical characterisation and for an optimisation process involving the compound formulation. All mechanical testing was performed 28 days after moulding, unless stated differently.

6.2 Results of general mechanical properties

The mechanical properties of the CDMC were varied with moulding conditions, glass fibre types and volume fractions. The properties were initially assessed by using flexural tests for E- and AR-glass fibre composites, with further tests being undertaken using tensile and instrumented impact tests for only AR-glass fibre 50/1 composites which exhibited superior properties to those with E-glass fibres.

6.2.1 Flexural properties of the E-glass fibre composites

The flexural stress-strain curves for the CDMC with 15%(vol.) E-glass moulded at 130 - 190 °C are presented in Fig. 6.2. The materials exhibit linear flexural stress-strain curves with the exception of the compound moulded at 130 °C. As moulding temperature increased towards 190 °C, the flexural strengths decreased. It has already been shown in

Chapter 5 that moulding at temperatures below 130 ℃ resulted in high water absorption and water retention linked to the probability of incomplete network formation. On this basis, therefore, it can be assumed that the optimum moulding temperature range for E-glass composites is around 130 °C.

The variations in modulus were less systematic. Modulus increased as the moulding temperature was increased from 130 ℃ to 150 ℃ but decreased from 150 ℃ to 190 ℃. The changes in modulus and strength are compared in Fig. 6.3 and the corresponding tested specimens are shown in Fig. 6.4 with a clear brittle failure when moulding temperatures exceeded 150 °C.

6.2.2 Flexural properties of the AR-glass fibre composites

The moulding temperature dependence of AR-glass fibres (50/1) composites was investigated by using a CDMC with 15%(vol.) AR 50/1 glass moulded over a temperature range 130 ℃ - 190 °C. A representative group of the flexural stress-strain curves is presented in Fig. 6.5. It can be seen that specimens moulded at 130 ℃ exhibit a high strain at failure. An overall comparison of flexural properties of the E-glass CDMC with different moulding temperatures is shown in Fig. 6.6. For this group of compounds, the modulus increases with moulding temperature until 170 ℃ and then falls at 190 ℃. Strength rises from 130 °C to 150 °C, but then begins to fall off. Fig. 6.7 shows the AR-glass specimens tested in flexure with moulding temperature changes. Fibre pull-out in these AR-glass fibre composites can be observed when the moulding temperature is below 150 °C.

The moulding temperature range for the best flexural properties with AR-glass fibre CDMC is in the range of 130 - 150 ℃ which is slightly higher than that of E-glass fibre CDMC.

6.2.3 Comparison of the E-glass and AR-glass fibre composites

The flexural stress-strain curves of the E and AR-glass fibre (50/1) composites are compared in Figs. 6.8 - 6.11 for moulding temperatures of 130 °C, 150 °C, 170 ℃ and 190 °C. For E-glass composites, the flexural stress-strain curves are linear until failure with the exception of compounds moulded at 130 °C. The moduli of both fibre composites are similar at the lower moulding temperatures, but AR-glass is significantly stiffer and stronger for the composites which were moulded at the temperatures over

150 °C. The comparison of composite strains at failure for both E- and AR-glass is listed in Table 6.1.

A general comparison of strength and modulus of the CDMC with AR and E-glass fibre for the moulding temperature range 130 - 190 ℃ is presented in Fig. 6.12 - Fig. 6.13. The AR -glass composites exhibit superior properties at all moulding temperatures apart from 130 °C.

The mechanical properties of the E-glass CDMC tend to be better at lower moulding temperatures (<130 ℃); AR-glass CDMC can achieve better properties at slightly higher moulding temperatures (140 - 150 ℃) for both flexural modulus and strengths. Overall the best moulding temperature for the material was selected at the range of 130 - 150 ℃ which was a compromise of material's water release, product appearance, mould-ability, ductility and final mechanical properties. Therefore, afterwards, most of specimens used for tests of fibre volume fraction and fibre lengths were moulded at 140 °C. The specimens moulded at this temperature normally exhibited good dimensional stability and appearance, and did not show evidence of over heating or excessively strong bonding between fibre and matrix.

6.2.4 Fibre volume fraction

Through the flexural property comparison, the AR-glass composites were found to possess better mechanical properties compared to the E-glass fibres composites. Therefore, further investigation such as volume fraction of glass fibre and fibre length was concentrated on the AR-glass fibres (50/1 and later on 62/2).

Volume fractions of the AR-glass fibre in the compound were prepared within a range of 5 - 22.6%(vol.) for the AR-glass 50/1. A further comparison of AR50/1 and AR 62/2 glass composites will be discussed in following Chapter. The flexural strength and modulus are shown in Fig. 6.14. The samples were moulded at 140 °C. The strength increased consistently with increase in fibre volume fractions, but the modulus was only slightly changed.

6.2.5 Retention of the flexural properties

The flexural property retention for the CDMC was studied in two steps: firstly, the flexural properties of the ceramic matrix were tested over a period of two months, and then the tests extended to its composites later for a period of one year.

The data for flexural property retention in Fig. 6.15 is for pure matrix. And the data in Fig. 6.16 is for the CDMC with 22.6%(vol.) of mixed glass fibre. For matrix, there was a very slight increase in both stiffness and strength with storage time. For the composite CDMC, properties exhibited a period of initial fluctuation but showed a promisingly stable value for the stiffness and strength after approximately 70 days.

6.2.6 Tensile properties

Tensile tests in this chapter concentrated on examining the variation of properties due to moulding temperatures and fibre volume fractions, for compounds with AR50/1 fibre.

- Moulding temperatures

The effects on the CDMC's tensile properties by moulding temperature were investigated over the range of 99 - 180 °C. Typical tensile stress-strain curves are presented in Fig. 6.17 with the key data in Table 6.2. It can be noticed that the modulus of the material increased with moulding temperatures until 150 °C. However, the tensile strength remained approximately constant until 180 °C, while strain to failure decreased progressively with increase in moulding temperatures.

- Glass fibre volume fraction

The effects of volume fraction on tensile properties of glass fibres (50/1) moulded at 140 °C are presented in Fig. 6.18. With a glass fibre volume fraction increase, both tensile strength and strain to failure are increased steadily as shown in Table 6.3, but modulus decreases.

6.2.7 Impact properties

Instrumented falling weight impact tests for the CDMC were carried out and some representative force-time and energy-time histories for a typical ceramic moulding composite with AR50/1 glass fibre are shown in Fig. 6.19. The typical force-time curve shows that the load rises with time until to the point 'I' at which a fracture was initiated. As the force continues to increase to the maximum point 'P', cracks may propagate and followed at 'D' where the striker penetrates the specimen. The specimen continues to resist the striker until complete fracture. The energy-time history curve shows how energy was absorbed during the impact test.

The ceramic matrix contributes very little in the development of impact energy. But the matrix in a composite can influence the damage mechanism in impact by the way of delamination, debonding and fibre pull-out, which are dependent on fibre/matrix interfacial shear strength, which is controlled by moulding temperatures. Therefore, the main testing results were related to the moulding temperatures and glass volume fractions.

- Moulding temperatures

The force-time history and energy absorption of the CDMC with 15%(vol.) glass fibre moulded at different moulding temperatures of 130-190 °C are presented in Fig. 6.20 and Table 6.4.

Over the range of moulding temperatures used, almost all the composites presented brittle failure although the amount of energy absorbed was the highest at the lowest moulding temperature.

- The volume fraction of glass fibre

The energy absorption of the materials with different volume fractions of glass fibre are listed in Table 6.5. These indicate that the more glass fraction in the material, the better impact properties can be achieved as shown in Fig. 6.21. The force-time curve was a double peak for the higher glass volume fraction CDMC, but not for lower volume fractions. Peak force is not a linear function of volume fraction of the glass fibre, i.e. the peak force of 15%(vol.) CDMC is higher than the peak force of 22.6%(vol.) CDMC although the latter absorbed more energy.

Impact properties are a reflection of the material toughness. Here since the glass fibre volume fraction had an influence on the impact properties. The material toughness should also be related to glass fibre volume fraction in the composite. Specimens were shown in Fig. 6.22 with 15 %(vol.) AR50/1 glass fibre which were completely shattered. And Fig. 6.23 shows the impacted CDMC with 22.6%(vol.) glass fraction shattered in few pieces. The composites with lower volume fractions of glass fibre shattered in a similar way but into much smaller pieces compared with the high volume fraction composite and was difficult to collect them after test.

6.3 Discussion

6.3.1 Chemical property of the E-glass CDMC

E-glass fibre is more sensitive to alkali attack at elevated temperatures compared to AR-glass. Corrosion of glass has been studied previously: mostly with soda-silica glass using various concentrations of NaOH water solutions (Charles, 1958) or acid (Metcalfe AG and Schmitz GK, 1972) as the reaction media. The former also used extracts from metallic silicate-based cements (with pH > 11) in ambient temperatures as the reaction media. In this research, the corrosive condition for glass fibre encountered during moulding is high temperatures (> 100°C) and high pH (>11). Information regarding to glass fibre in corrosive conditions at both high temperature (>100 °C) and alkaline (pH>11) condition has not been reported.

The reduction in strength for the E-glass composite was observed in their flexural, tensile properties when the moulding temperatures were higher than 140 °C (Fig. 6.2 - 6.3). There is evidence from SEM studies on the CDMC fracture surfaces, that fibre corrosion has occurred at the higher moulding temperatures (i.e. 160 °C) for this composite. It is illustrated by Fig. 6.24 which shows pitting on the fibre surfaces. It is believed to be due to such fibre corrosion.

Aluminium-silicate networks are inherently non-stable in an alkaline medium and glass corrosion in alkaline media at elevated temperatures is inevitable. The corrosion observed in the E-glass fibre CDMC moulded at 160 °C is very similar to the outer surface of glass fibre exposed to boiling water for extended time, which showed a degree of pitting corrosion (Hogg, 1981). The pitting corrosion happened on particular area of the surface of the E-glass fibres was indicated by arrows. This alkaline corrosion may cause

significant changes in the interface by damaging the surface of glass fibre. It also weakens the glass fibre considerably.

The strong alkali medium (Na^+-OH^-) constitutes a high pH environment at elevated temperatures, which enables the dissolution of the glass fibre silicate networks. The equilibrium for the following chemical reaction is dependent on the pH and will be driven towards the right.

$$\left[-Si-O^-Na^+\right]+H_2O \Leftrightarrow \left[-Si-OH\right]+Na^+OH^- \qquad \text{C6-1}$$

The build up of OH^- further increases pH and can accelerate attack of the silica network as shown in C6-2:

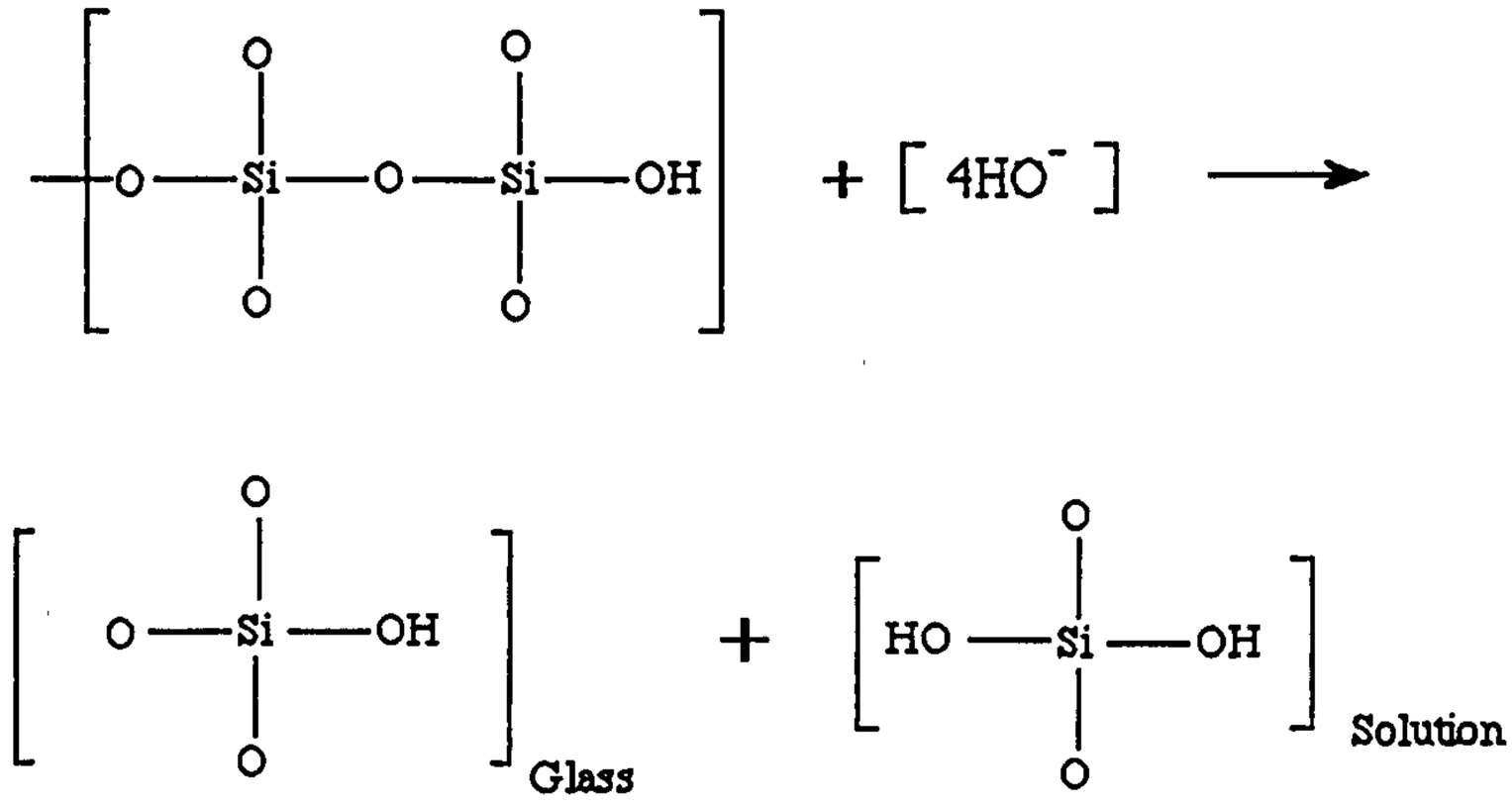

C6-2

The chemical reaction in an alkali environment involves a breakdown of the silica network by the OH^- ions, and eventually a congruent dissolution of all species in the glass. But at lower moulding temperature <130 °C, there is no observed evidence that severe corrosion happened to the E-glass fibre by alkalinity.

6.3.2 Mechanical properties of the AR-glass CDMC

When AR-glass fibre was used, they produced inferior results at the lower moulding temperatures (<130°C). When the temperature was raised to higher than 160 °C, the possible weak interface between the fibre and matrix started to disappear (interfacial bonding strength increased). This led to reduced strain before failure (Table 6.1 and 6.2). Both flexural and tensile stress-strain curves of the CDMC with the AR-glass fibre revealed an apparent ductility in the material processed at the lower moulding temperatures (i.e. 130 °C), but the materials became gradually brittle with rising moulding temperatures. For example, compared with the CDMC moulding at <130 °C, a shorter fibre pull-out level was observed in a tensile failed section of AR-glass CDMC moulded at 150 °C in Fig. 6.25. The insert shows the same specimen with much lower magnification. Although a higher moulding temperature gives benefits in production efficiency due to fast water release, it may not give enough time to allow the material to harden properly or to build up step by step. This may also lead to the production of a pores and a weak matrix and give more chance for the alkali to attack glass fibre vigorously.

6.4 Mechanical properties affected by fibre volume fraction

The flexural, tensile and impact testing results proved that all mechanical properties are influenced by the volume fractions of glass fibre. The flexural properties of the composite with 22.6%(vol.) Cem-FIL AR50/1 glass reached a strength of 82.0 MPa as shown in Fig. 6.14. The flexural modulus of the CDMC kept stable.

Compared with polymer composites, the tensile properties of the CDMC were less effected by the volume fractions of glass fibre. The matrix modulus, E_{CDMCm} is about 37 GPa and the modulus of AR-glass fibre (E_{ARf}) is about 80 GPa . The E_{ARf} is about 2 E_{CDMCm} . For phenolic or polyester DMC, the M_f (76 GPa) is around 20 M_m which is about 2 - 4 GPa for the pure resin cast plate. The expectation is to increase the strain to failure under the mechanical load in order to reduce the influence of flaws or defects remaining in the ceramic. Both stress and strain at failure of the CDMC were enhanced with an increasing fibre volume fraction as shown by the tensile results, in Fig. 6.18 and in Table 6.3. No significant improvements in the modulus were observed over the range of additional fibre fraction based on both tensile and flexural properties. Further increases in the fibre volume fraction could cause an increase in porosity in the composite owing to

the difficulties encountered in mixing during manufacture and in material flow during moulding.

The specimens with an increasing in volume fraction of glass fibre did show a significant improvement in the maximum strain at failure in comparison with the pure ceramic matrix. It was also suggested by Aveston et al. (1971) that the cracking strain of a ceramic matrix increases with fibre content and the presence of fibres delays the onset of matrix cracking in proportion to the fibre volume fraction.

6.5 Damage processes

Several factors contributed to the fracture mechanisms operating in the CDMC specimens including interfacial shear strength and residual stress.

6.5.1 Influence of the moulding temperatures

Some features of the damage behaviour are common to all the specimens moulded at the temperature range from 99 °C to 180 °C. Fig. 6.26 schematically shows the 3 different types of failure behaviours observed during the flexural tests.

Moulded at 160 - 180 °C, specimens presented a typical ceramic brittle failure (Fig 6.27-specimen moulded at 180 °C) on the fracture surfaces. SEM micro-graphs indicate the good bonding between fibre/matrix.

A tougher mode of failure was observed with panels moulded at 99 - 150 °C as shown in Fig. 6.28 and Fig. 6.29. Panels moulded at 99°C have complicated multi-delaminations. This might be caused by chopped fibres in the CDMC being distributed in two dimensions due to a pattern formed by flow to the cavity during moulding. More extensive fibre pull-out can be observed in these cases than those of specimens moulded at higher temperatures.

SEM analysis of polished specimens moulded at 99, 120 and 150 °C, illustrated pore link-up and apparent fibre debonding probably induced by matrix shrinkage before mechanical tests. Typical partial matrix cracking around the fibres is shown in Fig. 6.30. The specimen moulded at 150 °C and the circumferential crack patterns are an indication of

residual stresses arising from a fibre/matrix incompatibility or a mismatch during cooling after moulding in the interface owing to the difference in coefficients of thermal expansion. These could result in a lower interfacial shear strength due to the partial separation of fibre and matrix.

The partial separation between fibre and matrix may result from difficulties in removing the size coatings from the fibres at the lower moulding temperatures. The experimental works and SEM studies on the sizing surface of the glass fibre proved that the size on glass fibre would be pealed out partially when the glass fibre under pH >11 media and 99 °C for 24 hours. This is shown in Fig. 6.31.

Residual size could cover the surface of the fibre and act as a barrier layer to prevent the interaction between the fibre and ceramic matrix. When the moulding temperature was higher than 160 °C, the sizing system, composed of lower molecule weight polymers, may be assumed to be washed away, for it could not withstand the water/vapour (Plueddemann and Page, 1982; 1987) and an additional strong alkaline attack. Thus the glass fibre would present a bare surface to the silicate matrix slurry, and the fibre would become a nucleation point for accelerating the processes of the silicates polymerisation. This would explain the high bond strength as the moulding temperature increased. No evidence of fibre-matrix separation was found at the higher moulding temperatures as shown in Fig. 6.32.

6.5.2 Local fibre strength concentration

In general, composite consolidation degrades fibre properties and it becomes necessary to devise procedures that allow the determination of the characteristics of fibre strength S_c and a shape parameter for fibre strength distribution to be evaluated relevant to the fibres within the composite (Evens and Zok, 1994). In polymer composites, the matrix can be burned or dissolved without further degrading the fibres and then the bundle strength can be measured (Prow, 1986). But in ceramic composites, this process is impossible. An alternative to assessing strength in-situ uses study of the fracture surfaces of brittle fibres in brittle matrix.

The glass fibres in the CDMC SEM micro-graphs exhibit mirror zones on real fracture surfaces. A semi-empirical calibration has been developed that relates the mirror radius, a_m to in-situ individual fibre tensile strength, S_c given by (Evens and Zok, 1994):

$$S_c = 3.5(E_f \Gamma_f / a_m)^{1/2} \qquad \text{E8-1}$$

If AR-glass fibre E_f = 80 GPa,

$$S = 3.5\sqrt{\frac{80\Gamma_f}{a_m}} \qquad \text{E8-2}$$

Where Γ_f is the fracture energy of the fibre (Jamet, Lewis, Luh, 1984 and Eckel and Bradt in 1989), by measuring many fibres and then plotting the cumulative distribution, and the characteristic in-situ fibre strength, S_c can be ascertained. This fracture energy can be difficult to obtain in the case of chopped fibres randomly oriented in the CDMC. Some of these fibres have been displayed in Fig. 6.33 (A, B and C). Table 6.6 shows the relationship between mirror diameter a_m and the moulding temperatures. Fig. 6.34 schematically shows the fracture mirrors on top of the fibres.

6.5.3 Residual stresses

Analysis of the matrix SEM micrographs shows that although those voids in the specimens moulded at more than 170 ℃ varied in size and shape, there was no crack connected with them. The porosity allows shrinkage to be accommodated and hence no matrix cracking is nucleated. For the parts moulded at lower temperature such as <160 °C, cracks were observed both before and after the specimens were tested. There are three different matrix conditions:

- The specimens moulded at 160 - 180 ℃: significant level of pores/voids in the specimens, but almost no cracking associated with them.
- The specimens moulded at 130 ℃ - 150 ℃: contained few voids. There were also a few cracks associated with these voids which connected with the partial interfacial debonding. Almost all voids were connected with fibre dense zones.

- The specimens moulded at the temperature 99 ℃ - 120 ℃: presented more cracking associated with fibre bundles and interfacial debonding. The cracks could be induced by residual stresses resulted from the mismatch in linear thermal coefficients of the constituent. This may be accentuated by incomplete curing of the matrix structure which is not strong enough to provide resistance to stress concentrations.

Depending on the types of coupling agents, the bonds produced between fibre and sizing system only have limited resistance to water even at the ambient temperature. Previous work showed (Plueddemann, 1978, 1988) that silane could delay the time of failure in water by over-thousand-fold, but all bonds would ultimately fail in the extensive tests. The differences among formulations in terms of fibre and matrix were not that tremendous, but there were still two aspects have to be considered that impinge on stress that builds up in the material.

- Glass fibres have a dense structure (density: ~2.7). The density of the matrix is constantly changing due to water evaporation from about 35 - 40 %(wt) to about 25 to 0 %(wt.) which itself also varies according to moulding temperature. Therefore, the thermal coefficients of expansion of the matrix during cooling must change and result in stress concentration around fibres. The silicates depositing with water evaporation and matrix shrinkage, generated matrix cracks.

- When moulded below 160 °C, the size may protect the fibre from the corrosive matrix, which may produce lower bonding strength. The adhesion between fibre/matrix is not strong enough to prevent cracking, because the sizing system only provides a weak interface. When the interfacial strength of a fibre / matrix bond was exceeded by stress concentration produced by differences of coefficient of matrix expending/shrinking during a moulding or cooling, the cracks would occur around individual fibres or fibre bundles in the matrix. This has been proven beneficial for improving the toughness of the composites by many researchers (Ashby 1978; Aveston, Kelly 1973 and Haug and Schafer 1994).

In addition to the different thermal coefficients and the expansion/shrinkage of the matrix and glass fibre, the moulding process caused a water evaporation resulting in a large amount of volume reduction or shrinkage. The "clamping" of the fibres by the matrix was therefore conceivable. The stress generated by shrinkage of matrix, involving the water release process, therefore, needs more consideration. Here we can firstly work out the stress generated by the difference of thermal expansions between matrix and glass

fibres. The matrix shrinkage stress generated around the glass fibres may be solved in the future.

The difference in coefficients of thermal expansions between fibres and matrix leads to observable residual stresses in the composite specimens as a result of cooling from moulding to ambient temperatures. Phillips (1978) derived a expression for residual stresses in unidirectional brittle matrix composites (E6-3) and it may be used to work out of the thermal expansion of the composites as a brief indication of the thermal expansion:

$$\sigma_{residual} = \frac{E_f V_f (\alpha_m - \alpha_f)\Delta T}{1 + V_f\left(E_f / E_m - 1\right)} \qquad \text{E6-3}$$

If we use Ψ to represent E_f, V_f, and E_m, as following in E6-4,

$$\psi = \frac{E_f V_f}{1 + V_f\left(E_f / E_m - 1\right)} \qquad \text{E6-4}$$

Ψ is changes with V_f , the relationship between Ψ and fibre volume fraction V_f is listed in Table 6.7, which makes the following calculation easier if we have material's thermal data, α_m and α_f (coefficients of thermal expansions of matrix and glass fibre). Ψ is a number which connects with material's composition and elastic properties (unit GPa) for the interfacial area between glass fibre and matrix. If the elastic properties of fibre and matrix are fixed as in the situation of the CDMC, then:

$$\psi = f\left(V_f\right) \qquad \text{E6-4.1}$$

Therefore, the residual stress within the CDMC can be determined by material's composition, elastic properties and fibre/matrix thermal properties. Then E6-3 could be simplified as:

$$\sigma_{residual} = \psi(\alpha_m - \alpha_f)\Delta T \qquad \text{E6-5}$$

$$\sigma_{residual} = \psi(\alpha_m - \alpha_f)\Delta T = (\alpha_m - \alpha_f)\Delta T \cdot f(V_f) \quad \text{E6-5.1}$$

Where V_f is the fibre volume fraction, α_f , α_m are coefficients of the thermal expansions of the fibre and matrix, E_f and E_m are the elastic modules and ΔT is the temperature difference on cooling from the processing temperature to ambient temperature.

For our particular case of the CDMC, the matrix and fibre and other data are as indicated as following:

$E_f = 80$ GPa,

$V_f = 0.0\%, 5\%, 10\%, 15\%, 22.6\%$(vol.),

ΔT = moulding temperature 200 -- 20°C = (200 + 273)K - (20 + 273) K.

If average value of matrix :

$E_m = 35$ GPa, is taken for the pure ceramic matrix,

From E6-5 , for different volume fraction of glass fibre the $\sigma_{residual}$ would be changed if we just consider a single fibre or a single fibre bundle, it could be worked out as listed in Table 6.7. It is indicating that the less fibre involved in the materials, the less residual stress remained after the moulding or heat treatment.

Therefore, the lower the fibre volume fraction, the smaller the $\sigma_{residual}$, and the lower the moulding temperature, the smaller the $\sigma_{residual}$. The coefficient of thermal expansion α_m has been measured by NPL for the CDMC in the range of 50-200 ℃ and the result is 6.0×10^{-6} K^{-1}. Here, if it is in the temperature range of 50 to 200 °C (CMMT0918/2932):

For glass fibre: $\alpha_f = 3 \times 10^{-6}$ K^{-1} (50 to 200 °C)

For the matrix $\alpha_m = 6x10^{-6}\ K^{-1}$ (50 to 200 °C)

According to the standard theory (Fishbane, Gasiorowicz, Thornto, 1996), following simplified equation can be derived from E6-4 and E6-5 for the temperature range between 20 - 200 °C:

$$\sigma_{residual} = 1.42 \times 10^{-3} \psi = 1.42 \times 10^{-3} \cdot f(V_f) \qquad \text{E6-6}$$

The relationship among volume fraction of glass fibre, Ψ and $\sigma_{residual}$ of the CDMC has been listed in Table 6.7 and plotted in Fig. 6.35. It shows that the $\sigma_{residual}$ is about 20 MPa while the volume fraction is 22.6%(vol.). Since the matrix was shrinking during moulding, the residual stress generated is a clamping force around individual fibres or fibre bundles. This may be one of the major causes of matrix cracking after moulding.

6.6 Summary

General mechanical properties of the CDMC reinforced by E-glass and AR50/1 glass fibre were investigated and their flexural properties are compared. The results revealed that the properties of E-glass and AR50/1 glass CDMC are effected by material's moulding temperatures.

The CDMC moulded at lower temperatures (< 130 °C), were somewhat ductile. At higher moulding temperatures (>160 °C) the material tended to be brittle. Since the fibre sizing can be damaged in alkali media during moulding, it seems there is an optimum range of moulding temperatures for qualified products. This optimised moulding temperature range for AR-glass has been worked out through the moulding experiments in last Chapter in the range of 130 °C to 150 °C.

The fibres studied were initially E-glass fibres and AR-glass fibre 50/1. The E-glass fibre provided reasonable strength when moulded below 130 °C but there after strength decreased dramatically with moulding temperature raising. AR-glass fibres produced slightly inferior results in low moulding temperatures (99 ~120 °C) but improved properties at medium temperatures (130 ~150 °C). Combination of E-glass and AR (50/1) glass provide intermediate properties. The good bonding at moulding temperatures (160 ~ 190 °C) between glass and the silicate matrix resulted in a the very brittle composites.

The property affects of the volume fraction of glass fibre from 0 - 22.6%(vol.) were examined by using a CDMC with AR50/1 glass with the moulding temperature 140°C. Flexural, tensile and impact results revealed that the best results were obtained by the CDMC with 22.6%(vol.) AR50/1 glass fibre.

Table 6.1 The relationships of flexural strains at failure of the CDMC with 15%(vol.) AR 50/1 and E-glass fibre at moulding temperature 130 - 190 °C.

Moulding temperatures (°C)	CDMC flexural strain at failure (mm/mm)	
	E-Glass	AR-glass
130	0.0045	0.0035
150	0.0010	0.0016
170	0.0010	0.0007
190	0.0012	0.0013

Table 6.2 Tensile properties of the CDMC with 15%(vol.) AR50/1 GF effected by the moulding temperatures.

Moulding temperatures (°C)	Strain at failure (%)	Max. stress (MPa)	Modulus (GPa)
99	0.210	24.22	11.53
130	0.130	23.50	21.60
150	0.063	24.75	39.00
180	0.055	12.80	23.27

Table 6.3 Effects of volume fraction [%(vol.)] of the AR-glass fibre (50/1) on the tensile properties, moulding temperature 140 °C.

Volume fraction of AR50/1 in CDMC	Strain to failure %	Max. stress (MPa)	Modules (GPa)
Matrix	0.0239	10.59	37.88
5.0	0.0547	17.02	28.50
10.0	0.0872	19.52	24.23
15.0	0.1258	22.50	23.22
22.6	0.160	22.27	27.34

Table 6.4 Comparison of total energy absorption of the CDMC with 15%(vol.) AR50/1 glass fibre moulded at 130, 150, 170 °C. Total impacting energy was 5.9 J.

Moulding temperatures, °C	Impact energy absorption, E(J)
130	0.60
150	0.30
170	0.12

Table 6.5 Energy absorption of the CDMC with variation of fibre volume fractions. The total impacting energy 5.9 J.

Volume fraction of glass fibre in CDMC	Energy absorption, E(J)
0 %	0.02
5.0 %	0.16
10.0 %	0.15
15.0 %	0.60
22.6 %	0.73

Table 6.6 Mirror diameter $\mathbf{a_m}$ and the corresponding moulding temperatures of examined CDMC with 22.6(vol.) AR50/1 glass fibre. Individual fibre diameter was 14 μm.

Moulding temperature, °C	$\mathbf{a_m}$, μm
99	1 ~ 4
130	1 ~ 4
140	2 ~ 4
150	3 ~ 5
170	5 ~ 9
180	6 ~ 9

Table 6.7 The relationship between Ψ and volume fraction of glass fibre, V_f.

V_f(%(vol.).)	Ψ (GPa)	$\sigma_{residual}$ (MPa)
0	0	0
5	3.76	5.34
10	7.09	10.07
15	10.06	14.29
22.6	13.99	19.87
27	16.02	22.74
35	19.29	27.39
40	21.07	29.92

General mechanical tests of glass fibre reinforced ceramic moulding compound

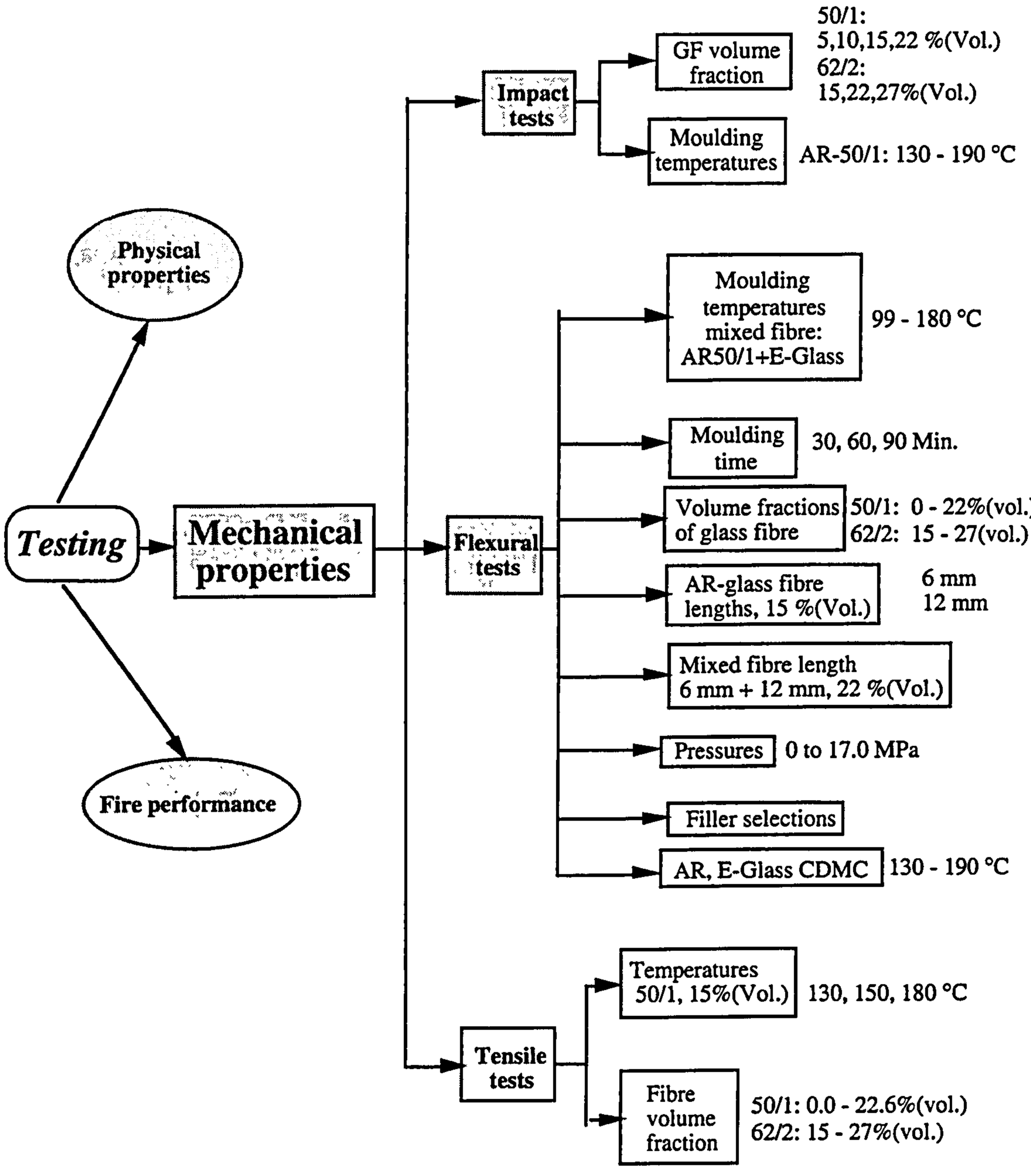

Fig. 6.1 The mechanical testing scheme of the CDMC throughout the research programme.

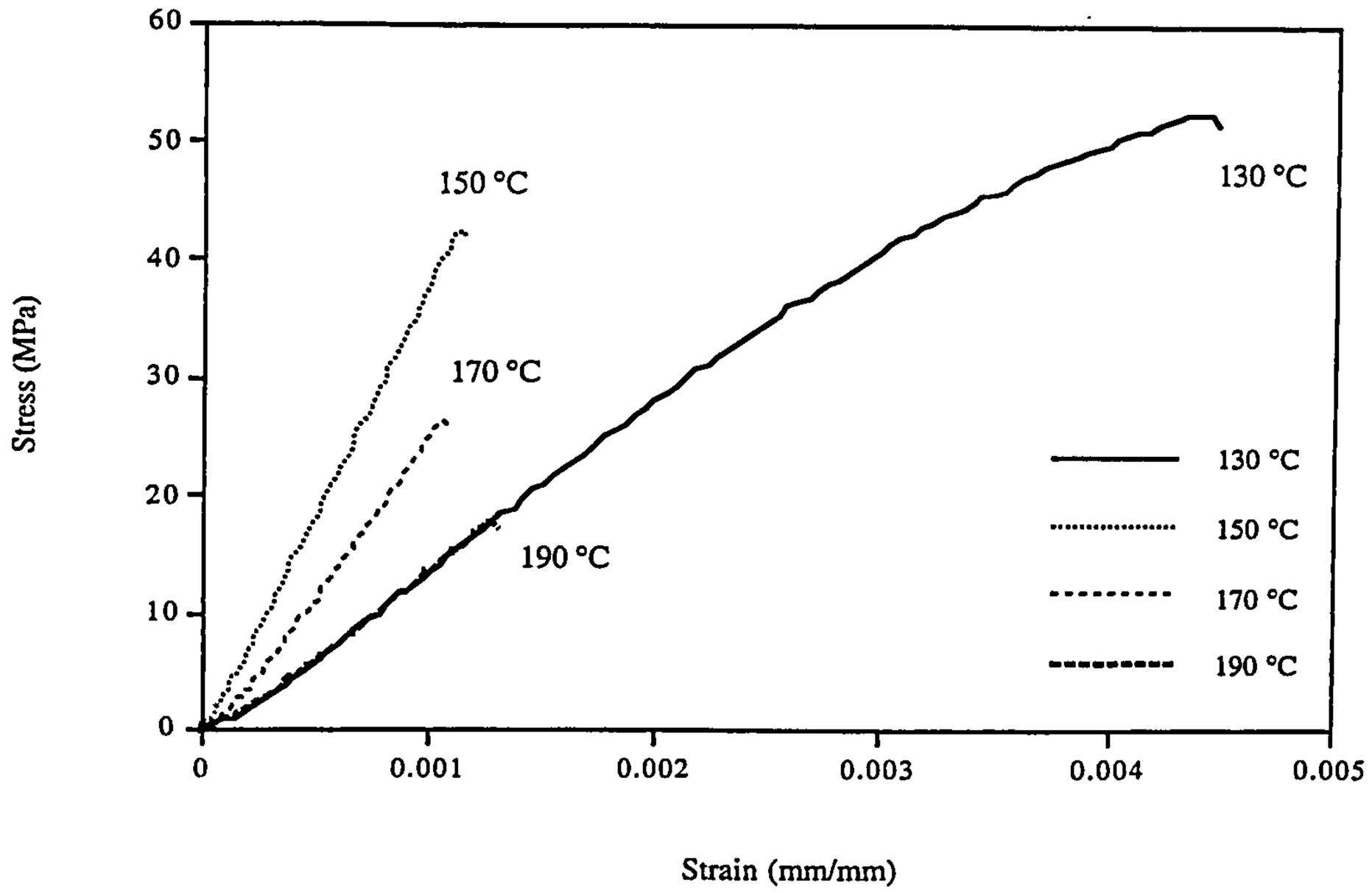

Fig. 6.2 The flexural stress-strain curves of the CDMC with 15%(vol.) E-glass fibre moulded at a temperature range from 130 ~ 190 °C.

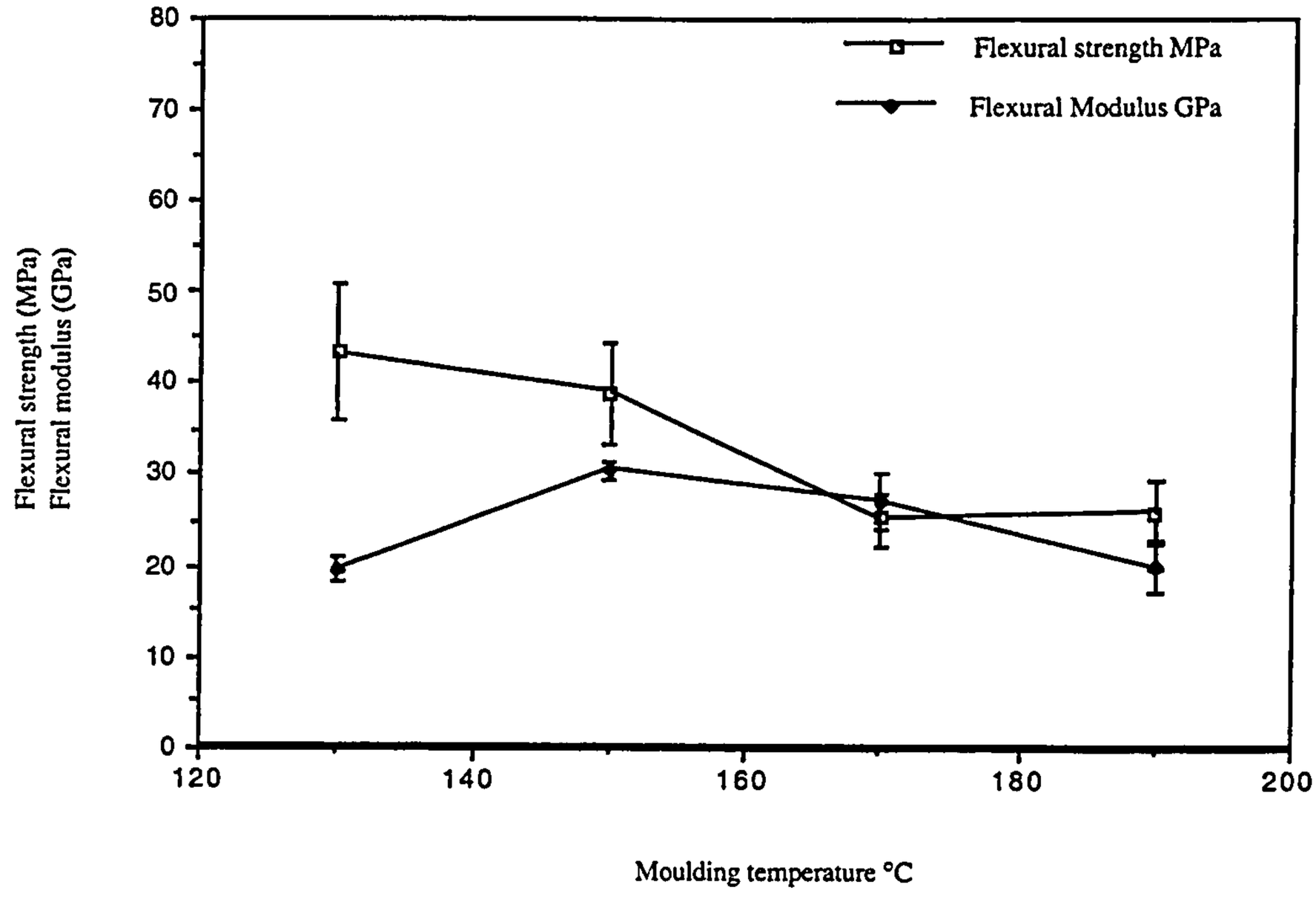

Fig. 6.3 The flexural properties of the CDMC with 15%(vol.) E-glass fibre roving (Tex 2450, chopped to 12 mm) moulded at 130 - 190 °C.

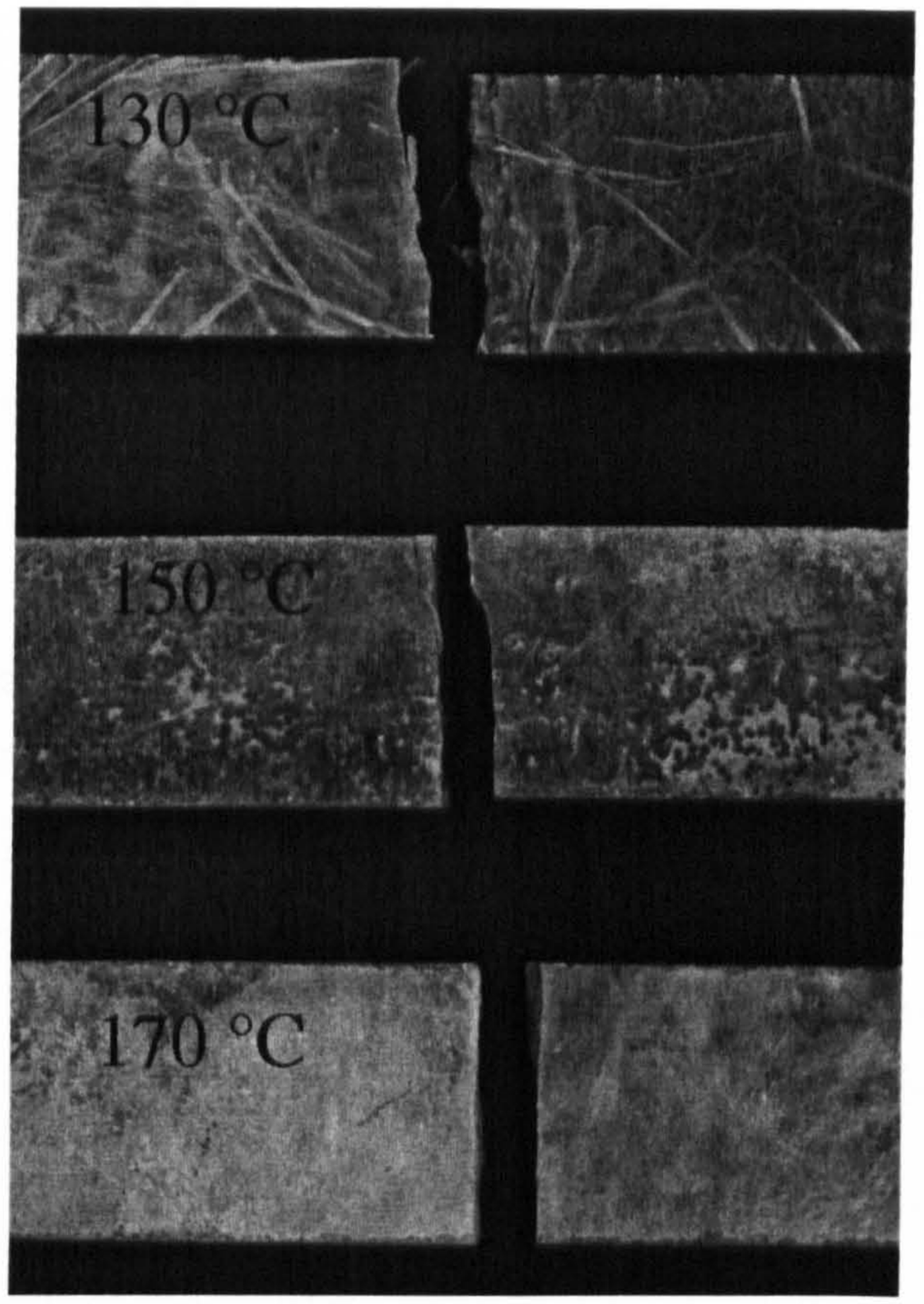

Fig. 6.4 Flexural failed specimens reinforced with E-glass fibre moulded at different temperatures.

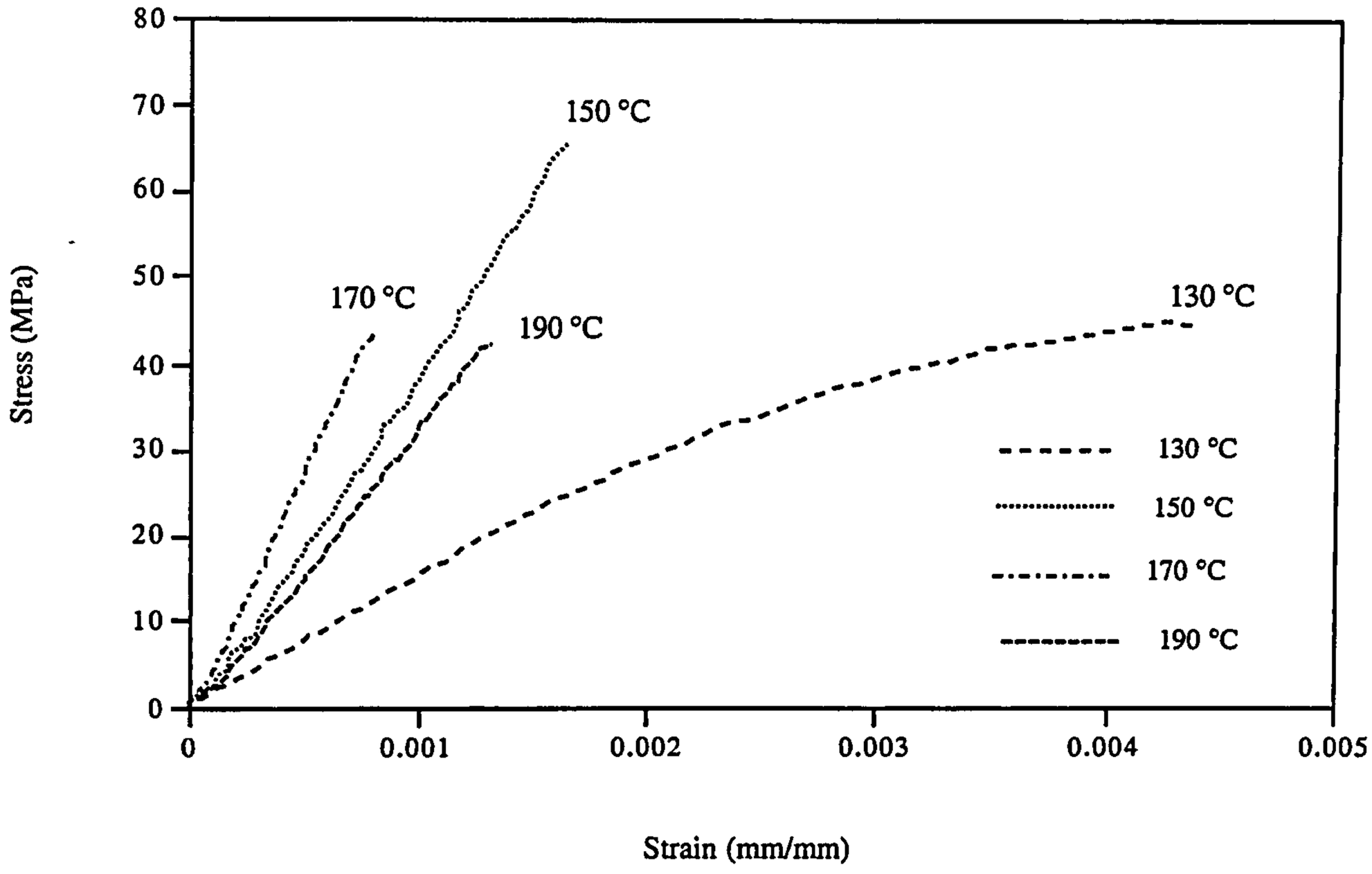

Fig. 6.5 The flexural stress-strain curves of the CDMC with 15%(vol.) AR-50/1 glass fibre, moulded at temperatures 130 ~ 190 °C.

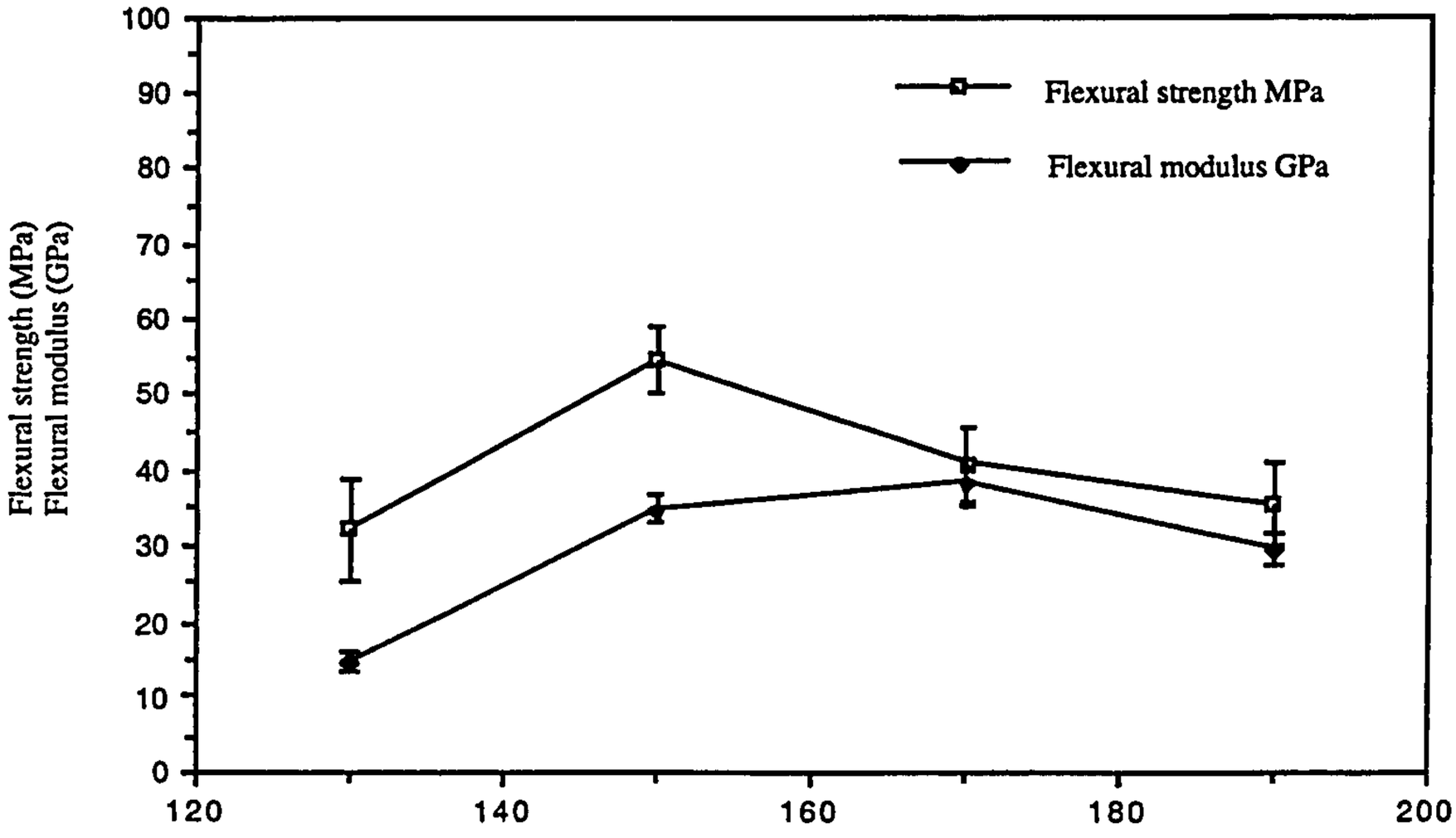

Fig. 6.6 The flexural properties of the CDMC with 15 %(vol.) AR50/1 glass effected by moulding temperatures from 130 - 190 °C.

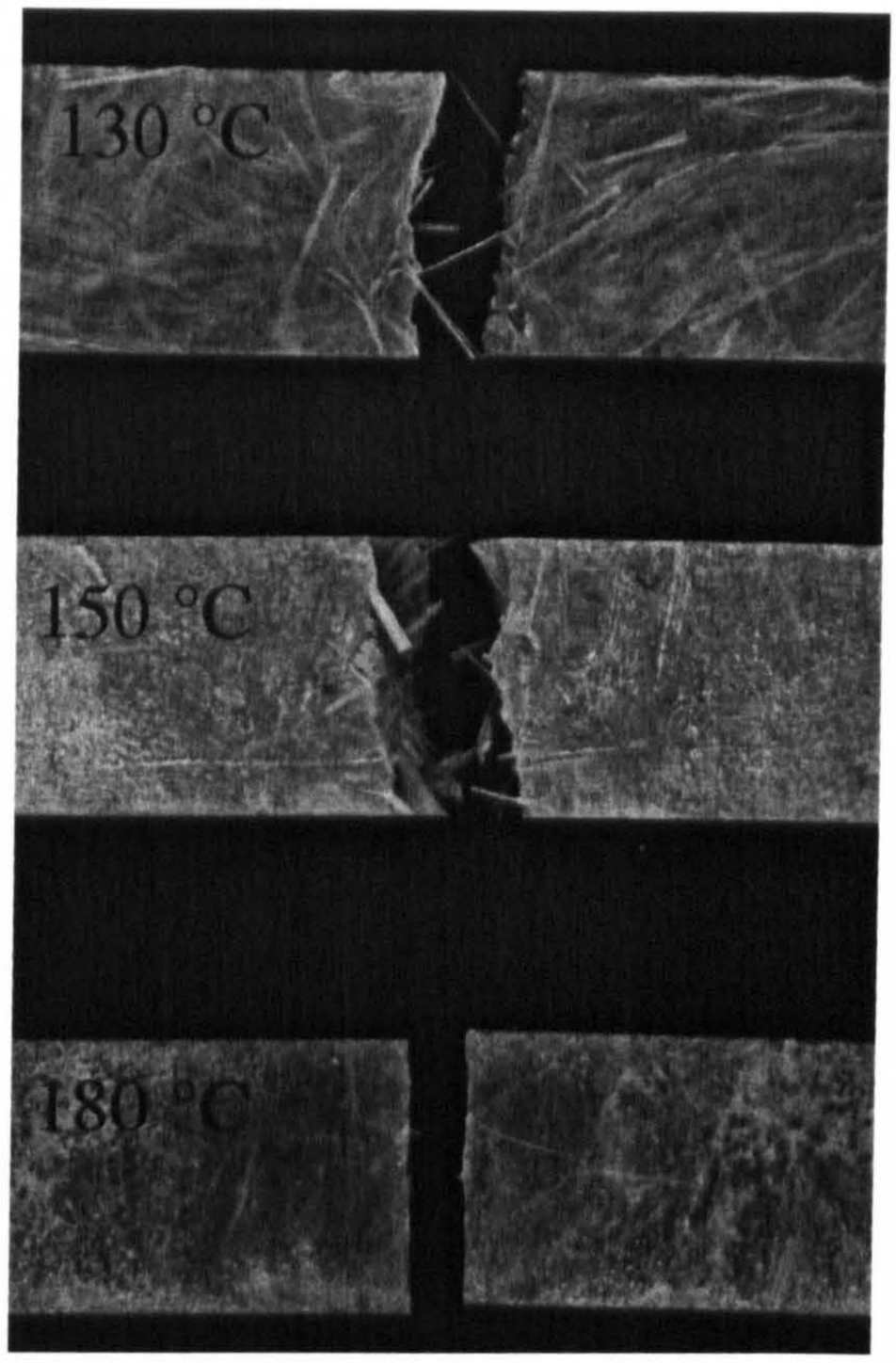

Fig. 6.7 Some flexural failed specimens of the CDMC reinforced with AR 50/1 glass fibre moulded at different temperatures.

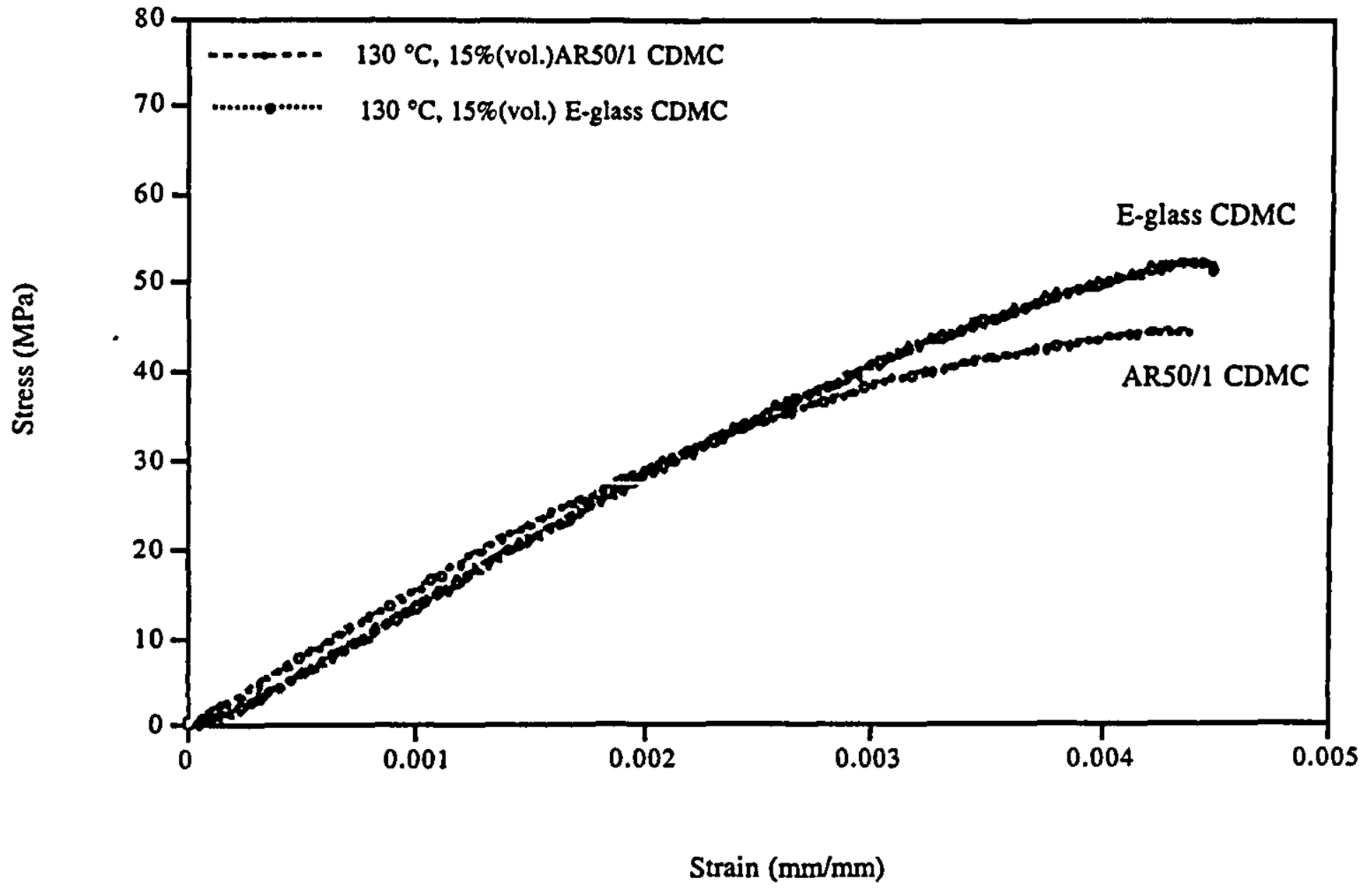

Fig. 6.8 Flexural stress-strain curve comparison of the CDMC with 15%(vol.) AR50/1 and E-glass, moulded at 130 °C.

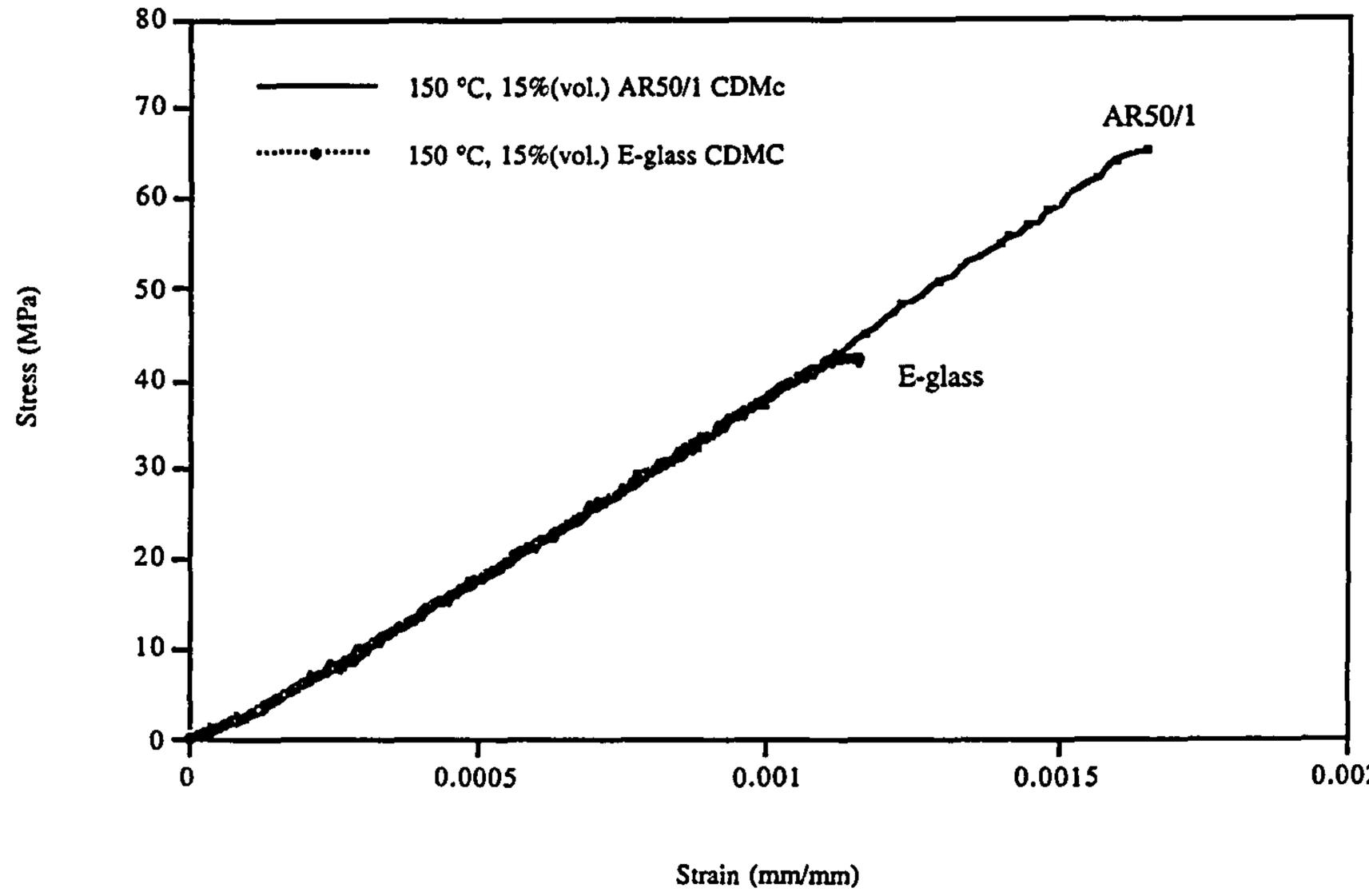

Fig. 6.9 Flexural stress-strain curve comparison of the CDMC with 15%(vol.) AR and E-glass fibre moulded at 150 °C.

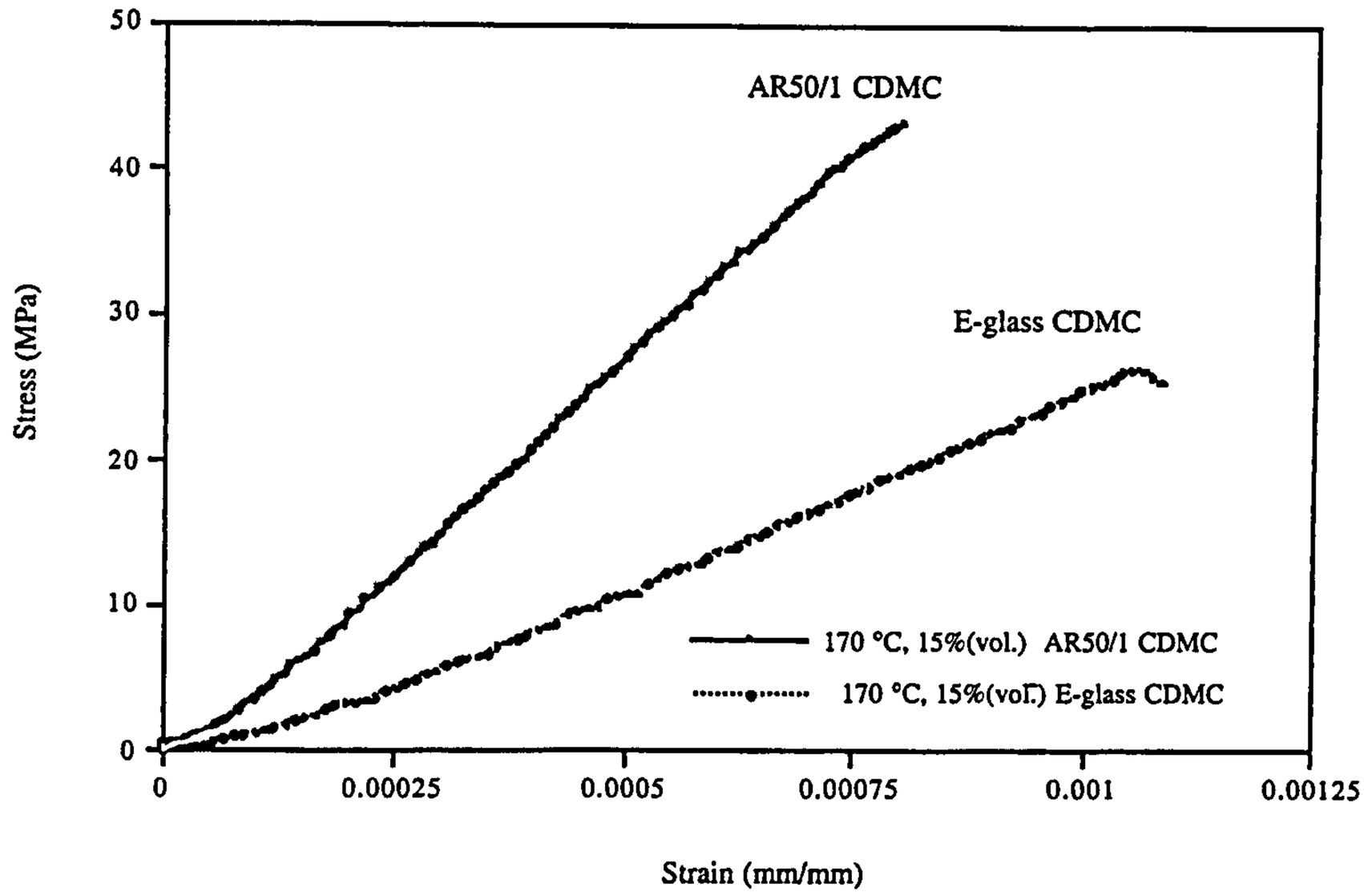

Fig. 6.10 Flexural stress-strain curve comparison of the CDMC with 15%(vol.) AR50/1 and E-glass fibre moulded at 170 °C.

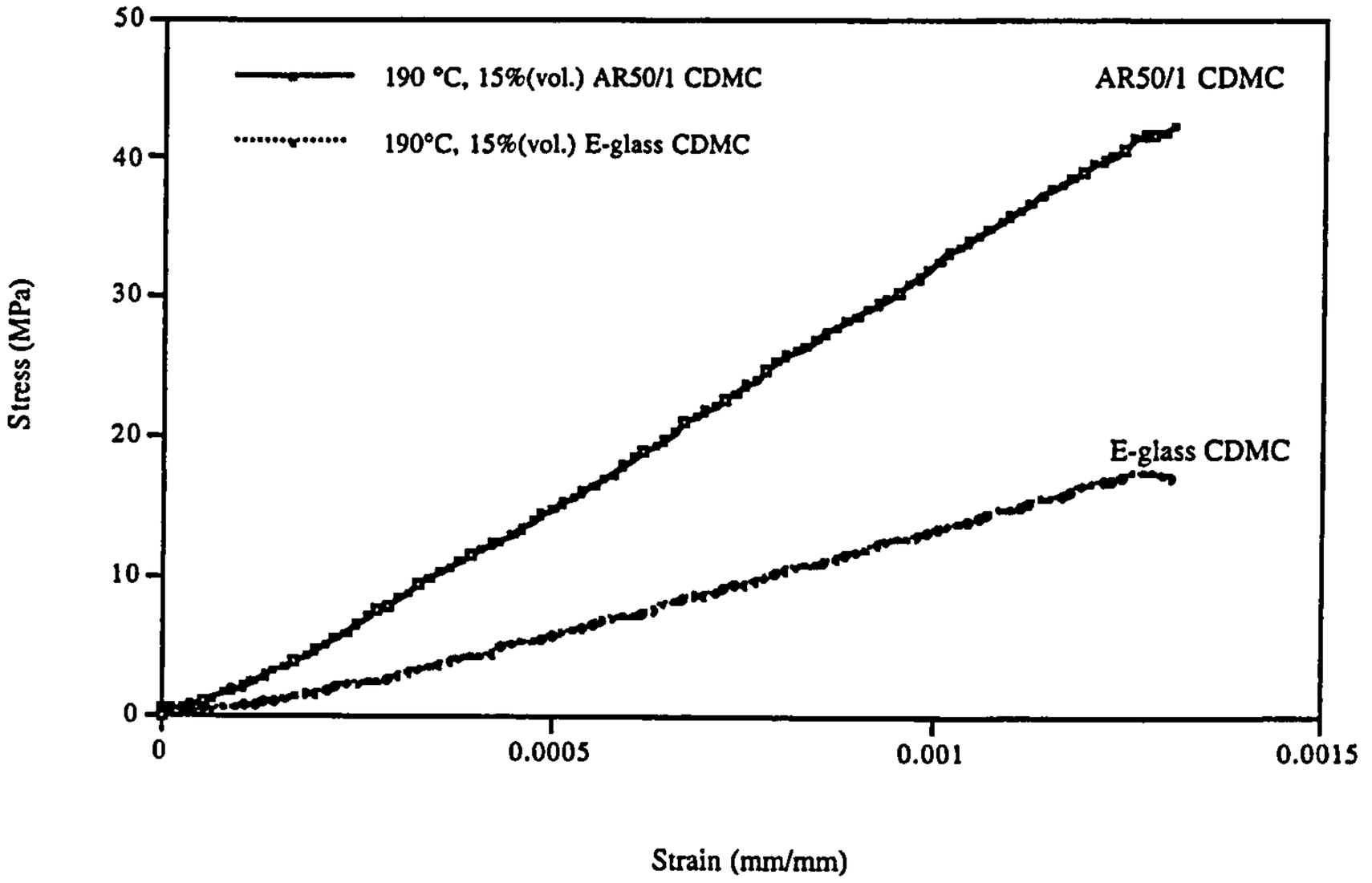

Fig. 6.11 Flexural stress-strain curve comparison of the CDMC with 15%(vol.) AR-glass 50/1 and E-glass fibre, moulded at 190 °C.

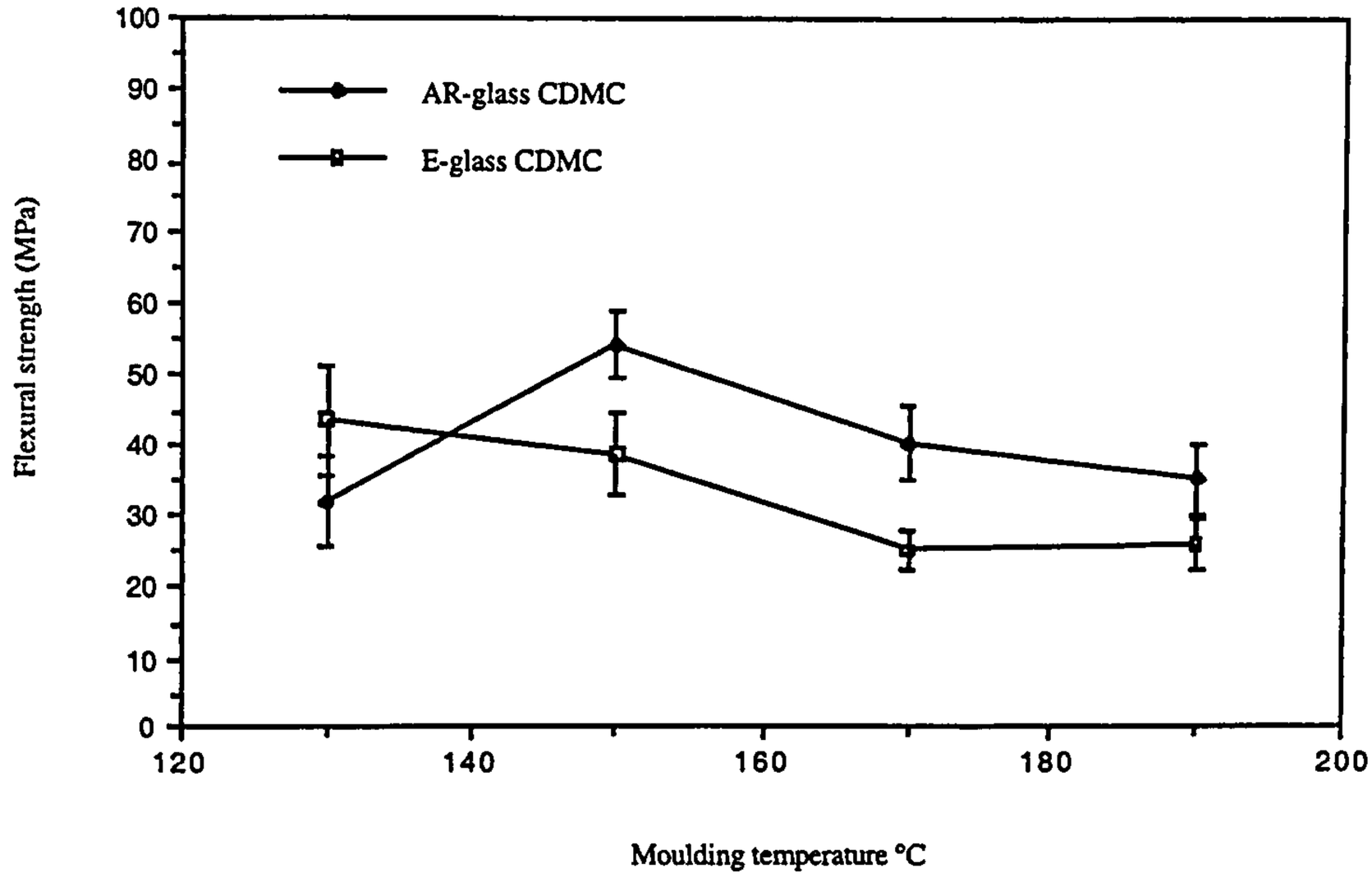

Fig. 6.12 The strength comparison of the CDMC with 15%(vol.) AR and E-glass fibre over the moulding temperature range 130 - 190 °C.

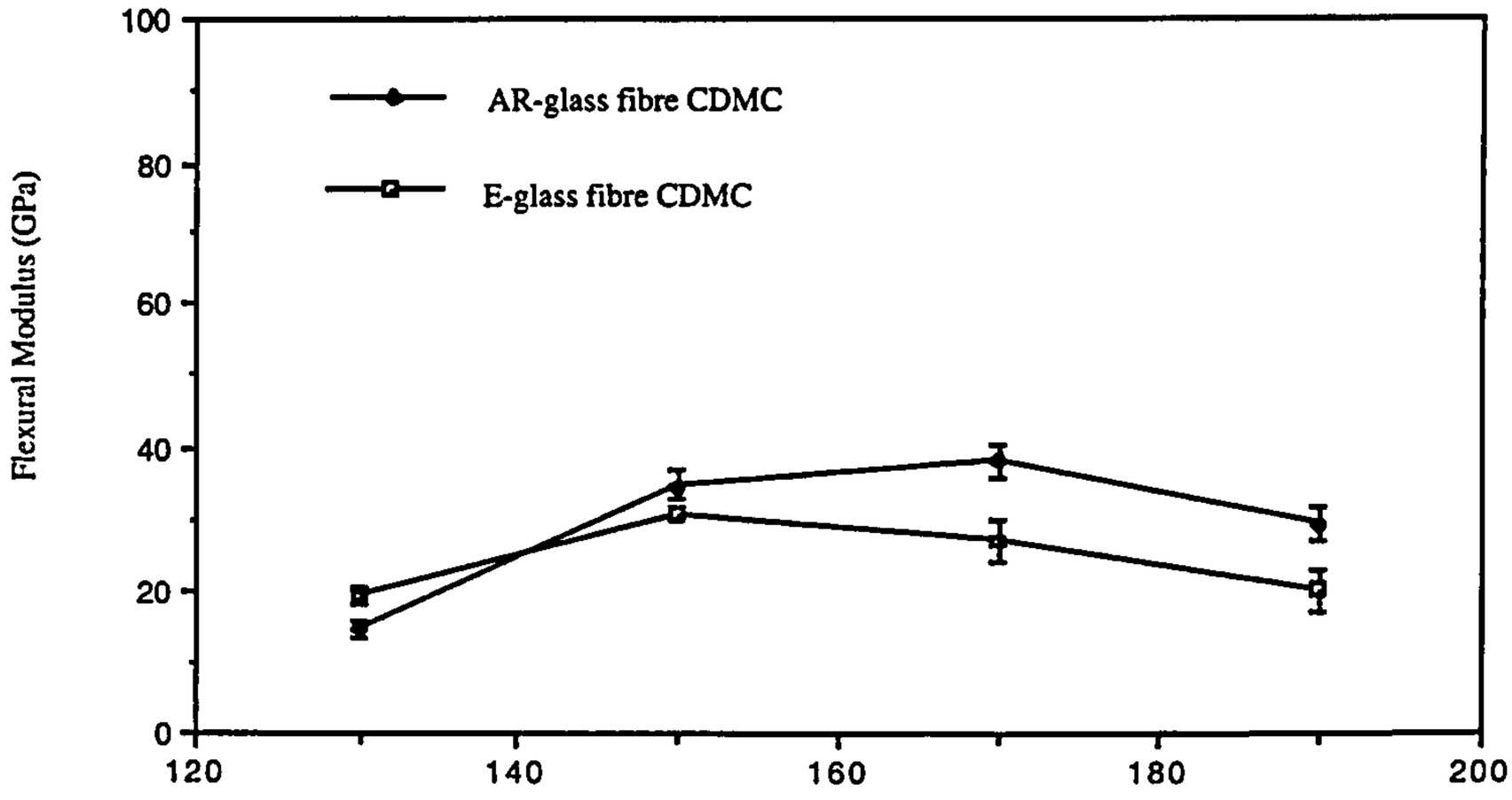

Fig. 6.13 The modulus comparison of the CDMC with 15%(vol.) AR and E-glass fibre over the moulding temperature range 130 - 190 °C.

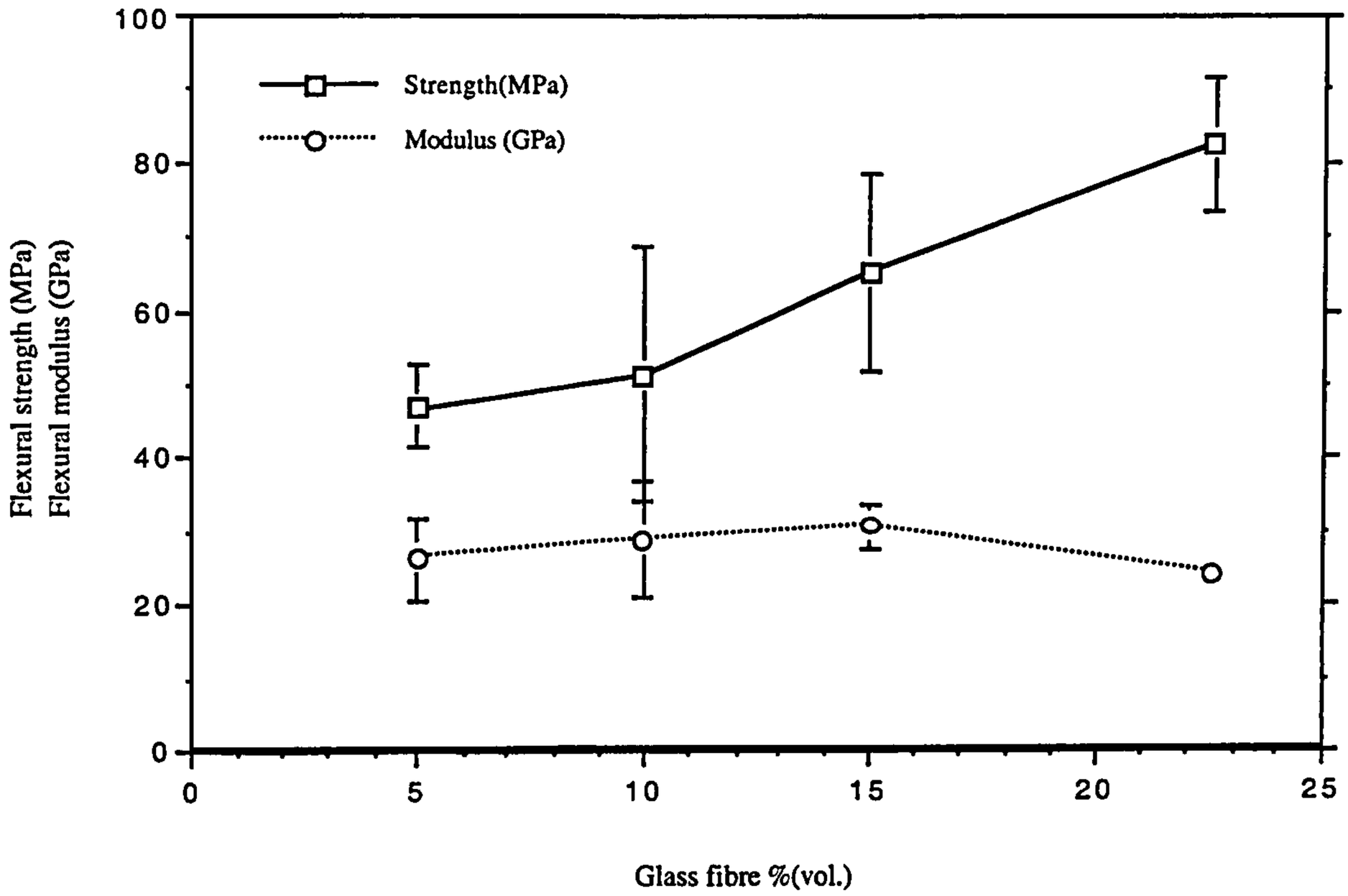

Fig. 6.14 The flexural properties of the CDMC with fibre volume fraction of 5 - 22.6%(vol.), AR50/1 GF (12 mm).

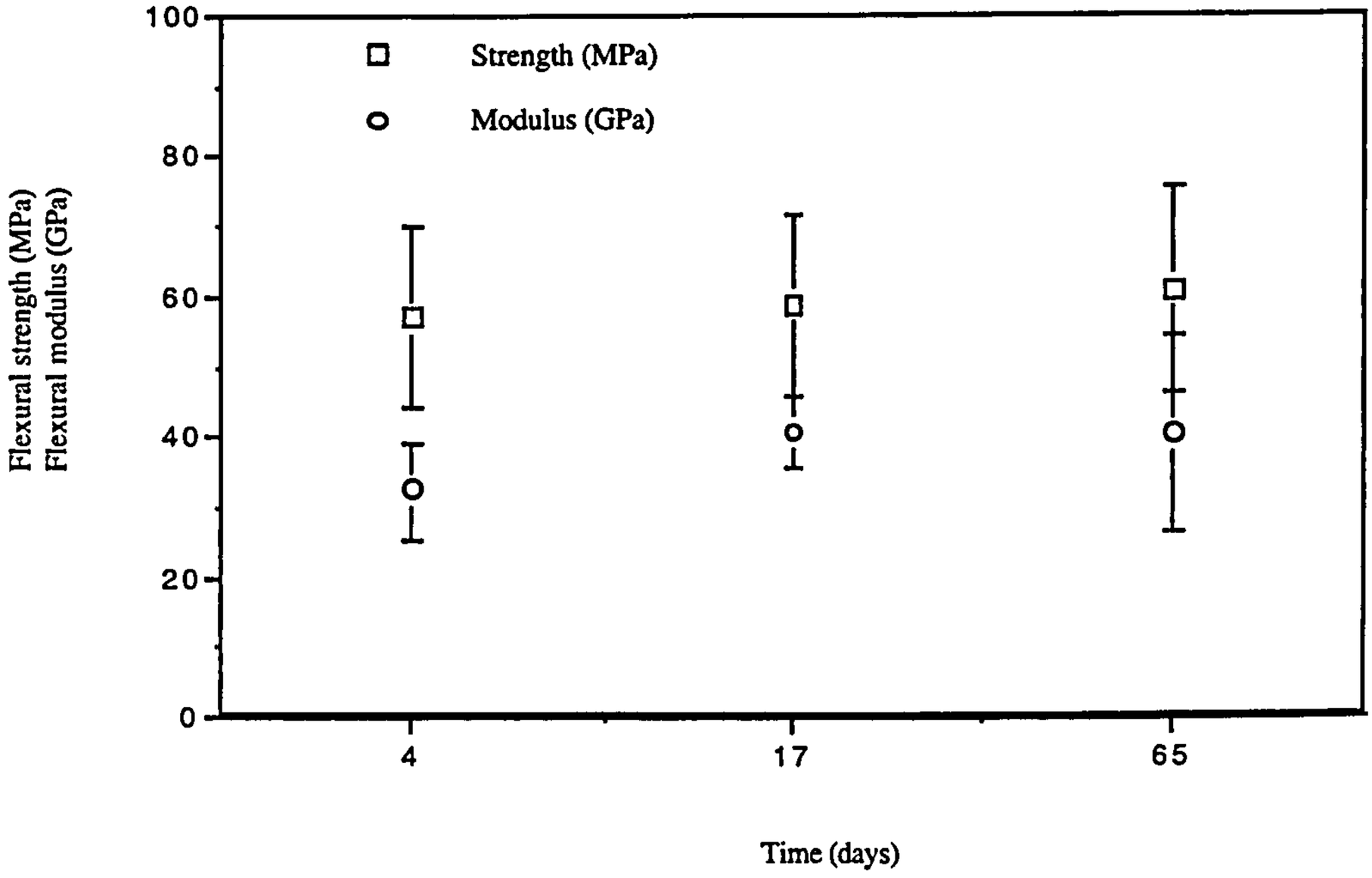

Fig. 6.15 The flexural property retention of the pure ceramic matrix. The time is the days after moulding.

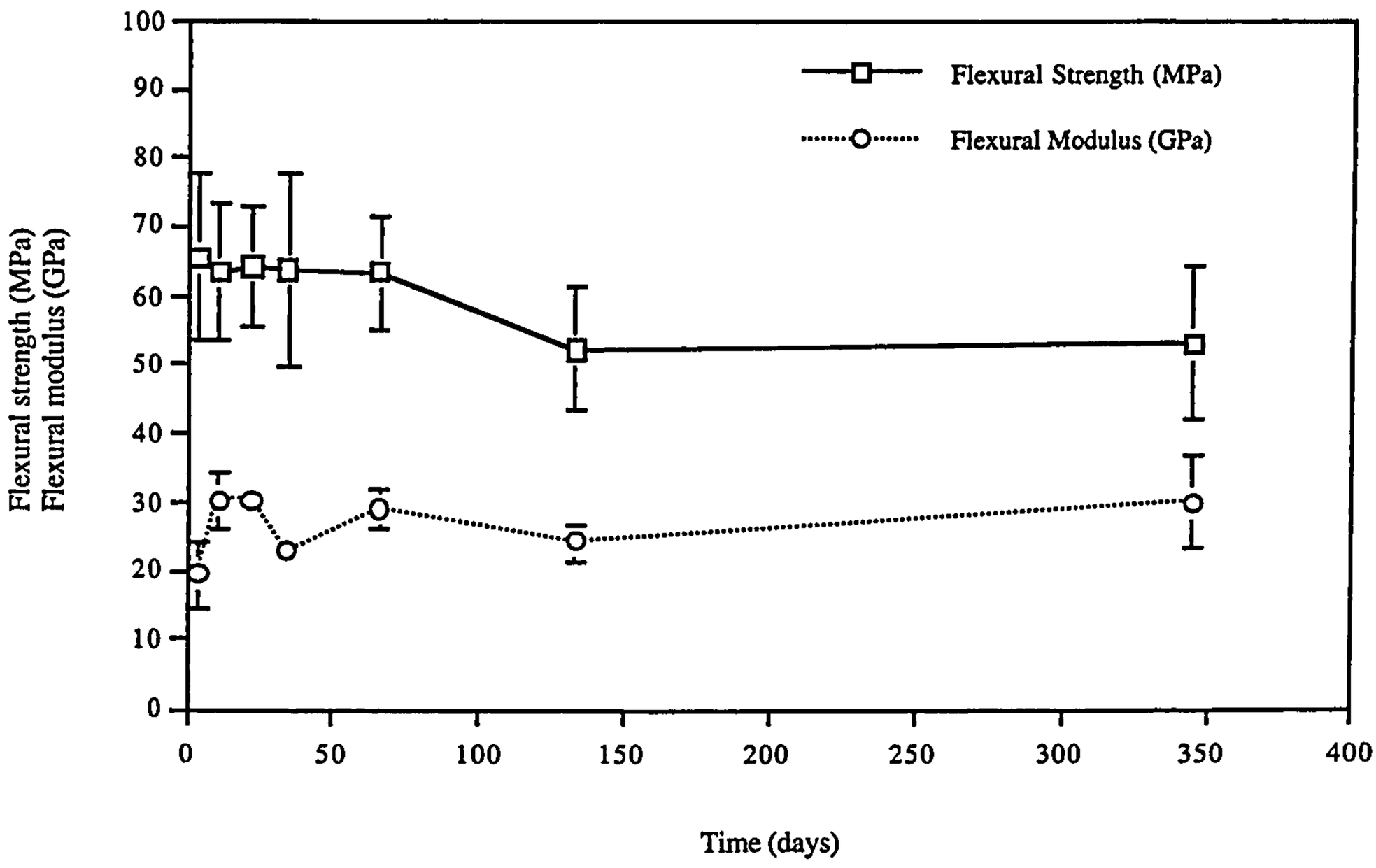

Fig. 6.16 The flexural property retention examined by using the CDMC with 22.6%(vol.) glass fibre. The time here is the number of days after the CDMC panel moulded.

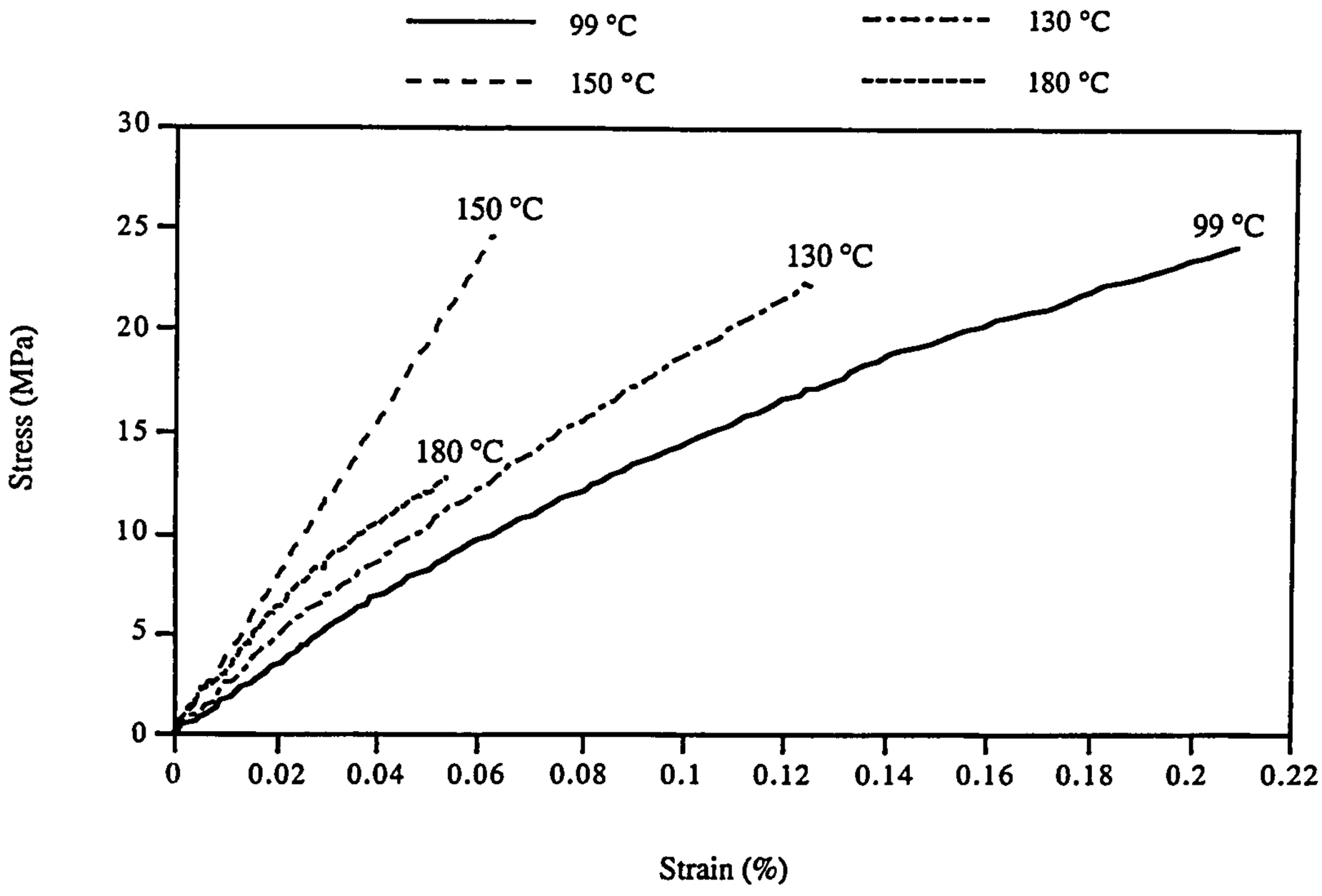

Fig. 6.17 The tensile stress-strain curves of the CDMC with 15%(vol.) 50/1 AR-Glass fibre moulded at the temperature of 99 - 180 °C.

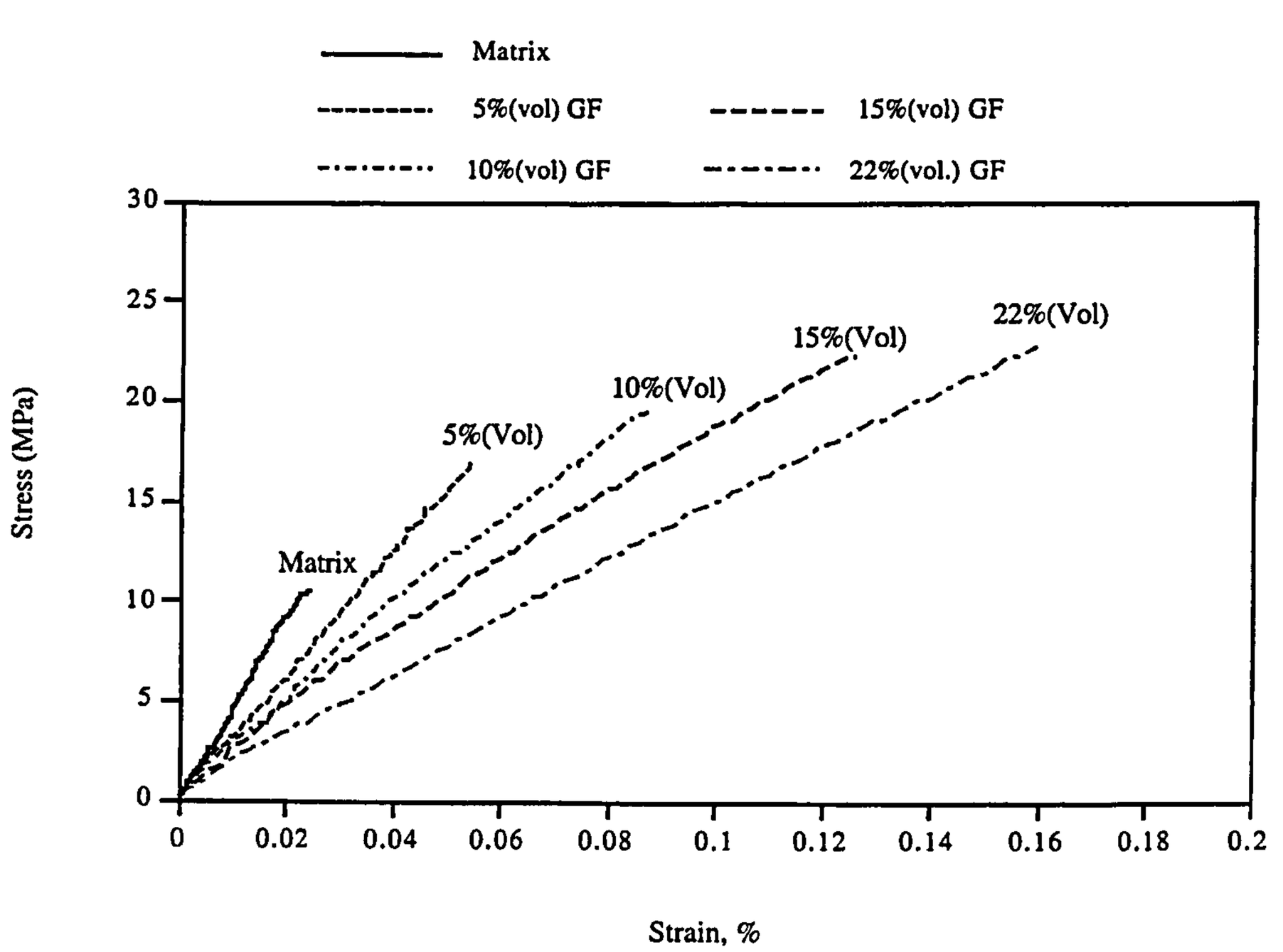

Fig. 6.18 The tensile stress-strain curves of the CDMC with glass fibre AR50/1 in volume fraction of 0 - 22.6%(vol.). Moulding temperature was 140 °C.

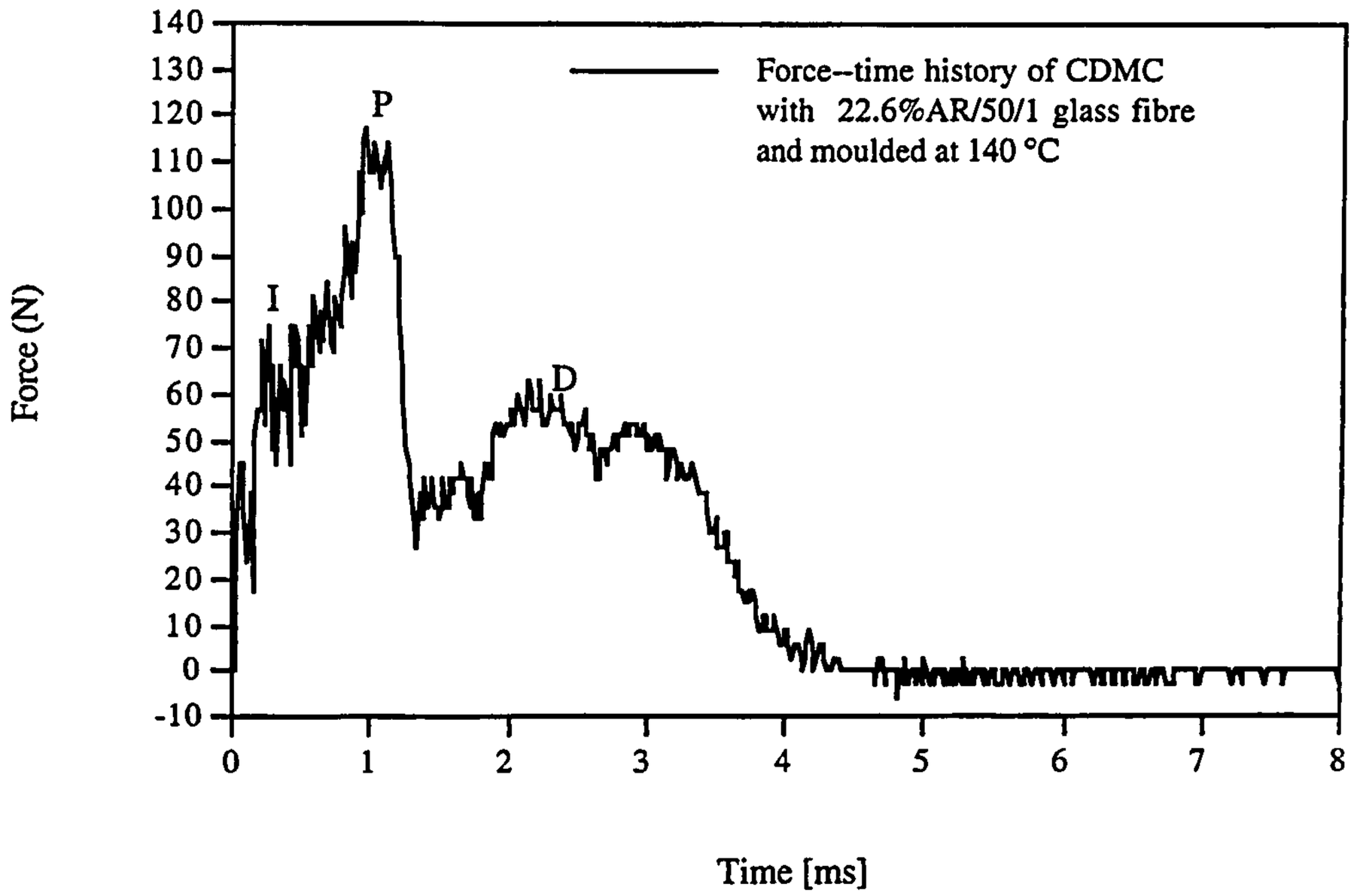

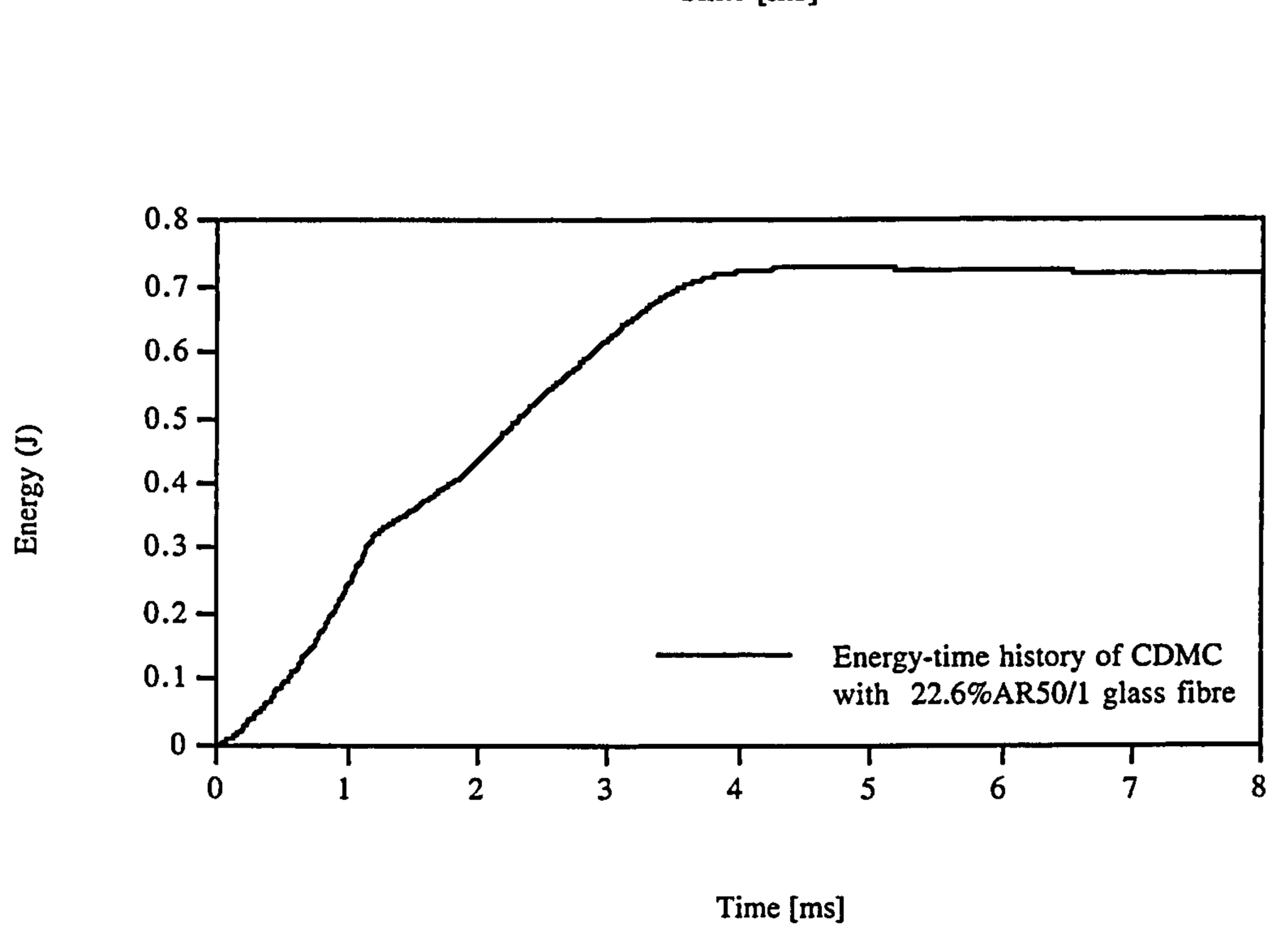

Fig. 6.19 The typical force-time and energy absorption - time histories of the CDMC with 22.6 AR50/1 glass fibre moulded at 140 °C.

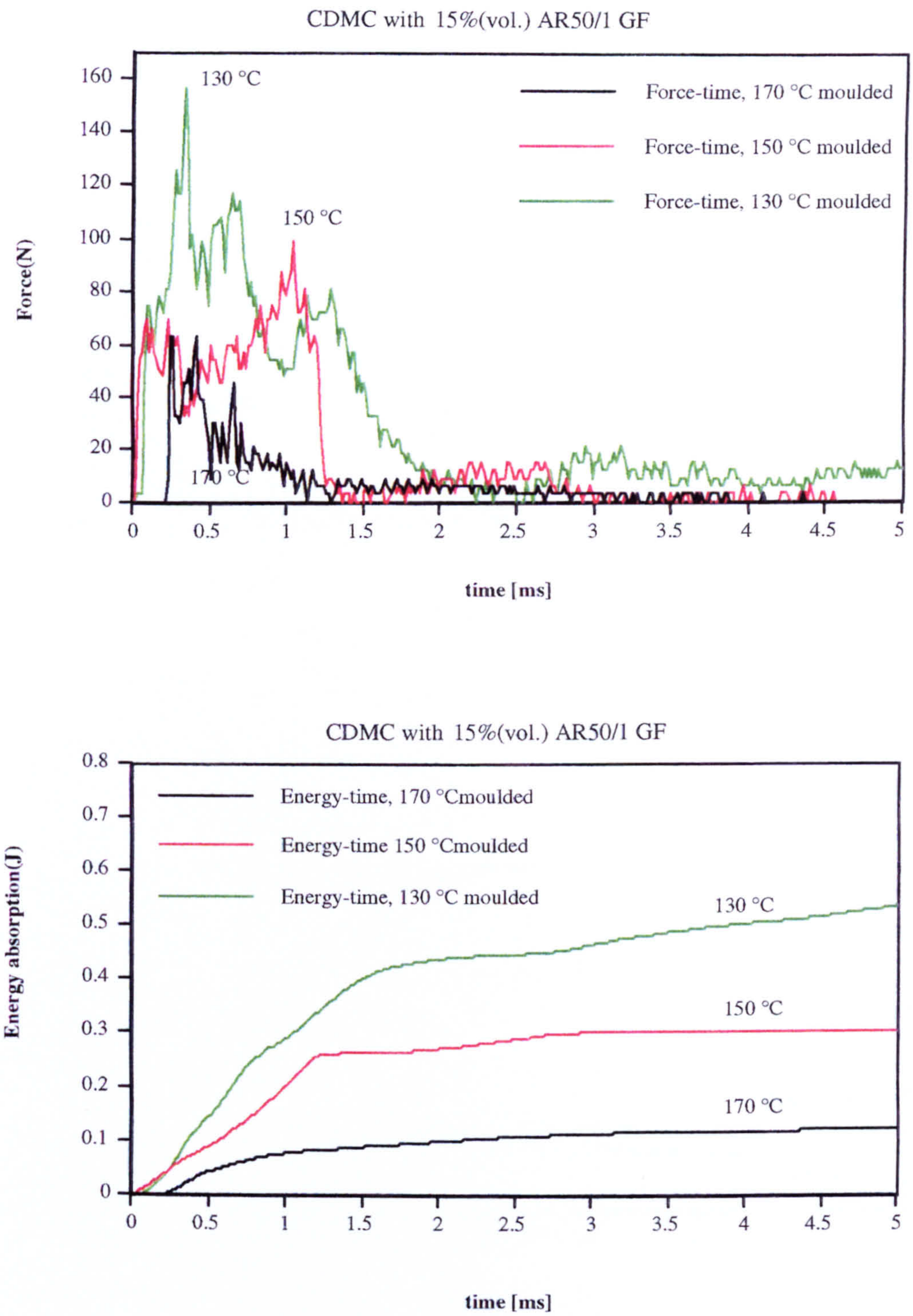

Fig. 6.20 The impact force-time and energy-time histories of the CDMC with 22.6 AR50/1 glass fibre moulded at 130 - 180 °C.

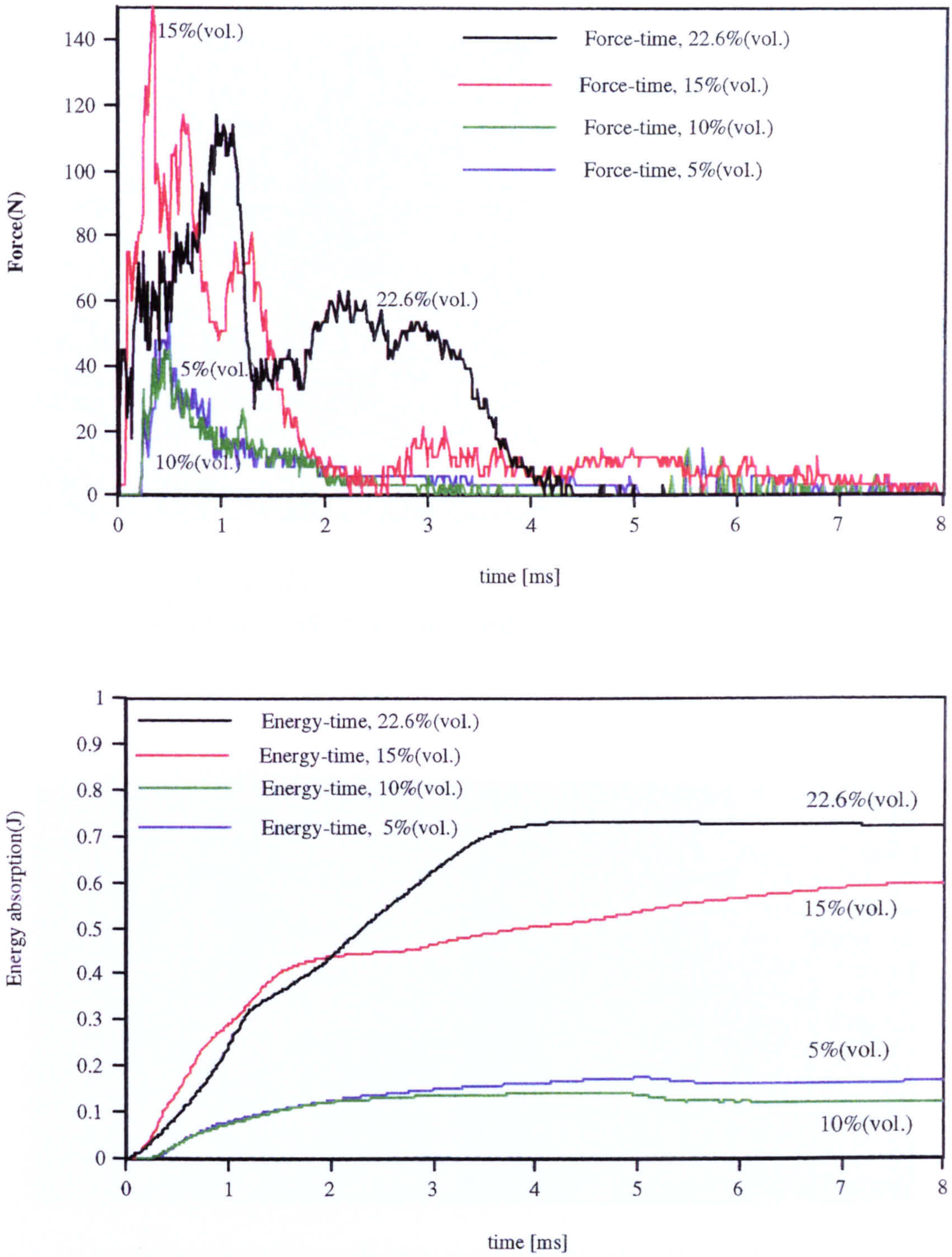

Fig. 6.21 The impact force-time (up) and energy-time (low) histories of the CDMC with 5% - 22.6%(vol.) AR50/1 glass fibre.

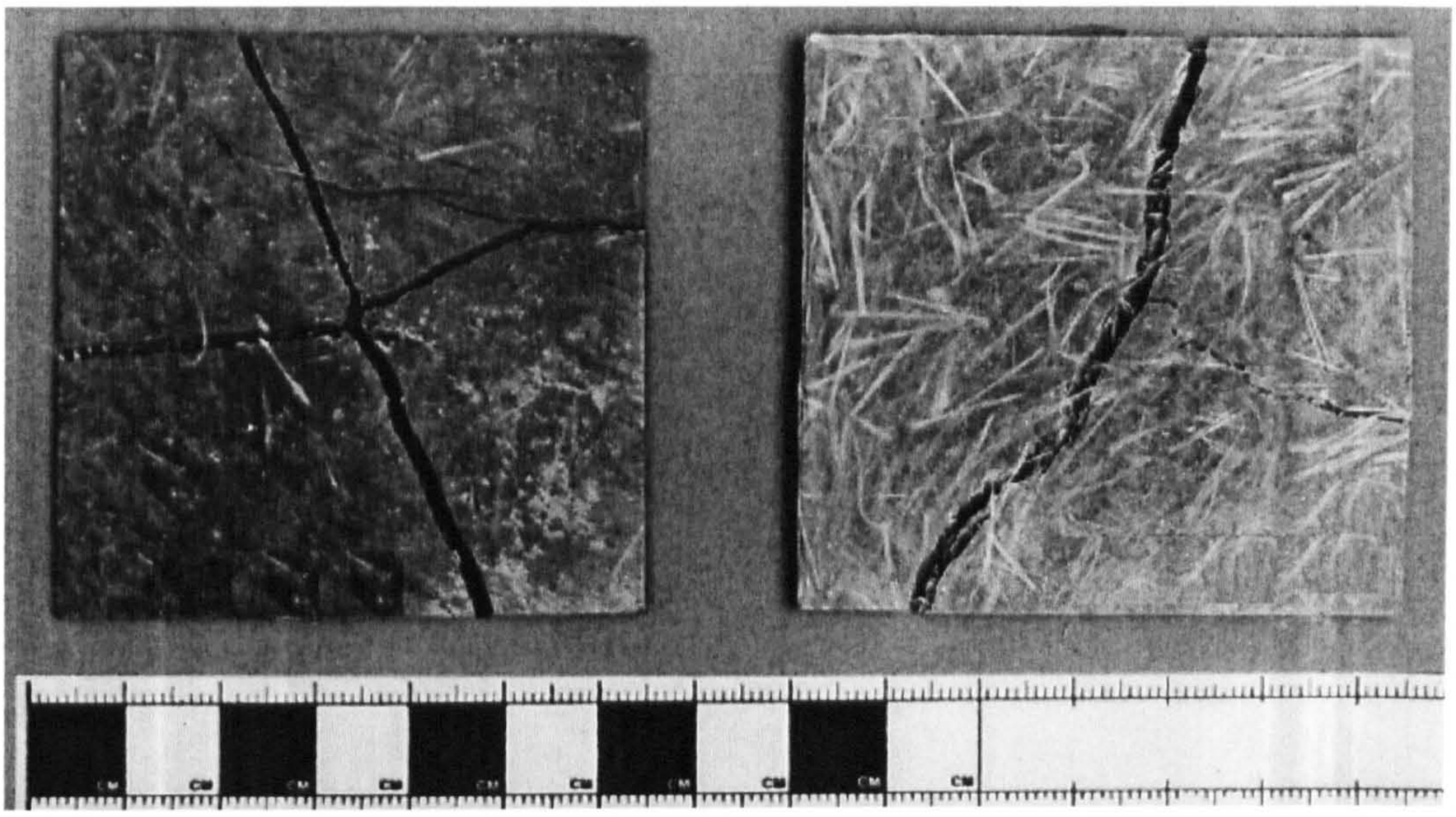

Fig. 6.22 Impacted specimens with 22.6%(vol.) AR50/1 glass fibre (12 mm). The specimens were shattered with impacting energy 5.9 J.

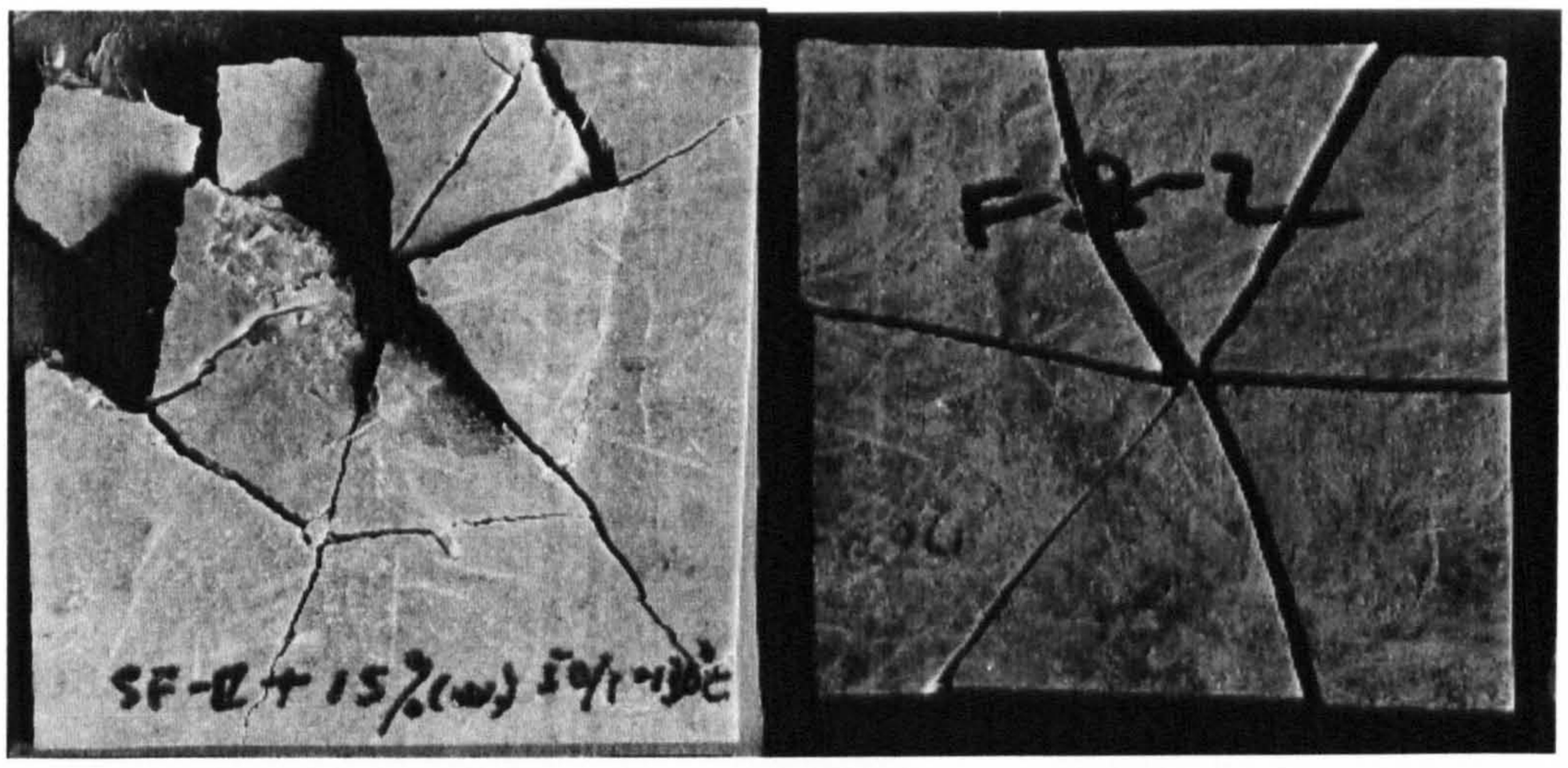

Fig. 6.23 Impacted specimens with 15% (vol.) AR50/1 glass fibre (12 mm).

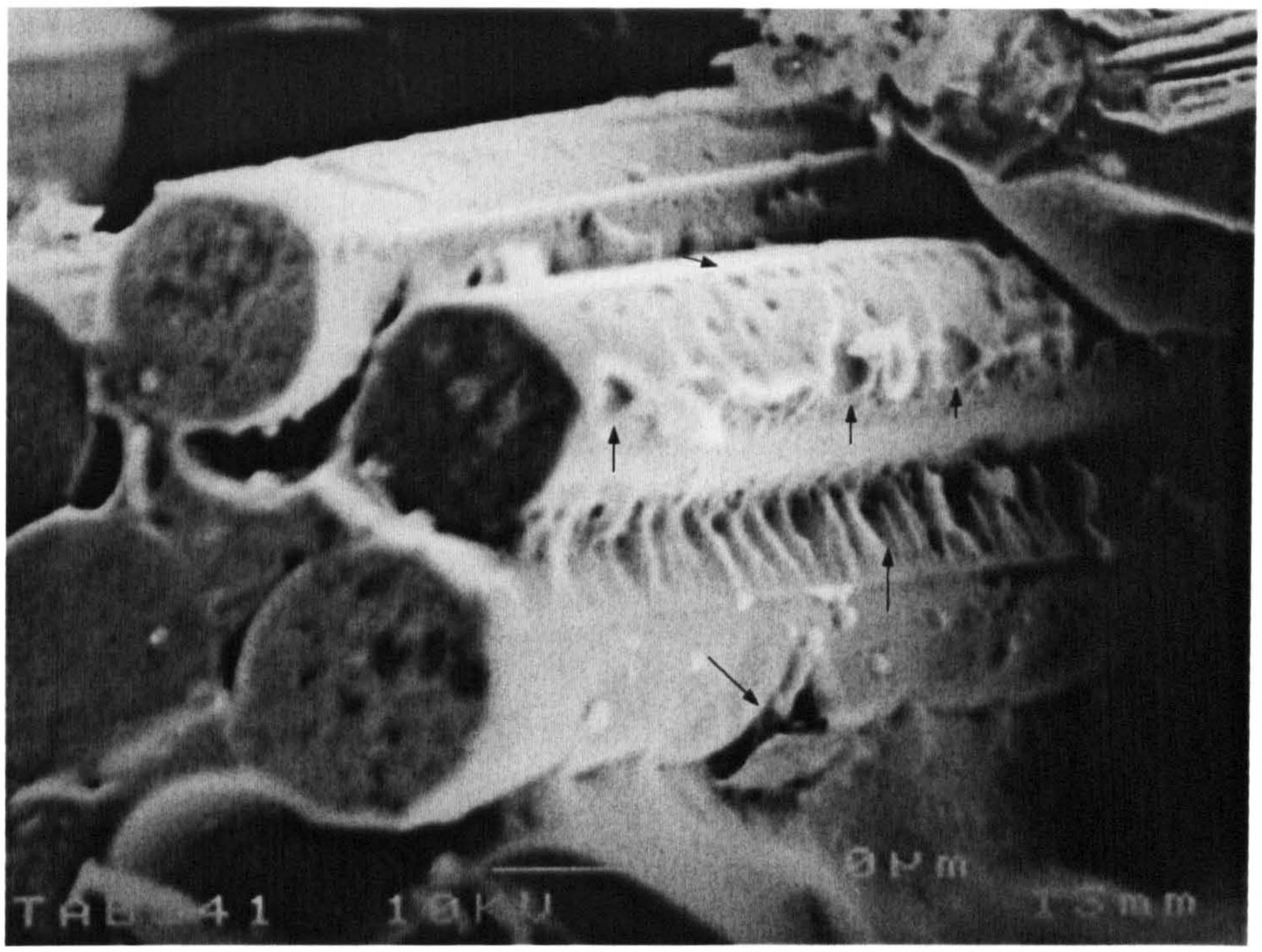

Fig. 6.24 A SEM image of E-glass fibre in the CDMC moulded at 160 °C. Severe corrosion has been observed on the surface of glass fibre caused by the alkali matrix system.

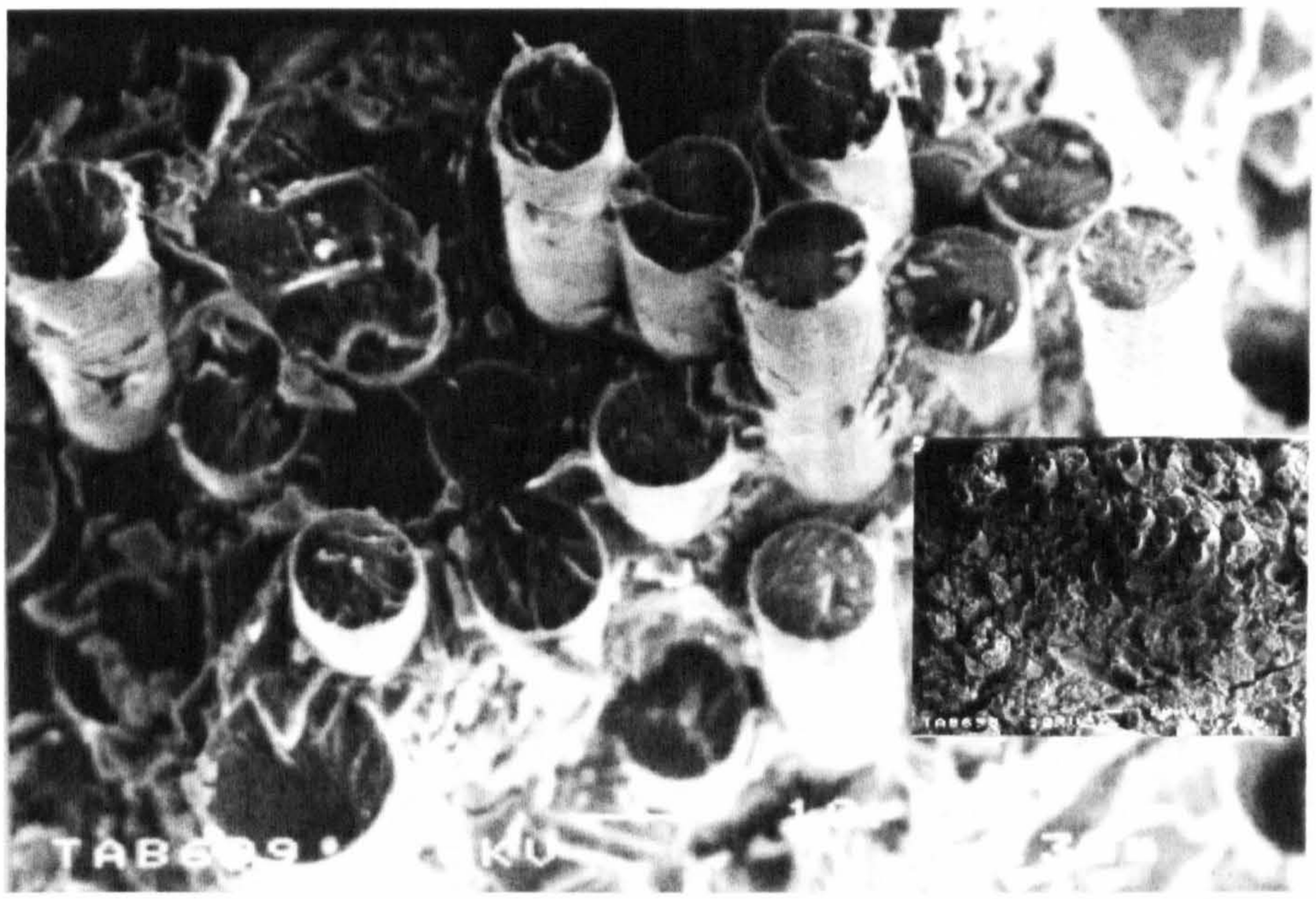

Fig. 6.25 Limited fibre pull-out in a tensile fractured section and studied by SEM. The specimens with AR-50/1 glass fibre 22.6% were moulded at 130 °C. Insert shows the same area on specimen with much smaller magnification.

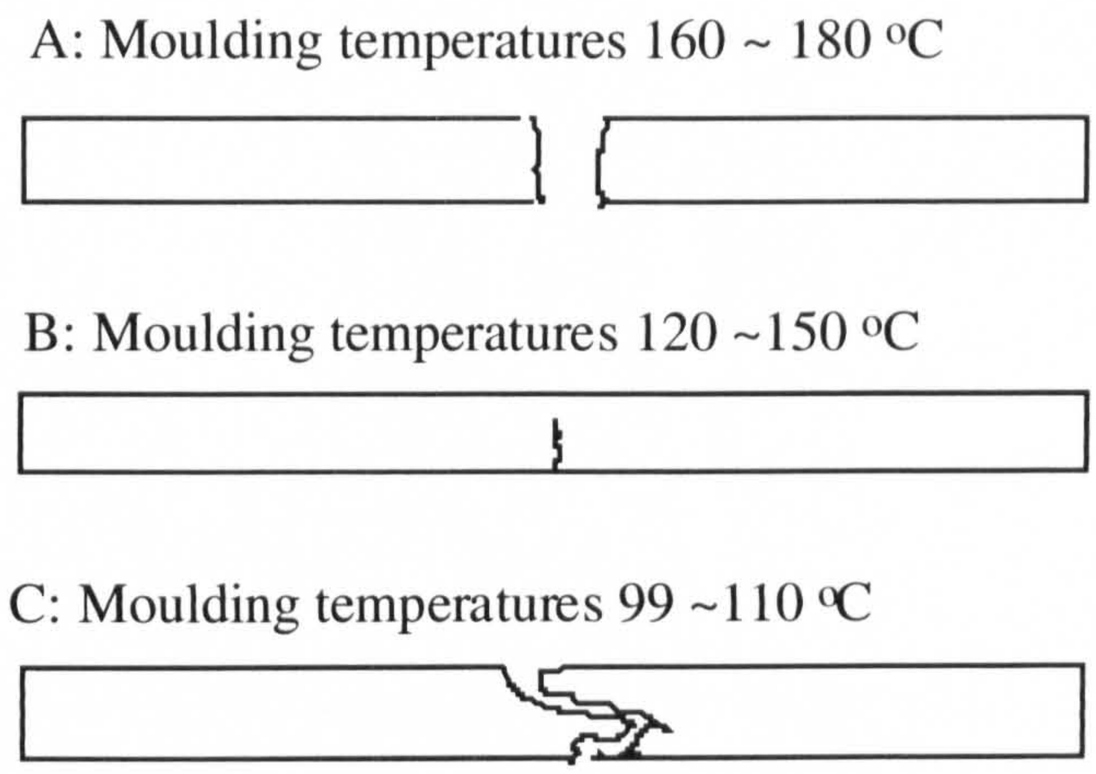

Fig. 6.26 Flexural test failure types of specimens moulded at different ranges of temperature for the CDMC with AR50/1 glass or E-glass.

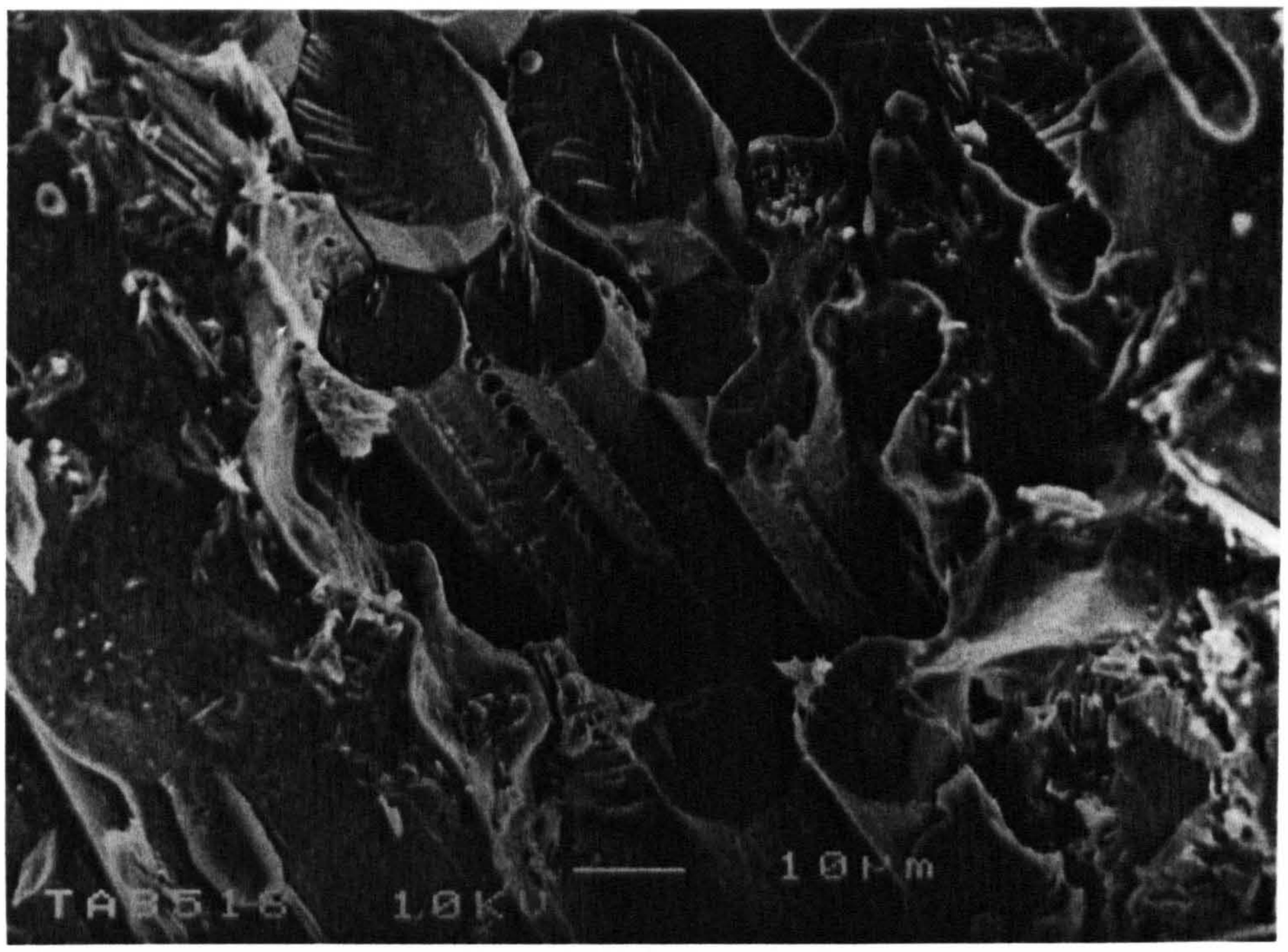

Fig. 6.27 Fractured surfaces of specimens with 22%(vol.) AR-glass fibre 50/1 after flexural tests, moulded at 170 °C.

Fig. 6.28 The SEM micrograph of a flexural fracture surface, specimen moulded at 99 °C, the CDMC with 22.6%(vol.) AR-glass fibre. Some fibres were pulled out completely.

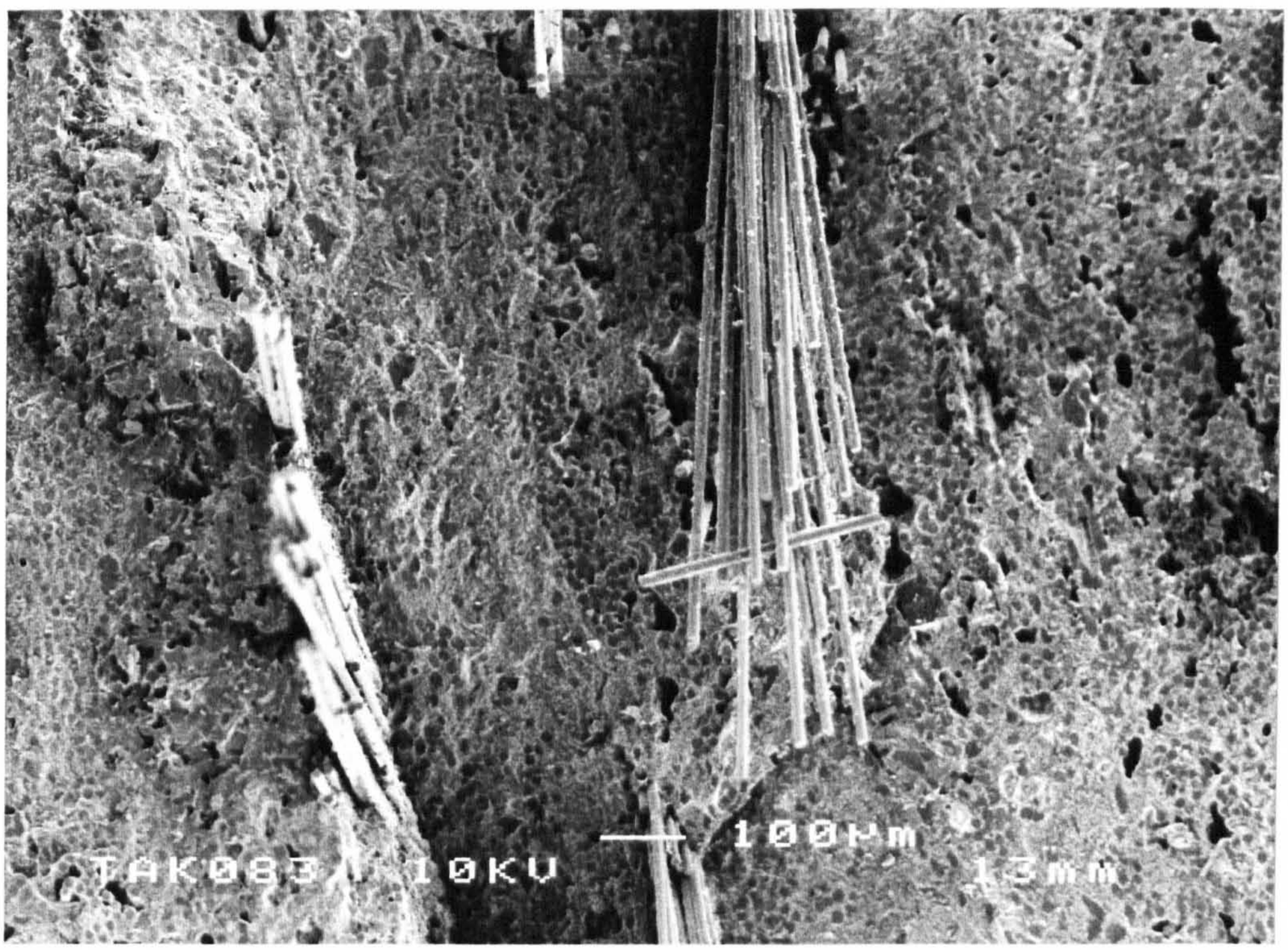

Fig. 6.29 SEM micrograph of the fracture surface from the tensile specimens with 22.6%(vol.) AR50/1 GF moulded 150 °C.

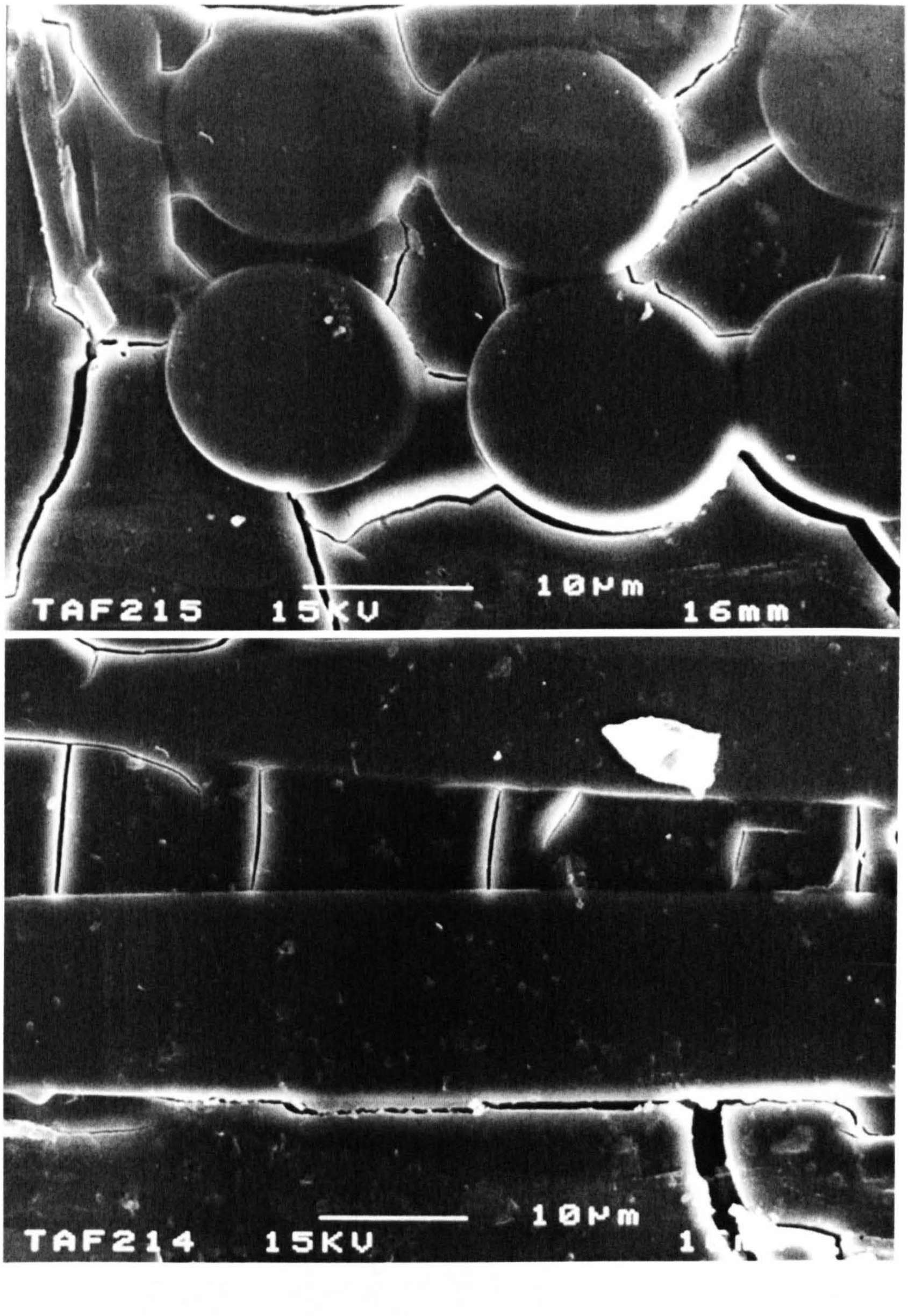

a.

b.

Fig. 6.30 (**a**. and **b**.) The SEM micrographs of matrix cracks and interfacial debonds caused by the thermal expansion and shrinkage or mismatching between fibre and matrix during the moulding and followed post curing. The sample specimen moulded at 150 ℃ with AR50/1 glass fibre was consistently polished until the thickness of specimen reached around 200 micron.

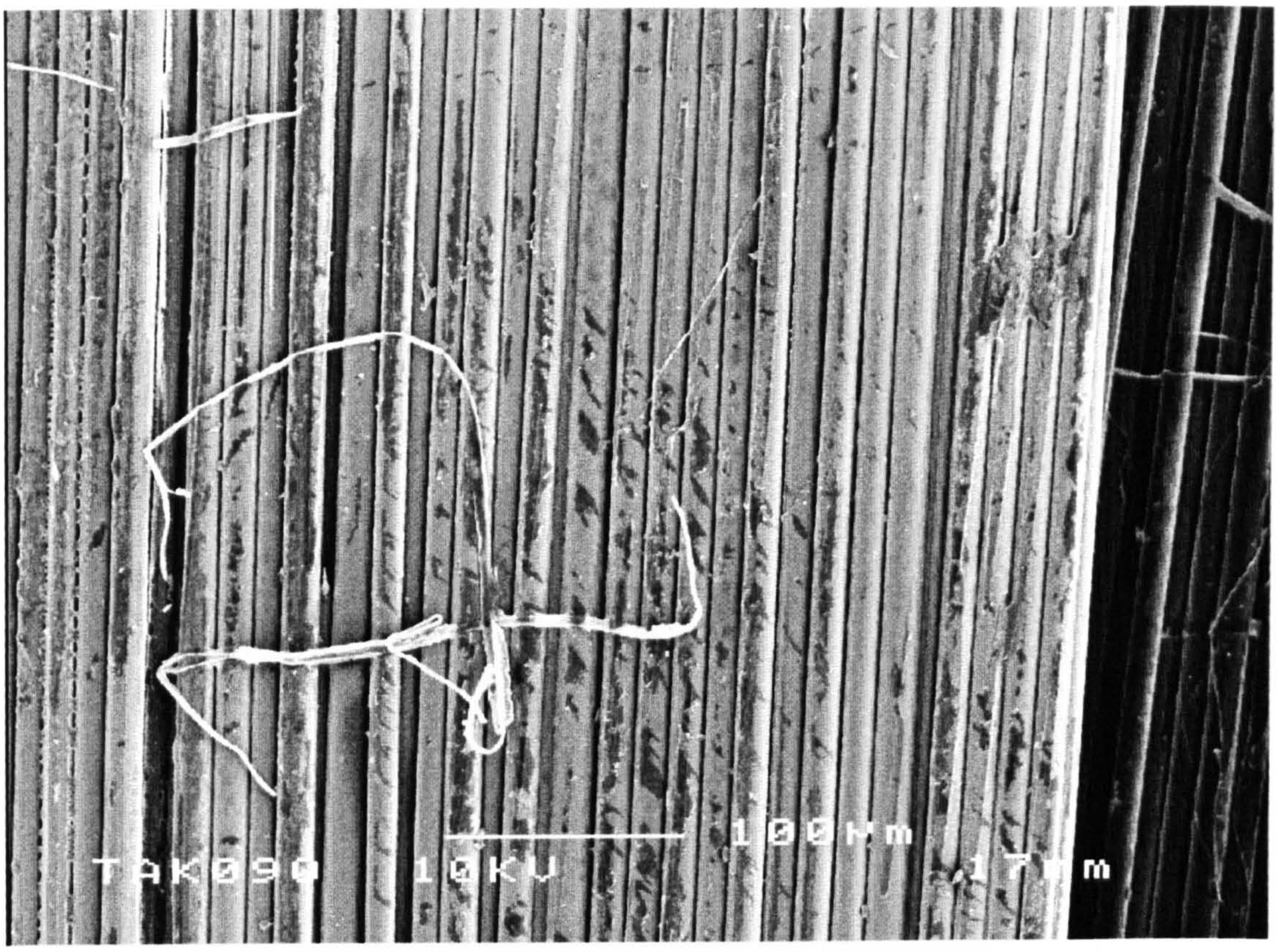

Fig. 6.31 AR glass fibre under alkali media of liquid sodium silicates (079) for 24 hours at the temperature 99 °C. Since some adhesive or binder around fibre is pealed off, the fibre surface becomes rough.

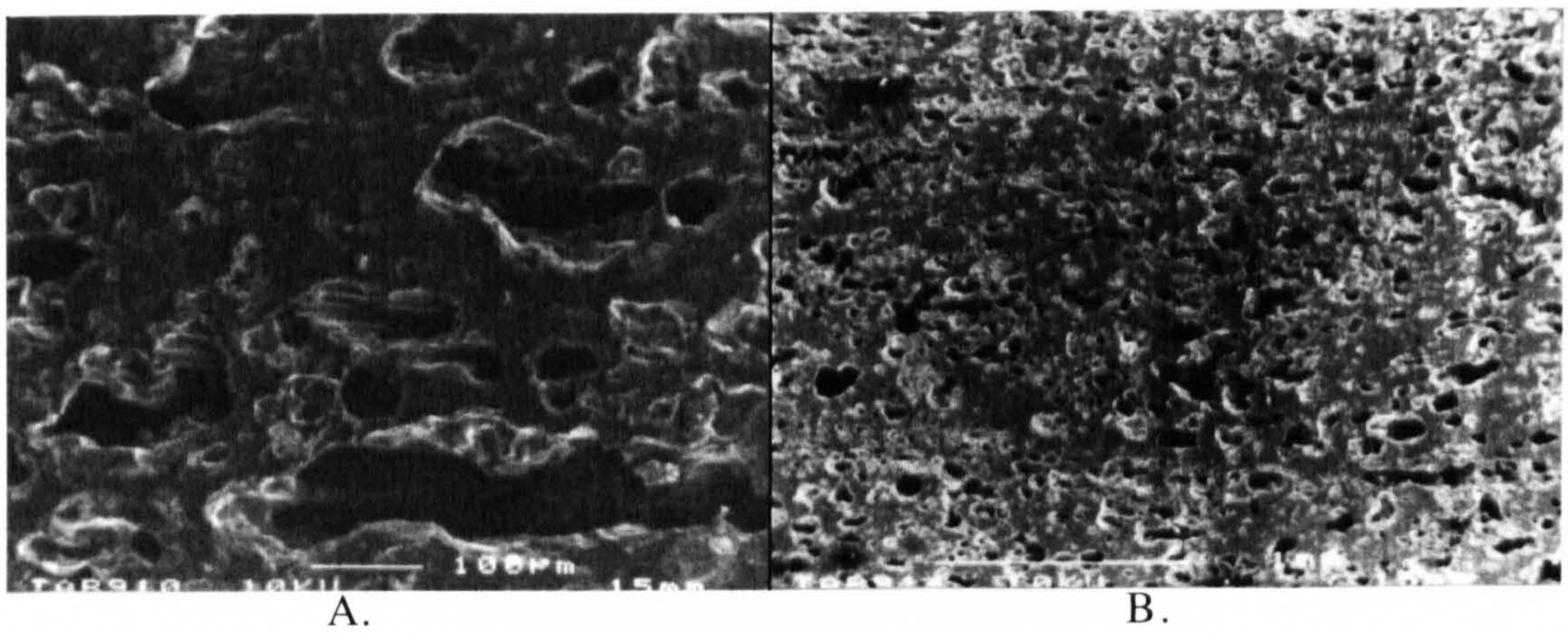

A. B.

Fig. 6.32 (left A, right B) The polished specimens moulded at 180 ℃ (A) and 170 ℃ (B). Although there were lots of voids, but the crack could not be observed.

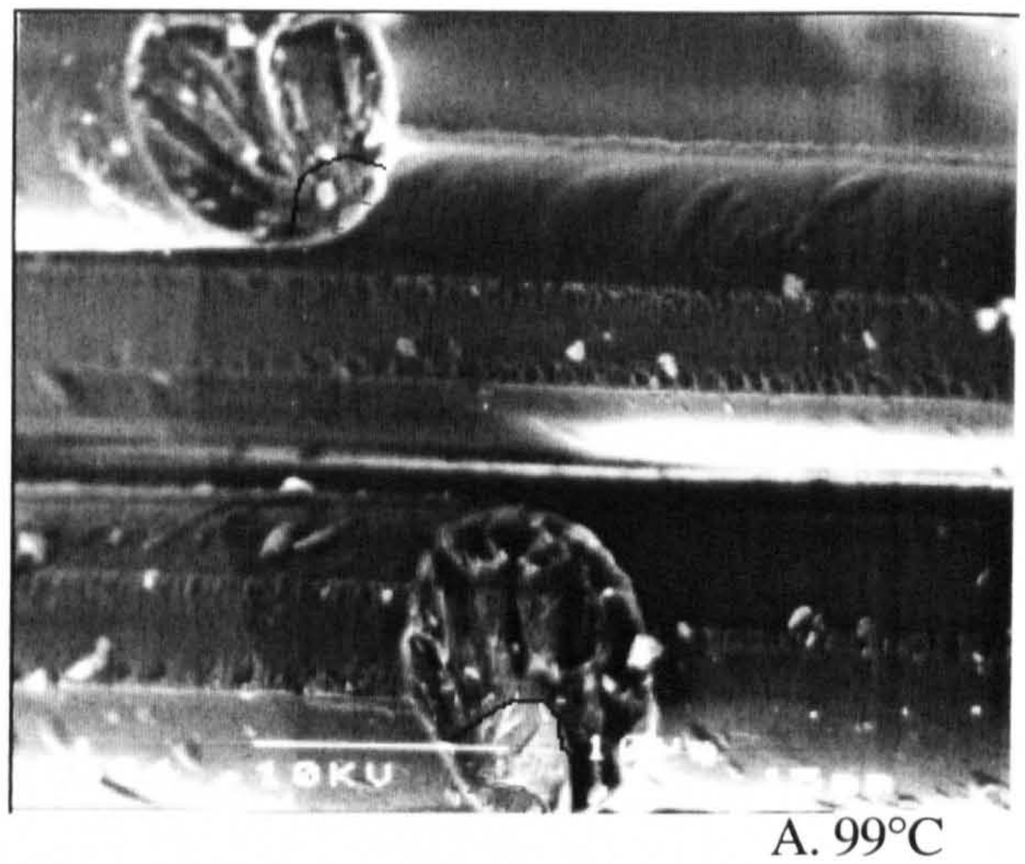

A. 99°C

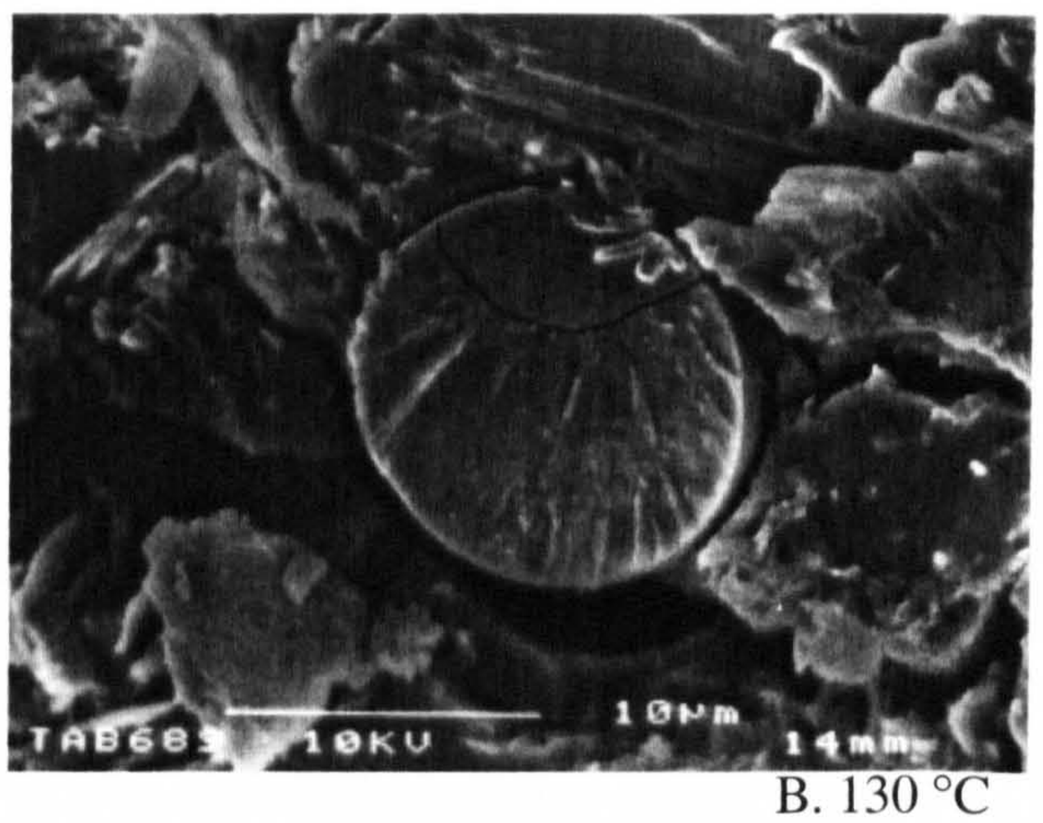

B. 130 °C

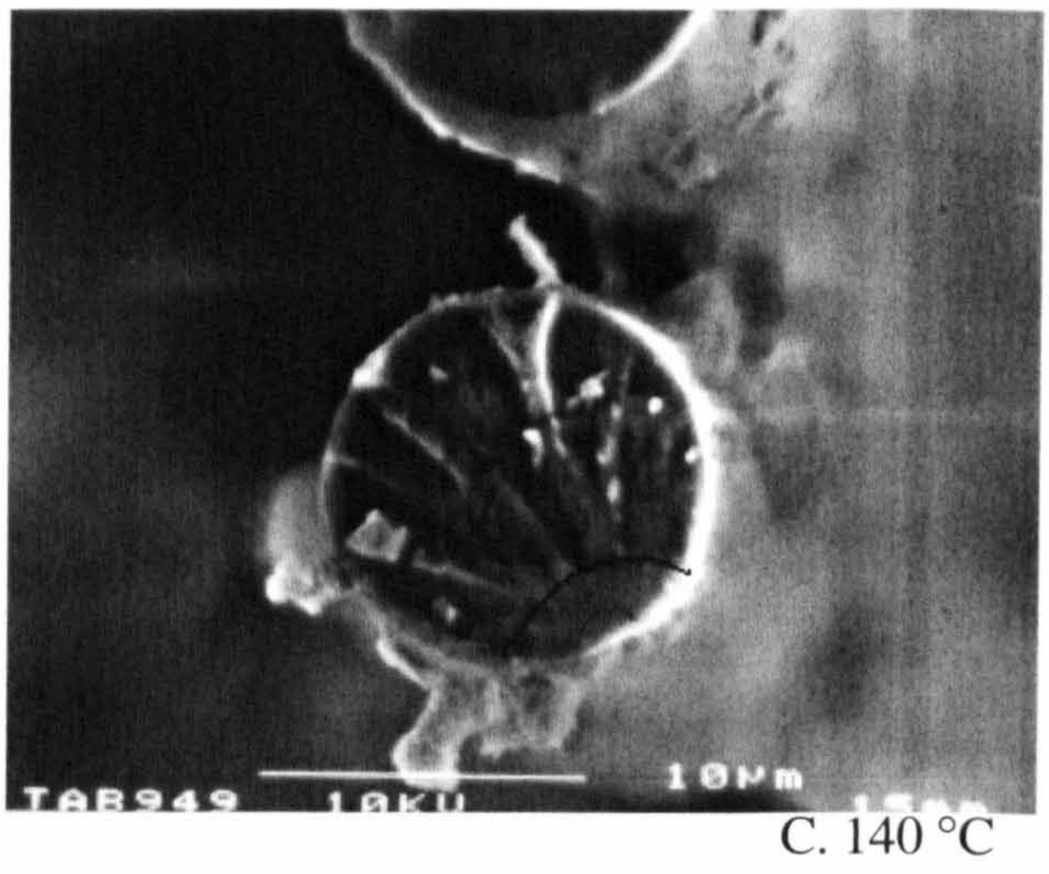

C. 140 °C

Fig. 6.33 The mirrors were observed at tensile specimens moulded at different temperatures 99 °C, 130 °C and 140 °C.

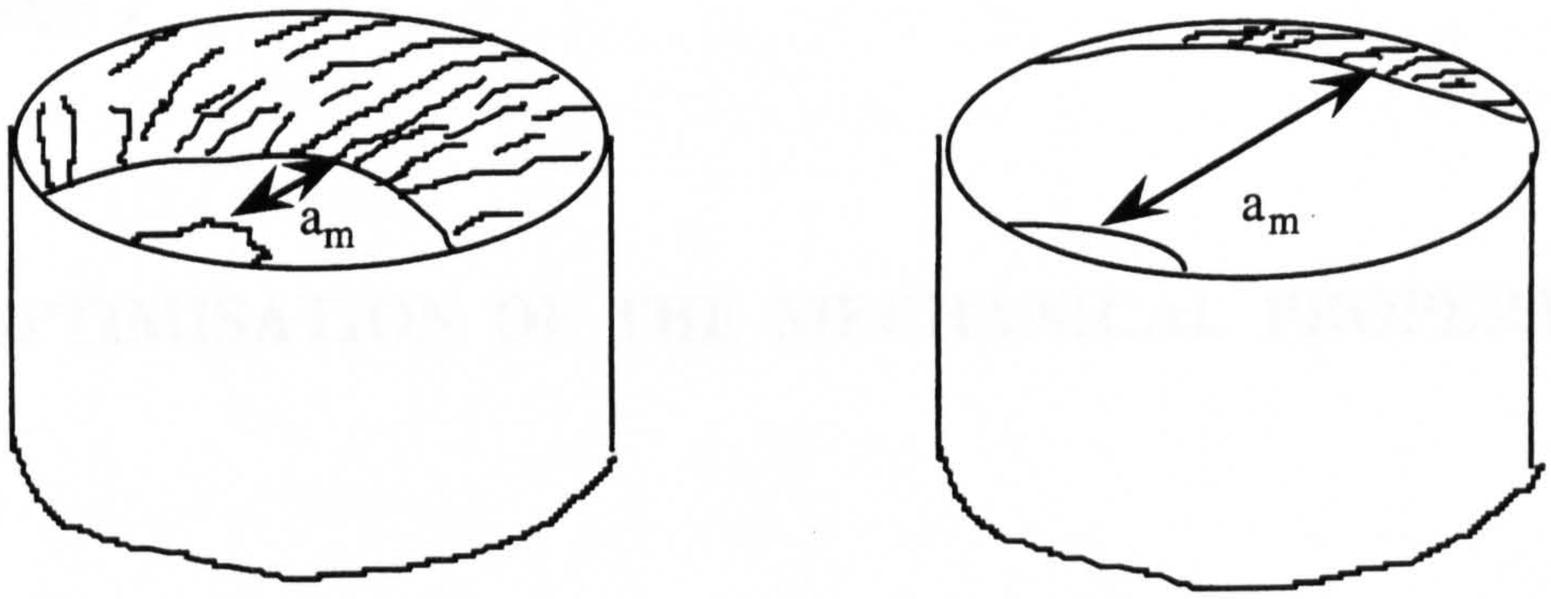

Fig. 6.34 A schematic illustration of two fracture mirrors and the dimensions $\mathbf{a_m}$ *in the* fibre tops from the CDMC fractured specimens which could be used to predict the in situ single fibre strength.

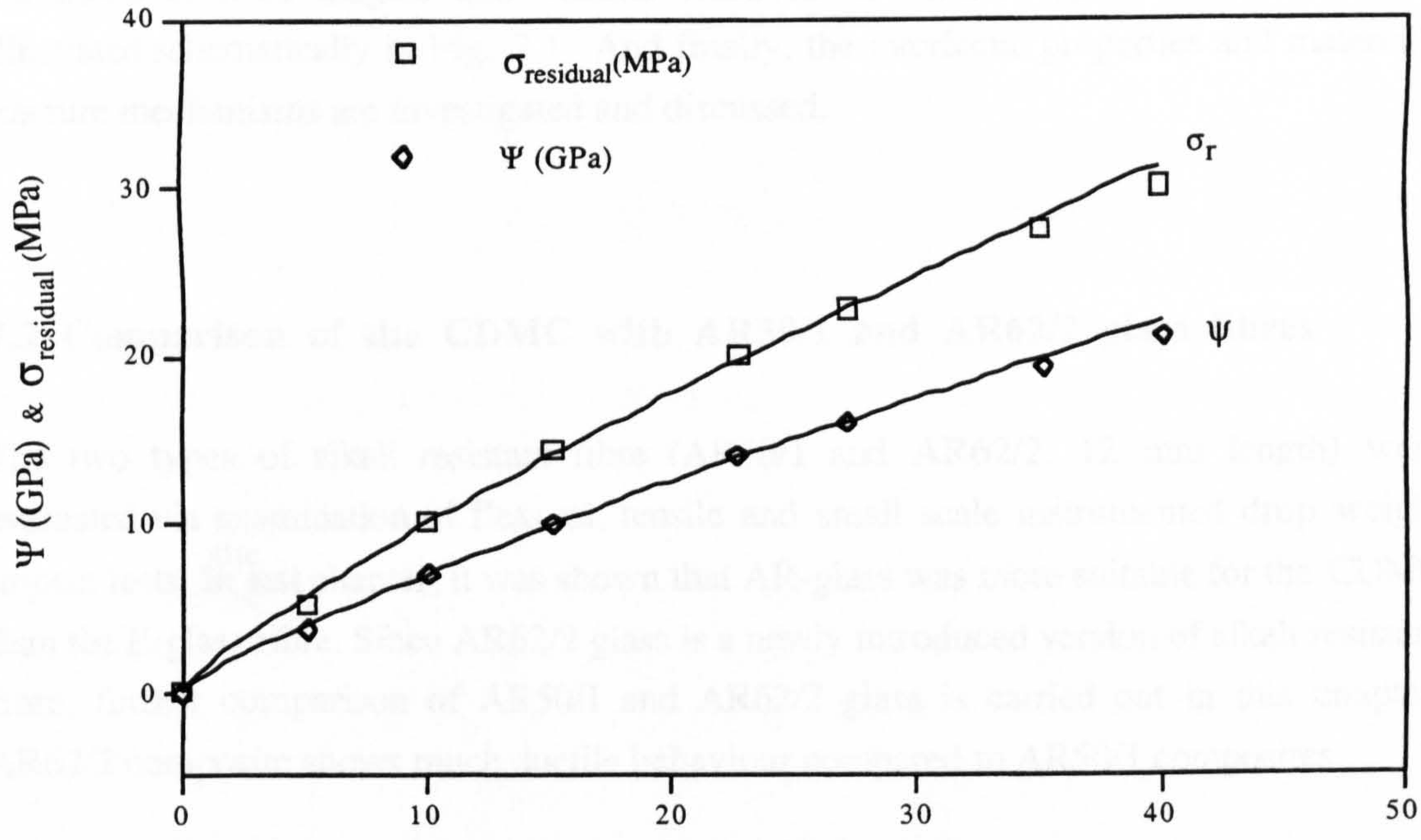

Fig. 6.35 The relationship between the matrix residual strength and the glass fibre volume fractions in the ceramic moulding composites.

Chapter 7

OPTIMISATION OF THE MECHANICAL PROPERTIES

7.1 Introduction

Optimisation of the mechanical properties for the CDMC is carried out by evaluating the combination of the matrix with different types and quantities of glass fibres. The objectives of this chapter are: firstly, to compare the flexural, tensile and impact properties of the CDMC with AR50/1 and AR62/2 glass fibres under selected moulding conditions (T_m = 140 °C, P_m = 8.0 MPa for 60 minutes), followed by a study of the effects in variations of fibre lengths and volume fractions of AR62/2 glass fibre. These are illustrated schematically in Fig. 7.1. And finally, the interfacial properties and material's fracture mechanisms are investigated and discussed.

7.2 Comparison of the CDMC with AR50/1 and AR62/2 glass fibres

The two types of alkali resistant fibre (AR50/1 and AR62/2, 12 mm length) were evaluated via examination of flexural, tensile and small scale instrumented drop weight impact tests. In the last chapter, it was shown that AR-glass was more suitable for the CDMC than the E-glass fibre. Since AR62/2 glass is a newly introduced version of alkali resistant fibre, further comparison of AR50/1 and AR62/2 glass is carried out in this chapter. AR62/2 composite shows much ductile behaviour compared to AR50/1 composites.

7.2.1 Flexural properties

The flexural stress-strain curves of the CDMC with AR 50/1 and AR62/2-glass fibres are illustrated in Fig. 7.2. It is found that although AR62/2 and AR50/1 glass CDMC have similar flexural strengths and moduli, the AR62/2 glass CDMC exhibited greater ductility,

and absorbed more energy during fracture. Although chopped glass fibres are randomly oriented, extensive fibre sliding, pull-out, and bridging could be still observed as shown in Fig. 7.3. The fibres with a good compatible surface treatment, 50/1 proceeded to fail in to a brittle fashion after being strained less than 0.25%. The compound with 62/2 fibre seemed to exhibit non-linear stress-strain characteristics after a strain of about 1.0% with considerable fibre pull-out.

7.2.2 Tensile properties

Tensile stress-strain curves of the CDMC with AR50/1 and AR62/2-glass fibres are compared in Fig. 7.4. The more ductile feature of the AR62/2 fibre CDMC is again observed in relative to the AR50/1 CDMC. For the AR62/2 glass CDMC, the initial elastic response was followed by matrix cracking which resulted in a fibre-matrix interfacial debonding and more absorbed energy. The tensile modulus of AR62/2 glass fibre CDMC is also significantly greater than that of 50/1 glass fibre CDMC. A comparison of tensile properties for AR50/1 and AR62/2 glass fibre composites is listed in Table 7.1.

In this comparison, it is difficult to understand why is that AR50/1 and AR62/2 glass composites exhibit different moduli, while the glass fibre and matrix composition are the same. The only difference between these two composites is in their sizing systems used on the fibres. The 50/1 fibre might use a different binder which results in a different bonding with the matrix compared with the 62/2 fibre, which might give different effects on the compound during moulding. But there is not enough evidence to cite that the interfacial differences or effects during moulding could determine the elastic moduli of the composites.

The micro fracture of the 62/2 glass CDMC also demonstrates different features to that of AR50/1 fibre. Much extensive fibre pull-out is observed in tensile specimens as shown in SEM micro-photograph in Fig. 7.5. The comparative SEM fibre pull-out for 50/1 fibre in CDMC was illustrated in last chapter (Fig. 6.25) with much shorter fibre pulled out after failure. This damage process also implies more energy absorption for the AR62/2 glass composite compared with the AR50/1 glass fibre composite during testing. This has been proved clearly by the following impact tests.

7.2.3 Impact properties

Force-time and energy-time histories of the CDMC with AR50/1 and AR62/2 glass fibres are recorded by computer and compared as shown in Fig. 7.6. The AR62/2 glass CDMC absorbed more energy compared to the AR50/1 glass CDMC. The values of energy absorption of the two composites are also listed in Table 7.2. The AR62/2 CDMC absorbed some 20 times more energy compared to the original AR50/1 glass CDMC.

With the same volume fraction of glass fibre and 15.9 J total impacting energy, the AR50/1 CDMC shattered during the impact, while the AR62/2 glass CDMC absorbed most of impact energy (15.0 J) without being fully penetrated as shown in Fig. 7.7. The AR50/1 glass CDMC is consistent with a good bonding between fibre and matrix which results in a brittle failure during impact. Although the AR62/2 glass fibre had a weaker bond with matrix, its composites achieved better impact properties.

7.3 **Mechanical properties of the CDMC with AR62/2 glass fibre**

Based on the above results, the CDMC with AR62/2 glass fibre produced better mechanical properties than that of AR50/1 glass composite. It was therefore necessary in this research to further investigate and evaluate the effects of AR62/2 glass fibre to the CDMC with variation in length and volume fractions in order to achieve optimum mechanical properties.

7.3.1 Flexural properties with different length and volume fraction

- Fibre length

The mechanical properties of the CDMC with different lengths of AR62/2 glass fibre were evaluated. Typical stress-strain curves of the material with 6 mm, 12 mm and 24 mm are shown in Fig. 7.8. The CDMC with 6 and 12 mm fibre length exhibit a more ductile behaviour with higher strain to failure in comparison with the 24 mm fibre composite. This ductile deformation was only achieved by the AR62/2 glass fibre.

One of the fractures of a specimen with 22.6%(vol.) glass fibre tested is shown in Fig. 7.9. The crack was generated in the tensile side of a flexural specimen with 12 mm AR62/2 glass fibres and fibre pull-out and bridging can be observed clearly.

Generally speaking, the longer the glass fibre in composites, the better the mechanical properties. However, for chopped fibre CDMC, the properties are also constrained by their compounding and moulding processes. Shorter fibres may be easier to flow or transfer to details within the mould chamber. Although longer fibres may be imagined to give better mechanical properties, they introduce difficulties during DMC manufacturing (mixing and moulding). Longer fibres may be more easily damaged and tangled together which hinders the materials flow during moulding when the fibre length far exceeds the thickness of the moulding cavity. These might be the reasons that longer fibre panels produced lower mechanical properties as shown in Fig. 7.10. Hence, it is not always the case that the longer the fibre in composites, the better mechanical properties produced.

- Volume fraction

It has been discussed in Chapter 6 by using 50/1 glass fibre that the flexural properties of the CDMC were effected by fibre volume fractions, and that 22.6%(vol.) compound generated the highest properties.

Flexural properties of the CDMC have been examined with different volume fractions of AR62/2 glass fibre (length 12 mm): 15%, 22.6% and 27%(vol.). The flexural stress-strain curves are shown in Fig. 7.11 and corresponding strength and modulus are shown in Fig. 7.12. Both stress-strain curves and overall flexural data indicate that 22.6%(vol.) glass fibre CDMC produced the highest flexural properties and these results are identical with the tensile and impact properties.

7.3.2 Tensile properties with different fibre volume fraction

Tensile properties of the CDMC with 15% - 27%(vol.) AR62/2 glass fibre were examined and their stress-strain curves are shown in Fig. 7.13.

The highest tensile properties achieved for the material are with 22.6%(vol.) AR62/2 glass fibre. This CDMC presented increased ductility (flexural strain to failure) over other volume fractions as listed in Table 7.3. The specimen fractures during tensile testing involved fibre pull-out and formed huge amounts of fibre bridging, randomly crossing cracks. The tensile specimens analysed by SEM showed even clear images of extensive fibre pull-out and bridging, as shown in Fig. 7.14. Fig. 7.15 shows three tensile specimens with different volume fractions that failed in a similar way with fibre pull-out, especially the one with 22.6%(vol.) AR62/2 glass. Fig. 7.16 schematically illustrates the chopped fibre pull-out and fracture along the tensile fractured area and left randomly oriented fibre bridging. The higher fibre volume fraction such as 27%(vol.) caused problems in obtaining an uniform compound prior to moulding and the disappointing mechanical properties are probably a consequence of the non-homogeneous compound with voids and areas of low fibre fraction.

Both flexural and tensile properties of the CDMC with AR 62/2 glass fibre are varied with fibre volume fraction ranging from 15 - 27%(vol.), as shown in Table 7.3. And the trends of strength and modulus developed are the same in both cases. Both maximum flexural and tensile properties were reached at the fibre volume fraction around 22.6%(vol.). These properties, are approaching the general properties of chopped glass fibre polyester and phenolic DMC as listed in Table 2.1.

The bridging effect is a very interesting phenomena for preventing specimen's catastrophic failure generated by progressive fibre pull-out. Many researchers believe that fibre debonding and fibre pullout may appear to be similar phenomena because the failure takes place at the fibre-matrix interface which significantly enhances fracture energy (Agarwal and Broutman, 1990). Fibre bridging can be enhanced to a certain extent by increasing fibre volume fraction as shown and indicated in Fig. 7.15. With volume fraction of glass fibre increased to more than 22.6%(vol.), the bridging demonstrated a strong effect. These phenomena could be also seen in the AR-glass fibre reinforced cementitious materials, steel fibre reinforced concrete, carbon fibre reinforced glass matrix and ceramic fibre reinforced ceramic matrix composites (Evens, Zok, 1994; Prow, 1986).

7.3.3 Impact properties with variations of fibre length and volume fractions

- Fibre length

The force - time and energy - time histories for the CDMC with 6, 12 and 24 mm fibres are shown in Fig. 7.17 and Fig. 7.18 and Table 7.4. Testing of different fibre lengths were undertaking using a striker, mass 0.78 kg, with an impact velocity of 3.6 m/s and total impact energy of 5.2 J. It is observed that 6 and 12 mm fibre reinforced CDMC absorb similar amounts of energy: 4.75 J (6 mm) and 4.87 J (12 mm) , but only 2.3 J is absorbed by 24 mm CDMC. The force-time traces differed with 6 mm CDMC having a lower and wider absorption pattern compared with a 12 mm fibre CDMC. For the 6 and 12 mm fibre CDMC with 15%(vol.) 62/2 glass fibre, the striker did not fully penetrate the panels.

The result of energy absorption of the composite with 12 mm fibre length is the best among the three lengths all with 15%(vol.) of glass fibre. If the fibre volume fraction is increased to around 23%(vol.) and the impact energy increases to 15.88 J, the maximum impact energy absorption reached 14.88 J. The 24 mm fibre CDMC has the lowest energy absorption amongst these three. The reason for this might be the problem encountered during the compounding and moulding process. The fibre tangling and an non-uniform distribution in the composite which has been mentioned before in this thesis. Based on this result, further investigation on the effects of volume fraction for AR62/2 glass fibre on impact properties was mainly using on 12 mm length reinforcement.

- Volume fraction

The impact properties of the CDMC with different volume fraction of glass fibre were investigated by adding 15%, 22.6%(vol.), 27%(vol.) AR62/2 glass fibre to the compound. The striker mass used was 2.32 kg which produced 15.88 J impacting energy. The impact force-time and energy-time comparisons for the composites with different volume fractions are shown in Fig. 7.19. The impact force-deformations of the CDMC are shown in Fig. 7.20. Slightly different energy absorption trends are developed here compared with flexural and tensile results. The specimen with 27%(vol.) glass fraction absorbed the same amount of energy with 22.6%(vol.) glass fibre specimen. The explanation may be that although 27%(vol.) glass composite can not reach same level of flexural and tensile properties as that of 22.6%(vol.), it still provides enough surface area increase inside the CDMC during impact to absorb equivalent energy. The impact damaged specimens with 22.6% and 27%(vol.) glass fibre fractions are shown in Fig.

7.21 - Fig. 7.22. None of these impacted specimen samples were shattered during test. These results represent a huge difference in behaviour compared with the AR50/1 and E-glass fibre CDMC.

Fig. 7.23 is a SEM fractograph of an impacted specimen with 15%(vol.) glass fibre and impacted with 5.2 J total impacting energy. This fracture may well represent an new impact damage phenomena for chopped fibre reinforced brittle matrix material. When the striker hit the specimen on the top surface, the surface contacting the striker provided resistance to the drop force and was subjected to a compressive load. Underneath, half of the thickness of the specimen was delaminated in a total of 5 layers. The surface of the specimen facing the striking force was subjected to a compression from the inside specimen while outer surface was under a tensile load and caused an enlarged tensile failure ring on the non striking face. The edge surrounding the striker circle was subjected to a shear force generated by the striker (diameter 20 mm) and the supporting ring (diameter 40 mm) of the specimen. Therefore, this impact failure might be summarised as a sequence of compression induced multi-delamination with shear followed with tensile failure. This involved composite deformation, matrix cracking, fibre debonding, fibre sliding and fibre pull-out & bridging, then fracture. At the same time as a result of these damage processes, a large amount of impact energy was absorbed by the composite.

The maximum energy absorption data for the CDMC is also compared with a energy absorption master curve generated from various polymer composite materials using glass fibre and carbon fibre reinforcements as shown in Fig. 7.24. The polymer matrices are thermoplastics and thermosets. An extensive amount of work at QMW has been undertaken to build up these master curves. For both carbon and glass fibre composites, if the specimens are of a similar size to those tested, a master curve can be constructed linking absorbed energy with specimen thickness multiplied by volume fraction (Babic, Dunn and Hogg, 1988). The use of the thickness multiplied by volume fraction allows for those unavoidable variations such as thickness, volume faction of reinforcement and type of reinforcement which make direct comparisons difficult. In these master curves, the range of results was expressed by a geometric variable, the specimen thickness, combined with a materials variable - glass fibre or carbon fibre volume fractions. Features related to resin type and fibre form therefore, can be ignored.

It is observed that the CDMC has lower energy absorption compared with glass fibre polymer composites, but has similar energy absorption with carbon fibre composites. The reason for this lower energy absorption may be due to different manufacturing processes

employed, different interfacial failure mechanism between fibre and matrix, and a different strains to failure of the fibres. A major difference is that the maximum tensile strain to failure of ceramic matrix is about 0.02% but the tensile strain to failure of polymer matrix is around ~1.0 - 2.0% about a hundred times higher. These may be one of the main reasons which affect the total energy absorption of the CDMC in comparison with the polymer composite master curves.

These impact results also show that the volume fraction of glass fibre gives relatively proportional effects on the impact energy absorption (Table 7.5) regardless of the difficulties in manufacturing process. However, it seemed that the fibre type played a key role. This further raises another issue of interfacial shear strength between fibre and matrix.

7.3.4 The elastic properties of the CDMC

In the CDMC, if we could restrict parameters such as fibre length to be 12 mm and assume most fibres have a 2-D in plane distribution of fibre orientations, we may use Cox's equation and the Halpin-Tsai equations to evaluate or to compare the theoretical Young's modulus with the measured elastic properties of the CDMC added with both AR50/1 and 62/2 chopped glass fibre in different volume fractions.

Based on the modified equations of "rule of mixtures" developed by Cox (1952), Halpin and Tsai (1969), for the CDMC reinforced by chopped glass fibre (or other types of chopped fibre such as carbon fibre, etc.), the reinforcing efficiency of short fibres is less than that of long fibres, it follows that the effective modulus of CDMC would be less.

For unidirectional aligned fibre material, the rule of mixtures (E7-1 and E7-2) developed by Halpin and Tsai:

$$E_{II} = E_f V_f + E_m (1 - V_f) \qquad \text{E7-1 (Halpin-Tsai)}$$

An extension indicated for short fibre composites of the Halpin-Tsai equation as shown in E7-2 expresses the longitudinal Young's modulus for only the parallel short fibre

arrangement. Where η is a general correction factor as explained in E7-3 and ξ is a geometrical parameter depending on fibre shape and arrangement which can be worked out by equation E7-4. Cox (1952) included other two additional terms η_0, η_l into equation E7-1 and shown as equation E7-5.

η - the correction factor;

η_0 - the orientation efficiency factor;

η_l - the fibre length factor;

ξ - is a geometrical parameter depending on fibre shape and arrangement. It depends on various characteristics of the reinforcing phase such as the shape and aspect ratio of the fibres, packing geometry and regularity and also on loading conditions.

Since these equations are all based on an assumption of $E_f >> E_m$, the suitability of these equations for the CDMC is questionable as $E_{m(CDMC)}$ is about $0.5\ E_f$ of the CDMC.

The extension for a fibre length of l with unidirectional orientation in composites can be expressed as :

$$E_{II} = \frac{E_m(1+\xi\eta V_f)}{1-\eta V_f} \qquad \text{E7-2 (Halpin, 1969)}$$

where
$$\eta = \frac{(M_f / M_m)-1}{(M_f / M_m)+\xi} \qquad \text{E7-3}$$

and
$$\xi = \frac{l}{r} \qquad \text{E7-4}$$

The Cox equation for 3-D or 2-D orientated short fibre distributions, assumed that the matrix and fibre deform elastically and the strains are equal (E7-5):

$$E = \eta_0 \eta_l E_f V_f + E_m (1 - V_f) \qquad \text{E7-5 (Cox, 1952)}$$

$$\eta_l = {E_{short}}/{E_{continuous}} = 1 - (\tanh \frac{1}{2}\beta l) \Big/ \frac{1}{2}\beta l \qquad \text{E7-6}$$

Where β is the angle related with the fibre orientation and position can be obtained by equation E7-7, and 2**R** is the inter fibre spacing and 2**r** is the fibre diameter. $\mathbf{G_m}$ is the shear modulus of matrix.

where $$\beta = \left\{ \frac{2G_m}{E_f r^2 \ln(R/r)} \right\}^{\frac{1}{2}} \qquad \text{E7-7}$$

and η_0 is given by equation (E7-8), related to fibre directions and dimensions:

$$\eta_0 = a_f' / a_f = \sum \Delta a_f \cos^4 \theta / a_f \qquad \text{E7-8 (Krenchel, 1964)}$$

The $\Delta \mathbf{a_f}$ is a total cross-sectional area of a group of parallel fibres lying at an angle θ to the applied load, it is equivalent to a group of fibres of area $\Delta \mathbf{a'_f}$ aligned in the direction of the applied load.

For unidirectional lamina : $\eta_0 = 1$.

When test at perpendicular to the fibres: $\eta_0 = 0$.

For 2-D in plane fibre orientation: $\eta_0 = 3/8$

For 3-D fibre orientation: $\eta_0 = 1/5$.

For a in-plane random fibre distributions: $\eta_1 = 0.99$.

When the fibre orientation is in 3-D, the η is given by equation E7-3 and ξ is given by equation E7-4.

For the CDMC with 12 mm AR glass fibre and fibre diameter is 14 μm:

according to E7-4:

$$\xi = \frac{l}{r} = \frac{12mm}{0.007mm} = 1714.29$$

The modulus of AR-glass fibre M_f and pure ceramic matrix M_m are:

$$M_f = 80 \text{ GPa},$$
$$M_m = 37.8 \text{ GPa},$$

Therefore, η in E7-3 is :

$$\eta = \frac{80/37.8 - 1}{80/37.8 + 1714.28} = \frac{1.12}{1716} = 6.53 \times 10^{-4}$$

Knowing ξ and η, it is possible to use the Halpin prediction for the modulus for the volume fraction of AR50/1 and AR62/2 glass fibres. They are also compared to the Cox model (E7-5) in Fig. 7.25. It shows that firstly, the two glass fibre composites do not fit with Halpin's equation at all. The elastic properties of the CDMC is closer to the Cox prediction but still does not fit well. The trends of the two elastic moduli of the CDMC are not linear since at lower glass fibre volume fraction, the elastic modulus tends to decrease and then increase with further increase in fibre volume fractions. The trend of AR62/2

CDMC is closer to the Cox prediction when the glass fibre V_f increase to more than 20%(vol.). The elastic modulus of the CDMC with AR50/1 is under the Cox prediction equation.

The fitting of the two curves for the 50/1 glass and 62/2 glass fibre composites are:

$$E_{50/1CDMC} = 0.071V_f^2 - 2.037V_f + 37.505 \qquad \text{E7-8}$$

$$E_{62/2CDMC} = 0.043V_f^2 - 1.007V_f + 37.365 \qquad \text{E7-9}$$

It is possible that the difference between the experimental results and predictions is because the two equation assumed that $E_f >> E_m$ (but for the CDMC $E_f = 2E_m$.). Two fitting lines have been drawn for the elastic data of the CDMC with AR50/1 and AR62/2 respectively. A second order power lines fit more suitable for prediction of the modulus with the volume fraction of moulding composites in this range of material's volume fraction. For higher glass fibre volume fraction (>23%(vol.), different mathematical equations may be developed based on the experimental results.

It may be possible to obtain a equation based on the Cox equation with some more correction factors. Factors such as voids, fibre lengths, matrix influences and possibly moulding conditions have to be considered and added to the equation and more wider range of chopped fibre ceramic composites should be investigated and compared. As an assumption, a new equation given as E7-10 for fibre volume fraction range from 0 ~ 27%(vol.) based on Cox prediction equation and preliminary equations E7-8 and E7-9, for AR50/1 and AR62/2 glass fibre composites. It is possible that when fibre volume fraction >27%(vol.), the n in equation 7-10 might be <2.

$$E = \eta_0 \eta_l E_f V_f^n + \eta_m \eta_v E_m (1 - V_f) \qquad \text{E7-10}$$

Where

n: n = 2 when volume fraction of glass fibre is 0 ~ 27%(vol.)

η_m = factor of matrix composition.
η_v = Factor of volume fraction of glass fibre.

Other factors should also be considered such as different residual stresses, interfacial properties and mismatch between fibre and matrix when the material is processed under different moulding conditions. The environmental conditions such as testing temperature and humidity may also have influence as well. These factors needed to be further investigated, but are outside the scope of this work.

7.4 Interfacial properties between glass fibre and matrix

The fibre/matrix interface is known to play a major role in ceramic composites ductility. This part of work is an attempt to obtain a value for the debonding load and interfacial shear stresses between fibre and matrix using an computer controlled indentation equipment.

The basic fracture mechanisms for ceramic composites are firstly matrix cracking, followed by fibre debonding, pull-out, bridging, splitting and fibre fracture. All these contribute to the work of fracture. The existence of interfaces contributed to these mechanisms of energy absorption and crack blunting by fibres, which are responsible for the ductility or fracture toughness of the composite materials (Chamis, 1994; Cooper and Kelly, 1969).

In the interface between glass fibre and ceramic matrix, after the first crack was formed across a fibre in ceramic matrix, the matrix stress was transferred to the fibres at the crack. Since the fibre is discontinuous and randomly oriented, whether they can support the stress or pull out from the matrix depends on the shear stresses developed on the fibre/matrix interface or on the strength of the interfacial bond (Majumdar AJ and Law V, 1973). If we assume that the shear stress developed at the interface is uniform along the fibre length, the load is then transferred from the fibre to the matrix and decreases linearly with distance from the crack. Therefore, since the ceramic matrix is brittle rather than ductile and does not show a yield stress, it leads to the result that the push-out or pull-out load is directly proportional to embedded fibre length. It has been reported that when resin and fibre become de-bond, then the fractional stress developed between fibre and matrix is roughly constant during pull-out or push-out (Kharrat, Carpenter, 1996).

7.4.1 Interfacial shear strength

The random fibre orientation in the composite does not allow a simple test such as interlaminar short beam shear strength or a transverse tensile tests to be undertaken that the indirectly gives a measure of the interfacial strength. Therefore, in order to measure the interfacial shear strength some trial experiments were carried out using a computer controlled micro-indentation system. Specimens used for indentation tests between single AR-glass fibre and the matrix effected by the moulding temperatures are listed in Table 7.6 and Table 7.7. Since the CDMC specimens moulded at lower temperatures less than 150 °C were too soft and could not be polished into required thickness, only the CDMC specimens moulded at 150 °C and 190 °C were tested. The result of interfacial shear strength of the CDMC moulded at 190 °C was higher between the fibre and matrix compared to the panel moulded at 150 °C.

The specimen thickness of 200 ~ 300 micron were polished. The indentor used was 20 micro-diameter, maximum load was 500 mN. One of the micro-indentation load - displacement curves of the glass fibre pushing out from the CDMC moulded at 150 °C is shown in Fig. 7.26. The debonding load for this particular glass fibre was around 260 - 280 mN. The average interfacial shear strengths at moulding temperatures of 150 °C and 190 °C are 22.20 MPa and 37.45 MPa respectively.

Consequently, if frictional forces play any part in the pull-out mechanism, it is essential to differentiate clearly between catastrophic and non-catastrophic debond in order to determine the true shear strength of the interface. It is sometimes preferable to ensure that the fibre and matrix interface has a low adhesive strength, so that it debonds easily. Since the ceramic composites' main priority is to raise its ductility, it can be done through promoting crack-deflection at the interface, to induce fibre pull-out by frictional sliding, which absorbs a substantial amount of energy.

Detailed analysis on the Hi-Nicalon/A-Si_3N_4 ceramic matrix composites has been undertaken (Monssef, Nakano, 1997) which concluded that if the fibre was subjected to an axial stress resisted by a contact shear stress, such as compressive stress, a radial compression is induced at the interface as a consequence of the so-called Poisson effect. This, in turn, modifies the resultant interfacial radial stress and the frictional stress would

take into account of all the contributions from the clamping stress at the fibre / matrix interface.

7.4.2 Fibre sliding and fracture

Fibre - matrix interface was highly effected by moulding temperatures. Based on the properties of the CDMC achieved in different moulding temperatures, the overall moulding temperature effects to features of interface were approximately estimated in Fig 7.27.

The tensile failed sections of the SEM fractograph for the specimens have been observed that much larger surfaces generated by fibres, an improvement in ductility and presented a consistent characterisation of interfacial mechanical properties. This has been described with two perimeters by previous researchers on this particular research field. One is associated with fracture and the other is with slip (Kerans and Parthasarathy 1991; Mackin, Warren and Evens, 1992). Fracture or debonding is considered to involve a de-bond energy, which is primarily a mode II (shear) fracture phenomenon. With a brittle matrix, mode II fracture typically occurs by the coalescence of micro cracks within material layers (Fleek, 1991). This was observed in the form of fracture marks on the sliding fibre surface which probably produced by the sizing layer or by absorbing locally concentrated fracture energy. These energy absorption marks were illustrated in the AR50/1 fibre surfaces in Fig. 7.28, Fig. 7.29, and Fig. 7.30 for a tensile failed section of the CDMC moulded at 130 °C.

This indicated that debonding occurred after the cracking process especially when the material was moulded at temperatures lower than 150 °C. The presence of a small fringe of striations on some fibres in the nucleation zones indicated the localised direction of crack growth. When a discrete de-bond crack exists, fractured sliding of the crack faces proceeds the shear resistance, such sliding occurs in accordance with a friction law (Marshall and Oliver, 1987):

$$\tau = \tau_o - \mu\sigma_{rr}$$

Where μ was the Coulomb friction coefficient, σ_{rr} is the compression nominal and τ_o is a term associated fibre roughness. For debonding and sliding to occur, rather than brittle cracking through the fibre, the debonding energy, τ_ι must not exceed an upper bound relative to fibre fracture energy τ_f . Fig. 7.30 is showing that some special marks of fibre

sliding on the surfaces of some AR fibre can be observed from its tensile failed specimen's SEM photograph.

7.4.3 The CDMC interfaces effected by moulding temperatures (assumptions)

Apart from the sizing systems which can only be controlled by the fibre manufacturer, the moulding temperatures were a major influence on the interfacial properties. At low moulding temperatures, a weak bonding can be produced; at medium moulding temperatures, an adjustable bonding can be produced and at high moulding temperatures, a strong bonding can be generated.

- Bonding at 99 - 120 °C

At this moulding temperature range, a coupling agent might provide a stable, water-resistant bonds across the surface of glass fibre. A non-polar end of the coupling agent would be assumed towards a silica matrix when the materials moulded at this temperature range. It was unlikely to produce a strong bond between a matrix and a glass fibre in a short term owing to the barrier of organic sizing system.

- Bonding at 170 - 180 °C

The over heated water forms vapour which may attack the sizing layer on the surface of a glass fibre with highly alkalinity when moulded at this temperature range. The sizing layers could be washed away (Cooper and Kelly, 1969) and high shear interactions between fibre / matrix during flow also tore the size structure apart as it formed during moulding. Then the full benefit of silanes might be lost (Plueddemann, 1988). It should be noted that most coupling agents were designed for producing a stable, water-resistant bond at the interface for composites prepared under low shear and pH neutral conditions. It should also be emphasised that at high alkali condition and elevated temperatures, and high shear force during moulding, Si-O-Si bonding could be hydrolysed (Hogg, 1981; Jang and Ishida, 1988). This would result in the matrix and glass fibre forming strong bonds directly through Si-O-Si chains. The interfacial bonding strength effected by the moulding temperatures ranging from 99 °C to 180 °C is shown in Fig. 7.31 schematically. The effects of sizing barrier, -Si-OH, -Si-O-Si- were briefly displayed.

- Bonding at 130 - 150 °C

The sizing system might be washed away and forming a partially bonded area. This could be very important in the range of the temperatures where the bond strength between fibre and matrix might be adjustable, and gives the opportunity to design the interfacial strength and performance for AR glass fibre.

For flexural and tensile specimens, moulded at temperatures 130 - 150 °C, the fibre pullout lengths at the resisting of tensile failure varied according to the fibre types. For the CDMC using 50/1 Cem-FIL fibre, the fibre pull-out was from 10 μm - 30 μm and for AR62/2 glass, the pull-out length is around 1.0 mm. The lower the moulding temperatures, the longer the fibre pulled out. The SEM study suggested that with temperature increase, the length of fibre pull-out would be decreased. The AR62/2 glass fibre composite specimens moulded at 130 - 150 °C exhibited 10 μm to several mm fibre pull-out length during tensile and flexural tests as observed in many of SEM photos in this Chapter.

7.5 Summary

The AR-glass fibre in composites was studied and revealed that optimum tensile, flexural and impact properties can be obtained with a chopped fibre of 12 mm and the fibre volume fraction of 22.6%(vol.). The use of the selected AR-glass fibre 62/2 resulted in the better flexural and tensile properties and a higher energy absorption in impact compared with AR50/1 and E-glass fibres. Some general properties of optimised glass fibre composites are summarised in Table 7.8.

Compared with AR50/1, AR62/2 fibre may give better heat resistance during moulding. In turn, it may provide suitable interfacial properties (relatively weak) for the CDMC when moulded at 130 - 150 °C and then increased ductility and energy absorption during impact. In general, the use of the AR-62/2 glass fibre resulted in improvements in tensile, flexural and impact properties, extended the tensile strain at failure and increased impact energy absorption. This improvement in failure process, a so called pseudo-plastic deformation, involves matrix cracking, fibre debonding, followed extensive fibre pull-out, then fibre fracture or bridging. Here the length of fibre pull-out may give certain contribution to this pseudo plastic deformation.

The CDMC properties are also effected by different lengths of glass fibres (tested by using AR62/2) and these were examined by adding 15%(vol.) different lengths of glass fibre. The CDMC with 6 mm fibre length generated highest modulus among them but lower average strength compared with 12 mm glass fibre. The longer fibres such as 24 mm, allowed certain forces to sustain by lowest stress and strain before rupture occurs. A combination of both 6 mm and 12 mm fibre might result in a synergistic improvement with both strain at failure and energy absorption being optimised.

The interfacial properties of this composite are crucial in determining the mechanical properties. The different moulding temperatures produced different interfacial shear strengths. It is observed and proved that the higher the moulding temperatures produced stronger interfacial bonding strength, while the lower moulding temperatures produced lower shear strength or weak bonding. The very weak bonding could be achieved by moulding process at low temperatures as low as 99 °C. 130 - 150 °C has been selected in the CDMC moulding process as the better moulding temperature range for overall mechanical properties. Some preliminary results were successful in indicating an interfacial shear strength of 22 to 37 MPa with 50/1 fibres depending on processing temperatures.

Table 7.1 The tensile properties of the CDMC with 22.6%(vol.) AR50/1 and 62/2 glass fibres respectively. The specimens were moulded at 140 °C.

	Glass fibre in the CDMC	
Composites	AR50/1	AR62/2
Tensile strength, MPa	22.27	51.0
Tensile modulus, GPa	27.34	42.9

Table 7.2 Energy absorption of the CDMC with AR50/1 glass fibre and AR62/2 glass fibre.

Composites	Energy absorption (J)
Total impacting energy (J)	15.9
AR50/1 CDMC	0.7
AR62/2 CDMC	14.9

Table 7.3 The tensile properties of the CDMC effected by volume fractions of the AR62/2 glass fibre (12 mm).

Volume fraction of AR62/2 in the CDMC	Tensile strength σ, MPa	Tensile modulus E, GPa	Strain to failure ε %
15%(vol.)	18.6	29.14	0.082
22.6%(vol.)	51.0	42.10	0.240
27%(vol.)	34.0	39.10	0.135

Table 7.4 Energy absorption of the CDMC panels moulded with different length of AR 62/2 glass fibre[(15%(vol.)], moulded at 140 °C. Total impacting energy was 5.12 J.

Fibre lengths, mm	Impacting energy(J)	Energy absorption(J)
6	5.12	4.75
12	5.12	4.87
24	5.12	2.30

Table 7.5 Energy absorption of the CDMC with different volume fraction of AR62/2 glass (12 mm) in impact tests. Effects of different fibre type, matrix systems to impact energy absorption were listed.

Glass fibre used	Impacting energy (J)	Energy absorption of different volume fraction of glass fibre (J)		
Glass fibre volume fraction, %(vol.)		15%	22.6%	27%
AR50/1 CDMC	5.12	0.27	0.73	0.84
AR62/2 CDMC	5.12	4.87	5.0	5.0
	15.90	11.34	14.88	14.99

Table 7.6 Specimens used for indentation test for interfacial shear strength between the single fibre and ceramic matrix.

Fibre diameter, μm	Thickness of specimen, μm	Moulding conditions	
		Temperature, °C	Pressure, Bar
14	300	150	80
14	300	190	80

Table 7.7 The interfacial shear strengths between single AR-glass fibre and the matrix effected by the moulding temperatures.

Moulding temperatures	Interfacial shear strength (MPa)
150 °C	22.20
190 °C	37.45

Table 7.8 The mechanical properties of two optimised glass fibre reinforced CDMC were listed. The CDMC were moulded with optimised moulding conditions.

Properties	CDMC with 22.6%(vol.)AR50/1 12 mm glass fibre	CDMC with 22.6%(vol.)AR62/2 12 mm glass fibre
Flexural strength (MPa)	82.0	120.0
Flexural modulus (GPa)	32.0	39.0
Tensile strength (MPa)	25.0	51.0
Tensile modulus (GPa)	39.0	42.90
Strain to failure in tension (%)	0.10	0.24
Energy absorption in impact test (J)	0.67	15.0-20.0
Density	2.30	2.30
Coefficient of thermal expansion, 25 - 400°C (10^{-6} K^{-1})	5.0 - 7.0	5.0 - 7.0
Specific heat (J/g °C), (20-280 °C)	1.5 - 2.0	1.5 - 2.0
Coefficient of thermal conductivity (W/m.K)	0.386	0.386

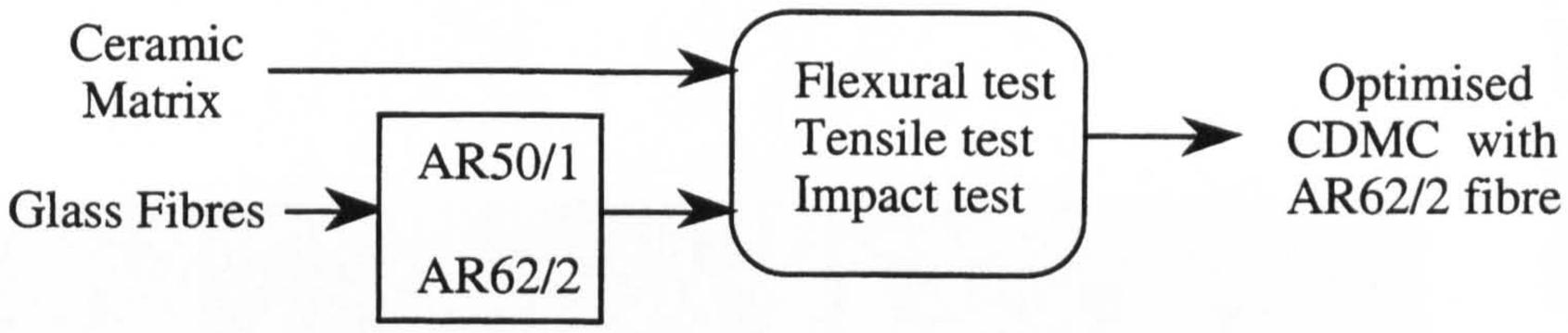

Fig. 7.1 The schematic view of the glass fibre optimisation for the ceramic moulding composites.

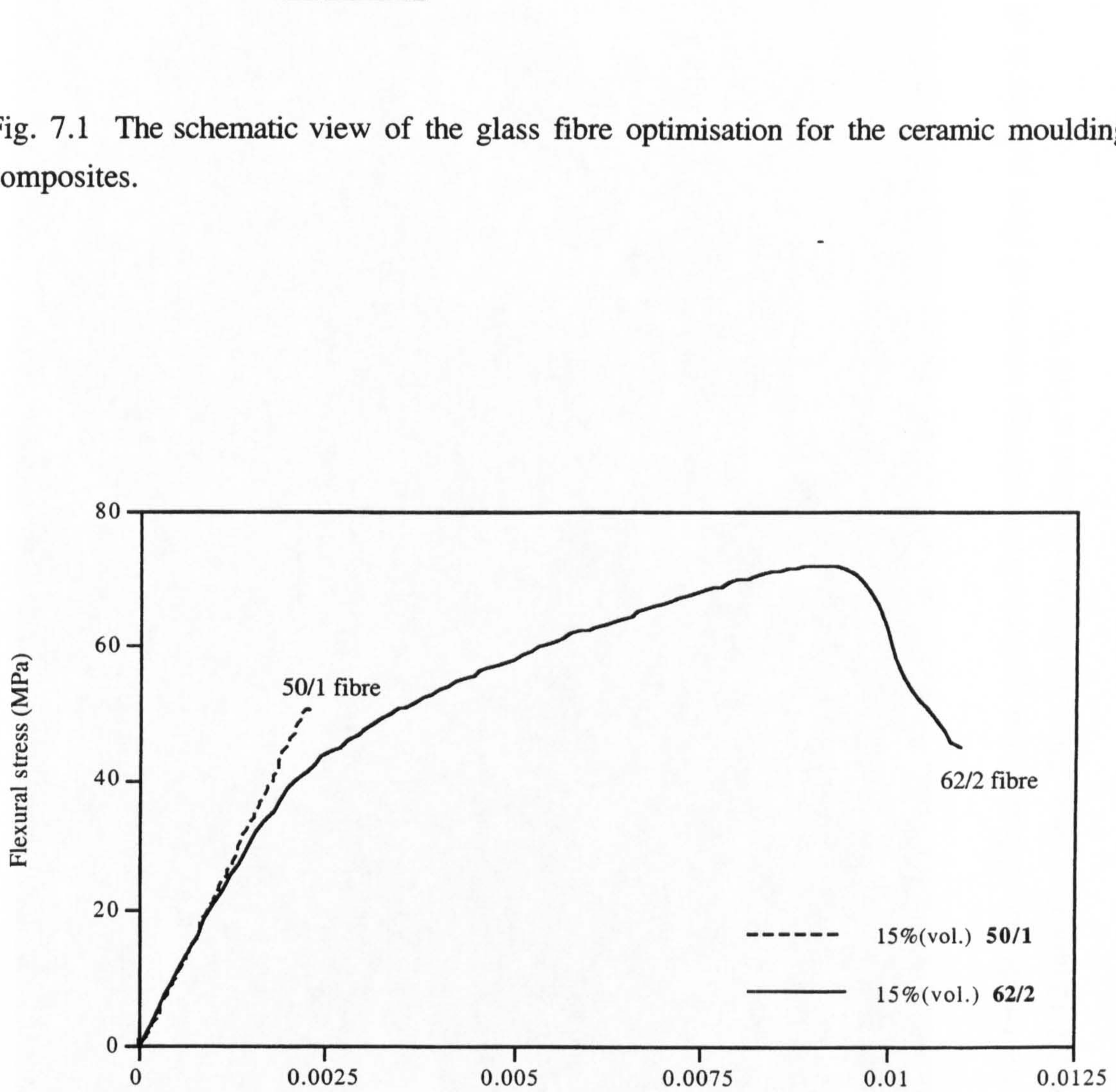

Fig. 7.2 The flexural stress-strain curves of 15%(vol.)AR-50/1 and 62/2 glass fibre composites, moulded at 140 °C.

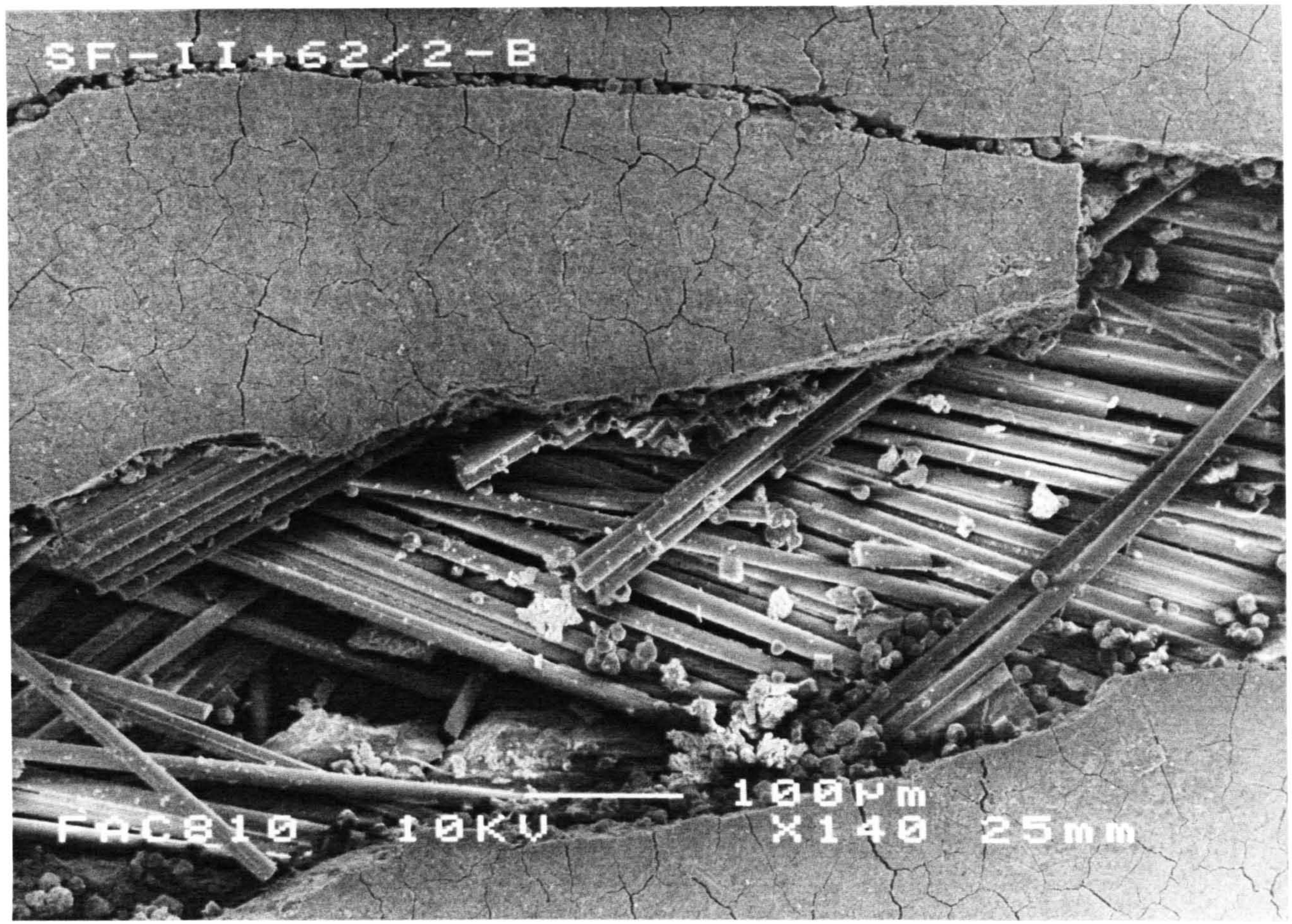

Fig. 7.3 Flexural fracture along the tensile side of flexural test specimen involved huge amount of fibre pull-out in all directions and bridging over the cracked area by chopped AR62/2-12 mm glass fibre. This CDMC was moulded at 140 °C.

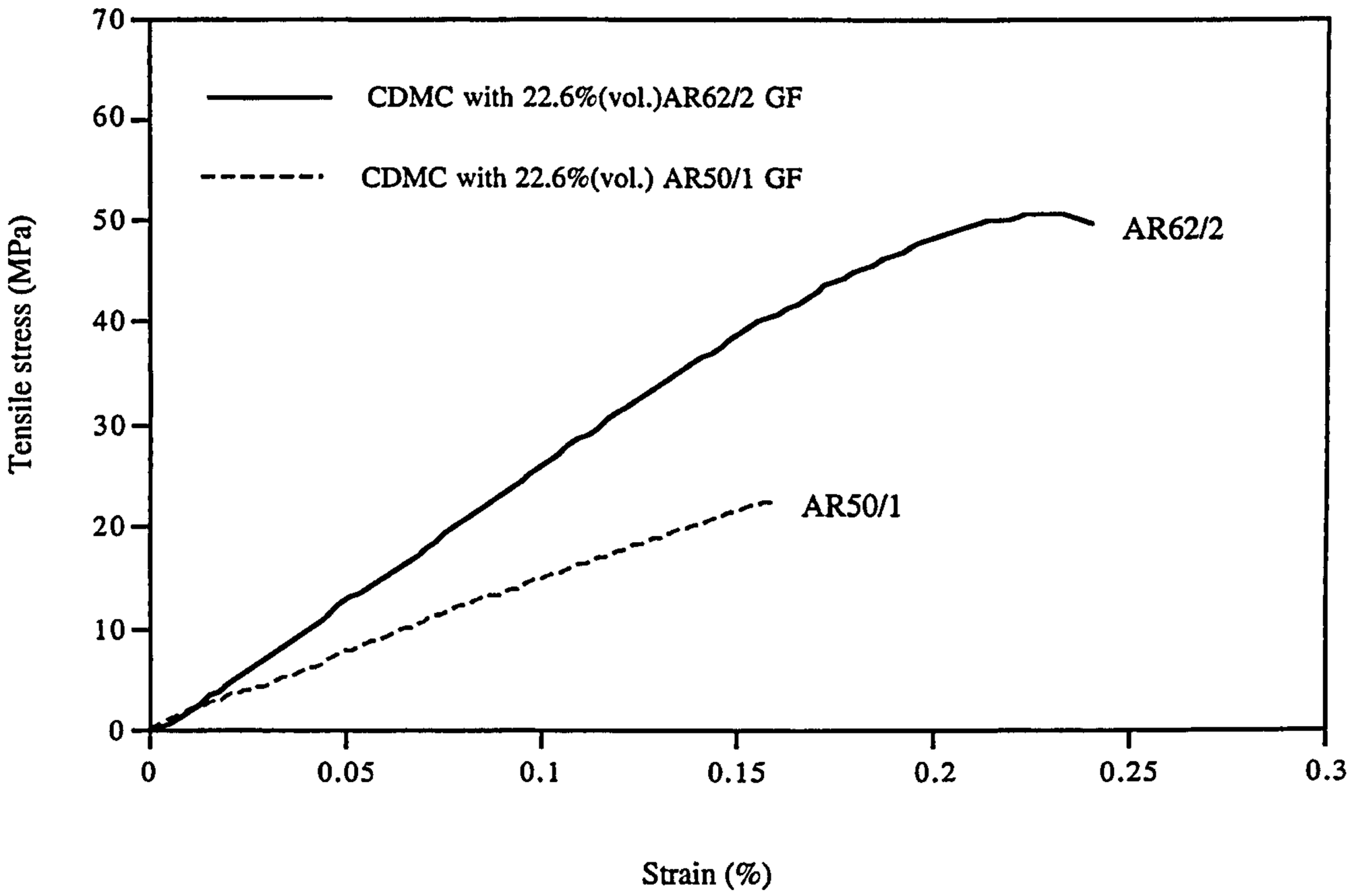

Fig. 7.4 Comparison of typical tensile stress-strain curves for 22.6%(vol.)AR50/1 and AR62/2 glass CDMC, moulded at 140 °C.

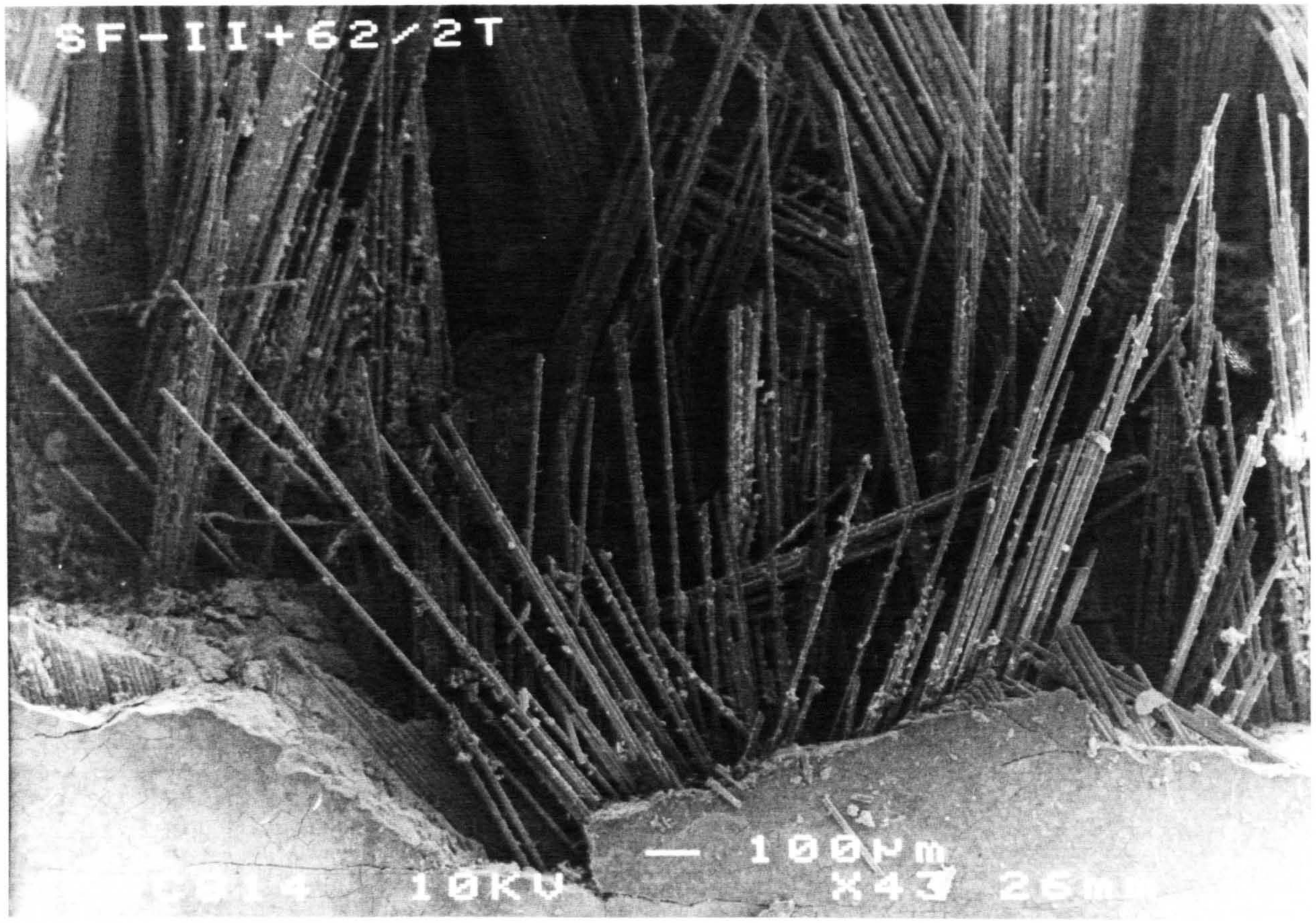

Fig. 7.5 An extensive fibre pulled out during the tensile test of the CDMC with 22.6%(vol.) AR62/2 glass fibre (12 mm), moulded at 140 °C.

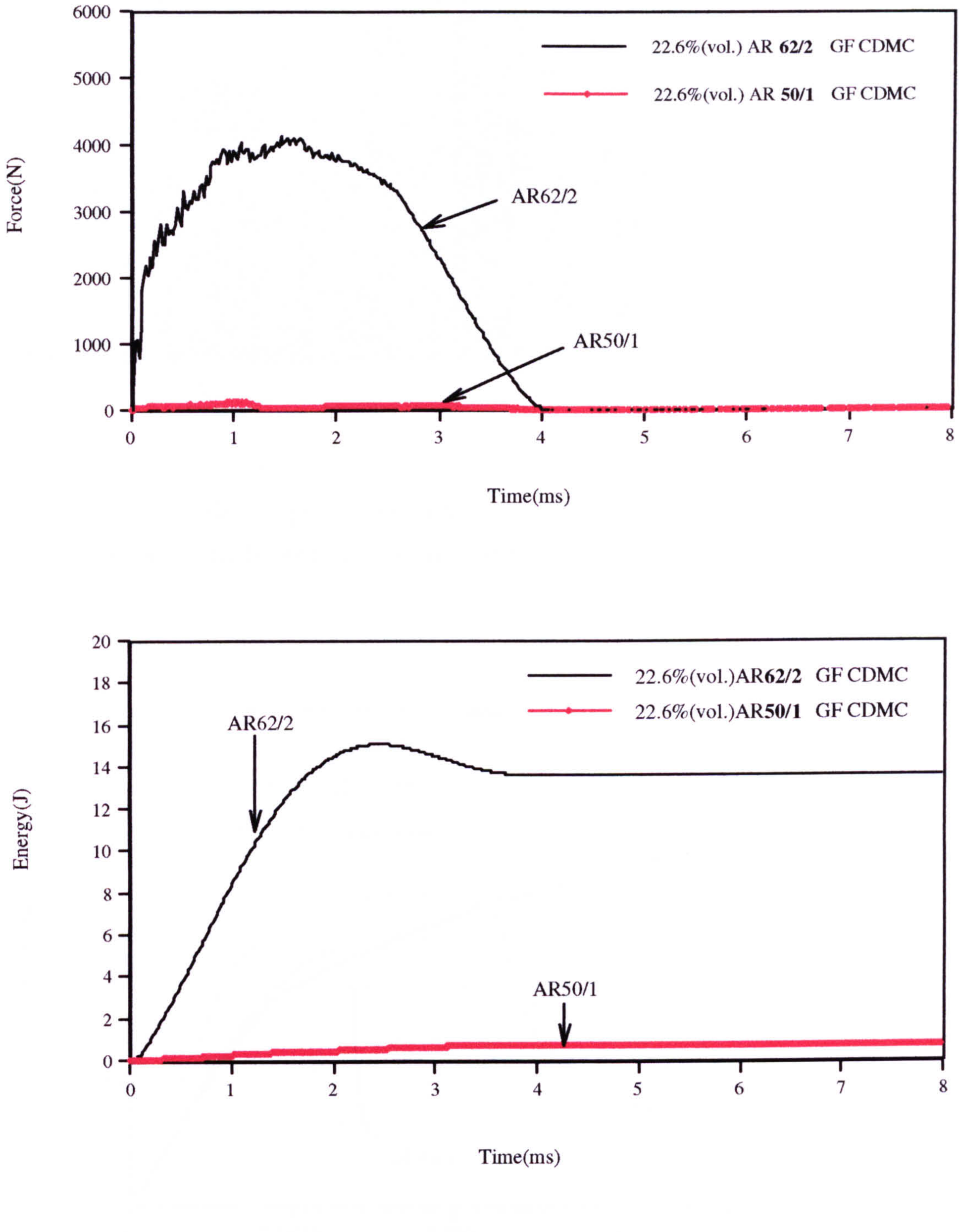

Fig. 7.6 Comparisons of the impacting force-time and energy-time histories of the CDMC with 22.6%(vol.) AR62/2 GF and 22.6%(vol.) AR50/1 GF. Moulding temperature was 140 °C.

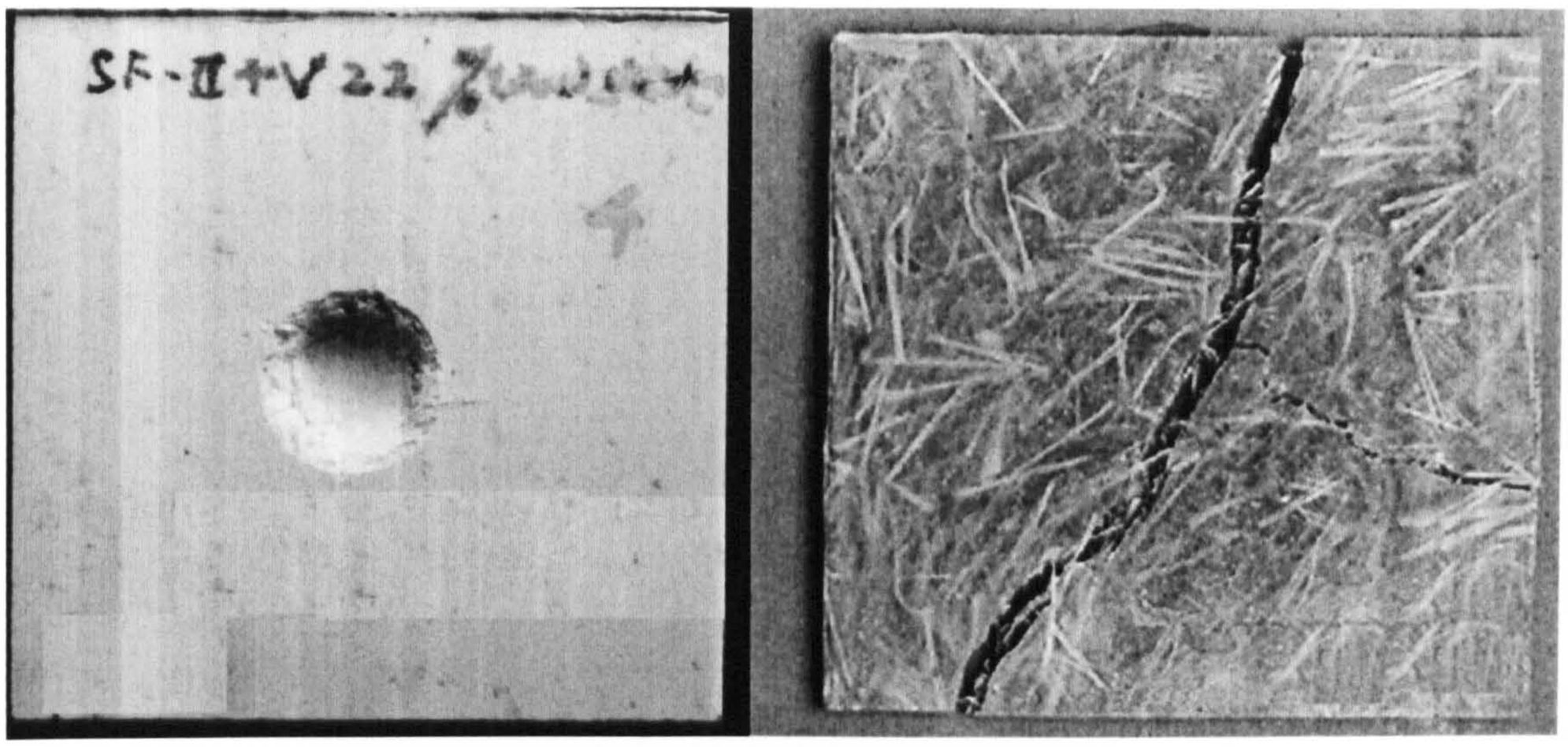

A. **B.**

Fig. 7.7 Comparison of the CDMC specimens after impact. The CDMC was reinforced by 22.6%(vol.) AR62/2 glass fibre (A.) and 22.6%(vol.)AR50/1 glass fibre (B.). Moulding temperature for both specimens was 140 °C.

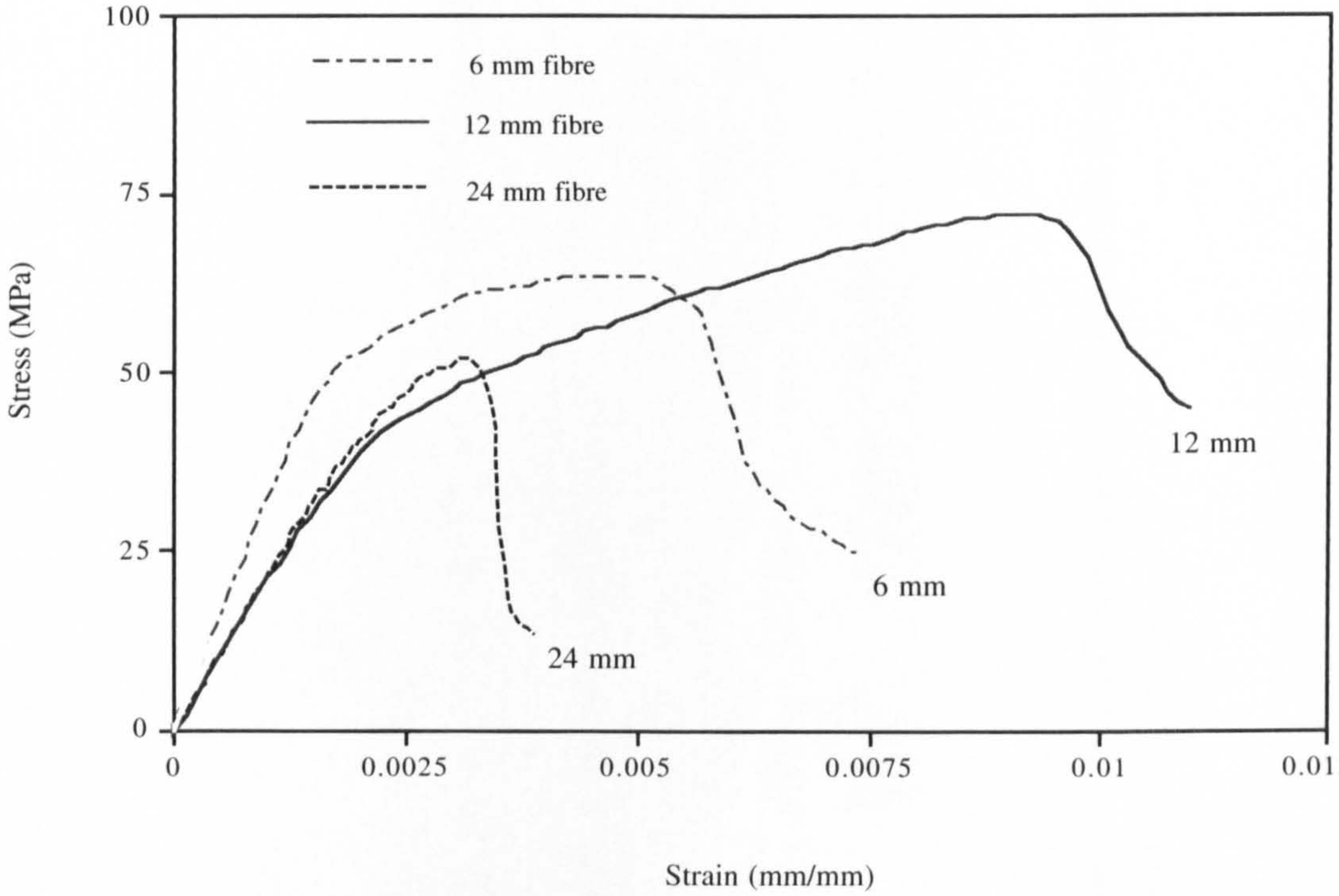

Fig. 7.8 Flexural stress-strain curves of the CDMC with different glass fibre lengths: 6, 12 and 24 mm, volume fraction of fibre was 15%(vol.), fibre type was AR62/2, moulded at 140 °C.

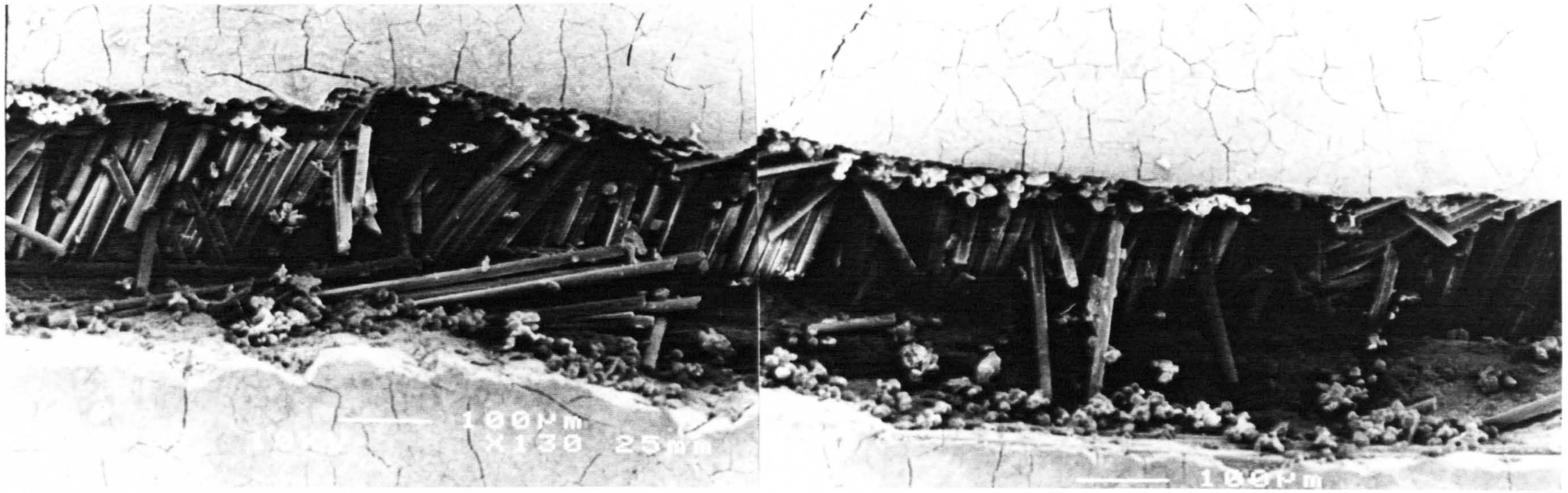

Fig. 7.9 Tensile side of a flexural failed specimen moulded at 140 °C, with 22.6%(vol.)AR62/2 glass. The bending fracture involved very much fibre debonding, pull-out and bridging.

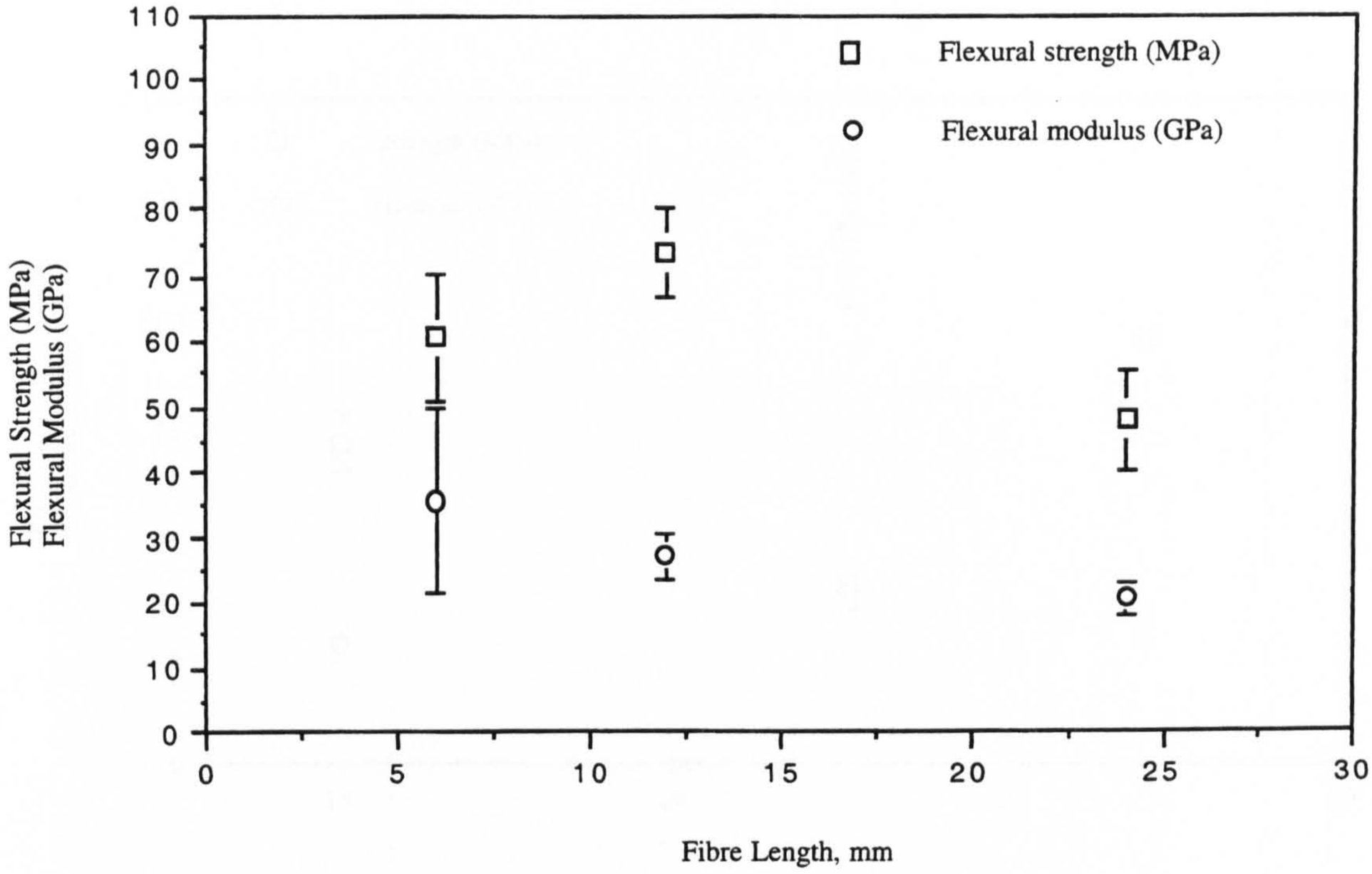

Fig. 7.10 Flexural properties of the CDMC effected by lengths of the glass fibre AR62/2, moulded at 140 °C.

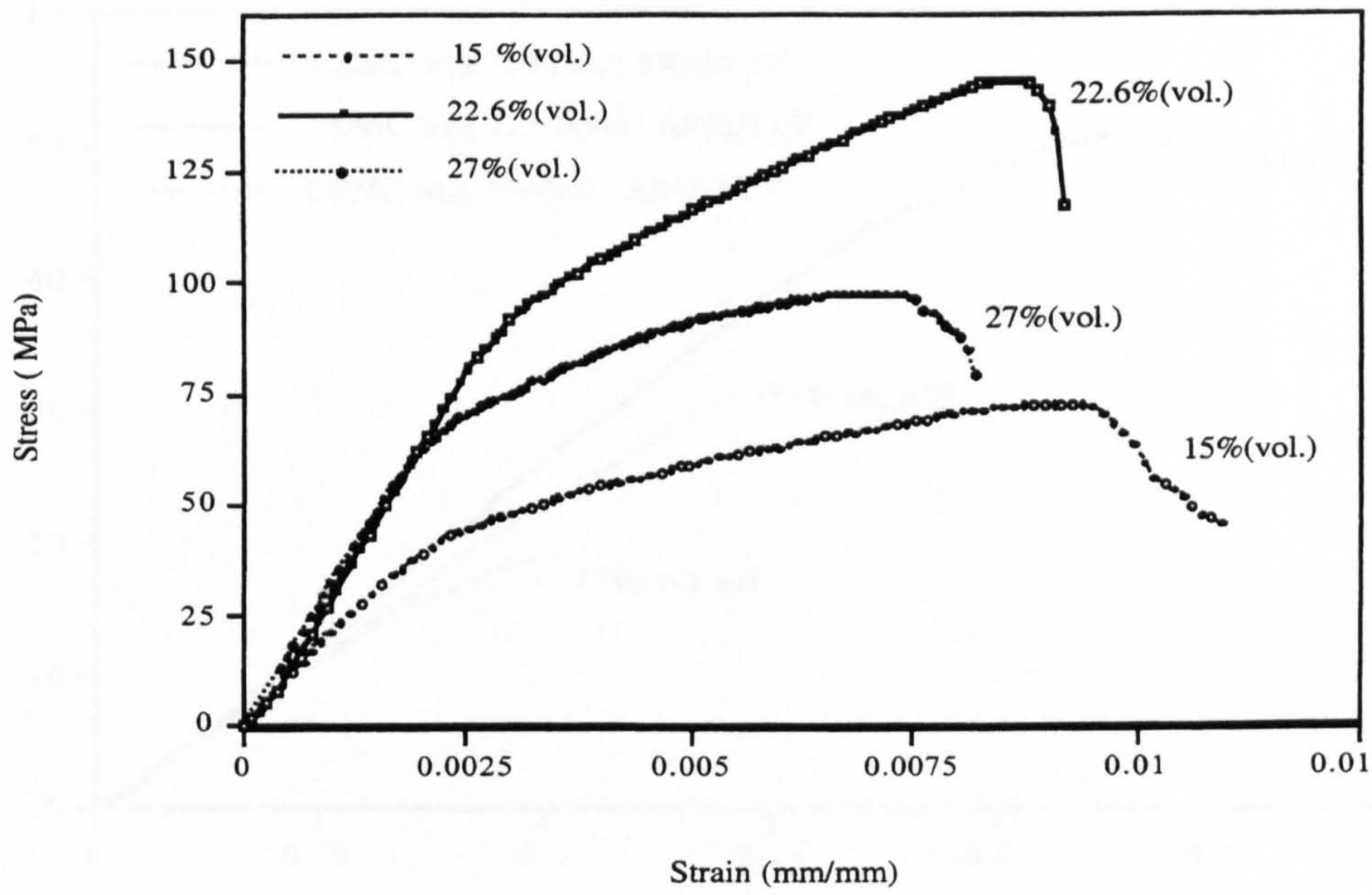

Fig. 7.11 Flexural stress-strain curves of the CDMC with glass fraction: 15% - 27%(vol.). Fibre type was AR 62/2, moulded at 140 °C.

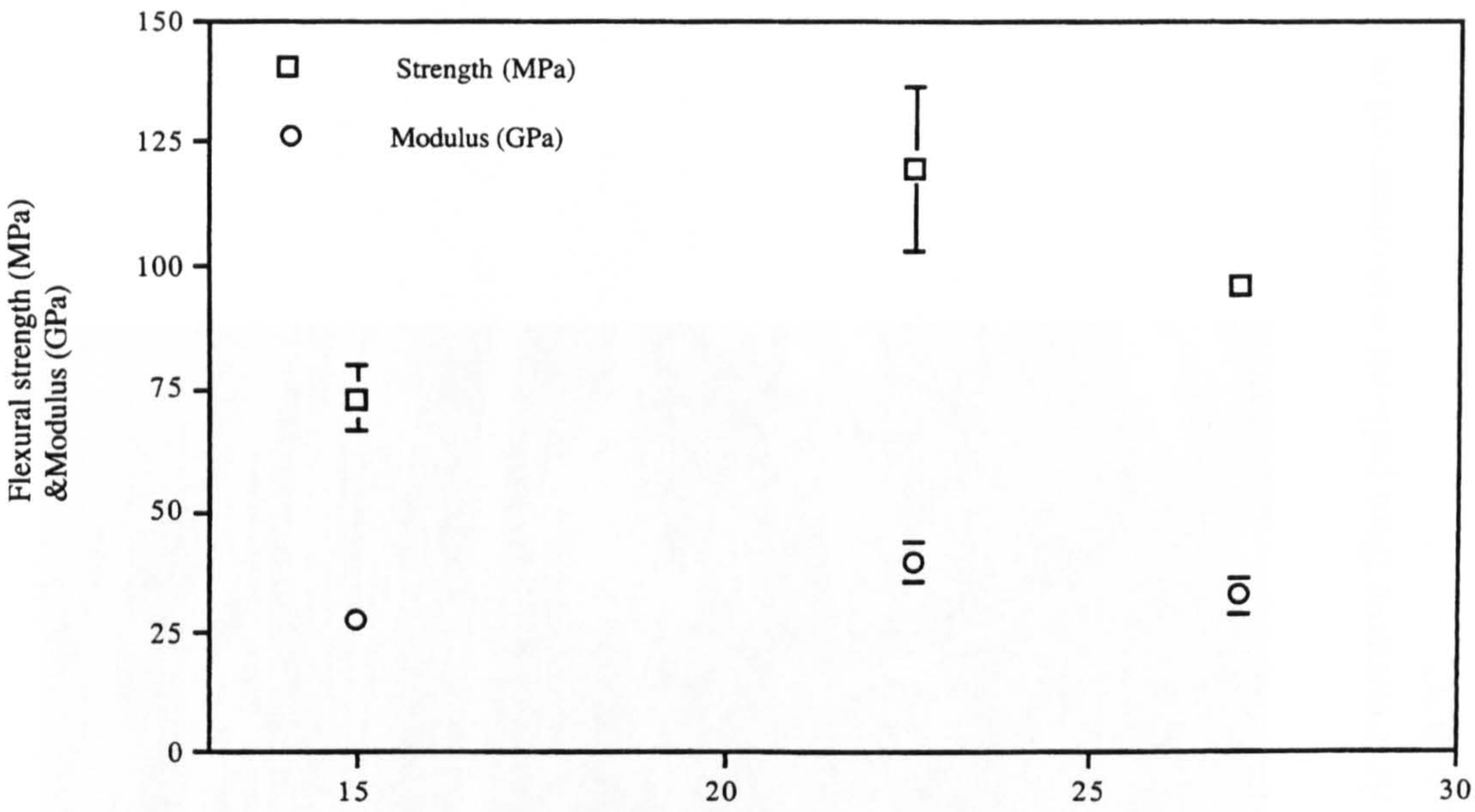

Table 7.12 Flexural properties of the CDMC effected by volume fraction of the AR62/2 glass fibre (12 mm): 15%, 22.6%, 27%(vol.). Moulding temperature 140°C.

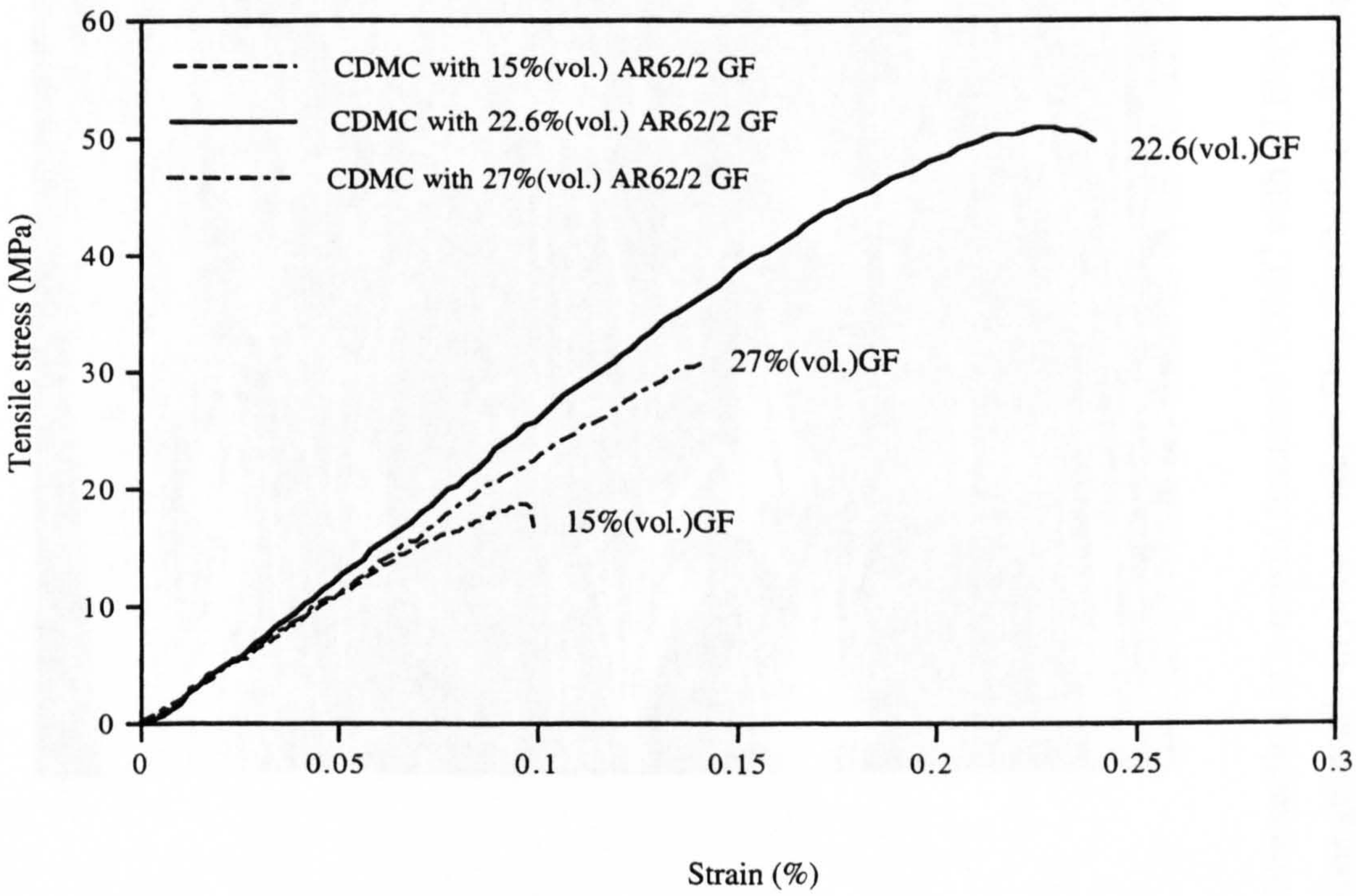

Fig. 7.13 Tensile stress-strain curves of the CDMC with AR 62/2 glass in volume fractions from of 15% - 27%(vol.), moulded at 140 °C.

Fig. 7.14 A failure section of a tensile fractured CDMC with 22.6%(vol.) 62/2 AR-glass fibre. An extensive fibre pull-out was observed in different directions generally in-plane random fibre distributions. This specimen was moulded at 140 °C.

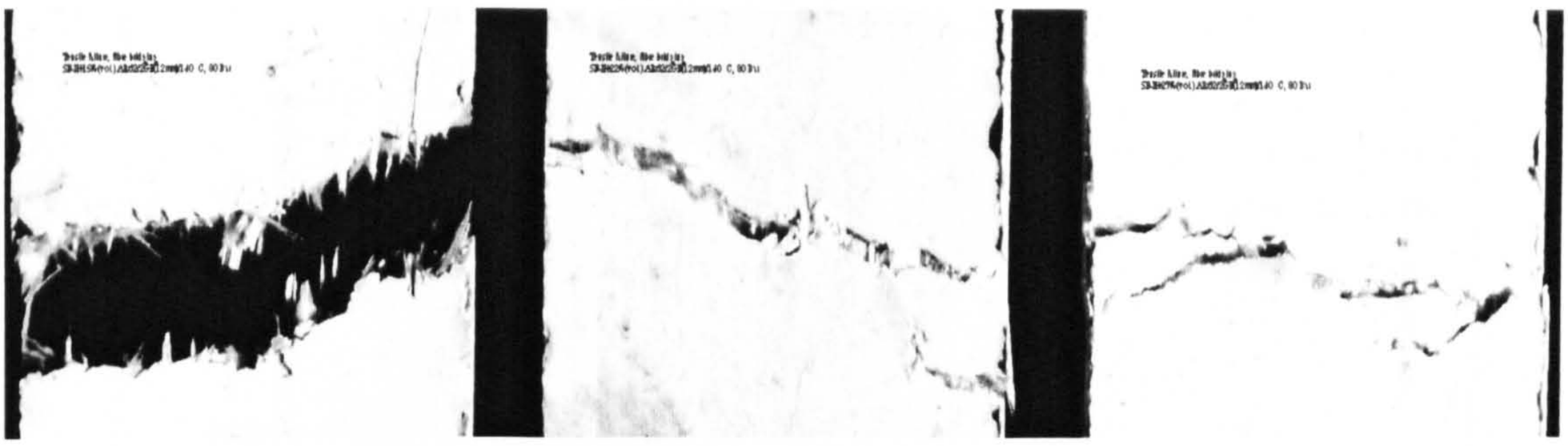

A. 15%(vol.)AR62/2 B. 22%(vol.) AR62/2 C. 27%(vol.)AR62/2

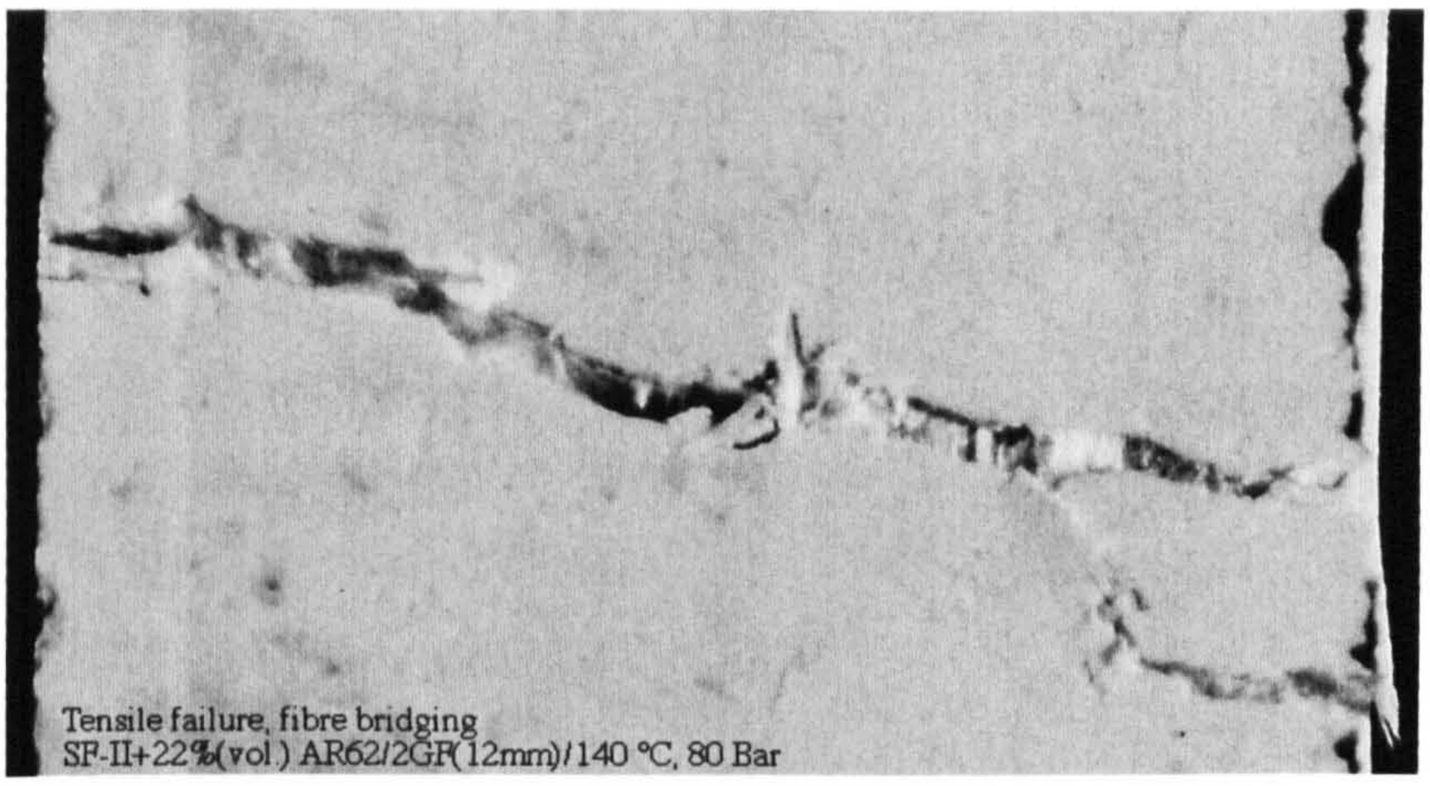

D. Enlarged B.

Fig. 7.15 The views of the tensile failed specimens with different volume fraction of glass fibre from left to right A [15%(vol.)], B [22%(vol.)], C [27%(vol.)]. and D is the enlargement of B. The width of the tensile specimens were 25.0 mm and thickness was 4.0 mm.

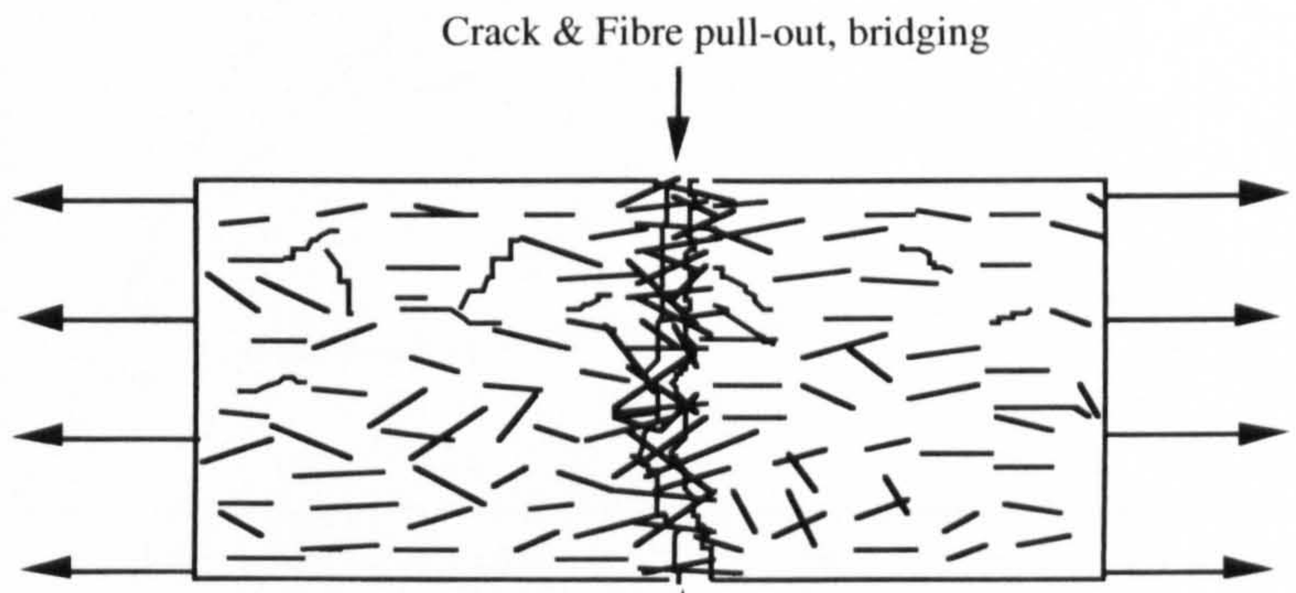

Fig. 7.16 A schematic illustration of the fibre pull-out in tensile crack, fibre pull-out, failure and formed the bridge by groups of fibre bundles along the tensile failed section, corresponding to the case of Fig. 7.15.

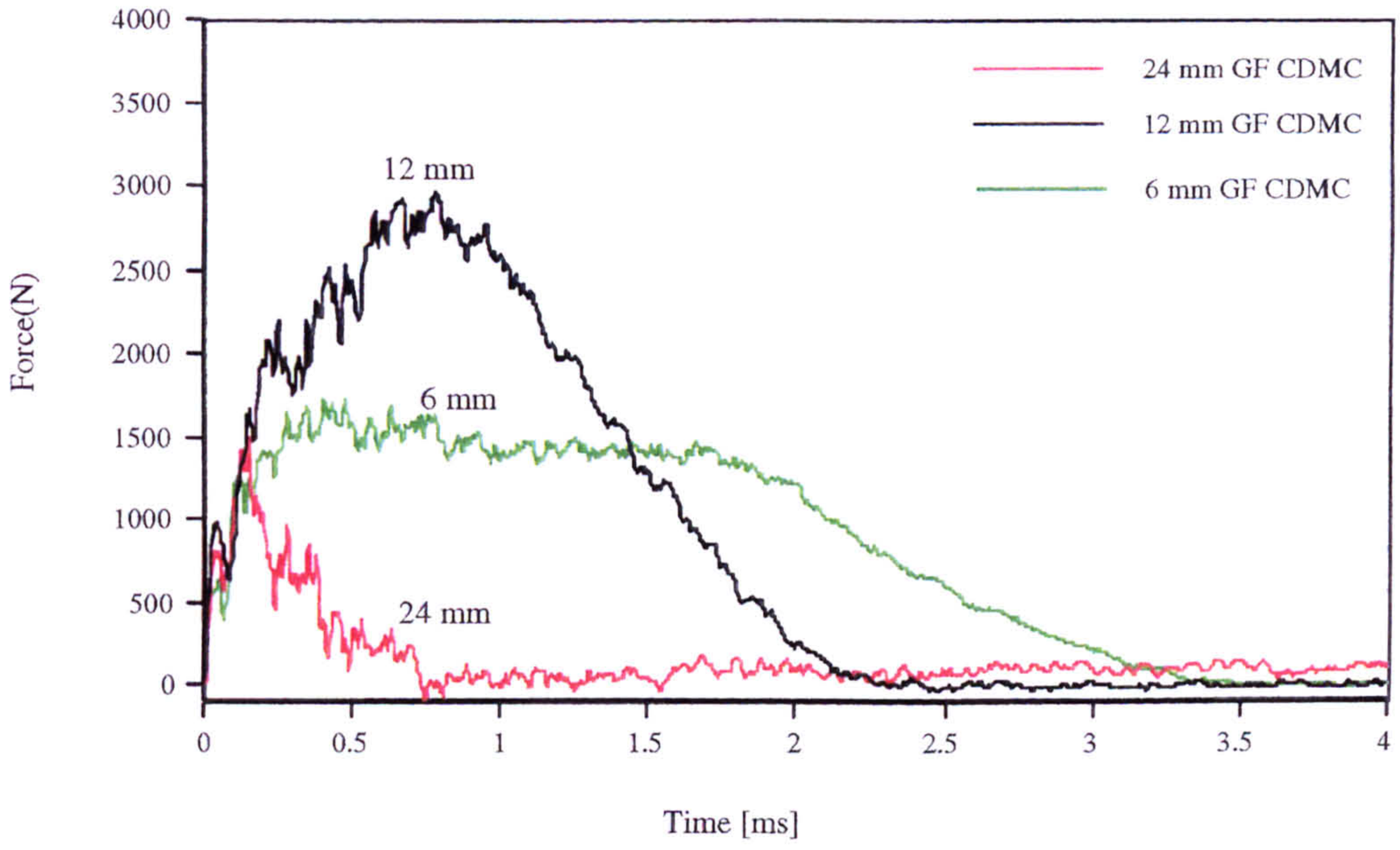

Fig. 7.17 The impact force-time histories of the CDMC panels with 15%(vol.) AR-62/2 GF and different fibre lengths, moulded at 140 °C.

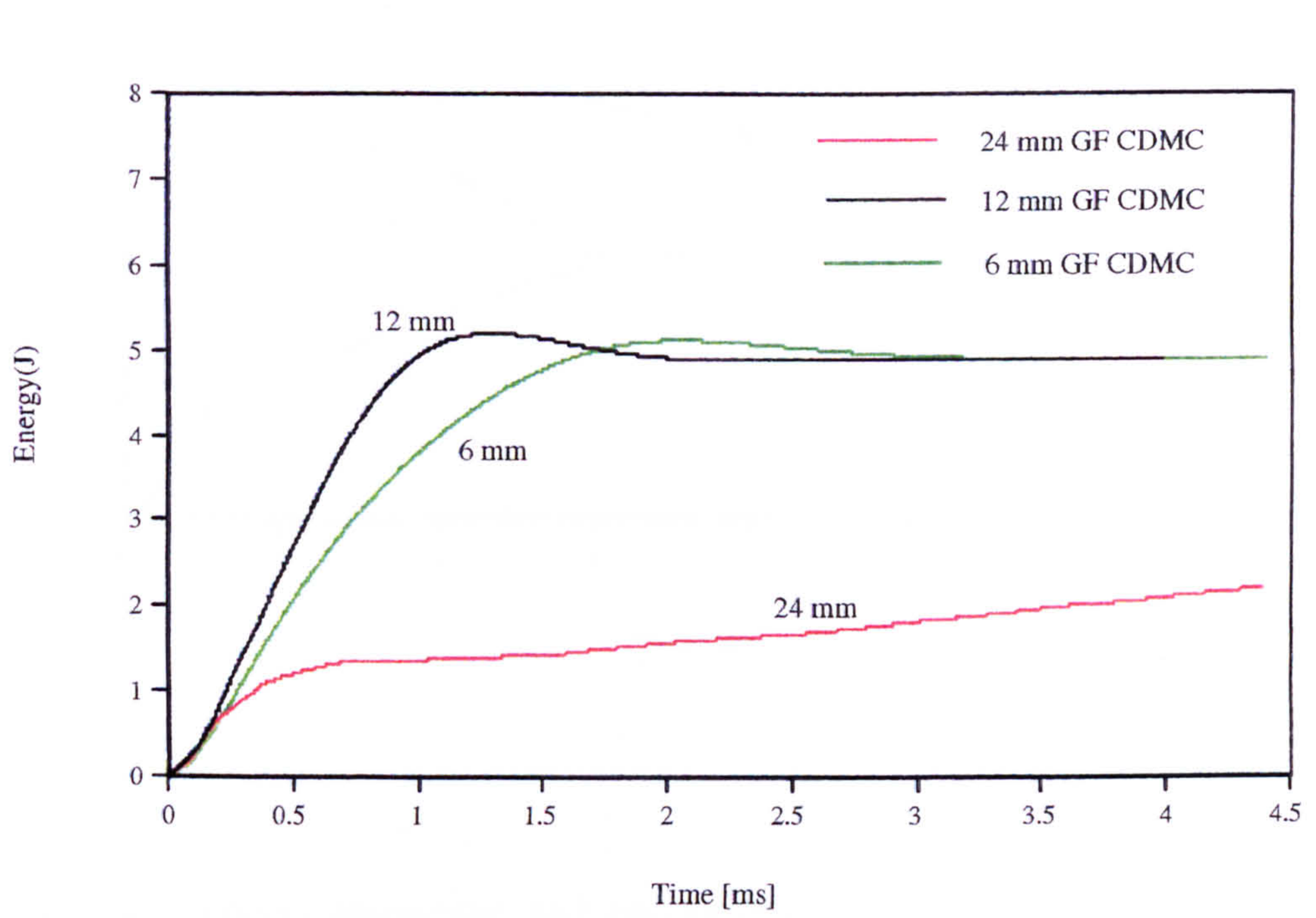

Fig. 7.18 The impact energy absorption-time histories of the CDMC with AR62/2-glass fibre and different fibre lengths, moulded at 140 °C.

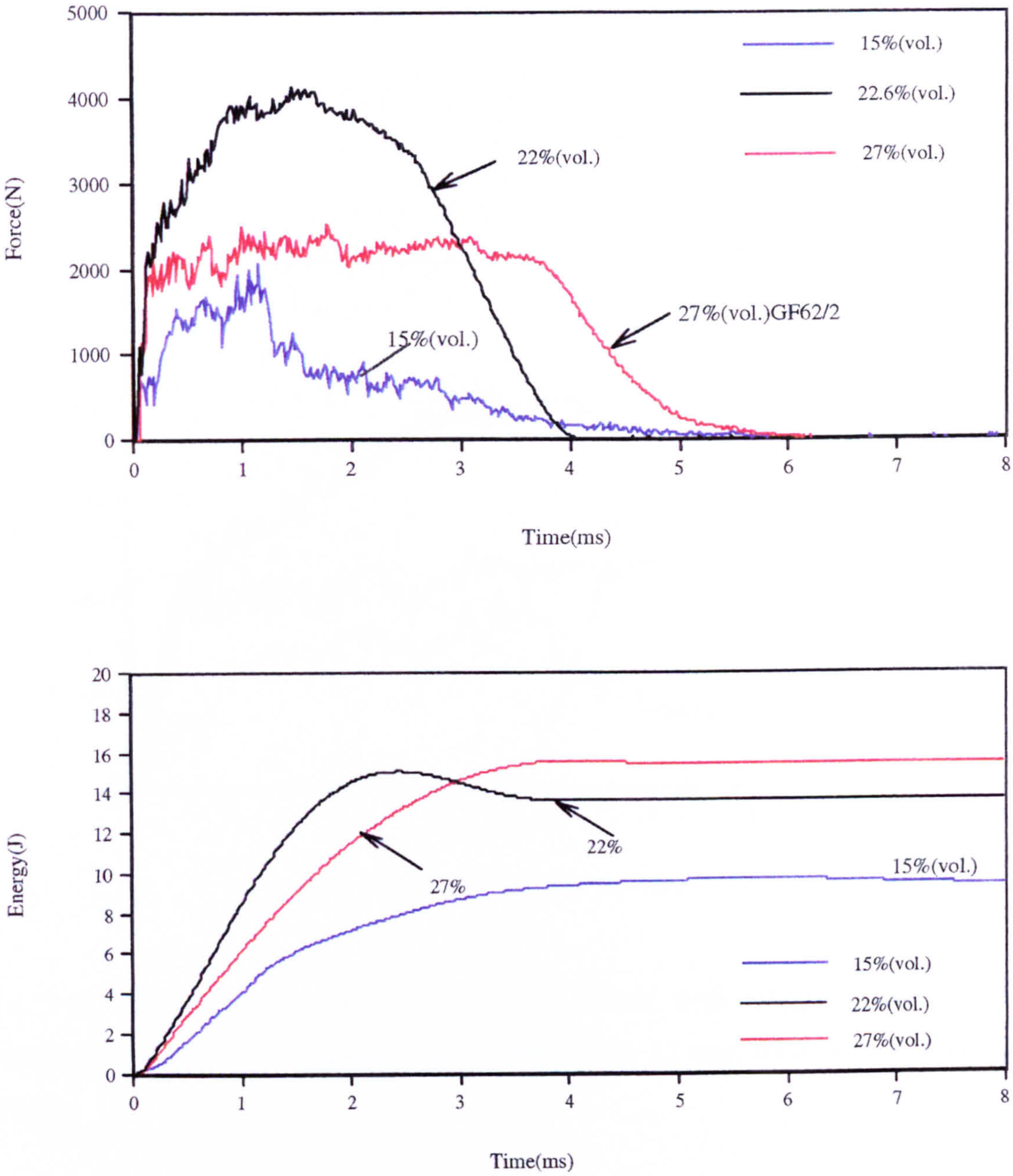

Fig. 7.19 The impact force-time and energy-time histories of the composites with different volume fraction of AR62/2 glass fibre (12 mm) under total impacting energy 15.9 J. The materials was moulded at 140 °C.

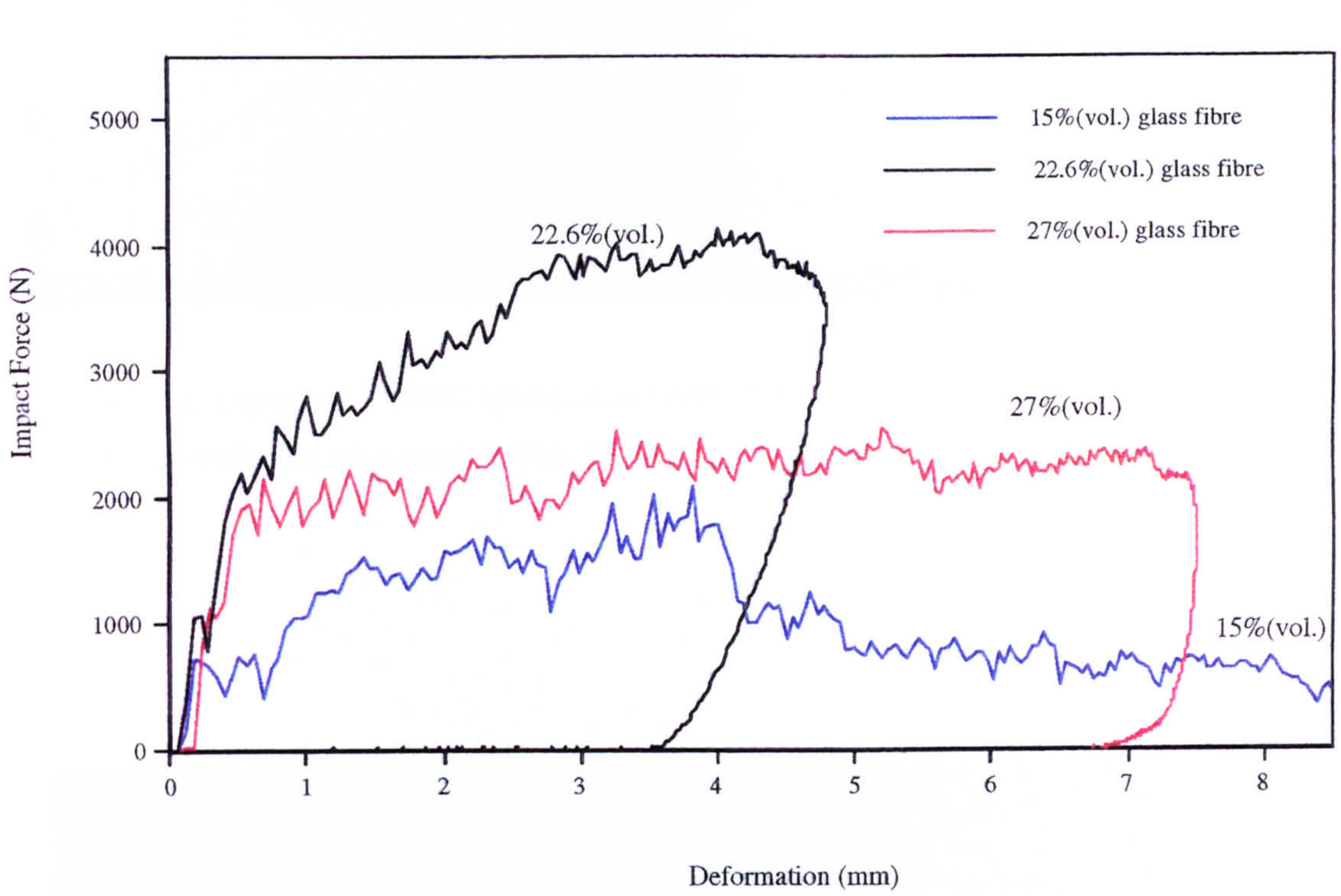

Fig. 7.20 The force-deformation curves of the CDMC with different AR-glass fibre volume fractions obtained during impact, fibre length 12 mm, total impacting energy 15.9 J.

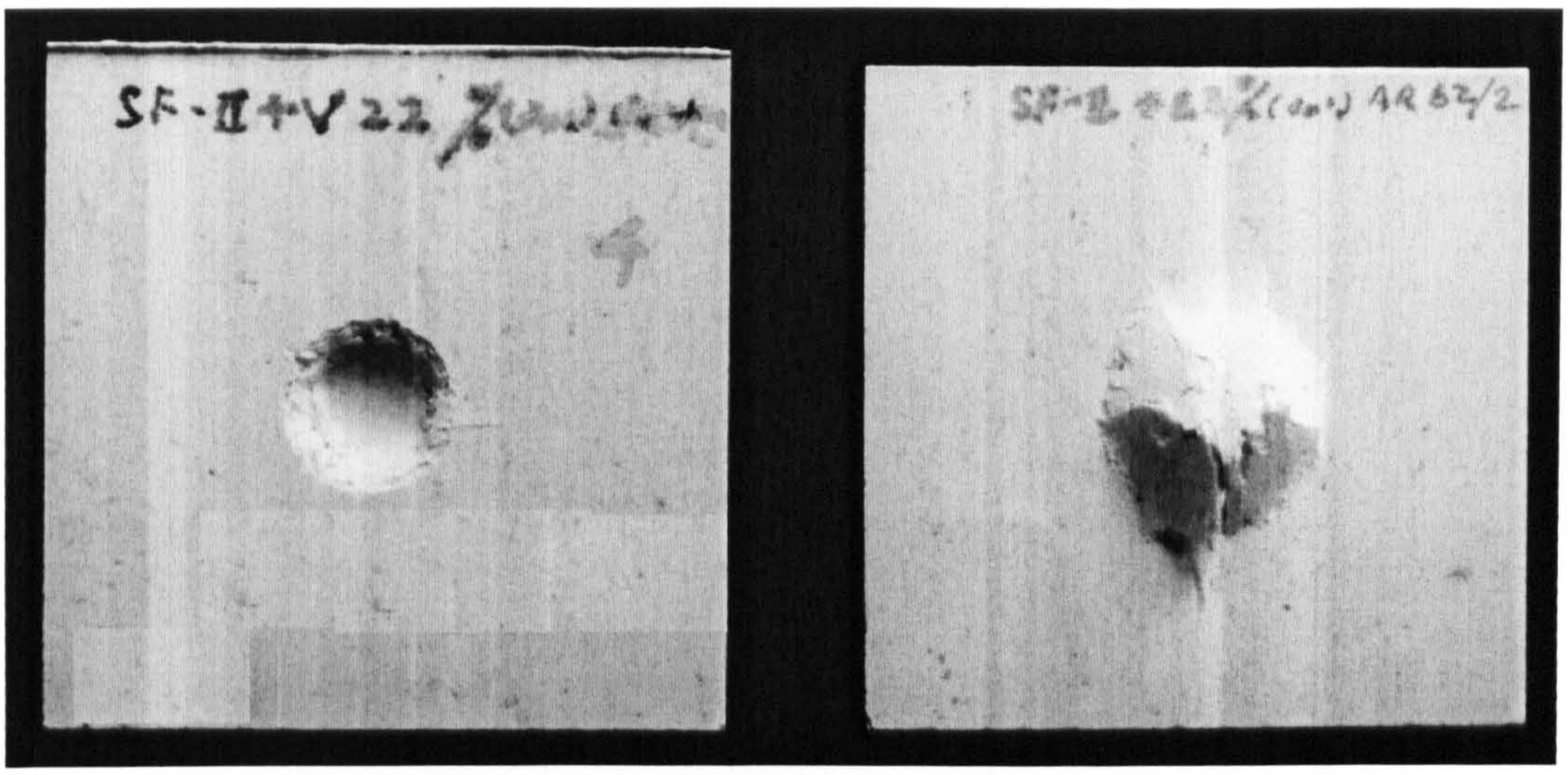

Fig. 7.21 The impacted CDMC specimens with 22.6%(vol.) AR62/2 glass fibre moulded at 140 °C. Total impacting energy was 15.9 J.

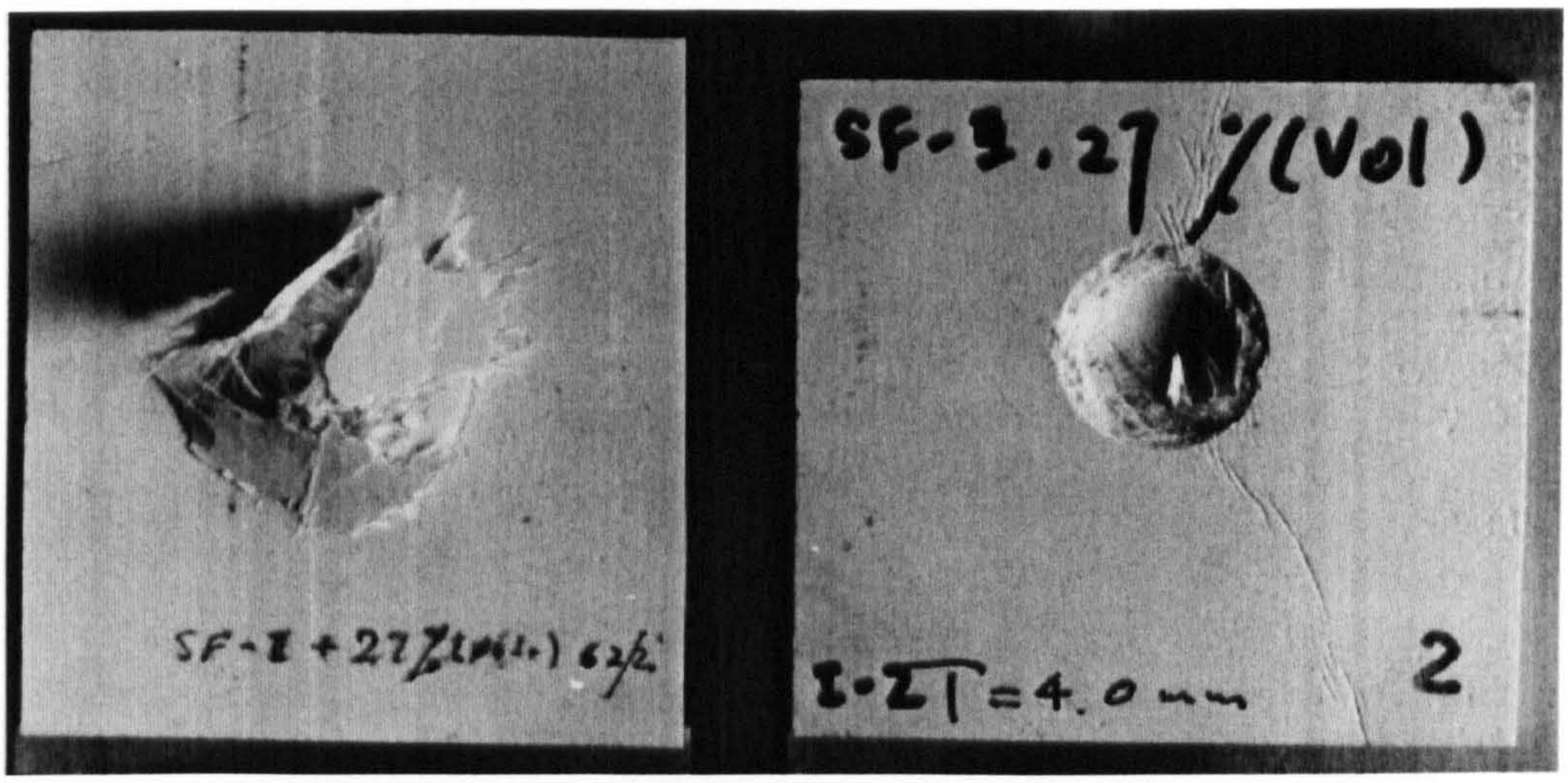

Fig. 7.22 The impacted specimens of the CDMC with 27%(vol.) of AR62/2 glass fibre. The total impacting energy was 15.9 J.

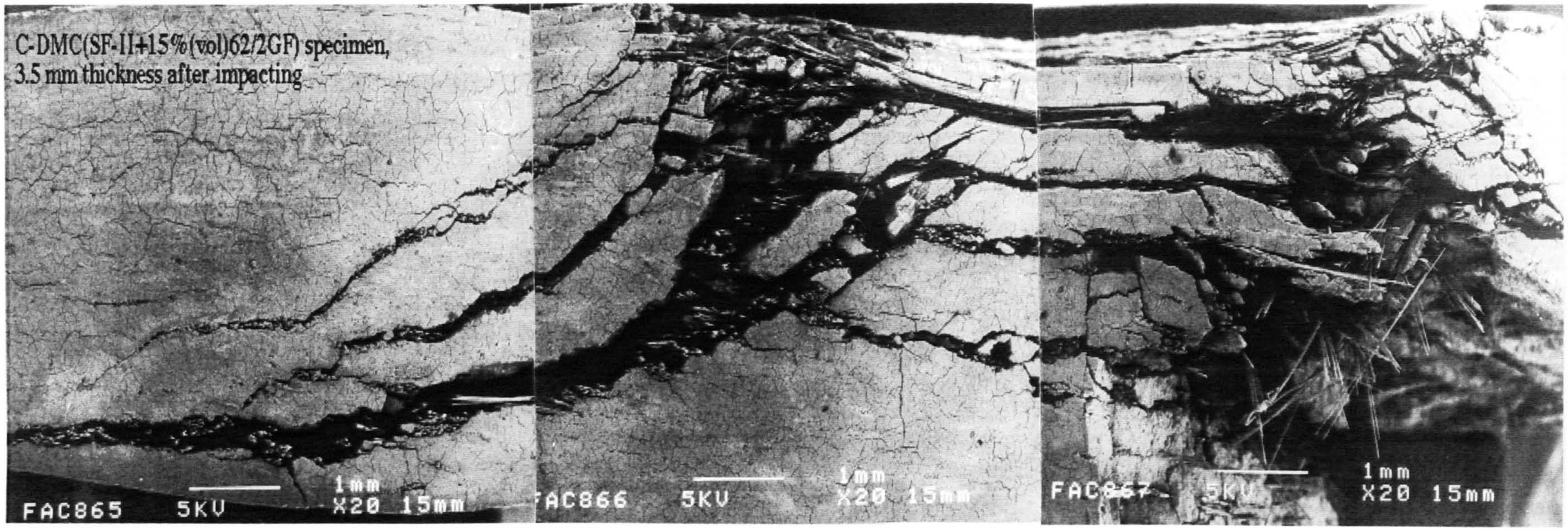

Fig. 7.23 The impact fractured cross section morphology of the CDMC with 15%(vol.) AR62/2 glass fibre after impact. The impacting energy 5.8 J. This specimen was moulded at 140 °C.

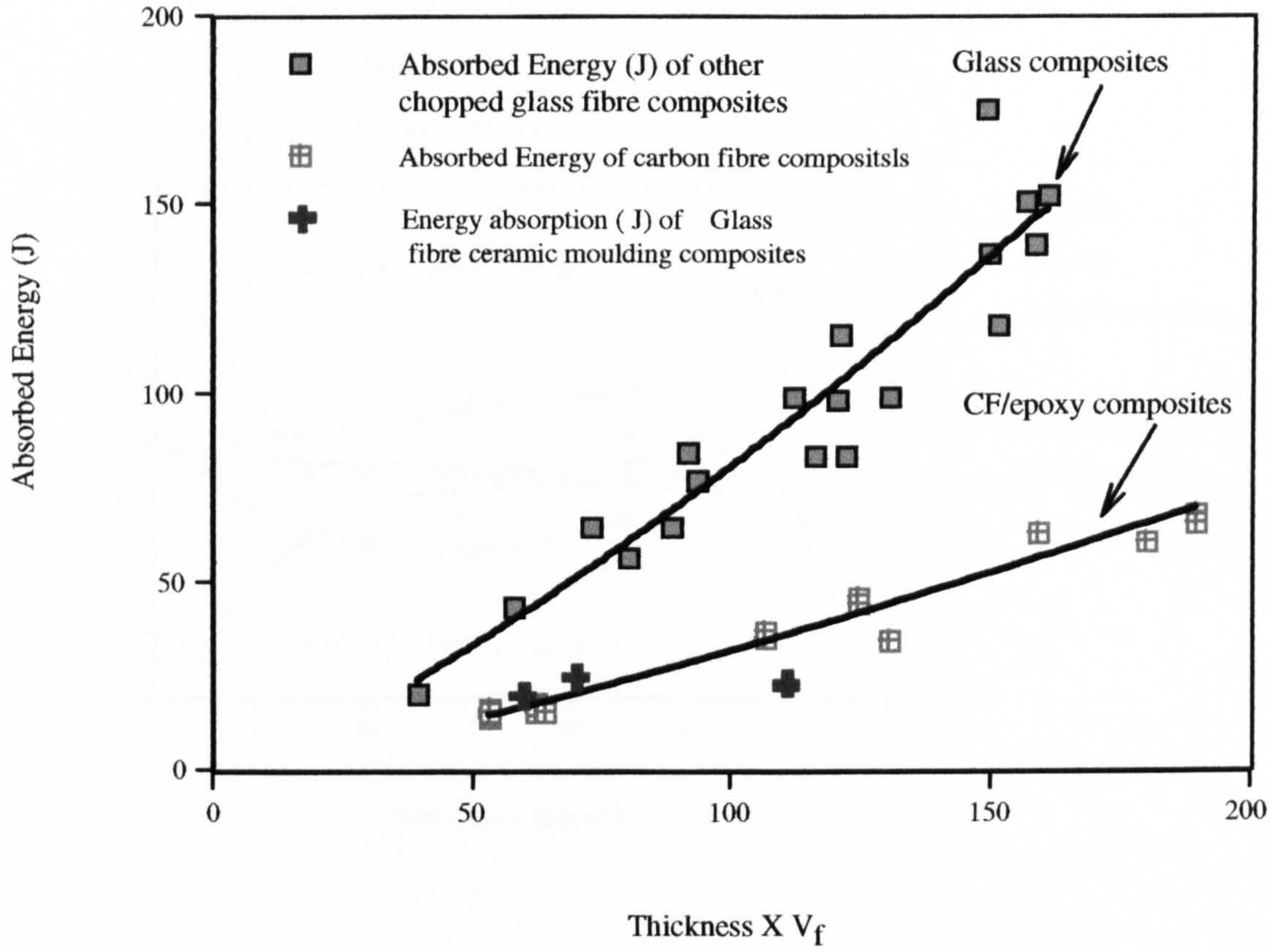

Fig. 7.24 The maximum impact energy absorption data of the CDMC in two fibre composite master curves, absorption energy to thickness (mm) multiplied by V_f . A very wide range of glass fibre or carbon composites falls on these master curves, irrespective of the matrix types (thermoset, thermoplastic) and reinforcement types (woven fabrics, CSM, UD stacks).

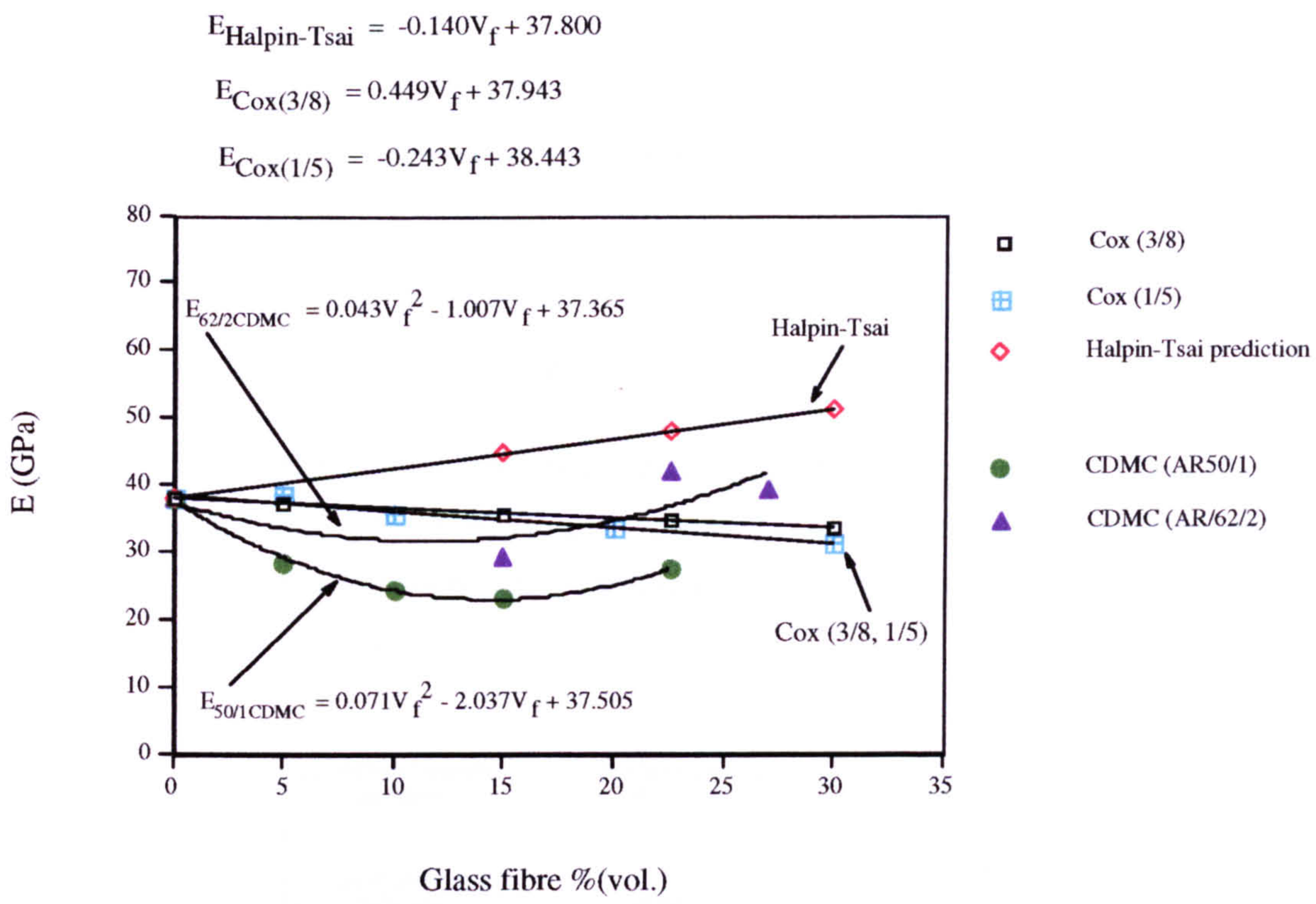

Fig. 7.25 Comparison of elastic properties of the CDMC reinforced by AR50/1 and 62/2 glass fibres in volume fractions with the Cox and Halpin-Tsai prediction equations for short fibre composite materials.

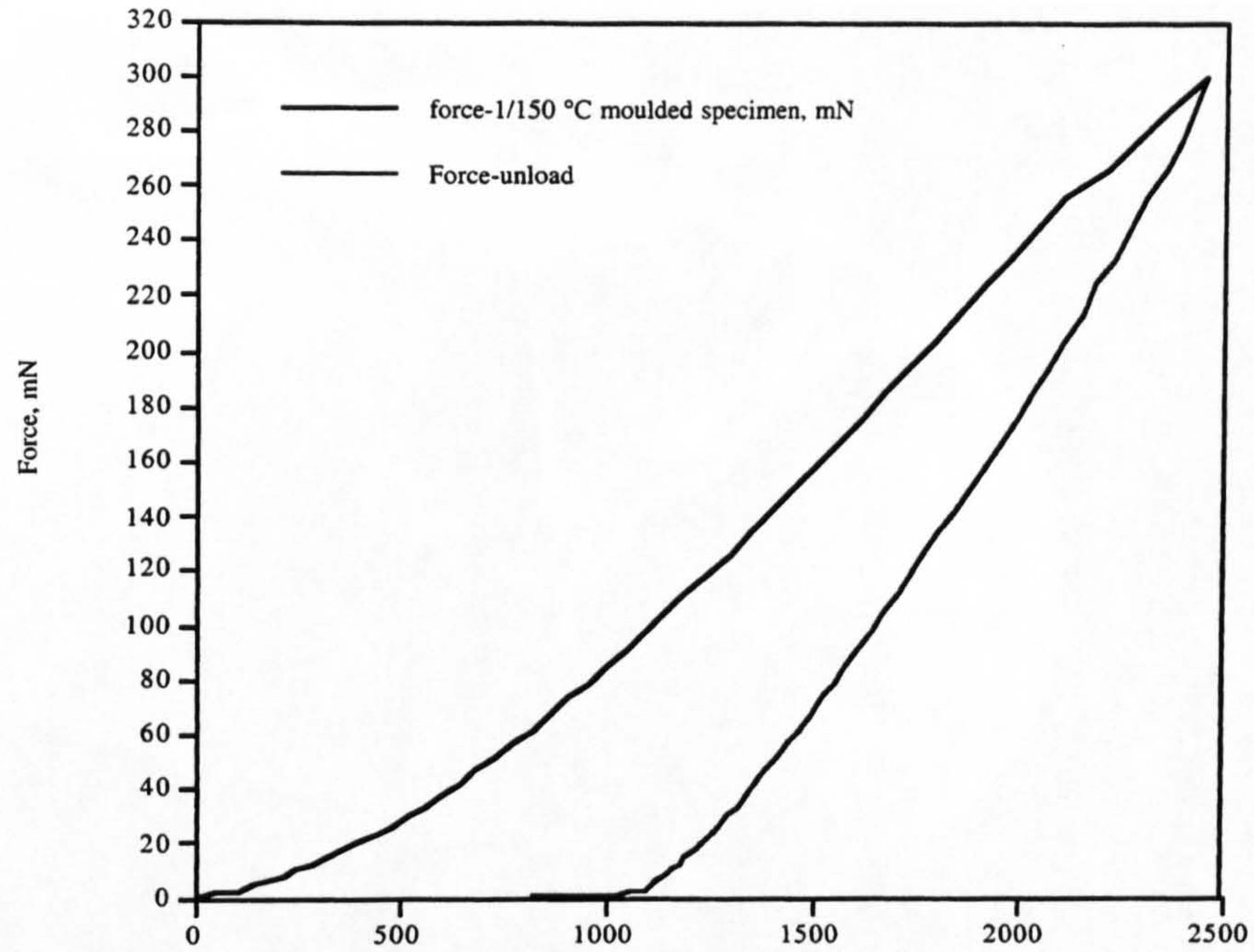

Fig. 7.26 An illustration of micro-indentation load - displacement of the glass fibre push-out from the CDMC. The 200~300 micrometer thickness specimens moulded at 150 ℃ and 190 °C. The indentor used was 20 micro diameter, maximum load was 500 mN.

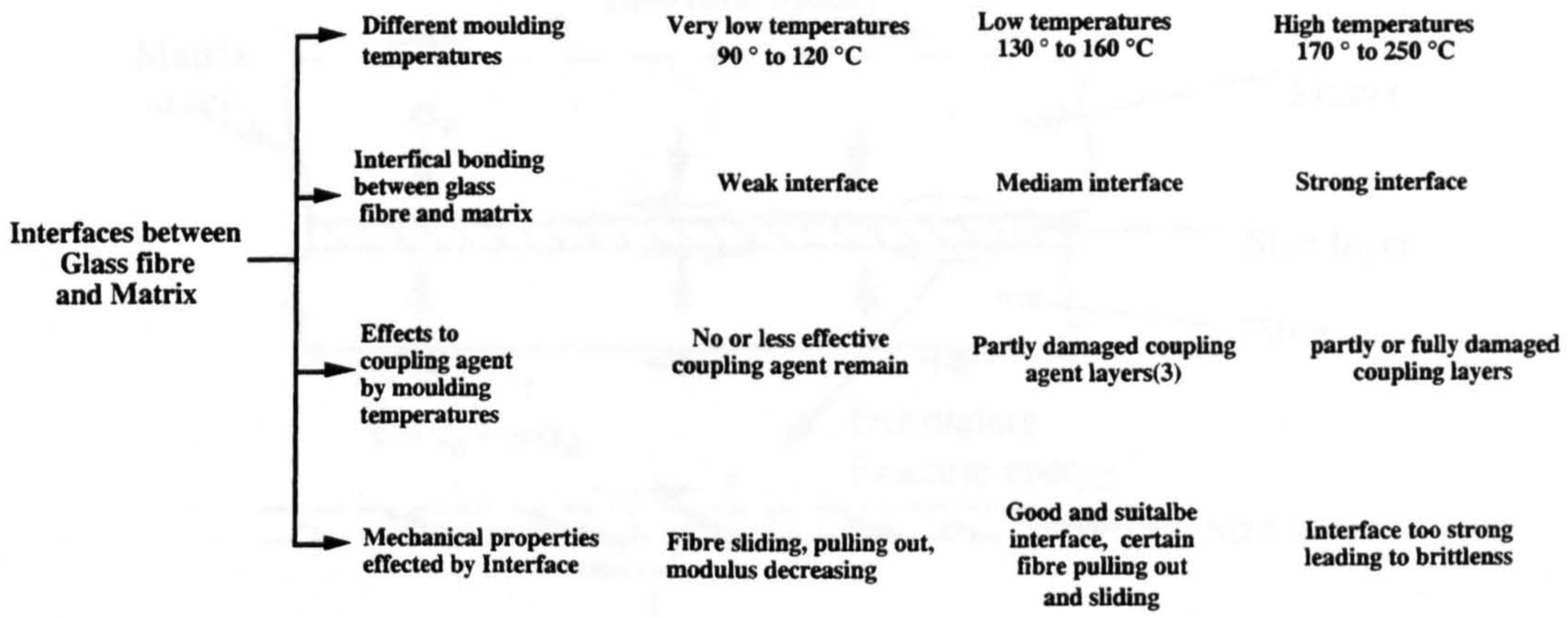

Fig. 7.27 A schematic drawing of the trends in mechanical properties and interfacial strength effected by the moulding temperatures.

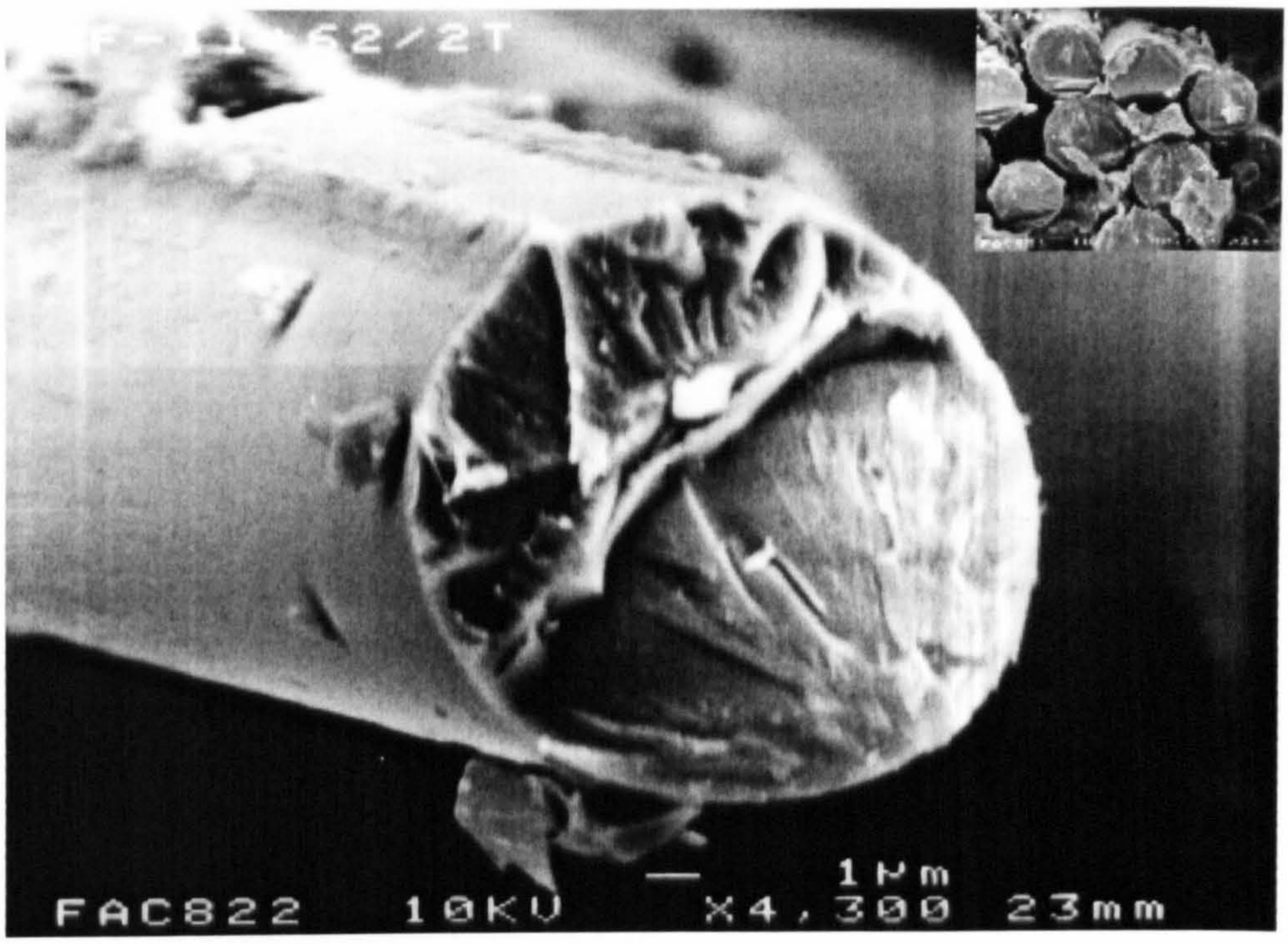

Fig. 7.28 A tensile fractured single fibre in the tensile failed specimen moulded at 140 °C. The glass fibre was 62/2, 12 mm length, 14 μm. The insert is in lower magnification of part of the same specimen.

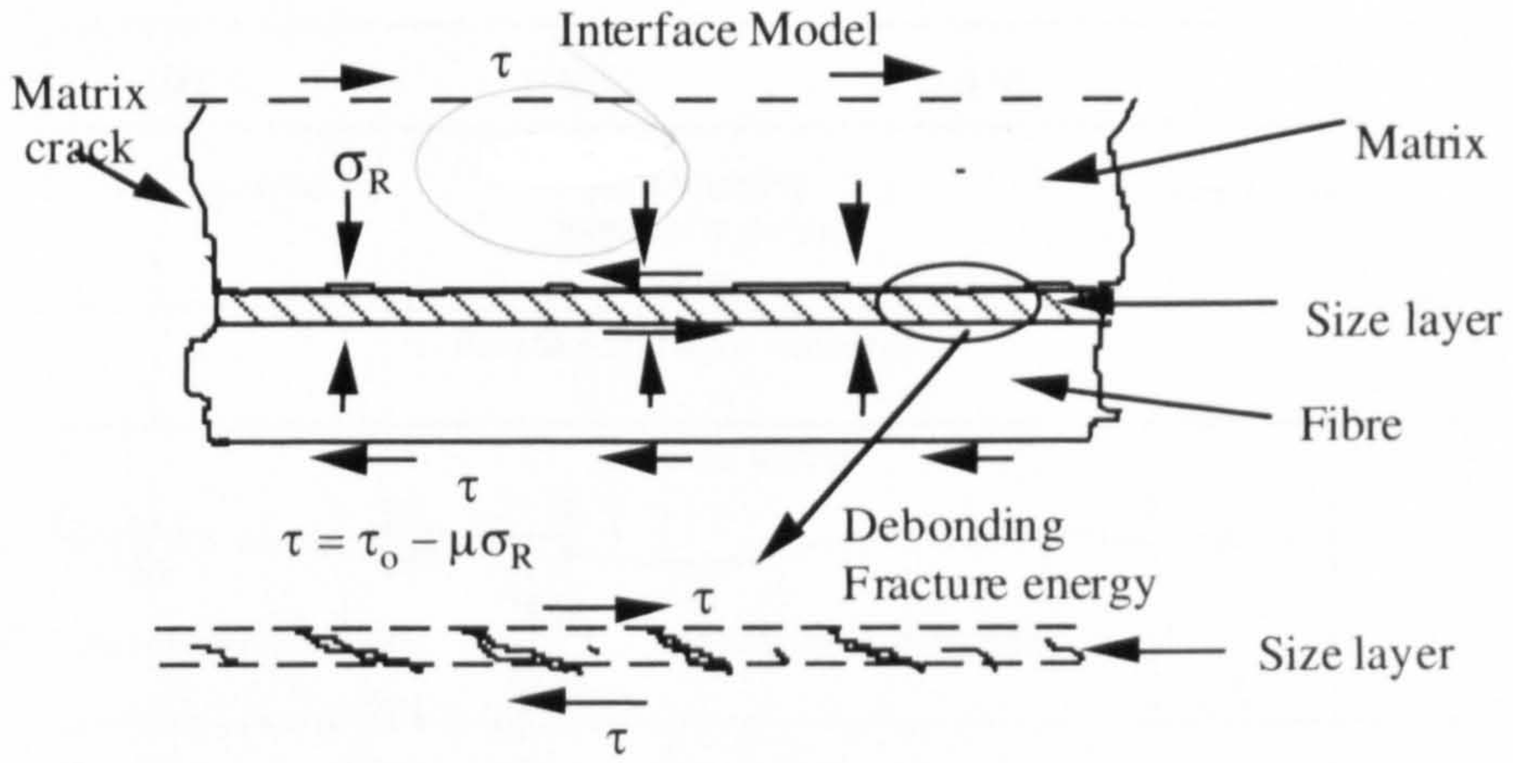

Fig. 7.29 The fibre sliding model could be an indication of the location of debonding and frictional sliding. The cross-hatched region was a thin fibre coating or sizing system (Marshall and Oliver, 1987).

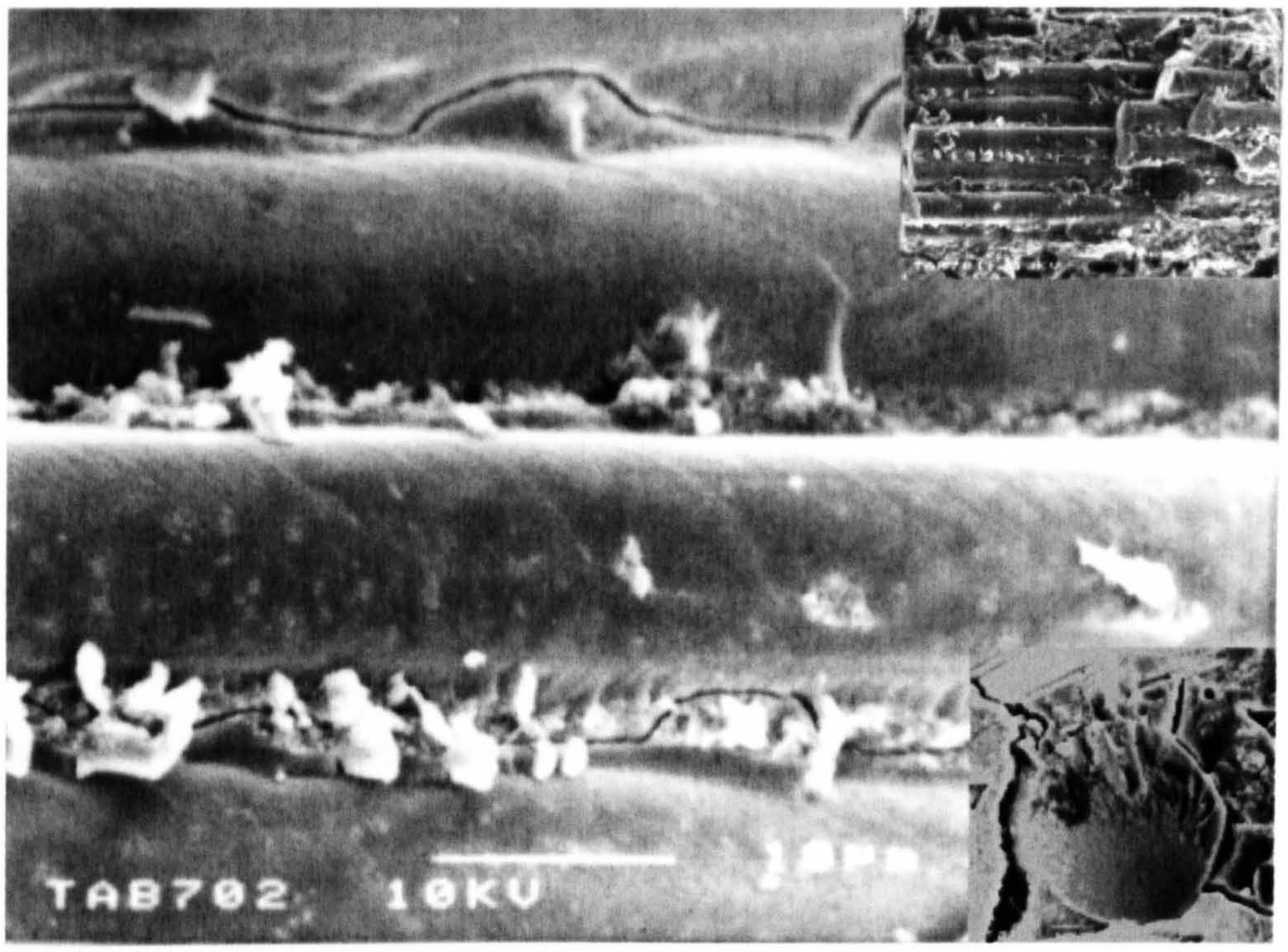

Fig. 7.30 A practical fibre sliding in a surface section of a tensile failed specimen with AR 50/1 glass fibre, moulded at 130 °C. The cross-hatched region/marks are probably a thin sizing film scratched by the debonding. And the matrix cracking was also observed in the tensile tested specimens moulded at low temperature (130 °C). Up insert is same specimen in lower magnification, lower insert is a single fibre fracture in higher magnification.

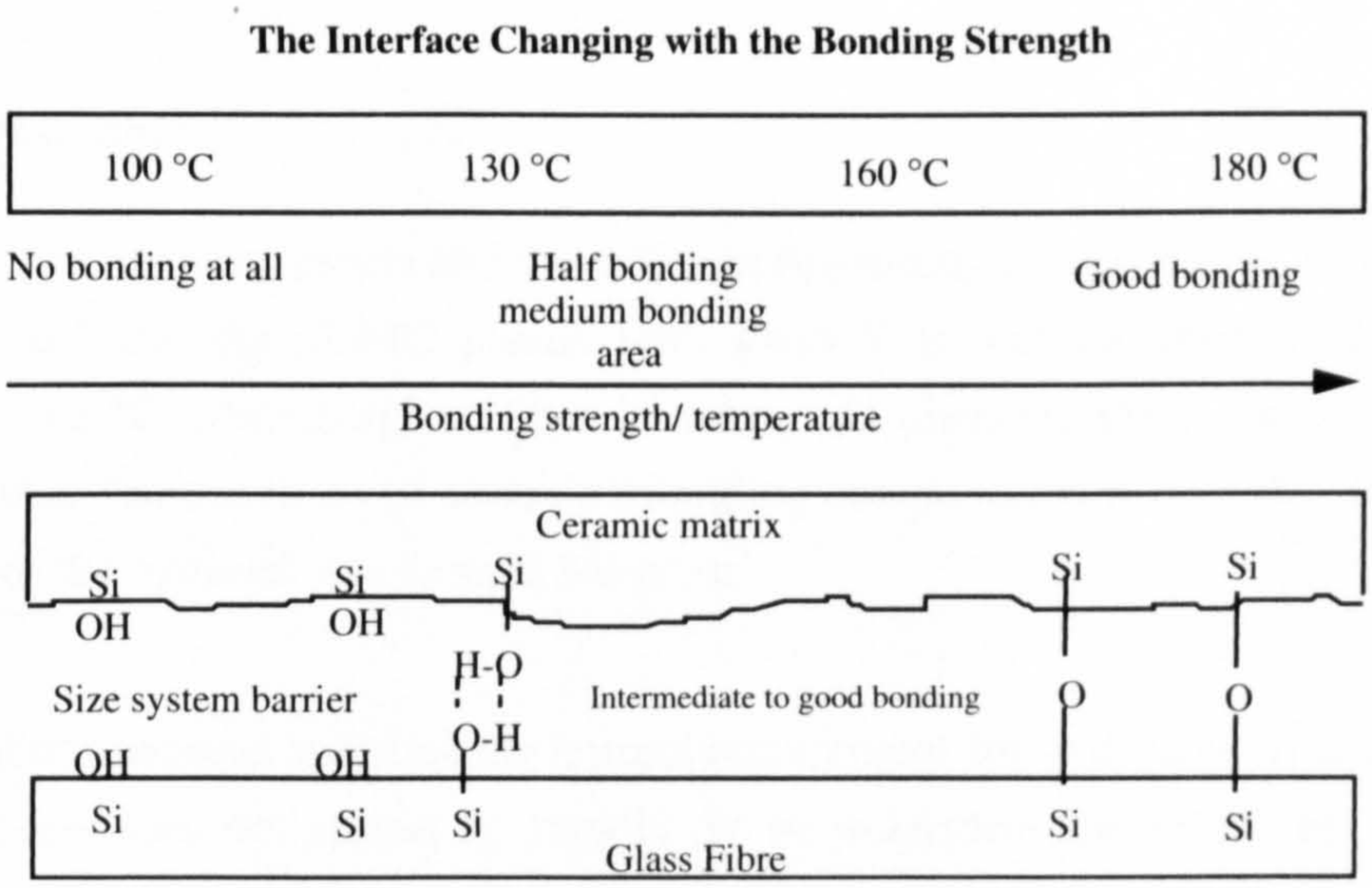

Fig. 7.31 A schematic show of the interfacial bonding strength effected by the moulding temperatures ranging from 99 °C to 180 °C, briefly the effect of sizing barrier, -Si-OH, -Si-O-Si- were displayed.

Chapter 8

FIRE PERFORMANCE

8.1 Introduction

In this Chapter, two main tests have been carried out: a fire resistance test which measures the temperature transmission with time through a fire barrier panel; and a material's reaction to fire test by using a Cone Calorimeter.

The fire resistance and Cone Calorimeter tests are newly developed small scale testing methods for material's fire and thermal properties. The IMO test uses a small scaled furnace to measure the fire resistance or resistance to fire penetration and is a effectively scaled version of BS476, Part 20. The Cone Calorimeter test measures a material's basic reaction to heat/fire. Both tests were considered to have merit for the study of material variables in this programme. Three types of panels were investigated by these testing methods: the CDMC panels; a phenolic/NCF laminate and a phenolic DMC panels.

8.2 Fire resistance

The CDMC and phenolic panels and the different fire testing conditions are listed in Table 8.1. These included the CDMC panels with glass fibre volume fraction 22.6%(vol.) moulded at 140 °C; phenolic/glass fibre laminate and phenolic DMC panels with glass fibre 25%(wt.). The thickness of ceramic moulding compound is from 3.0 - 3.4 mm and the density of the material was around 2.0 g/cm^3.

For a typical fire resistant material, the normal requirement for resistance to fire has to be such that a fire does not spread so rapidly as to jeopardise the safety of passengers (BS6853, 1987) if part of a transport system, or occupants if in part of a building. To simulate the real fire, a group of gas burners in a furnace was used. The test exposed one side of the CDMC plate to a rising temperature while the temperature rise on the unexposed face of the plate was recorded continuously.

Dehydration is the initial reaction of a normal material to fire or heat and this occurred in the matrix of the CDMC panels during the fire test. The temperature inside the furnace would reach nearly 1000 ℃ within a few minutes after the ignition of fire. As the temperature increased, the matrix started to lose physically contained moisture in the temperature range 100 ℃ - 200 °C, followed by chemically bonded water, which was released before 500 °C. One of the test results of a typical CDMC with 22.6%(vol.) glass fibre listed in first row in Table 8.1 is displayed in Fig. 8.1, together with the standard temperature rise curve (shown as IMO curve) generated by the gas burner inside the furnace.

The CDMC panel lost its chemically bonded water at around 250 to 300 °C, forming water vapour on the surface of the panel (which could reduce the heat transfer during firing). No shrinkage crack or fissures occurred during the test. No crack was observed on an unexposed surface of the panel from room temperature to 500 ℃ as shown in Fig. 8.2. However, the inner face of the panel exposed to the furnace fire may have cracked a few times when the furnace temperature rose to above 800 °C. No crack occurred on the unexposed face of the panel during the whole test. The furnace temperature rose from room temperature to 960 °C during a 60 minute period in the fire test. The test resulted in a rise of temperature in the immediate vicinity of the inside surface of the specimen according to a specified temperature - time curve. This temperature / time curve simulates the conditions imposed in practice by burning cellulose or hydrocarbons.

The 3.0 mm thickness panel retained structural integrity despite a maximum temperature difference of 500 ℃ between exposed and unexposed faces at the end of the test. The temperature gradient here was nearly 170 °C for each mm for this sample.

After the fire test had finished, the specimen was cooled down rapidly to room temperature. The difference in thermal expansion (or contraction) among fibre, fillers and matrix produced stresses causing propagation of existing cracks. During the monitored 60 minute test, no surface cracks or through thickness cracks were visible on the unexposed face of specimen. It was only after the test and surface shrinkage that a few fissures less than 0.5 mm were observed while the tested sample cooled down to a room temperature. The higher the firing temperature reached, the more cracks on the exposed surface; and the longer the firing time, the greater the distortion. These are shown in Fig. 8.2 when the final temperature was over 1000 ℃ for 80 minutes with large cracks produced on the exposed surface during cooling.

The samples from exposed and non-exposed faces of the CDMC panel that had experienced over 1000 ℃ were collected, then the microstructures of panel were examined by SEM. The levels of damage for both fibre and matrix were checked in these exposed and un-exposed faces. Their micrographs were obtained and shown in the left side of Fig. 8.3/A and Fig. 8.3/B; on the right sides are their original state of glass fibre surfaces before fire in relevant magnification. The thermal erosion on the surfaces of glass fibres can be observed on both sides of the panel after firing around 1000 °C. On the non-exposed surface of the CDMC, the fibre still remained its shape and a certain smoothness. A slight surface erosion had taken place by the intensive heat blast[Fig. 8.3/(A) left]. The exposed face had more thermal erosion which resulted in rough surfaces on glass fibres [Fig. 8.3/B (left)]. Despite the thermal erosion, the glass fibres, still retained their basic shape and this helped the composite panel kept its integrity and certain mechanical properties.

8.3 Comparison of the CDMC with phenolic composites

The temperature curves of fire resistance for the CDMC and for a glass phenolic laminate against time have been compared in Fig. 8.4. The phenolic / glass (NCF) laminate had been tested was just for comparison. At the start of the fire test in first 10 - 20 minutes, the same water evaporation took place from both materials. This process delayed the temperature increase in samples for certain period of time by absorbing a large amount of heat.

The glass/phenolic laminate absorbed more heat energy from temperatures 100 to 400 ℃ through water loss and degradation or decomposition of its polymer constantly. The curve for temperature rise is almost as same as for the CDMC at the starting few minutes. Then followed temperature drops due to the phenolic matrix decomposition (burning out) around temperature 140-400 °C. However, one of the major advantages for ceramic moulding composites here is that no chemical is released during the whole firing process apart from water vapour (or moisture contained). But the phenolic laminate panel with 8.0 mm thick generated lot of smoke and burnt during almost the whole test period, especially a few minutes after the test started. With a thickness of only around 3.0 mm the CDMC panel achieved better fire resistance than 8 mm thick glass/phenolic laminate.

From a structural point of view, the 3.0 mm ceramic composite structure suffered less damage compared to the phenolic composite. It was observed that at the same temperature range, the phenolic based glass fibre laminates with thickness 8.0 mm failed and was penetrated by fire less than 30 minutes into the fire test. A damaged phenolic composite is shown in Fig. 8.5 with a completely damaged structure (delamination) and a burnt out of resin matrix.

8.4 Constant firing temperature

An alternative fire resistance test used constant furnace temperature at 700 °C. At this stable working temperature as shown in Fig. 8.6, the test was allowed to be continued for an extra 20 minutes before firing stopped. The impermeability of the CDMC panel was examined by noting any gaps, cracks or fissures that were visible on the unexposed face of the specimen (BS476, part 20, 1987).

A slight distortion and a few micro-cracks on the exposed surface of the CDMC were observed after the fire test (Fig. 8.7). This may be due to the shrinkage caused by further release of water (or moisture), or more likely, the micro-cracking process took place during cooling down to the room temperature.

8.5 Material reaction to fire

The characteristics and levels by which the material behaves in a fire situation can be applied to many application areas. All of these can be well judged by measuring the following capabilities of the material: ignite-ability, rate of flame spreading on a surface, rate of heat release, smoke generation, the nature of combustion gases and their proportions under given exposed conditions and the release of harmful products. Since the fire is a very complex phenomenon, its behaviour and effects depend upon a number of interrelated factors. The philosophy of "reaction to fire" is explained in ISO/TR 3814 and ISO/DIS5660.

The stability of a CDMC was measured by the Cone Calorimeter. There was no ignition recorded on the CDMC and the mass loss was only small amount of water physically and chemically combined with ceramic matrix. For few specimens, there are tiny areas (<1

cm^2) where the surface rose up a few millimetres in extended testing times. An increase in thickness would in turn, increase the thermal insulation performance.

The test results of heat reaction include a total heat release (THR), a heat release rate (HRR), a CO production rate and a yield, a CO_2 production rate and a yield, the effectiveness of heat combustion, mass stability, mass loss rate and a rate of smoke released. In order to have better understanding of the fire performance of the material under the cone radiator, we compared them with a group of phenolic DMC under similar or lower heat flux condition. The results proved that the overall fire performance of the CDMC is better than those of the phenolic DMC which has always been considered as one of the best polymer composites in aspect of fire performance. The phenolic DMC with about 25%(vol.) of glass fibre was given as a sample plate by the TBA, a British composites manufacturer. The results of the Cone Calorimeter study are presented in Fig. 8.8 - Fig. 8.17.

- The total heat released and the heat release rate (THR, HRR)

The THR is calculated by measuring oxygen concentration and flow rate in the combustion product stream. In the THR vs. time curves, the heat release rate for the CDMC was almost zero compared with the heat released from the phenolic DMC, as shown in Fig. 8.8.

- CO production rate and yield

CO yield during tests for the CDMC was zero. The CO production rate for the phenolic DMC is much higher compared to that of the CDMC, although both materials gave very low rate of the CO production, displayed in Fig. 8.9 and 8.10. The higher CO production rate for the P-DMC is due to a incomplete burning of the phenolic resin structure.

- CO_2 production rate and yield

The CDMC kept at vary low level of CO_2 production. CO_2 production rate for phenolic DMC at first 200 seconds was quite high and gradually levelling off.

The general trend of CO_2 generated in different materials is the same with those results achieved in CO production rate. Phenolic DMC generated much more CO_2 compared with those of CDMC, shown in Fig. 8.11 and 8.12. Trends of curves were similar between CO_2 production rate and HRR, since CO_2 generated was covering the main stream of burned gases which was detected from the exhausting system.

Naturally, the CO_2 yield for phenolic DMC is much higher than that of the CDMC especially at the period of 1200 seconds. After this, the phenolic matrix was burned off.

- The effective heat of combustion (EHC)

The CDMC is almost zero compared with the phenolic DMC in the effective heat of combustion. The EHC of phenolic DMC is around 15 to 25 MJ/kg. The EHC curves of the CDMC and the phenolic DMC are shown in Fig. 8.13.

- Mass stability (MS) and mass loss rates (MLR)

The CDMC lost mass (water release) slowly during test. Stability and mass loss rates are shown in Fig. 8.14 and Fig 8.15. A phenolic DMC loses its mass constantly during the whole test of 1200 seconds after the initial sharp loss at 200 seconds. The mass loss became slow after 400 seconds for the CDMC and gradually levelled off and kept stable. The DSC results indicated a loss of water in the CDMC after 110 ℃ from the matrix. DSC results also show a loss peak at 250 ℃ for water from the fillers. These water emissions account for the small mass loss observed in the Cone Calorimeter tests. Weight loss in the phenolic composites is primary result of thermal decomposition of the polymer.

- Rate of smoke released (RSR)

Rate of smoke release for the CDMC was zero at all the time during the test. For a phenolic DMC, the rate of smoke release at first 200 seconds is high, after this the release rate decreased to very low level as shown in Fig. 8.16.

- Specific extinction area (SEA)

The CDMC has the constant extinction and never being ignited actually during the fire test in Cone Calorimeter. Specific extinction area for the CDMC and the P-DMC is illustrated in Fig. 8.17. However, the phenolic DMC contains the phenolic matrix. Under intensive radiation, it ignited and kept burning until the polymer burned off. But phenolic composites have a common advantage over most of other polymers, as they are self extinguishing when the outside heat/fire source is removed.

8.6 Summary

Overall heat resistance of the CDMC is much better in comparison with the phenolic DMC and other polymer composites. The types of composites tested are listed in Table 8.2. The average results of different composites as a total feature are listed in Table 8.3. It appeals that the smoke emission (m^2/kg) of the CDMC is 8 m^2/kg; compared with polyester SMC/DMC (239 m^2/kg); fire retardant GRP (993.7 m^2/kg). Very small amount of smoke emission in CDMC might come from the sizing system coated outside of glass fibre (about 0.3% in the total CDMC composition). The peak release rate for the CDMC is 2.0, compared with polyester SMC/DMC (282.3); phenolic SMC/DMC (224); fire retardant GRP (180).

One of samples of the fire proof CDMC after Cone Calorimeter test under the heat flux of 75 kW/m^2 for over 1.0 hour is shown in Fig. 8.18. On the left hand side the sample shows exposed face to a cone heat (cone radiator temperature is around 900 - 1000 ℃ with heat flux >75 kW/m^2), and the right hand side sample shows the unexposed face. The Al foil was used for a preventing of the heat loss. Under this heat flux, the sample's dimension kept stable, no sign of crack occurred.

The fire resistance of the CDMC tested shows that the ceramic moulding compound products can perform exceptionally well in delaying the temperature rise on the unexposed face without combustion on the inner face. Naturally the ceramic panels would outperform any equivalent polymeric composites panels such as the phenolic matrix composites.

The CDMC is effectively incombustible. the heat release measured was negligible and only trace amount of smoke and carbon dioxide were produced. The results were effectively constant for all compositional changes.

Table 8.1 A list of dimensions and testing perimeters of the CDMC and other composite samples for the fire penetration test.

Type of panels	Dimension (mm^3)	Temperature range in fire test	
		Starting(°C)	End(°C)
CDMC with 22.6%(vol.) GF	300x170x3.0	20	960-1100
CDMC with 22.6%(vol.) GF	300x170x3.0	20	700
Phenolic based DMC with 20%-25%(wt.) GF	300x170x4.0	20	960
Glass/phenolic laminate	300x170x8.0	20	900

Table 8.2 A list of different materials subjected to the Cone Calorimeter tests. The dimension of sample was 100 x100 mm^2.

DMC	Matrix	Thickness (mm)	Heat flux (kW/m^2)
CDMC with 15%(vol.) GF	Ceramic resin	3.5	75
UP DMC with 28%(wt.) GF	UP resin	4.0	75
Phenolic DMC with 20-25%(wt.) GF	Phenolics	4.0	75
Fire retardant GRP	UP resin	4.0	75
PVC foam	PVC	10	75
PMMA	PMMA	4.0	75

Table 8.3 A listed summary of the Cone Calorimeter tests for the CDMC, P-DMC, UP-DMC, PVC foam and PMMA.

Materials	Time to ignition (s)	Peak heat release rate (kW/m^2)	Total heat released (kJ)	Smoke emission (m^2/kg)	Mass loss (%)
CDMC	No ignition	2.0	0.0	0.8	
P-DMC	48	224	309.8	239	
UP-DMC	34	282.3	760.8	985	
UP/CDMC-2.0% UP	No ignition	3.0	0.2	15	19.64
PVC Foam	1.0	272.6	153.5	1232.3	84.12
PMMA	24.0	794	583.7	176	96.91

During the testing, the Cone Calorimeter operated with the heat flux of 75 kW/m^2.

The materials tested were the CDMC, the phenolic DMC, the polyester DMC, the polymer added CDMC, the PVC and PMMA.

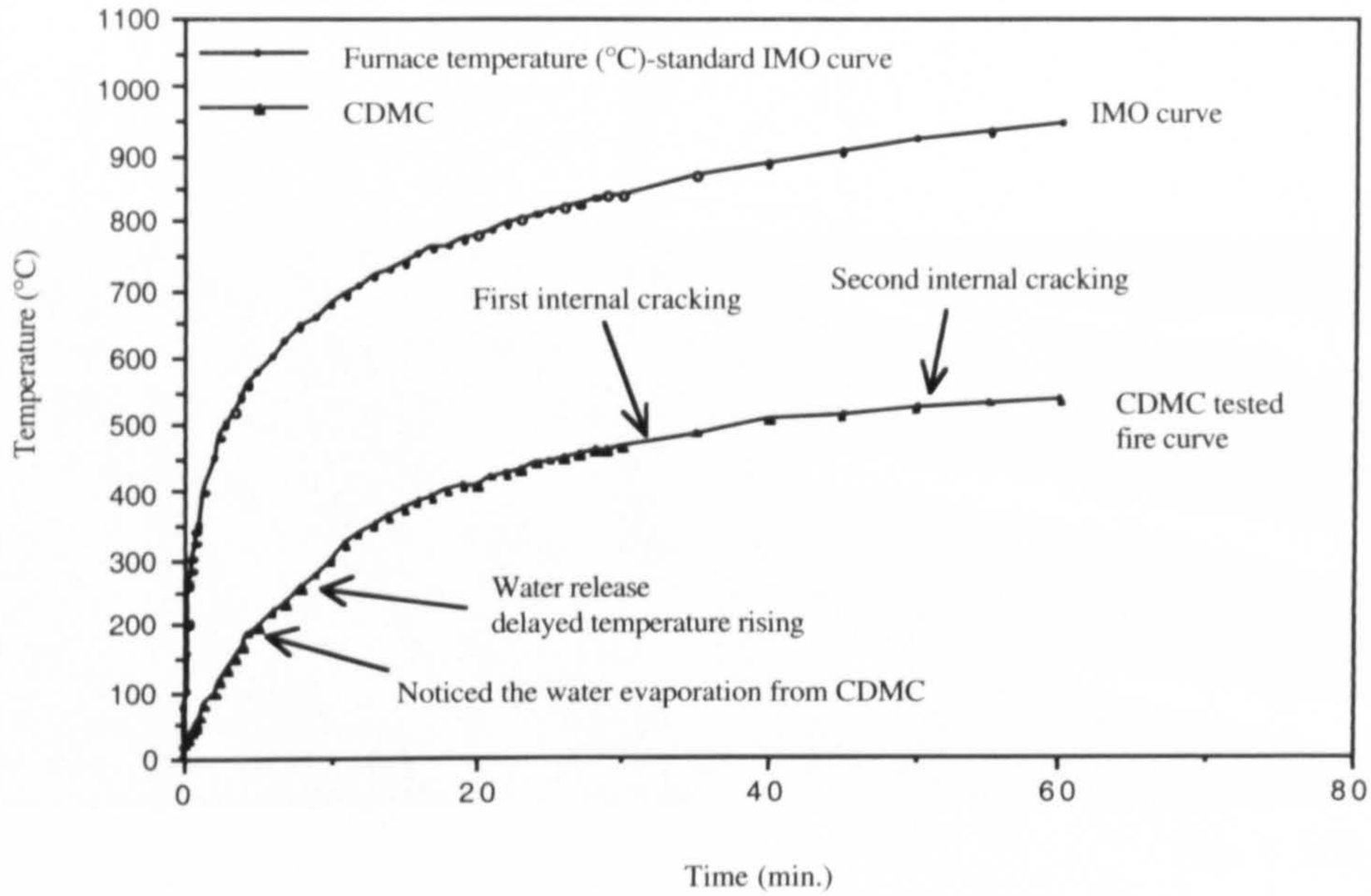

Fig. 8.1 IMO fire penetration test results of the CDMC. The thickness of specimen was 3.1 mm.

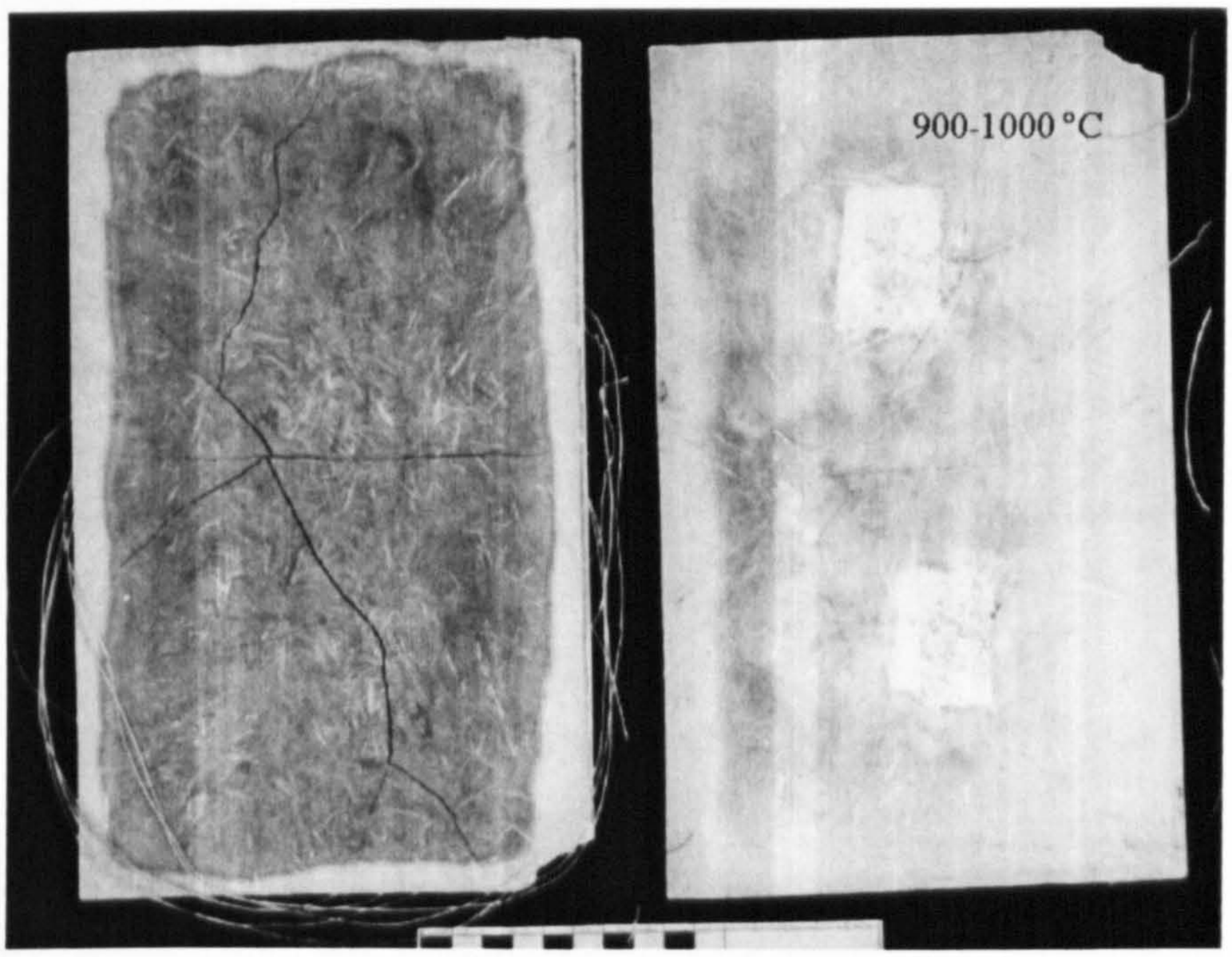

Fig. 8.2 The surfaces of specimen after fire resistance test. The left sample panel is the exposed surface which under the maximum temperature of 1000 ℃ for over 1.0 hour. The right hand is the same panel non-exposed surface.

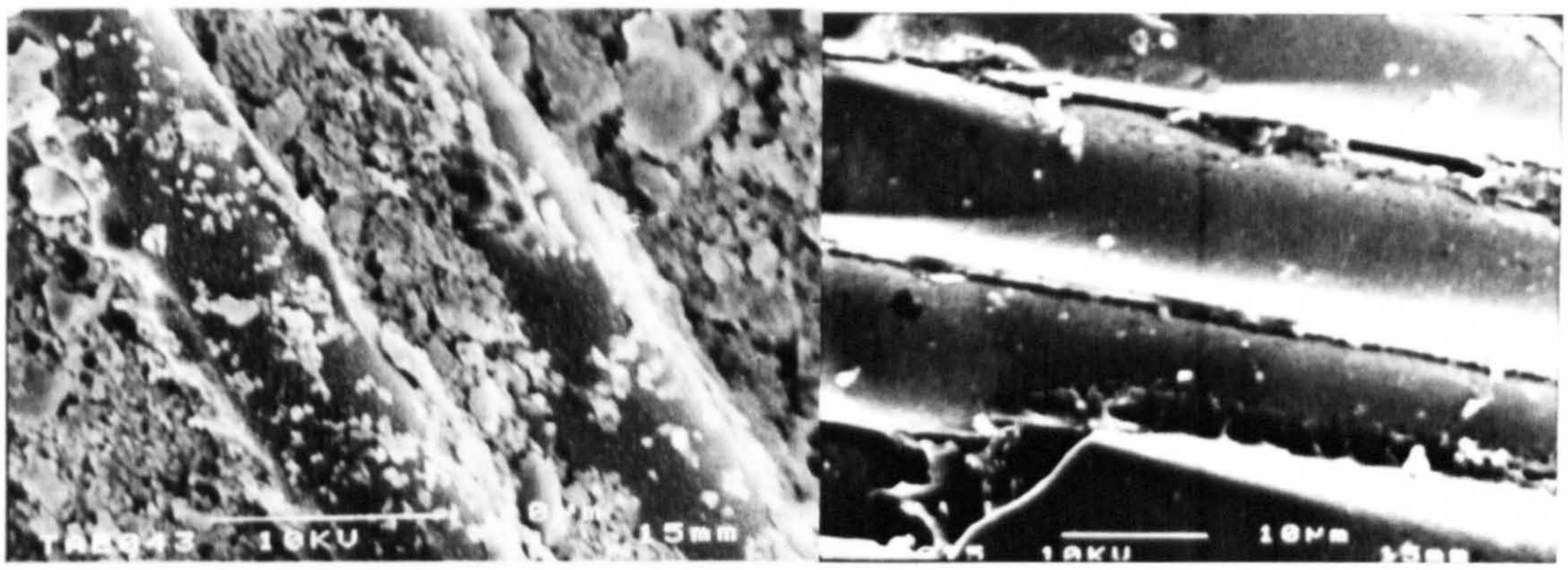

Fig. 8.3/A

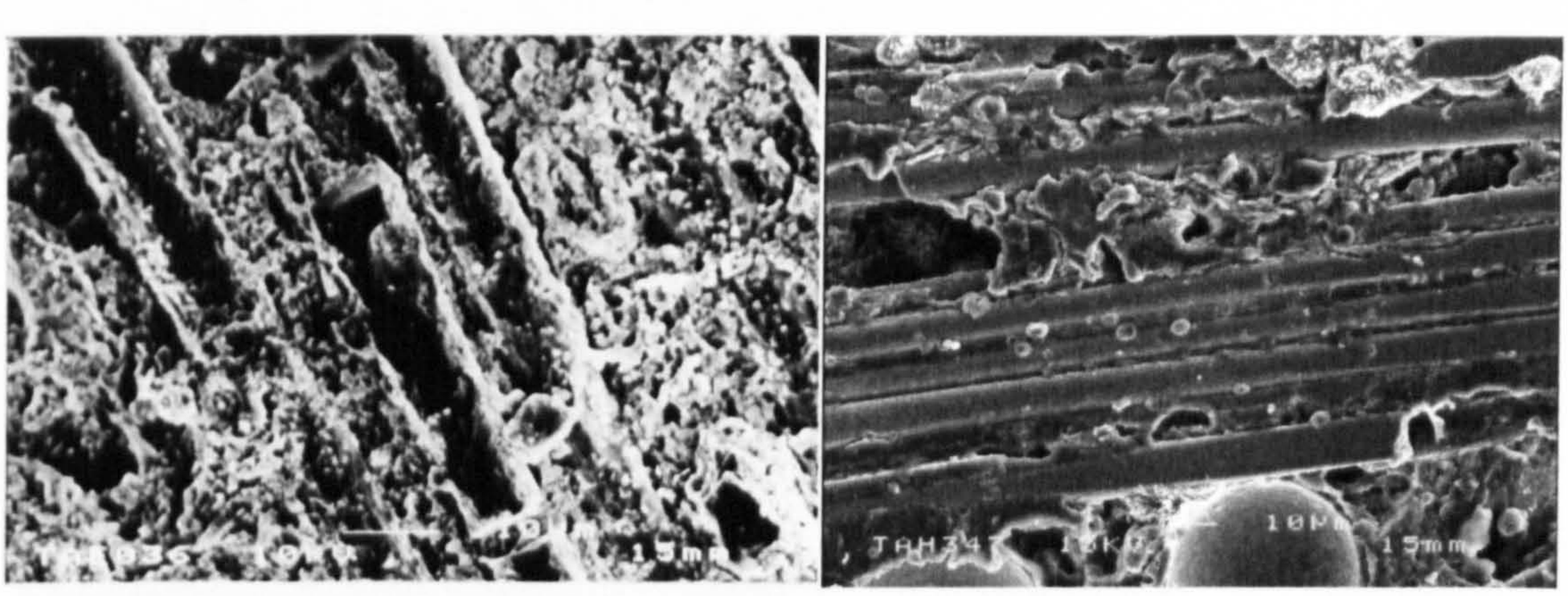

Fig. 8.3/B

Fig. 8.3 (A and B) SEM graphs of the CDMC subjected to a fire for about 100 minutes. The furnace temperature raised up to about 1100 °C. Fig. 8.3/A shows the comparison of original glass fibres (right) and fired fibres(left) near the unexposed surface in the cross section of the tested panel. Fig. 8.3/B shows original fibres (right) and fired fibres (left) in the exposed surface facing fire.

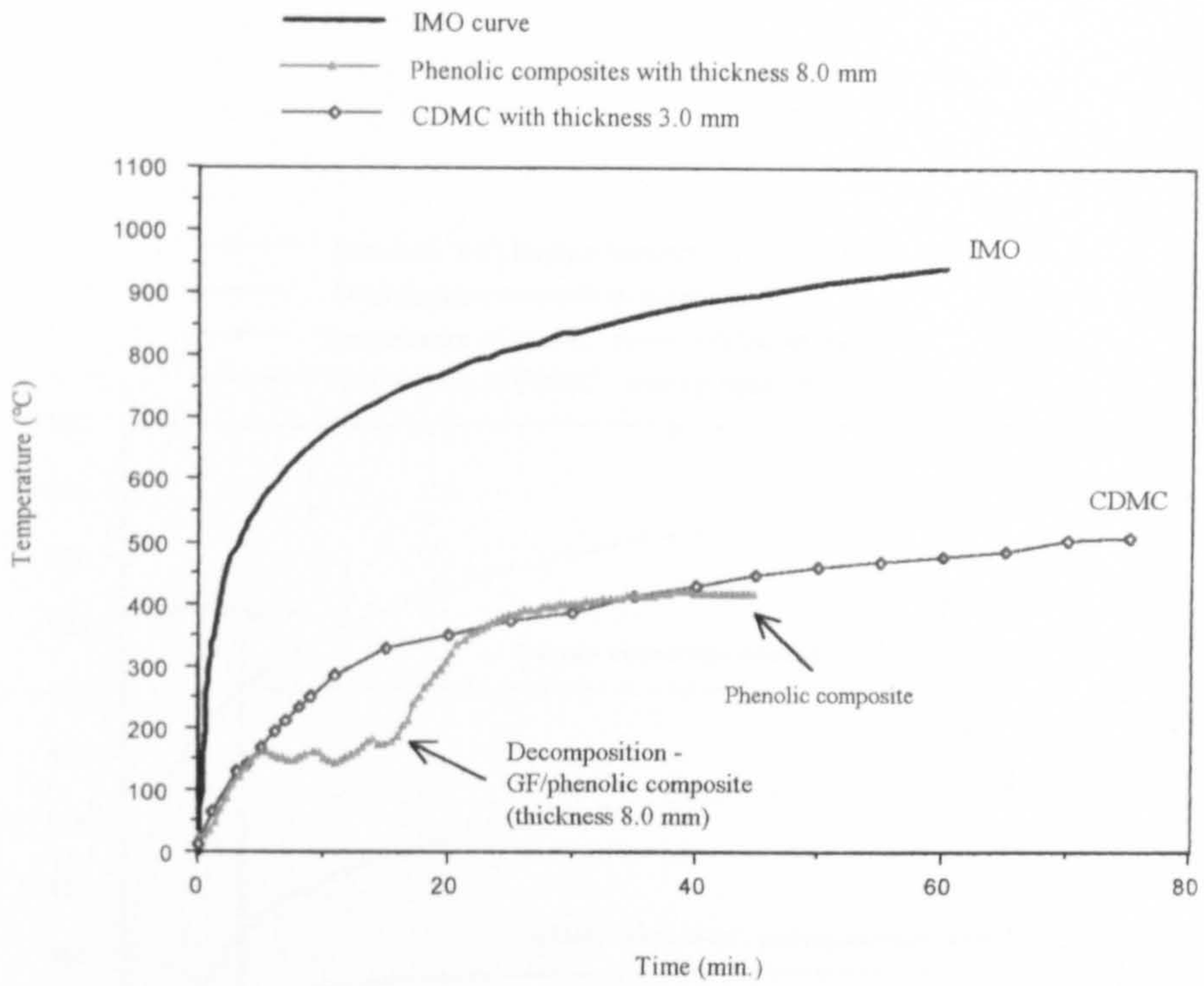

Fig. 8.4 The results of fire penetration test of the CDMC (thickness 3.1 mm), and glass fibre/phenolic composite (thickness 8.0 mm).

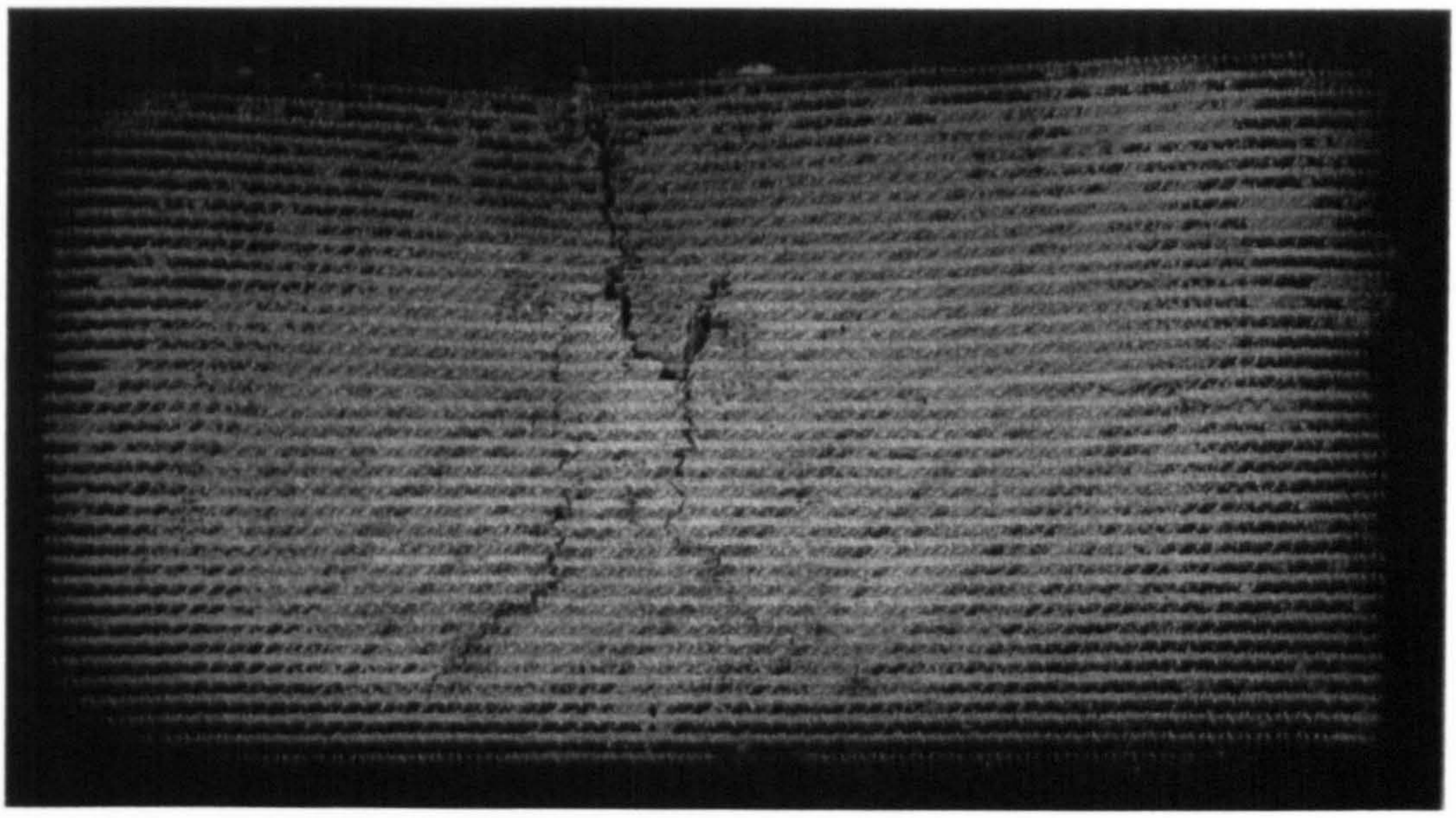

Fig. 8.5 The resin matrix was completely burned out in the specimen of phenolic composite after a fire test for just 40 minutes.

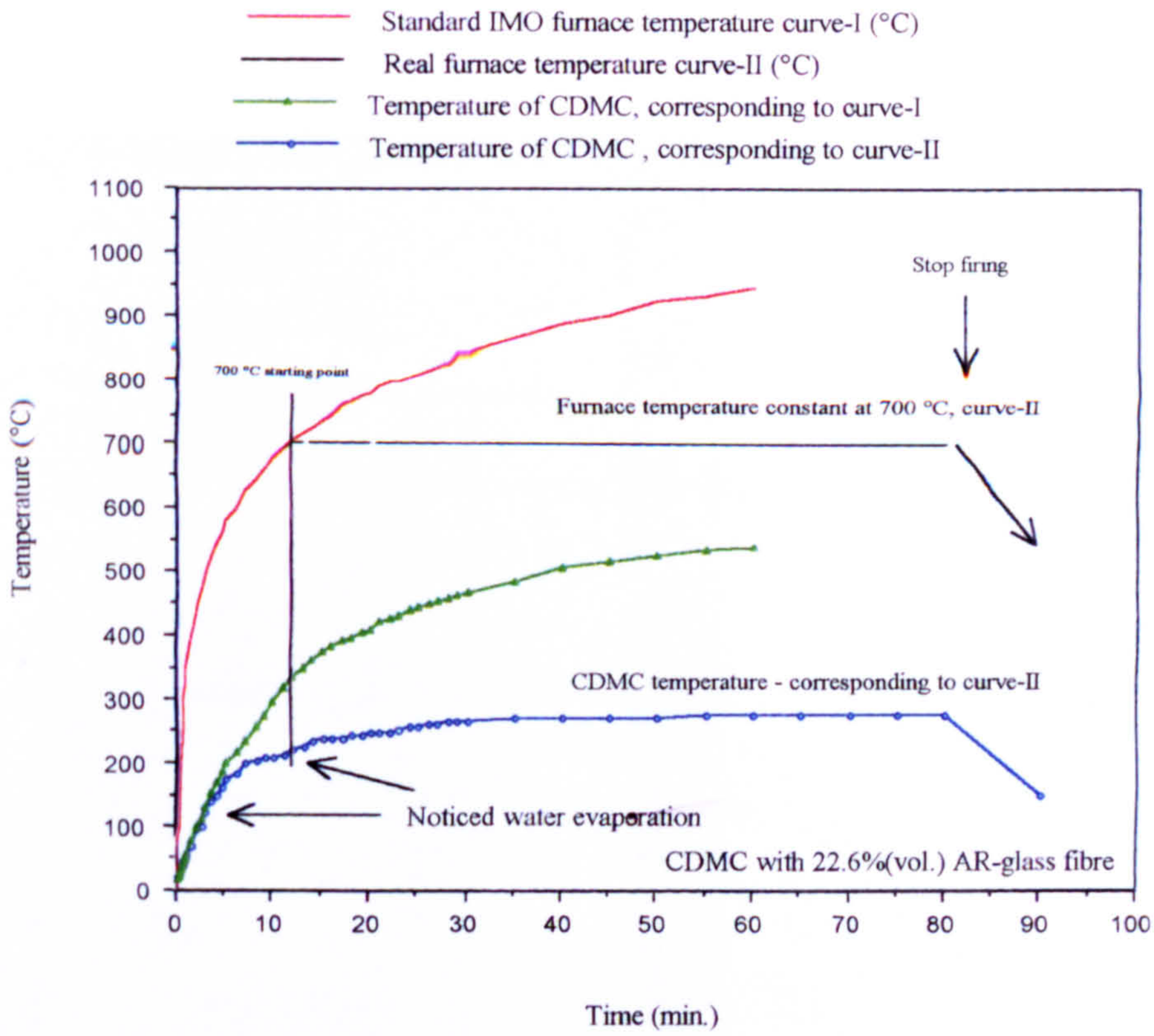

Fig. 8.6 IMO fire penetration test for the CDMC, the temperature of the panel non-exposed to fire was measured while the temperature inside the furnace stabled at 700 °C. Curve I was standard IMO temperature raising curve inside the furnace; curve II was stabilised temperature curve (700 °C) inside the furnace for this particular test.

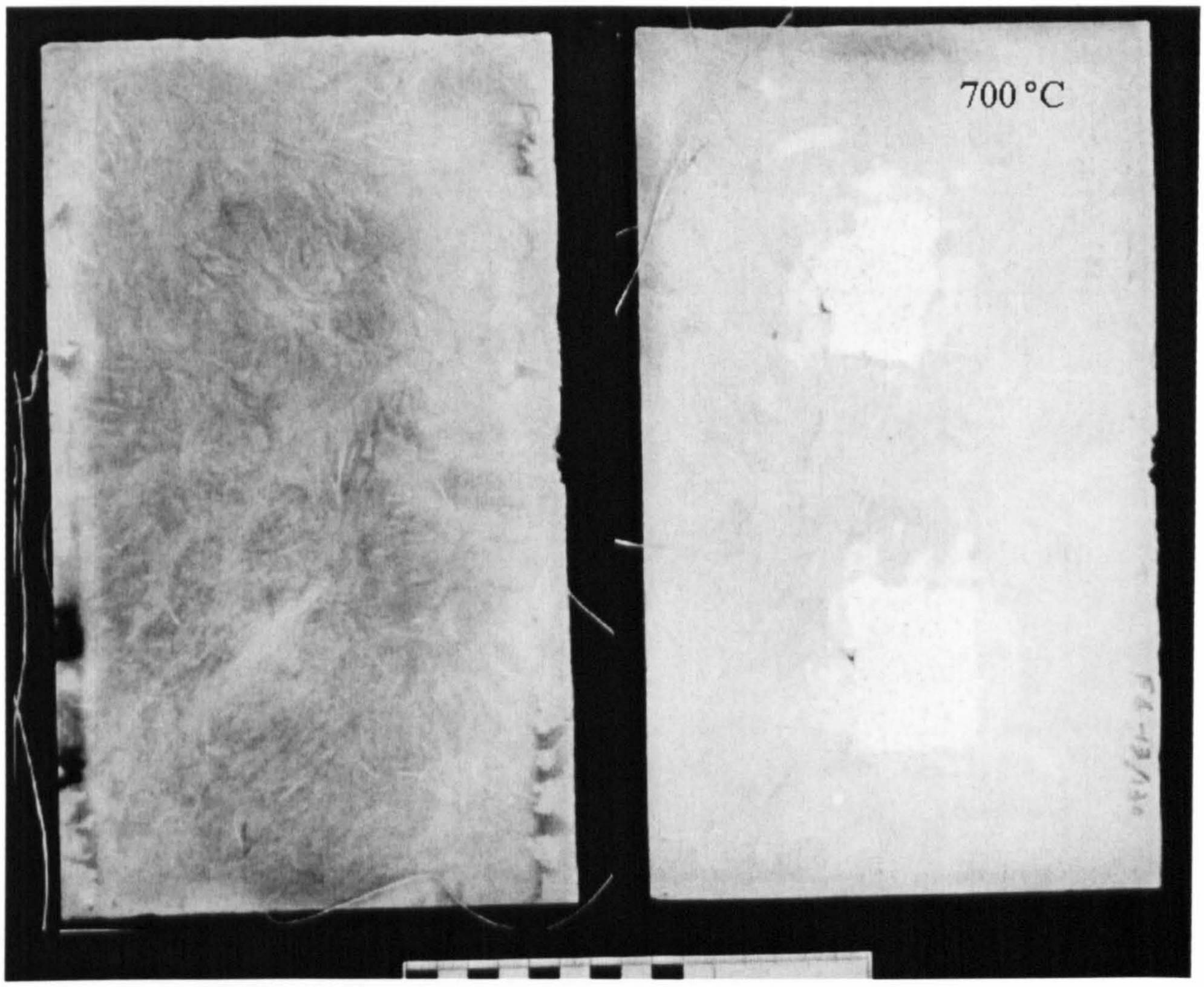

Fig. 8.7 This fire tested specimen is corresponding to Fig. 8.6. The panel had been subjected to a temperature of 700 °C for more than 80 minutes. And this picture indicates the status of the panel after fire test. Left is the surface exposed to fire, right hand is the non-exposed surface.

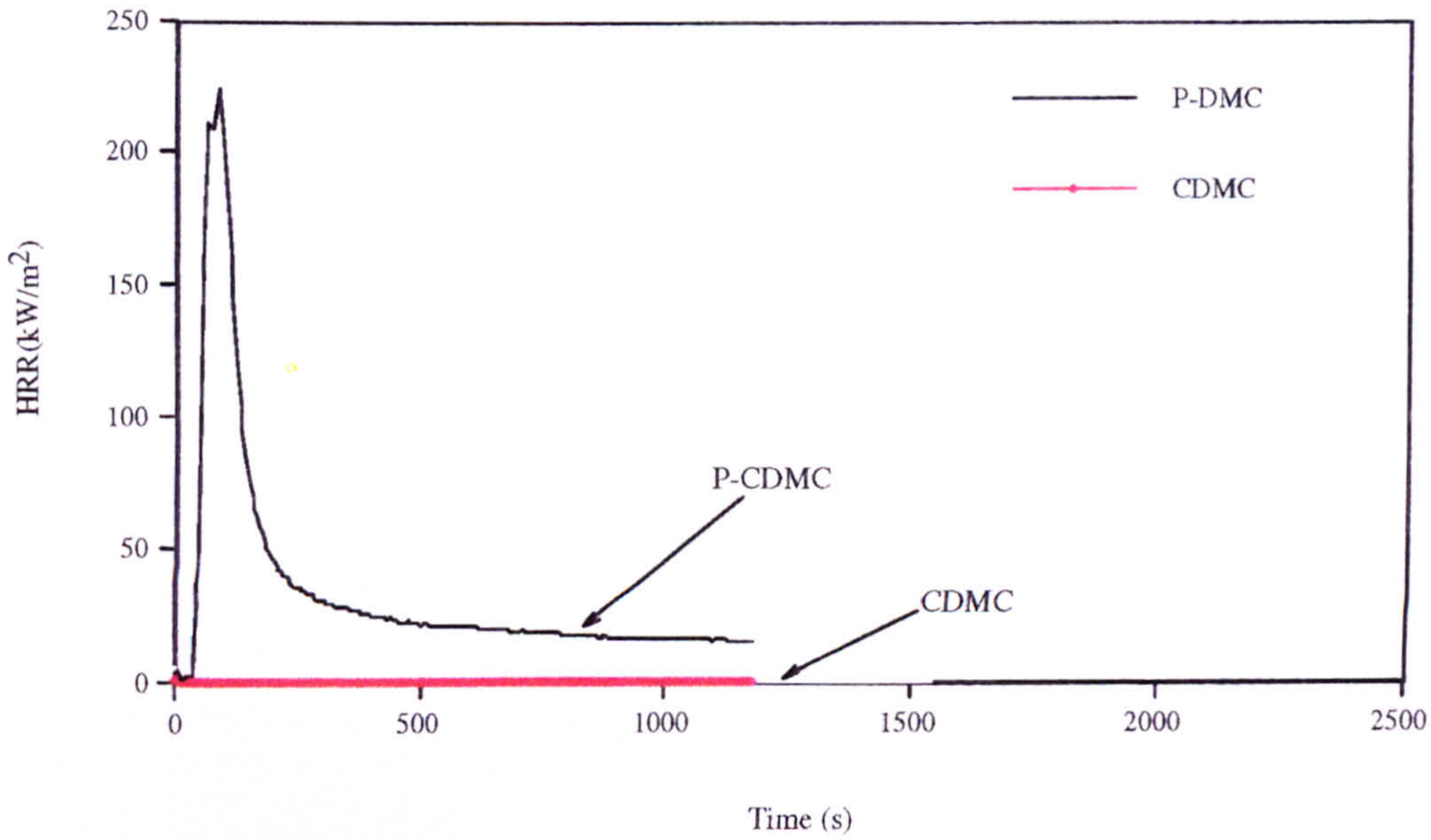

Fig. 8.8 Heat release rate of the phenolic DMC and the ceramic DMC.

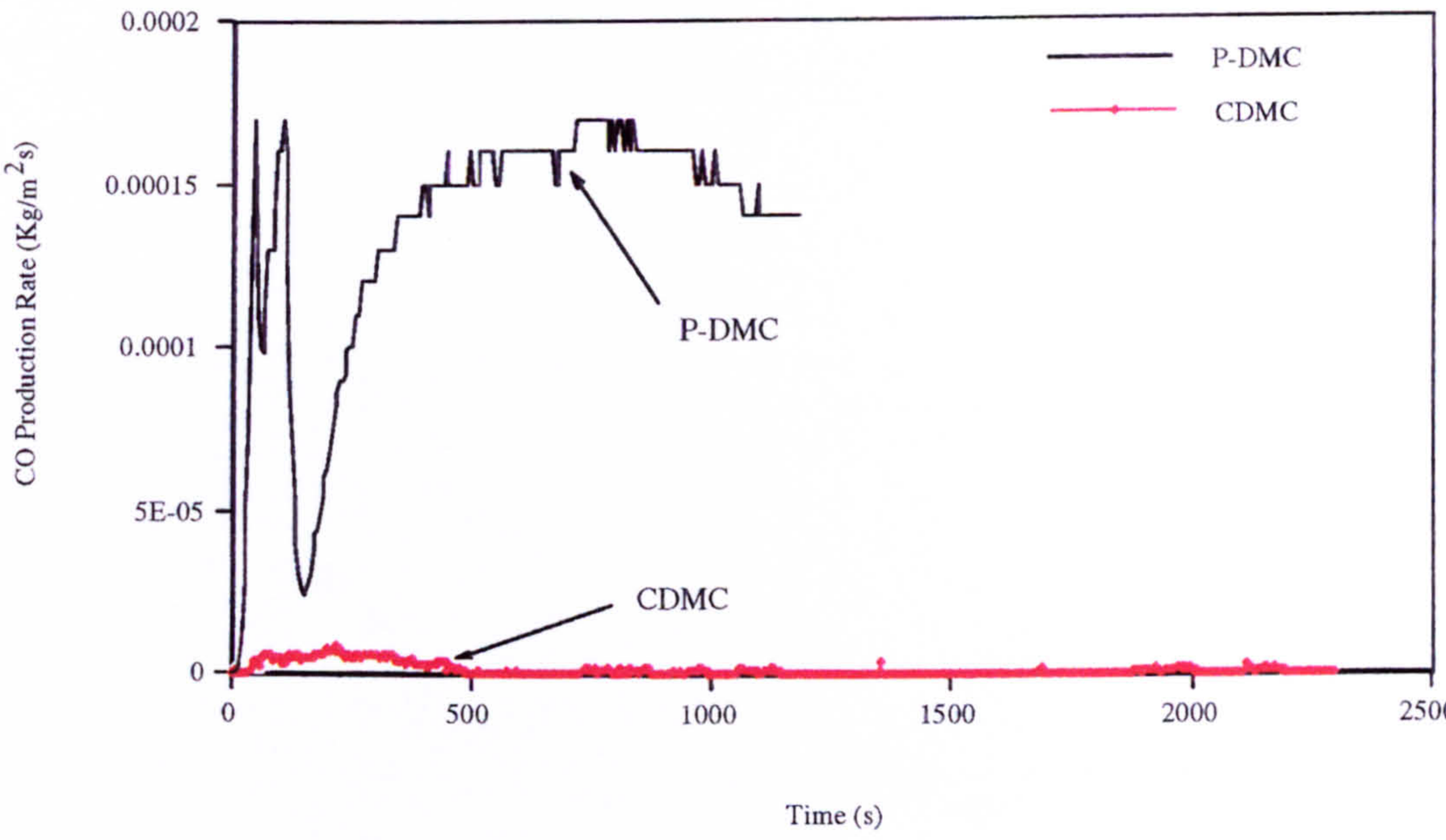

Fig. 8.9 The figure showed the CO production rates (kg/m^2) for the phenolic DMC and the CDMC.

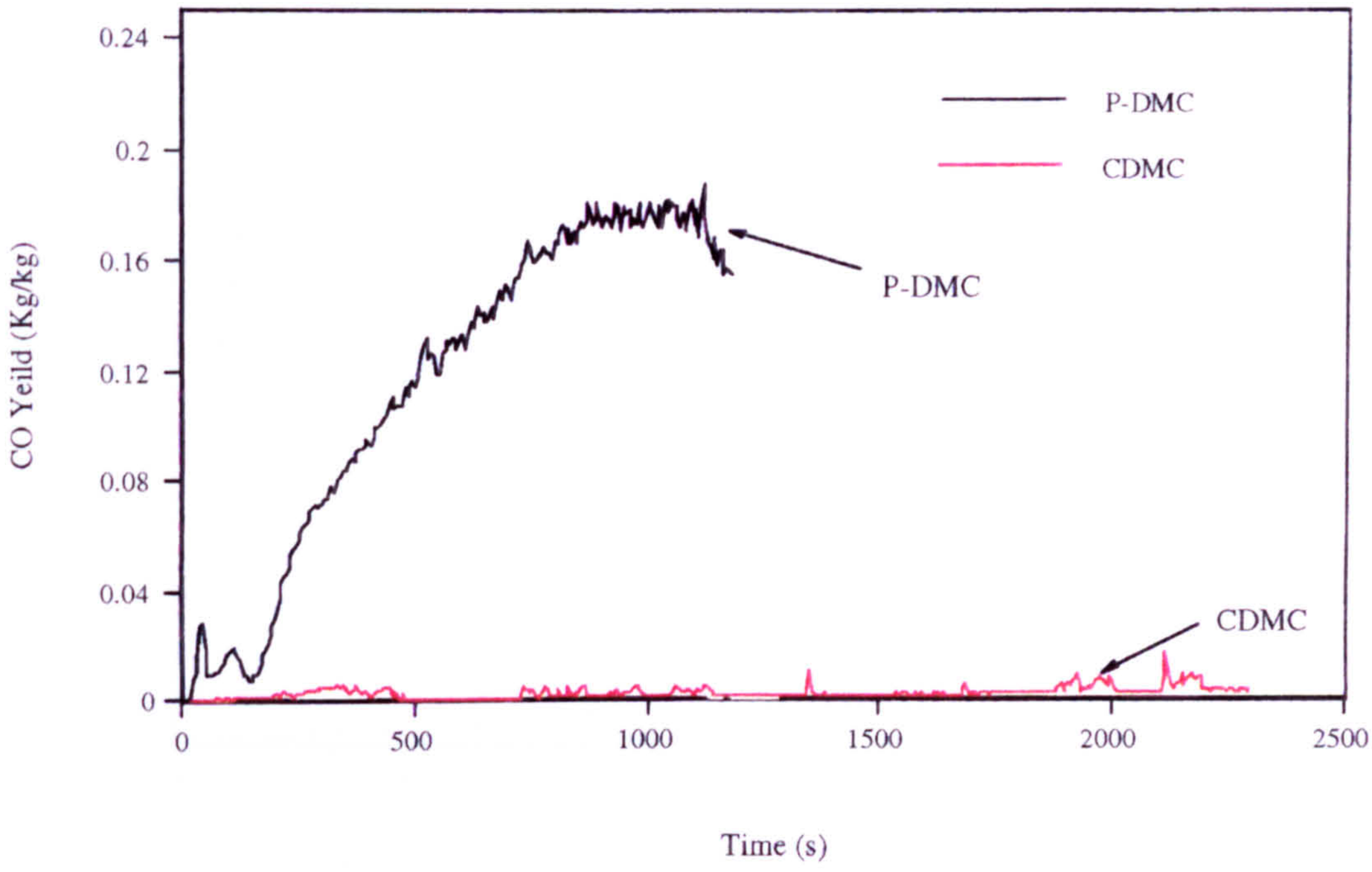

Fig. 8.10 CO yields for the phenolic DMC and the CDMC.

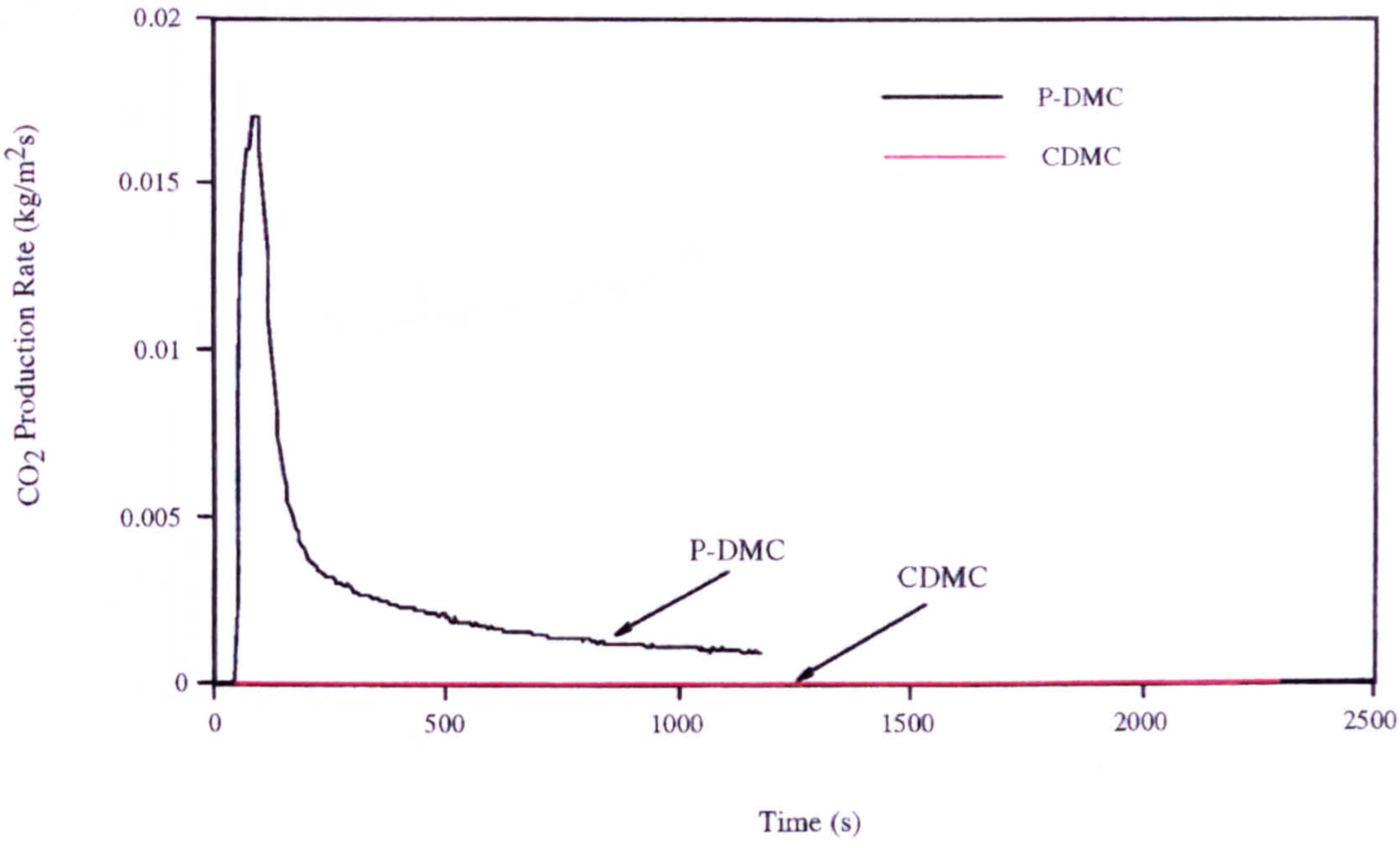

Fig. 8.11 CO_2 production rates for the phenolic DMC and the CDMC.

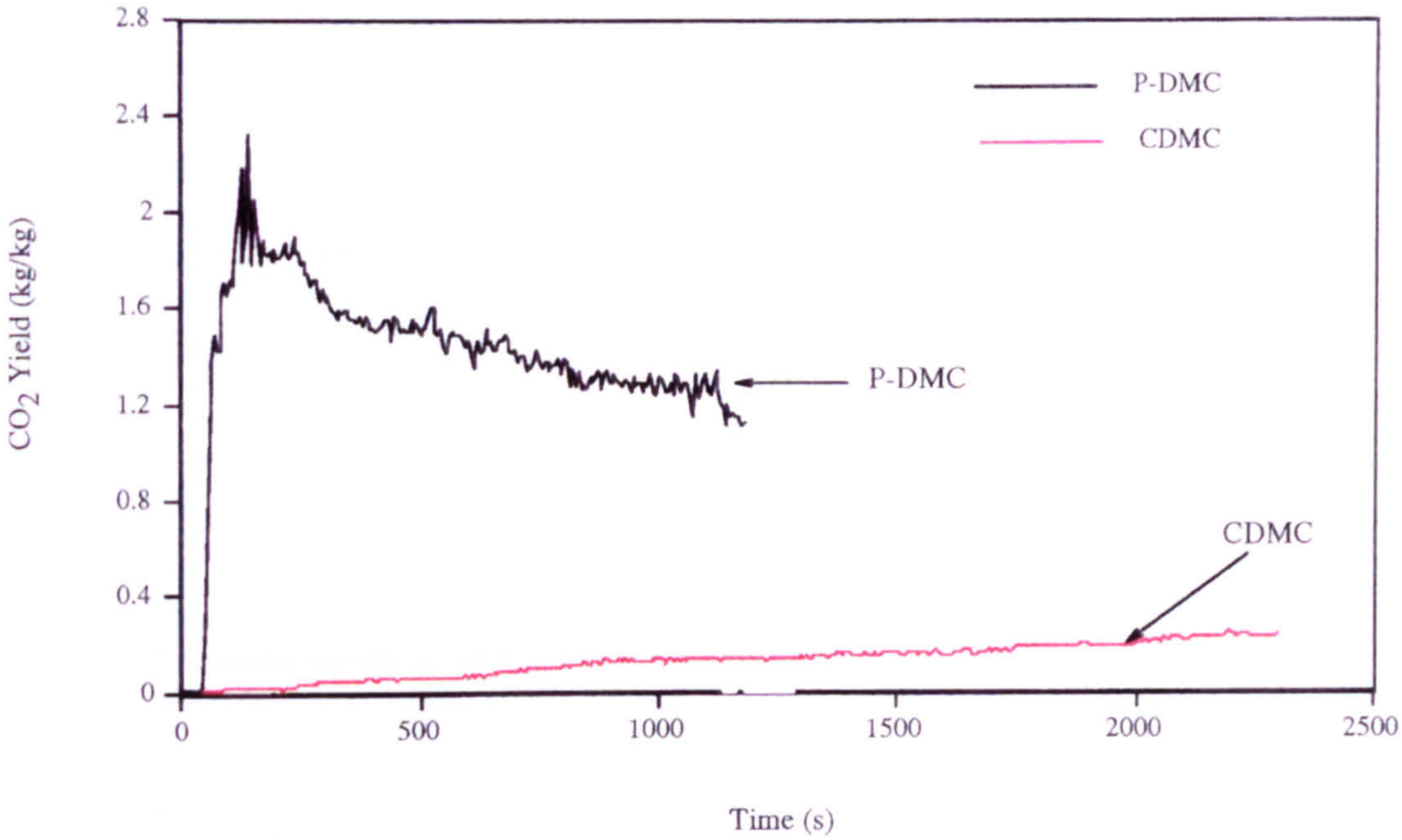

Fig. 8.12 CO_2 yield for the P-DMC and the CDMC.

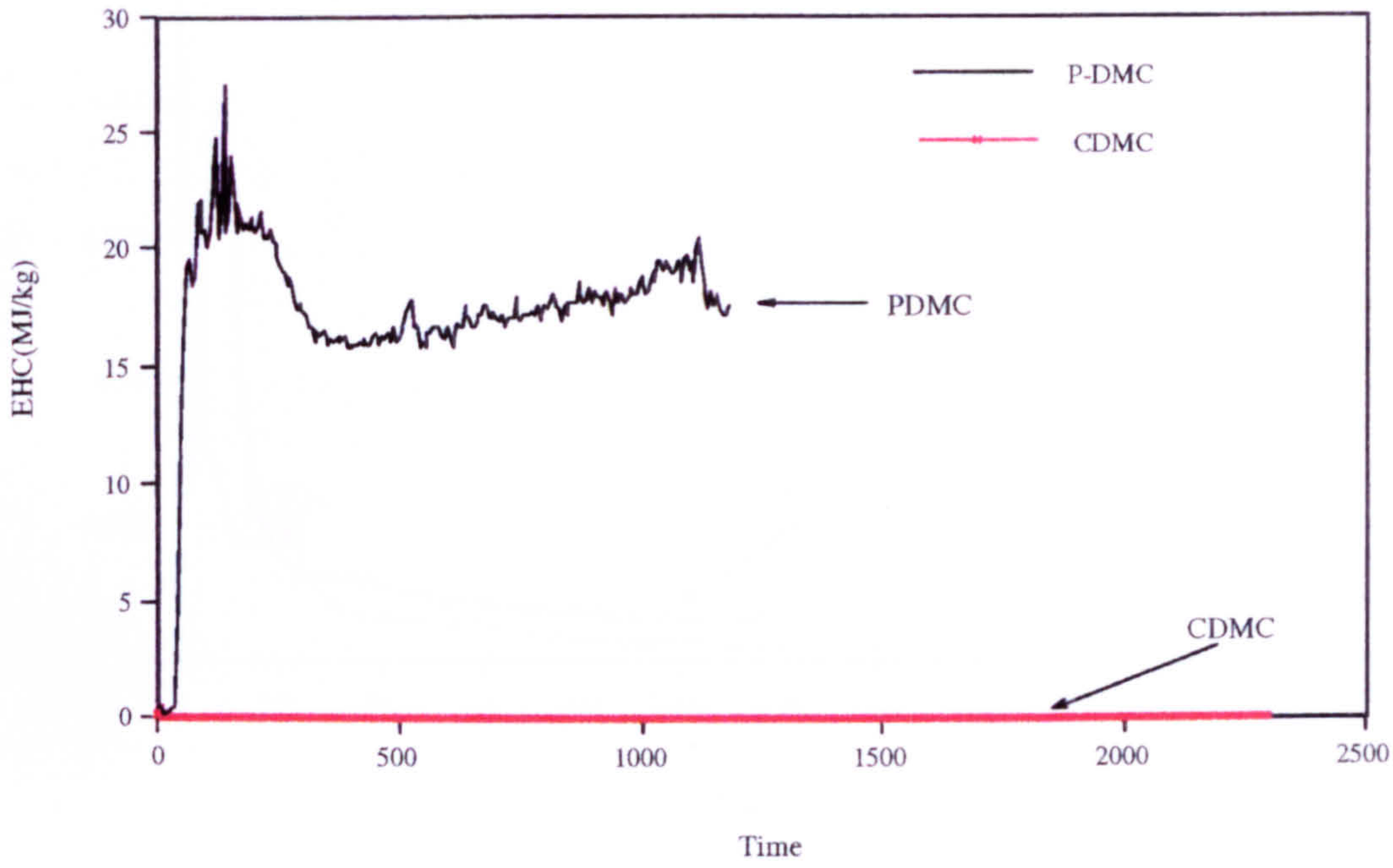

Fig. 8.13 Effective heat of combustion (EHC) for the P-DMC and the CDMC.

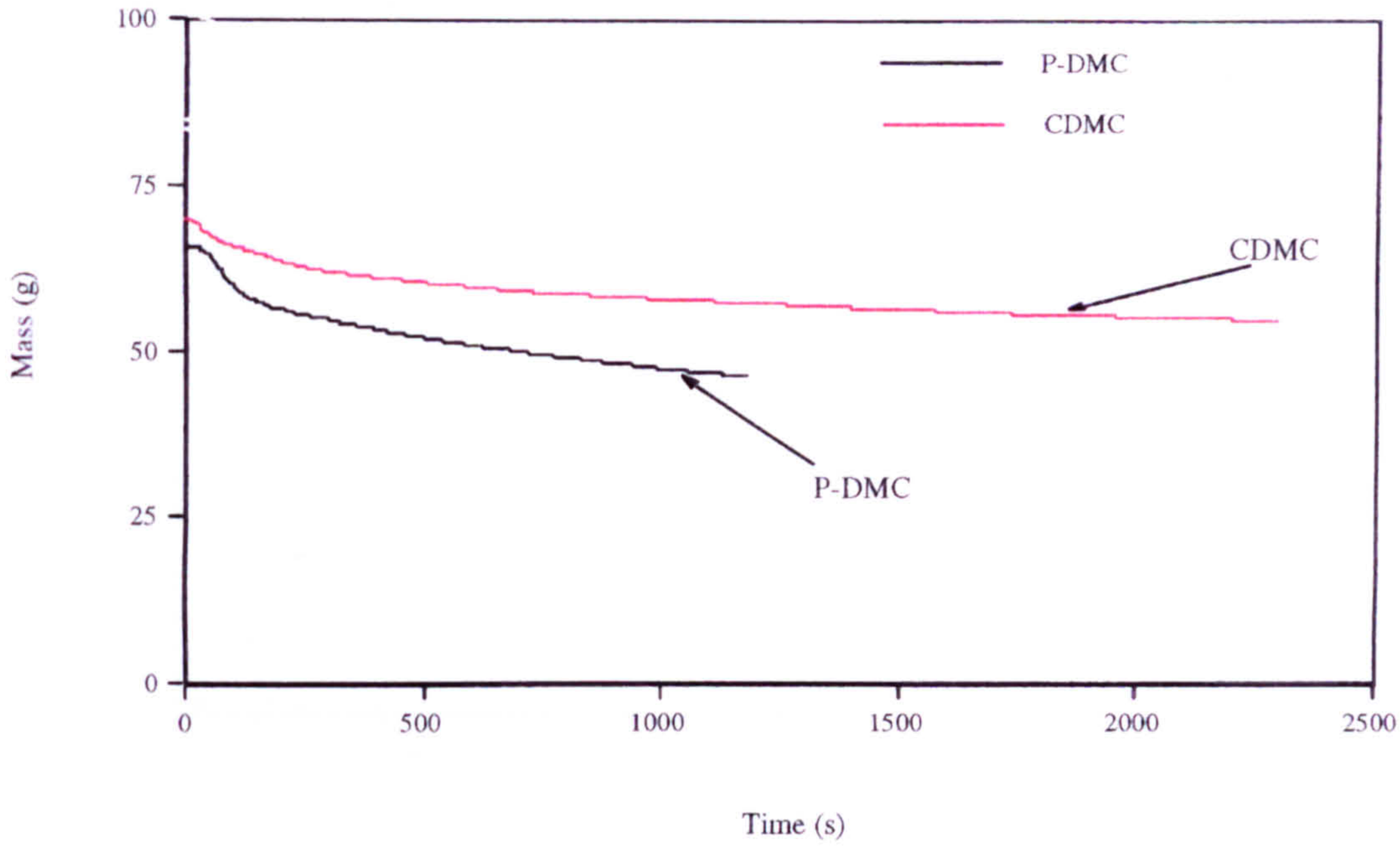

Fig. 8.14 Mass stability (MS) of the P-DMC and the CDMC.

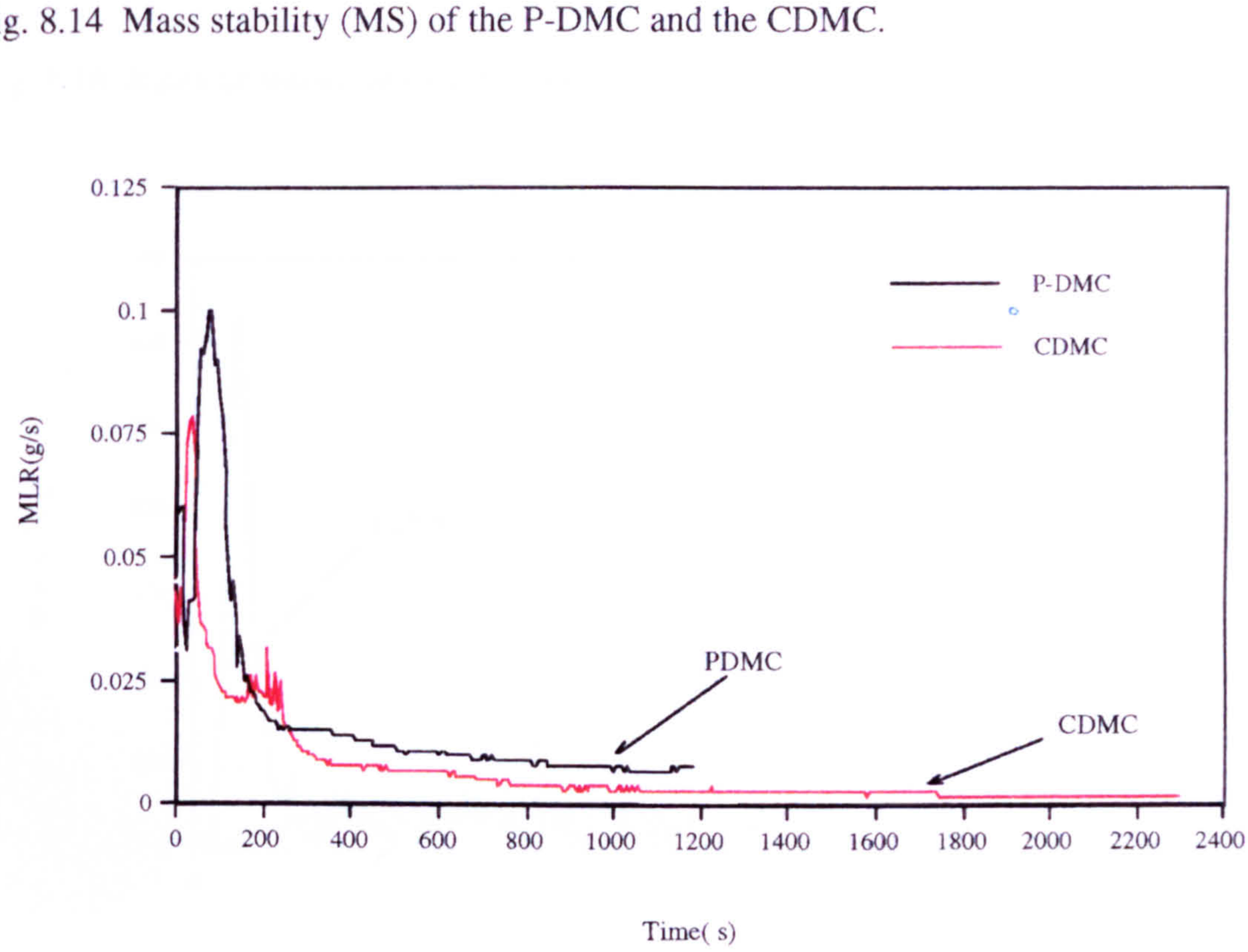

Fig 8.15 Mass loss rates (MLR) for the P-DMC and the CDMC.

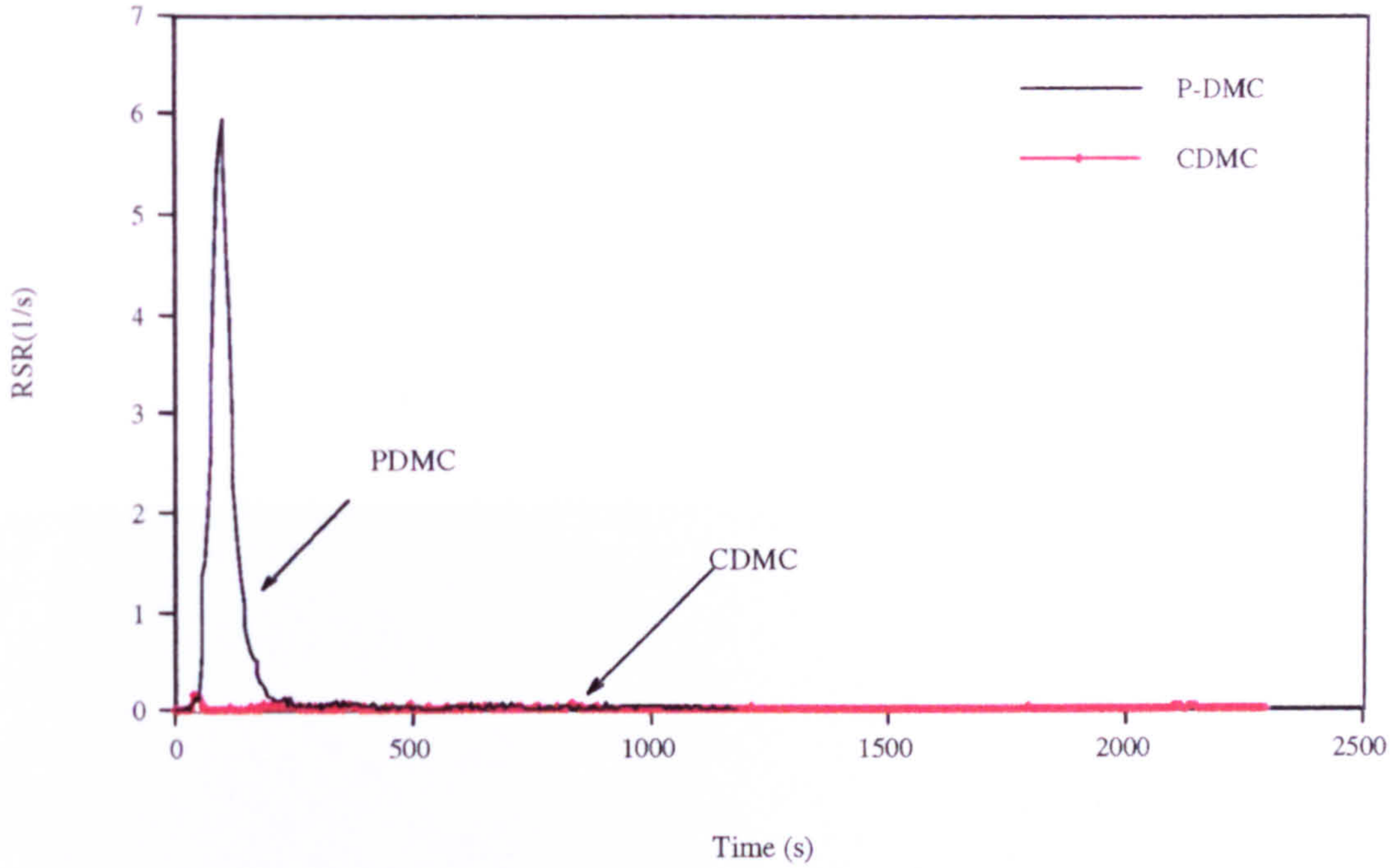

Fig. 8.16 Rates of smoke released (RSR) for the P-DMC and the CDMC.

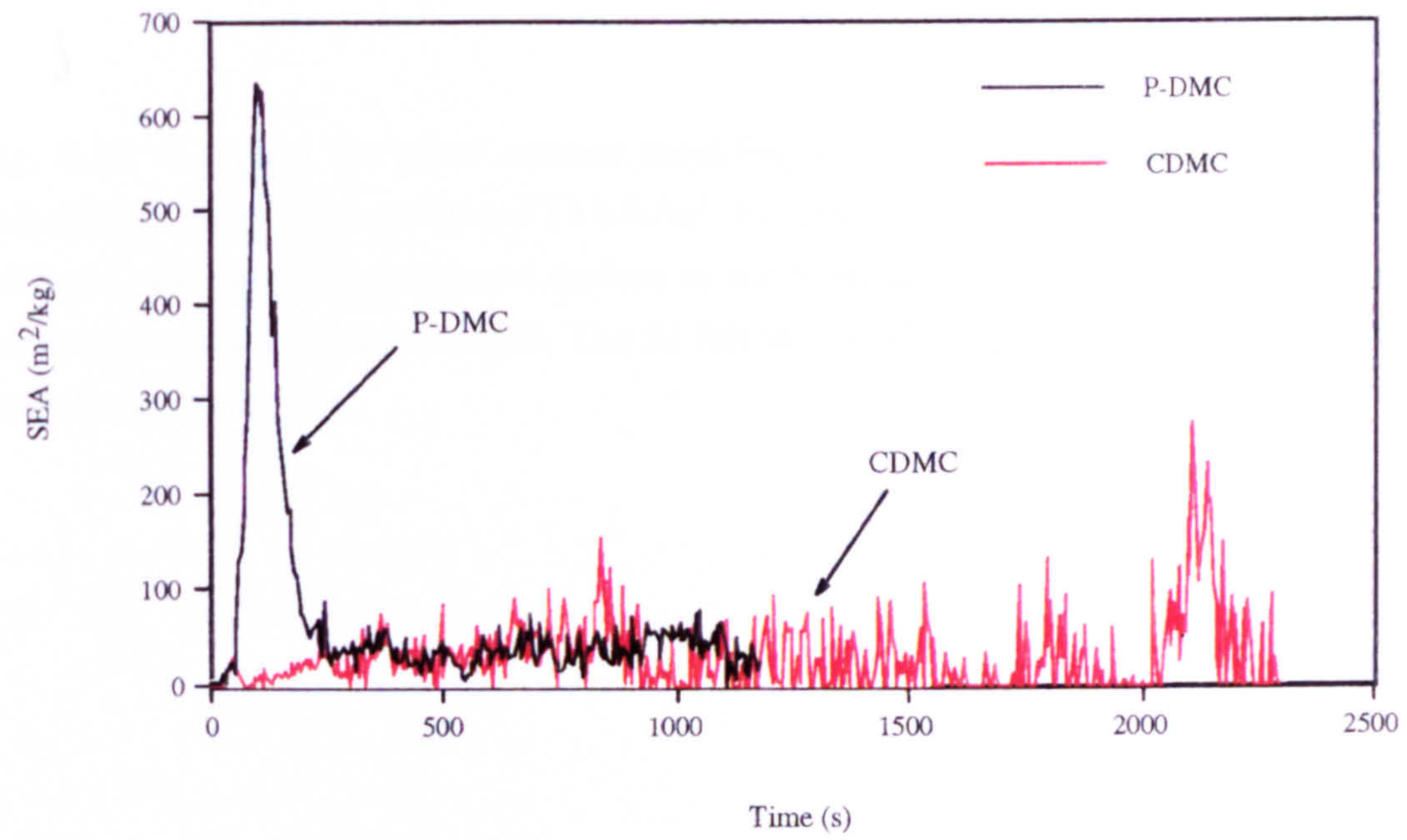

Fig. 8.17 Specific extinction area (SEA) for the P-DMC and the CDMC.

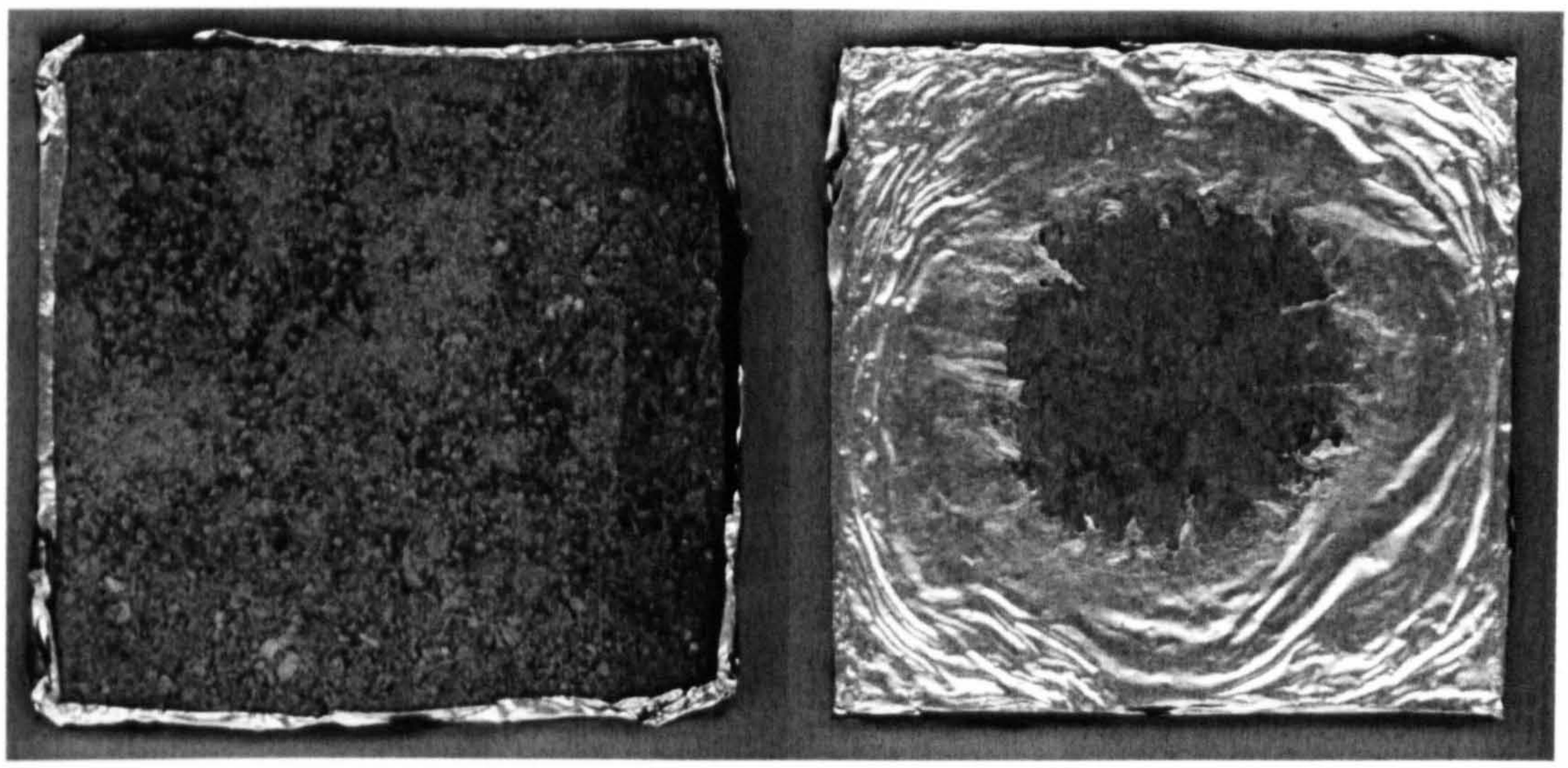

Fig. 8.18 A typical fire proof ceramic moulding composite sample tested by the Cone Calorimeter under the heat flux of 75 kW/m^2 for more than one hour. The sample on the left hand side shows the exposed surface to the heat, and the right hand side shows the unexposed surface of same sample. The Al foil was used for insulation and was molten in central area during test.

Chapter 9

POTENTIAL APPLICATIONS

9.1 Introduction

In order to validate the applicability of the ceramic dough moulding compound, a number of test components were manufactured. A combination of samples with complex shapes was produced using wherever possible standard moulds and moulding procedures that would be compatible with current practices in the polymer composites industry.

The parts selected for this study include a simple single curvature heat shield, a complex heat protection cup, both based on current automotive products, and a double curvature track line fairing which is a test aerospace component.

9.2 The heat shield

The heat shield was intended to be a direct equivalent of a current production item manufactured from a phenolic moulding compound. A schematic drawing of the heat shield is shown in Fig. 9.1 and the tooling used for moulding heat shield is shown in Fig 9.2. The real part is equipped with a thin aluminium foil layer on one surface to provide heat reflectivity.

The heat shield is produced using a simple metal tool with minimal pressure induced by clamping a shell female tool surface to a solid male tool. To produce the same part from the CDMC, no change in tooling was considered. The aluminium foil was laid down on the female shell tool and acted as a release film. A charge of the CDMC, of 40 - 50 g was applied by hand onto the tool, covering approximately 60 -80 % of the tool. A release film of PTFE was applied to the surface of the male tool. The tool was then closed manually and the complete tool and moulding compound assembly was placed in a heated oven at

140 ℃ for 30 - 60 minutes to cure the part. The part demoulded easily after cooling to room temperature, and two heat shield products are presented in Fig. 9.3.

Examination of a cross section of a moulded heat shield revealed good bonding between the aluminium foil and the moulding compound, as shown in Fig 9.4. The CDMC was observed to contain a high level of porosity which was expected due to the minimal pressures applied in the moulding operation.

The test parts were examined by an automotive component supplier and subjected to environmental testing and basic operational trials. The results of those trials are proprietary to the company but the basic outcome was that the CDMC heat shield outperformed existing phenolic parts and passed all durability tests that could be required for commercial use of the system. Long term environmental cycling did not result in any degradation of the CDMC but did cause slight corrosion in the aluminium foil which is indicated in Fig. 9.5.

9.3 The heat shield cup (HSC)

The second part to be produced was another heat shield but this time a more complex item resembling a cup in shape. Matched metal tooling for this part was supplied by a commercial manufacturer. The production item again was a phenolic moulding compound but this time produced under high pressure. The procedures for moulding were to apply a charge of the CDMC , of 100 g, to the female tool by hand, position the male tool section onto the female and close the tool slowly in a heated pressure at temperatures of 140 ℃. The mould was held at that temperature after closing for 1.0 hour.

This part was moulded easily and the final product was of high quality with low void content. The complex shape of the part was readily adopted by the moulding compound.

The problem with this part was that a method for achieving good release from the tool was not available in the time scale and no complete part could be lifted from the tool without damage. Mouldings had to be undertaken using a release film which did not conform with the tool shape resulting in parts that failed to meet aesthetic standards due to creasing and wrinkling in the film, as indicated in Fig 9.6.

However, the exercise did confirm that well consolidated parts of complex shape were feasible if the mould release problem is solved.

9.4 The track line fairing

The track line fairing is a test part used in a development of aerospace materials and simulates a full scale fairing used in aircraft to house moving mechanisms associated with flaps and other control surfaces. There is no equivalent commercial product but the tooling that was available, a matched set of monolithic graphite tools have been used previously to mould test parts from Carbon-PEEK thermoplastic composites.

The original tool had been slightly damaged and as such a complete fairing could not be produced. However, by again applying a charge of more than 300 g of material covering 60 % of the surface, and closing the tool slowly at 140 °C, a fully consolidated part was achieved. The tool closure pressure was around 8.0 MPa (80 Bar) during moulding. A release spray of PTFE worked adequately in this situation. The successfully moulded part is shown in Fig. 9.7.

9.5 Summary

All moulding trials showed that parts of varying complexity could be moulded by using the CDMC. The degree of porosity and strength in the moulded parts depended on the applied temperatures and pressures. The compound was capable of flowing and faithfully reproducible for the details of the mould. However, when using metal tools, it became apparent that mould release was a major problem and this issue, which was outside the scope of this programme, needs to be addressed if the material has any significant commercial future.

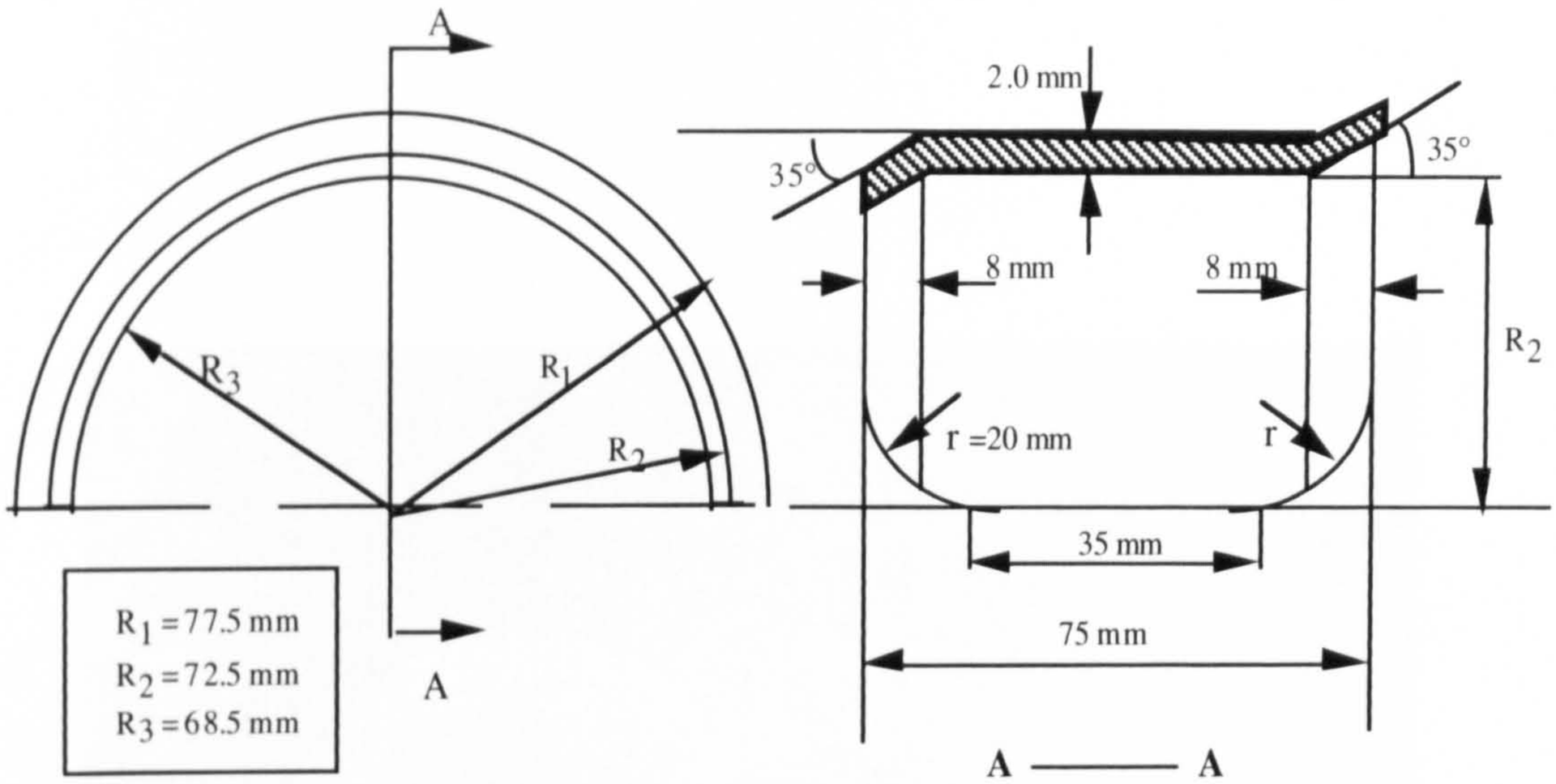

Fig. 9.1 A schematic drawing of the heat shield.

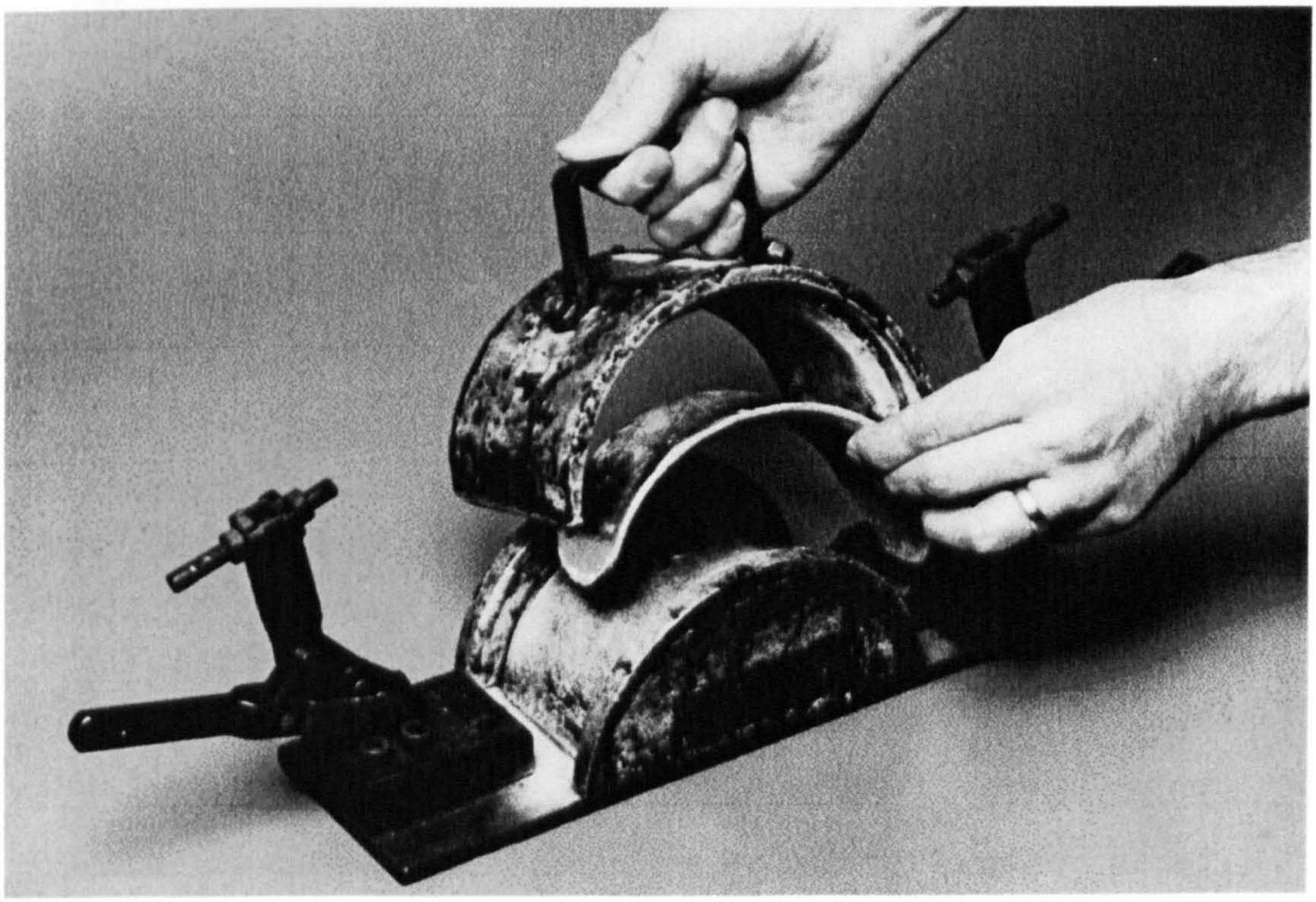

Fig. 9.2 The tooling used for manufacturing the heat shield.

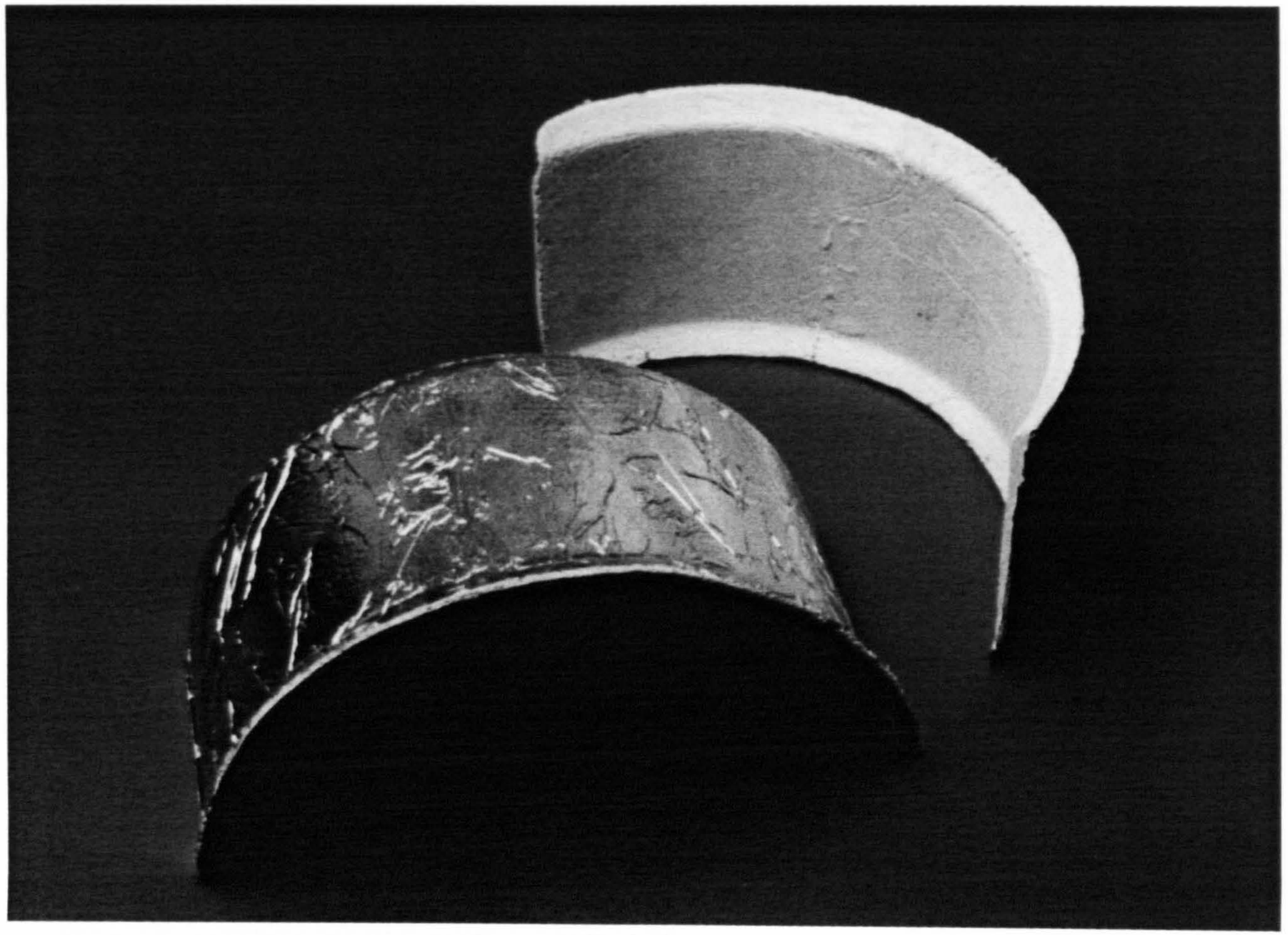

Fig. 9.3 Some of the heat shields made from the CDMC.

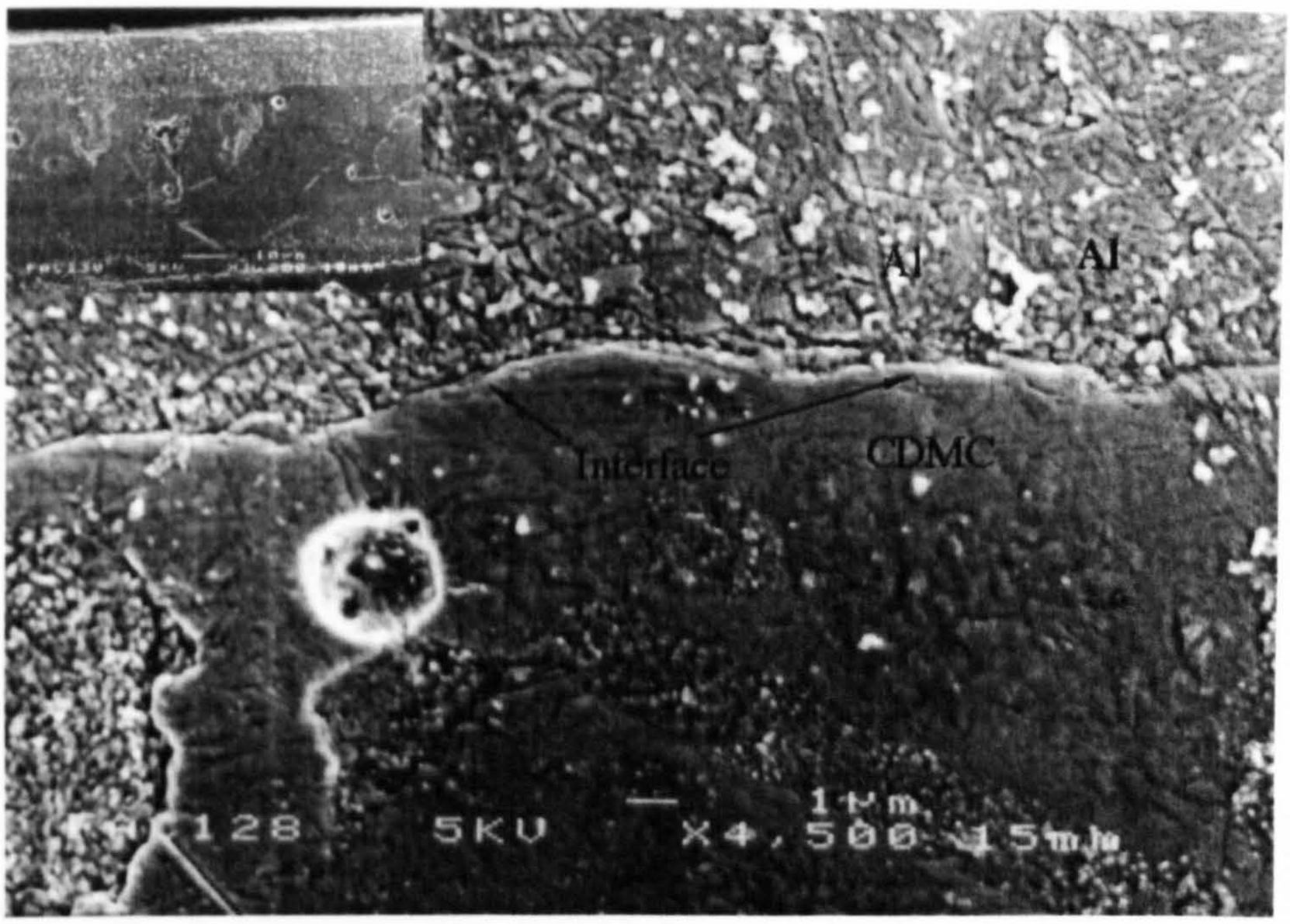

Fig. 9.4 The interface between the ceramic matrix and Al foil, shows a good bonding. The heat shields without environmental tests generally presented good interface.

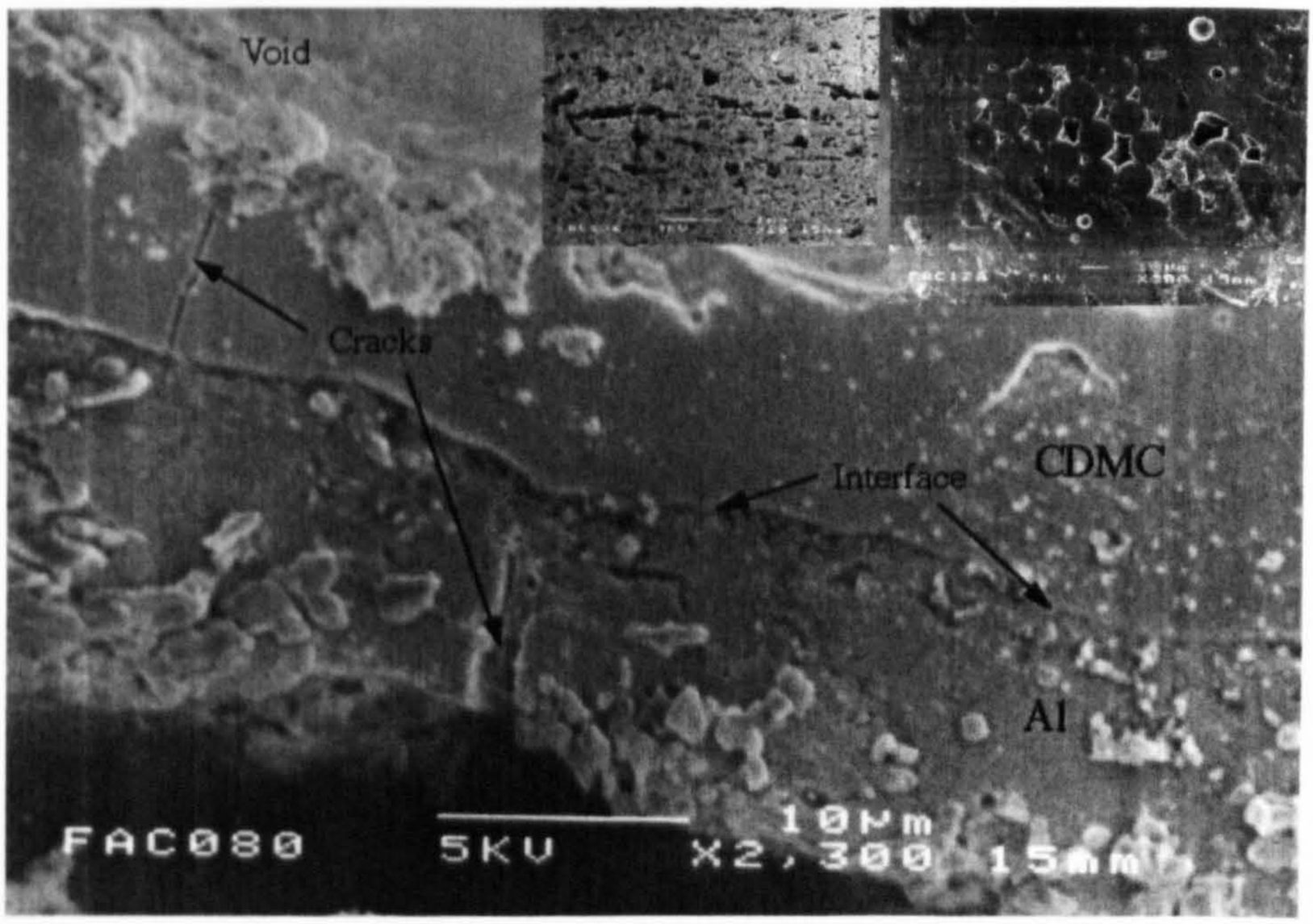

Fig. 9.5 SEM examination of the CDMC heat shield after standard industrial heat and chemical corrosion tests for car components. The Al foil was corroded and few cracks were generated from the Al foil and might extend to the interface between Al film and ceramic matrix. On the top right hand, both present the pores matrix and glass fibre bundle remained in an original conditions inside the tested specimen.

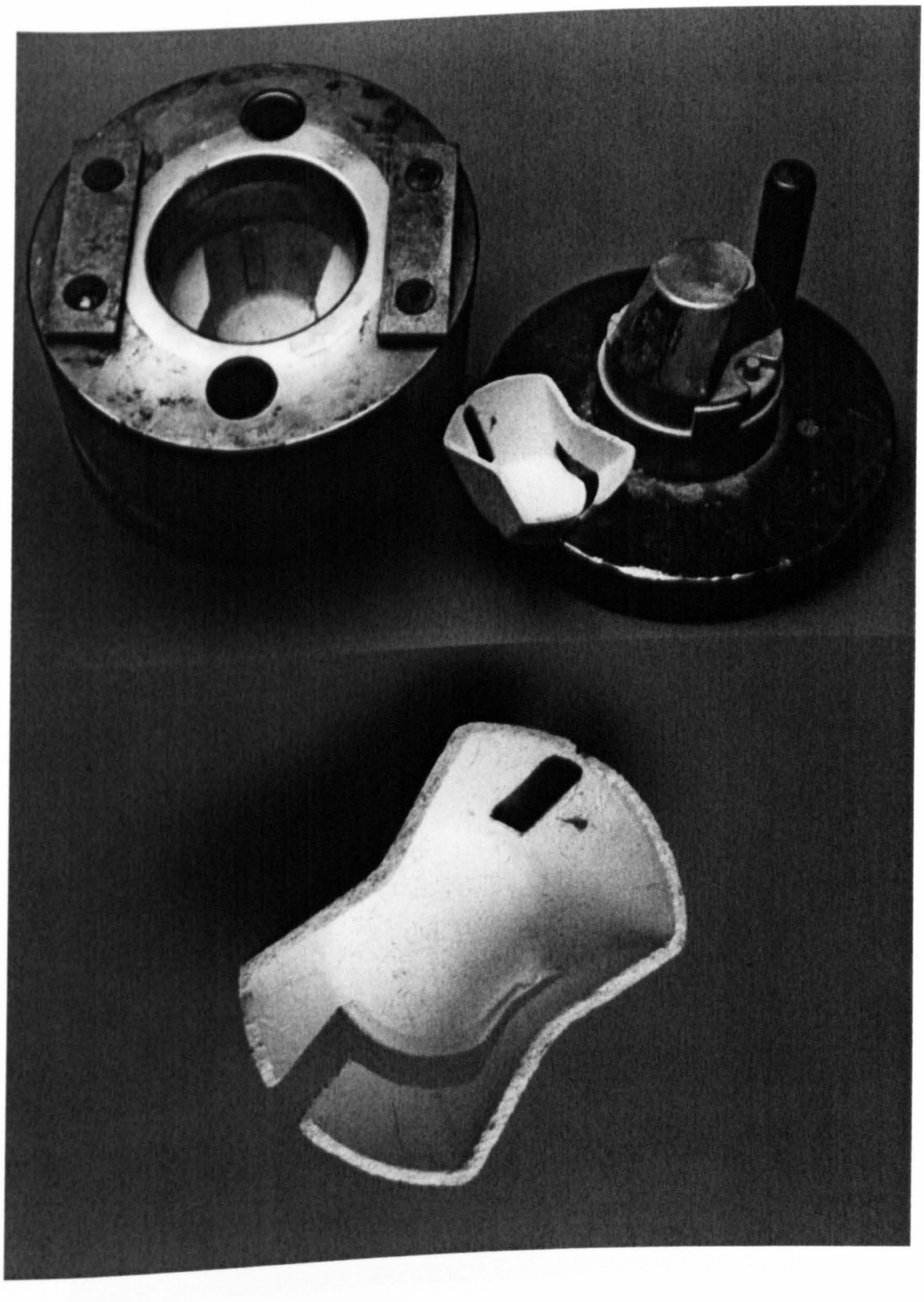

Fig. 9.6 A few HSCs moulded from the CDMC, top photo shows two halves of complicated moulds used.

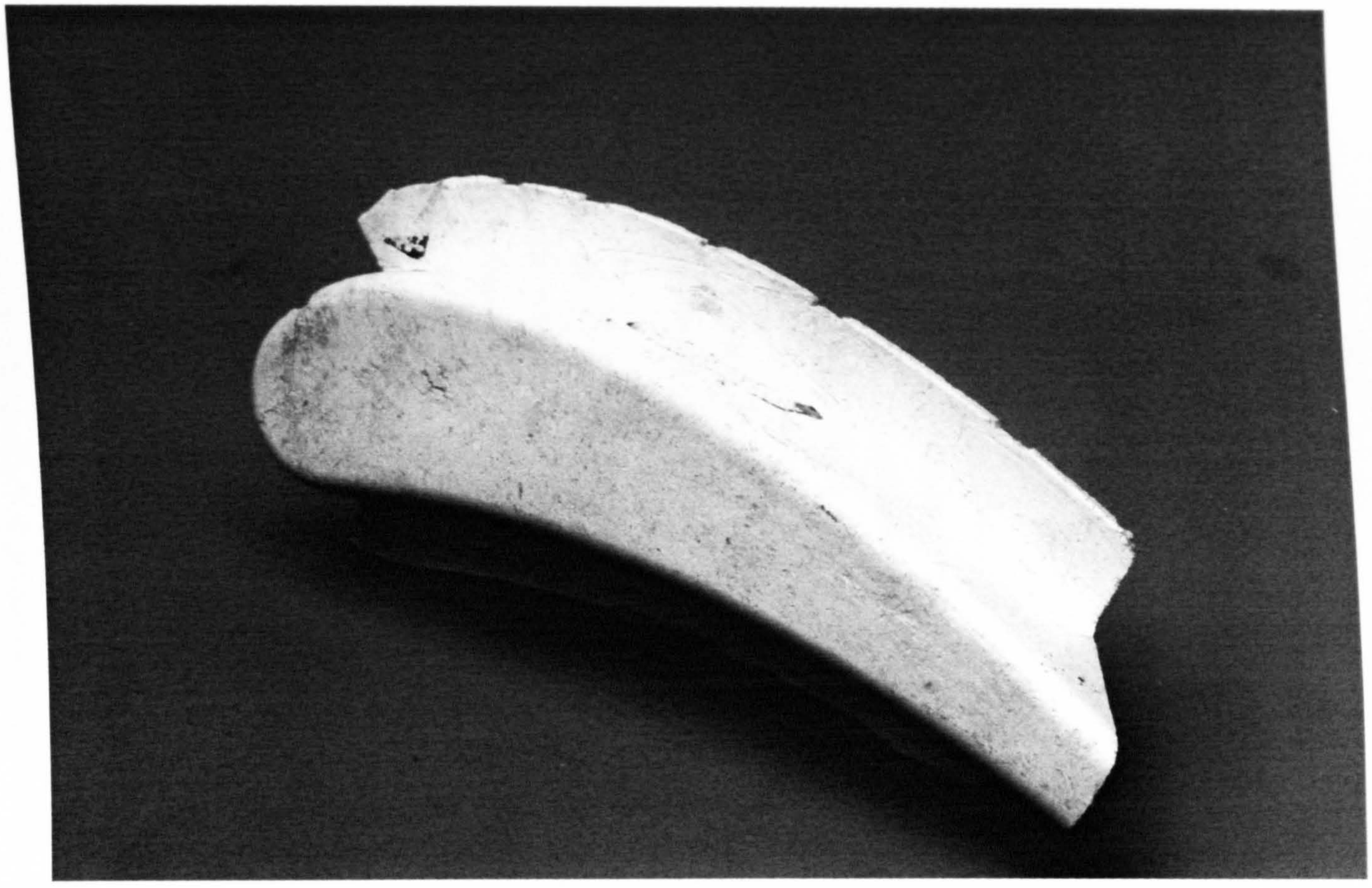

Fig. 9.7 A photo of a fairing moulded from ceramic moulding compound. The mould used was a pair old graphite moulds for making advanced polymer composites at elevated temperatures.

Chapter 10

CONCLUSIONS

10.1 Overview of the research

A silicate based glass fibre moulding compound is a composite which combines exceptionally high thermal resistance and reasonable mechanical properties. It overcomes some of the difficulties in manufacture of traditional ceramic composites with complicated shapes. With chopped fibre reinforcement, a CDMC can be designed with different functions as application requires. Compared with the traditional ceramics and glasses, the CDMC possesses the features of using low cost raw materials, low cost in manufacture, improved ductility and design versatility.

As the reinforcement in the CDMC, the chopped AR-glass fibres were used in consideration of the cost. The continuous development of AR-glass fibres have provided suitable low cost alkaline resistant reinforcement for the composite. Liquid metallic silicates as the main binder, with additional mineral fillers which functionalised for special properties, constitute of the matrix system.

The chopped fibre composites are an ideal choice for products with complicated shapes or details which require fire and heat resistance. The un-cured composites can flow within a closed mould, and form the desired shape under certain temperatures. The mechanical properties of the moulded parts depend on the formulation of the composites, and the processing routes. The strength of the moulded parts was not only dependent on the formulation of the composites, but also on the manufacturing methods and the moulding conditions. This is due to the changes in physical properties such as water content and density in the moulded parts.

Through this research, a formulation for optimum processibility and mouldibility of the material has been achieved by using the traditional DMC manufacturing and moulding processes. More freedom in material selection, design of fibre matrix combination, viscosity control and moulding process has been realised.

10.2 Background of the research

Polymer dough moulding composites have been well developed for more than 40 years. The raw materials are normally glass / carbon fibres with polymer matrices such as unsaturated polyester, epoxy or phenolics. More and more thermoplastics are also used as matrix systems in order to provide special mechanical properties and functionality. These composites have been used in many areas and occupy big share in plastics and metallic application markets.

The polymer based composites can only work within the temperature range 100 - 200 °C, which is a limiting temperatures for their applications. However, there is a market requirement for materials possessing a working temperature over 200 °C, even up to 1000 °C. This is the major reason for developing ceramic silicate based composites. Metallic silicates are one of the many choices for the matrix with low cost and easy proccessibility at relatively low moulding temperatures. For their new material concept with new processing route, problems encountered at the early stages of the research was that no background information was available for processing.

10.3 Materials and compounding

Material selection and compounding are so important that they determine the basic mechanical and thermal properties. After the confirmation of the basic composition of the ceramic dough moulding compound, a traditional DMC processing route for the CDMC was investigated in the early stage of this research.

Since the compounding process involves the matrix flow in the processing equipment, and more importantly wetting out the reinforcing fibres, the rheological properties of the ceramic matrix was investigated and it was identified as a Non-Newtonian slurry with an important property of plastic deformation. The viscosity increment of the matrix during

moulding is an apparent reflection of the silicate polymerisation, which makes the compounding and moulding process possible. A viable matrix has been formulated by following the viscosity effects generated by hardeners and mineral fillers. Many formulations were developed with different advantages at the early research stage and, later, mechanical and thermal properties were studied. A general formulation was concentrated on in order to produce the best viscosity - processing relationship and compatibility with the new chopped glass fibre, AR62/2.

The viscosity of the matrix slurry played an important role in processing the CDMC. And the viscosity increase for CDMC is ideal for the stage of moulding. The matrix initial viscosity was, as expected, low enough to wet out the chopped glass fibre. Then the viscosity of premixed paste (>$1x10^6$ cps = $1x10^3$ kg/m·s = $1x10^3$ Pa·s) can increase shortly for following moulding.

The followings are some important factors for material's viscosity:

- The viscosity increase rate in the compounding has been matched to the moulding requirements. With Fabutit 320, the viscosity of the matrix slurry was low (3000 to 5000 cps), providing good condition for matrix to impregnate the fibre. About 30 to 40 minutes after mixing, the viscosity started to increase until it reached 1.0 x 10^7 cps after more than few hours (or few days depending on formulation and environmental condition) when it is ready for moulding. The viscosity of the matrix continues to raise very slowly in two to three months which would be the suitable time for the moulding process.

- The fillers also influence the viscosity. Different fillers have different influences on the viscosity of the matrix system.

The required viscosity increase rate for the CDMC in the compounding and moulding is adjustable. The use of glass fibre and mineral fillers keeps costs low, while the use of the ceramic matrix is environmentally clean and safe.

10.4 Moulding

The CDMC is mouldable using selected moulding conditions. At lower temperatures of 99 - 120 °C, qualified products were difficult to obtain. This was linked to distortion of products if proper fixture was not employed after moulding. At medium temperatures of 130 - 150 °C, the moulded products had a smooth surface finish. The moulding pressure can give contribution to control its porosity, density and surface quality, especially within the range of 8.0 MPa to 12.0 MPa. These controls in turn give qualified products. The voids in the composites would remain at a minimum at this temperature and pressure range. Some thermal / shrinking residual stresses also generated micro-cracks in matrix and around fibres or fibre bundles, providing opportunities for the material to divert fracture energy and to increase the interfaces by fibre sliding and pull-out.

The moulding conditions were optimised through investigation of a temperature range of 99 - 190 °C. By increasing the moulding temperatures, the de-watering time and the time for closing the mould was reduced. But there was an increment in porosity. This also resulted in a better interfacial bonding and lad to a material brittleness. The cause of this phenomenon of porosity may be due to the matrix shrinkage while water evaporating and rapid hardening at the elevated moulding temperatures.

The severe corrosion presented when the moulding temperatures over 160 °C for E-glass fibre. This type of corrosion has not been observed with AR-glass fibres in this concerned temperature range. However, an interfacial diffusion or good interfacial bonding between fibre and matrix has taken place for both E-glass and AR-glass when moulding over 170 °C.

10.5 Mechanical properties

- General mechanical properties

The range of moulding temperatures for an ideal ceramic DMC was further defined by a compromise between brittleness and ductility.

Moulding temperatures influence the mechanical properties of the CDMC. When moulded at lower temperatures (< 130 °C), the CDMC demonstrated more ductile properties. At higher moulding temperatures (>170 °C), the material tended to be brittle. Since the fibre sizing may be damaged in alkali media, there is an optimum range of moulding temperatures for achieving the best mechanical properties. This optimised moulding temperature range for AR-glass is in the range of 130 °C to 150 °C.

The mechanical properties of the CDMC moulded at lower temperatures are also effected by time and post-curing. There were optimum properties after about 28 days of post curing in an ambient temperature. The properties of the CDMC moulded at higher temperatures appeared more difficult to control both in the moulding process and surface quality of the products.

The mechanical properties effected by volume fraction of glass fibre were examined by use of a CDMC with AR50/1 glass fibre with a volume fraction range 5%(vol.) - 22.6%(vol.). The maximum strength of the material was reached by adding fibre volume fraction of 22.6%(vol.). More volume fractions of glass fibre such as 30%(vol.) have been tried and resulted in an uncompleted wetting out during compounding. Therefore, the properties of the CDMC effected by volume fraction of glass fibre were constrained below the 30%(vol.).

The resistance of sizing to alkali becomes a key issue in developing the mechanical properties. The CDMC with E-glass fibre when moulded at the temperature higher than 160 °C, severe corrosion occurred. The sizing agent around glass fibre sheath was damaged or washed away by alkalinity, which resulted in a fibre and matrix fused together. The modulus of the CDMC with E-glass fibre approached the modulus of pure matrix, while the strength decreased tremendously. Because of this, from this step forwards, the E-glass fibre was given up as the candidate reinforcement for the CDMC.

Instrumented falling weight impact tests were performed on the plates of the CDMC with AR50/1 glass fibre. The CDMC was moulded at different moulding temperatures and added with different volume fraction of the glass fibre. The key parameters studied were the force-time histories and energy absorption during impact fracture. The plates when moulded at lower temperature (99 - 150 °C) were not completely shattered and absorbed some energy, while the plates moulded at higher temperatures (160-190 °C) completely shattered and absorbed much less energy.

The fracture mechanism of the CDMC was also analysed by the fracture pattern for flexural tested specimens. Individual glass fibre fractured end with mirror morphology after tensile fracture is studied. The fibre/matrix mismatching by thermal expansion/shrinkage was played an important role when all these materials moulded at different moulding temperatures. The related interfacial shear strength between glass fibre and matrix was studied by the fibre push-out test using a micro-indentation machine. The results revealed that the higher interfacial shear strength was achieved when the moulding temperature was set higher.

- Optimised mechanical properties

In order to optimise the mechanical properties, a new type of AR-glass fibre, AR62/2 was introduced and supplied by the fibre manufacturer which provided better processibility. The CDMC with this fibre achieved better mouldibility and good appearance compared with AR50/1 glass fibre. It is revealed that the better mechanical properties were also achieved by the CDMC with AR62/2 glass fibre.

With different fibre lengths, the CDMC revealed that optimum tensile, flexural and impact properties can be obtained with a chopped fibre length of 12 mm (AR62/2 fibre). The fibre volume fractions of the material were also examined from 15% to 27%(vol.) by using 12 mm fibre. It is found that the composite with fibre volume fraction of 22.6%(vol.) demonstrated the best mechanical properties under the moulding temperature 140 ~ 150 °C and pressure 8 - 10 MPa.

Maximum flexural properties were reached at the volume fraction of 22.6%(vol.), with the value of 120 MPa for flexural strength and 39.7 GPa for modulus. The highest tensile properties of the CDMC were obtained with 22.6%(vol.) glass fibres as well. It presented increased ductility (maximum strain to failure) over other volume fractions. The higher fibre volume fraction such as 27%(vol.), caused problems in obtaining an

uniform compound prior to moulding. The disappointing mechanical properties are probably a consequence of the non-homogeneous compound with areas of low fibre fractions. Tensile stress-strain curves are also obtained with different volume fractions. Tensile fractures revealed extensive fibre pull-out and fibre bridging, randomly crossing cracks, which provided the possibility for preventing catastrophic failures.

The behaviour of the interface is affected by sizing on the fibre and the moulding temperatures. The exact mechanism of sizing under different temperatures is beyond our control and knowledge due to commercial confidentiality. It seemed that within the examined range of moulding temperatures (99 ℃ - 190 °C), different interfacial shear strengths were produced. It has been proved that higher moulding temperatures produced stronger interfacial bond strength, while under the lower moulding temperatures produced lower interfacial shear strength or weak bond. The very weak bond could be achieved by moulding process at low temperature as low as 99 °C. The temperature range of 130 - 150 ℃ has been selected for the CDMC moulding as the better temperature range for overall mechanical properties. Some preliminary results were successful in indicating an interfacial shear strength of 22 to 37 MPa with 50/1 fibre, which is depending on the processing temperatures.

At higher moulding temperatures, the strongly bonded CDMC becomes brittle regardless of the glass fibre used. The problem here may be the weak interface (sizing) disappeared and then a strong interface formed. The fibre / matrix interface in the composites played an important role in determining the mechanical properties, especially the impact properties.

The impact properties of the CDMC with different volume fraction of glass fibre of 15-27%(vol.) were examined. The specimen with 27%(vol.) glass fraction absorbed similar amount of energy with 22.6%(vol.) specimens. Quite different with flexural and tensile properties, the material's impact properties are a dependent of fibre volume fraction and the type of glass fibre.

The maximum energy absorption data for the CDMC has been compared with an energy absorption master curves generated from varies polymer composite materials with glass fibre and carbon fibre reinforcements. For general glass fibre/polymer composites, if the specimens are of a similar size to those tested, a master curve can be constructed linking absorbed energy with specimen thickness multiplied by volume fractions. It is observed

that the value of energy absorption of the CDMC is more close to the mast curve of the carbon fibre / polymer composites and lower than glass fibre / polymer composites.

From the observation of large amount of SEM graphs of the AR62/2 glass fibre CDMC, it could be further explained that the matrix cracks generated by partially fibre / matrix de-bonding might be caused by the difference in coefficient of the thermal expansion during moulding at certain temperature range. This thermal mis-match between fibre and matrix, later led to the fibre sliding, fibre pull-out when specimens under the mechanical load. These processes are followed by fibre bridging, which may prevent the CDMC from catastrophic failures such as shattering in impact tests as well.

The optimised glass fibre (12 mm AR62/2 fibre) in formulation, together with the optimised range of moulding conditions for compounding / manufacturing ideal CDMC provide a base platform for the design of the CDMC with proper ductility and functionality.

There are some evidences that the elastic properties of the composites are determined by fibre volume fractions. And the failure of fibres and specimens may be attributed to void content (negative effect) and residual stresses (positive effect).

Although the research was mainly emphasised on the CDMC processing, the problem of "brittleness in ceramics" has also been studied. However, over 30 years research into improving ceramic toughness, it seemed that ceramic matrices combining with fibres has been one of the best routes to solve the problem. The interesting thing is that the theories which have been developed seemed compatible with this CDMC composites involved in this research work.

Generally speaking, the improvement in the mechanical failure processes for the CDMC as so called pseudo plastic deformation involves matrix cracking, fibre de-bonding, followed extensive fibre pull-out, then fibre fracture or bridging. This research work has primarily proved that through these mechanisms, the fibre reinforced mineral silicate composites can stop the catastrophic failure or shattering under mechanical loads or under different impacting forces.

10.6 Fire and thermal properties

Fire and thermal properties of the CDMC were investigated by using fire penetration test and material's reaction to fire / heat by the Cone Colorimeter test. Meanwhile, a phenolic based DMC and other polymers were also tested at same conditions for comparison.

The data of fire resistance for the CDMC tested shows that it performed exceptionally well in delaying the temperature rise on the unexposed face without combustion on the inner face. It is natural that the ceramic panels would outperform any equivalent polymeric matrix composite such as the phenolic matrix composites. Although fire retardant GRP has improved fire properties, such as peak heat release rate, total heat release and oxygen index, these sacrifice the properties of smoke emission, and toxicity, etc.

The CDMC also shows the better mass stability in resistance of the fire penetration compared to those polymer matrix DMC. There was no ignition for the CDMC in comparison with a polyester SMC/DMC, the phenolic SMC/DMC, and a fire retardant FRP/GRP. Compared with their original composites, the fire retardent polyester DMC and phenolic SMC/DMC need a longer ignition time due to 30 - 70% fillers in their matrix systems.

Among the data generated by cone calorimeter tests for the phenolic DMC, polyester DMC, PVC and PMMA, the CDMC is superior in almost all aspects. As a result of this, the overall fire and thermal properties of the CDMC outweigh the most known competitive composite systems based on polymeric matrix.

10.7 Potential applications

Potential applications have been investigated in Chapter 9 and moulding trails of a few products were discussed. The moulding for them were quite successful and samples of the moulded parts have been produced.

Since the fire and thermal properties of the CDMC are superior to those of phenolic DMC or polymeric composites, the working temperature can be raised to 600 - 700 °C. Meanwhile, through the formulation design, the CDMC can be thermally stable and non-flammable in fire at elevated temperatures while absorbing large amount of heat energy.

10.8 Future work

Future work should involve:

Simulation of compound flow during moulding, interfacial properties, toughness measurement, mould design and release agents for the industrialisation.

- Moulding

Viscosity: matrix viscosity requires to be known at moulding temperature range for simulation of compound flow during moulding.

Moulding temperatures: detailed relationship between moulding temperatures and durability of fibre / matrix interface.

Mould release: suitable release agents need to be investigated or developed for moulding complicated components.

Mould design: based on the feature of the CDMC.

- Mechanical properties

Interfacial properties: investigating the interfacial functions of the ceramic moulding composites. Measurement of toughness of the materials: relationship with interface.

Environmental test: weather conditions and chemical corrosive conditions.

- Material's elastic modulus

A suitable equation can be developed in order to evaluate elastic properties of the chopped fibre ceramic composites. In a broad category, the chopped fibre reinforced cement, concrete, glass and most of ceramics should also fit into the same equation. It may be developed into two direction, one is the $E_f >> E_m$, such as ceramic matrix with carbon fibres or SiC fibres, the other one should be E_f is similar to E_m. , as ceramic matrix with glass fibre and other similar modulus fibres.

For example, glass reinforced ceramics such as glass and cementatious materials should belong to the class of E_f similar to E_m ; carbon fibres (Bahl, Shen, Lavin and Ross, 1998) or SiC fibre (Yang HH, 1992) or other high modulus fibre reinforced glass and low modulus ceramics should still belong to the $E_f >> E_m$ category. But whether or not Cox or Halpin-Tsai equations are suitable for this category remains to be a question and should be investigated.

Through the development of the CDMC, a new and simple manufacturing process has been established with a group of low cost raw materials. Compared with advanced ceramic materials and their manufacturing routes, the CDMC is much more economical and efficient. It can also be a competitive material to polyester and phenolic moulding composites due to its fire resistance and thermal insulation properties at elevated temperatures.

References

Agarwal BD, Broutman LJ, " Analysis and Performance of Fibre Composites: fibre debond and fibre pullout", Second Edition, pp 327-329, John Wiley & Sons, Inc., 1990.

Ali MA, Majumdar AJ, Singh B, "Properties of glass fibre cement-the effect of fibre length and content", *Journal of Materials Science* , 1732 - 1740, Volume 10, 1975.

Ambroise J, Dejean J and Pera J, "Study of fibre matrix interfaces in metakaoline-OPC /blended cement GRC composites", Materials Research Society "*Bonding in Cementitious Composites*" Symposium Proceedings. P175, Volume 114, December 1987, Boston, USA.

Ashby MF and Jones DRH, "Chapter 13: Fast Fracture and Toughness", Engineering Materials 2: An Introduction to Microstructures, Processing and Design. pp 121-128, ISMST, Volume 39, 1978.

Ashby MF and Jones DRH, "Chapter 14: Micro-mechanisms of fast fracture", Engineering Materials 2: An Introduction to Microstructures, Processing and Design. pp 129 - 134, ISMST, Volume 39, 1978.

ASTM 1354, "Heat and visible release rates for materials and products using an oxygen consumption calorimeter", American Society for Testing and Materials, 1990.

ASTM D790-91: "Standard test methods for flexural properties of unreinforced and reinforced plastics and electrical insulating materials". pp269-278, 1991.

ASTM D792-86: "Standard test methods for specific gravity (relative density) and density of plastics by displacement", pp 299-320, 1986.

ASTM: STP. 452, 1969, pp. 90-106.

Aver R. G. and J. D. F. Ramsay, *Journal of Colloid Interface Science*, Volume 42, P597, 1973.

Aveston J, Cooper GA and Kelly A, " The properties of fibre composites", conference proceedings. National Physics Laboratory (IPC), pp 15, 1971.

Aveston J., A. Kelly, "Theory of multiple fracture of fibrous composites", *Journal of Materials Science* , vol. 8, P352-362, 1973.

Aveston J, Mercer RA and Sillood JM, *Conference Proceedings*, National Physics Laboratory (IPC), P 93, 8/9 April 1974.

Babic L, Dunn C & Hogg PJ, "Damage development and its significance in GRP subjected to impact", Plastics and Rubber Processing and Applications 12(1989) 199-207.

Bahl OP, Z Shen, Lavin JG and Ross RA, "Manufacture of carbon fibres", Carbon Fibre, third edition, revised and expanded, edited by Jean-Baptiste Donnet, Tong kuan Wang and Jimmy C M Peng and Serge Rebouillat. P31, 1998.

Banas RP, et al., "Lessons learned from the development and manufacture of ceramic reusable surface insulation(RSI) materials for space shuttle orbiters," NASA/LARC conference "Shuttle Performance: Lessons Learned," Langley Research Centre, March 8-10, 1983.

Barby D, Parfitt GD and Sing KSW, "Silica: Characterisation of Powder Surfaces", pp 353, Academic, New York, 1926.

Bentur A, Mindess S, "Fibre Reinforced Cementitious Composites", pp 218-279, Elsevier Applied Science, London and New York, 1990.

Breuer H, "1,2,4-Oxadiazolonylancetyl cerphalosporins", 1995 US Pat. 3, 929,782.

Brookfield Engineering laboratories Catalogue "Brookfield viscometer/rheo-meters", INC.

Brookfield Engineering Laboratories, INC. "A Guide to Getting More from Your Brookfield Viscometer", 1990.

Brunauer S, Emmett PH and Teller E, Journal of American Chemical Society, 60, 309 (1928).

Brunauer S, "The Absorption of Gases and Vapours", Physical Absorption, Vol. 1, Princeton University Press, Princeton, N. J., 1495.

BS 2782: Part 10: Method 1003: 1977 EN61. British Standard Methods of testing Plastics. Part 10, glass reinforced plastics. Method 1003. Determination of tensile properties.

BS 2702: Part 10: Method 1005, 1977 EN63. British Standard methods of testing Plastics. Part 10. Glass reinforced plastics. Method 1005. Determination of flexural properties. Three point method.

BS 2728: Part 3: Method 353A: 1991, ISO6603-1, 1985. "Methods of testing Plastics, Part 3. mechanical properties". Method 353A. Determination of multi-axial impact behaviour by the falling dart method.

BS 476: "Fire tests on building materials and structures, Part 20, Method for determination of the fire resistance of elements structure (General principles)", 1987.

BS 6853, "Fire precautions in the design and construction of railway passenger rolling stock", 1987.

Burnaner S, "The Absorption of Gasses and Vapours", Physical Absorption, vol. 1, Princeton University press, Princeton, N. J., 1945.

Bushby AJ, PhD thesis: "Structure and Properties of Glass Fibre Reinforced Cements", pp 15-21, 1991.

Buzagh A, "Von Colloid Chemistry", 2nd ed., Wiley, New York, 1950, pp. 307-326.
Caletka R., Radkokhimiya, 12(4), 549 (1970).

Callister WD, Jr., "Materials Science and Engineering: An Introduction" Third Edition, p 377-397. John Wiley & Sons. INC, 1993.

Cem-FIL International Ltd "Data sheets of AR glass fibre", 1996.

Chamis CC, " Mechanics of load transfer at the interface", Chapter 2, Vol. 6, *Composite Materials*, 1994.

CMMT 0918/0932: NPL Test Report: Thermal expansion of ceramic matrix composites (Commercial restricted), 1998.

Chant JM, Bleay SM, Harris B, Russell-Floyd R, Cooke RG and Scott VD, *Journal of Materials Science*, vol. 30, 2769-2784, 1995.

Claymore Systems: "Data sheet-1 and Data sheet-2", 1994.

Cooper GA, Kelly A, "Role of the interface in the fracture of fibre-composite materials", Interfaces in Composites, ASTM STP 452, American Society for Testing and Materials, 1969, pp. 90-106.

Cox HL, "The elasticity and strength of paper and other fibrous materials." British Journal of Applied Physics. 3, 72-9, 1952.

Crosfield Chemicals: "Data sheet 2",1994.

Crosfield Chemicals: "Categories of Crosfield Soluble Silicates for the Foundry Industry", 1995.

Dainippon Ink and chemicals, Inc., "Manufacturing methods of organic composites", **JP** 5898302 A2 830611, 1994.

Dando NR, Cleaver TR, Pearson A, Stinson JM, Kolek PL and Martin ES, "Aluminium trihydroxide(ATH) as a filler for polymer composites: improvements in thermal stability by controlled precipitation" 50th Annual Conference, Composites Institute, The Society of the Plastics Industry, Inc. 30th January -1st February, 1995.

Darby D, Griffiths T, Jacques AR, Pawson D and Thompson R, "The modern Inorganic Chemistry Industry: 'silicon compound", The Chemical Society, London, UK. 1977.

Dubinin MM, "Adsorption in micropores", Journal of Colloid Interface Science, 23, 487-499, 1967.

Dubinin MM, Adv. Colloid Interface Sc., 2, 217 (1968).

Eckel A. J. and Bradt RC, "Strength distribution of reinforcing fibres in a nicalon fibre/chemically vapour infiltrated silicon carbide matrix composite", Journal of American Ceramic Society, 72, pp. 435, 1989.

El-Shamy TM, Lewins J and Douglas RW, "Kinetics of the reaction of water with glass", Glass Technology, volume 13, No 3, pp 81, 1972.

El-Shamy TM, Lewins J and Douglas RW, "The dependence on the pH of the decomposition of glasses by aqueous solutions", Glass Technology, volume 13, No. 3 1992.

Ellsworth, Mark W., "'Inverse' organic-inorganic composites materials", *Chemical Materials*, , 5(6), pp 839-844, 1994.

Evans AG, Zok FW, *Journal of Materials Science* 29, pp 3857-3896, 1994.

Everett DW. and Stone FS, "The Structure and Properties of Porous materials", Proc. 10 th Sump. Colston Research Society, University of Bristol, March 24-27, 1958.

Fincke H; Bohr H; Staeger S, ICI, "Mehrschichtige platte", **DE** 2540017 760422.

Fishbane, PM; Gasiorowicz, S; Thornto, ST; Chapter 21 "Properties of Solids: 21.1 The nature of solids", Physics, for Scientist and Engineers, Second Edition. pp 563-577, 1996.

Fleek N. A., Proc. R. Soc. A432 (1991) 55.

Fu Yan, Xie P, Gu P and Beaudoin JJ, "Characteristics of shrinkage compensating expansive cement containing a pre-hydrated high alumna cement-based expansive additive", Cement and Concrete Research, Vol. 24, NO. 2 pp. 267-276, 1994, Elsevier Science Ltd., 1994.

Grayson Martin, editor, "Encyclopaedia of Glass, Ceramics, Clay and Cement", published by John Wiley & Sons, Inc., pp 198-230, 1985.

Greenwood NN And Earnshaw A, "Chemistry of the Elements", p 379-419, 1984.

Halpin, JC and Tsai, SW, "Environmental factors in composite materials design," Air Force Materials Laboratory Technical Report AFML-TR-67-423, 1967.

Hardt DE, "Process control of thermosetting composites: Context and review", *Advanced Composites Manufacturing,* edited by Gutowski TG, John Wiley & Sons, Inc., 1997.

Haug T and Schafer W, "Fibre reinforced ceramics for aerospace applications," Advanced Materials and Structures from Research to Application, SAMPE European Chapter, 163-173, 1992.

Hayami H, "Flame-retardant resin composition and insulated electrical wire employing the same" **US 5236985 A**, 1993.

Hendrdkus V, "Moulded building materials and their manufacture", NL 88-339 880211, 1995.

Hideo H, Takaaki S, Shgigemi K, "Manufacturing of inorganic foamed articles for thermal insulators", JP 02263775 A2 901026, Application: JP 89-85989 890404.

Hogg PJ, Ahmadnia A, Davies P and Croquette JP, "The Development of Fire performance test methods for glass fibre composite materials". Seventh European conference on Composite Materials, Volume 2, ECCM-7, 14-16 May, 1996. London, UK.

Hogg PJ, PhD Thesis, P 67 - 70, 1981.

Holmes ST, "Porous foamed silicate products", **US. Pat. 3.095, 312** (1963).

Hull D. and T. W. Clyne. Chapter 10, page 237 - 270, " An Introduction to Composites Materials". -2nd Ed, 1996.

Iler RK, "Polymerisation of Silica", Chemistry of Silica, p 223-227, Second Ed. 1984, New York.

Iler RK, "Chemistry of Silica", pp 641~645, 1984, New York.

Iler RK, "Colloid Chemistry of Silica and Silicates", Cornell University Press, Ithaca, pp 39, New York, 1955.

Iler RK, Matijevic E, Ed., "Surface and Colloid Science", Vol. 6, p.11, Wiliy, NY., 1973.

IMO resolution A517(13), "Recommendation on fire test procedures for 'A', 'B', and 'F' class divisions', International Maritime Organisation, 1984.

Industry Overview: "FRP materials, manufacturing methods and markets." Engineering & Manufacturing Solutions for Industry, Composites Technology, Yellow Pages, 1999.

Iribarnegaray JE, Minones TJ, Garcia SF, and San Pedrero P, "Chemistry and Physical Chemistry" Anwendungstech. Grenzflaechenaktiven Stoffe, Ber, Int. Kong. 6th 1972, Carl Hauser Verlag, Munich, 1973.

Ishchenko SS, Filippovich AY, Veselovskii RA, " Water state in the systems based on the water glass and isocyanates", Inst. Dhim. Vysokomol. Sodden., Kiev, USSR, 57(9), 1002-6, 1991.

Ishikawa, Iakeshi, "Heat and fire-resistant expanded inorganic-polymer", **JP 58005932 B4 830202**, 1994.

ISO 179/1982: "Plastics-Determination of Charpy impact strength of rigid materials".

ISO 3261, " Fire tests - Vocabulary", 1975.

ISO/TR 3814/ISO 5660/DIS: "Fire Tests - Reaction to Fire - Rate of Heat Release from Building Products (Cone Calorimeter).", International Organisation, 1992.

Jamet J. F., D. Lewis and E. Y. Luh, Ceram. Eng. Sc. Proc. 5(1984) 625.

Jang Jyongsik and Hatsuo Ishida, "Hydrothermal stability and disruption behaviour of the mixed silane with a crosslinking additive on E-glass fibres", ICCI-II, 365 - 380, 1347 June, 1988, Ohio, USA.

Kazufumi S, Toshio T, Kiichi M, Ichiro K, Akira K, Masayuki K, "Coloured high strength composite for building materials" JP 5-163051/A2 930629, Heisei, 1994.

Kansal P, Laine RM, "Pentacoordinate silicon complexes as precursors to silicate-glasses and ceramics", Journal of The American Ceramic Society. Vol. 77, No 4, P. 875-882, 1994.

Kelly A and Macmillan NH, "Strong Solids", 3rd Ed. (Clarendon Press, Oxford, 1986).

Kharrat M, Carpenter L, Chateauminois A and Kapsa P, "Evaluation of the fibre/matrix interfacial shear strength using reduced micro-indentation curves.", Vol. 2 ECCM-7, 14-16 May 1996, London, UK.

Kirk, "The Encyclopaedia of Chemical Technology", 2nd ed., Vol. 18, pp. 246-286, 1969.

Kiyomoto, M; Omiya-shi, SK; at al., "Hydraulic compositions and high-strength composite materials", **EP No. 0431 503 A2**, 1989.

K&K-Greeff Univar plc.: Data Sheets, 1996.

Larner A. L. J., K. Speakman and A. J. Majumdar, "Chemical interactions between glass fibre and cement", *Journal of Non-Crystalline Solids* , 20 (1976) 43 - 74.

Lee FM, "The chemistry of cement and concrete", Third edition, Edward Arnold (Publishers Ltd), 1970.

Linsen BG and Heuvel VAD and Flood EA, "The Solid-Gas Interface", pp 1025, Vol. 2, Dekker, New York, 1967,.

Mackenzie KJD, Brown IWM, "Process for manufacturing ceramic-like materials and products". NZ 212330, 1989.

Mackenzie KJD; Brown IWM, Ranchod P, Meinhold RRH, "Silicate bonding of inorganic materials, Part I. Chemical reactions in sodium silicates at room temperatures", *Journal of Materials Science*, (1991), 26(3), 763-768.

Mackenzie KJD, Brown IWM, Ranchod P, Meinhold RH, "Silicates bonding of inorganic materials, Part II. Chemical reactions in sodium silicates at high temperature", *Journal of Materials Science*, Vol. 26. No. 3 pp. 769-775, 1991.

Mackenzie KJD; Meinhold RH; "A glass-bonded ceramic material from chrysotile(white asbestos)", *Journal of Materials science,* Vol. 29, No 10. pp. 2775-2783, 1994.

Mackin T, Warren P and Evans AG, Acta Metall. Mater. 40 (1992) 1251.

Majumdar AJ, Nurse RW, "Glass fibre reinforced cement-Invited review", *Building Research Establishment*, 5th October, 1973.

Maringer MF, Biggs JW, "Flame retardant polymeric compositions", **US 5225469** A, 1993.

Marshall, DB; and W. C. Oliver, "Measurement of Interfacial mechanical properties in fibre reinforced ceramic composites", *Journal of America Ceramic Society*, vol. 70 pp 542-548, 1987.

Masayuki K, Hiroshi S, Kiichi M, Kazufumi S, Akira K, "High strength composites", **JP 05097495** A2 930420.

Matsushita, N, Takanori K, Satoshi E, Miyoko I**, JP 55038862 800318**, 1993.

Metcalfe AG, Schmitz GK, " Mechanism of stress corrosion in E-glass filaments", Glass Technology, volume 13, No 1 1972.

Monssef DH, Nakano K, "The modelling of shear stress transfer in hi-nocalon/A-Si_3N_4 ceramic-matrix composites by the use of micro-indentation tests" , Composites Science and Technology, Elsevier Science Limited, 19th March, 1997.

Mookerjee SK and Niygi SK, Cent, Glass and Ceram. Res. Inst. Bull. 22, 1 (1975).

Murphy J, "The Reinforced Plastics Handbook", 1st Edition, Page 30, 31, 144. Elsevier Advanced Technology, 1994.

Nguyen DT, Veinot DE, James F**,** "Inorganic intumescent fire protective coatings and multi-layer composites", **US 4,888,057**, 1989.

Nicholas KEI, "The CO_2 Silicate Process in Foundries", British Cost Iron Research Association (BCIRA), Alvecharch, UK, 1972.

O'Connor KM, Krizek RJ, and Atrmotzidis DK, "Micro-characteristics of chemically stabilised granular materials", Proceedings of the American Society of Civil Engineers, 104(GT7), 939(1978).

O'Connor KM, Krizek RJ, Asce M and Atmatzidis DK, "Micro-characteristics of chemically stabilised granular materials", Journal of the Geothchnical Engineering Division, pp 13894, GT7, July 1978.

Okkerse C and Linsen BG, "Porous Silica", "Physical and Chemical Aspects of Absorbents and Catalysts", Chapter 5, pp 219. Academic, New York, 1970,.

Olivares HF, Oteiza I and Villanueva LD, "Fire behaviour of sisal short fibres reinforced gypsum", *Fire and Materials*, Vol. 18, pp 77-80, 1994. pp 417-519, John Wiley & Sons, Inc., 1985.

OMYA Croxton+Garry: "Trihyde on-4608", Technical data, 1996.

Paul KT, " Cone calorimeter: initial experiences of calibration and use", Fire Safety Journal 22(1994) 67-68.

Pepplinkhouse HJ and Davern WA, "Acoustic tiles from solid wastes", Journal of Australian Ceramic. Society 11 (1975) 42.

Perumalsamy N, Surendra B, Shah P, "Fibre reinforced Cement Composites", McGraw-Hill, Inc. New York, pp 180-201, 1992.

Plaisted AC and L. L. Pearson, Ger. **Pat. 2, 258, 111**, 1973.

Plueddemann EP and Page P, *SPI 42* nd Ann. Tech. Conf. Reinf. Plast. 21-E(1987).

Plueddemann EP, "Silane coupling agents", "Additives for Plastics", Vol. I, pp 146, Academic Press, New York(1978).

Phillips DC, "Fracture toughness testing of high performance laminates" Proceedings of the International Conference on Testing, Evaluation and Quality Control of Composites, UK, 1983.

Philips DC, Journal of Material Science, 9 (1974), 1874.

Plueddemann EP, "Present status and research needs in silane coupling", *Interfaces in Polymer, Ceramic, and Metal matrix Composites(ICCI-II)*, pp 17 - 33, June 1988.

Plueddemann EP, "Silane Coupling Agents", pp 17, *Plennm Press*, New York (1982).

Porter RA and Weber WJ, Jr., Inorg, "The interaction of silicic acid with iron (III) and uranyl ions in dilute aqueous solution", Nucl. chem., 33, 2443 (1971).

Prow KM, J. Materials Science vol. 21, pp 3590, 1986.

Remmey Jr. Bickley G, "Firing Ceramics". Advanced Series in Ceramics- Vol. 2. Published by World Scientific, pp 30-31, 1994.

Roberts M, "Organic ester hardeners in self-hardening sodium-silicate-bonded sands", Foundry Trade Journal, 133(2925), 783, December 28, 1972.

Sakae S, Keigo S, Akira T, "Fire-resistant flexible building boards", JP 01264977 A2 891023; application JP 88-90343 880414.

Sanders DM and Hench LL, "Environmental effects on glass corrosion kinetics", Journal of American Ceramics Bulletin, 52(1973) 662.

Sanders DM and L. L. Hench, "Mechanisms of glass corrosion", Journal of American Ceramic Society. 56 (1973) 373.

Sarvarant L, Mikkola E, "Fire mortar composites in fire conditions", *Fire and Materials* Vol., 18, pp 45 - 50 (1994).

Schwartz M, "'Composite Materials Handbook: 1.10, Chapter 1. pp 9-15", Second Edition, McGraw-Hii, Inc., 1992.

Shchetanov BV, Mizyurina GT, Gribkov VN, Shalin RE, Kachanov EB, "Process for manufacturing a heat-insulating material", **US 5556586**, 1996.

Sakae S, Keigo S, Hideo K, Akira T, Terumaro N, "Thermal insulator-moulding frames for buildings", JP 04071802 A2 920306(JP 90-184486 900712).

Silvaperl: "Light weight aggregates and fillers", Technical data, 1998.

Smith RA and Pater A, "Overview of Tradition Ceramics", *Engineering Materials Handbook*, p10-12, Volume 4, ASM International, 1993.

Smith CG, Peters JF, "Composites utilising fillers of surface-modified hollow microspheres", **US**. 4508556A 850402, 1994.

Snyder LR, "Principles of Adsorption Chromatography", Dekker, New York, pp 156, 1968.

Soroushian P and Bayasi Z, "Silica fume effects on the pull-out behaviour of randomly oriented steel fibres from concrete." Materials Research Society: "Bonding in Cementitious Composites", Symposium Proceedings, P 205, Volume 114, December 1987, Boston, USA.

Standard for 1952, Vol. 4, America Society Testing Materials, Philadelphia, pp 195.

Taniguchi K et al., Inst. Chem. Res. Kyoto Univ., 49, 212(1971), Nipping Kayak Zasshi, 91(6), 529(1970).

Taylor HFW, "'Chapter 19: X-ray diffraction', The chemistry of cements", Volume 2, pp 197-219. Academic Press, London 1964.

Terufusa W, Mitsuo K, Yasushi I and Masahiro I, "Sintered ceramic articles having three-dimensional porous network and manufacture of the articles", **JP** 63256578 A2 881024, 1994.

Terufusa W, Mitsuo K, Yasushi I and Masahiro I, "Sintered honeycomb-shaped ceramic articles and their manufacture", **JP** 63256576 A2 881024, 1994.

Tredway WK, Musson CW and Chen OY, "Fibre-reinforced glass matrix composites with secondary matrix reinforcement", **US** 552215, 1996.

Monroeville KGL and Damle SB, "Intumescent flame retardant composition", **US** 5227416 A.

Vail JG, Reinhold P, "Soluble silicates", ACS Monograph Series , New York, 1952, Vol. 1, pp 158; Vol. 2, 549.

Winyall ME and Acker EG, " Process for preparing silica gel", **US** Pat 3, 501, 269, 1970.

Wu Hanyang, "Thickening and diluting analysis of black talc slurry", Taoci Zazhi pp 27-29 (4), 1993.

Wuestefeld Aloys, "Fine-grained granules of expanded Perlite or vermiculite", DE 3314135 A1 841025.

Yanakiev Y, Radovanov I, " Refractory composite based on sodium meta-silicate", Tekh, Misul, 27(5), pp 49-52, 1990.

Yang HH, " 2. Chemical and physical properties of Kevlar fibre", Kevlar Aramid Fibre, P30-31, John Wiley&Sons, 1992.

Williams DB, "Practical Analytical Electron Microscopy in Material Science", page 55-101. Phillips Electronic Instruments Inc. Electron Optics Publishing Group, 1984.

Williams DB and C. Barry Carter, " Transmission Electron Microscopy: Spectrometry IV", page 599-685. Plenum Press, New York, 1996.

Goldstein JI, Newbury DE, Echlin P, Joy DC, Fiori C, Lifshin E, "Scanning Electron Microscopy and X-Ray Microanalysis", page 366-405. Plenum Press, New York, 1939.

Newbury DE, Joy DC, Echlin P, Fiori CE, Goldstein JI, "Advanced Scanning Electron Microscopy and X-Ray Microanalysis", page 236-313. Plenum Press, New York, 1986.